

NASA Contractor Report 3164

Selected Advanced Aerodynamics
and Active Controls Technology
Concepts Development on a
Derivative B-747 Aircraft

Final Report

Staff of Boeing Commercial Airplane Company
The Boeing Commercial Airplane Company
Seattle, Washington

Prepared for
Langley Research Center
under Contract NAS1-14741



National Aeronautics
and Space Administration

**Scientific and Technical
Information Office**

1980

Page intentionally left blank

FOREWORD

This document constitutes the final report for advanced research conducted under the requirements of the Statement of Work for Contract NAS1-14741. The report covers work conducted from May 1977 through June 1979. The NASA Technical Monitor for the contract was Mr. D. B. Middleton of the Energy Efficient Transport Project Office at Langley Research Center.

The investigations were conducted within the Product Development Department of the Boeing Commercial Airplane Company 747 Division. Contractor personnel who participated and their area of contribution are:

MANAGEMENT

G. W. Hanks	Program Manager
J. D. Warner	747 Technology
M. A. Booth	747 Technology
R. L. Allison	Technical Manager

AERODYNAMICS

A. H. Eldridge	Manager
E. Dickson	Wing Tip Extensions and Performance
P. A. Podenski	Winglet Design

ENGINEERING DESIGN

R. H. Weiland	Manager
E. Bulger	Structural Design
H. W. Kassel	WLA System Installation Design

FLIGHT CONTROLS

D. E. Chichester	Manager
E. P. Nolte	WLA System Control Law Synthesis, Analysis, and Simulation
W. C. Stain	Stability and Control
C. I. Svensson	WLA System Mechanization Concept

STRUCTURES

J. R. Fuller	Manager
B. R. Perkin	Manager

Flutter

M. J. Walter	Manager
B. W. Dickerson	Flutter
R. T. Wagner	Flutter

Loads

S. R. Perin	Manager
M. T. McIntosh	Lead Loads Analyst
A. R. Schwinkendorf	Dynamic Loads
R. S. Winters	Static Loads Data Analysis

Stress

T. J. Comerford	Lead Stress Analyst
D. R. Lake	Stress and Structural Sizing

WEIGHTS

D. A. Abrams	Manager
T. L. Clark	Weight Estimates
D. E. Nelson	Weight Estimates

Page intentionally left blank

CONTENTS

	Page
1.0 SUMMARY	1
2.0 INTRODUCTION	5
2.1 OBJECTIVES AND SCOPE	6
2.2 STUDY APPROACH AND GROUND RULES	7
2.2.1 Approach	7
2.2.2 Ground Rules	9
2.3 REPORT ORGANIZATION	10
2.4 UNITS OF MEASUREMENT	10
3.0 SYMBOLS AND ABBREVIATIONS	11
4.0 WING TIP EXTENSIONS	23
4.1 PRELIMINARY TREND STUDIES	23
4.1.1 Lift-to-Drag Ratio Improvement	24
4.1.2 Loads and Twist	24
4.1.3 Flutter	24
4.2 ANALYSES OF TWO WING TIP EXTENSION CONFIGURATIONS	29
4.2.1 Lift-to-Drag Ratio Improvement	29
4.2.2 Loads and Twist	29
4.2.3 Structural Resizing	30
4.2.4 Weights	34
4.2.5 Stability and Control	36
4.3 INSTALLATION DESIGN CONCEPT	38
4.3.1 Extension Configuration and Construction	38
4.3.2 Extension/Wing Splice	38
4.3.3 Wing Structural Revision	40
4.3.4 Control Systems Revision	40
4.3.5 Electric and Electronic Systems	40
4.4 INTERIM ASSESSMENT	40

	Page
5.0 WING TIP WINGLETS	41
5.1 TEST CONFIGURATION SELECTION	42
5.1.1 Aerodynamic Design	43
5.1.2 Preliminary Trend Studies	54
5.2 TEST DATA ANALYSIS	62
5.2.1 Aerodynamics	62
5.2.2 Flutter	62
5.3 ANALYSES OF TWO WING TIP WINGLET CONFIGURATIONS	74
5.3.1 Lift-to-Drag Ratio	74
5.3.2 Loads and Twist	76
5.3.3 Structural Resizing	80
5.3.4 Weights	84
5.3.5 Stability and Control	84
5.4 INSTALLATION DESIGN CONCEPTS	88
5.4.1 Z9 Winglet Construction	89
5.4.2 Wing Structural Revisions for Z9 Winglet Installation	89
5.4.3 Systems Revisions for Z9 Installation	89
5.4.4 Control Systems Revision for Z9 Installation	90
5.4.5 Z13 Winglet Construction	90
5.4.6 Wing Structural Revisions for Z13 Winglet Installation	90
5.4.7 Systems Revisions for Z13 Installation	90
5.4.8 Control Systems Revisions for Z13 Installation	90
5.5 INTERIM ASSESSMENT	90
6.0 WING LOAD ALLEVIATION	91
6.1 AILERON CONFIGURATION DEFINITION	94
6.1.1 Aileron Effectiveness	94
6.1.2 Bending/Torsion Trades	96
6.1.3 Wing Box Weight Trends	100
6.1.4 Selection and Rationale	105

	Page
6.2	STRUCTURAL BENEFITS 106
6.2.1	Loads 106
6.2.2	Wing Resizing 109
6.2.3	Weights 114
6.2.4	Actuator Sizing 117
6.2.5	Gust Loads With Wing Load Alleviation 118
6.3	CLOSED-LOOP DYNAMIC ANALYSES 121
6.3.1	Rate/Position Limit Effects on Gust Load Alleviation . . . 124
6.3.2	Maneuver Load Control/Gust Load Alleviation Effects on Flutter 129
6.4	SYSTEM CONFIGURATION DEFINITION. 131
6.4.1	Study Approach and Criteria 131
6.4.2	Control Law 133
6.4.3	System Mechanization and Installation 146
6.5	RECOMMENDED DESIGN APPROACH AND ASSESSMENT. 159
6.5.1	Recommended Design Approach. 159
6.5.2	Assessment 162
7.0	FINAL CONFIGURATION STUDIES 165
7.1	WING TIP (WTE/WTW) COMPARISONS WITH AND WITHOUT MANEUVER LOAD CONTROL 166
7.1.1	Basic Concepts 166
7.1.2	Loads and Twist 169
7.1.3	Flutter 171
7.1.4	Structural Resizing with MLC 178
7.1.5	Weights 183
7.1.6	Aerodynamics 190
7.1.7	Stability and Control 194
7.1.8	Installation Design 195
7.2	BENEFITS OF WING LOAD ALLEVIATION FUNCTIONS 201
7.2.1	Maneuver Load Control/Gust Load Control for Wing Tip Extensions and Wing Tip Winglets 201
7.2.2	Flutter Mode Control 202

	Page
7.3 FINAL EVALUATION	207
7.3.1 Performance Comparisons	207
7.3.2 Economic Comparisons	210
7.3.3 Operational Considerations	217
7.3.4 Retrofit Feasibility	219
7.4 RESULTS SUMMARY	220
8.0 CONCLUSIONS AND RECOMMENDATIONS	221
8.1 CONCLUSIONS	221
8.2 RECOMMENDATIONS	223
8.2.1 Final Configuration	223
8.2.2 Phase II	224
9.0 REFERENCES	225
APPENDIX A METHODOLOGY	A-1
APPENDIX B SUPPORTING DATA	B-1
APPENDIX C WIND TUNNEL TESTING	C-1

FIGURES

	Page
1 Study Configurations	5
2 Program Outline	6
3 Baseline 747 Model-200B for EET Studies.	9
4 1.83-m (6-ft) Tip Extension Geometry	25
5 3.66-m (12-ft) Wing Tip Extension Geometry	26
6 Effect of 1.83-m (6-ft) Tip Extension on Drag.	27
7 Performance Trends for Wing Tip Extensions	28
8 Effect of Wing Tip Extension Length.	28
9 Performance Trends for Wing Tip Extensions	30
10 Effect of Wing Tip Extensions on Wing Design Bending Moment	31
11 Wing Twist Increment for Tip Extensions	31
12 Structural Sizing of Wing with 1.83-m (6-ft) WTE	32
13 Structural Stiffness of Wings with Tip Extensions	33
14 Structural Sizing of Wing with 3.66-m (12-ft) WTE.	35
15 Effect of 1.83-m (6-ft) WTE on Static Longitudinal Stability	37
16 Longitudinal Speed/Trim Stability with 1.52-m (5-ft) WTE	37
17 Attachment Concept for 1.83-m (6-ft) WTE.	39
18 Winglet Configurations Tested in BTWT	42
19 Design Iteration	43
20 Winglet Geometry Comparison	45
21 Effect of Winglet Planform on Section Normal Force Coefficient	46
22 Winglet Z9 and Z10 Geometry	46
23 Winglet Z9 and Z13 Incremental Drag	47
24 Effect of Suboptimum Winglet Loading.	48
25 Winglet Z11 Geometry.	49
26 Winglet Z12 Geometry.	50
27 Winglet Z13 Geometry.	51
28 Wing-Winglet Junction Details	52
29 Optimum Versus Suboptimum Winglet Loadings	53

	Page
30	Winglet Trend Study Geometry 54
31	Winglet Trend Study—Aeroelastic Twist Increments 55
32	Performance Trends with Span and Cant Angle 56
33	Wing Twist Increment for Winglet Trend Study 57
34	Winglet Panel Weight Comparison 58
35	Wing Box Weight Increments for Winglet Trend Study 59
36	Effect of Wing Tip Winglet Cant Angle. 60
37	Effect of Wing Tip Winglet Span 61
38	Velocity-Damping Trends with Cant Angle 61
39	Effect of Winglets Z9, Z10, and Wing Mod on Drag. 63
40	Effect of Winglets Z11, Z12, and Z13 on Drag 64
41	Effect of Winglet Z13 on Drag 65
42	Winglet Flutter Analysis Development Summary. 66
43	Pretest Flutter Analysis Predictions Versus Wind Tunnel Results 67
44	Wing Tip Normal Force Loading Effect. 68
45	Winglet Normal Force Variation with Airspeed 69
46	Preliminary Aerodynamics for Winglet Flutter Analysis 70
47	Correlation Results with Preliminary Methodology. 71
48	Final Aerodynamics for Winglet Flutter Analysis 71
49	Structural Degree-of-Freedom Effects. 73
50	Z9 Winglet Correlation Results with Improved Methodology. 73
51	Simulated Z13 Winglet Correlation Results with Improved Methodology 74
52	L/D Comparison, WTW Z9 and Z13 75
53	Effect of Winglets on Wing Design Bending Moment 76
54	Wing Twist Increment for Winglets 77
55	Effect of Stiffness on Wing Bending Moment Ratio for Z13 WTW . . . 78
56	Effect of Stiffness on Wing Bending Moments Increment for Z13 WTW 79
57	Structural Sizing of Wing with Z9 Winglet Prior to Flutter Sizing 80
58	Structural Sizing of Wing with Z13 Winglet Prior to Flutter Sizing 81

	Page
59	Effect of Flutter Sizing on Wing with Z13 WTW 82
60	Structural Stiffness of Wing with Z13 Winglet 83
61	Effect of Winglets on Static Longitudinal Stability. 85
62	Longitudinal Speed/Trim Stability with Z13 WTW 86
63	Effect of Z13 WTW on Static Lateral/Directional Stability 87
64	Attachment Concept for Z9 Winglet (Preliminary). 88
65	Attachment Concept for Z13 Winglet (Final) 89
66	Maneuver Load Control Concept 91
67	Final WLA Control Law (MLC Only) 92
68	Wing Section Aerodynamic Effectiveness Due to Outboard Ailerons 95
69	Aileron Effectiveness on Airplane Coefficients 96
70	Effect of MLC Aileron on Base Design Bending Moment 97
71	Effect of MLC Aileron on Base Torsion 98
72	Incremental Wing Loads Due to Aileron and Retrim 99
73	Illustration of Bending Moment Alleviation Above Aileron Roll-Reversal Speed 100
74	Effect of Tab Chord Ratio on Wing Box Weight 101
75	Effect of MLC Aileron Configuration on Front Spar Web Sizings . . . 102
76	Airplane Weight Trends for Variations in MLC Aileron Tab Span . . . 104
77	MLC Aileron Configuration Selection 105
78	Wing Structural Resizing Procedures. 107
79	Effect of MLC on Base Design Bending Moments 108
80	Incremental Wing Twist for MLC on Base Wing 109
81	Structural Stiffness Ratios of Basic Wing with MLC 109
82	Wing Stiffness Design Change Effects 110
83	Structural Sizing of Basic Wing with MLC 111
84	Effect of MLC on Wing Panel Sizing for Ultimate Gust Loads 112
85	Fatigue Stresses at Specific Locations 113
86	Effect of MLC on Fatigue Sizing 114
87	Wing Mass (Weights) with MLC 115
88	Effect of Aileron Deflection Capability on MLC Benefits 117
89	Effect of WLA on Wing RMS Bending Moments Due to PSD Gust. . . 119
90	Effect of WLA on Wing Design Bending Moment Envelope 120

	Page
91	Design Envelope Gust Method for WLA System with Position Limits 122
92	Effect of WLA Rate and Position Limits on Wing RMS Bending Moments Due to PSD Gust 123
93	Power Actuator Model 124
94	WLA Stability Evaluation with Blowdown in Large Amplitude Gust . . 126
95	WLA Aileron Response to Turbulence 127
96	WLA Elevator Response to Turbulence 128
97	MLC/GLA Control Law and Gain Schedules for Flutter Analysis . . . 129
98	Flutter Stability Comparisons for MLC and GLA with WTW 130
99	Final Control Law Diagram 133
100	Effect of WLA on Airplane Short-Period Characteristics 134
101	Final WLA System Stability at V_B 135
102	Final WLA System Stability at V_C 135
103	Step Column Maneuver Response, Final Control Law 136
104	Effect of Control Law on Bending Moment Power Spectrum Near Wing Root 137
105	Effect of Control Law on Bending Moment Power Spectrum Near Outboard Aileron 138
106	Effect of MLC Gain on Gust Loads 139
107	Effect of Elevator on Wing Root Bending Moment Power Spectrum 140
108	Discrete Gust Response, Final Control Law 141
109	Autopilot Performance with WLA 142
110	Flaps-Down Roll Control with WLA 143
111	Wing-Root Bending Moment Power Spectrum 144
112	First Cycle MLC Filter Frequency Response 145
113	Interim Control Laws, CL2 146
114	Final WLA System Mechanization 147
115	WLA Control System Installation 148
116	Existing Outboard Aileron PCU and Lockout Mechanism 149
117	Outboard Aileron Electrohydraulic PCU Installation 150
118	Local Structural Revisions for MLC Aileron Installation 150

	Page	
119	Outboard Elevator Electrohydraulic Power Control Unit (PCU) Installation	151
120	Final WLA System Reliability (MLC Only)	153
121	Preliminary WLA System General Arrangement	154
122	Progression of WLA System Reliability	155
123	Electrohydraulic Actuation, Outboard Aileron	157
124	Integrated Hydromechanical Actuation, Outboard Aileron	158
125	Fuel Saving with WLA	163
126	Winglet Force Vector Illustration	167
127	Span Loadings	167
128	Effect of Aeroelasticity on WTE/WTW Loads	168
129	Effect of Aeroelasticity on Wing Bending Moments for Z13 WTW	170
130	Effect of Aeroelasticity on Wing Bending Moments for 1.83-m (6-ft) WTE	170
131	Effect of MLC on Wing Bending Moments for Base Wing and Wing with 1.83-m (6-ft) WTE and Z13 WTW	172
132	Effect of Combined WTW or WTE and WLA on Wing Bending Moment Envelope	173
133	Effect of Combined WTE or WTW and WLA on Wing Elastic Twist	173
134	Flutter Comparisons for Extensions and Winglets	174
135	Configurations for Final Flutter Analyses	175
136	Flutter Stability Comparisons for Final Configurations	176
137	MLC Effect for a 1.83-m (6-ft) Wing Tip Extension	176
138	MLC Effect for a 2.74-m (9-ft) Wing Tip Extension	177
139	MLC Sizing Effect for Wing Tip Winglets	178
140	Structural Sizing of Wing for 1.83-m (6-ft) WTE and MLC	179
141	Effect of MLC on Wing Structural Stiffness Requirements for 1.83-m (6-ft) WTE	180
142	Wing Structural Modifications Required to Add WTE/WTW without MLC to Baseline Wing	181
143	Wing Structural Modifications Required to Add WTE + MLC to Baseline Wing	182
144	Wing Structural Modifications Required to Add WTE + MLC to a Zero-Margin Baseline Wing	183

	Page
145	Weight Comparison of WTE/WTW without WLA 184
146	Weight Comparison of WTE/WTW with MLC 185
147	Change in Wing Box Weight Distribution for WTE without WLA 188
148	Change in Wing Box Material Distribution for Z13 WTW without WLA 188
149	Wing Box Mass (Weight) Distributions for WTE's + MLC. 189
150	Wing Box Mass (Weight) Distribution for Z13 WTW + MLC 190
151	Lift-to-Drag Comparison, WTE Versus WTW 190
152	WTE/WTW Relative Aerodynamic/Structural Efficiency 191
153	Effect of 1.83-m (6-ft) WTE on Initial Buffet 192
154	Effect of Winglet Z13 on Initial Buffet 192
155	Estimated Approach Speed Improvement Due to WTE 193
156	Estimated Approach Speed Improvement Due to Winglets. 194
157	Effects of WTE/WTW on Flight Control System and Flying Qualities. 195
158	Airplane Modifications for 1.83-m (6-ft) WTE Installation. 196
159	Airplane Modifications for 2.74-m (9-ft) WTE Installation. 196
160	WTE Installation Design Concepts 197
161	New Variable Camber Flap Drive for 2.74-m (9-ft) WTE 198
162	747 Wing Leading-Edge Variable Camber Flap Mechanism 198
163	Stiffener Reinforcement for Retrofit 199
164	Airplane Modifications for Z13 WTW Installation 200
165	Effect of MLC on Wing Structural Stiffness Requirements for 1.83-m (6-ft) WTE. 203
166	Wing Structural Modifications Required to Add WTE/WTW without MLC to Baseline Wing 204
167	Wing Structural Modifications Required to Add WTE + MLC to Baseline Wing 205
168	Flutter Modes for the 747 EET/Z13 Winglet Configuration 205
169	Outboard Aileron Frequency Response 206
170	Block Fuel Savings 207
171	Percent Block Fuel Savings 208
172	Block Fuel Trades with Zero Fuel Weight 208

	Page
173	Full Cost Savings per Trip Comparison 209
174	Fuel Cost Savings per Year--747-200B with 1.83-m (6-ft) WTE . . . 209
175	Fuel Cost Savings per Year--747-200B with Z13 Winglet 210
176	Effect of EET Modifications on Maximum Payload 211
177	Study Prices for 747 EET Modifications 212
178	Structural Complexity Comparison of WTE/WTW 213
179	After Tax Return on Modification Investment 215
180	WTE/WTW Price/Payback Comparison for Current Fuel Price 216
181	WTE/WTW Price/Payback Comparison for Escalated Fuel Price . . . 217
182	Wing Bending Moment Envelope Ratio for Reduced Takeoff Gross Weight with WLA System Inoperative. 218
183	Increased Semispan Operational Concerns 219

TABLES

	Page
1 Wing Tip Extension (WTE) Weight Summary	36
2 Preliminary Versus Improved Methodology Summary	72
3 Z13 Wing Tip Winglet—Weight Summary.	84
4 Weights for WLA System and Aileron/Tab Changes	102
5 Weights Breakdown for Final WLA System.	116
6 Gain and Phase Margins.	132
7 Weight Breakdown for Variable Camber Flaps on 2.74-m (9-ft) WTE	187
8 Mass (Weight) Breakdown for 2.74-m (9-ft) WTE	187

1.0 SUMMARY

Wing tip extensions, wing tip winglets, and the use of active outboard ailerons for wing load alleviation were studied as possible ways to improve fuel efficiency of the Boeing 747. The general approach was to improve the cruise lift-to-drag ratio (L/D) by means of wing tip modifications while using a wing load alleviation system to minimize the associated structural weight increase. The existing wing jig shape and cruise Mach number were retained. Potential fuel savings of the concepts were determined by detailed analyses based on wind tunnel test data. The analyses included structural resizing to determine the airplane weight increment associated with each concept. Key results were:

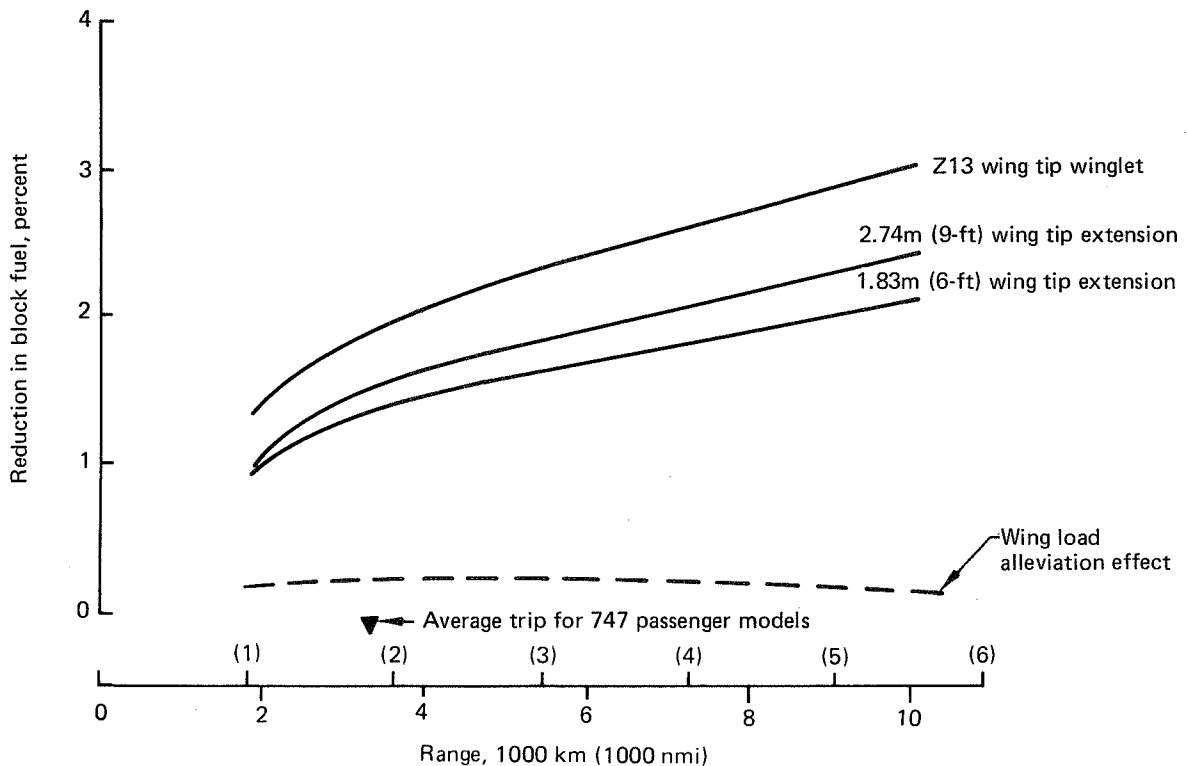
Wing Tip Modifications—A wing tip winglet was designed that performed very well during wind tunnel testing at the cruise Mach number, achieving 96% of the drag improvement predicted by subsonic-flow theory. Flutter model testing disclosed that winglet aerodynamic effects introduced a symmetric flutter mode and a wing tip flutter mode that required increased wing stiffness to restore predicted flutter speeds to acceptable levels.

Wing tip extensions up to 3.66m (12ft) per side were compared with the best winglet configuration tested, which had a span of 4.27m (14ft) canted 30 deg out from vertical. With aeroelastic losses included, a 3.2% increase in fullscale, maximum trimmed L/D was estimated for this winglet. Trend data indicate this is slightly more L/D improvement than could be achieved with a tip extension having the same panel length. Further, the winglet achieves the L/D improvement with less increase in wing semispan (gate clearance) and with lower bending moments on the inboard portions of the wing.

When the L/D improvement was adjusted to reflect the effects of the added wing tip panel and wing box reinforcement weights on fuel efficiency, the optimum WTE without WLA was found to be about 2.74m (9ft). Although the weight benefits of the reduced bending moments for the winglet were offset by heavier attachment structure and by the flutter weight penalty, estimated fuel savings for a fixed payload were greater for the best winglet than for the best wing tip as shown on the next page.

Wing Load Alleviation—The outboard ailerons on the 747 are presently used as low-speed roll control surfaces. Although wing torsion loads are increased, the symmetrically deflected ailerons are effective in reducing wing bending moments in maneuvers, even at flight conditions where they are aeroelastically reversed as roll control surfaces. An aileron balance tab was evaluated as a means for minimizing the torsion increases, but the existing (untabbed) aileron configuration appeared preferable and was retained for the system concept definition and structural benefit studies.

Outboard wing acceleration was the only feedback parameter retained in the final system configuration, which provides both maneuver load control and damping of the first wing bending mode. A fail-operational mechanization concept was selected that utilized in-line monitoring techniques with triplicated sensors, dual-dual computers, dual electronic channels, and new electrohydraulic dual-tandem actuators. Estimated reliability for this concept approaches that of a dual yaw damper system.



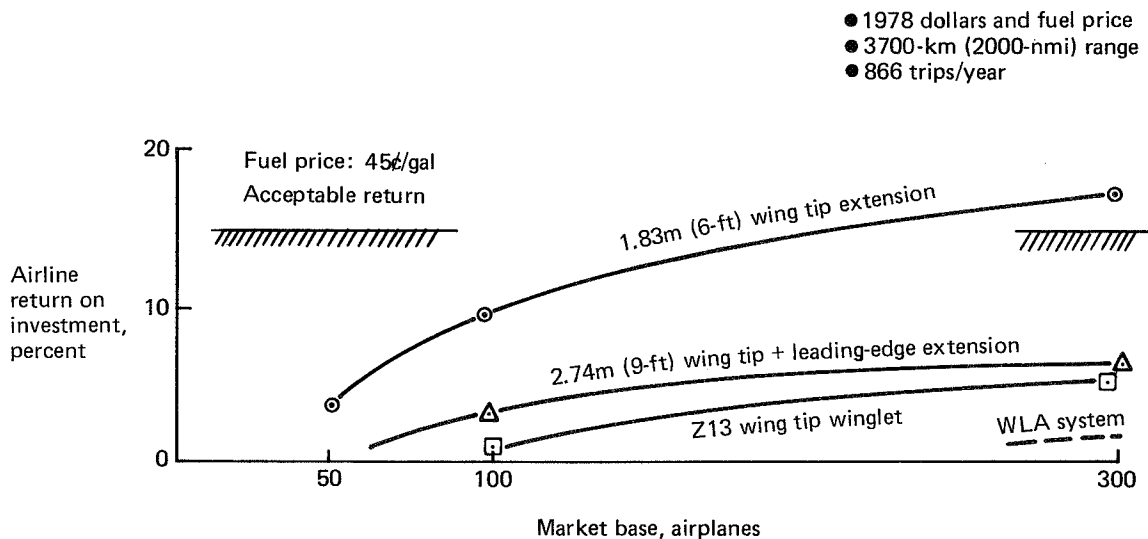
Block Fuel Savings for 747 EET Study Concepts

Wing structure resizing analyses showed that a net airplane operational empty weight (OEW) reduction equivalent to 2.5% of the wing structural box weight could be achieved with the final system configuration. About four-fifths of the benefit accrues from the maneuver load control function. Resizing of the wing with wing load alleviation also caused a slight reduction in cruise L/D due to increased aeroelastic washout. The net improvement in fuel efficiency attributable to wing load alleviation was estimated to be about 0.2%.

Wing Tip Modifications Combined With Wing Load Alleviation—A 1.83-m (6-ft) wing tip extension and the best winglet were analyzed and tested in combination with the existing outboard ailerons deflected symmetrically. Aileron effectiveness for the rigid wing was about the same with either tip extensions or winglets. Static aeroelastic effects appeared more favorable for the winglet, but increased requirements for flutter stiffness probably would offset the apparent advantage in ultimate load sizing. Use of a flutter mode control system to damp the symmetric mode could be beneficial, especially in combination with wing load alleviation, but would require an extensive development and test program. Outboard aileron span extension was not evaluated for either configuration. The fuel savings shown above for wing load alleviation were determined for the basic wing, but they are considered representative of the additional fuel savings that could be attained if wing load alleviation were combined with a wing tip modification.

Economic Comparisons—Retrofit of a tip extension or winglet appears impractical with or without wing load alleviation, so fleet implementation costs for all concepts were estimated assuming production line installation. Amortization of development

and engineering flight test program costs were excluded. Production costs were greater for the winglet than for a tip extension due to the larger size of the winglet and increased complexity in the wing-winglet juncture region. Wing box modification costs were excluded from the wing load alleviation system costs on the assumption that the system would be installed concurrent with a wing tip modification. Estimated purchase price curves (derived for this study as a function of market base) and fuel cost savings were used to compute airline return on investment comparisons of the individual concepts. Comparisons for a typical 1978 fuel price are shown in the following figure. Escalation of fuel prices relative to the general inflation rate also was considered, but it did not alter the economic rankings.



After-Tax Return on Modification Investment

The most economically attractive study configuration was a 1.83-m (6-ft) tip extension without leading-edge flaps and without a wing load alleviation system. Since payload capability is volume-limited rather than weight-limited on typical passenger routes, the structural weight reduction provided by the wing load alleviation system could not be converted to increased revenue, and the associated fuel savings were not sufficient to provide a favorable economic return. The economic return for a wing load alleviation system could be more favorable for other specific 747 applications or for airplanes designed for outboard aileron actuation at high speeds. While the winglet has excellent potential for fuel savings, it appears doubtful that recurring production costs could be reduced sufficiently for the winglet to become economically competitive with a simple wing tip extension. Furthermore, an extensive development and flight test program, including additional flutter research and testing, would be required before committing such concepts to production.

Phase II Recommendations—Flight testing of maneuver and gust load alleviation concepts has been accomplished on the B-747 as part of a separate Boeing-funded IR&D program and, in combination with a tip extension, on the L-1011 as part of the NASA (LRC)EET program. Application of a tip extension is an option for normal growth of the B-747. Near-term commercial application of winglets to the B-747 appears unlikely. As a result, no further NASA/Boeing 747 EET Phase II work is recommended in these technical areas. Application of winglets to other models (e.g., KC-135) with different wing lift distribution (tips more heavily loaded) and structural characteristics (not flutter critical) may allow more benefits to be derived. Each configuration requires tailoring of the winglet design for the specific application.

2.0 INTRODUCTION

This study was conducted as part of the NASA-LRC Energy Efficient Transport (EET) element of the Aircraft Energy Efficiency (ACEE) program. The overall objective of the ACEE program is to improve the fuel efficiency of air transportation to conserve petroleum fuel. The 747 EET study was concerned with aerodynamic improvements in the form of wing tip modifications to improve lift-to-drag ratio (L/D) and in the application of active controls for wing load alleviation to minimize the structural weight increment associated with the wing tip modifications. The study concepts, illustrated in Figure 1, were analyzed individually and in combination.

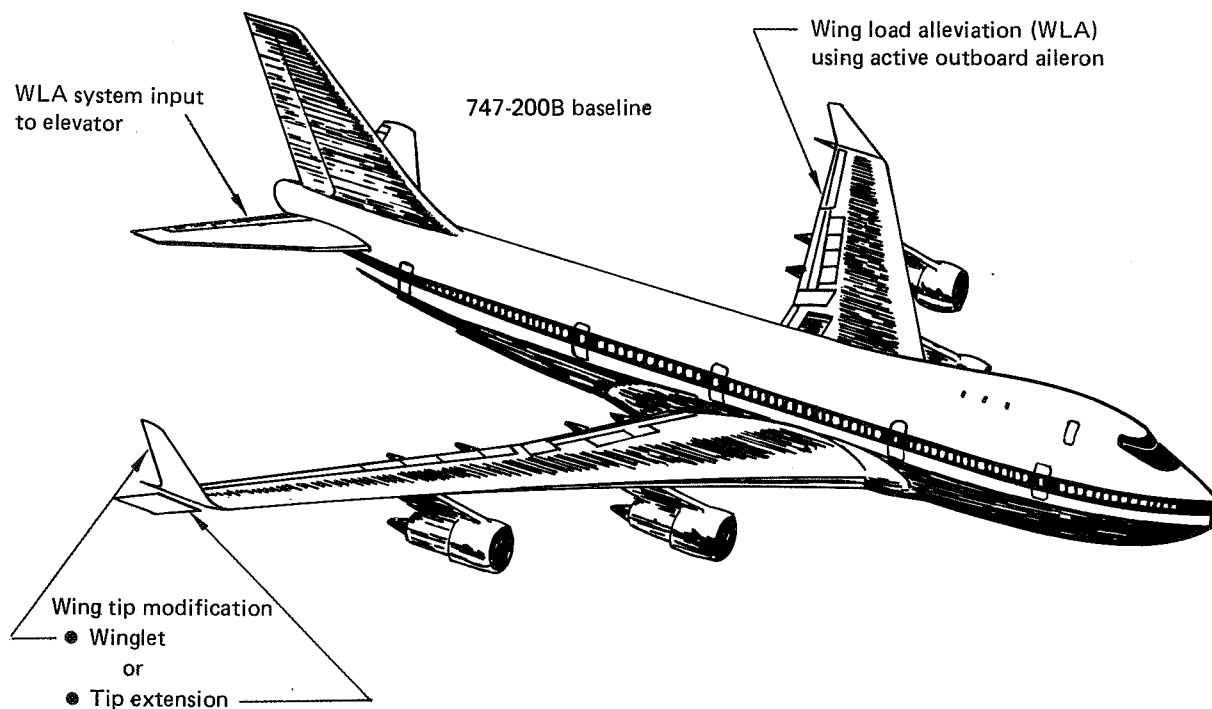


Figure 1. Study Configurations

The winglets and tip extensions decrease induced drag, thereby improving the L/D. Tip extensions increase the real aspect ratio of the wing, while winglets increase the effective aspect ratio and also produce a forward-acting force via the forward inclination of the winglet normal force vector (similar to a sail). Tip extensions differ aerodynamically from a new wing of increased span in that the twist distribution of the existing wing is not reoptimized for the WTE. The study ground rule of maintaining existing wing jig twist to minimize changes to production tooling (an important economic consideration) tended to reduce the L/D benefits of both the WTE and WTW.

The wing load alleviation concept studied was to use the outboard ailerons to shift the wing lift distribution inboard in maneuvers and low frequency gusts, and to damp the first wing-bending-mode response to higher frequency gusts. The elevator was used to compensate for the pitching moments induced by the ailerons.

Relative benefits of the concepts will vary from aircraft to aircraft. For example, winglets should be more effective on the KC-135 than on the B-747 because of the heavier wing tip aerodynamic loading on the KC-135. Structural weight benefits of WLA could be greater for airplanes such as the L-1011 already equipped with high-speed outboard ailerons.

The 747 EET program was planned for accomplishment in two phases. The first phase, a 2-year study program, was completed as described in this report. Concepts identified as having potential for near-term commercial fleet implementation were to be identified in the Phase I study. At the conclusion of Phase I, a recommendation was to be made regarding continuation of the program into a Phase II activity for further development and flight test verification. Although continuation of the 747 EET program into Phase II has not been recommended, a valuable data base has been generated that can continue to be used for reference on new and derivative airplane programs.

2.1 OBJECTIVES AND SCOPE

Objectives—Specific objectives of the 747 Phase I study, reported herein, were to 1) examine feasibility, benefits, and costs of wing tip extensions (WTE), wing tip winglets (WTW), and a wing load alleviation (WLA) system employing active outboard ailerons, and 2) make a recommendation regarding continuation of the program into Phase II.

Scope—Figure 2 illustrates the scope of the Phase I program. The 2-year study program consisted of analyses and wind tunnel tests. No flight testing was conducted and, apart from wind tunnel model parts, no hardware was developed. Emphasis was

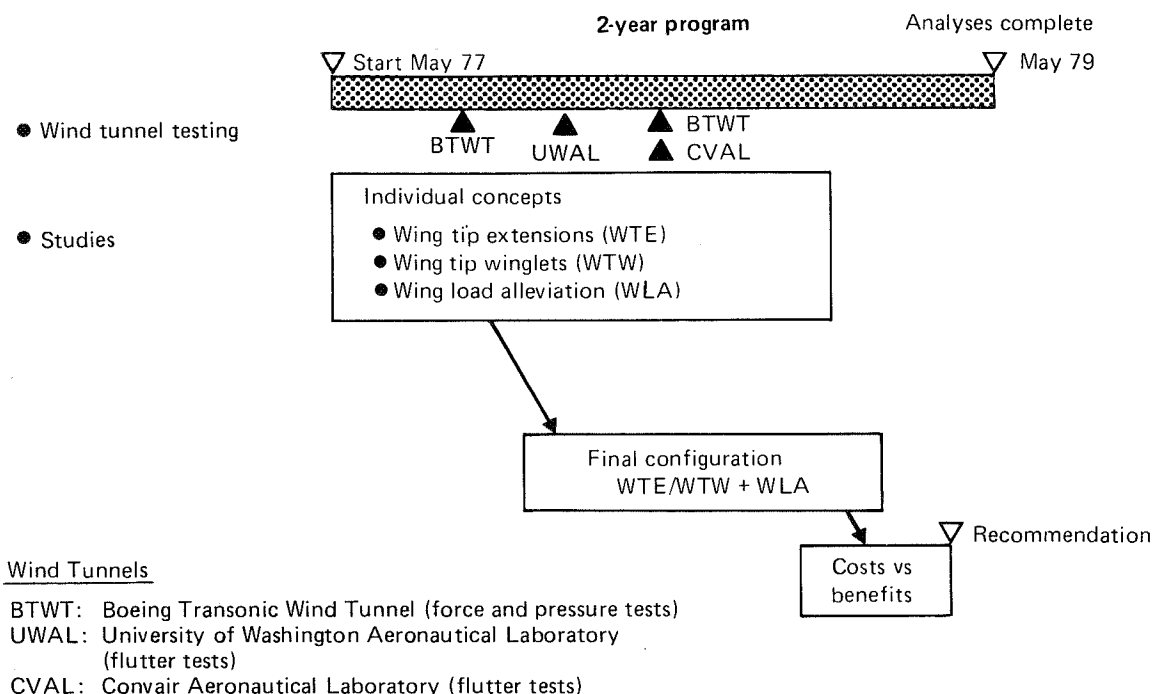


Figure 2. Program Outline

on those factors that would affect the economic trades [e.g., lift to drag ratio (L/D) improvement, structural weight, system reliability, and general design complexity], rather than on detailed structural design or control system development, which were planned for accomplishment during Phase II.

The two high-speed wind tunnel tests were accomplished in the Boeing Transonic Wind Tunnel (BTWT) to obtain force and pressure data for winglets and for symmetrically deflected outboard ailerons. Low-speed configuration (flaps down) testing was deferred to Phase II. Flutter testing of winglets was accomplished in the University of Washington Aeronautical Laboratory (UWAL) and the Convair Aeronautical Laboratory (CVAL) using a low-speed flutter model dynamically scaled to represent high-speed conditions.

Engineering analyses were conducted to determine loads, structural sizing (including flutter stiffness requirements), weights, L/D, performance, and stability and control effects for the various concepts. Preliminary engineering design studies were accomplished to the extent necessary to develop conceptual layouts and work statements for pricing and to support the analytical effort.

Production costs were estimated. Price curves based on these costs were used in addition to performance estimates to determine airline return on investment. The total package of technical and economics data was considered in making the Phase II recommendation.

2.2 STUDY APPROACH AND GROUND RULES

2.2.1 Approach

The original plan was to study the WTE/WTW/WLA concepts individually, and then select either a WTE or WTW for more detailed analysis in combination with WLA as a "final" configuration. As the study progressed, several factors evolved which led to a decision to carry both WTE and WTW configurations to the end of the Phase I study.

Structural resizing studies were concerned primarily with maneuver load control (MLC), although gust load alleviation (GLA) potential was analyzed for the basic wing, and a brief flutter mode control (FMC) feasibility study was conducted for the wing with winglets. The final control law provided some GLA capability, but since the design objective was to provide MLC, only the maneuver load capability was considered in the structural sizing of the WTE/WTW configurations.

In the following discussions, the acronym WLA is used as a general term encompassing both MLC and GLA. When consideration was limited to maneuver load control only, the acronym MLC is used.

Winglet Selection—The L/D improvement achieved in BTWT testing of the first winglet design was no better than for a 1.83-m (6-ft) WTE, although a winglet of that size was known to have considerably more potential. In addition, a flutter problem was identified in flutter model testing of the winglet, which required modifying available flutter analysis computer programs before the required wing stiffness increase (flutter weight penalty) could be estimated. It was decided to alter the study approach so as to put more emphasis on winglet aerodynamic design/test and flutter analysis while carrying both the winglet and tip extensions in combination with maneuver load control for comparison. Selection of the wing tip configuration for Phase II was deferred to the end of Phase I.

Accordingly, three winglets were designed and tested in the second BTWT entry. Performance test data were reviewed and the best winglet (designated Z13) was selected while loads and stability/control testing were in progress for the 1.83-m (6-ft) WTE/MLC configuration. Loads and stability/control testing was then conducted for the Z13 WTW with and without MLC.

Benefits Analyses—Structural resizing and performance analyses were completed for the 1.83-m (6-ft) WTE and Z13 WTW without MLC, and for the basic wing (no WTE/WTW) and the 1.83-m (6-ft) WTE with MLC. Resizing analyses were partially completed for a 3.66-m (12-ft) WTE, for the first winglet design without MLC, and for the best winglet (Z13) with MLC.

Section 6.0 discusses investigations wherein the basic wing (no WTE/WTW) was resized with and without MLC using consistent methodology and ground rules to provide a basis for assessing WLA benefits. The methodology and ground rules for analyzing all of the configurations with WLA also were consistent, but differed in some respects from those used for analyses without WLA. Consequently, the benefits of MLC combined with tip extensions and winglets should not be inferred from comparison of the results in Sections 4.0 and 5.0 (WTE/WTW without MLC) against the results in Section 7.0 (WTE/WTW with MLC) because of the previously noted differences in methodology and ground rules and also because:

- Final structural sizing was not completed for the WTW/MLC configuration for reasons discussed in Section 7.0
- The existing aileron span, which was retained throughout this study, may not be optimum for the WTE/MLC configuration

Rather than expend the resources necessary to complete final WTW/MLC sizing and aileron span optimization for the WTE/WTW configurations, a judgement was made that a valid Phase II recommendation could be based on the assumption that MLC would offer benefits for both the WTE and WTW comparable to those determined in Section 6.0 for the basic wing.

Results shown for the 1.83-m (6-ft) WTE combined with MLC were obtained from detailed analyses based on wind tunnel testing with the existing aileron. The data shown for a 2.74-m (9-ft) WTE were, in general, estimated from the 1.83-m (6-ft) WTE, 3.66-m (12-ft) WTE, and MLC studies. Based on separate Boeing studies, it was determined that leading-edge flaps probably would not be required for the 1.83-m (6-ft) WTE, but would be required for a 2.74-m (9-ft) WTE. A leading-edge flap installation was included in cost and weight estimates for the 2.74-m (9-ft) WTE.

WLA System Studies—The WLA system control law and mechanization concept development studies for the MLC and GLA functions were conducted for the basic wing (no WTE/WTW) only. However, a brief flutter mode control feasibility study was conducted for the WTW configuration and structural weight benefits of WLA were examined for both the 1.83-m (6-ft) WTE/MLC and Z13 WTW/MLC configurations. The rationale was that wing structural dynamic modes of interest to the MLC/GLA functions would not differ enough between WTE/WTW configurations to alter the selection of a control law concept or the number/type of sensors required. Different filter gain/phase characteristics might be required in the detailed design, but these differences were assumed to be unimportant for the feasibility/costs/benefits study. Flutter mode control was considered only for the wing with winglet since there was no flutter weight penalty for the basic wing or the WTE configurations with or without MLC/GLA.

The MLC/GLA system development was approached by arbitrarily selecting a configuration for the first cycle of studies, analyzing that configuration to determine where improvements were necessary, conducting trade studies of alternate configurations, and then defining an improved configuration for final system performance, cost, and reliability estimates. Although design emphasis was on MLC for the final WLA system, the selected system configuration (using wing accelerometers) also was effective in damping the first wing bending mode in gusts.

2.2.2 Ground Rules

The following ground rules were established:

Baseline Airplane—The 747-200B configuration illustrated in Figure 3 was defined as the baseline airplane. At the operating weights indicated, the baseline wing has positive structural margins of safety at design load conditions.

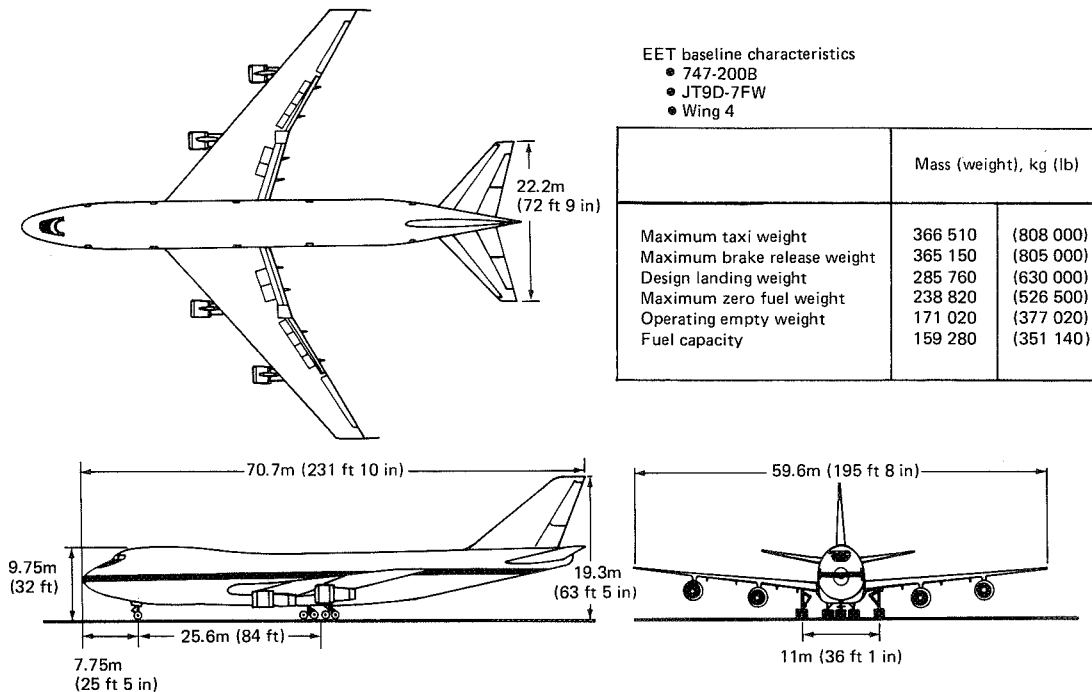


Figure 3. Baseline 747-200B Model for EET Studies

Basic Wing Geometry—To minimize changes to production tooling, no changes in wing planform, airfoil section, or jig twist were allowed inboard of the tip modification. This reduced the benefits attainable from all WTE/WTW/WLA concepts because all caused more washout at cruise flight conditions, which has an adverse effect on L/D. The requirement to retain jig twist is an important distinction between studies of tip extensions and new wings with increased span, since jig twist could be revised to optimize cruise twist for a new wing.

Flight Envelope—No changes to the speed/altitude/maneuver envelope were allowed.

Performance Comparisons—Fuel efficiency was expressed in terms of block fuel savings for a given range with a fixed payload. The maximum taxi weight was unchanged although the operating empty weight was modified to reflect the structural/system weight changes for the various concepts.

WLA Control Surface—Consideration was restricted to the outboard aileron as the primary wing load control surface. The elevators were used to compensate pitching moments introduced by the ailerons; their application to add pitch damping for GLA also was considered.

Structural Resizing—Consideration was limited to wing structure only. Ground rules for treatment of the structural safety margins inherent in the baseline wing differed, depending on the configuration, as follows:

- **WTE/WTW Without WLA**—Absorb the existing margins as required and "beef-up" only where required to bring negative margins back to zero. This ground rule was adopted to determine if retrofit was practical; i.e., in a retrofit program, material can be added in some areas by means of doublers, but it is generally impractical to remove material.
- **Structural Benefits of WLA (Basic Wing)**—First define a zero margin baseline without WLA, then resize to zero margin with WLA to determine WLA benefits.
- **WTE/WTW With WLA**—Resize to zero margins.

2.3 REPORT ORGANIZATION

Results of the individual concept studies (WTE/WTW/WLA) are presented in Sections 4.0, 5.0, and 6.0. Comparisons of WTE versus WTW with and without WLA and the final cost/benefit comparisons are contained in Section 7.0. Selected discussions of methodology and supplemental data are supplied in Appendices A and B.

WTE/WTW study emphasis in Section 7.0 is on comparisons of results, whereas Sections 4.0 and 5.0 discuss how the results were obtained. Appendix C describes the wind tunnel models and facilitates and summarizes the conditions tested, while the actual test data are presented in the other sections or in Appendix B as necessary to support those discussions.

The principal discussions of WLA, both from the systems and structures points of view, are contained in Section 6.0. Weight and performance benefits of WLA for the WTE/WTW configurations are presented in Section 7.0.

2.4 UNITS OF MEASUREMENT

Results are expressed in International System (SI) units with the corresponding U.S. customary units shown in parenthesis; e.g. 1.83-m (6-ft) WTE. Exceptions are made in the case of airspeed, weight, and mass. Airspeed is expressed only in knots, which is universally understood in the aviation industry and is used for instrument markings. Weight, a force, has not been expressed in the SI unit (newton) because guidelines for SI usage encourage reference to the mass of an object rather than the weight. Accordingly, weight is expressed only in the U.S. customary engineering unit for force (pound) and the corresponding mass is expressed only in the SI unit for mass (kilogram).

3.0 SYMBOLS AND ABBREVIATIONS

A

$\bar{\alpha}$	sting pitch angle
A	cross sectional area
\bar{A}	ratio of root-mean-square value of load to root-mean-square gust velocity
A/A _B	cross sectional area ratio—modified/baseline, both at same η station
\bar{A}/\bar{A}_0	ratio of root-mean-square value of load from closed-loop dynamic analysis to root-mean-square value of load from controls fixed dynamic analysis (root-mean-square gust velocity equals 1.0 ft/sec)
ac	alternating current
ACEE	aircraft energy efficiency
AND	airplane nose down
ANU	airplane nose up
AR	aspect ratio
ATR	Austin Trumbull Radio (ARINC standard for electronic box size)
\bar{A}_Y	ratio of root-mean-square value of load Y to root-mean-square gust velocity
A ₀	component area on baseline wing sized to MS = 0
\bar{A}_δ	ratio of root-mean-square value of control surface angle δ to root-mean-square gust velocity

B

b	wing span
b _{WTW}	winglet span
b/2	wing semispan

B	baseline
BASIC	antisymmetric basic flutter mode
BBL	body buttock line
BIT	built-in test
BM	bending moment
$BM(t)/BM_0$	ratio of time variant BM to reference BM
BTWT	Boeing Transonic Wind Tunnel

C

c	chord
\bar{c}	wing mean aerodynamic chord
cg	center of gravity
$cC_{N\alpha}/(cC_{N\alpha})_{REF}$	normalized static normal force distribution
$C/4$	quarter chord
C	coefficient
C_{ℓ}	rolling moment coefficient
C_{ℓ}	section lift coefficient
CARSRA	Computer Aided Redundancy Systems Reliability Analysis (computer program)
C_c	chordwise force coefficient
C_D	drag coefficient
C_{D_i}	induced drag coefficient
C_{ℓ_E}/C_{ℓ_R}	ratio of elastic to rigid rolling moment
$C_{\ell \dot{p}}$	roll damping coefficient
$C_{\ell \beta}$	lateral stability coefficient
$C_{\ell \delta}$	lateral control effectiveness
\mathcal{C}	centerline

C_L	lift coefficient
CL2	Control Law 2
C_m	airplane pitching moment coefficient
c_m	wing section moment coefficient
$C_{m\delta}/C_{n\delta}$	ratio of section moment to section normal force
C_N	normal force coefficient
C_p	pressure coefficient
CPU	computer processor unit
c_{root}	root chord
c_t/c_a	tab-to-aileron chord ratio
CVAL	Convair Aeronautical Laboratory (General Dynamics Low-Speed Wind Tunnel)
$C_{y\beta}$	sideforce due to sideslip coefficient
$C_{\eta\beta A}$	section normal force due to aileron deflection
$C_{N\alpha}$	variation normal force due to angle of attack
$C_{\eta\beta}$	directional stability coefficient

D

D/A	digital-to-analog conversion
dB	decibel
dc	direct current
deg	degree
DFR	detail fatigue rating

E

E	Young's modulus of elasticity
---	-------------------------------

EAS	equivalent air speed
EET	energy efficient transport
EI	bending stiffness
EMS	elastic mode suppression

F

f_b	bending stress
fps	feet per second
ft	foot
ft^2	square foot
fwd	forward
FAA	Federal Aviation Administration
FAR	Federal Airworthiness Regulation
FCS	flight control system
flaps 30	Flaps set at detent 30, the landing flap position. It is one of several specific flap settings identified on the flap control and provides flap action approximately equivalent to a hinged flap at 30 deg down.
FMC	flutter mode control
F_N	static normal force

G

g	acceleration due to gravity
g	flutter mode damping
gal	gallon
g_m	antisymmetric minimum damping
g_{min}	minimum damping
G	shear modulus of elasticity

GAG	ground-air-ground cycle
GJ	torsional stiffness
GLA	gust load alleviation

H

HAA	high angle of attack
HF	high frequency
\bar{h}	hinge line
Hz	hertz

I

in	inch
in • lb	inch pound
inbd	inboard
I_M/I_A	model-to-airplane inertia ratio
IR&D	independent research and development
I_X	bending moment of inertia = ΣAZ^2
I_0	I_X for baseline wing sized to MS = 0

J

J	torsion moment of inertia = $\frac{4A^2}{\Sigma \frac{\Delta S}{t}}$
J_0	J for baseline wing sized to MS = 0

K

kg	kilogram
kg/cm	kilogram per centimeter

km	kilometer
kn	knot
ksi	kips per square inch
K_a	WLA system aileron gain
KCAS	knots calibrated airspeed
K_e	WLA system elevator gain
KEAS	knots equivalent airspeed
K_M/K_A	model-to-airplane stiffness ratio
K_W	WLA system gain for lateral control prioritization

L

lb	pound
lb-in	pound-inch
L/D	lift-to-drag ratio
LH	left hand
L_M/L_A	model-to-airplane length ratio
LRU	line replaceable unit
LVDT	linear variable differential transformer

M

m	meter
m ²	square meter
max	maximum
ms	margin of safety
M	Mach number
MAC	mean aerodynamic chord

MLC maneuver load control
MTW maximum taxi weight

N

nmi nautical mile
 n_z normal load factor (vertical acceleration)
 $n_{z_{cg}}$ load factor (vertical acceleration) at cg
 $n_{z_{wing}}$ load factor (vertical acceleration) at wing station 1180
N newton
N•M newton meter
NP static neutral point
NU nose up
N(Y) number of exceedances of the indicated **value of load**
Y per unit time

O

OB outboard
OEW operational empty weight
ONSB antisymmetric outboard nacelle side bending flutter mode

P

Pa pascal
PCU power control unit
PSD power spectral density
psi pounds per square inch

Q

q_M/q_A	model-to-airplane dynamic pressure ratio
QSAE	quasi-static aerodynamics with aeroelastic effects included

R

rad	radian
rad/sec	radians per second
R	radius
R&D	research and development
RH	right hand
RMS	root mean square
R/O	round off
ROI	return on investment

S

s	second
δ_{FRL}	stabilizer position relative to fuselage reference line
δ_p	stabilizer trim setting relative to pilot index
S	wing area
S&C	stability and control
SI	International System of Units
S_{ref}	reference area

T

t	skin thickness
---	----------------

t/c	airfoil thickness-to-chord ratio
TE	trailing edge
TED	trailing edge down
TEU	trailing edge up

U

UAL	United Airlines
UWAL	University of Washington Aeronautical Laboratory
U_{σ}	design gust intensity level for PSD design envelope analysis

V

V	velocity
V_{∞}	freestream velocity
V_A	design maneuver speed
Vac	volts alternating current
V_B	design speed for maximum gust intensity
V_C	design cruise speed
V_D	design point dive speed
Vdc	volts direct current
V-g	velocity-damping
V-f	velocity-frequency
V_F	flutter speed
V_F/V_{REF}	flutter velocity ratio
VIZ	flow visualization
V_M/V_A	model-to-airplane velocity ratio
V_{MO}	maximum operating speed

V_{REF}	reference velocity
V_S	stall speed
V/V_{REF}	velocity ratio
V_2	takeoff reference speed

W

w_{gust}	vertical gust velocity
WBL	wing buttock line
WDP	wing design plane
WL	waterline
WLA	wing load alleviation
W_M/W_A	model-to-airplane weight ratio
WS	wing station
WTE	wing tip extension
WTW	wing tip winglet

X

X	longitudinal axis/distance/force
X/C	chordwise location in percent chord

Y

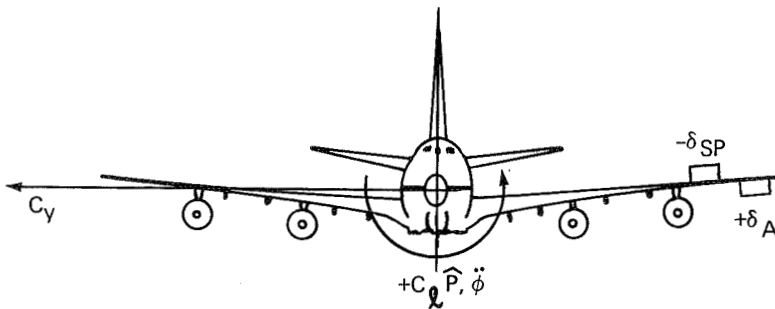
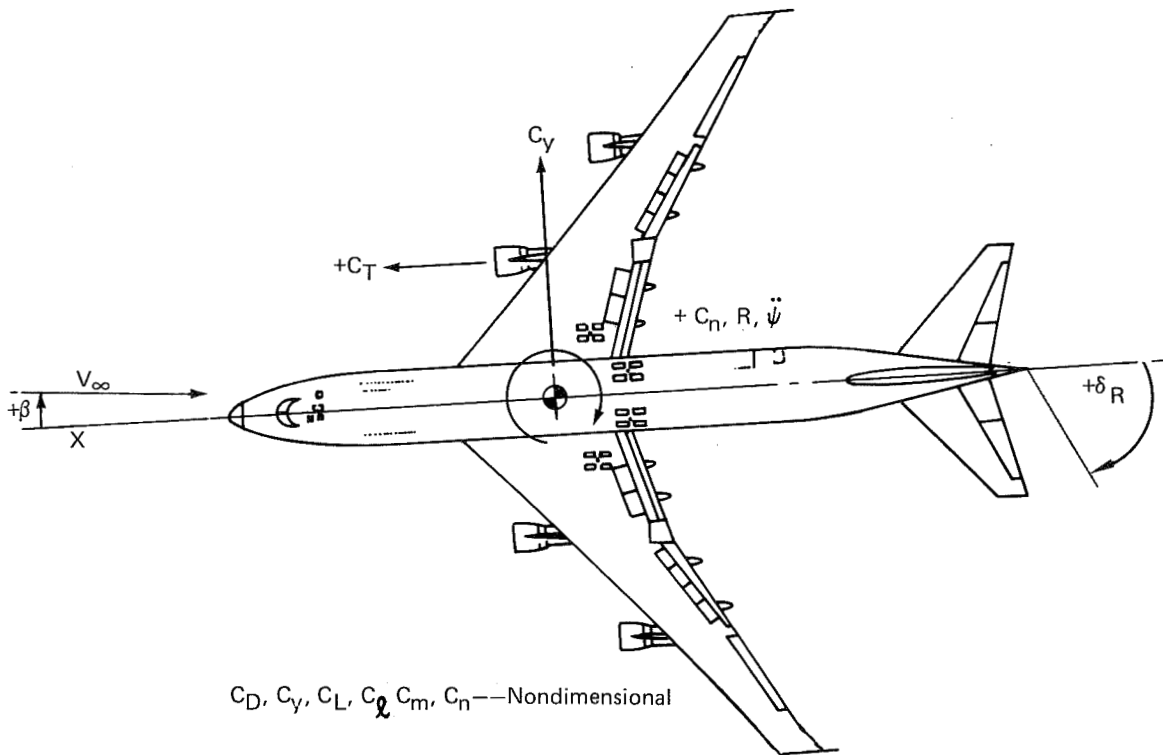
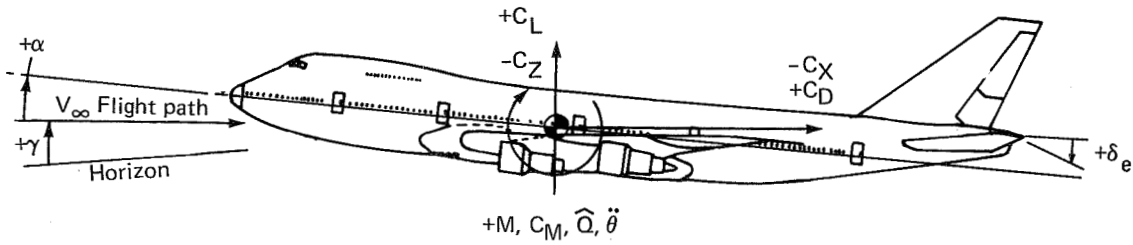
Y	lateral axis/distance/force
---	-----------------------------

Z

z/c	vertical location in percent chord
Z	vertical axis/distance/force
Z-XX	winglet configuration designation

GREEK SYMBOLS

α	angle of attack
α_w	wing angle of attack
β_{WTW}	winglet incidence angle
δ	deflection angle
$\dot{\delta}$	angular deflection rate
δ_a	aileron deflection angle
δ_{a_c}	aileron deflection command
$\dot{\delta}_{a0}$	outboard aileron rate
δ_{e_c}	elevator deflection command
δ_{e_O}	outboard elevator deflection
$\dot{\delta}_{e_O}$	outboard elevator rate
δ_T	tab deflection
Δ	incremental
ΔP	differential pressure
$(\Delta W)/Y$	weight distribution
η	wing spanwise location expressed as a fraction of basic wing semispan = $\frac{2Y}{b}$ ($\eta = 1.0$ at existing wing tip, $\eta > 1.0$ at tip of wing with WTE)
$\eta_{winglet}$	winglet spanwise location expressed as a fraction of winglet span
σ_{cg}	standard deviation
$\dot{\theta}_{cg}$	pitch rate at cg
Λ	sweep angle
σ_w	RMS vertical gust intensity
$\phi_{\bar{A}_0}^2$	normalized power
ω	vibrational frequency



SIGN CONVENTIONS

4.0 WING TIP EXTENSIONS

This section discusses the addition of wing tip extensions (WTE) to the baseline wing without wing load alleviation (WLA). Comparisons with wing tip winglets (WTW) and discussions of WTE combined with WLA are contained in Section 7.0.

Two wing tip extensions were analyzed in detail. One was a 1.83-m (6-ft) WTE previously tested in a Boeing High-Speed Wind Tunnel test (BTWT 1441). The second was a 3.66-m (12-ft) WTE selected for analysis on the basis of preliminary (quick-look) trend studies that considered flutter and the effects of increased aeroelastic washout on lift to drag ratio (L/D). Although L/D continues to increase for semispan increases to 3.66m (12 ft), the maximum studied, the detailed analyses showed net fuel efficiency to be little better for the 3.66-m (12-ft) WTE than for the 1.83-m (6-ft) WTE when structural weight effects also were included.

Based on results of the trend studies and subsequent detailed analyses, a 2.74-m (9-ft) WTE was selected as the optimum semispan increase for a WTE without WLA. A longer tip extension could be optimum with WLA, depending upon the extent to which the WLA system negates the added weight penalty. However, concerns regarding flutter, the need for leading-edge flaps, and gate/maintenance hangar access increase with the length of the WTE.

The L/D estimates shown in the figures in this section are about 0.1% higher than the final results shown for the WTE versus WTW comparisons. This is because, to be consistent with the WTW analyses, a more detailed analysis was used for the final comparisons. Based on the final analyses, an L/D improvement of about 1.9% was estimated for the 1.83-m (6-ft) WTE. While not specifically analyzed without WLA, a 2.6% improvement in L/D can be inferred from interpolation of the available data. The net improvement in fuel efficiency also depends on the added weight of the added tip panel and wing structural reinforcement and varies with trip distance. Final comparisons of fuel savings are contained in Section 7.3.1.

4.1 PRELIMINARY TREND STUDIES

The study plan called for detailed analyses of a 1.83-m (6-ft) WTE and an alternate WTE to determine net fuel efficiency improvement considering both L/D and weight effects. Estimation of the weight effect requires extensive structural resizing analyses, and could be done for only one alternate configuration due to time and budget constraints. The purpose of the preliminary trend studies was to provide guidance in selecting the alternate configuration so that resources would not be wasted on detailed analyses of a configuration having no chance of being better than a 1.83-m (6-ft) WTE.

Prior studies had shown that aeroelastic washout negated much of the potential L/D benefit of a WTE. Hence, elastic wing twist was computed for 1.83- and 3.66-m (6- and 12-ft) extensions, using loads developed from the prior 1.83-m (6-ft) WTE test and extrapolated to 3.66m (12 ft). Baseline wing stiffness was assumed; i.e., no structural resizing for the twist calculation nor for the preliminary flutter trend analyses.

These preliminary trend study results showed no reason to limit the semispan increase to less than 3.66m (12 ft), the maximum considered in the study. Because a significant portion of the loads analysis was completed for a 3.66-m (12-ft) WTE as a fall out of

the trend study, detailed analyses were continued for that configuration, as reported in Section 4.2.

4.1.1 Lift-to-Drag Ratio Improvement

The configurations analyzed for the trend study are shown on Figures 4 and 5. The BTWT 1441 1.83-m (6-ft) tip extension has a constant chord, thickness, and jig twist that are the same as the existing 747 wing section at wing buttock line (WBL) 1169. The 3.66-m (12-ft) tip extension also has a constant thickness/chord ratio and jig twist that are the same as the existing wing section at WBL 1169, but has a tapered chord. Aerodynamically, differences due to a tapered planform versus constant chord planform were found to be negligible for the 1.83-m (6-ft) tip.

The experimental increments shown on Figure 6 for the 1.83-m (6-ft) WTE were used as a basis for predicting drag for longer tip extensions. Twist of the basic-model wing (W46, no WTE) corresponds to the 1-g cruise twist, taking into account the elastic twist of the model. No additional twist was designed into the WTE (fig. 4). This wind tunnel model configuration represents a flight cruise condition with no additional penalties due to aeroelastic twist because of the WTE ("existing twist"). A brief study was made to optimize the twist on the wing tip for minimum induced drag, but the optimization had little effect on drag and resulted in a twist distribution that would be impractical to manufacture. As a result, no additional jig twist was designed into the wing tip extensions.

Figure 7 shows that $(L/D)_{\max}$ increases with the length of the WTE. The aeroelastic twist penalty for the baseline wing stiffness (no resizing) also is shown. From an aerodynamic standpoint alone, not considering weight effects, there was no apparent reason not to consider span extension up to 3.66m (12 ft) or more per side.

4.1.2 Loads and Twist

The 1.83- and 3.66-m (6- and 12-ft) tip extensions were analyzed using baseline wing stiffness to support the span extension trend studies. The load results for these studies are presented and discussed in Section 4.2.2.

4.1.3 Flutter

Preliminary flutter analyses using conventional methods for planar wings were conducted on WTEs to explore feasibility of the wing tip extension concept for lengths up to 3.66m (12 ft). Simple constant chord extension increments of 0.91m (3 ft) were added to the standard airplane antisymmetric flutter analysis. Identical weights and stiffnesses were used for each increment, based on the nominal airplane wing tip properties. The aerodynamic spanwise lift distribution was adjusted for each increment by the theoretical change of the baseline airplane experimental lift distribution.

Results of these analyses showed the relative effects of WTEs on the 747 wing flutter modes. The critical antisymmetric wing flutter mode is referred to as the BASIC mode and is characterized by wing bending and torsion and aft fuselage bending.

Figure 8 shows the relative change in minimum damping of the antisymmetric BASIC mode as a function of WTE length for the nominal airplane with full wing fuel and full payload.

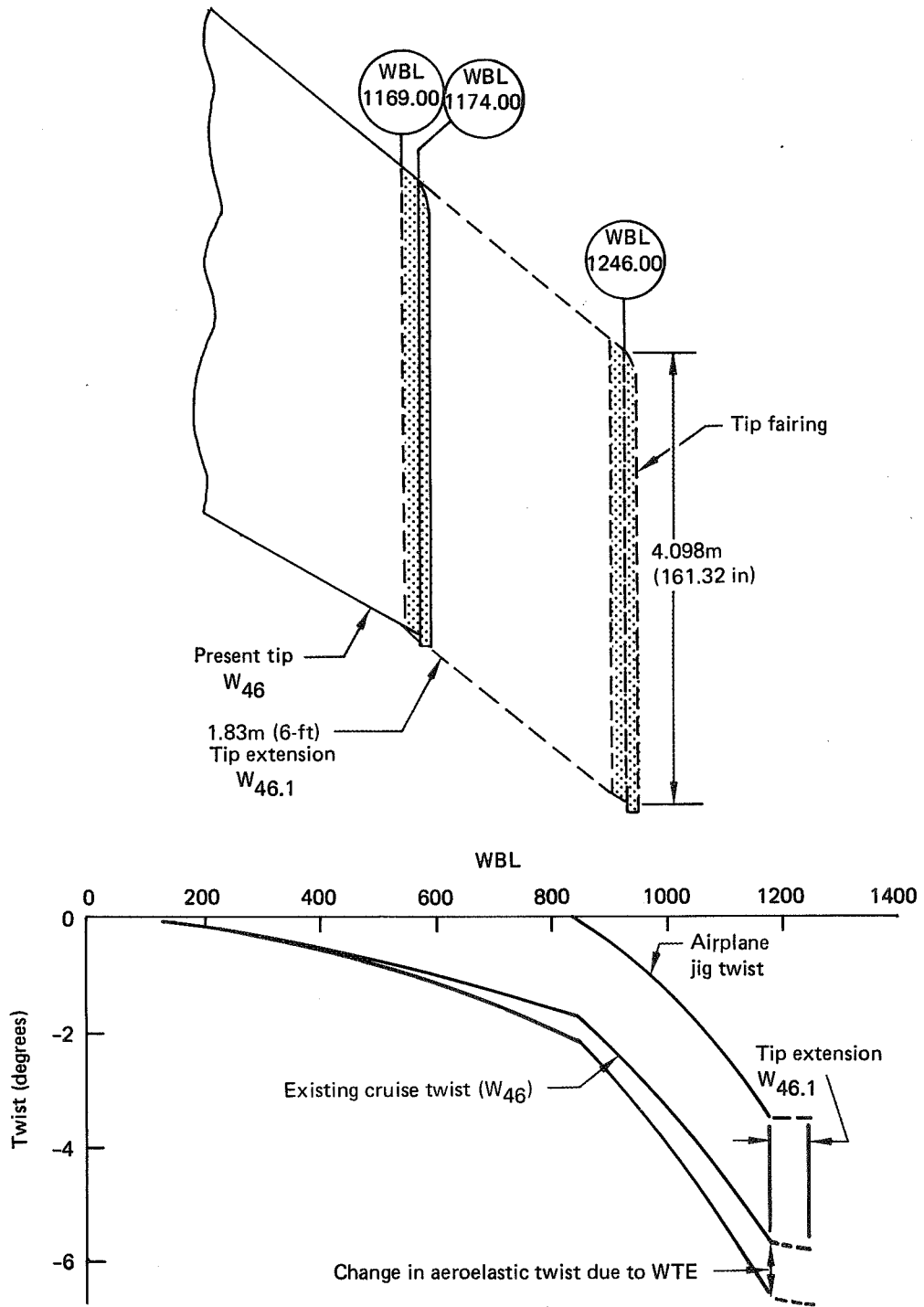


Figure 4. 1.83m (6-ft) Tip Extension Geometry

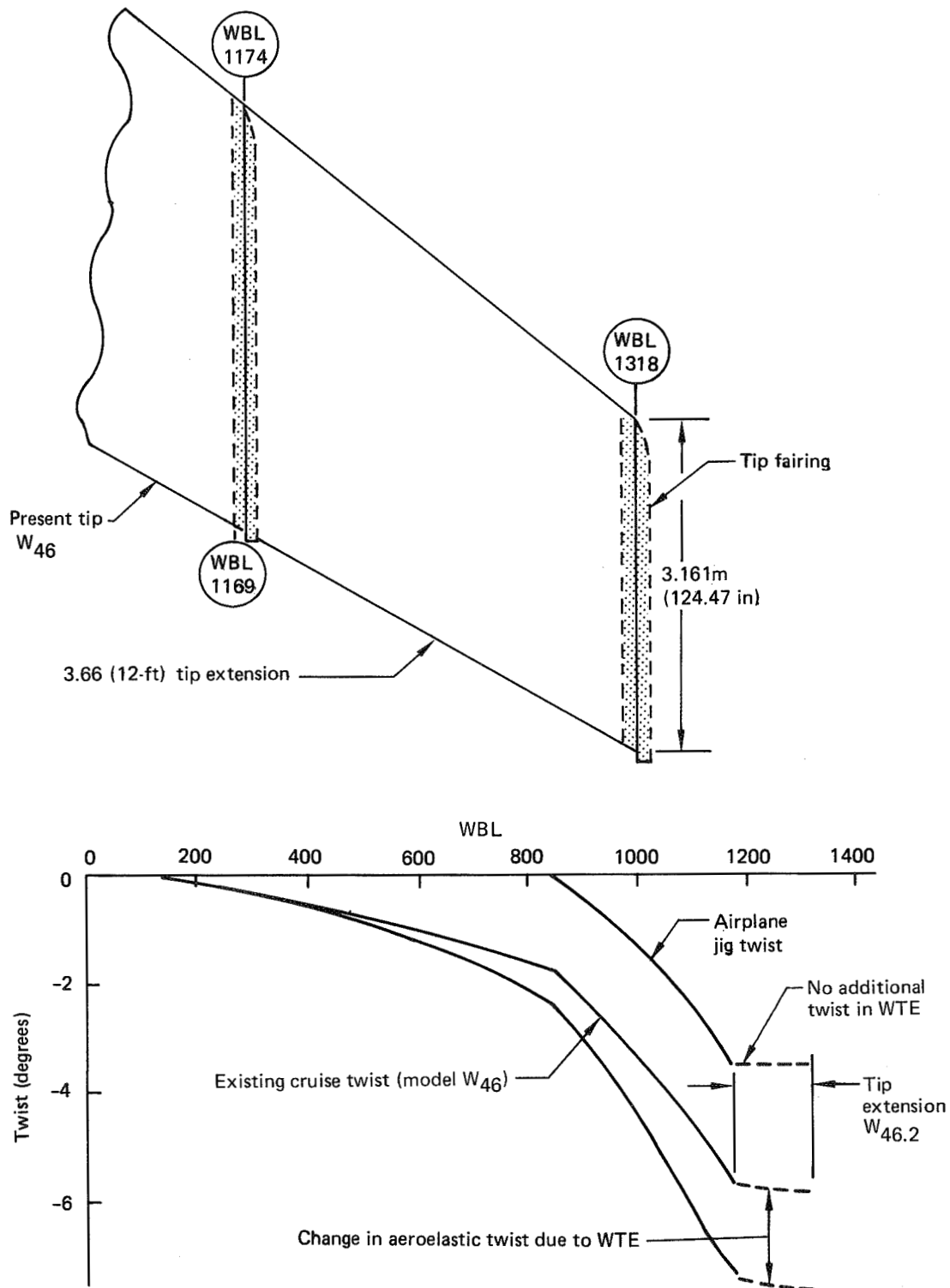


Figure 5. 3.66m (12-ft) Wing Tip Extension Geometry

- Wind tunnel data (BTWT 1441)
- Untrimmed (tail off)
- BTWT Reynolds number
- $S_{ref} = 0.46 \text{ m}^2 (4.95 \text{ ft}^2)$
- $\Delta C_{DWTE} = C_{DWTE_{on}} - C_{DWTE_{off}}$

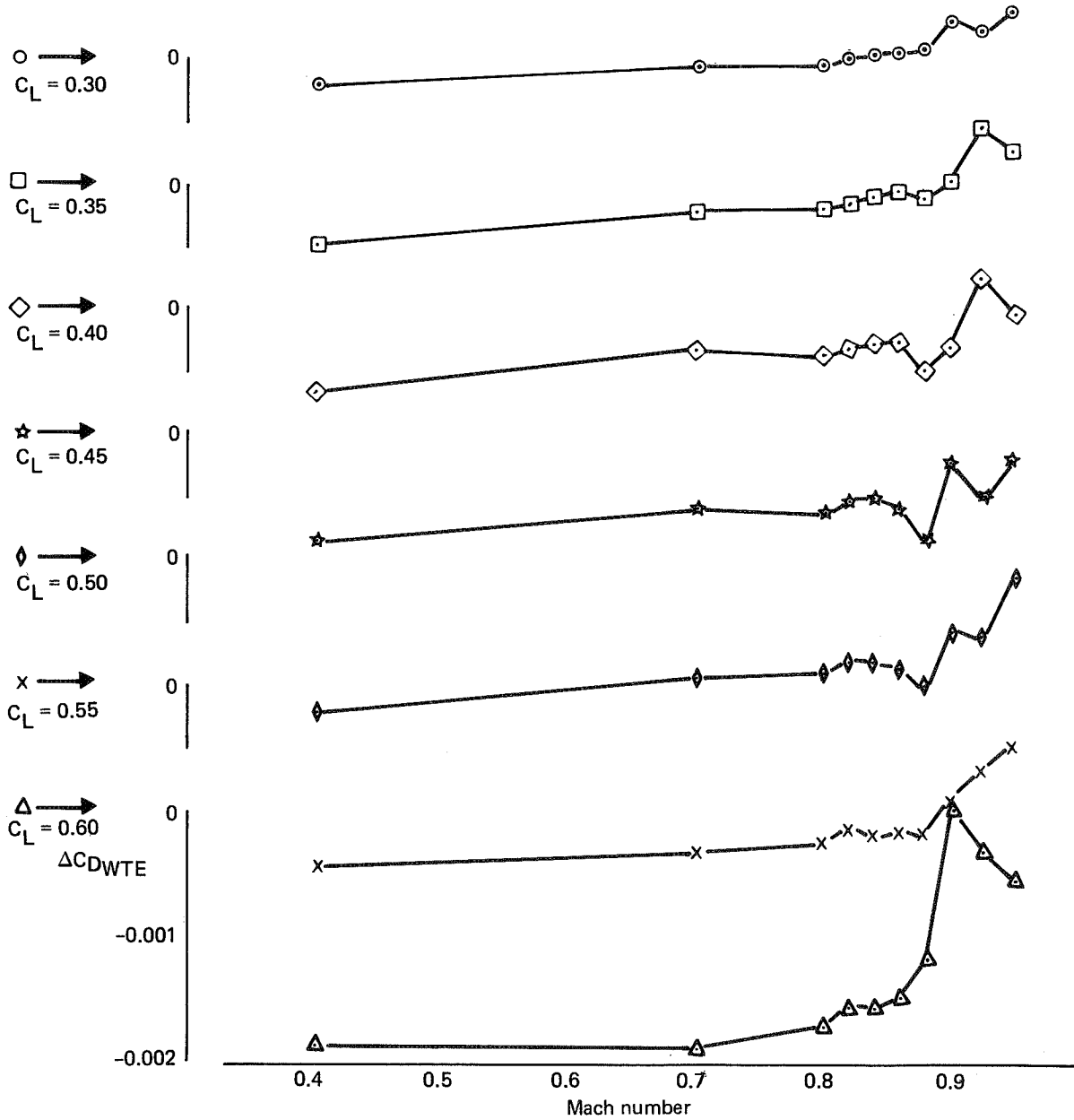
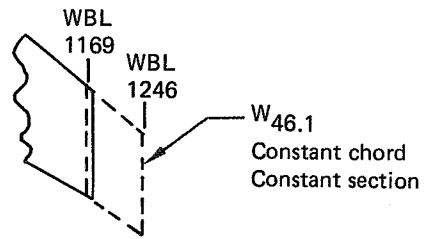


Figure 6. Effect of 1.83m (6-ft) Tip Extension on Drag

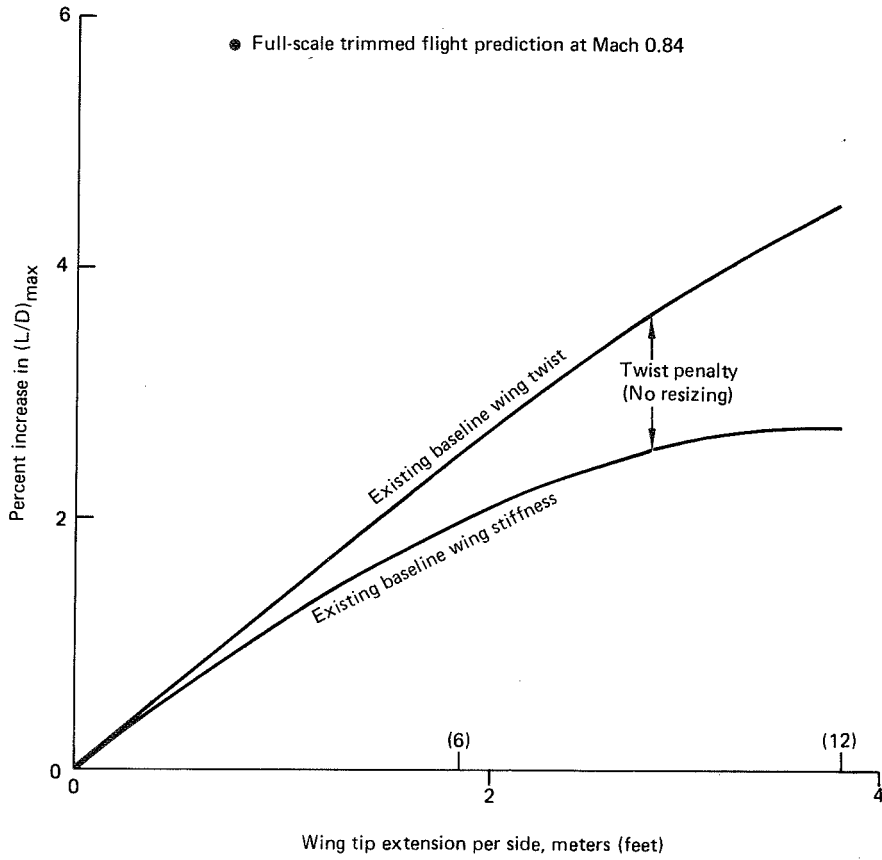


Figure 7. Performance Trends for Wing Tip Extensions

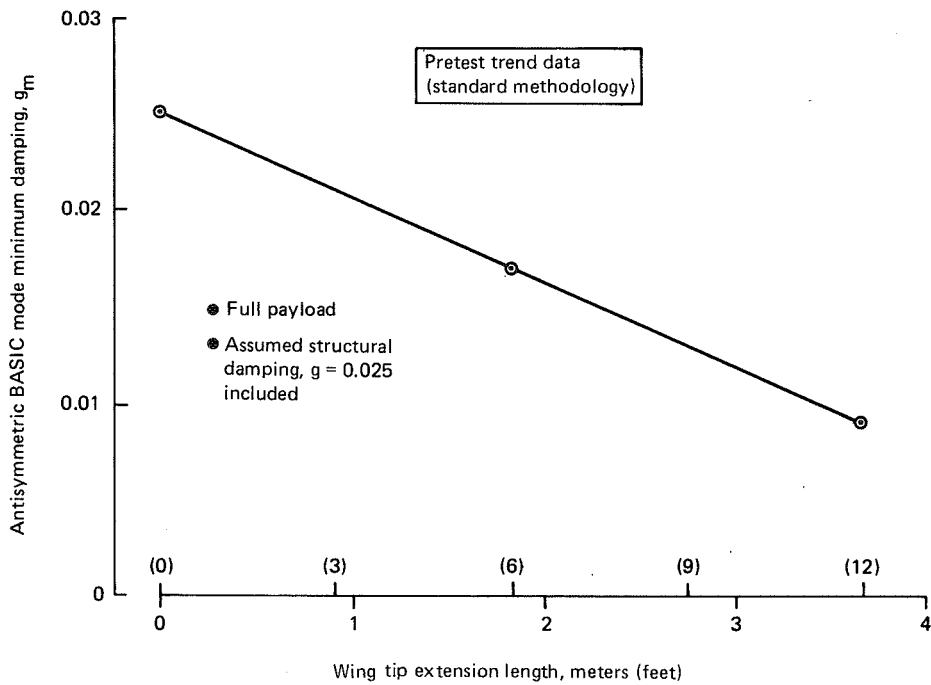


Figure 8. Effect of Wing Tip Extension Length

The trend results of Figure 8 show that a minimum damping decrease of 0.008 would be expected for a 1.83-m (6-ft) extension. This is considered acceptable without additional wing stiffness requirements for flutter. Longer extensions, while feasible, require further analyses (including symmetric analyses) and wind tunnel data to determine stiffness requirements. Symmetric mode analyses were conducted during final configuration flutter investigations, which are discussed in Section 7.1.3.

4.2 ANALYSES OF TWO WING TIP EXTENSION CONFIGURATIONS

This section discusses detailed analyses conducted for 1.83- and 3.66-m (6- and 12-ft) WTEs. Wind tunnel data used in the 1.83-m (6-ft) WTE analyses were obtained from a prior Boeing test (BTWT 1441). Aerodynamic data from loads testing of this WTE were extrapolated for use in the 3.66-m (12-ft) WTE study.

In general, the analyses to determine fuel savings consisted of loads definition and ultimate and fatigue sizing, based upon comprehensive sets of design loads, flutter stability checks, cruise twist, and weights estimates for the resized wing. L/D computation accounted for twist effects, and fuel savings estimates accounted for L/D and weight effects. However, the structural loads and sizing cycle was abbreviated for the 3.66-m (12-ft) WTE after it became apparent from preliminary weights data that fuel savings would be only slightly more for the 3.66-m (12-ft) than for the 1.83-m (6-ft) WTE.

The effects of tip extensions on stability and control and on the flight control system were determined only for the 1.83-m (6-ft) WTE. Preliminary design studies concerned with the tip attachment concept and equipment relocation, which formed a basis for cost estimation, also concentrated on the 1.83-m (6-ft) WTE. In these areas, considerable background information and drawings were available from prior studies.

4.2.1 Lift-to-Drag Ratio Improvement

Figure 9 shows percent increase in $(L/D)_{\max}$ as a function of length of the WTE. Structural resizing decreased the twist penalty slightly, as seen by comparing these results with those on Figure 7.

The L/D equivalent of the increased operating empty weight (OEW) was obtained using a trade factor of 0.2% L/D decrease per 453.5 kg (1000 lb) of airplane mass (weight) increase. This trade factor is valid for nontakeoff gross weight limited missions [e.g., 5556 km (3000 nmi)]. Net $(L/D)_{\max}$ indicates that a 2.74-m (9-ft) tip extension is near optimum. Comparisons with winglets are shown in Section 7.1.6.

4.2.2 Loads and Twist

This section shows the load results used for the tip extension studies. Maneuver conditions critical for design of the wing structure were analyzed for the baseline wing with 1.83- and 3.66-m (6- and 12-ft) tip extensions (WTE). Fatigue analyses were conducted only for the 1.83-m (6-ft) WTE, although approximate fatigue material requirements were estimated for the 3.66-m (12-ft) WTE. Required weight and stiffness increases were determined, and the analysis was cycled to determine final load results.

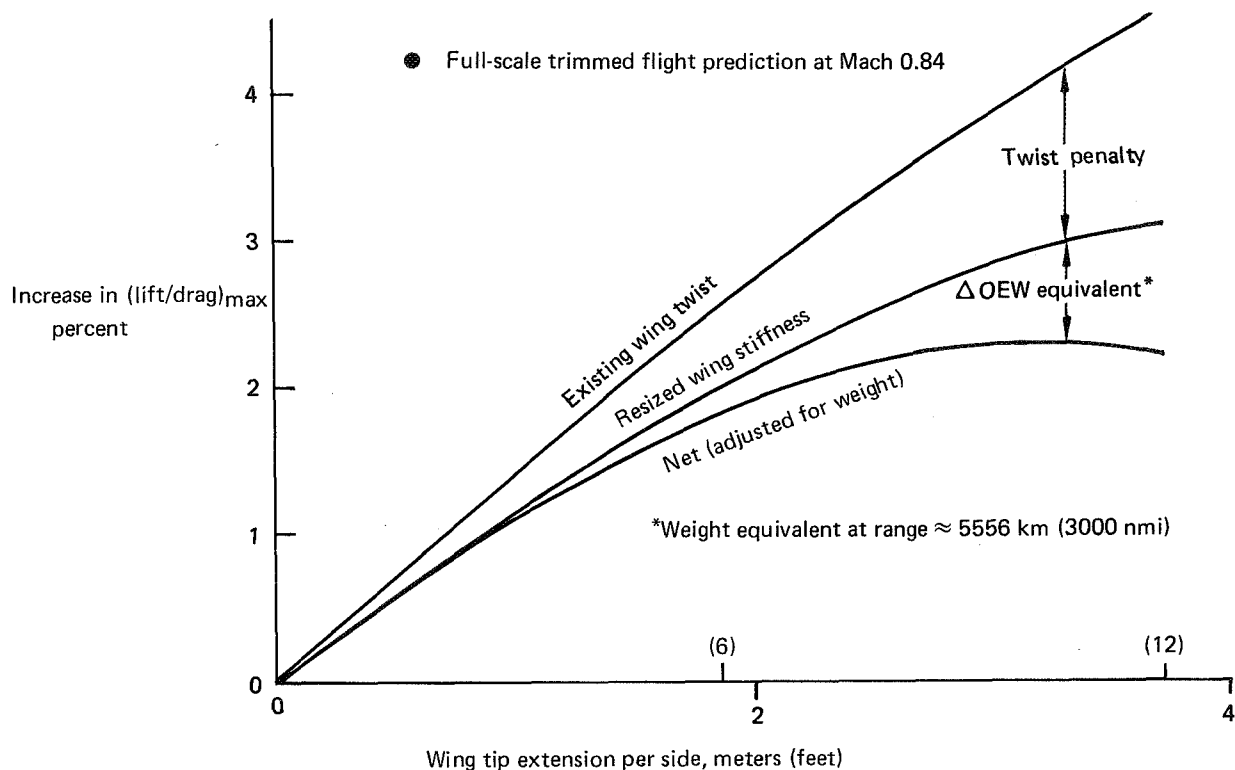


Figure 9. Performance Trends for Wing Tip Extension

The aerodynamic forces used for the analysis were based on wind tunnel test data for a 1.83-m (6-ft) tip extension (BTWT 1441 test) and extrapolated for analysis of the 3.66-m (12-ft) tip configuration. A sample incremental span loading for the 1.83-m (6-ft) tip extension, as determined from the wind tunnel data, is contained in Appendix B.

Figure 10 shows the effect of the WTEs on wing design bending moment and Figure 11 shows wing twist data for a typical cruise condition. As expected, the WTEs increased wing design bending moment and also increased wing tip washout for the cruise flight condition. The effect of the required increased stiffness was small for the 1.83-m (6-ft) tip extension because the baseline wing had excess structural margins that were absorbed as required when the 1.83-m (6-ft) tip extension was added. For both configurations, final load results were obtained in one loads-stiffness iteration cycle.

The tip extension configurations were not critical for flutter or gust; therefore, the stiffness for maneuver and fatigue design gave the final load and twist results for these configurations.

4.2.3 Structural Resizing

The wing box spar webs and panels (skins, stringers, spar chords) were analyzed for ultimate loads, fatigue loads, and flutter stiffness requirements. The ultimate stress analysis methods used were identical to those used in the 747-200B certification stress analysis, and included correction factors obtained from full-scale wing static destruction tests.

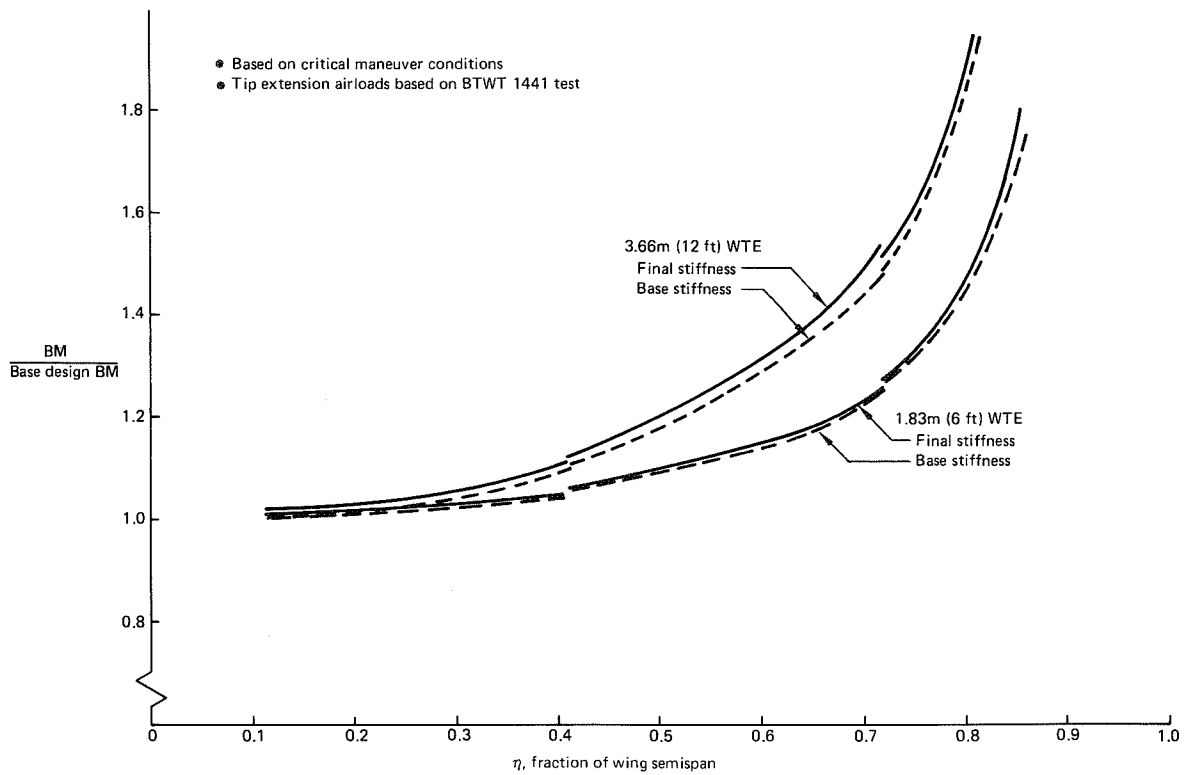


Figure 10. Effect of Wing Tip Extensions on Wing Design Bending Moment

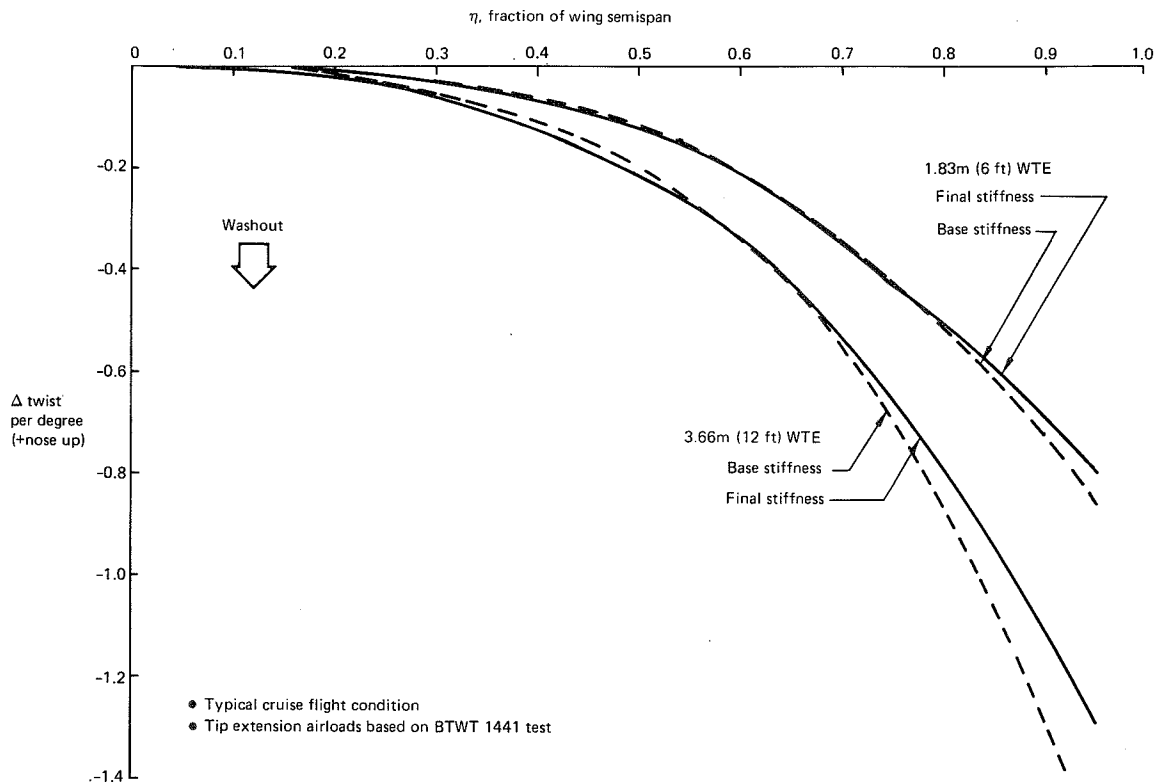


Figure 11. Wing Twist Increment for Tip Extensions

The fatigue analyses were based on a life goal of 20 years, using the typical 3-hour average flight length of the 747-200B. The analyses used a Boeing-developed fatigue analysis method that utilizes detail fatigue ratings. All significant flight and ground loads were included or estimated in the analyses.

Panel skin/stringer areas were resized using the existing ratio of skin area/stringer area, which maintains the fail-safe capability of the structure.

To determine the changes required to retrofit a tip extension, the wing box structure was resized to bring all negative margins of safety (MS) up to zero (MS = 0, "beef-up" only). No material was removed where positive margin of safety remained. Since resizing affected the wing stiffness (EI and GJ), a new set of loads, based on the new stiffness, was used for the final sizing analysis. Results are shown in Figures 12 and 13.

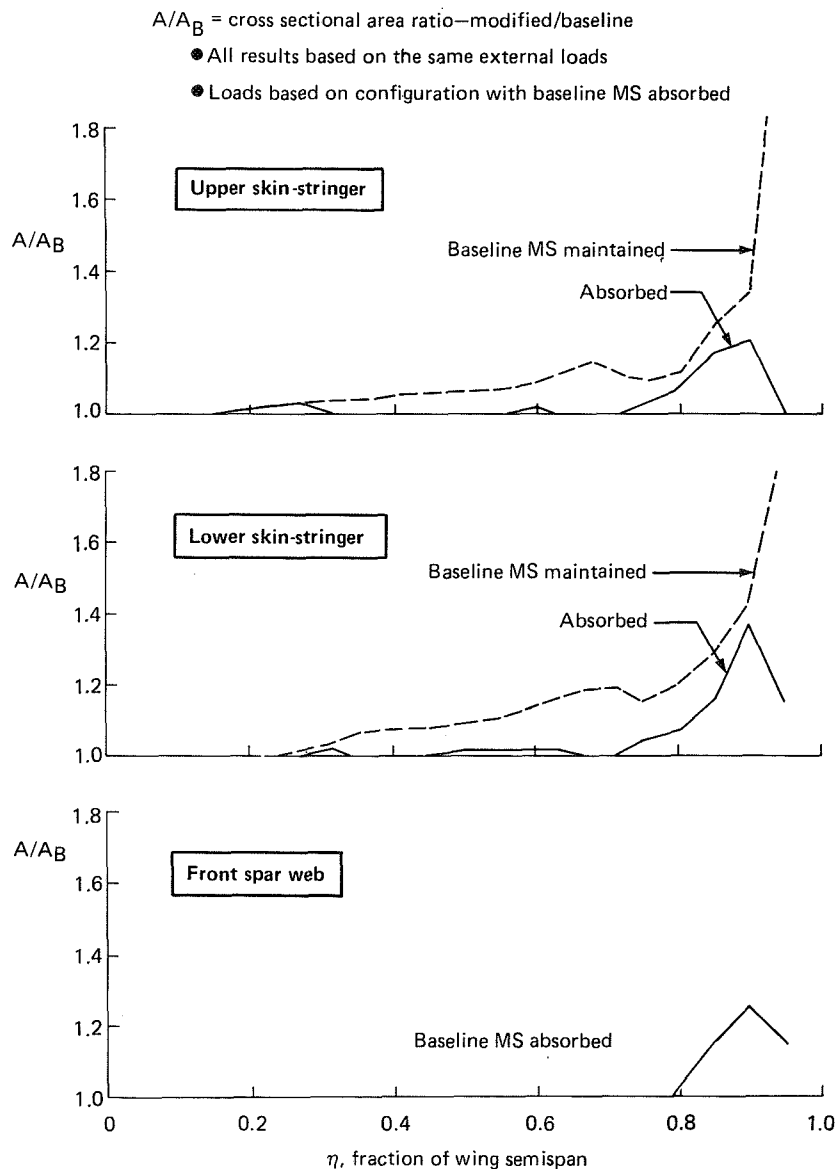


Figure 12. Structural Sizing of Wing With 1.83m (6-ft) WTE

$$\frac{EI}{EI_B}, \frac{GJ}{GJ_B} = \text{stiffness ratios—modified/baseline}$$

Baseline MS absorbed, fatigue changes not included

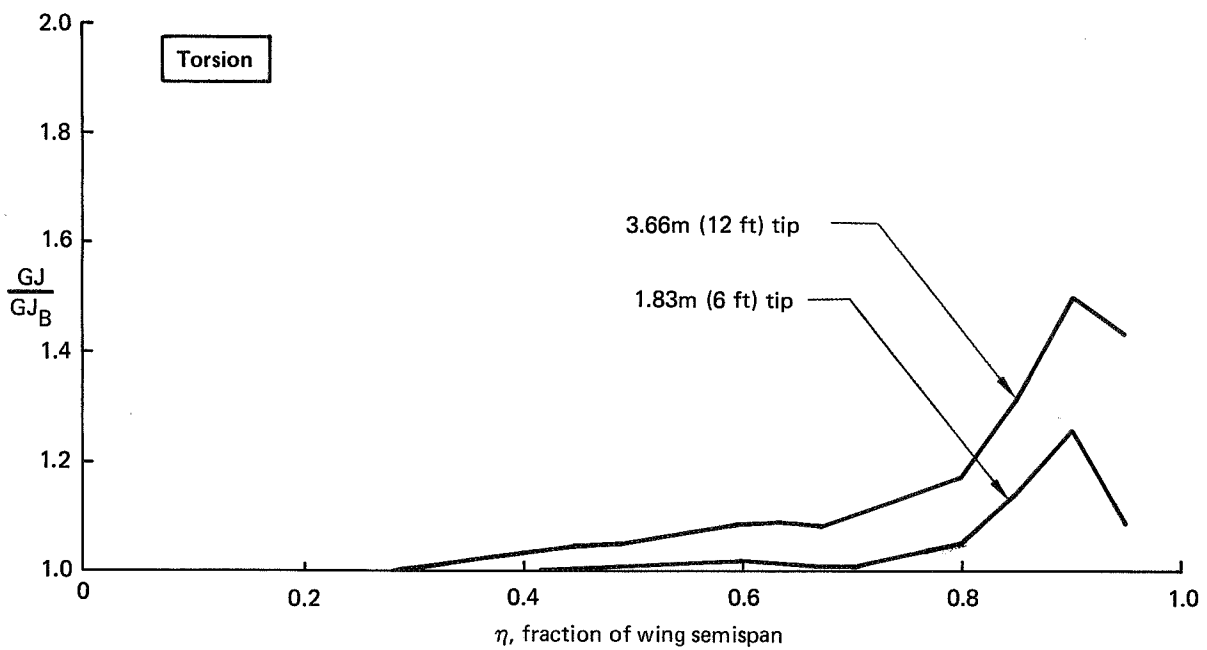
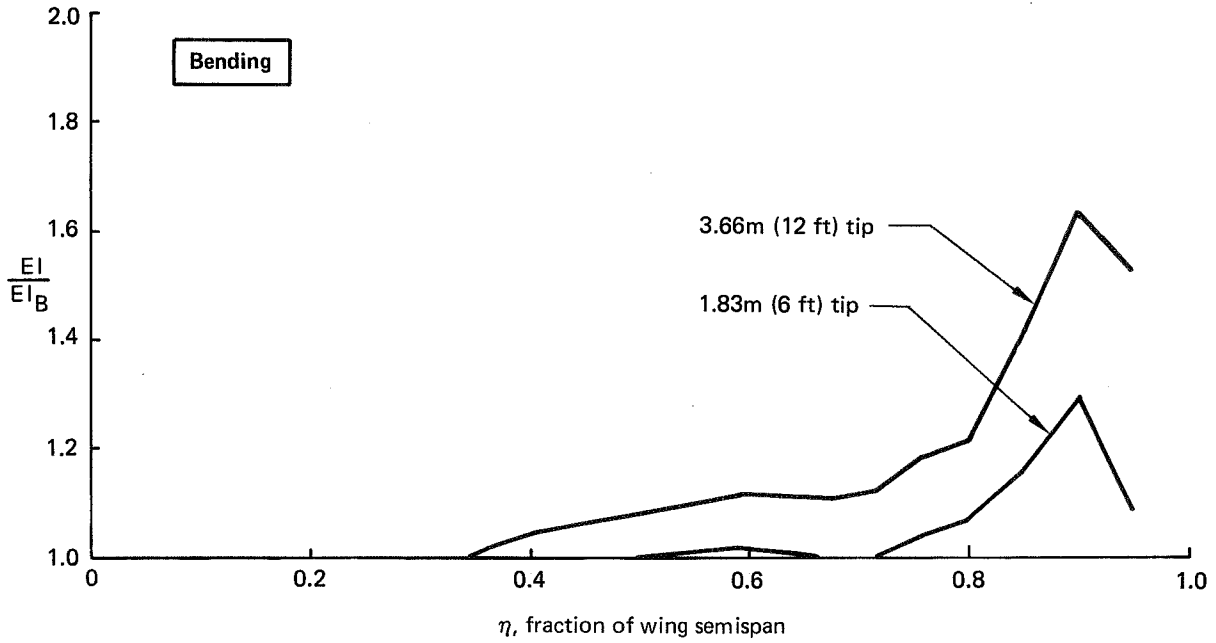


Figure 13. Structural Stiffness of Wings With Tip Extensions

No material was required for flutter on the wing with the 1.83-m (6-ft) tip extension. Mid-and rear-spar webs on the wings with tip extensions did not require any strength increase.

To provide an indication of the weight penalty associated with installing a tip extension on a wing initially having a zero margin of safety in the upper and lower panels, these panels were resized (using the same external loads) to have margins of safety equal to those of the baseline wing. Critical spar web loads were not calculated; therefore, spar web gages were not increased above the "beef-up"-only sizing. If spar web gages had been increased to maintain their baseline margin of safety, the weight impact would have been small. If loads with a tip extension produced a smaller sizing, then no material was removed from these sections. Sizing results are shown in Figures 12 and 14.

The 3.66-m (12-ft) tip configuration sizing shown in Figures 13 and 14 was obtained from using ultimate maneuver loads only. Airplane performance based upon this sizing indicated that little benefit could be obtained relative to the 1.83-m (6-ft) tip. Therefore, fatigue and flutter analyses were not accomplished, although a fatigue weight increment was estimated. If more weight were added to satisfy flutter requirements, the performance would only be further reduced.

A study indicated that retrofitting a tip extension is not practical because of the extensive wing structural changes required.

4.2.4 Weights

Wing tip extension panel weights were estimated from a configuration description and layout drawings. The panel/attachment configuration description was based on a prior Boeing study of a 1.83-m (6-ft) extension. The weight of the tip for that study was calculated from drawings and was used to verify the current study estimate. The weight buildup of the 1.83-m (6-ft) extension is as follows:

	<u>Mass/airplane</u> kg	<u>Weight/airplane</u> (lb)
Extension of wing box	243	(535)
Extension of leading edge (no leading-edge device)	82	(180)
Extension of trailing edge	38	(84)
Additional access doors	7	(16)
Deletions from baseline	-54	(-120)
Miscellany and round off (systems relocation, etc.)	2	(5)
Total 1.83-m (6-ft) WTE	<u>218</u>	<u>(700)</u>

The weight of the 3.66-m (12-ft) extension was estimated to be twice that of the 1.83-m (6-ft) extension. Wing box weight increments were estimated from the stress sizings.

Table 1 compares weight increments of the 1.83- and 3.66-m (6- and 12-ft) WTE with the existing margins of safety absorbed and maintained.

A/A_B = cross sectional area ratio—modified/baseline

- All results based on the same external loads
- Loads based on configuration with baseline MS absorbed
- Fatigue sizing not included

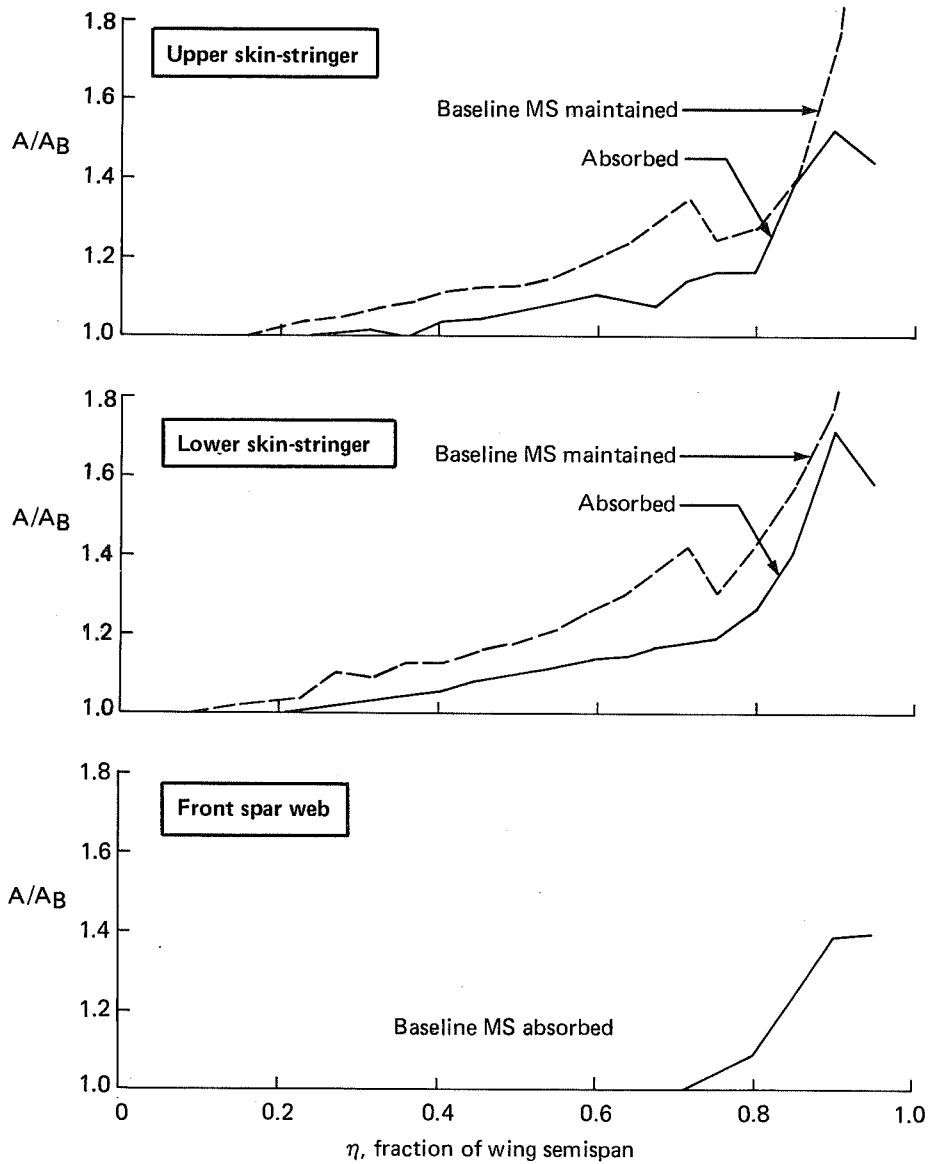


Figure 14. Structural Sizing of Wing With 3.66m (12-ft) WTE

Table 1. Wing Tip Extension (WTE) Weight Summary

	Increment per airplane, mass (weight), kg (lb)			
	1.83m (6-ft) WTE		3.66m (12-ft) WTE	
	Absorb existing MS	Maintain existing MS	Absorb existing MS	Maintain existing MS
Wing tip installation	317 (700)	317 (700)	635 (1400)	635 (1400)
Wing box reinforcement for:				
• Static loads	190 (420)	1360 (3000)	1168 (2575)	2710 (5975)
• Fatigue	45 (100)	0 (0)	230 (500)	0 (0)
• Flutter	0	0	0	0
Total delta increase/airplane	553 (1220)	1678 (3700)	2030 (4475)	3345 (7375)

4.2.5 Stability and Control

The addition of a WTE changes the stability and control characteristics of the basic airplane to the extent that minor modifications to the longitudinal flight control system may be required. Some lateral-directional stability and control characteristics are slightly degraded, but no aileron span extension or other lateral control system revisions are considered necessary. Results of this task were derived from analyses of data for 1.52- and 1.83-m (5- and 6-ft) tip extensions obtained from prior wind tunnel tests. Similar effects are expected with longer extensions.

As shown in Figure 15, a WTE results in an increase in rigid airframe longitudinal stability due to additional lifting capability aft of the quarter chord of the mean aerodynamic chord (MAC). This stability increase is largely offset by aeroelastic losses, but the net result is an increase of approximately 2-3% MAC, flaps up. The corresponding increase for flaps 30 (landing flaps) is 3% MAC. The increased stability will result in increased stick forces to maneuver. However, the stick forces per g can be reduced to present levels, if desired, by minor modification of the feel system.

The WTE tends to increase longitudinal static stability relative to the basic airplane, except for indication of tuck (airplane tendency to nose down with increasing Mach number) at speeds a little above the cruise Mach number which can be inferred from the wind tunnel data comparisons in Figure 16. If more extensive investigations (including aeroelastic and feel system effects) indicate improvement is required, some compensation can be gained through changes such as adjustment of the elevator rigging.

Stabilizer trim requirements to trim with the wing tip extension are generally more airplane nose down (stabilizer leading edge up) during cruise. The difference is

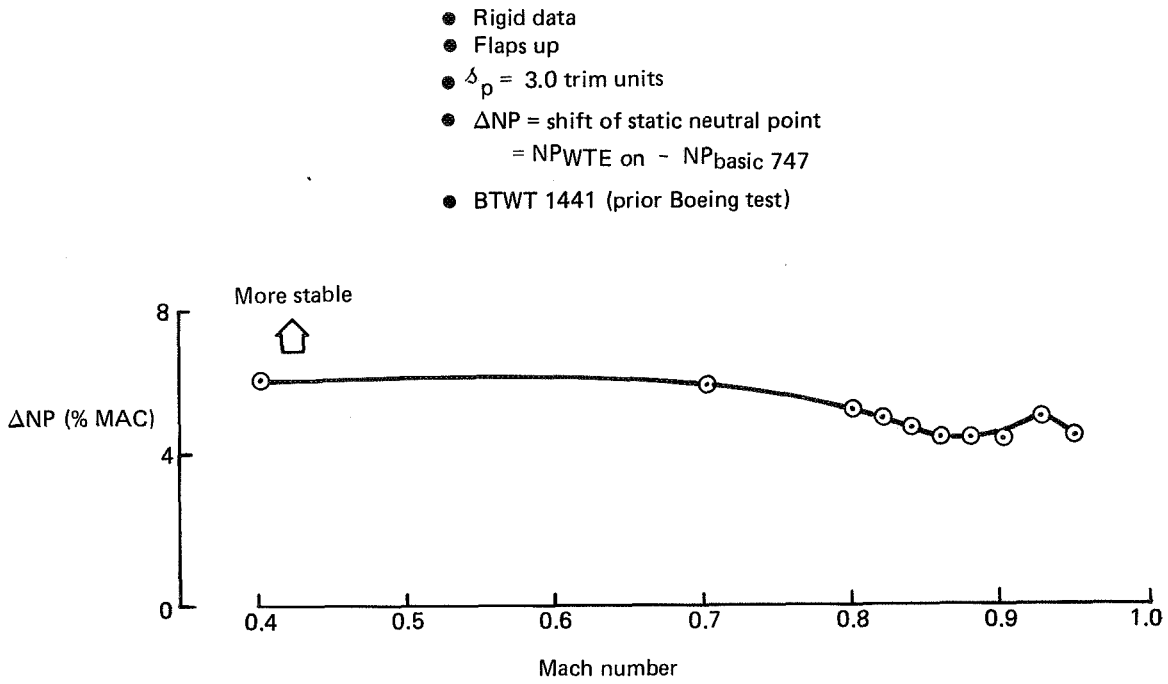


Figure 15. Effect of 1.83m (6-ft) WTE on Static Longitudinal Stability

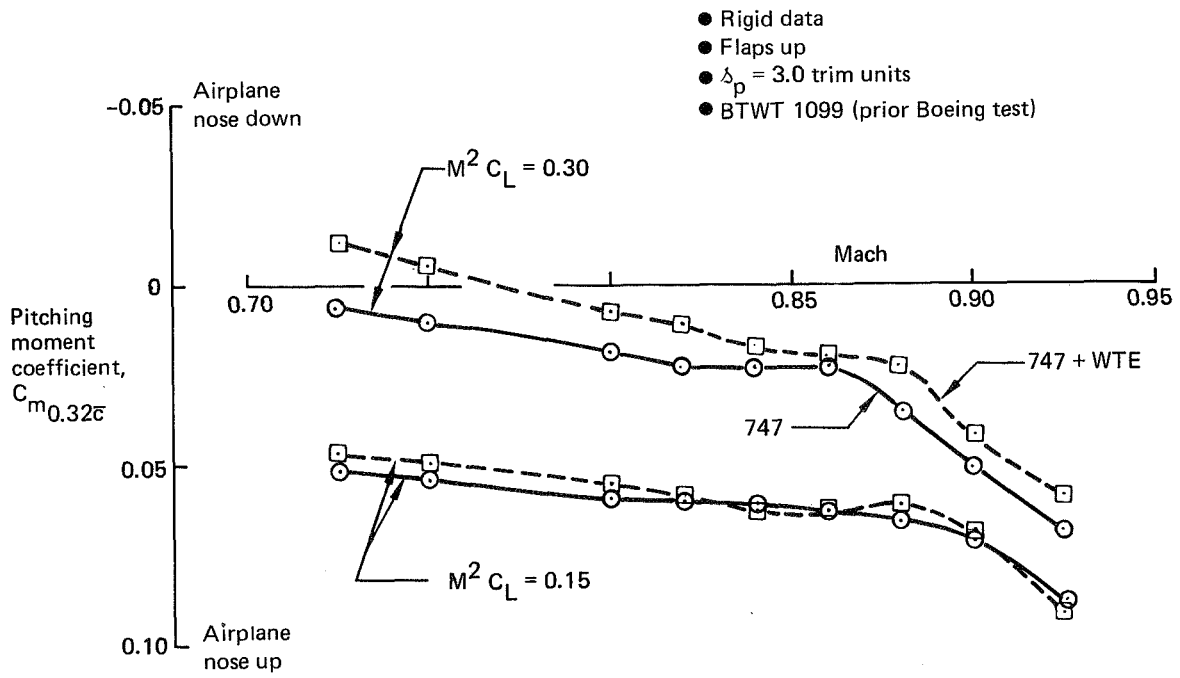


Figure 16. Longitudinal Speed/Trim Stability With 1.52m (5-ft) WTE

approximately 1/4 unit at maximum operating speed. Landing trim is more airplane nose up by approximately 3/4 unit at the approach reference speed. Approximately 1/2 unit more airplane nose up trim is required for takeoff.

The addition of a WTE to the 747 has only small effects on lateral-directional stability derivatives. The tip is expected to increase roll due to sideslip ($C_{l\beta}$) by 2-3%, increase roll due to outboard aileron (C_{lA_0}) by 3-4%, and increase roll damping ($C_{l\dot{\beta}}$) by 2-3%. The impact of a tip extension on yawing moment and side force derivatives is negligible.

The effects of these changes on lateral-directional static stability characteristics (i.e., engine-out control, cross wind capability, rudder induced sideslips) are minimized by the fact that the increases in $C_{l\beta}$ and $C_{l\dot{\beta}}$ are offsetting when the flaps are down. For flaps up flight, where the outboard aileron is locked out, the wheel required in side-slip will increase by 2-3%, which is negligible.

For flaps-down flight, the 2-3% increase in roll damping and 3-4% increase in aileron effectiveness combine to cause a loss in roll performance of approximately 1%. Flaps up, maximum roll rate will be reduced 2-3%. Both changes are considered acceptable (though undesirable), so an aileron span extension is not mandatory to meet flying qualities requirements with the WTE.

The predicted increases in $C_{l\beta}$ and $C_{l\dot{\beta}}$ have offsetting effects on Dutch roll characteristics, with the net effect being no noticeable change in either damping or period. Spiral stability will be very slightly increased.

The flight control system modifications to compensate for the stability and control effects of wing tip extensions are noted in Section 4.3.4.

4.3 INSTALLATION DESIGN CONCEPT

The design studies were concerned primarily with establishing feasibility and providing preliminary design work statements for use in obtaining cost estimates. Emphasis was on production-line installation for future deliveries, although feasibility of retrofit also was studied and found to be impractical. Three-view drawings illustrating the WTE/WTW configurations considered as final configuration candidates are presented in Section 7.1.8.

4.3.1 Extension Configuration and Construction

Previous studies of wing tip extensions determined that it was possible to simplify construction and minimize fabrication costs if the extension had a constant chord, thickness, and twist, the same as the existing wing section at WLB 1169. The extension construction is the same as the inboard wing, namely sheet stiffener and honeycomb panels. The existing tip fairing is retained and, by revising existing attachment hole locations, is installed 1.83m (6 ft) outboard.

4.3.2 Extension/Wing Splice

Existing wing spar and skin panel lengths are the maximum capable of being handled without affecting major assembly fixtures and manufacturing equipment. The wing and extension, therefore, are fabricated as separate units, then spliced at the locations shown in Figure 17.

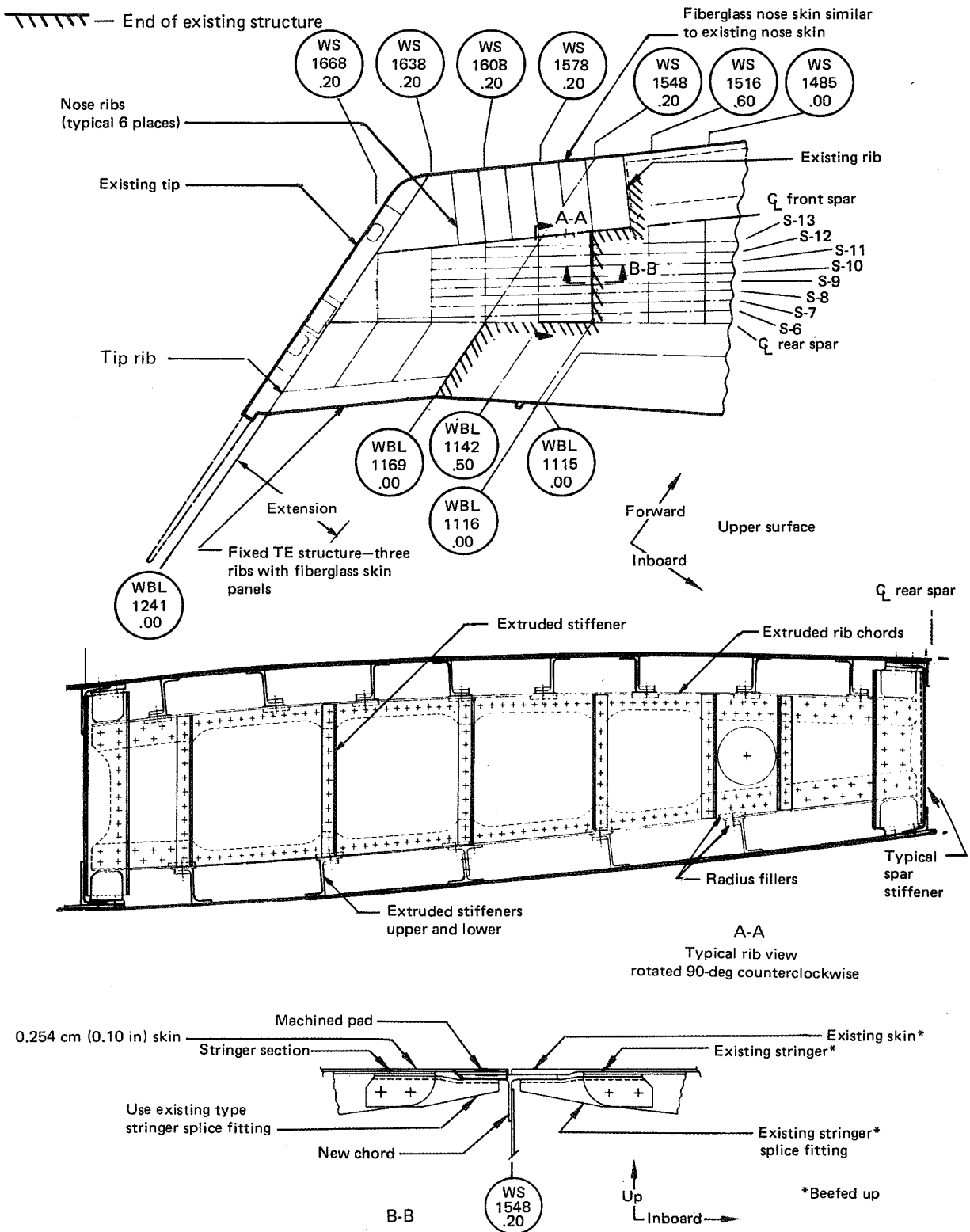


Figure 17. Attachment Concept for 1.83m (6-ft) WTE

4.3.3 Wing Structural Revision

The inboard wing box is reinforced to carry the increased loads from the increased span. Reinforcing is achieved by revising the machining of the skin, stringers, and front spar. The same skin/stringer thickness ratio is maintained, as in the existing wing, to satisfy fail-safe requirements. Existing raw plate material and extrusions can accommodate the thickness increase of the revised parts.

4.3.4 Control Systems Revision

Some relatively minor changes to the elevator and stabilizer control systems may be required. For example, the elevators can be rigged with additional downrig (more trailing edge down) to improve cruise static (speed) stability and mistrimmed dive recovery. The elevator feel system may be revised to maintain stick control force at the current force level. The stabilizer limit switches are relocated to provide increased electrical trim capability. To accommodate the revised takeoff trim range, the stabilizer greenband is modified and the greenband warning switches are relocated.

4.3.5 Electric and Electronic Systems

These systems, presently located in the tips, are simply moved outboard and similarly located.

4.4 INTERIM ASSESSMENT

Selection of the best WTE is a compromise between a number of factors, including performance, manufacturing cost, gate/taxiway clearance, flying qualities, and the extent of the development program required to address technical concerns such as flutter or buffet.

A 1.83-m (6-ft) WTE provides improved fuel efficiency and probably would not require leading-edge flaps or flutter material. Access to some existing gates would be lost, taxiway clearances would be reduced, and some minor modifications would be required to maintenance facilities. Minor flight control system revisions would be required (e.g., revised trim limits), but effects on flying qualities would be minimal with no aileron modifications required.

A 2.74-m (9-ft) WTE appears to be near optimum with respect to improved fuel efficiency for application without WLA, but leading-edge flaps would probably be required to avoid undesirable buffet, which would increase manufacturing costs. Still larger span extensions might give better fuel efficiency with WLA, but they would increase concerns regarding flutter, buffet, and gate/taxiway clearance and might require extension of the aileron span.

The 1.83-m (6-ft) WTE has economic and operational advantages, while the 2.74-m (9-ft) WTE has performance advantages; therefore, both should be considered in the final comparisons with winglets.

There is nothing unique about wing design, manufacturing, or FAA certification of tip extensions. No certification rule revisions or new special conditions should be necessary and certification of the modification should be routine.

5.0 WING TIP WINGLETS

This section discusses the addition of wing tip winglets (WTW) to the baseline wing without wing load alleviation (WLA). Comparisons with wing tip extensions (WTE) and discussion of WTW combined with WLA are provided in Section 7.0.

The winglet studies were similar to the tip extension studies in that detailed analyses (including structural sizing) to determine potential fuel savings were conducted for two configurations, Z9 and Z13 (sec. 5.3); however, the winglet studies required a much larger effort than did the tip extension studies. Several winglets had to be designed and tested in the Boeing Transonic Wind Tunnel (BTWT) before satisfactory performance was achieved; flutter model testing was necessary and analytical tools had to be modified in the areas of aerodynamic design, loads, and flutter. The winglet design and test data analysis activities are discussed in Section 5.2.

Flutter testing showed that the winglets caused a symmetric flutter mode and a wing tip flutter mode to appear that are not present for the baseline wing. Testing with the winglets replaced by equivalent masses, showed the modes resulted from aerodynamic rather than mass effects. Flutter speeds with these modes were greatly reduced relative to the flutter speed for the antisymmetric flutter mode of the baseline wing.

These modes and the attendant reduction in flutter speed were not predicted by the conventional flutter analysis methods used prior to the winglet test. When the problem appeared, the flutter study plan was expanded to improve the winglet flutter analysis. As discussed in Section 5.2.2, the improved analysis gave a reasonable degree of correlation with the test results and was then used as part of the final structural sizing cycle for the Z13 WTW.

Flutter sizing required addition of a significant amount of stiffness material. The added flutter weight, when translated in terms of equivalent L/D, reduced the L/D benefits of the Z13 WTW by about 0.5%. Complete L/D, weight, and performance data are presented in Section 5.3.

The Z13 WTW gave the best performance of the configurations tested, achieving 96% of the potential predicted by subsonic theory. A full-scale increase in maximum trimmed cruise L/D of 3.2% (which includes the adverse effects of increased aeroelastic washout of the basic wing) was estimated. This is a significant improvement and is better than that attained by any other winglet tested to date on a 747 model. Having a full-chord planform and a reasonable thickness-to-chord ratio, the Z13 is better with respect to wing/winglet attachment design than the partial-chord designs (Z11 and Z12) that were tested. Hence, the Z13 WTW was selected as the "final" winglet configuration for comparison with tip extensions and for combination with WLA.

A preliminary design installation concept was devised that used three steel fittings to attach the wing spars to the winglet spars. This concept was judged to be unsatisfactory with respect to stress and manufacturing aspects, so a concept employing multiple spars in the wing/winglet juncture region was adopted for the final winglet (Z13) attachment design.

5.1 TEST CONFIGURATION SELECTION

A number of winglet configurations had been wind tunnel tested on 747 models prior to this program. The best of these (Z4) was similar to the winglet developed for the NASA/Boeing KC-135 Winglet Flight Test Program. This design, which had a span equivalent to 13.5% of the wing semi-span, and associated design methods were used as a starting point for design of the first 747 EET winglet (Z9). The Z4 had failed to achieve its theoretical performance potential at cruise Mach, so modifications intended to correct these deficiencies were incorporated into the Z9, which was designed to achieve optimum loading. When the Z9 also failed to meet its performance potential, the winglet design and test activities were expanded to enhance development of a successful winglet. Based upon available time, resources, and tunnel occupancy, three winglets (Z11, Z12, Z13) were designed for the second BTWT entry. A suboptimal loading philosophy was adopted for the aerodynamic design of these winglets, and a radius blend was incorporated in the wing-winglet juncture region. The winglets tested and their design pressure loadings are illustrated in Figure 18.

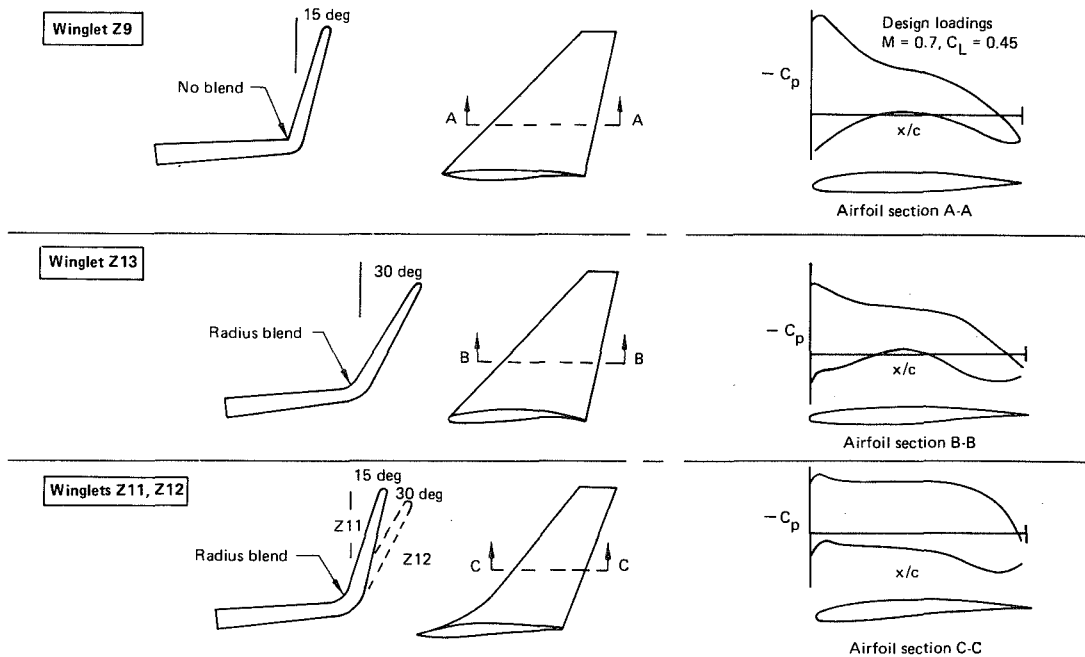


Figure 18. Winglet Configurations Tested in BTWT

The winglet aerodynamic design procedure is discussed in Section 5.1.1. Aerodynamic design was initiated on the Z11 winglet and a brief trend study (sec. 5.1.2) was conducted. The primary purpose of the trend study was to determine if the 30-deg cant angle being considered for the Z12 and Z13 (to aid in alleviating transonic interference effects in the wing-winglet juncture) would result in an excessive structural weight penalty or aggravate flutter. The trend studies indicated only a small weight increase with the increased cant angle, so aerodynamic design of the Z12 and Z13 configurations proceeded using 30 deg of cant.

Fabrication of winglet models Z11, Z12, and Z13 was more detailed than for the Z9. Closer tolerances were held on the leading edges and the wing-winglet juncture blend was machined as an integral part of the winglet.

5.1.1 Aerodynamic Design

This section describes how the winglet design cycle was carried out and reviews the Z9 winglet design, its problem areas, and the revised approach used for winglets Z11, Z12, and Z13.

The winglet design method was based primarily on two computer programs: A372, a vortex lattice program capable of designing the winglet camber surface and A230, an inviscid, subsonic potential flow program that calculates surface pressure distributions. Details of these programs and the paneling models used are in Appendix A.

The winglet design and iteration process is shown in Figure 19. Winglet span, cant angle, and loading (C_N) are the significant parameters affecting induced drag. Winglet planform and airfoil shape are significant parameters affecting viscous and compressibility drag. Winglet interference drag is a strong function of Mach number, cant angle, winglet loading, planform shape, and winglet chordwise location on the wing tip. All these factors influence the selection of winglet planform and cant angle. (The drag trend portion of Section 5.1.2 discusses the effect of span and cant angle on induced drag.)

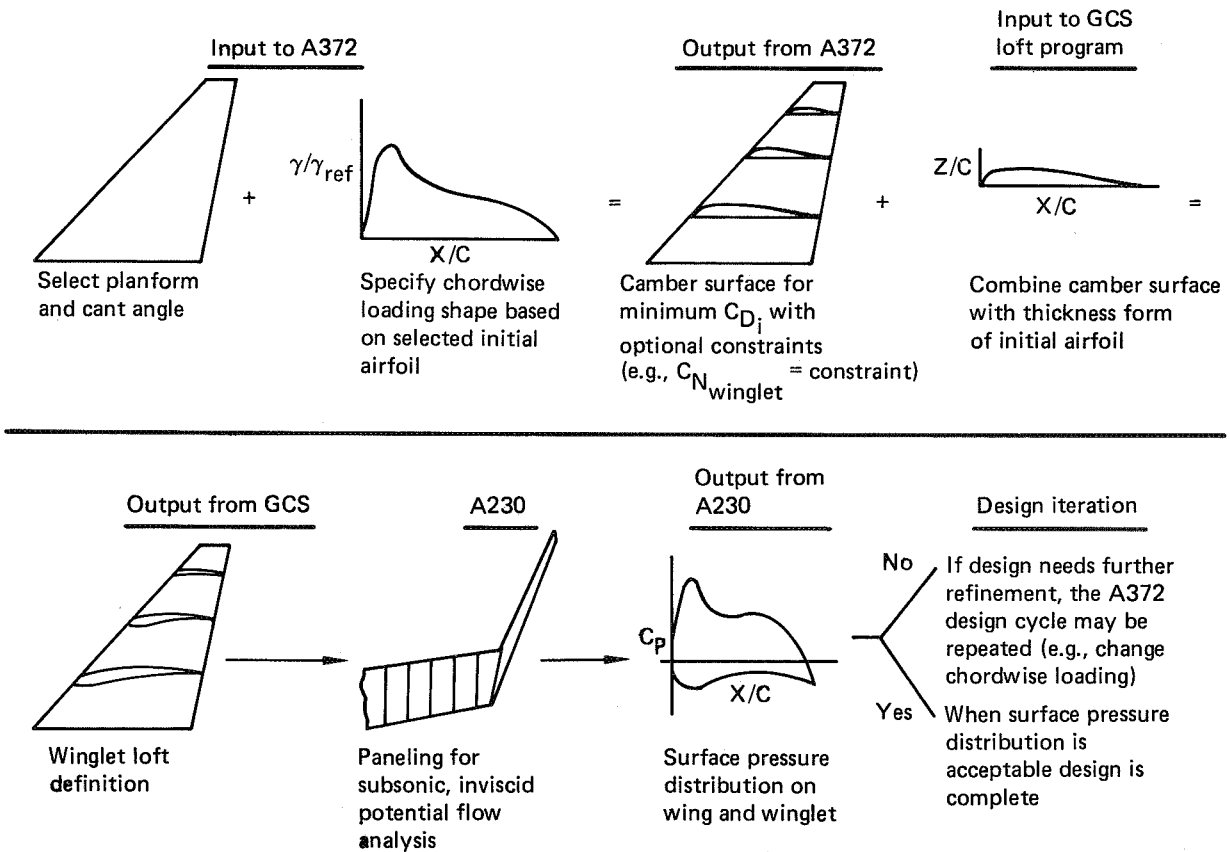


Figure 19. Design Iteration

Initial airfoil selection is an important element of a successful winglet design. A preliminary design run using computer program A372 is made to determine the required section lift coefficient for the airfoil. The initial airfoil selection was based on the required section lift, winglet planform sweep, and cruise Mach number.

The chordwise vorticity distribution of the initial airfoil section was determined for use in the A372 design program. As a design tool, A372 allows the winglet camber surface to be determined for a prescribed section chordwise loading shape. The designed camber surface corresponds to minimum induced drag for the wing and winglet with optional constraints (e.g., specified normal force on winglet surface). The design of the winglet in combination with an existing wing will produce no change in wing geometry and yields a prescribed geometry for the winglet camber surface. An important feature of the A372 computer program is that the camber surface for the winglet is designed in the curvilinear flow at the wing tip.

The designed winglet camber surface then is combined with the thickness form of the initial airfoil section to make a winglet loft. The resultant winglet definition is paneled for analysis in the A230 potential flow program. The A230 surface pressure distributions on the wing tip and winglet are evaluated for interference effects and suitability of winglet section pressure characteristics. If the interference between wing and winglet is excessive or the winglet section pressure distribution requires modification, iteration will be needed. An iteration could involve a change in the section chordwise loading shape input to A372 or a change in the airfoil thickness distribution. When the A230 analysis yields acceptable surface pressure distributions the design is complete.

The winglet design method described in the preceding paragraphs has several limitations. The A372 camber surface design is for incompressible conditions. This may result in excessive winglet root loading at cruise Mach number (0.84). Additionally, the winglet camber surface resulting from an A372 design run may be unacceptably defined over approximately one third of the inboard span (design surface indicated is impractical to loft because of sharp spanwise changes in twist and camber). This results in a necessary modification to the inboard camber geometry. The modification can be made with relatively small changes to the winglet span load, although the time required may be significant. Another limitation involves the lack of analysis capability at cruise Mach number. The A230 analysis is essentially limited to predicting subsonic surface pressure distributions.

Z9 was the first winglet designed in the 747 EET development program. Previous 747 studies were done on a partial wing tip chord winglet Z4 (similar to Z11 in planform shape). The Z9 winglet was a full wing tip chord winglet of trapezoidal planform. The previous-study winglet (Z4) did not meet its goal for cruise drag reduction. The main problem area was excessive winglet section loading. Winglet Z9 was designed to have essentially the same optimum span loading as the earlier study winglet, but with approximately 27% greater planform area (fig. 20). This increased area resulted in a theoretical required section lift coefficient that was 20% less than the previous winglet at midspan (fig. 21). The camber surface (chordwise loading shape) of the Z4 winglet was modified to reflect the increased planform area of Z9 and used to define the Z9 winglet geometry (fig. 22). As shown on Figure 23, the Z9 winglet did not perform as well as expected; cruise drag reduction was only 20% of estimated. Excessive leading-edge velocities caused significant wave drag and the larger planform resulted in undesirable wing tip interference losses. The experimental results of the 747 EET winglet testing are discussed in Section 5.2.1.

Planform characteristics		
Parameter	Winglet	
	Z ₄	Z ₉
Λ c/4 (degrees)	35	38
Aspect ratio	2.0	1.6
(t/c) _{max}	0.07	0.087
C _{tip} /C _{root}	0.35	0.23
b, m (ft)	4.03 (13.21)	4.01 (13.16)
S _{ref} , m ² (ft ²)	7.99 (86.0)	10.15 (109.3)
Cant (degrees)	15	15

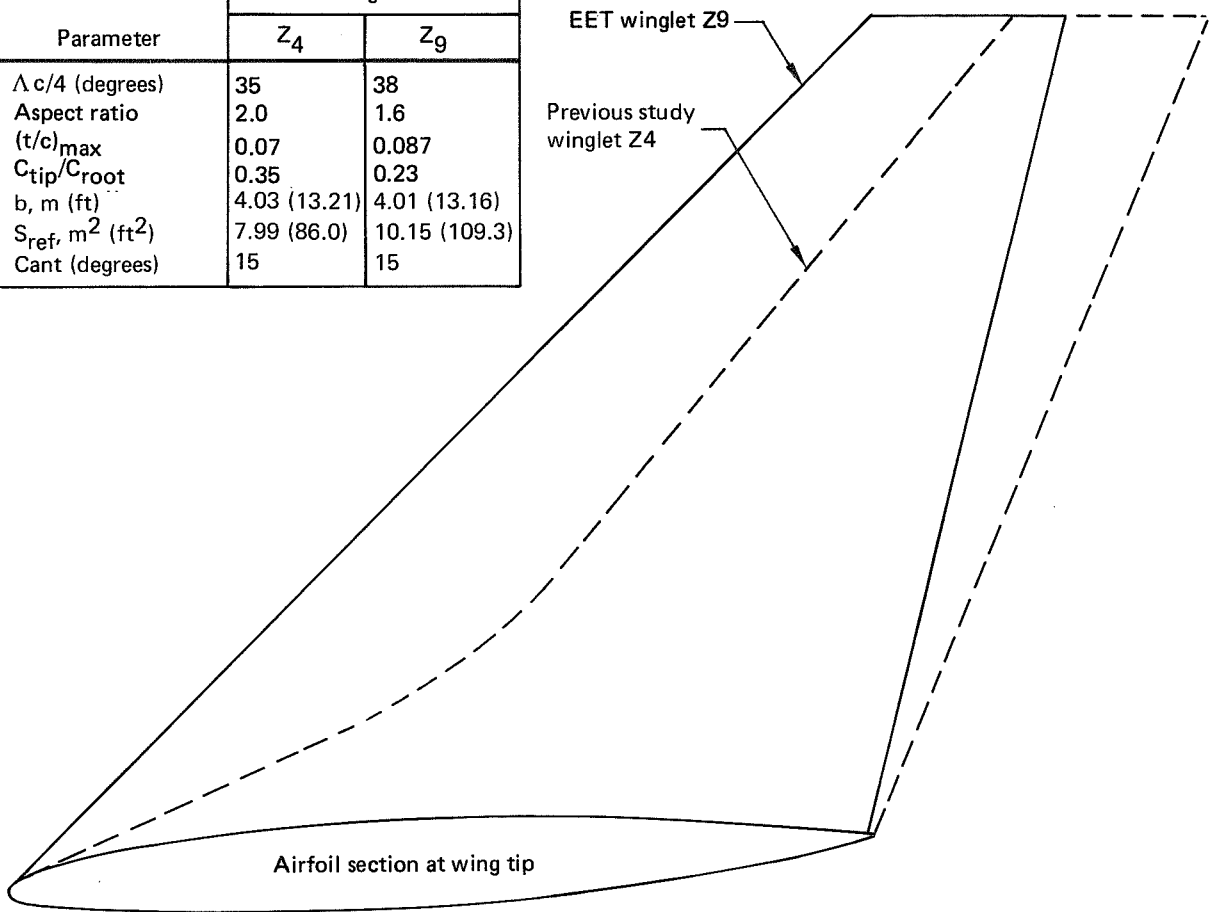


Figure 20. Winglet Geometry Comparison

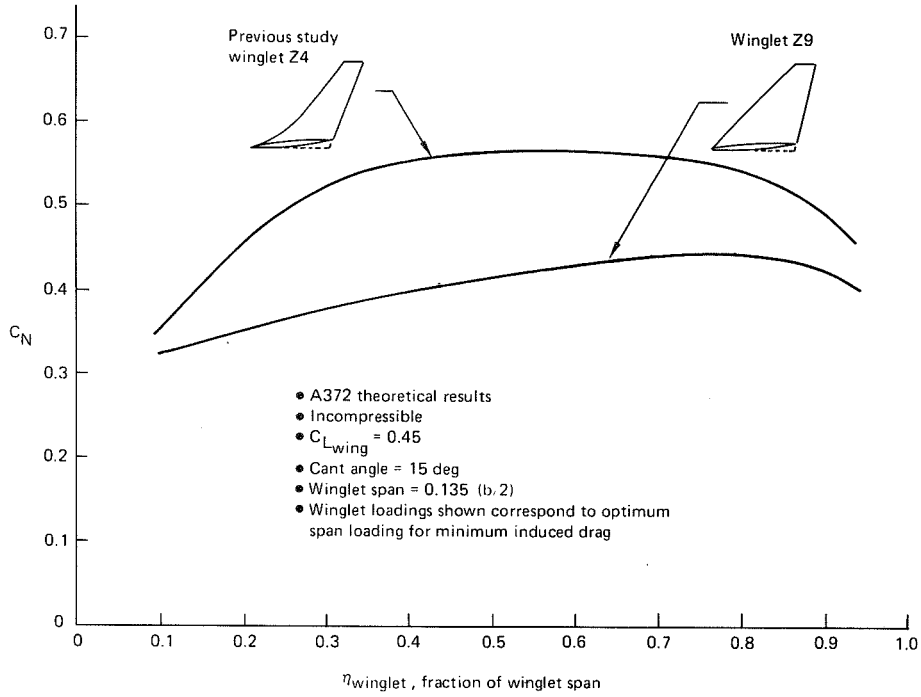


Figure 21. Effect of Winglet Planform on Section Normal Force Coefficient

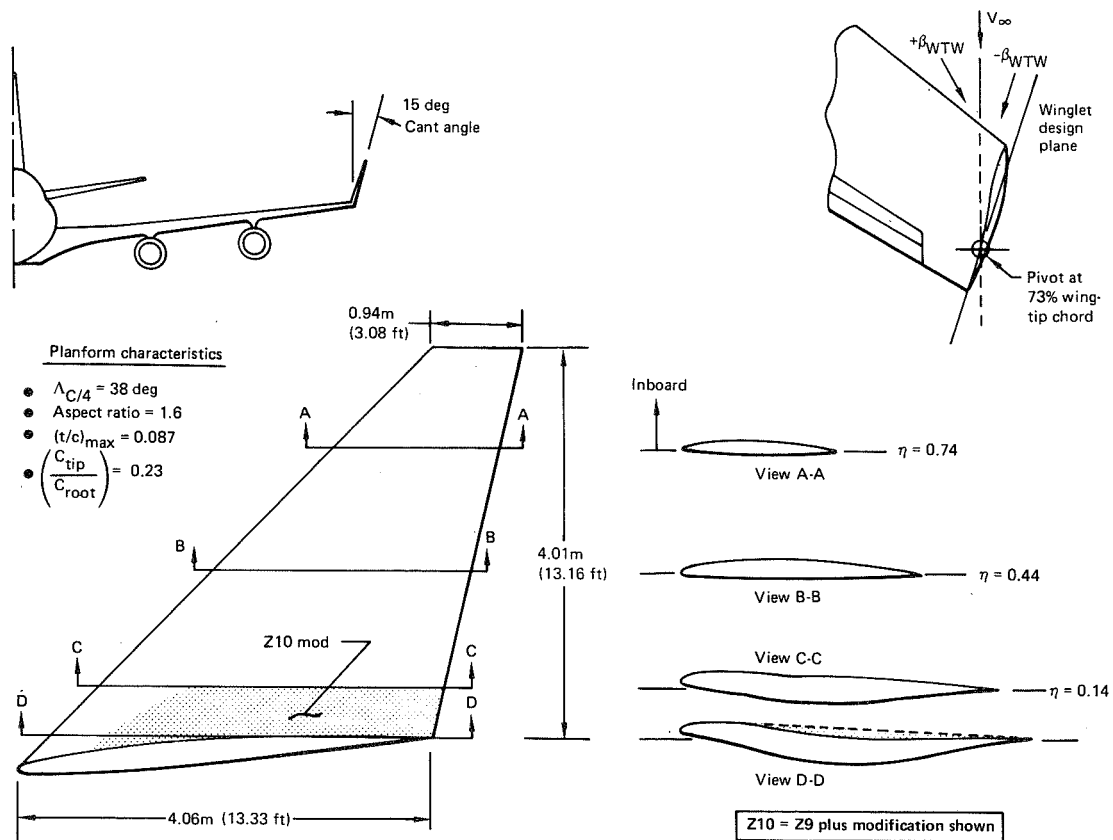
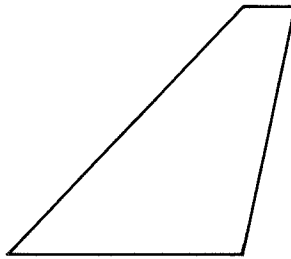


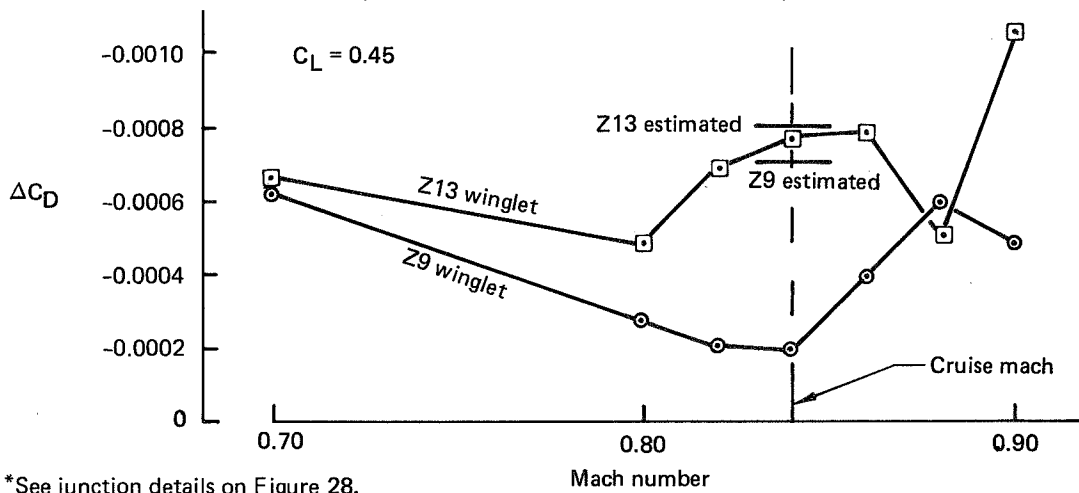
Figure 22. Winglet Z9 and Z10 Geometry

Z9/Z13 planform



	Z9	Z13
Cant angle (degrees)	15	30
(t/c) _{max}	0.087	0.075
Junction blend*	No	Yes
Loading concept	Optimum	Suboptimum
Tested during	BTWT 1599	BTWT 1642
β_{WTW} (degrees)	-1.5	0

Trimmed wind tunnel drag increment



*See junction details on Figure 28.

Figure 23. Winglet Z9 and Z13 Incremental Drag

Both Z4 and Z9 winglets had extensive root section tailoring (fig. 22) to help minimize wing tip interference, while maintaining the optimum winglet span load for minimum induced drag. The partial wing tip chord winglet had better wing tip interference characteristics and less wetted area, while the Z9 planform was structurally simpler to integrate onto the wing tip, with lower section lift coefficient required.

An A372 analysis was made to determine the effect on induced drag for winglet loadings less than optimum. The results shown in Figure 24, indicated that a 20% decrease in Z9 winglet C_N would ease the section design requirement with less than a 6% decrease in the favorable induced drag increment.

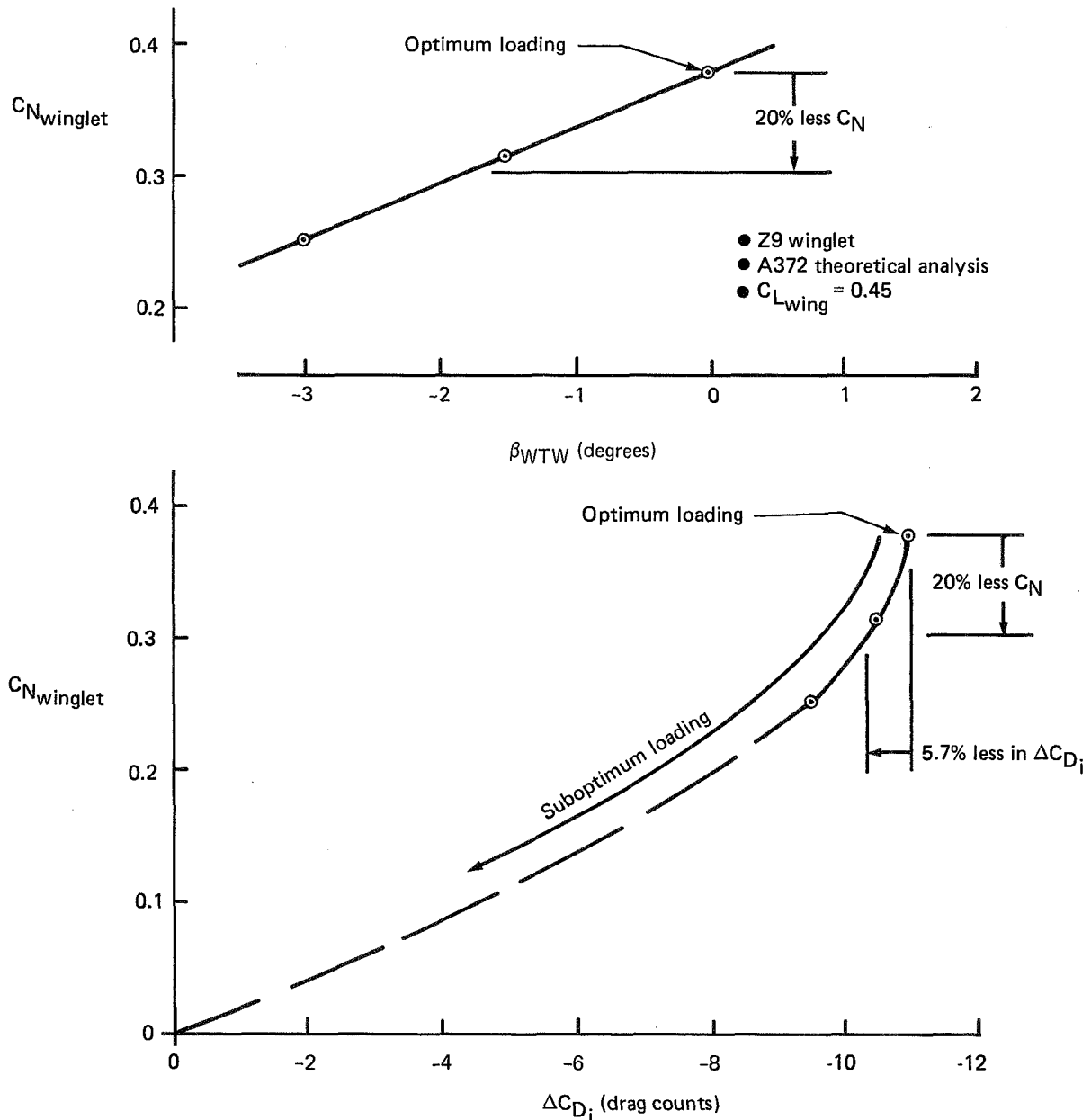


Figure 24. Effect of Suboptimum Winglet Loading

The information gained from the winglet Z4 and the Z9 loading study was used to develop three new winglet configurations. Winglets Z11 and Z12 were partial wing tip chord planforms with leading-edge strakelets blending into the wing tip and were canted outward 15 and 30 deg respectively (fig. 25 and 26). Winglet Z13 had the same planform as Z9, but was canted at 30 degrees (fig. 27).

Several design features were common to the three new winglets. First, a blended wing/winglet junction (fig. 28) was modeled from a successful KC-135 winglet configuration. Second, the winglet loadings were chosen to be approximately 20%-25% less than the corresponding optimum loadings (fig. 29). Section design, rather than winglet incidence reduction, was used to accomplish the suboptimum loading. Third, the extensive tailoring of the winglet root camber used on the previous winglets was eliminated. The suboptimum loading (and greater cant angles on Z12 and Z13) decreased the wing/winglet interference, which permitted more conventional root camber details than the previous winglets.

Winglet Z11 was designed using experimental pressure data from the partial wing tip chord winglet (Z4) as a starting point. Two dimensional transonic airfoil analysis and design techniques were applied, considering previous airfoil section geometry, corresponding experimental pressure data, and new design requirements that included reduction of inboard winglet surface velocities to sonic, or lower, over the entire chord. A new airfoil design with low leading-edge loading and increased aft loading (overall lift reduced by approximately 20%) was developed. The new airfoil was used

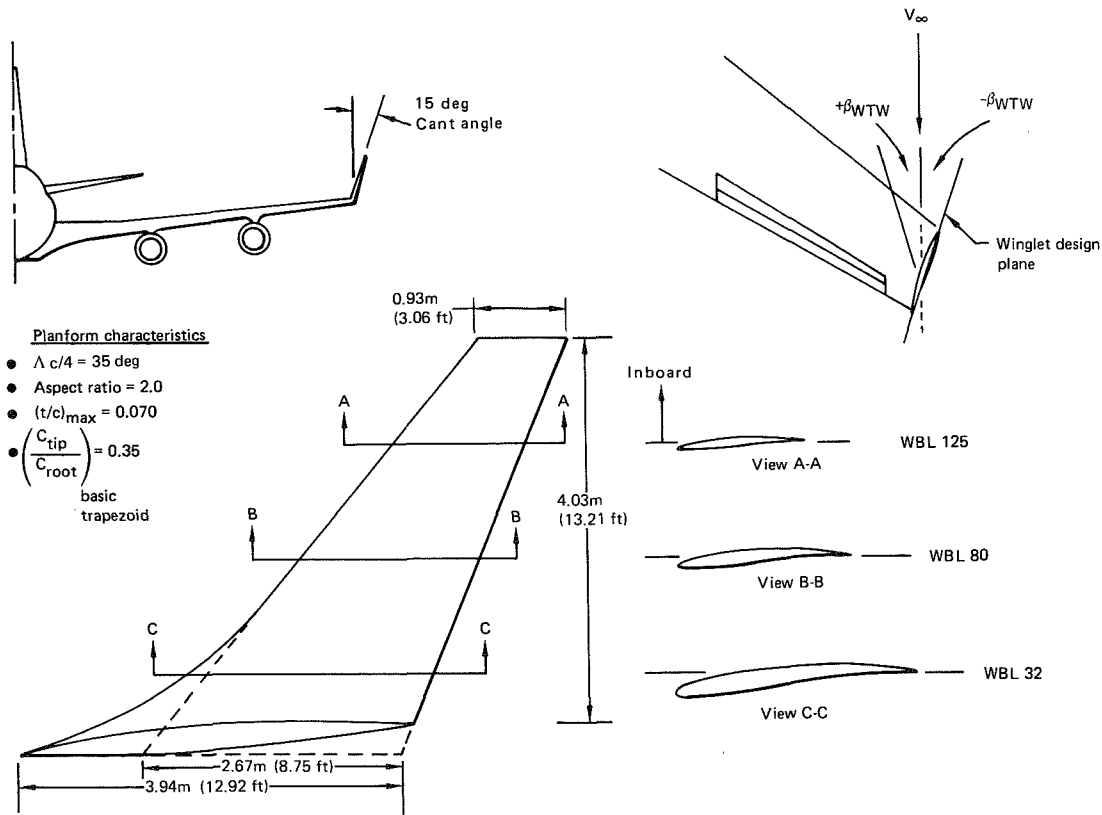


Figure 25. Winglet Z11 Geometry

in the A372 design cycle previously described. Winglet Z12 was obtained by repositioning the winglet Z11 at 30 deg cant and changing the winglet incidence to give the same winglet loading as Z11.

The initial airfoil for winglet Z13 was derived from an advanced technology airfoil that had been successfully applied in a previous 747 wing study. The airfoil section was scaled down in thickness and camber with considerable leading-edge droop added to reduce the leading-edge loading. This airfoil modification was accomplished using two dimensional, transonic airfoil analysis and design methods. The airfoil developed was used as the initial airfoil section for the A372 design cycle.

Of the three new winglet designs, experimental performance of Z13 was the best, with a cruise drag reduction that was 96% of the pretest estimated value (fig. 23). Z13 was designed using the design tools available, but it would be desirable to have a transonic flow analysis method (e.g., FL-27) to refine the design.

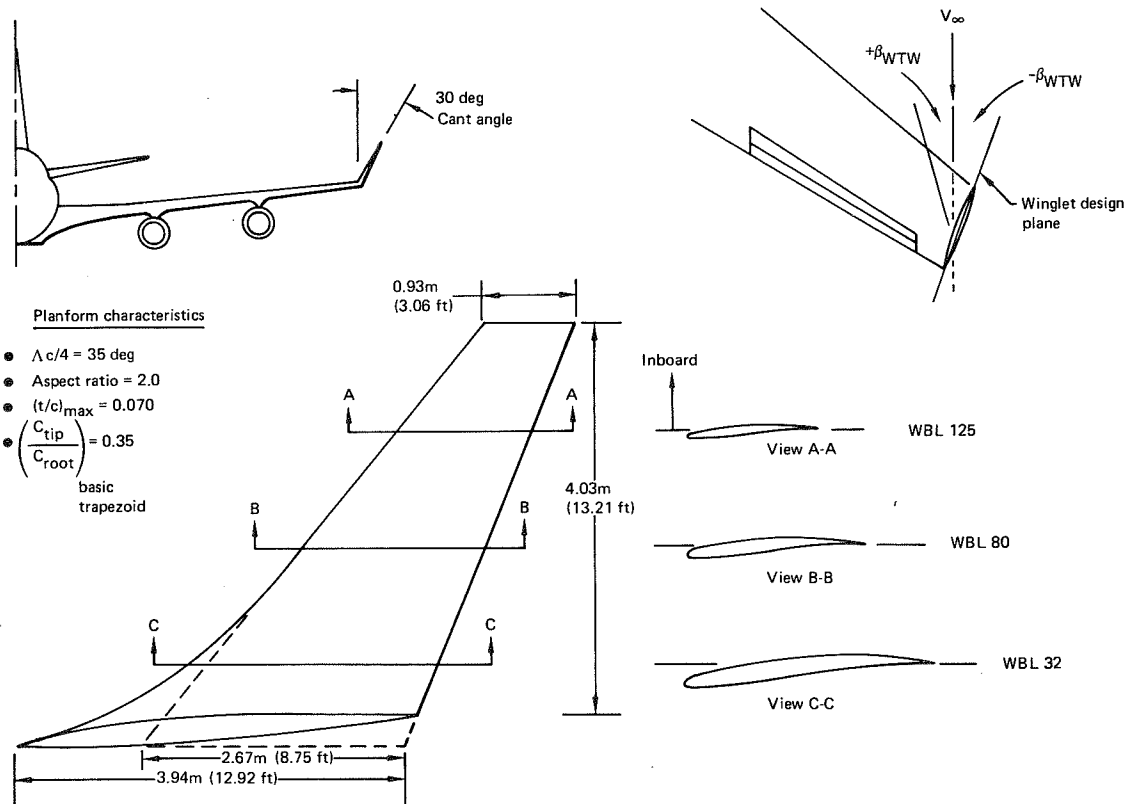


Figure 26. Winglet Z12 Geometry

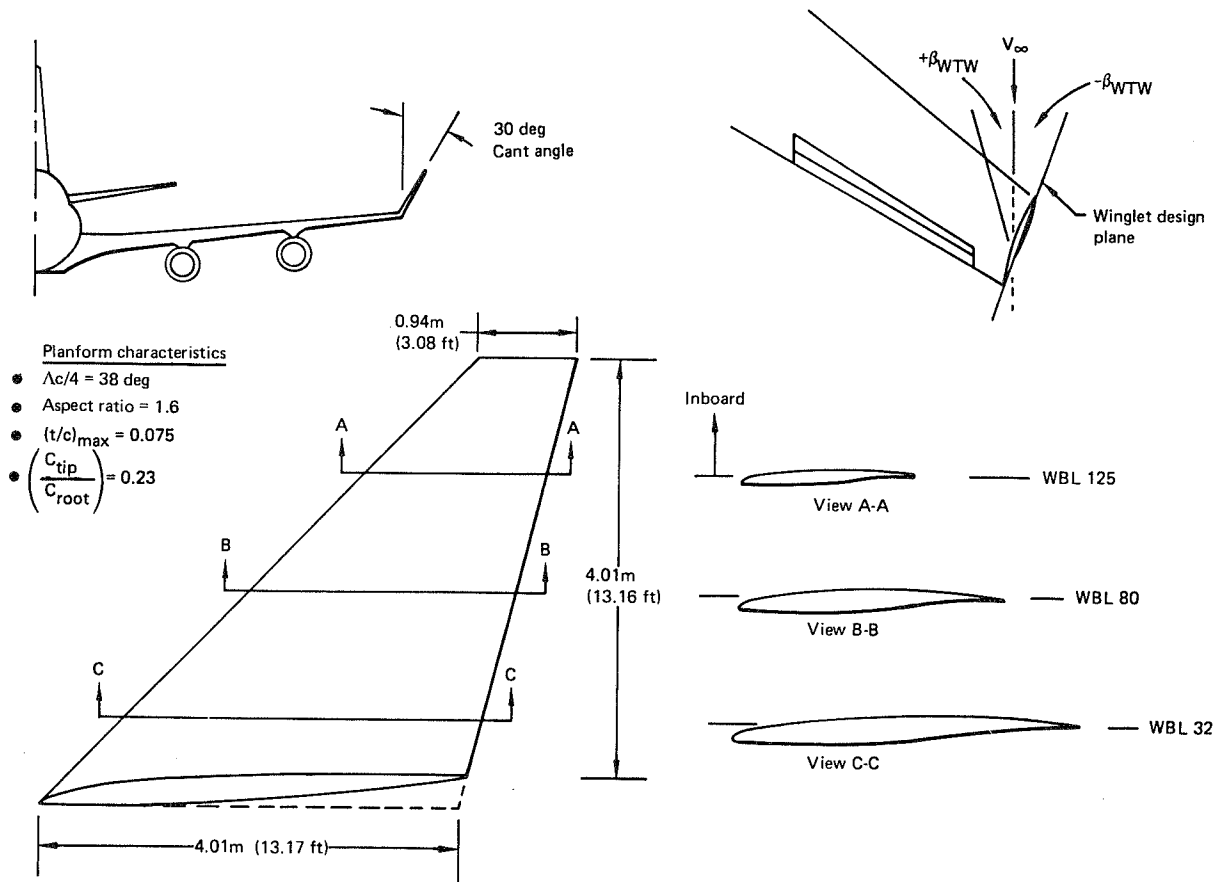
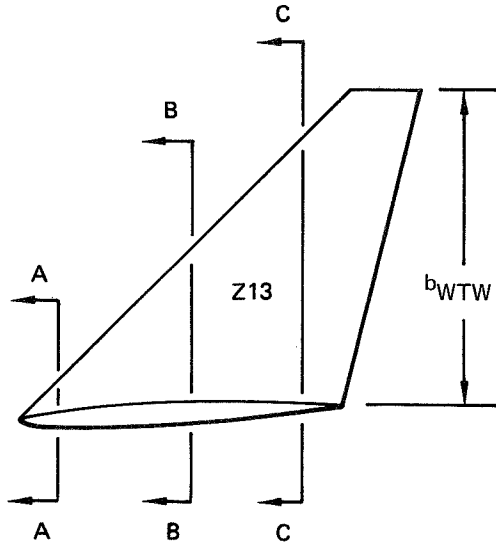


Figure 27. Winglet Z13 Geometry

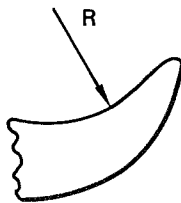
Z13 winglet

Not to scale

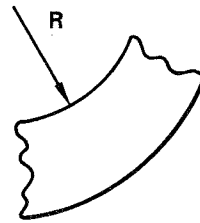


Note: Z13 wing-winglet junction is similar to the Z11-Z12 junction detail

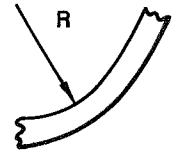
$$R = 0.09 b_{WTW}$$



View A-A

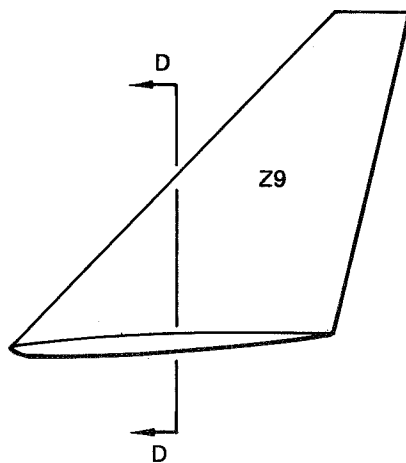


View B-B



View C-C

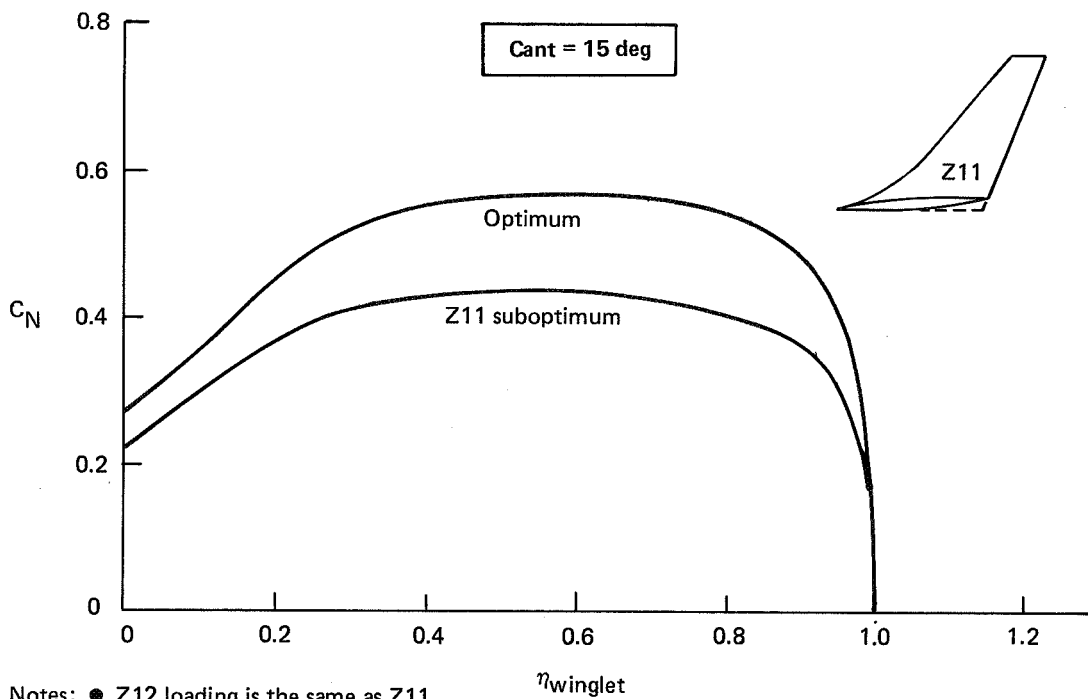
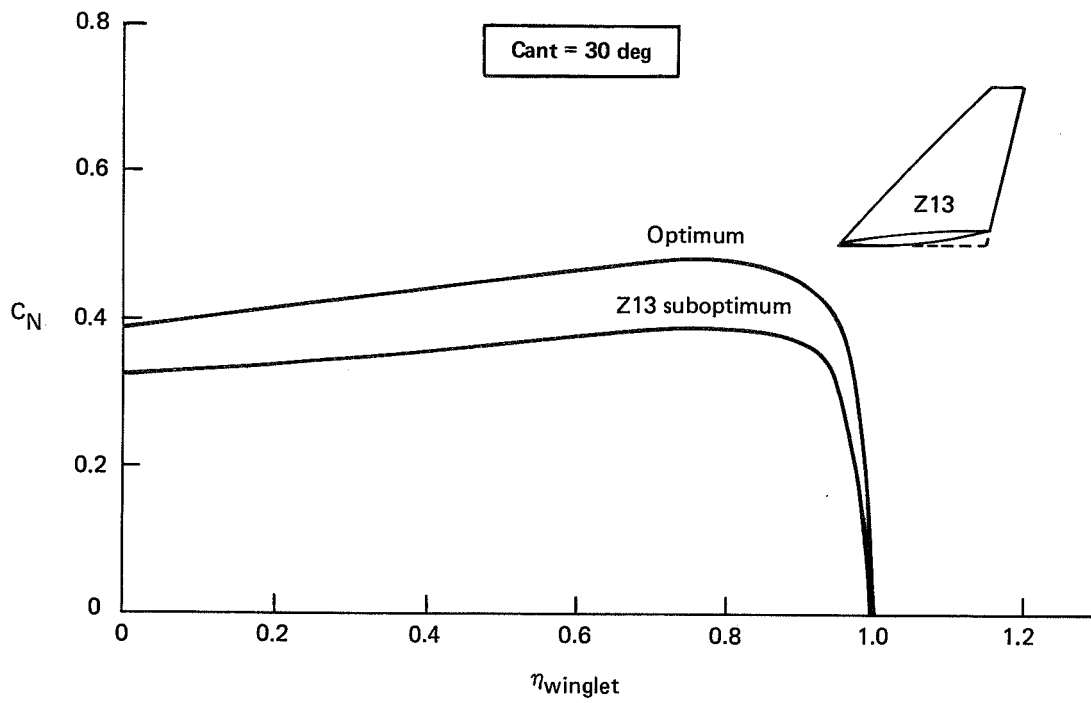
Z9 winglet



Inboard junction not blended

View D-D

Figure 28. Wing-Winglet Junction Details



Notes: ● Z12 loading is the same as Z11

● $C_{L_{wing}} = 0.45$

Figure 29. Optimum Versus Suboptimum Winglet Loadings

5.1.2 Preliminary Trend Studies

Drag Trends—Prior to the second phase of wind tunnel testing, a winglet trend study evaluated the sensitivity of induced drag to winglet span and cant angle. Figure 30 shows the planforms evaluated. Computer program A372 was used to determine the induced drag savings with optimum winglet loadings. Each span/cant angle combination involved both a design run and an analysis run. The design mode was run to give the optimum loadings for cruise, followed by the analysis mode to yield wing/winglet loadings (as a function of angle of attack) for use in assessing the aeroelastic twist penalty due to increased wing tip loading with winglets (fig. 31). The aeroelastic twist increment due to winglets then was analyzed in A372 to give an induced drag penalty.

Dimensions

Configuration	Span at leading edge, m (ft)	Reference area, m ² (ft ²)
Z9 planform	4.26 (14.0)	10.15 (109.3)
Shorter span	3.23 (10.6)	7.58 (81.6)
Longer span	5.62 (18.5)	13.55 (145.8)

● Tip chord = 0.94m (3.1 ft) ● Root chord = 4.06m (13.3 ft)

Planforms

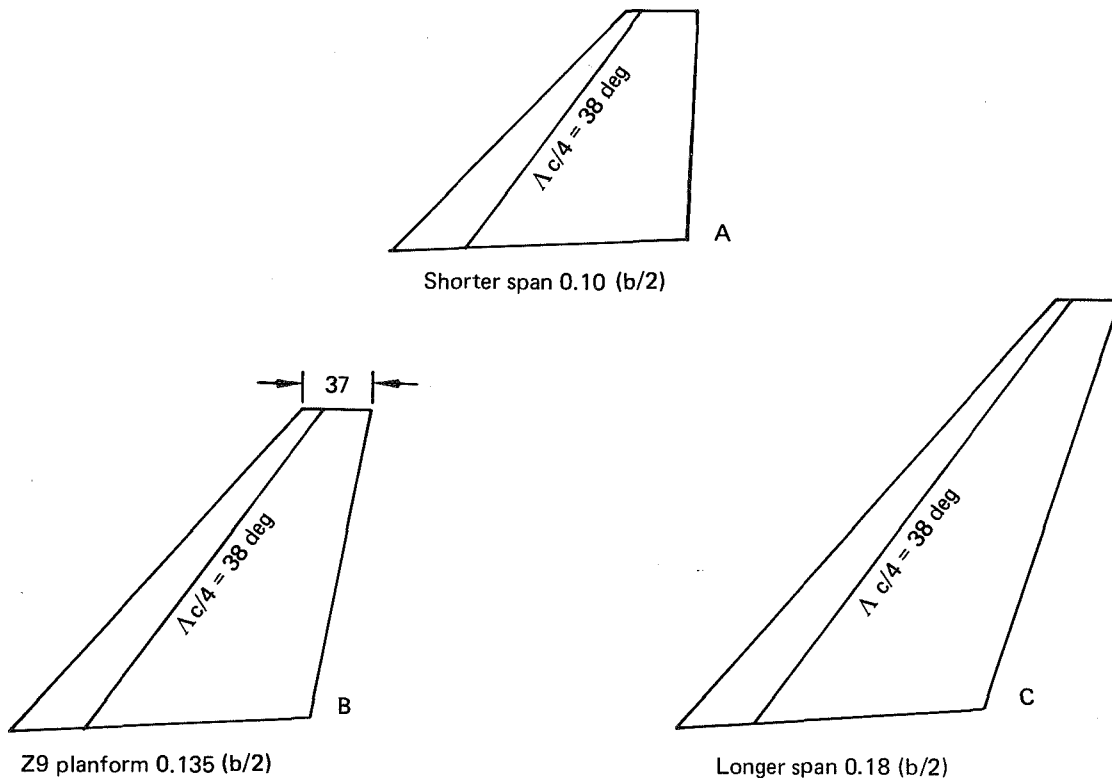


Figure 30. Winglet Trend Study Geometry

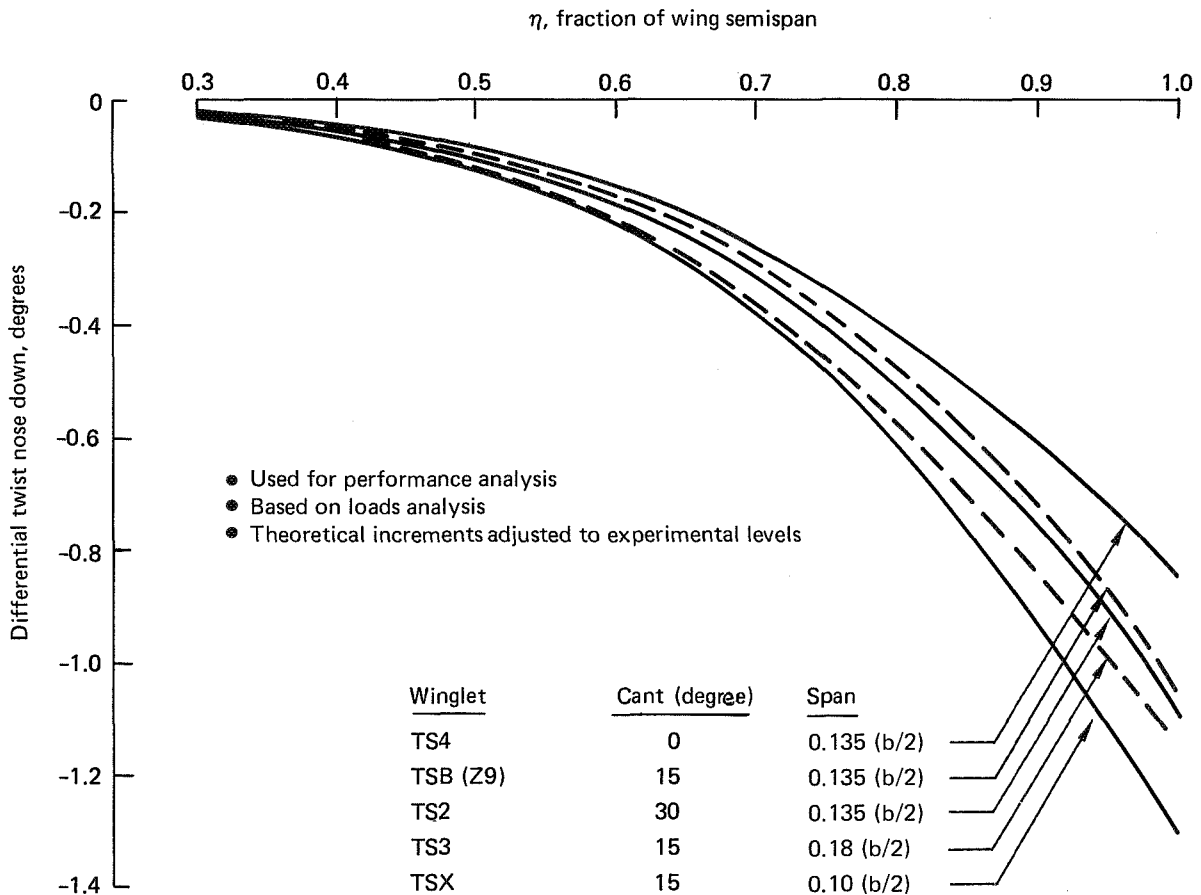


Figure 31. Winglet Trend Study—Aeroelastic Twist Increments

The results of the winglet trend study (fig. 32) show, as expected, that drag benefits improve with cant angle. Because weight and twist effects were not significant enough to influence the selection, winglets Z11 and Z13 were designed for 30 deg cant. Winglet span was not increased beyond 0.135 b/2 because of flutter considerations.

Twist Trends—Preliminary trend studies were performed using theoretical estimates of the aerodynamic loads for various winglet configurations. Wing twist results for the typical cruise condition are shown in Figure 33. As expected, these results show that increasing winglet span or cant increases wing tip washout. Final load results based on wind tunnel data for the Z9 and Z13 winglet configurations are contained in Section 5.3.2.

Weight Trends—Weight estimates of the winglet panels Z9, Z11, Z12, and Z13 were made, using wing weight estimation methods applied to the actual weight of an existing winglet design (KC-135). To obtain weight trends, the method uses an empirical wing weight equation that has parameters such as wing area, aspect ratio, sweepback angle, taper ratio, and thickness ratio as variables. Using the KC-135 winglet weight and geometry as a basepoint, weight estimates of the 747 configuration were made. The results are shown in Figure 34. Winglet attachment weights were not estimated for the trend study.

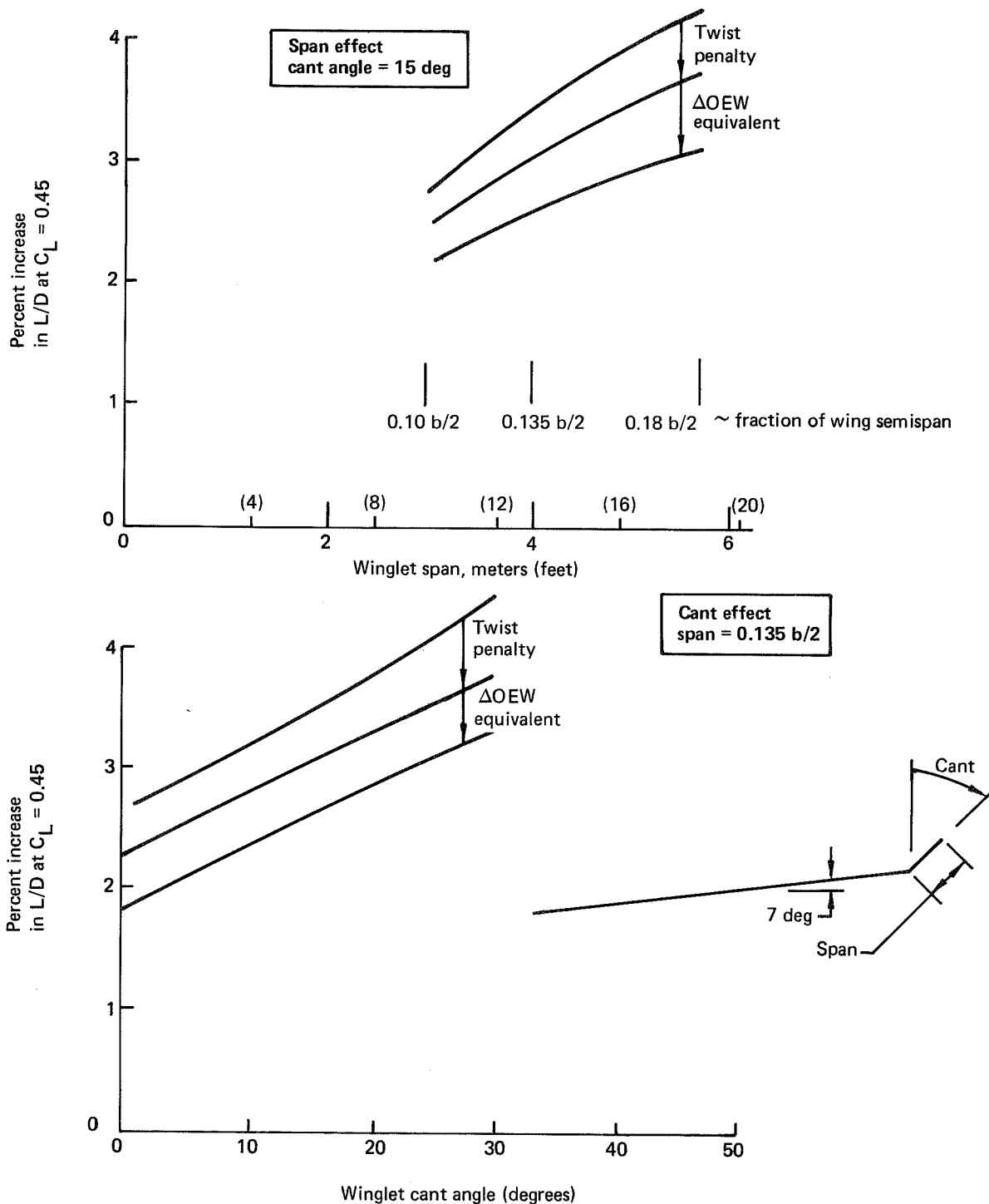


Figure 32. Performance Trends With Span and Cant Angle

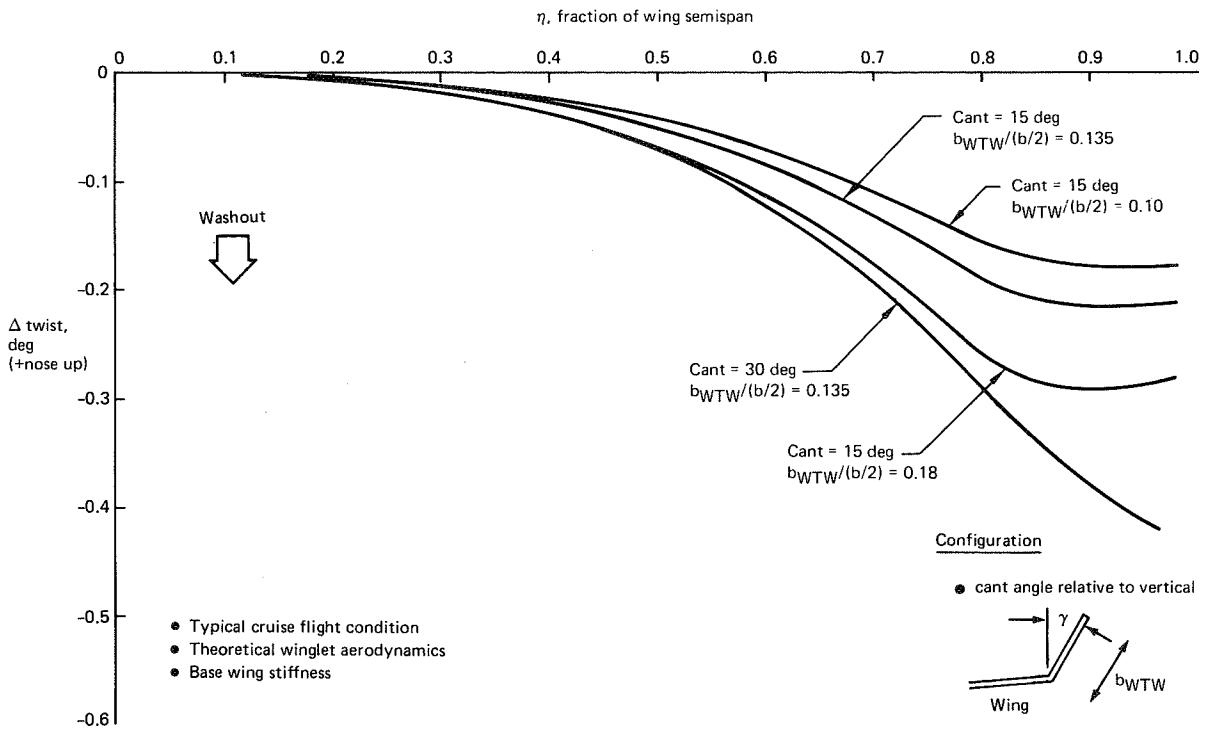


Figure 33. Wing Twist Increment for Winglet Trend Study

The effects of winglet span and cant angle on wing box weight were estimated from Boeing wing sizing data, maintaining the existing wing box structural margins of safety. Results are shown in Figure 35. The "bucket" in the cant angle trend curve was unexpected. Bending moments were verified to increase with cant angle and no problem was apparent in the resizing or weights computations. Because the pending design decision was whether or not to increase the cant angle from 15 to 30 degrees, the trend data were interpreted as showing weight to be relatively insensitive to small variations in cant angle, but strongly influenced by span variations. Winglet span for the second BTWT entry was maintained at 0.135 $b/2$ and two cant angles (15 and 30 deg) were tested. The weight difference between the 15 and 30 deg cant angles was confirmed by subsequent detailed analyses of the Z9 and Z13 configurations. The trend with reduced cant was not further examined.

Flutter Trends—Pretest flutter studies, using standard analysis methods, were conducted on Z9 winglets to explore wing tip winglet concept feasibility and to establish preliminary design estimates of acceptable geometric limits and sensitivity to payload variations. These analyses included standard three-dimensional lift and moment aerodynamics, but did not include oscillatory aerodynamic terms similar to those found necessary in T-tail analyses. The types of additional aerodynamic terms used in subsequent studies are described in Figure A-9 of Appendix A.

The configurations analyzed included the Z9 winglet (planform identical to the Z13 final configuration) at cant angles of 0, 15, and 30 deg and two other winglets with greater and lesser span at a cant angle of 15 deg. These latter two configurations maintained the quarter chord sweep and taper ratio of the Z9 planform. The mass properties were adjusted to account for the change in winglet size.

Configuration	Panel area, m ² (ft ²)	Span at leading edge, m (ft)	Thickness ratio, t/c max	Taper ratio, λ	Panel weight (lb/airplane)
Z9 family	10.15 (100.3)	4.26 (14.0)	0.087	0.23	1,000
Shorter span	7.58 (81.6)	3.23 (10.6)	0.087	0.23	680
Longer span	13.55 (145.8)	5.67 (18.5)	0.087	0.23	1,360
Z11 and Z12	7.95 (85.6)	4.18 (13.71)	0.070	0.35	870
Z13	10.26 (110.4)	4.18 (13.72)	0.075	0.23	1,010

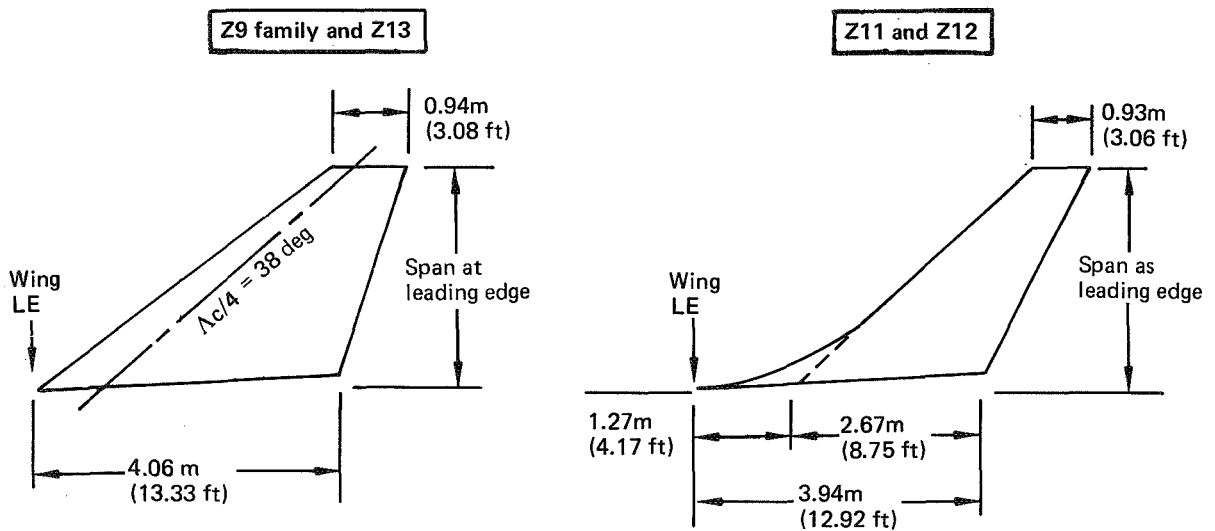


Figure 34. Winglet Panel Weight Comparison

- Existing margin of safety (MS) maintained
- Flutter and fatigue not considered

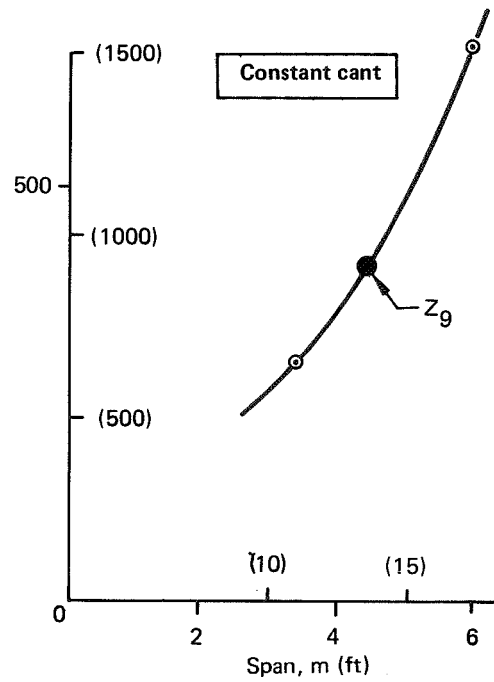
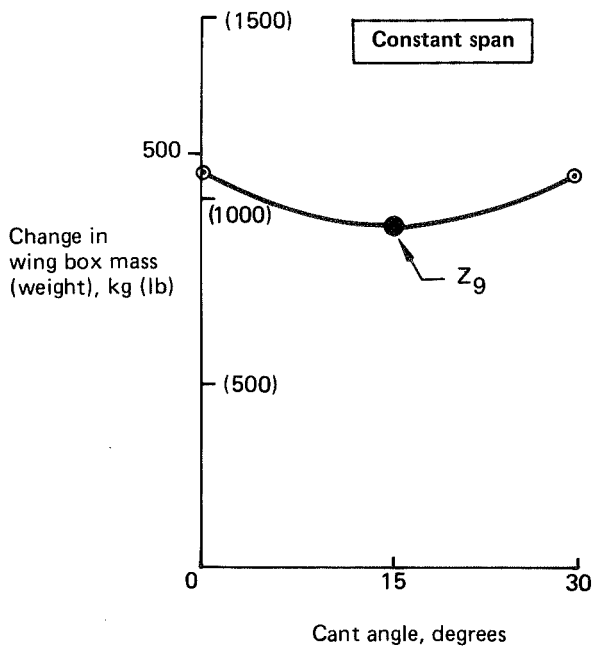
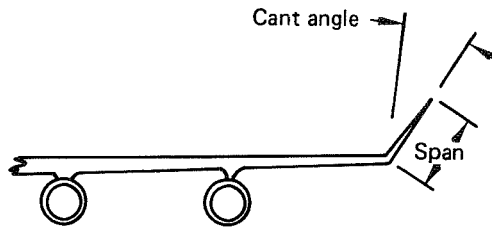


Figure 35. Wing Box Weight Increments for Winglet Trend Study

The critical antisymmetric BASIC flutter mode showed a minimum damping sensitivity to both the cant and span variations. Figure 36 shows the increase in antisymmetric BASIC mode minimum damping with an increase in cant angle for the empty payload configuration. The trend was similar for a full payload configuration. The change in damping with the variation of cant angle is not considered significant. Figure 37 shows the decrease in antisymmetric BASIC mode minimum damping with an increase in winglet span for the empty payload configuration. Again, a full payload configuration had similar characteristics. The degradation in damping with the increased span is significant.

From these studies, it was decided that a deficiency in methodology existed because of the general lack of flutter sensitivity to a major aerodynamic addition. This decision was confirmed by the results of the wind tunnel flutter test and by application of analytical techniques developed after the pretest studies.

Figure 38 shows the results of the standard and improved methodology for a cant angle variation. The standard methodology yielded only the antisymmetric results. The improved methodology results in symmetric and wing tip flutter modes (as seen during flutter testing) and also shows that cant angle is still not a significant parameter. Section 5.2.2 contains a more detailed explanation of the methodology differences.

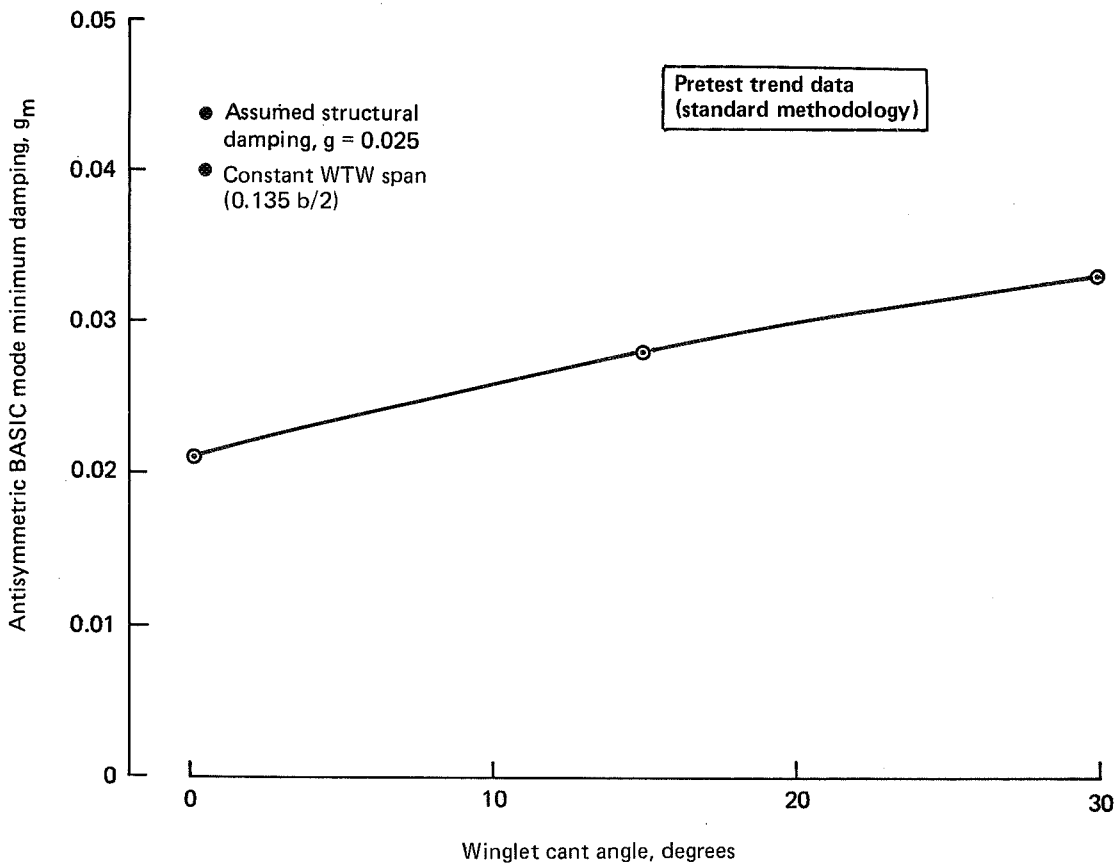


Figure 36. Effect of Wing Tip Winglet Cant Angle

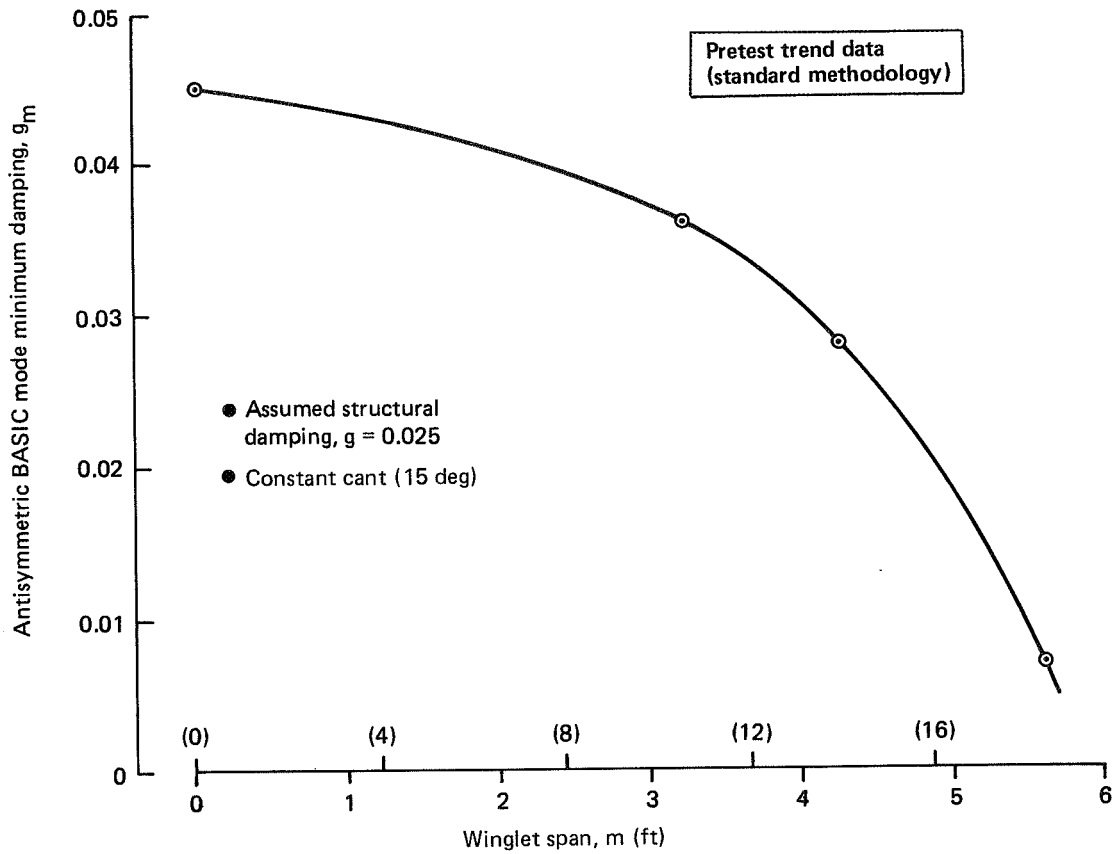


Figure 37. Effect of Wing Tip Winglet Span

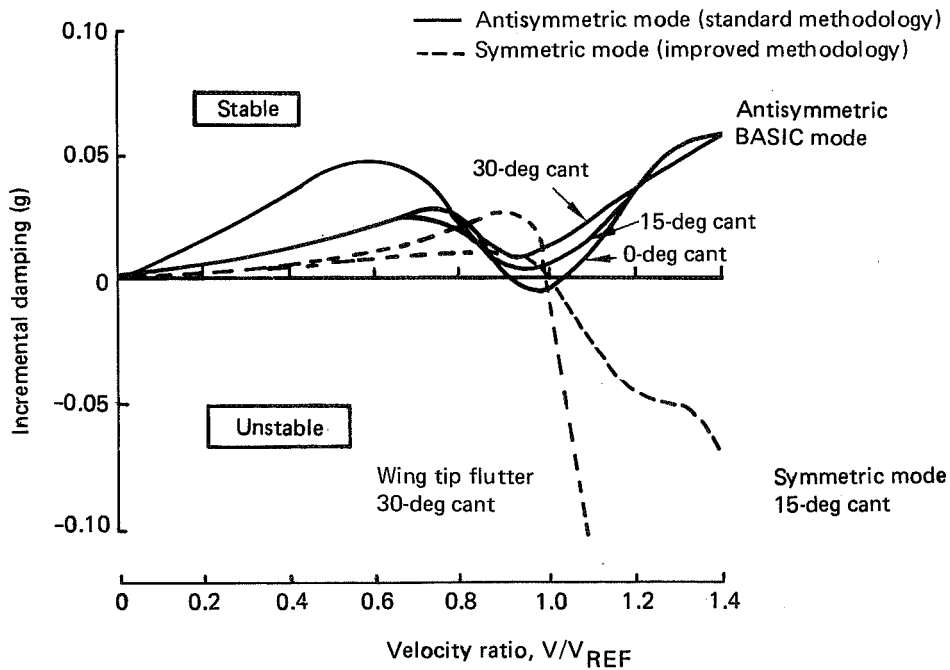


Figure 38. Velocity-Damping Trends with Cant Angle

5.2 TEST DATA ANALYSIS

This section discusses winglet aerodynamic and flutter testing and correlates the results with theoretical predictions. The aerodynamics portion (sec. 5.2.1) presents BTWT test data for the various winglet test configurations. The flutter portion (sec. 5.2.2) describes the evolution of the flutter analysis used for final structural resizing of the wing with winglets.

5.2.1 Aerodynamics

Force and Moment Data—Figure 39 shows drag improvements due to winglets Z9 and Z10. The measured drag reduction due to the Z9 winglet approaches the estimated value at $M = 0.70, C_L = 0.45$, but deteriorates with increasing Mach number. Modifications to the winglet (Z10) resulted in some improvement, but when tested together with a wing tip modification, little or no benefit was obtained from the wing tip modification.

Figure 40 shows a comparison of winglet Z11, Z12, and Z13 measured drag increments with pretest estimates. Both Z11 and Z12 fall below the estimated level by a significant amount, while Z13 performs very near its estimated level at cruise ($C_L = 0.45, M = 0.84$). The Z13 winglet was favored for ease of installation over the partial chord design (Z12), and was, therefore, selected for further performance, loads, and stability and control testing. Figure 41 shows the winglet Z13 drag increment compared to the pretest cruise incremental drag estimate, as a function of both Mach number and C_L .

Pressure Data and Flow Visualization—These data are presented in Appendix B.

5.2.2 Flutter

Results of Convair Aeronautical Laboratory (CVAL) wind tunnel flutter testing of the 747 EET with wing tip winglets confirmed the necessity for improved flutter analysis techniques to account for aerodynamic surface extensions that project out of the main wing plane. Initial flutter studies using standard 747 flutter analysis methods showed a modest degradation of antisymmetric wing/nacelle flutter modes. However, it was believed that the addition of a major surface area at the tip of the wing would have significant flutter stability effects. The CVAL 731-2 wind tunnel flutter tests subsequently confirmed the existence of two unique winglet induced symmetric flutter modes and provided the necessary experimental results to begin improved methodology development.

Development proceeded in two stages, guided by experimental evidence that the problem was primarily aerodynamic rather than structural. Preliminary results showed that an empirical correlation could be achieved with selected math model modifications. However, this was accomplished at the expense of rationality by increasing the airloads unrealistically in the wing tip/winglet area. Improved methodology was subsequently able to restore rationality to the wing tip aerodynamic loading. Reasonably correlated flutter solutions were obtained using conventional strip-theory/Theodorsen flutter methods modified with experimental steady-state airload data on the wing and winglet surfaces. The methodology developed was subsequently applied to the final configuration winglet studies to assess the structural weight increments related to flutter clearance. Consideration of the more complex surface theories was ruled out of preliminary design level studies, based on efficiency, economy, and the success of the simpler approach.

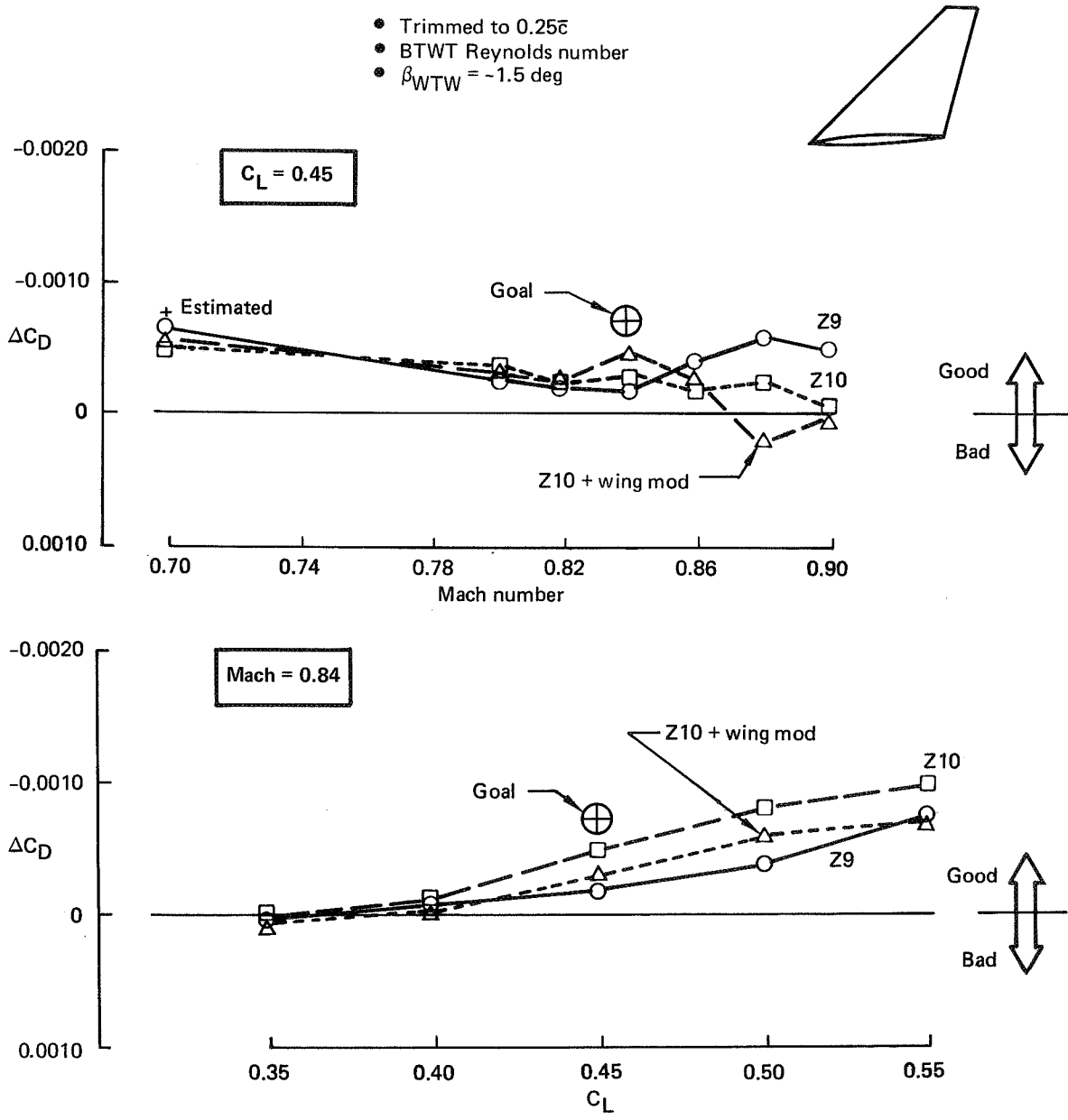


Figure 39. Effect of Winglets Z9, Z10, and Wing Mod on Drag

- Wind tunnel drag levels
- $C_L = 0.45$
- Trimmed to $0.25\bar{c}$

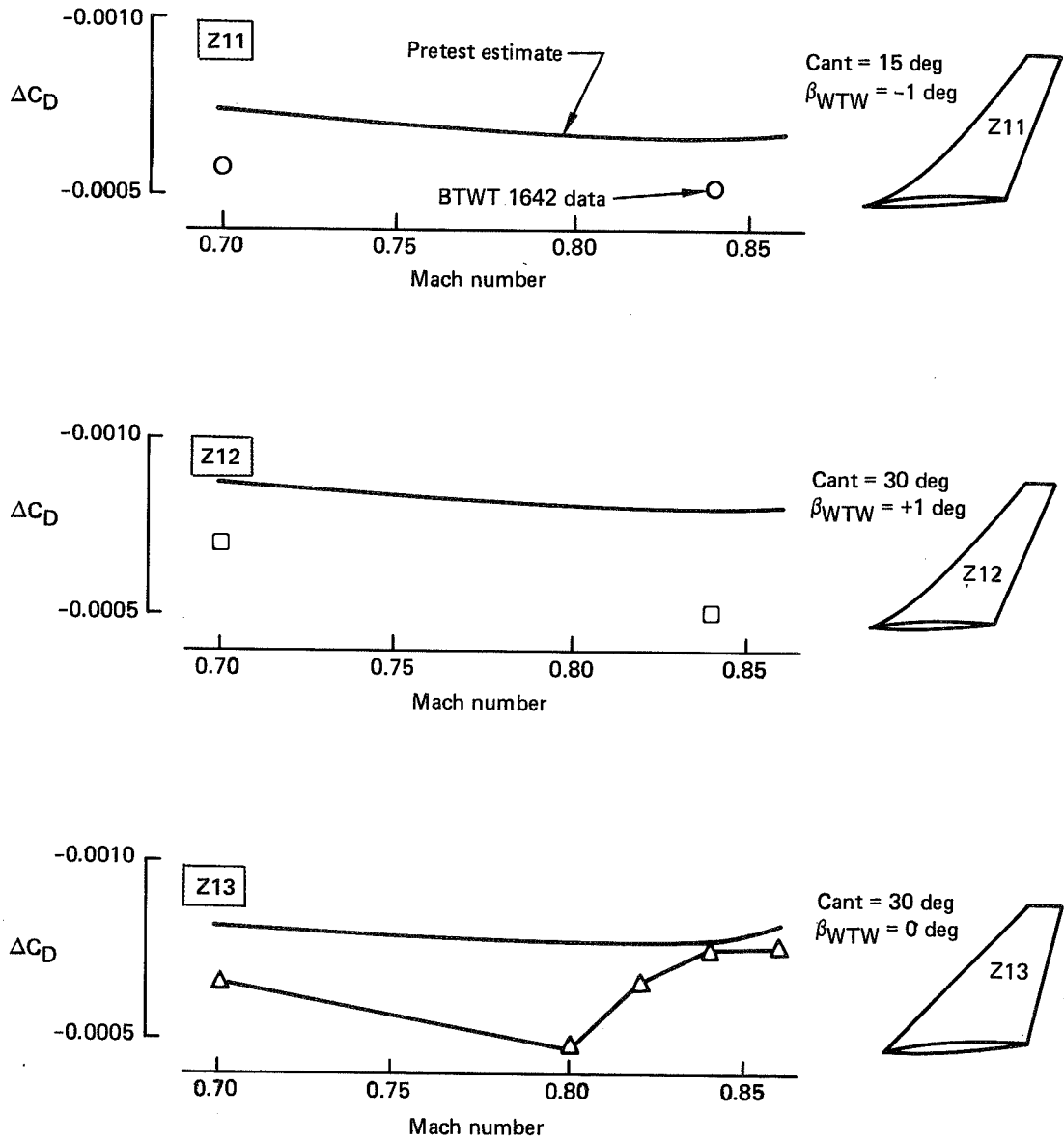


Figure 40. Effect of Winglets Z11, Z12, and Z13 on Drag

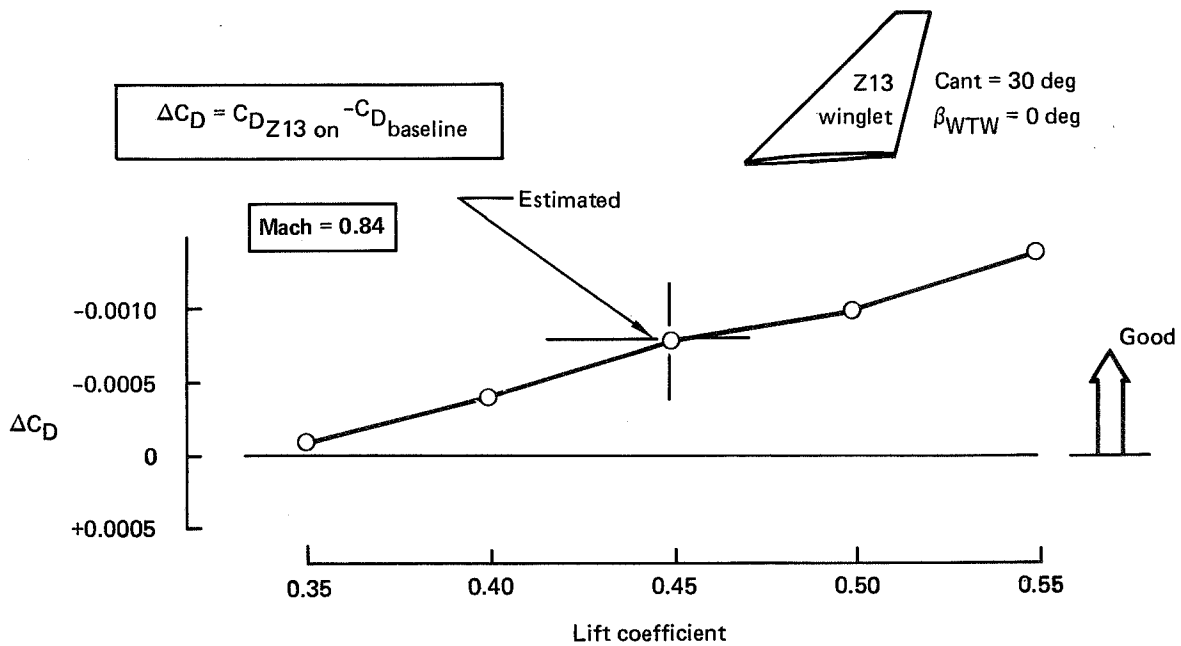
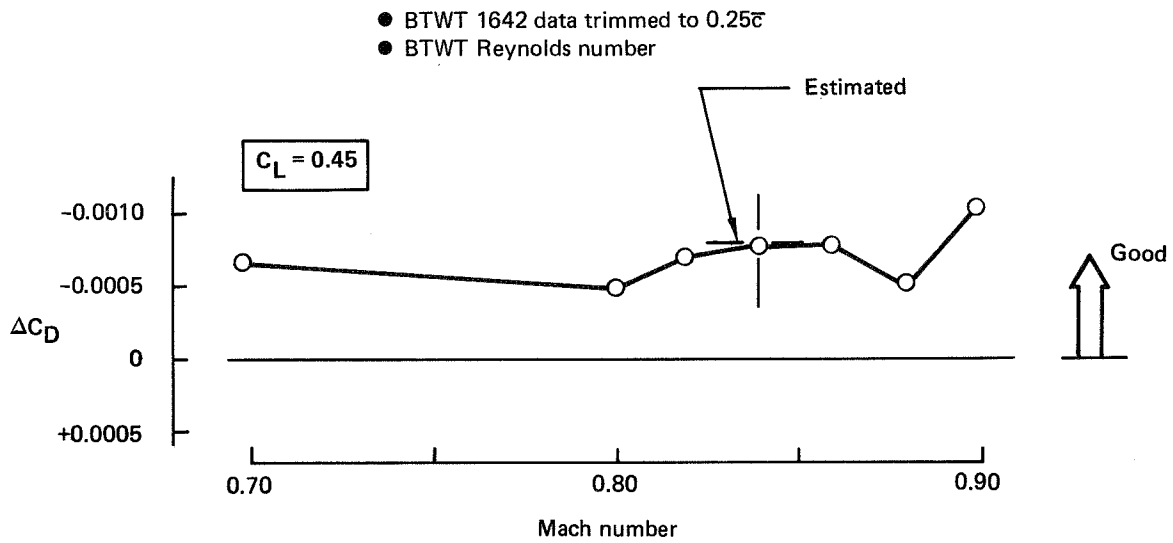


Figure 41. Effect of Winglet Z13 on Drag

A summary of the wing tip winglet flutter analysis development effort for the 747 EET Phase I program is shown in Figure 42. From this work, it has been concluded that strip-theory/Theodorsen methods can give satisfactory winglet flutter results when supported with wind tunnel test data and when generalized air forces are modified to include the effects of static air forces on the winglet. The number and complexity of potential flutter modes that can be involved in a winglet design will necessitate further coordinated test/analysis development prior to flight. Consideration of maneuver load deformations and compressibility effects are some of the potentially critical problem areas not addressed in this study. Detailed discussions of methods and results are presented in the following paragraphs.

Early pre-wind-tunnel-test investigation of winglet effects on flutter were based on standard Boeing 747 analysis techniques. The structural modes were based upon an elastic axis stick model built up of finite elements. The aerodynamic math model was based upon classical strip-theory/Theodorsen unsteady air forces with oscillatory derivatives modified with the use of steady-state lift distributions derived from wind tunnel pressure model tests. Figures A-6 and A-7 of Appendix A illustrate the structural and aerodynamic models. Results of these pretest evaluations showed modest degradation of the familiar 747 flutter modes, but unique winglet induced modes did not appear. The Flutter Trends portion of Section 5.1.2 summarizes results used to help scope geometric constraints during the early stages of winglet definition.

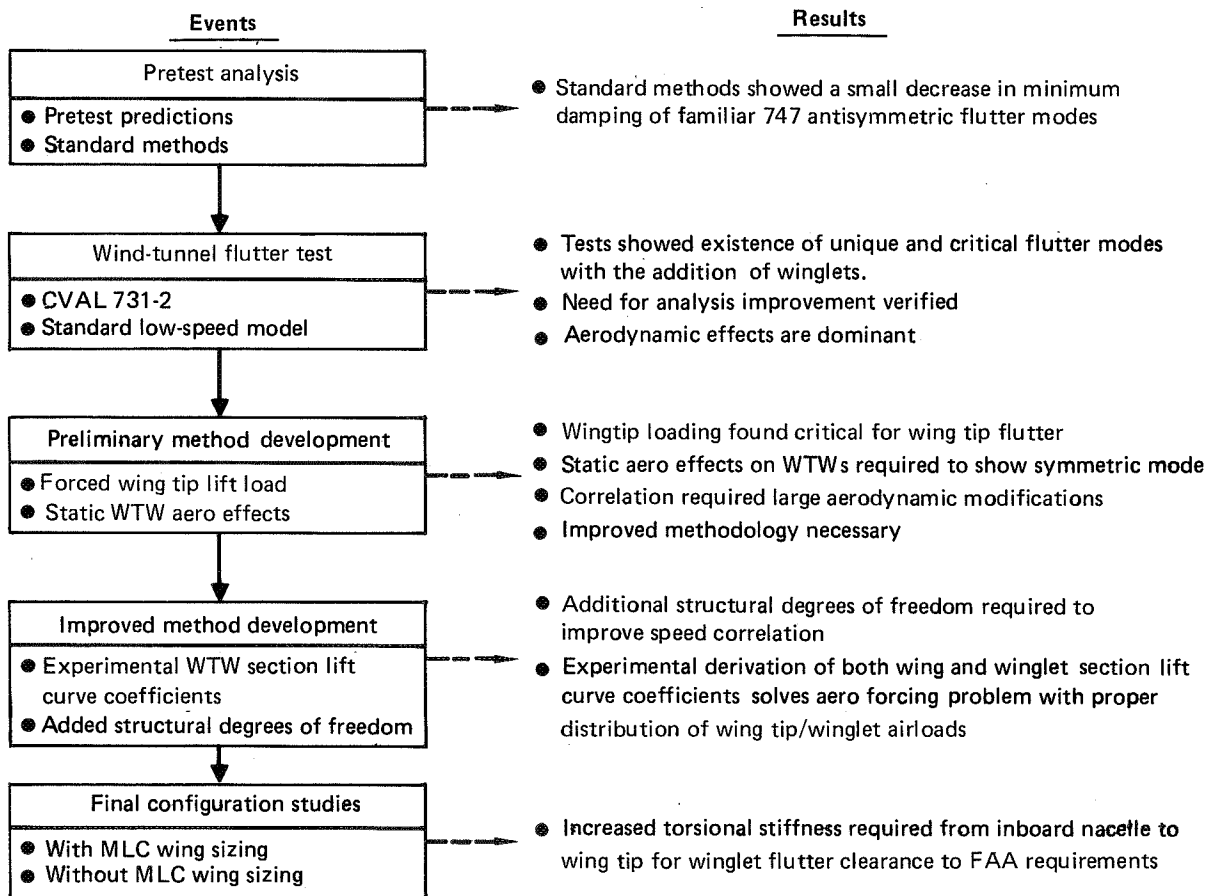


Figure 42. Winglet Flutter Analysis Development Summary

Verification of unique flutter modes caused by the addition of winglets was obtained in low-speed flutter model tests at the CVAL wind tunnel in San Diego. Detailed descriptions of the CVAL 731-2 flutter test program and results are described in Section 2.0 of Appendix C. The most significant result is presented in Figure 43, which shows the wind tunnel test results superimposed for comparison with the pretest flutter analysis predictions. Two winglet unique flutter modes were revealed experimentally. This included a high frequency (5.2 Hz) wing tip flutter mode and a lower frequency (2.3 Hz) symmetric wing flutter mode. Because outboard nacelle strut side bending frequency has been a significant parameter in 747 wing flutter stability, the wind tunnel results show the flutter speed ratios for each mode as a function of this strut frequency ratio. The nominal strut frequency, ω_{REF} , refers to the natural vibration frequency of the outboard nacelle/strut package when excited in the side-bending direction. Off-nominal frequencies are referred to as soft ω/ω_{REF} ratios less than 1.0 and stiff for ω/ω_{REF} ratios greater than 1.0. Results shown are for the original baseline Z9 (15-deg cant) winglet configuration with an operating empty weight (OEW) airplane, and full standard wing fuel (inboard mains full, outboard mains full, normal reserves full, extended range fuel tanks empty).

This configuration was selected for analysis/test correlation studies to develop the winglet flutter methodology. The pretest analysis results show two antisymmetric flutter modes at off-nominal strut frequencies. The antisymmetric outboard nacelle side bending (ONSB) mode appears at less than nominal strut frequencies and is characterized by relative lateral motion between the outboard nacelle and the wing. The mode appearing at above nominal strut frequencies is referred to as the

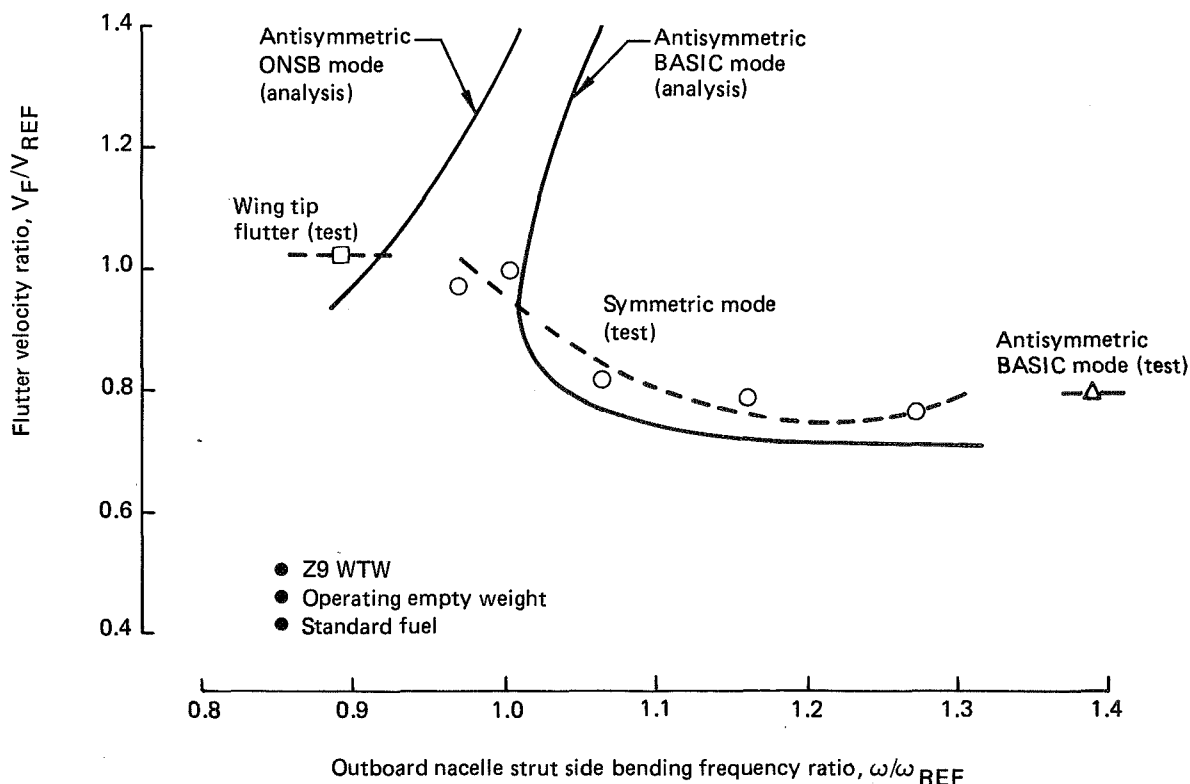


Figure 43. Pretest Flutter Predictions Versus Wind Tunnel Results

antisymmetric BASIC mode and it involves wing bending/torsion and aft body side bending motions. With the Z9 winglet addition, the antisymmetric BASIC mode appears only at a relatively stiff strut frequency (much higher than nominal), but a critical symmetric mode is introduced in the strut frequency range of interest (near nominal). At a relatively soft strut frequency (lower than nominal) the analysis predicts the antisymmetric ONSB flutter mode would be encountered, but test results showed the presence of a high frequency wing tip flutter. This wing tip flutter would be expected to be insensitive to strut frequency tuning and must be considered design critical along with the symmetric mode at the nominal strut frequency. In summary, Figure 43 presents results that verify the existence of two design-critical flutter modes and illustrates the need for improved analysis methods to predict these modes.

The area of emphasis for analysis improvement was guided by experimental evidence from the CVAL tests indicating that the aerodynamic effects of the winglet addition were the dominant factors (fig. C-11, Appendix C). Pretest methodology used a standard 747 wing lift distribution and a value of 2π for the lift curve coefficients on the winglet aerodynamic panels. The aerodynamic improvement investigations initially centered on the development of a wing normal force distribution reflecting experimental derivation of induction effects for both winglets and nacelles. Wind tunnel rigid pressure model test data from BTWT test 1599 at Mach = 0.40 were used to derive the sectional lift curve coefficients that were inserted into the unsteady aerodynamic formulation. This approach resulted in the appearance of the wing tip flutter mode.

As expected, this wing tip flutter appeared in either symmetric or antisymmetric solutions and was essentially independent of outboard nacelle strut side bending frequency. Flutter speed levels were found to be quite sensitive to the wing tip normal force loading, as shown in Figure 44. This is the limited region where significant winglet induction effects are seen in the pressure distribution data.

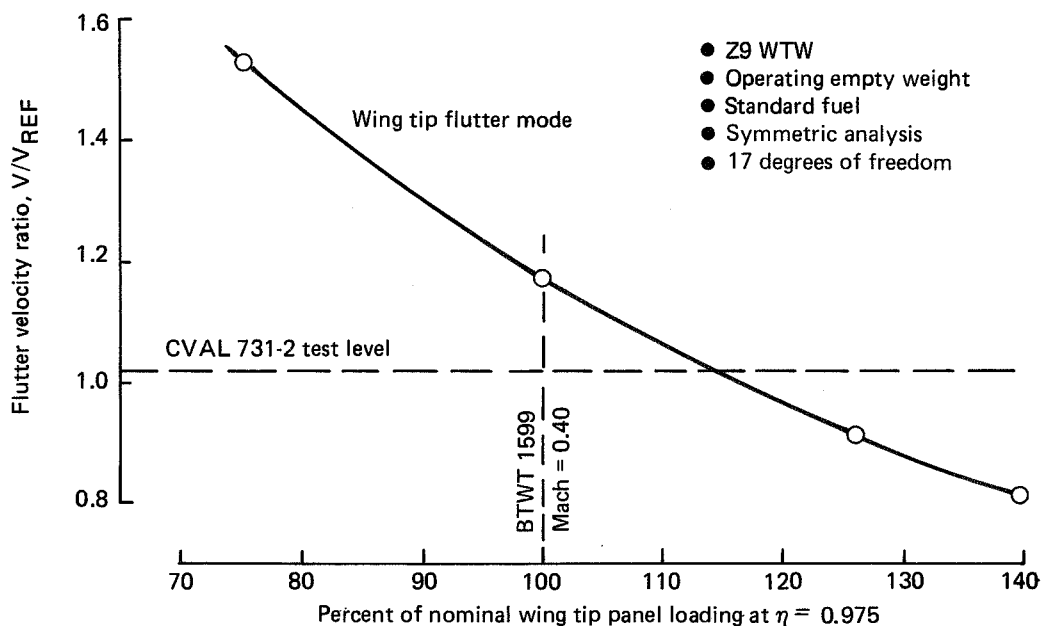


Figure 44. Wing Tip Normal Force Loading Effect

A major deficiency still existed due to the absence of the symmetric mode flutter. Experience with T-tail type flutter analysis on other programs had revealed the importance of certain static air forces effects on these surfaces, so programming was initiated to incorporate these effects. The general level of the winglet normal force was guided by balance data information from earlier wind tunnel investigations in the University of Washington Aeronautical Laboratory (UWAL) 1215 flutter test. Figure 45 shows the limiting behavior of the winglet normal force as air speed was increased. The static air force effects included both normal force (out-of-plane) and chord force (in-plane) aerodynamics on the winglets. Figure A-9 of Appendix A defines the five specific components considered by the program for calculating the additional increments to the overall oscillatory generalized air force terms in the flutter equations. The resultant flutter solutions with static effects on the winglet now showed the existence of the symmetric flutter mode as observed in the CVAL 731-2 flutter test. Figures B-18 and B-19 of Appendix B show the velocity-damping (V-g) results with and without this static effect on the winglets.

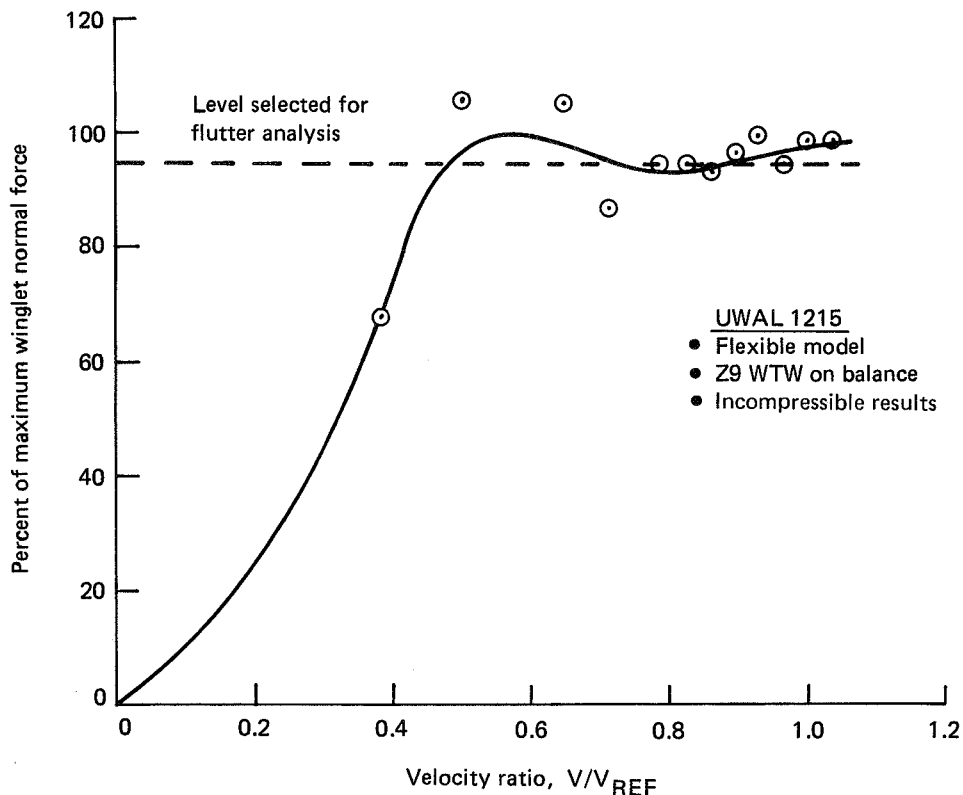


Figure 45. Winglet Normal Force Variation With Airspeed

Preliminary tuning to obtain an empirical match of flutter speeds proved quite difficult because improvement in one mode generally caused an unfavorable trend in the other mode. In addition to the main wing tip loading effect of Figure 44, the amount of static normal force on the winglet was a powerful parameter. Figure A-10 of Appendix A shows the effects of this parameter on the two flutter modes of interest. Preliminary correlation tuning utilized a forced aerodynamic loading on the main wing tip, 2π lift curve coefficients on the winglets, and an excessive amount of static air load used in the calculation of the T-tail type air force increments added to

the regular airforces matrices. Figure 46 shows the preliminary aerodynamics used to obtain correlation with the flutter test results. The comparison of analysis and test results using this preliminary methodology is shown in Figure 47. The tuning criterion emphasized best correlation for the critical symmetric mode in the nominal strut frequency region and accepted some compromise elsewhere.

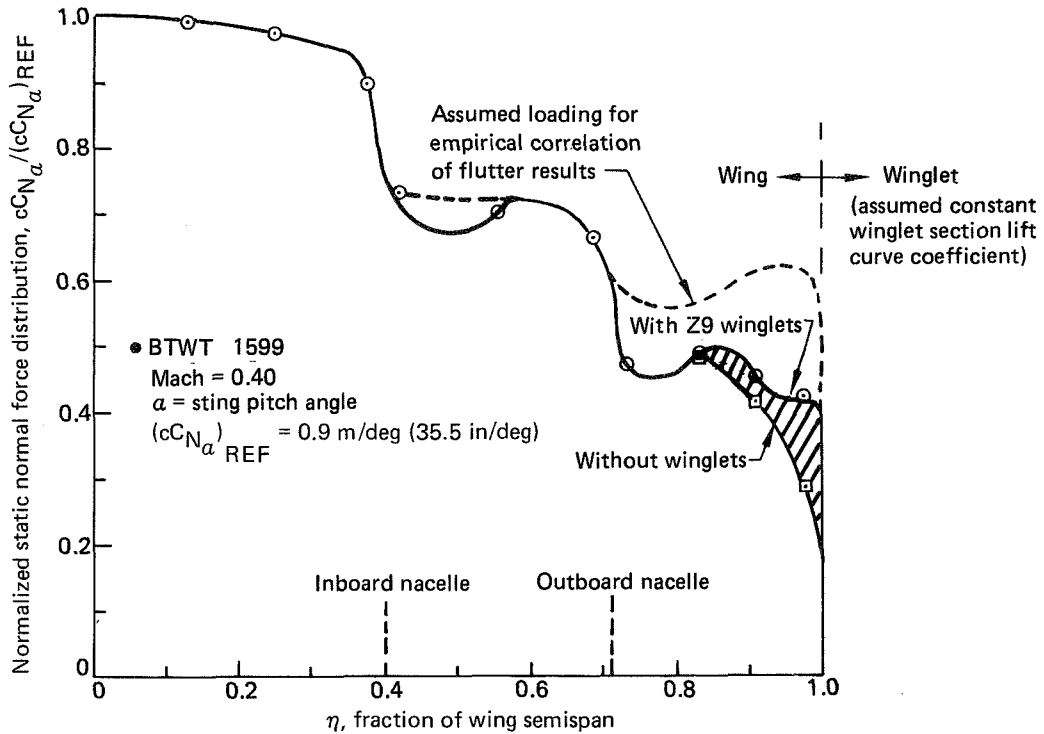


Figure 46. Preliminary Aerodynamics for Winglet Flutter Analysis

A 17 degrees-of-freedom structural model was used throughout the preliminary methodology development studies. The method was used to predict preliminary stiffness requirements for flutter with winglets. The basic conclusion, however, was the need for an improved methodology yielding comparable correlation results without forced aerodynamic loadings.

Although the improvement emphasis still centered on obtaining a rational aerodynamic representation, the presence of the high frequency 5.2 Hz wing tip flutter mode caused some concern that important higher frequency modes might influence the solution. The addition of more structural degrees-of-freedom was considered for further investigation. In the aerodynamic investigations the arbitrary use of assumed section lift curve coefficients on the winglets was found to cause irrational distributions of lift in the vicinity of the wing tip/winglet junction. It was decided that a more rational distribution could be obtained by considering the wing/winglet as a single surface with a large dihedral break. Using this concept, an overall array of section lift curve coefficients was derived from a continuous normal force distribution from the main wing root to the winglet tip, as shown in Figure 48. Again, the BTWT 1599 wind tunnel data were used, but without any excessive forcing in the tip area. Some smoothing over the "bucket" areas (around nacelles and at the winglet interface) was used for mathematical conditioning purposes. The winglet airloads used to compute the static effects increments were reduced by 63% to a more acceptable level. Table 2 summarizes the differences between the preliminary and improved methodology.

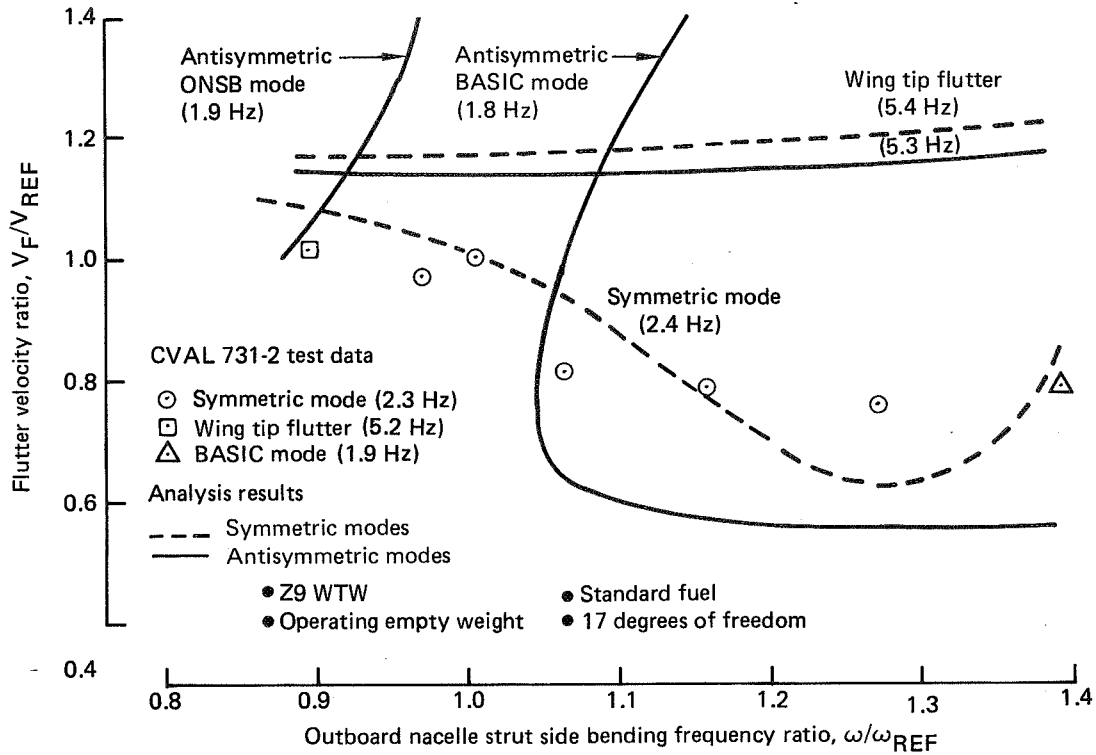


Figure 47. Correlation Results With Preliminary Methodology

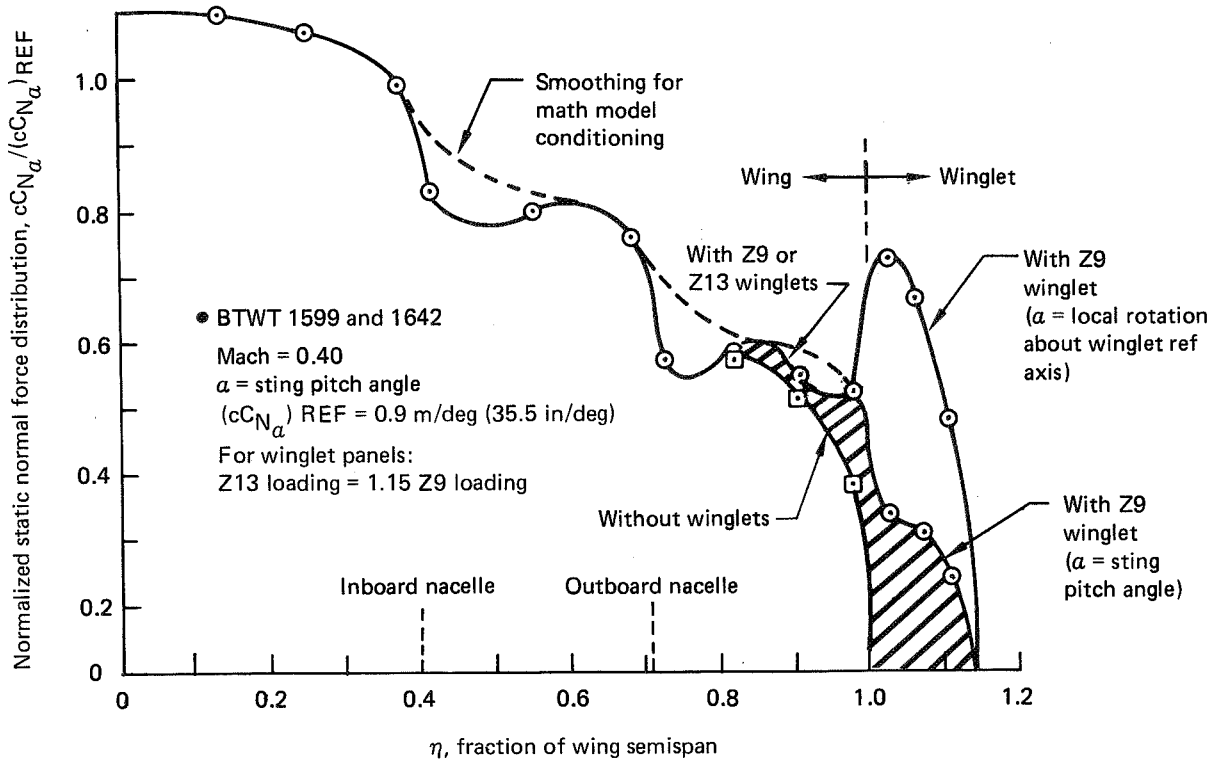



Figure 48. Final Aerodynamics for Winglet Flutter Analysis

Table 2. Preliminary Versus Improved Methodology Summary

Method 	Preliminary	Improved
<u>Structural model</u>		
• Finite element stick model	Yes	Yes
• Selected degrees of freedom	17	24
<u>Aerodynamics</u>		
• Modified strip theory with Theodorsen unsteady effects	Yes	Yes
• Static winglet airload effects	$\alpha = 7.5$ deg	$\alpha = 2.8$ deg
• Wing section lift curve coefficients from experimental cN_{α} distribution	Modified distribution	Experimental distribution
• Winglet section lift curve coefficients	2π	Experimental distribution

Results of these changes in methodology yielded reasonable correlation with the CVAL test data without excessive forcing of the experimental aerodynamic data. Figure 49 shows the effects of added structural freedoms with the flutter speeds starting to converge at 20 degrees-of-freedom. The 24 degrees-of-freedom solution was accepted as a reasonable limit. The vibration solution covers still-air modes up to twice the frequency of the wing tip flutter and yields a reasonable flutter speed correlation with the test data when used in conjunction with the revised aerodynamics. Figure 50 shows the Z9 winglet correlation results using the improved methodology. Corresponding velocity-damping and velocity-frequency trend plots are shown in Figures B-20 and B-21 of Appendix B for the symmetric case at nominal strut frequency.

The improved methodology for winglet flutter analysis was subsequently used for final configuration flutter analyses on the Z13 winglet configuration with 30 deg of cant. Figure 51 shows the configuration validation run using CVAL 731-2 wind tunnel results for the Z9 winglet rotated to a 30-deg cant angle. See Appendix C, Section 2.2, Figure C-1 for test results. Although the method does not predict the symmetric mode flutter speed very well at the higher strut frequency, the more critical wing tip flutter mode is predicted quite well at the nominal strut frequency condition. The method adequately predicts the shift of the critical flutter mode from the symmetric mode with the Z9 winglet to the wing tip flutter mode for the Z13 winglet. The wing tip flutter frequency increase from 5.2 Hz for the Z9 winglet (15-deg cant) to 5.6 Hz for the Z13 winglet (30-deg cant) also was predicted analytically. The velocity-damping and velocity-frequency trend plots associated with both symmetric and antisymmetric solutions for the Z13 winglet are contained in Figures B-22 through B-25 of Appendix B. Critical still-air mode shapes and frequencies associated with the Z13 WTW symmetric mode flutter and wing tip flutter are shown in Figures B-26 and B-27 of Appendix B.

The improved methodology subsequently was used for assessment of flutter stiffness requirements to clear the required FAA margins on a purely structural basis. Increased torsional stiffness was required to clear the Z13 wing tip flutter and symmetric flutter modes to 1.2 VD margins. Figure B-28 of Appendix B shows typical

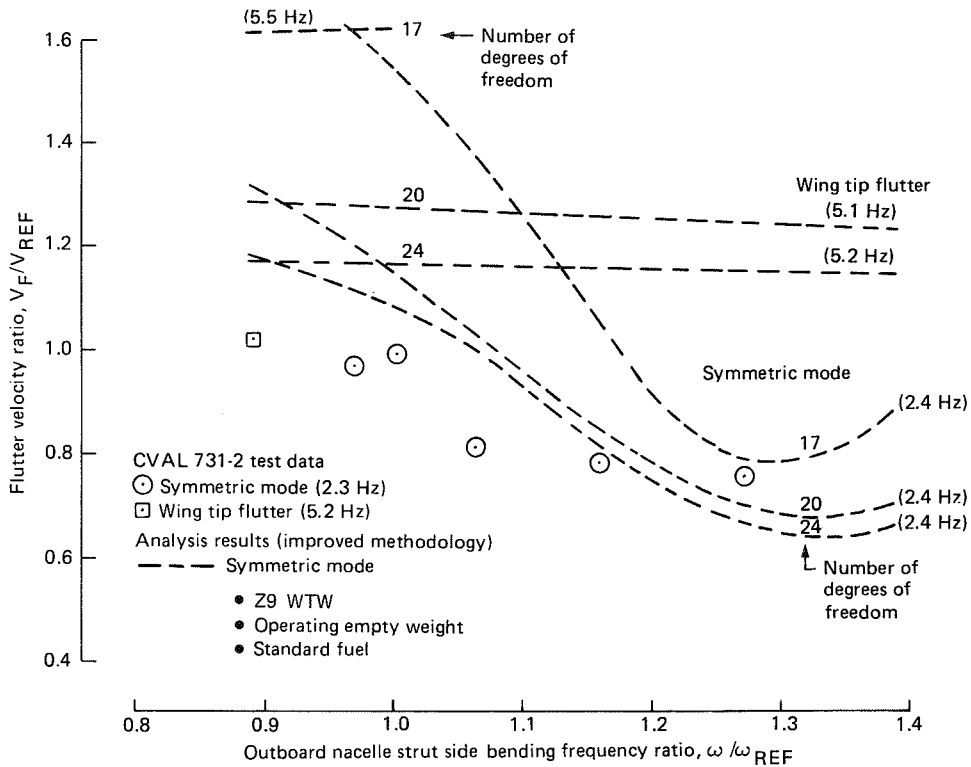


Figure 49. Structural Degree-of-Freedom Effects

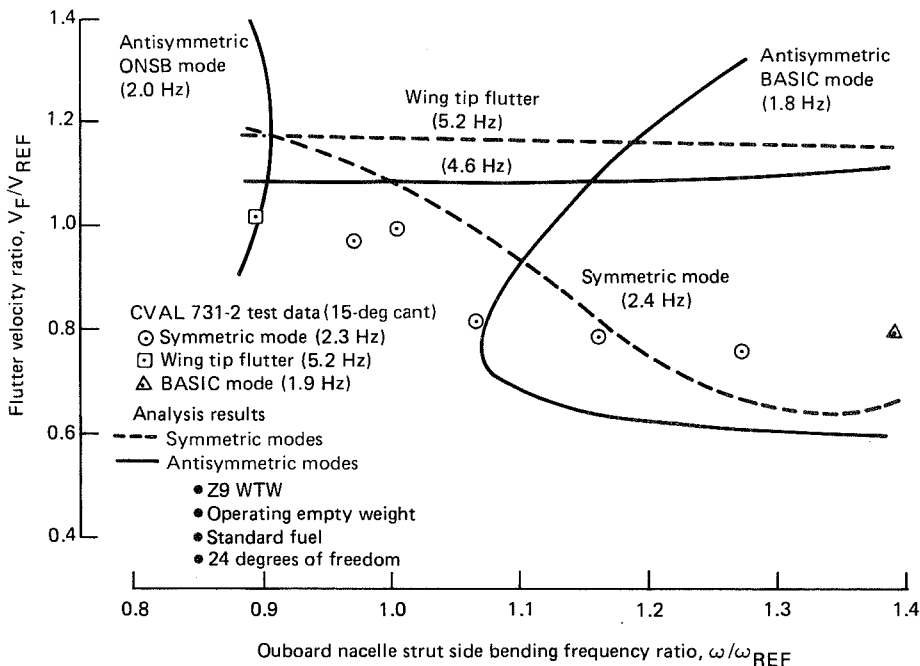


Figure 50. Z9 Winglet Correlation Results With Improved Methodology

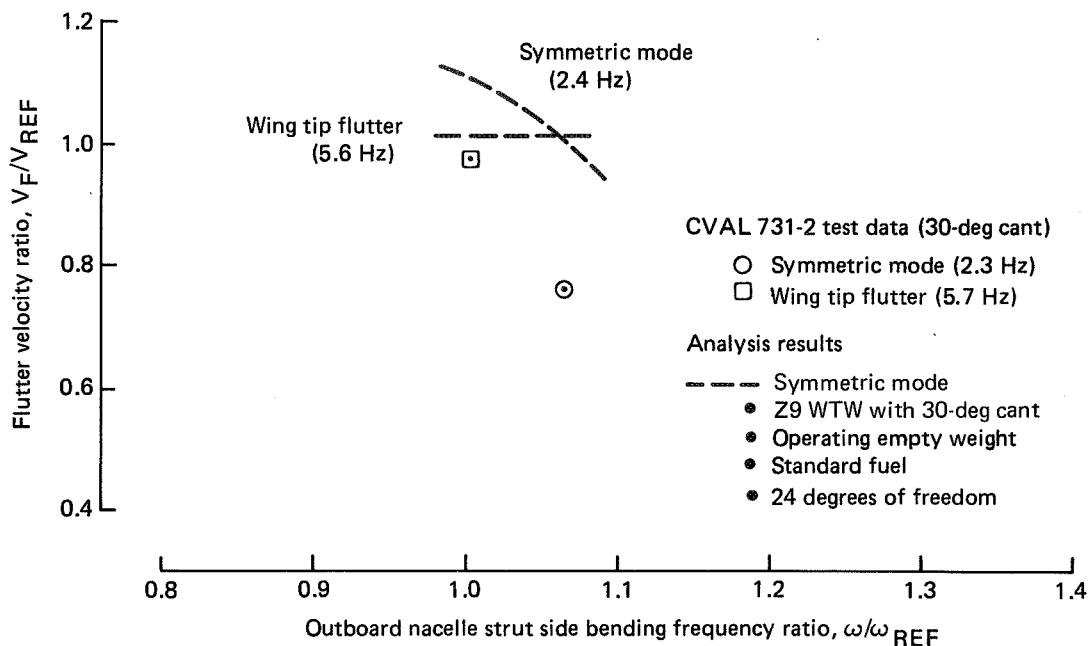


Figure 51. Simulated Z13 Winglet Correlation Results With Improved Methodology

distribution of stiffness increases and resultant flutter speed increases obtained for Z13 winglet flutter modes. Other studies using the improved methodology are discussed in Sections 6.3.2 and 7.1.3, Final Configuration Studies covering the Z13 WTW configuration with a baseline wing and also with a wing resized for the maneuver load control (MLC) system.

5.3 ANALYSES OF TWO WING TIP WINGLET CONFIGURATIONS

This section discusses detailed analyses of the Z9 and Z13 winglet configurations. These analyses were similar to those described in Section 4.2 for the 1.83-m (6-ft) and 3.66-m (12-ft) WTE (e.g., structural sizing, etc.). The preliminary decision to define structural sizing, weights, and performance for both a WTW and WTE combined with WLA was based on structural sizing/weights for the Z9 WTW and L/D for the Z13 WTW. Final comparisons (sec. 7.0) were based on the complete set of Z13 analyses.

5.3.1 Lift-to-Drag Ratio

Figure 52 shows percent increase in L/D at $C_L = 0.45$ for the Z9 and Z13 winglets. The L/D equivalent of the increased OEW (no flutter penalty) was obtained using trade factors which are valid for nontakeoff gross weight limited missions [e.g., 5556 km (3000 nmi)].

The superior performance of the Z13 winglet when compared to the Z9 winglet is evident. The Z13 winglet achieved most of its theoretical potential (without twist or weight penalties).

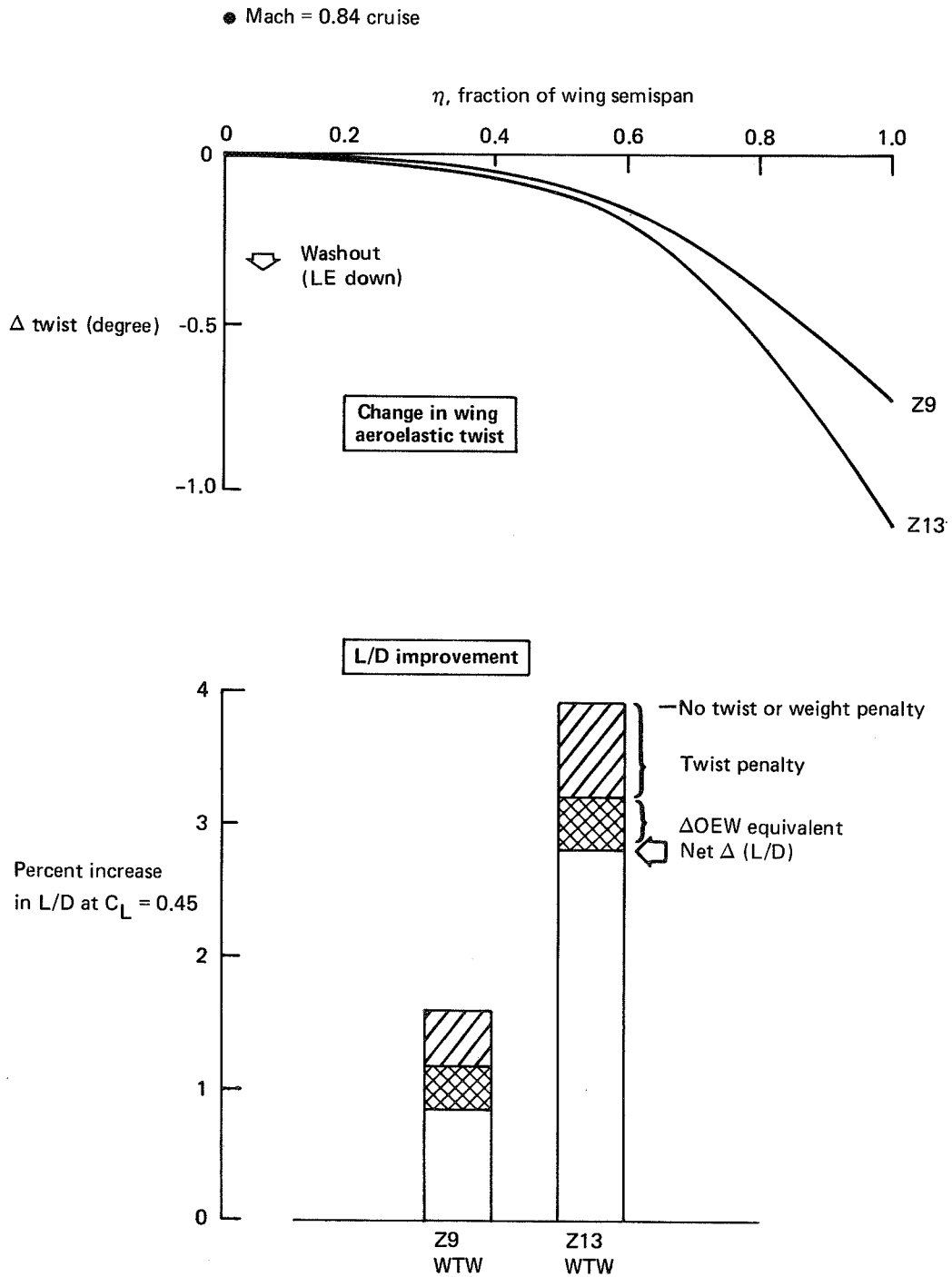


Figure 52. L/D Comparison, WTW Z9 and Z13

5.3.2 Loads and Twist

This section contains the load results used for analysis of the Z9 and Z13 wing tip winglet configurations. Maneuver and fatigue conditions critical for wing structure design were analyzed for the wing with the Z13 winglet. The Z9 winglet was analyzed for design maneuver conditions only since its aerodynamic performance did not warrant a full structural analysis. The load results were processed to determine required stiffness increases and the analysis was cycled to determine the final load results.

The aerodynamic forces used for the analysis were based on wind tunnel test data. Wing and winglet pressures were measured for the Z9 winglet configuration (BTWT 1599 test) and wing pressures only were measured for the Z13 winglet (BTWT 1642 test). A sample of the incremental span loads and winglet force coefficients as determined from these tests is shown in Appendix B. The Z13 winglet forces were derived using the Z9 data.

Figure 53 shows the effect of the winglets on wing design bending moment and Figure 54 shows wing twist data for a typical cruise condition. The effect of the winglets is to increase wing bending moment over the outboard wing with a small reduction near the root and also to increase wing washout. The Z13 winglet, which had the larger cant angle, gave the highest wing loads and the most wing washout. The effect of increased stiffness for strength design was small because the base wing had excess structural margins, which were absorbed when the winglet was added. Final load results were obtained in one loads stiffness iteration cycle.

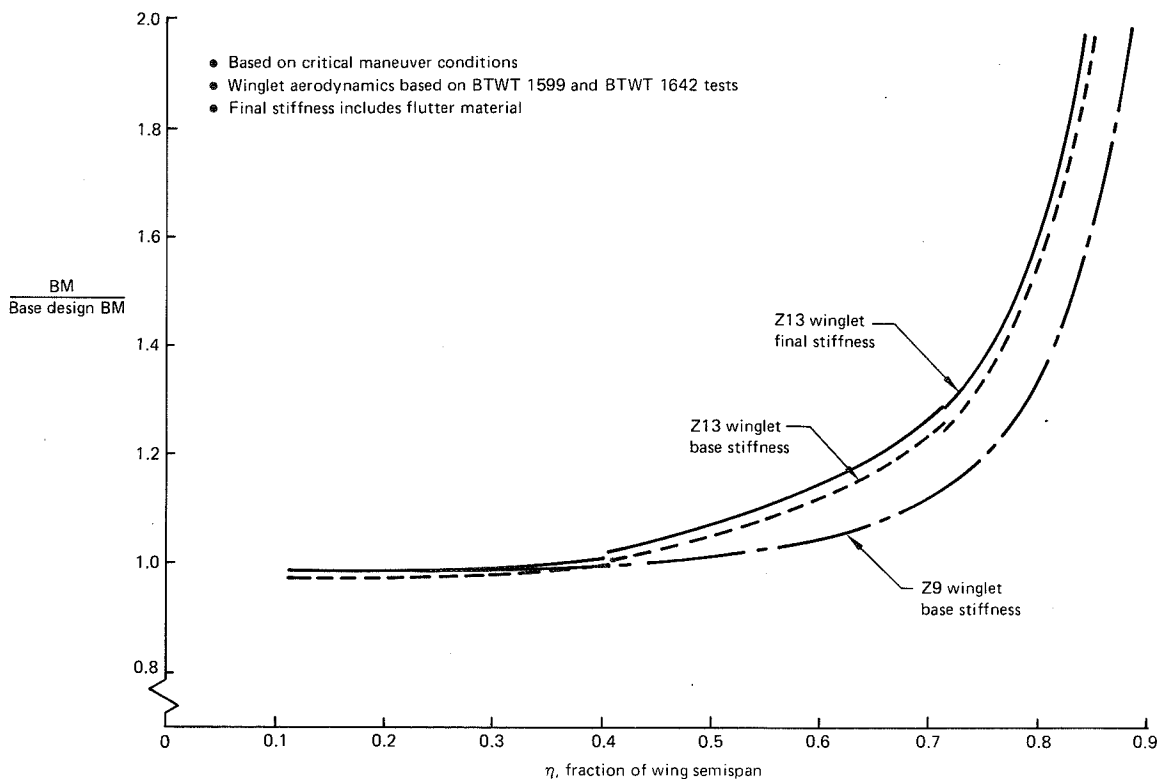


Figure 53. Effect of Winglets on Wing Design Bending Moment

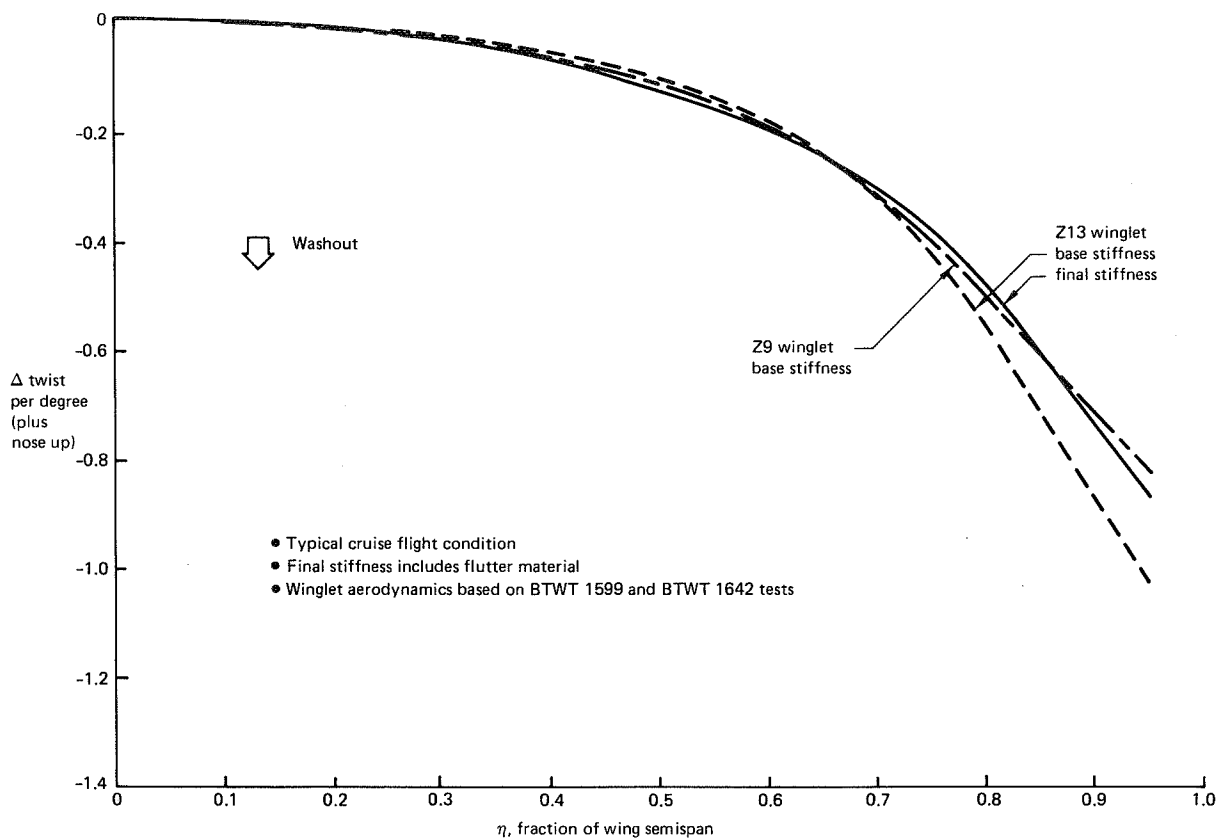


Figure 54. Wing Twist Increment for Winglets

A flutter analysis of the Z13 winglet configuration showed that a stiffness increase was required to prevent wing flutter for this configuration. Load and twist results for this stiffness are shown in Figures 53 and 54 and represent the final load results for the Z13 winglet configuration.

The bending moment reduction near the wing root does not occur when the wing is assumed rigid, as shown in Figures 55 and 56. The load reduction at the root due to wing flexibility is caused by a combination of aerolastic effects, which are discussed in detail in Section 7.0. Figure 56 demonstrates the significance of the choice of stiffness on the wing load due to the winglet. These results show that if existing wing structural margins were maintained rather than absorbed, a significantly higher load would result.

Local winglet loads were derived for design of the winglet to wing attachment fittings based on a limited survey of symmetric maneuver, lateral gust, and lateral maneuver conditions. The critical condition was a rudder maneuver II condition, as defined by FAR25.351(a)(3), which produced an ultimate design winglet pressure of 22 060 Pa (3.2 psi).

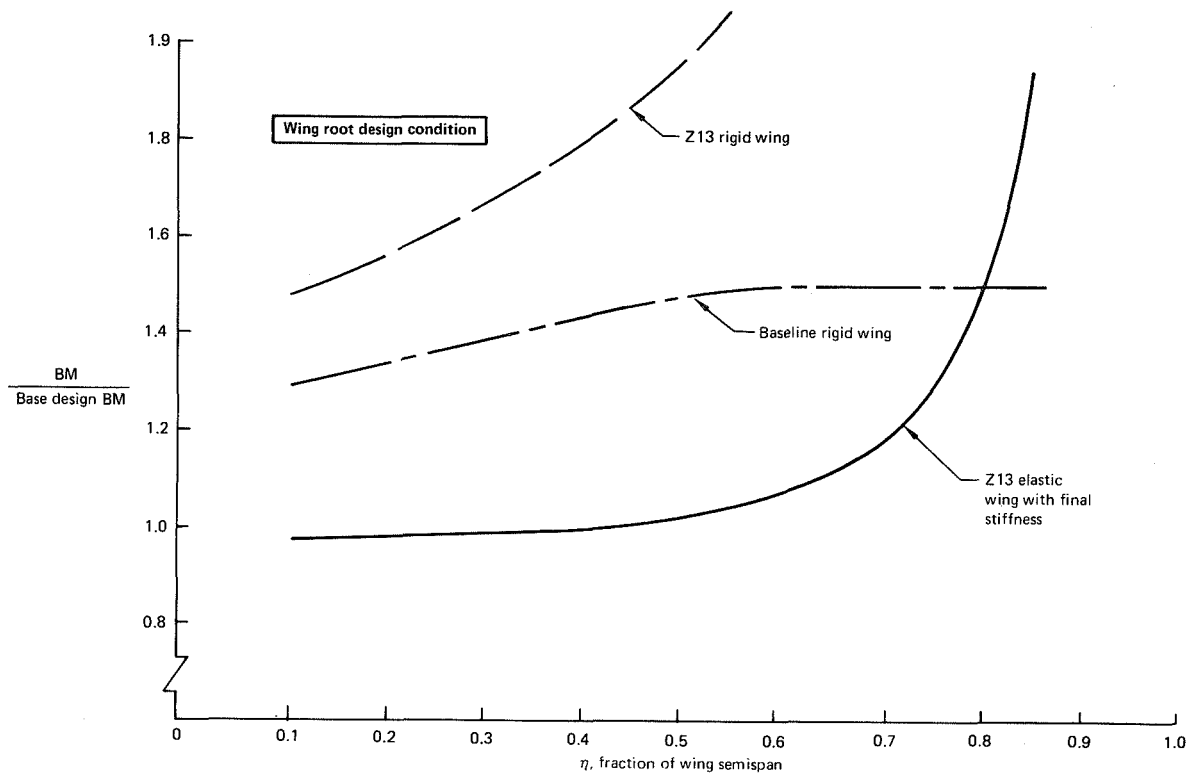


Figure 55. Effect of Stiffness on Wing Bending Moment Ratio for Z13 WTW

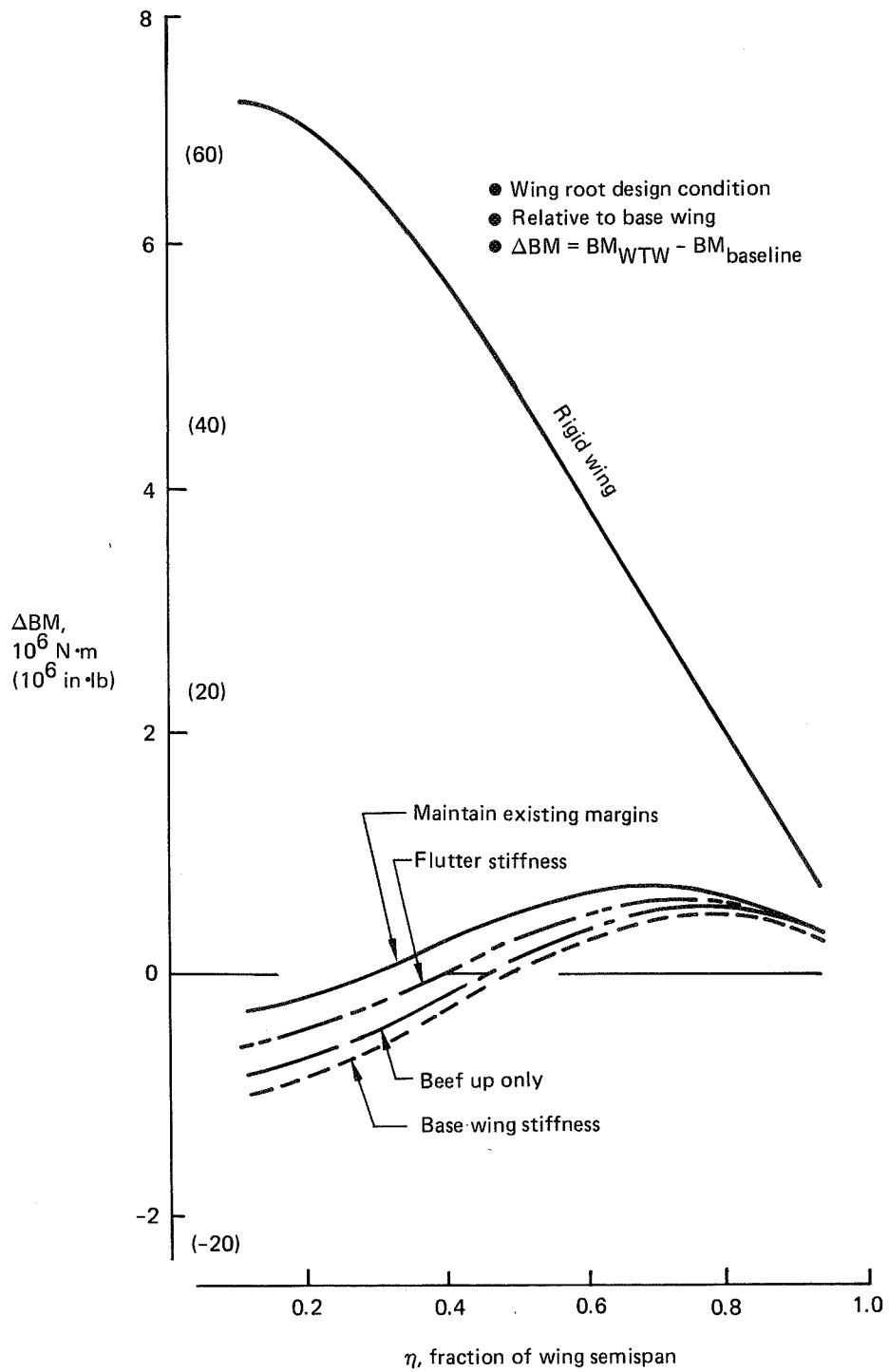


Figure 56. Effect of Stiffness On Wing Bending Moments Increment for Z13 WTW

5.3.3 Structural Resizing

The wing boxes with Z9 and Z13 winglets were resized using the same general procedures given in Section 4.2.3. Sizing results presented in Figures 57, 58, 59, and 60, when compared with the tip extension sizings in Section 4.2.3, indicate that winglets cause fewer wing box structural revisions for ultimate loads than do tip extensions, but require large stiffness increases for flutter stability.

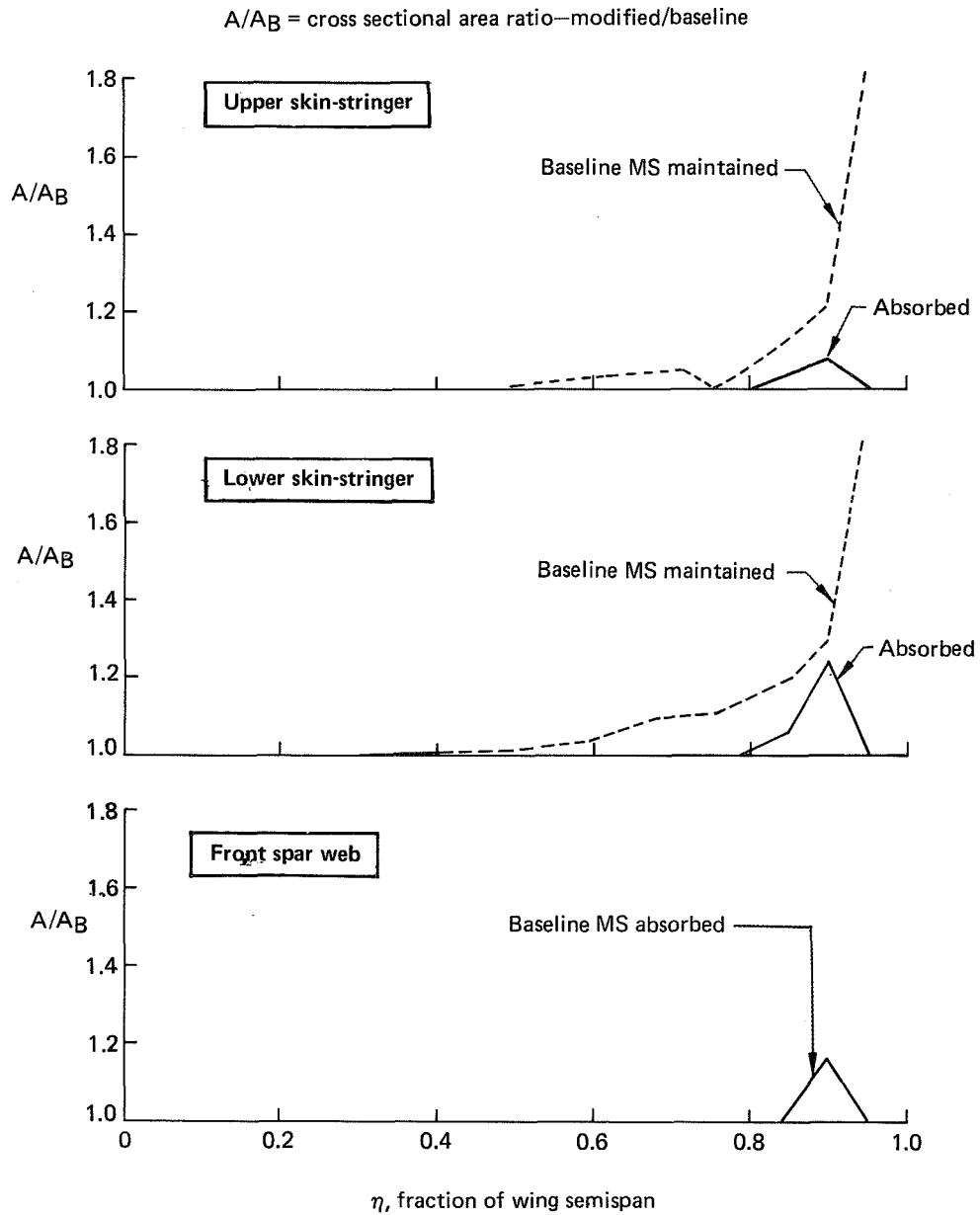


Figure 57. Structural Sizing of Wing With Z9 Winglet Prior to Flutter Sizing

The Z9 winglet configuration sizing shown in Figure 57 was obtained from flaps-up maneuver loads only. The overall performance with this winglet configuration indicated little or no benefit. Consequently, the study was shortened by deleting further structural sizing studies.

Mid- and rear-spar webs on the wings with winglets do not require any strength increase for ultimate or fatigue loads. A study indicated that retrofitting a winglet is not practical because of the extensive wing structural changes required.

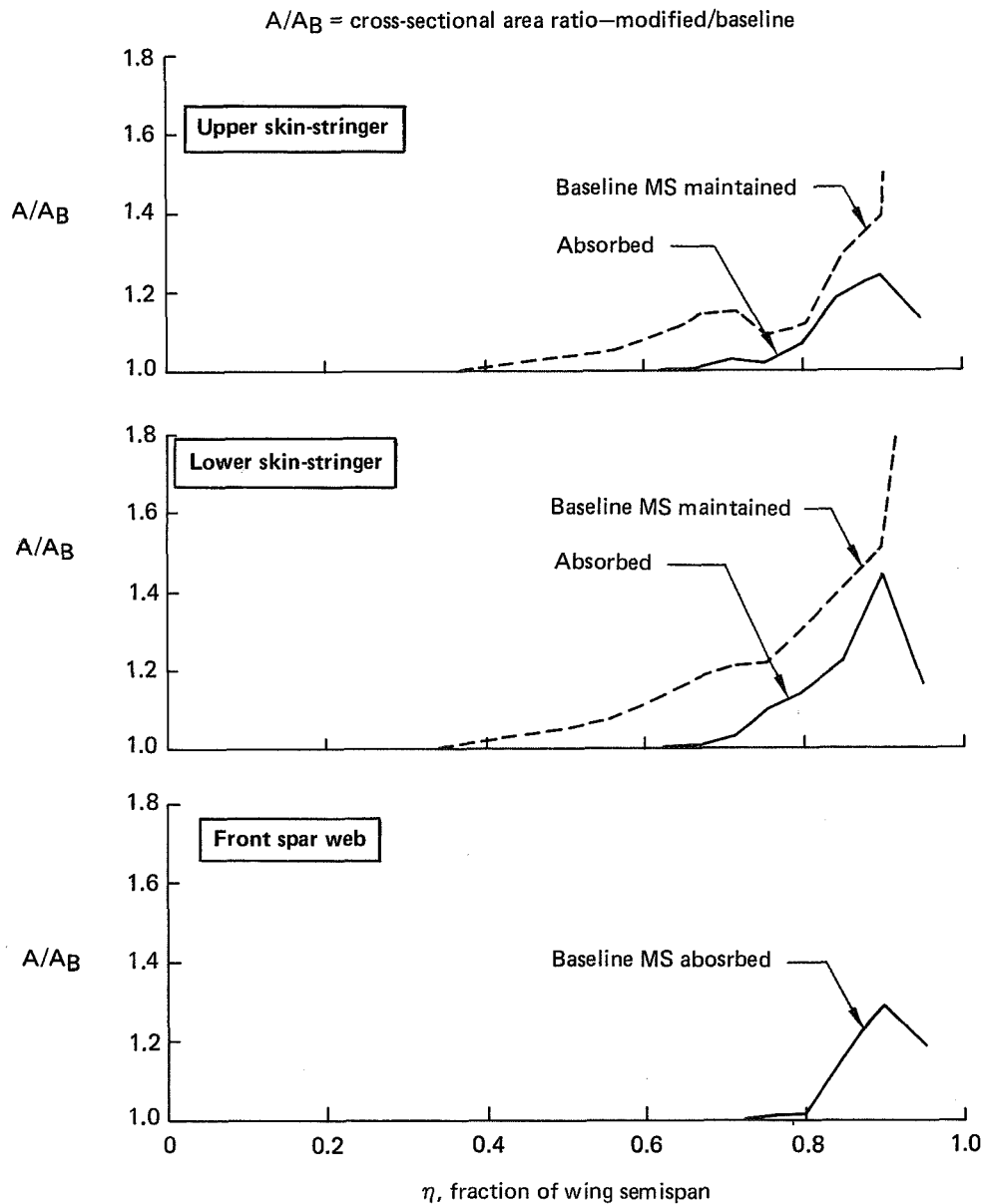


Figure 58. Structural Sizing of Wing With Z13 Winglet Prior to Flutter Sizing

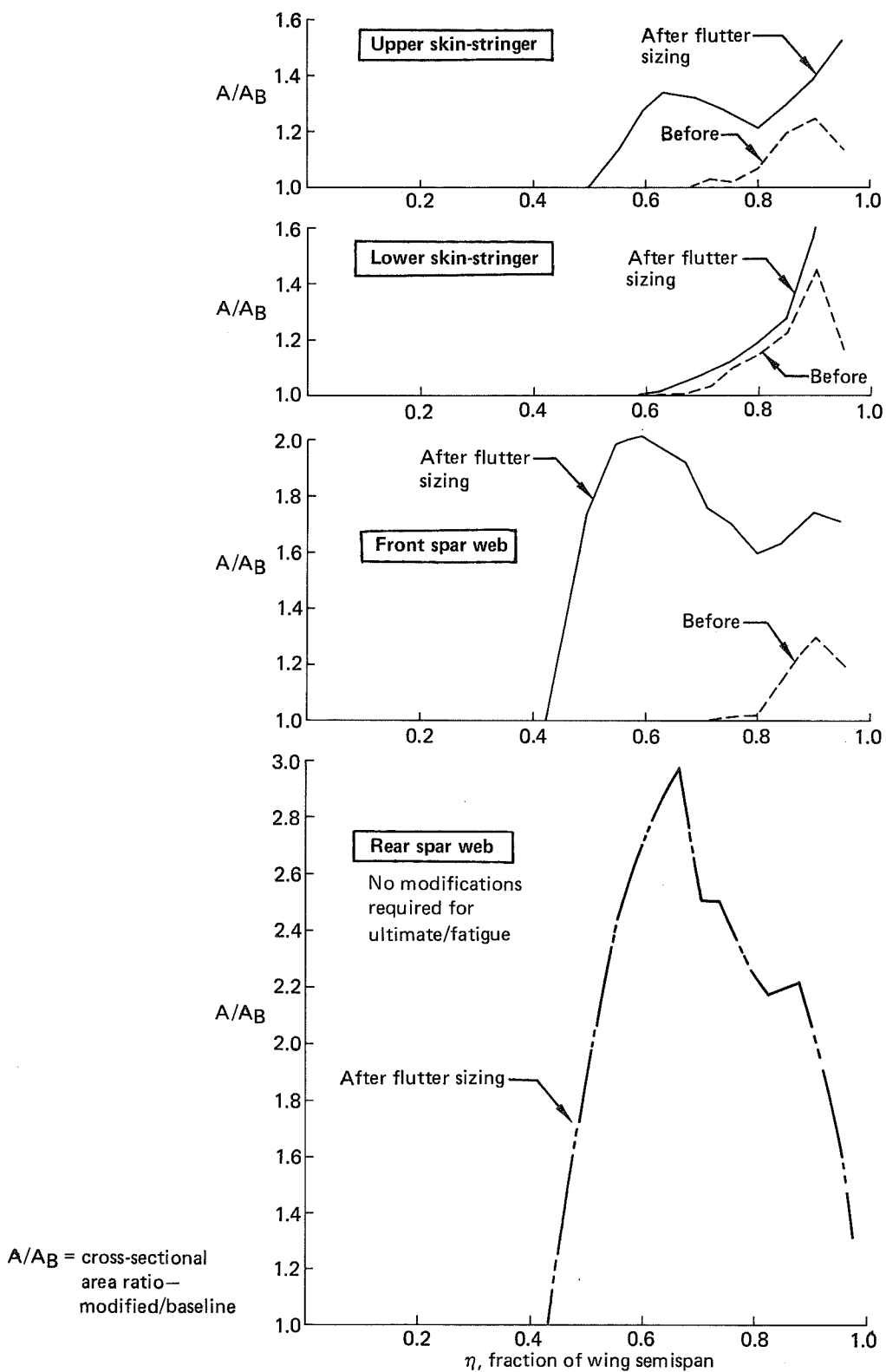


Figure 59. Effect of Flutter Sizing on Wing With Z13 WTW

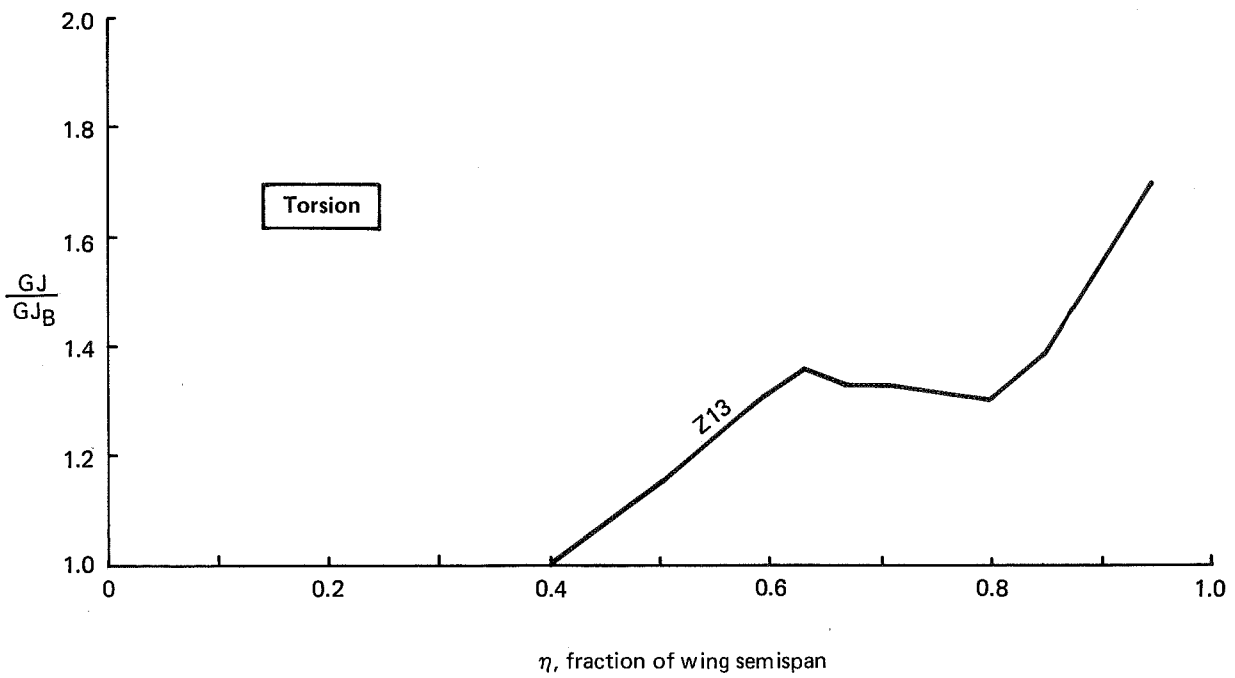
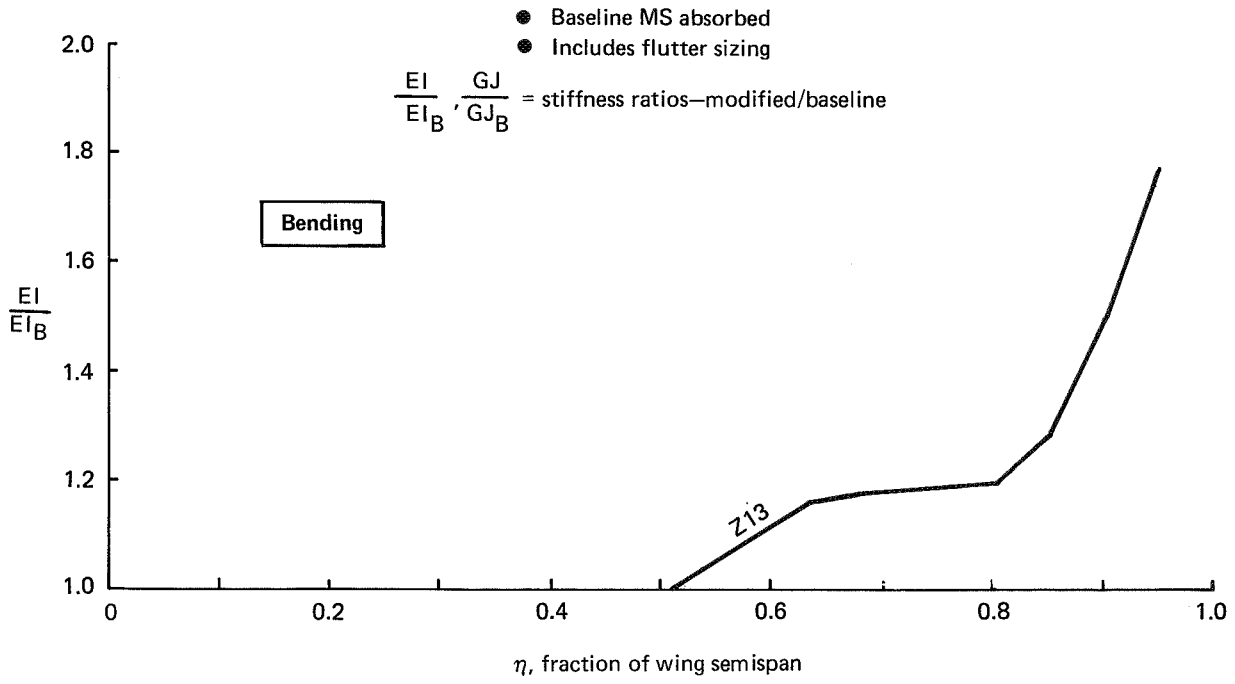


Figure 6D. Structural Stiffness of Wing With Z13 Winglet

5.3.4 Weights

Weight of the winglet panel (Z13) was estimated using Class I wing weight estimation methods (sec. 5.1.2) applied to an existing KC-135 winglet weight. The winglet attachment weight increment was estimated from preliminary configuration descriptions, layout drawings, and structural sizing information. The effects of winglet Z13 on wing box weight, maintaining and absorbing existing structural margins of safety, were estimated from the structural sizing studies discussed in the preceding section.

A tabulation of the weight effect of the Z13 winglet is contained in Table 3, based on structural sizing with existing margins absorbed and maintained.

Table 3. Z13 Wing Tip Winglet (WTW)—Weight Summary

	Increment per airplane—mass (weight), kg (lb)			
	Absorb existing margins of safety		Maintain existing margins of safety	
Winglet installation				
Winglet panel	458	(1010)	458	(1010)
Winglet attachment	185	(410)	185	(410)
A. Structural panels = 182				
B. WS 1548 rib modification = 42				
C. Rib installation = 83				
D. Spar webs = 39				
E. Spar splices = 5				
F. Spar forgings = 243				
G. Parts deleted from baseline = -188				
H. Miscellaneous and roundoff = 4				
Wing box reinforcement				
• Maneuver and gust loads	218	(481)	1041	(2296)
• Fatigue	0	(0)	0	(0)
• Flutter	903	(1991)	523	(1154)
Total delta increase/airplane	1764	(3892)	2207	(4870)

5.3.5 Stability and Control

Both longitudinal and lateral-directional stability and control characteristics of the basic 747 are affected by the addition of wing tip winglets. The Z9 and Z13 winglets have similar effects. With either, minor revisions to the longitudinal flight control system are possibly required and airplane crosswind capability is slightly reduced.

Wing tip winglets increase the rigid airframe longitudinal stability due to increased wing lifting effectiveness aft of the quarter chord. As shown in Figure 61, the Z13 configuration is slightly more stable than the Z9. Aeroelastic losses are expected to offset a major part of the increase in stability. Increased stick forces to maneuver will result because of the increased stability, however, present force levels can be retained by minor modification of the feel system.

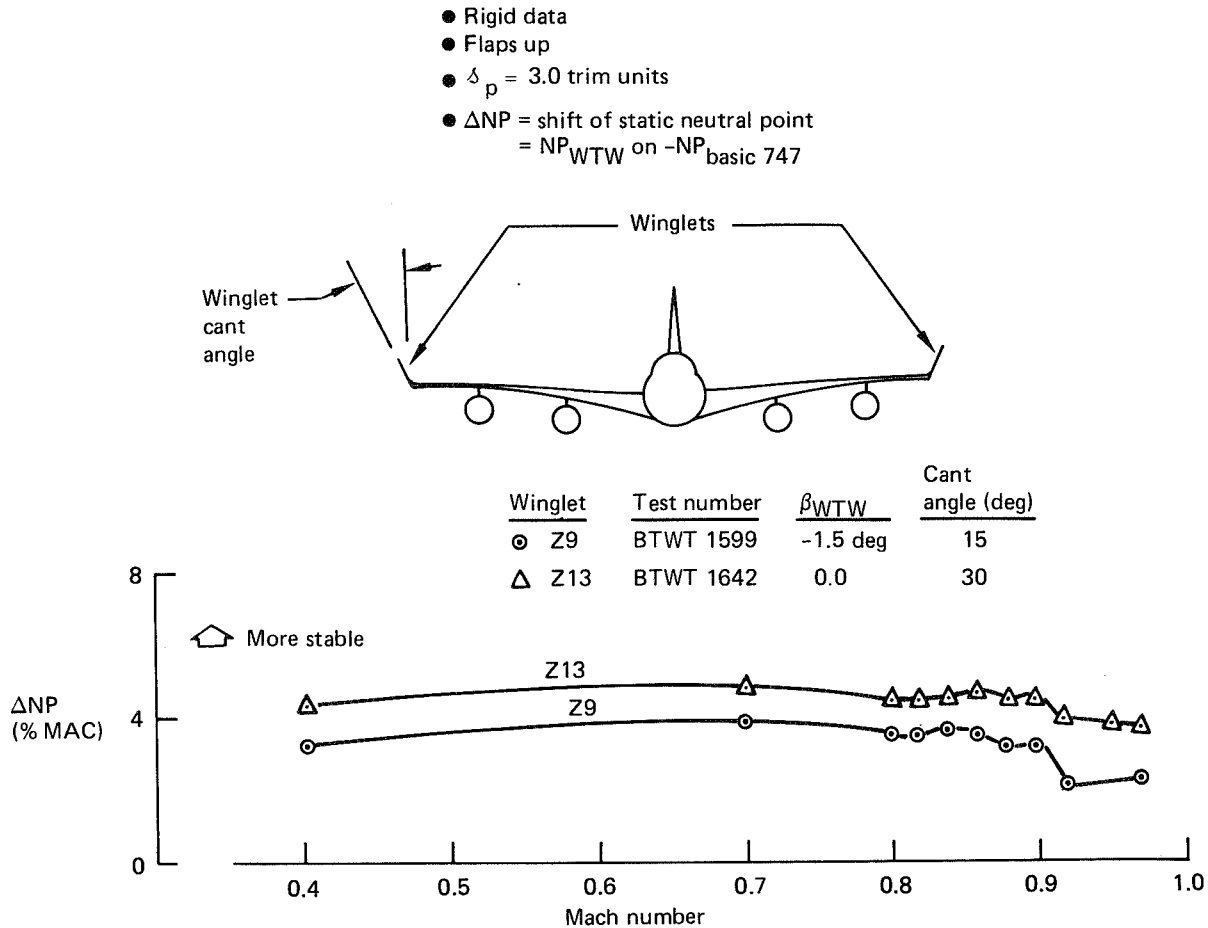


Figure 61. Effect of Winglets on Static Longitudinal Stability

As illustrated in Figure 62, winglets have a negligible effect on FAA speed stability. The stabilizer required to trim with winglets is more airplane nose up during cruise and is similar in magnitude for both the Z9 and Z13 configurations. This difference is equivalent to approximately 0.2 unit with the effects of aeroelastics included.

Wing tip winglets produce significant changes in lateral-directional stability derivatives. The changes for the Z9 winglet are similar to those shown in Figure 63 for the Z13 winglet. In the cruise Mach number range, side force due to sideslip ($C_{y\beta}$) and directional stability ($C_{n\beta}$) are increased approximately 15%. Dihedral effect ($C_{l\beta}$) is increased approximately 35%.

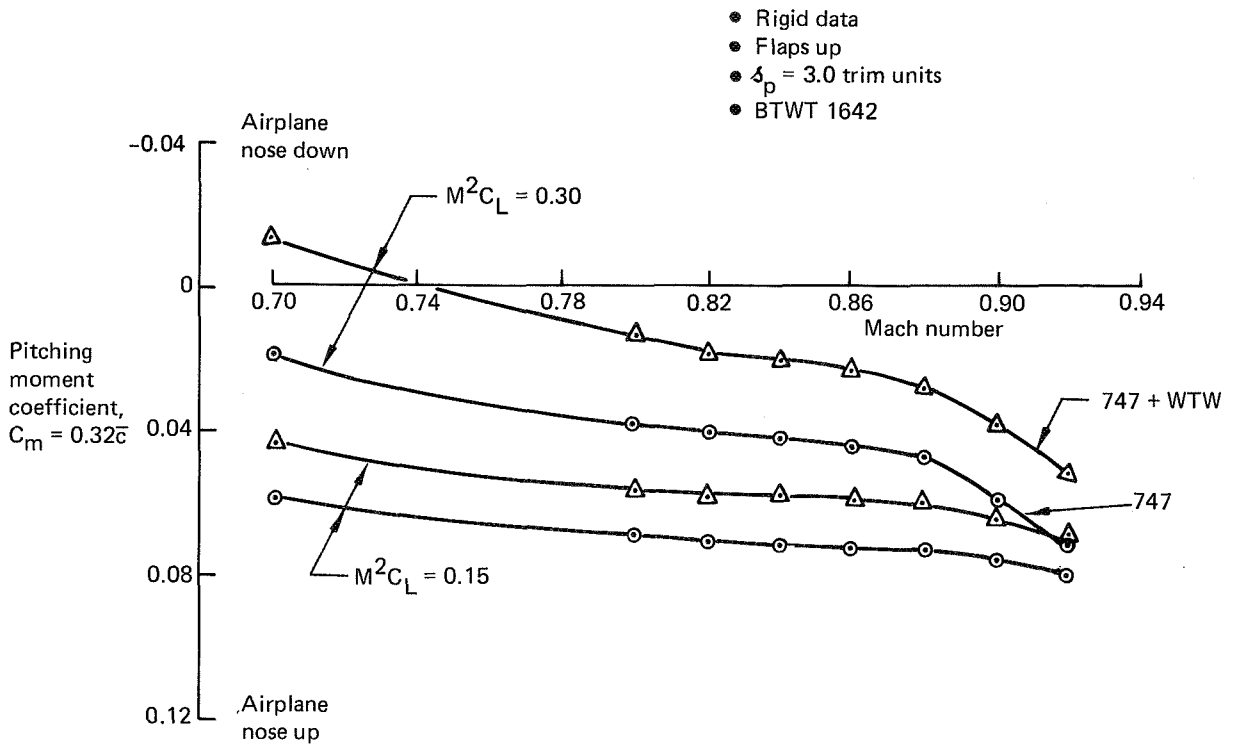


Figure 62. Longitudinal Speed/Trim Stability With Z13 WTW

The combination of increased directional stability ($C_{n\beta}$) and increased dihedral effect ($C_{\ell\beta}$) requires approximately 10 deg more wheel for maximum sideslip, flaps up, low -speed. Maximum sideslip is reduced by about 1 deg. These effects reduce crosswind capability during takeoff by approximately 4 to 7 knots depending on cg location. The resultant capability, however, is still sufficient to meet normal operation or FAA crosswind requirements.

Engine out lateral control requirement to meet the Boeing tameness criteria is adversely affected by the increase in $C_{\ell\beta}$. Tameness is a measure of the ability to maintain heading by using wheel only (no rudder pedal input) during a $1.4 V_S$ takeoff climbout after a critical engine failure. Although decreased sideslip results from the increase in $C_{n\beta}$, the disproportionately larger increase in $C_{\ell\beta}$ requires more lateral control for balance. The FAA air and ground minimum control speeds are virtually unchanged due primarily to the smaller sideslips encountered in these maneuvers.

The increases in $C_{\ell\beta}$ and $C_{n\beta}$ caused by the winglets have somewhat offsetting effects on Dutch roll characteristics, resulting in a slight reduction in damping ratio accompanied with a small decrease in period. The net effect on the Dutch roll oscillations is negligible.

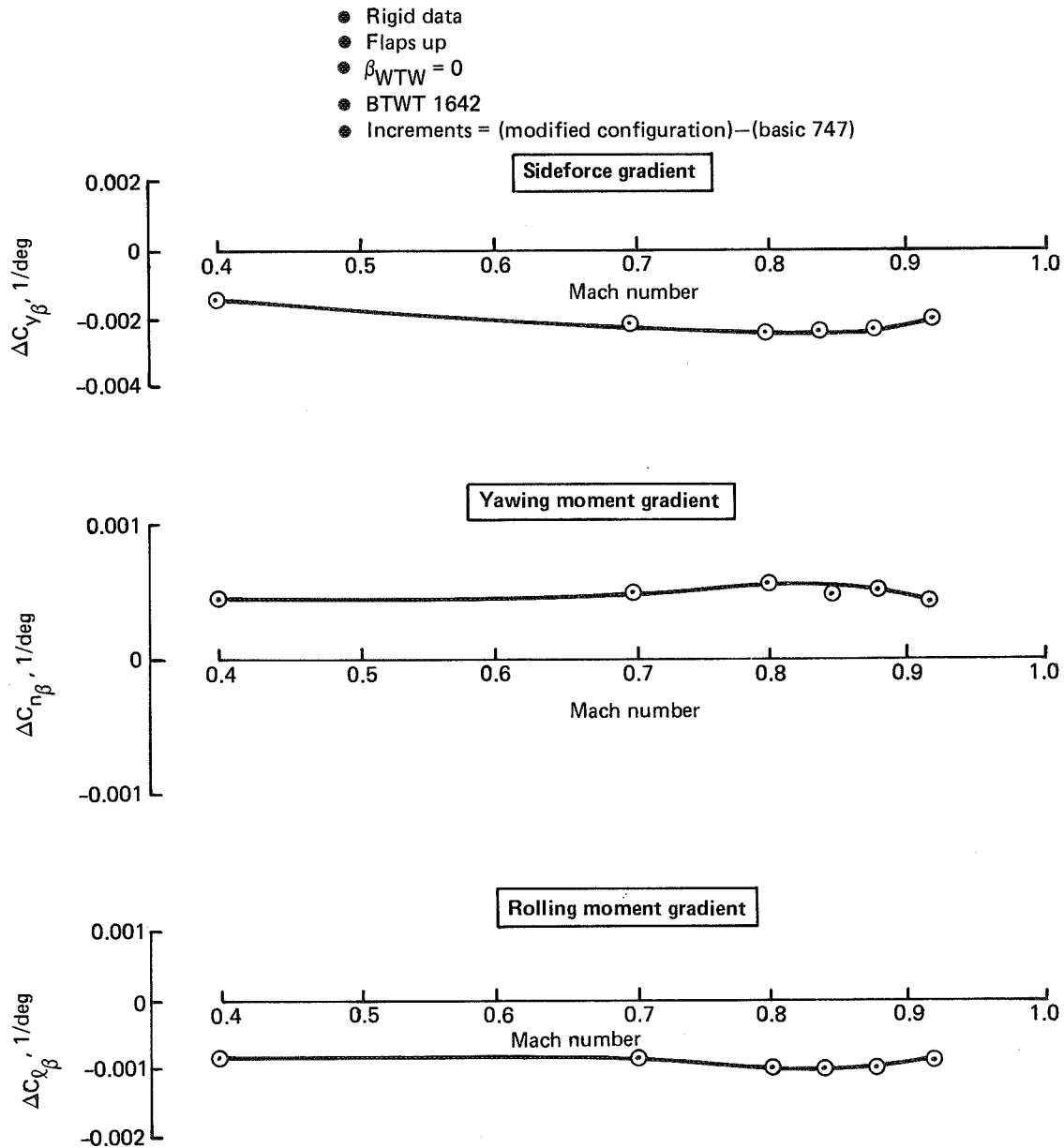


Figure 63. Effect of Z13 WTW on Static Lateral/Directional Stability

The revisions to the flight control systems which may be necessary to compensate for the longitudinal stability and control effects of WTWs are the same as those noted in Section 4.3.4 for WTEs, i.e.,

- Modified pitch feel system
- Re-rig of the elevators
- Revised stabilizer trim greenband for takeoff

These recommendations are based on flaps-up test results. Flaps down testing and further study is necessary to quantify the effects and define the primary flight control system with the flaps extended.

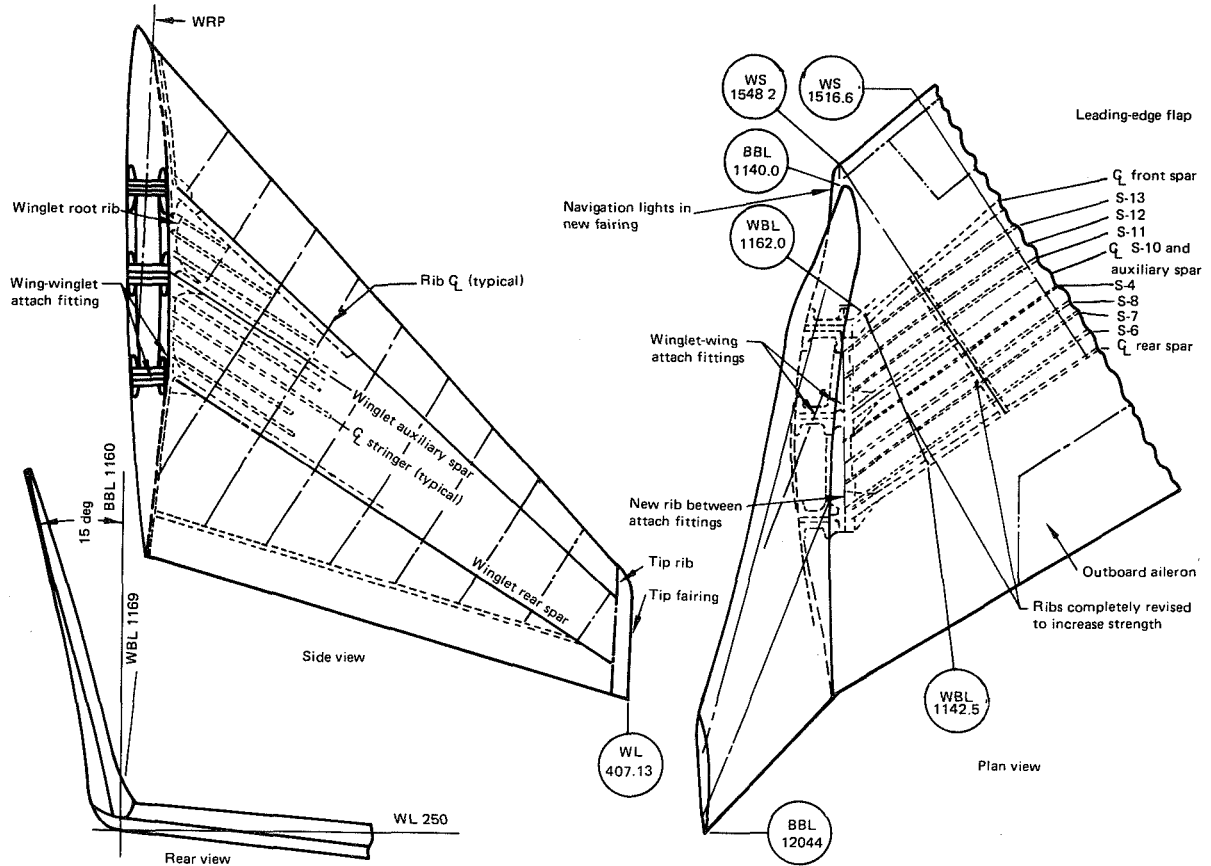


Figure 64. Attachment Concept for Z9 Winglet (Preliminary)

5.4 INSTALLATION DESIGN CONCEPTS

Installation design feasibility studies were made for two wing tip winglet configurations. The first, Z9, consisted of conventional skin and stiffener construction with the front and rear spar locations determined to facilitate splicing alignment with the wing spars. An auxiliary spar was installed to transfer the large bending moment at the winglet root into the wing tip and provide a fail-safe concept. Complex machined fittings were required to tie together the spars and root rib in the winglet and the wing spars to the tip rib (fig. 64). Attachment of the winglet to wing fittings required the use of large bolts and, while adequate, provided a relatively flexible load path.

The second configuration, Z13, rectified the flexible winglet/wing attachment of Z9 by using a multispar configuration, as shown in Figure 65, for the lower portion of the winglet and the outboard portion of the wing. The winglet cant angle also was increased from 15 to 30 deg. A three view of the 747 with the Z13 installed is shown in Section 7.1.8.

Both winglet configurations had approximately the same effect on flight controls and other system installations in the wing tip. The spars, machined from aluminum forgings in the Z13 configuration, did not require relocation of the magnetic compass sensor, as was required by the large volume of steel in the Z9 attachment fittings.

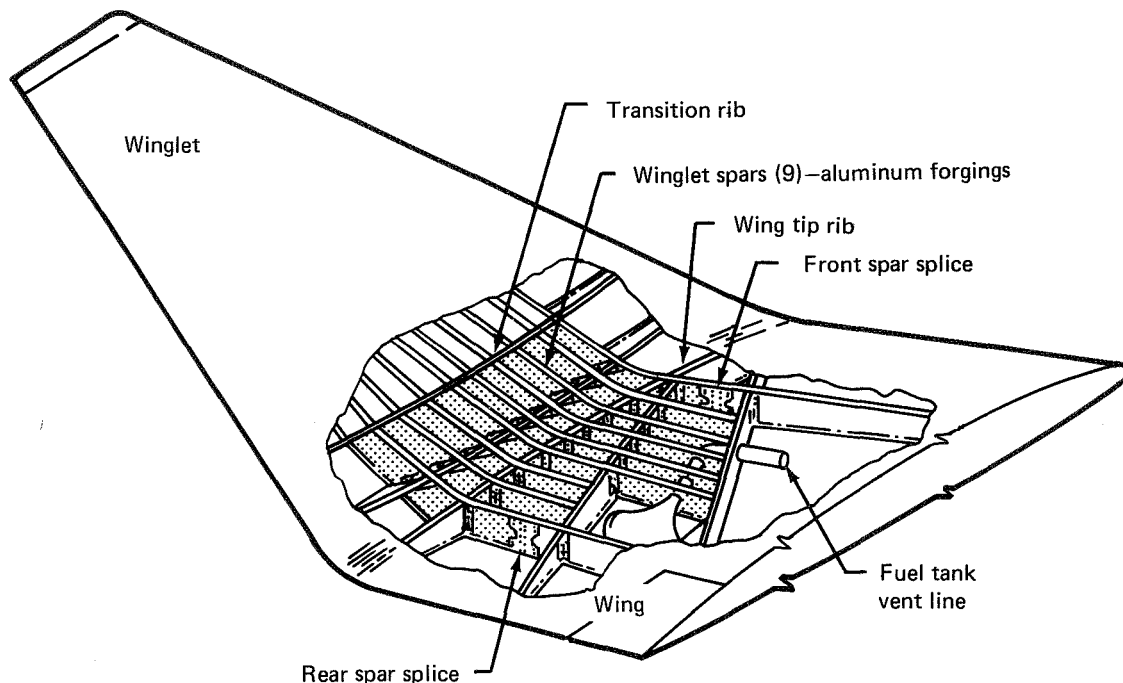


Figure 65. Attachment Concept for Z13 Winglet (Final)

Both winglet configurations were fabricated as separate units then spliced to a suitably prepared wing. Wing reinforcement was approximately the same for both winglets and the same retrofit problems prevailed as were outlined for the tip extension.

5.4.1 Z9 Winglet Construction

The winglet structure consisted of a main box section with conventional aluminum skin stiffeners and spars construction. The leading edge was fabricated from formed aluminum sheet and the trailing edge from fiberglass honeycomb panels. The lower end of the spars were spliced to steel fittings, which also spliced the root rib (fig. 64).

The winglet was attached to mating fittings in the wing tip by large diameter bolts. All fittings were of fail-safe design, ensuring that, in the event of one fitting failure, the remaining pair together with the adjacent structure, was capable of redistributing and reacting the design load.

5.4.2 Wing Structural Revisions for Z9 Winglet Installation

Outboard of WS 1548, the honeycomb panels were replaced by sheet-stiffener construction, with the exception of the panel attached to the fuel tank vent scoop. An auxiliary spar was added to back up the middle attachment fitting. In addition to reinforcing the front and rear spars (for the increased winglet root loads), the wing structural box also was revised inboard. The basic plate and extrusion blanks were capable of accommodating the increased thicknesses.

5.4.3 Systems Revisions for Z9 Installation

Due to the volume of steel in the wing-winglet attachment fittings the magnetic compass sensor was relocated to the fin front spar. The high frequency antenna was replaced by a shunt antenna located on the fin leading edge.

5.4.4 Control Systems Revision for Z9 Installation

Changes to the control systems were relatively minor; the same as for the wing tip extension (sec. 4.3).

5.4.5 Z13 Winglet Construction

Construction of winglet Z13 differed from Z9 in its attachment to the wing. As shown in Figure 65, a multispar arrangement replaces the three spars with steel fittings and, thus, provides greater capability for carrying the increased loads at the winglet root/wing tip junction. The front and rear spars were spliced to the wing spars, while the others terminate at the WS 1548 rib, except in the region of the fuel tank vent scoop. The spars were fabricated from aluminum forgings and extended up to the transition rib. The leading edge, trailing edge, and box structure, above the transition rib, were all of the same construction as the Z9 winglet.

5.4.6 Wing Structural Revisions for Z13 Winglet Installation

Inboard of WS 1548, wing structural changes were similar to those required for the Z9 winglet installation and were accommodated within the existing skin plate and extrusion blanks.

5.4.7 Systems Revisions for Z13 Installation

System revisions are the same for the Z13 winglet as for the Z9 except that, by use of aluminum forgings in lieu of steel fittings, the magnetic compass sensor did not require relocation.

5.4.8 Control Systems Revisions for Z13 Installation

Changes to the control systems were the same as for the WTE and the Z9 installation, (sec. 4.3).

5.5 INTERIM ASSESSMENT

High-speed test results have shown that a winglet can provide a significant L/D improvement for the 747 wing although, due to relatively light tip loading, potential benefits are less than for some other airplanes such as the KC-135. Flutter is the primary technical concern for winglet application to the 747, and the increase in wing-box weight associated with the increased stiffness required to achieve satisfactory flutter speeds detracts from the performance benefits.

Operational concerns regarding gate access, taxiway clearances and required maintenance facility modifications are the same as for a tip extension having the same semispan increase. Minor flight control system revisions would be required (e.g., revised trim limits). Effects on longitudinal flying qualities would be minimized. The combined effects of increased lateral and directional stability would adversely affect cross-wind landing capability and engine-out control speeds.

Wing design and manufacture would be considerably more complex than conventional wing tips, particularly with regard to working out the loft lines, details, and tooling in the wing/winglet junction region. Extensive engineering development and engineering flight test would be required, but FAA certification should be routine.

6.0 WING LOAD ALLEVIATION

This section discusses development of the wing load alleviation (WLA) system configuration and shows the potential weight benefits of maneuver load control (MLC) and gust load alleviation (GLA) for the basic wing without wing tip extensions (WTE) or wing tip winglets (WTW). Application of WLA in combination with tip extensions and winglets and the feasibility of flutter mode control (FMC) with winglets are discussed in Section 7.0. The WLA studies for the basic wing were restricted to consideration of the MLC and GLA functions using the outboard aileron as the primary WLA control surface. The distinction between the WLA functions is as follows:

- **MLC**—Reduction of the maneuver loads used for structural design. Maneuver loads for this study were computed for steady-state maneuvers at limit load factor. The concept of using active outboard ailerons to reduce maneuver loads is illustrated in Figure 66. Actuation of the ailerons shifts the lift distribution inboard which reduces wing bending moments. The resulting nose up pitching moment reduces the balancing tail load, which further reduces the wing design loads. As discussed in Section 6.1.1, the 747 outboard aileron can be used as a MLC surface even at flight conditions where it would be reversed as a roll control surface due to aeroelastic effects.

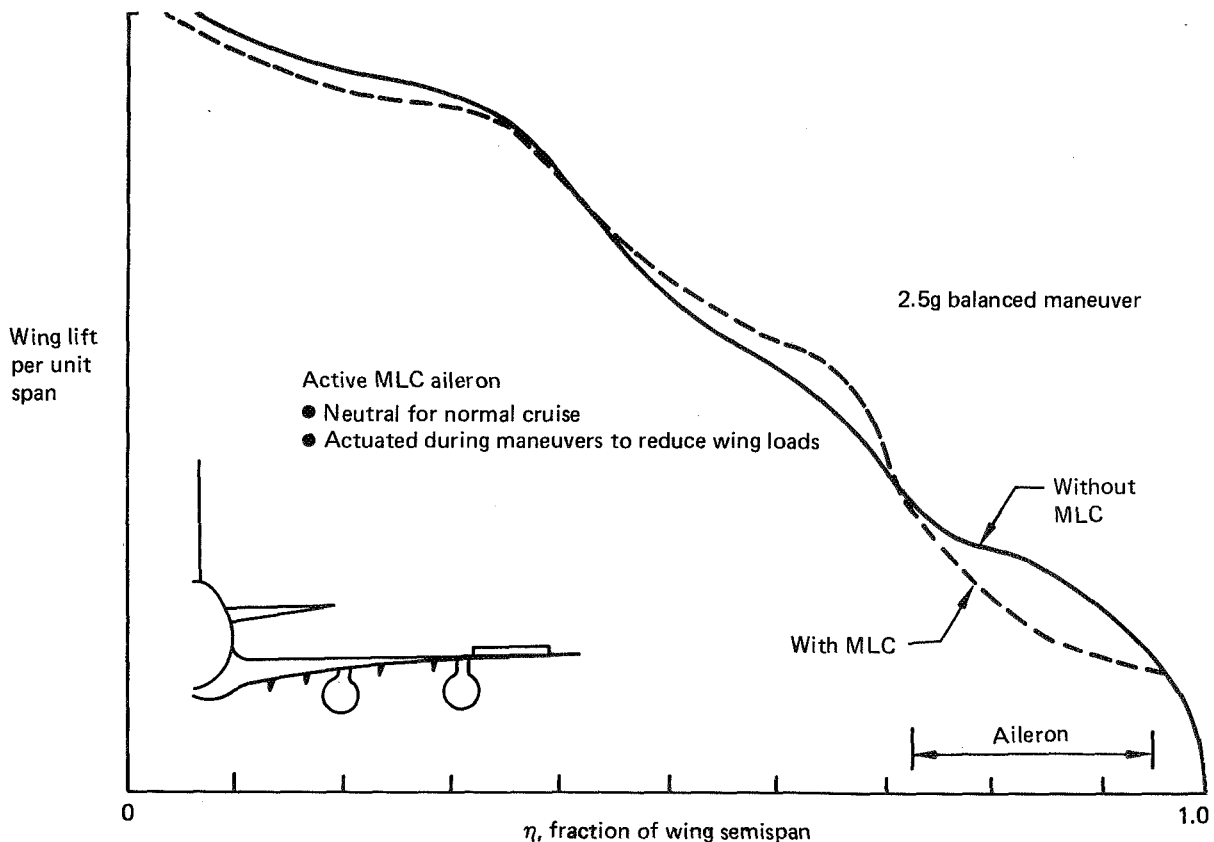


Figure 66. Maneuver Load Control Concept

- **GLA**—Reduction of the gust loads used for structural design. Gust loads for this study were computed by means of a power spectral density (PSD) design envelope analysis. The final WLA control law (fig. 67) employs wing acceleration feedback to the ailerons. Though MLC was the primary objective in the control law design, alleviation of gust-induced bending moments is provided at lower gust frequencies directly from the aileron effect on quasi-steady state lift distribution. Additional GLA is provided through elastic mode suppression (EMS) of the first wing bending mode.
- **EMS**—Elastic mode suppression of the first wing bending mode was studied as a means for implementing the GLA function and has been retained in the final control law. However, the objective of the MLC/GLA functions is to reduce design loads rather than to provide EMS per se. In the case of flutter mode suppression, the term "flutter mode control" has been used rather than EMS to avoid confusion with other applications of EMS.

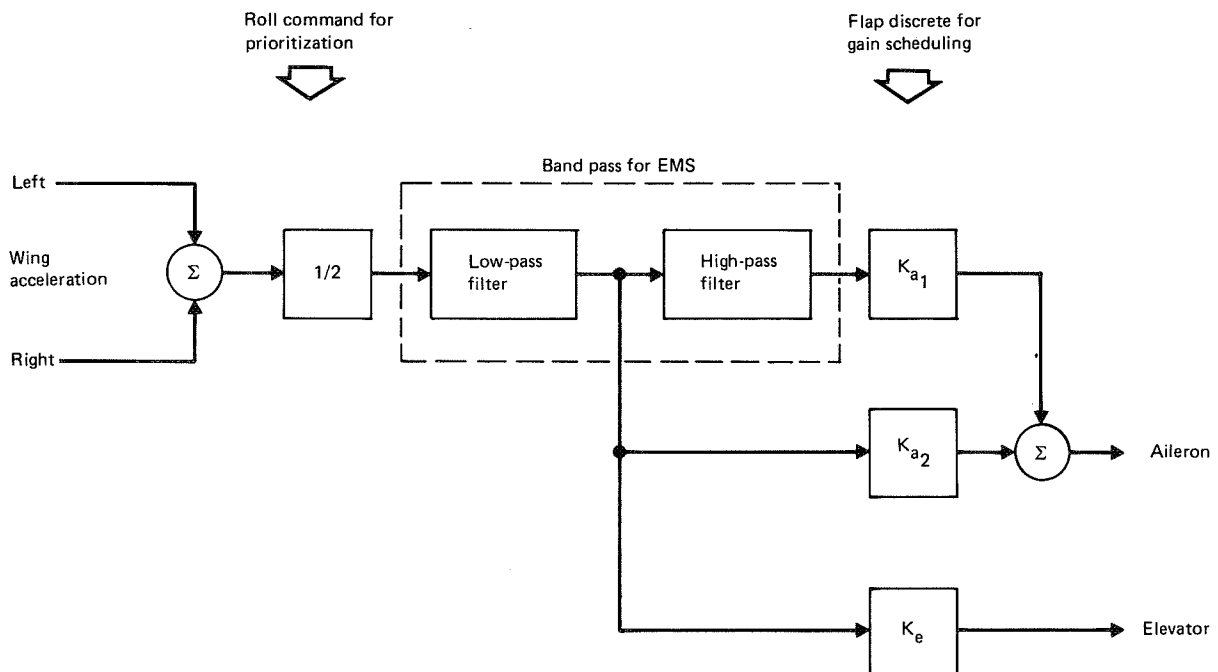


Figure 67. Final WLA Control Law (MLC Only)

The WLA studies were accomplished, based on the aerodynamic and structural dynamic characteristics of the basic wing (no WTE/WTW). Objectives of the first series were:

- MLC aileron configuration definition (plain vs. tabbed)
- Weight benefits assessment for the MLC and GLA functions
- MLC/GLA control law development
- System mechanization concept development

The existing aileron span and chord were retained. A balance tab was tested and analyzed as a means for minimizing the increased torsion loads associated with MLC; but a plain aileron was selected for use in the structural benefits assessment and final WLA system studies. Both plain and tabbed aileron configurations were flight tested as part of the Boeing WLA Demonstrator program to obtain flight data for correlation with wind tunnel and analytical results.

The potential weight benefits of the MLC and GLA functions were computed for an ideal system independent of the control law development. This was done by first sizing the structure to accommodate maneuver loads (only) computed with the MLC aileron deflected to the hinge-moment limit, and then resizing with baseline gust loads (i.e., controls-fixed at neutral in gusts) also included. Closed loop analyses (sec. 6.2.5 and 6.3.1) were conducted to evaluate performance of an actual system.

Two series of WLA system configuration studies were conducted. The first series, in combination with the structural benefit studies, was directed toward developing an understanding of the potential benefits and problem areas associated with the MLC and GLA functions and with the preliminary system mechanization concept. The preliminary mechanization concept and control law were subsequently adopted for further development and implementation in RA-001 (the Boeing flight test 747 aircraft) as part of the Boeing WLA Demonstrator Program. Ground rules for the preliminary system mechanization were:

- Actuators—Use existing power control units (PCUs) and off-the-shelf WLA servos, if possible
- Redundancy—Dual channel, fail passive. One reason for studying this concept was that a triple-channel fail-operative system reverts to this configuration after the first channel failure.

A second series of WLA system configuration studies was then conducted to simplify the control law, improve system reliability, and develop an installation concept more suitable for a production system. Ground rules for the final system mechanization were:

- Actuators—Consider new PCU with integrated WLA series input
- Redundancy—Fail-operational with dual actuators and in-line monitoring

The GLA function required several additional sensors while providing little additional weight benefit; therefore, the requirement for GLA was deleted from the final WLA system. Although the requirement was for MLC only, the final control law (fig. 67) also provides EMS of the first wing bending mode through the use of wing accelerometers. Use of wing accelerometers simplifies the problem of designing the MLC filter to avoid adverse effects on gust loads. Although the final control law has a favorable effect on gust loads, baseline gust loads (i.e., controls-fixed in gusts) were used for structural sizing of the final configurations (WTE/WTW with MLC). Retention of the gust material improves structural safety margins following WLA system failure.

A new aileron PCU incorporating electrical summing of the roll control and WLA commands was incorporated into the final configuration because it was found to be lighter, cheaper, and more reliable than the existing PCU with mechanically summed WLA servo inputs. Technical feasibility of the electrical summing concept was confirmed by the supplier (Hydraulics Research Inc.) of the WLA servos used in the 747 WLA Demonstrator. With a new PCU installation, the option exists for installing more powerful actuators, if desired. Trade studies (sec. 6.2.4) showed that increased MLC aileron deflection offers little additional weight benefit for the basic wing. However, there might be advantages for a WTE configuration if aileron span were increased (with associated increases in aileron stiffness and PCU force capability).

The final mechanization, discussed in Section 6.4.3, approaches the reliability of a dual, independent yaw damper system through the use of a fail-operational concept employing in-line monitoring techniques. The mechanization incorporates triplicated sensors (with signal-select) dual-dual computers, dual servo electronics, and dual WLA servo (T-valve) inputs to dual-tandem PCUs.

An assessment of WLA benefits is provided in Section 6.5.2. The recommended system design approach and the relationships between structural sizing, system reliability, and operational restrictions associated with system failures are discussed in Section 6.5.1.

6.1 AILERON CONFIGURATION DEFINITION

It was recognized that although the outboard aileron would provide wing load relief in terms of bending moment reduction it would cause an increase in torsion loads, particularly in the immediate region of the outboard aileron. An aileron balance tab was tested and evaluated as a means for reducing the adverse effects on torsion.

A study involving wind tunnel testing of both a plain (untabbed) aileron and a tabbed aileron was conducted to determine aileron and tab force data to aid in selecting the best configuration for wing load relief. The tab studies were conducted to determine the torsion load relief available and to evaluate the adverse effect of the tab on wing bending moment relief.

A theoretical study was conducted to determine the best tab chord to use for optimum wing box weight reduction. Use of the plain aileron configuration to angles higher than normal blowdown angle also was considered in the total configuration definition.

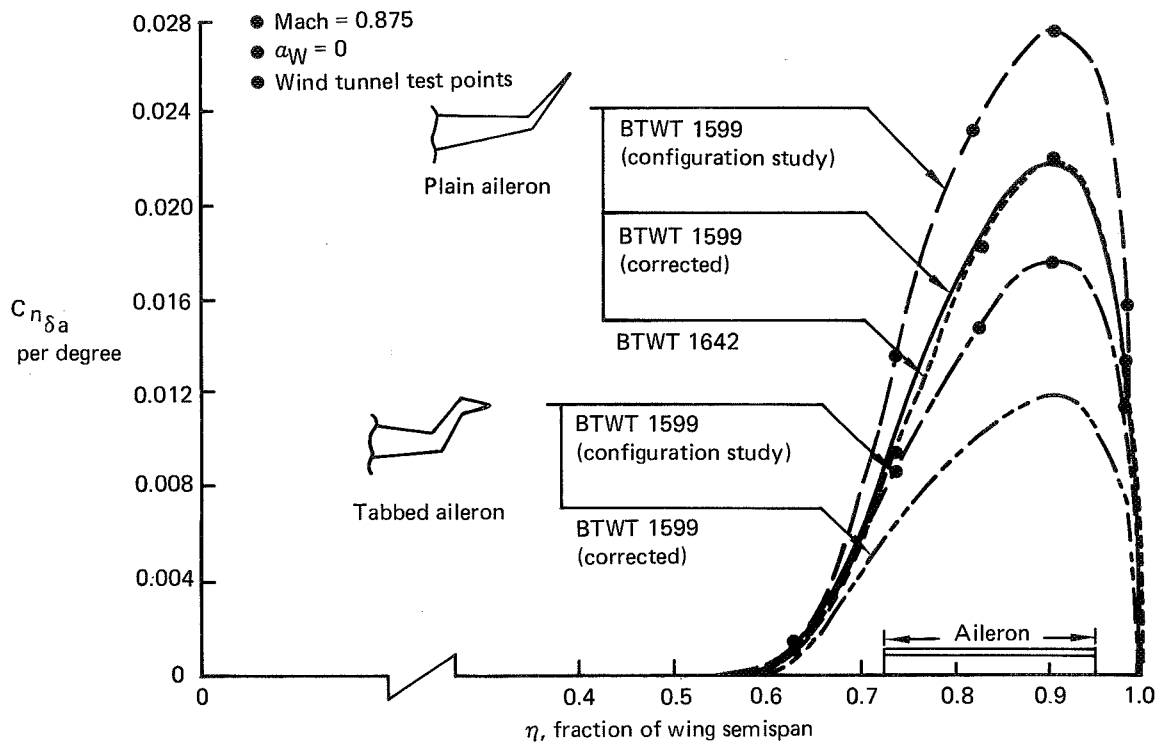
The studies showed that after taking all factors into account, the best aileron configuration for the 747 EET was a plain (untabbed) aileron using the existing actuators.

6.1.1 Aileron Effectiveness

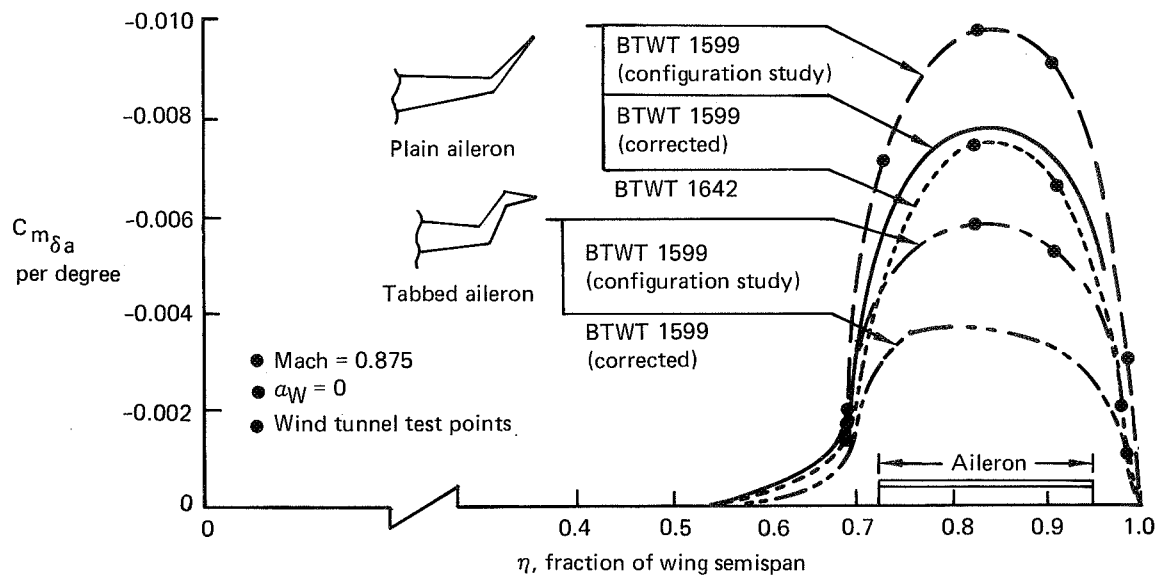
Aileron effectiveness for plain and tabbed ailerons was based on wind tunnel pressure data from the first EET wind tunnel pressure test (BTWT 1599). These results were used in the WLA configuration studies reported in Section 6.1.2 and the structural benefits analysis reported in Section 6.2. Wing, aileron, and tab pressures were measured for a plain outboard aileron and for the aileron with a 30% chord full span balance tab (tab to aileron gearing, -1:1). Similar data were measured for the plain aileron only during the second EET wind tunnel test (BTWT 1642) for use in analysis of the final EET configurations.

Significant differences were noted between the two sets of test results, as can be seen from the sample data shown in Figure 68. Following a review of measurements made during and after the tests, it was concluded that the aileron was misrigged during the BTWT 1599 test, causing the aileron effectiveness to be overpredicted. When the difference in rigging was accounted for, satisfactory agreement was achieved.

The required correction for aileron rigging provided some calculated improvement in tab effectiveness because it resulted in a calculated reduction in the aileron effectiveness increment only, with no change to the tab increment; thus the tab was calculated to be relatively more effective. For the data shown in Figure 68, the



A. Wing Section Lift Due to Outboard Ailerons



B. Wing Section Moment Due to Outboard Ailerons

Figure 68. Wing Section Aerodynamic Effectiveness Due to Outboard Ailerons

chordwise center of pressure of the combined aileron/tab pressure distribution ($0.25 + C_{m\delta}/C_N\delta$) was shifted forward approximately 2% of the wing chord due to the calculated correction. This was not considered enough to justify a reanalysis of the tabbed aileron configurations.

The final tab effectiveness was only about half the theoretical estimate. For the Mach 0.875 condition, the tab was predicted to shift the center of pressure forward approximately 10% of the wing chord relative to the plain aileron, but the corrected wind tunnel results showed only about a 5% shift.

The load alleviation benefits of a tabbed aileron configuration will be determined by flight test during the company-funded WLA demonstrator program using the 747 flight test airplane.

Aileron Effectiveness Vs Angle of Attack—The aileron was demonstrated to remain effective and reasonably linear at all angles of attack tested, including beyond the stall break in the airplane lift curve, as indicated in Figure 69. This is a desirable characteristic of the ailerons which would not be characteristic of a configuration employing spoilers for WLA.

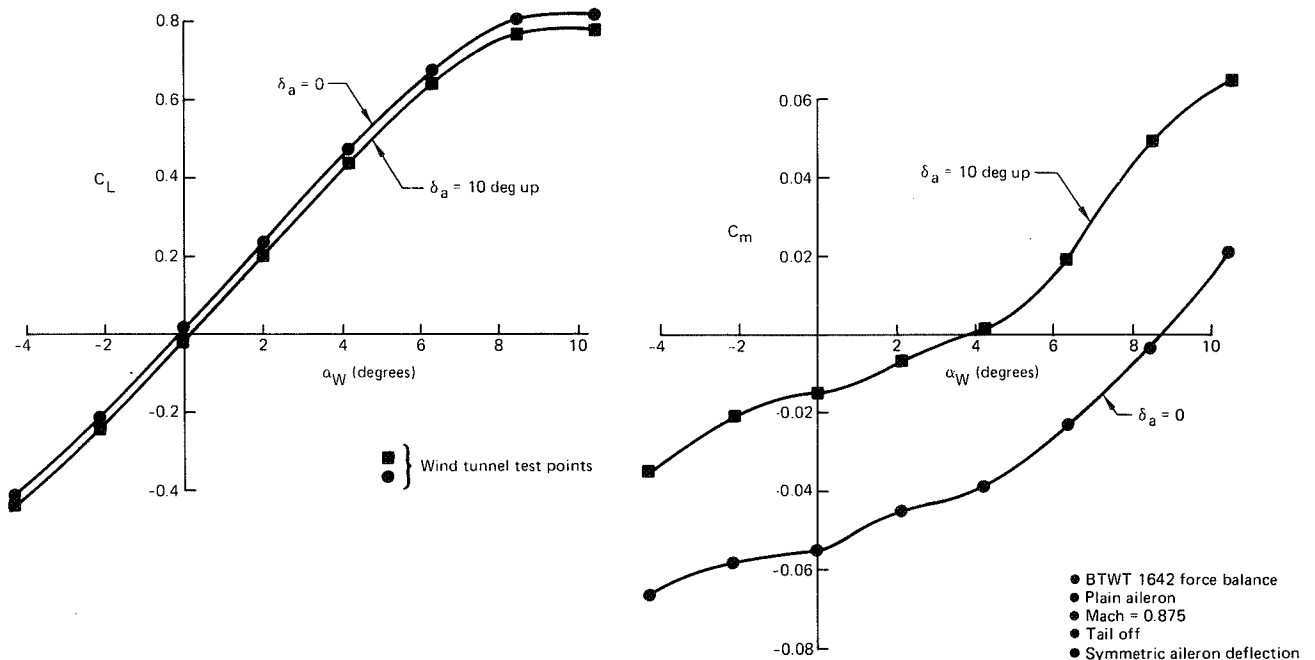


Figure 69. Aileron Effectiveness On Airplane Coefficients

6.1.2 Bending/Torsion Trades

This section discusses the load results used for the WLA aileron configuration selection studies. A limited set of flaps-up, 2.5-g maneuver conditions based on previous analysis experience was analyzed using outboard ailerons for the wing load alleviation. Aileron aerodynamic effectiveness was based on wind tunnel test data from the first EET wind tunnel test (BTWT 1599) (sec. 6.1.1).

Figures 70 and 71 show the wing bending moment and torsion ratios for the aileron configurations tested. The base notations refer to the existing wing with existing safety margins. Included are results for the plain and tabbed ailerons deflected to mechanical limits (25 deg up) and for the plain aileron deflected to the existing actuator blow-down limits. These figures also show results for unalleviated flaps-down maneuver and gust conditions. As expected, the tab reduced the torsion load increase, and less bending moment reduction was obtained. For all configurations analyzed, the bending moment alleviation achieved was maximum near the aileron and was reduced inboard. Based on the estimated wing box weight savings for these configurations, the plain aileron deflected to the existing actuator limits was selected as the WLA configuration and was recommended for both flaps-up and down maneuvers. Final maneuver load results for this configuration, based on an expanded set of conditions, are reported in Section 6.2.1. Also, because the unalleviated gusts loads became critical when the maneuver loads were relieved, the gust analysis was extended to determine the potential weight savings benefit of a GLA system.

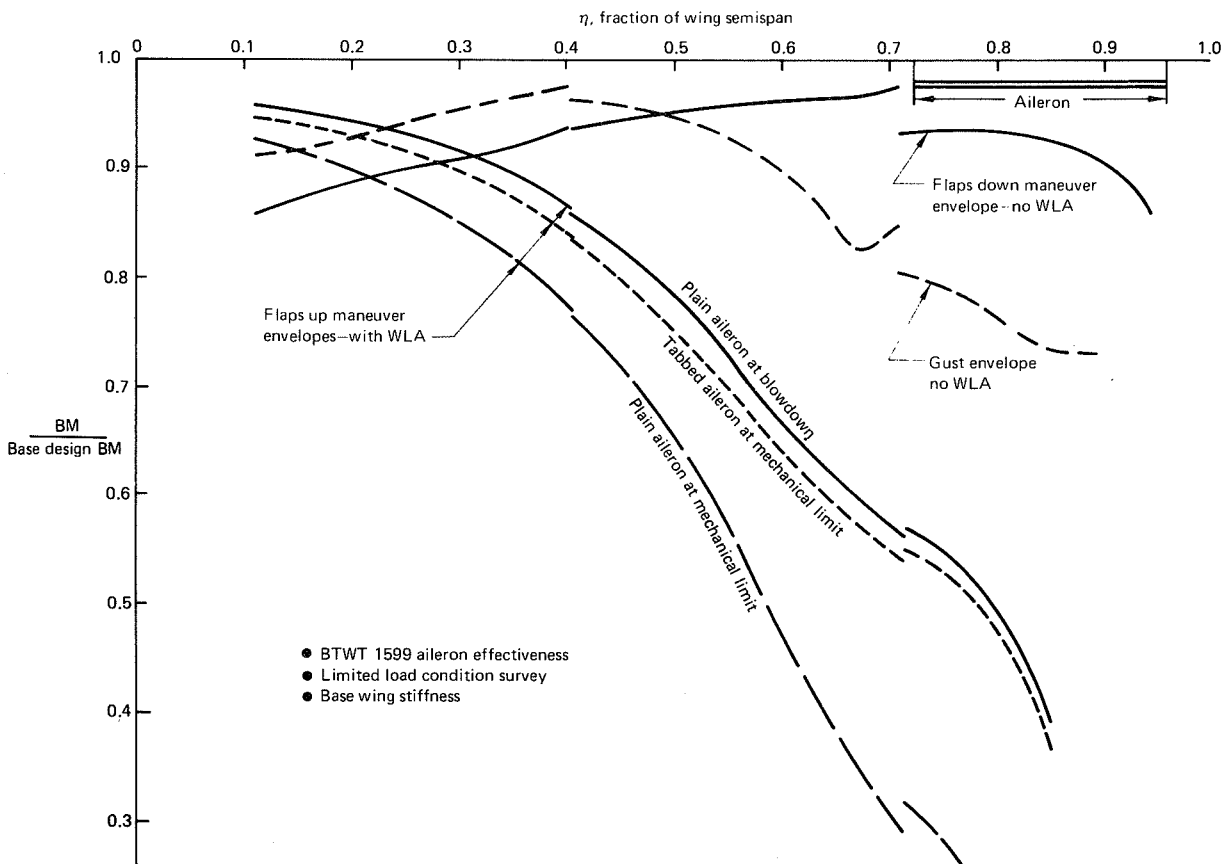


Figure 70. Effect of MLC Aileron on Base Design Bending Moment

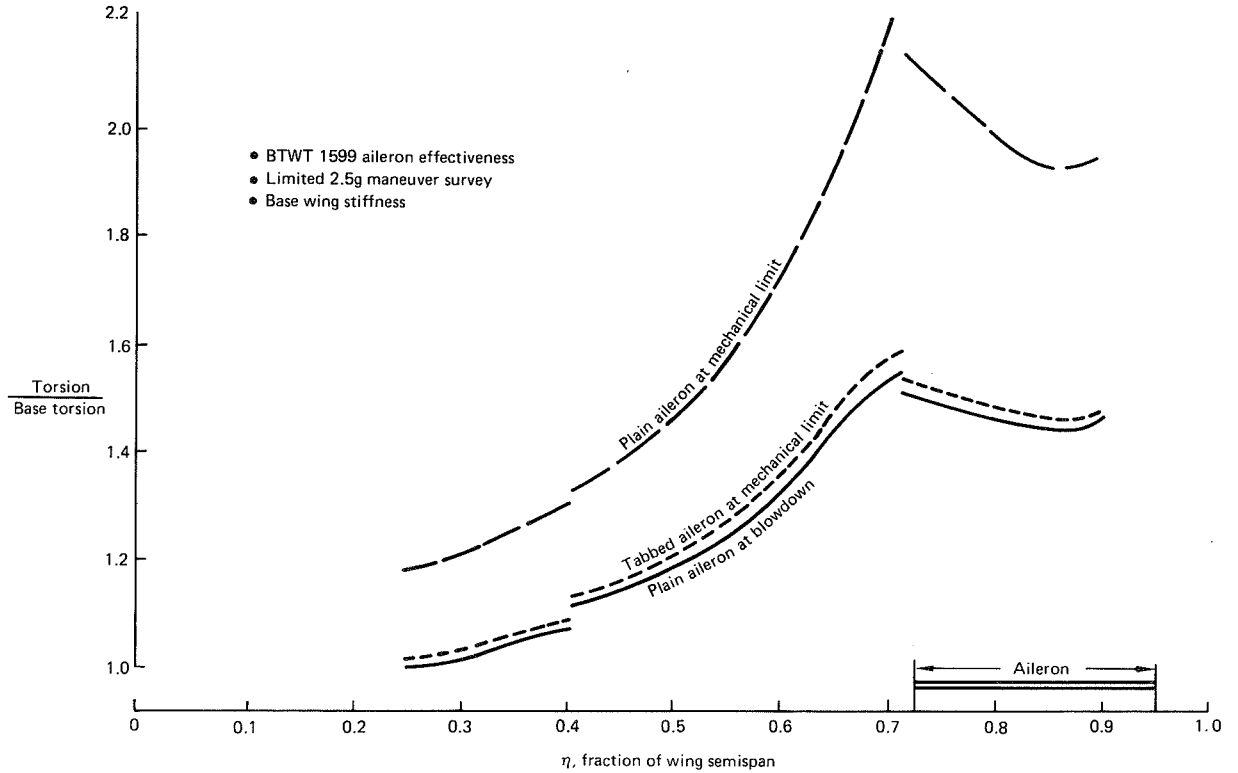


Figure 71. Effect of MLC Aileron on Base Torsion

Figure 72 depicts how the ailerons work to change wing loads for the wing root design condition. The moment curve on this figure shows that the incremental moment due to aileron deflection, when determined at constant angle of attack, reverses at $\eta = 0.25$, but when combined with retrim loads as required to maintain a constant load factor maneuver, no reversal occurs. The load reversal near the wing root at constant angle of attack is related to the roll reversal phenomenon. Figure 73 shows that the aileron significantly reduces wing bending moment over most of the wing, and retrim is a secondary effect that produces additional load reduction and eliminates the load reversal characteristics near the wing root. Thus, the plain outboard ailerons of the 747, which were originally designed for low-speed roll control, can be used symmetrically at high speed for maneuver load alleviation with no net load reversal characteristic.

Results of the structural analyses and the related weight reduction trends for the various WLA configurations analyzed are summarized and discussed in Section 6.1.3.

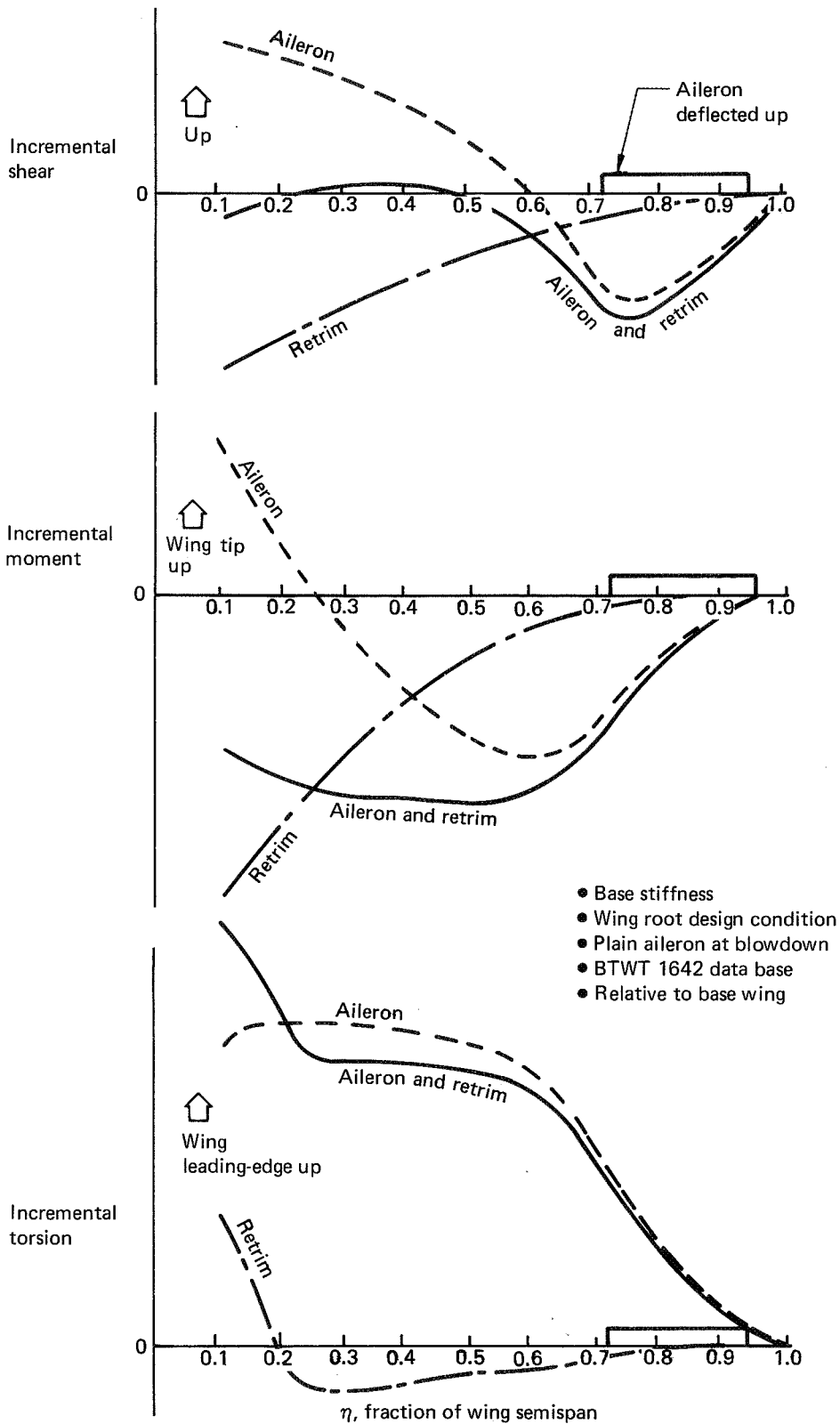


Figure 72. Incremental Wing Loads Due to Aileron and Retrim

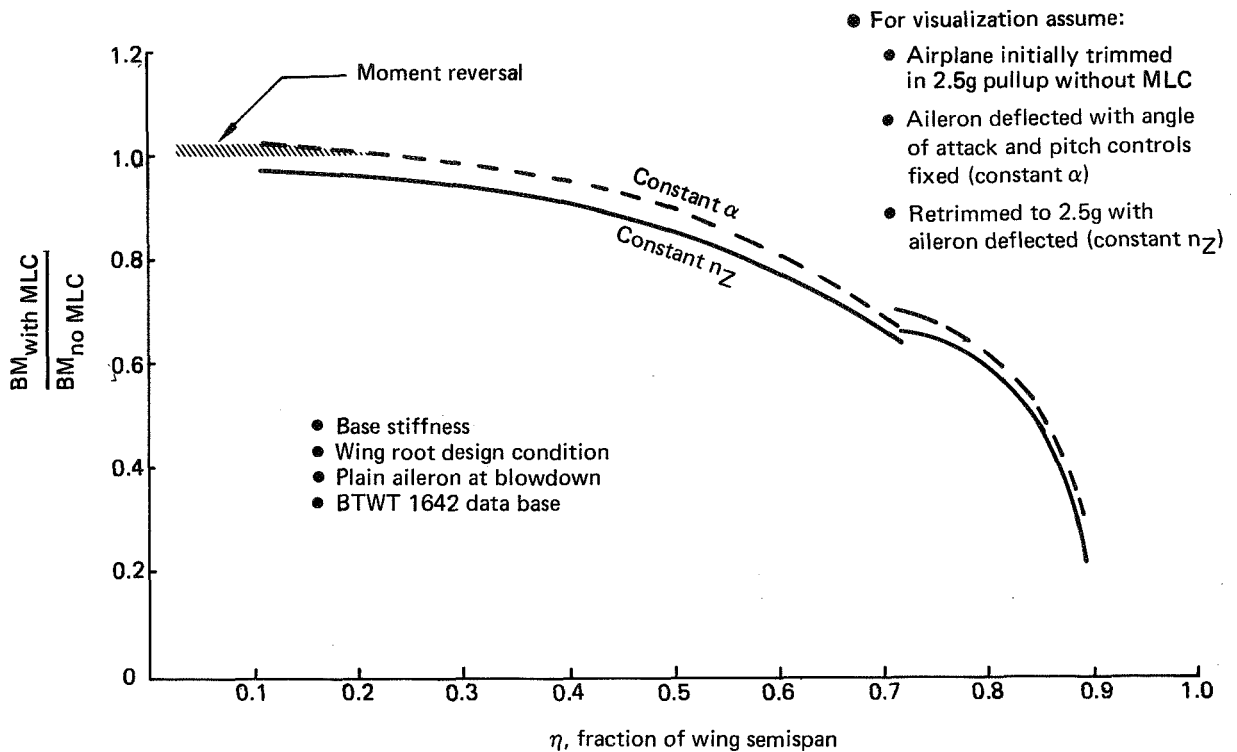


Figure 73. Illustration of Bending Moment Alleviation Above Aileron Roll-Reversal Speed

6.1.3 Wing Box Weight Trends

Trade studies were conducted to determine the best aileron configuration to be used for wing load alleviation. Use of the outboard aileron as a maneuver load alleviation device to reduce wing bending moment has the undesired effect of increasing wing torsion. In an attempt to reduce this effect, a tabbed aileron configuration was investigated.

Early studies involved investigation of the best tab chord to use. These studies were conducted using the 2.5-g maneuver condition for determination of design loads. The wing was resized, maintaining constant skin/stringer area ratios, using the changes in loads determined for the various aileron tab chord dimensions. Figure 74 shows the results of this study. Two sets of aerodynamics were used, a preliminary set of theoretical aerodynamics and the first wind tunnel test entry (BTWT 1599) aerodynamics. The upper curve shows the trend in wing box weight with increasing tab chord, assuming a constant aileron blowdown angle of -14 deg. Actually, the aileron

- 2.5g maneuvers
- Loads based on existing structure
- Resized maintaining constant skin/stringer area ratios

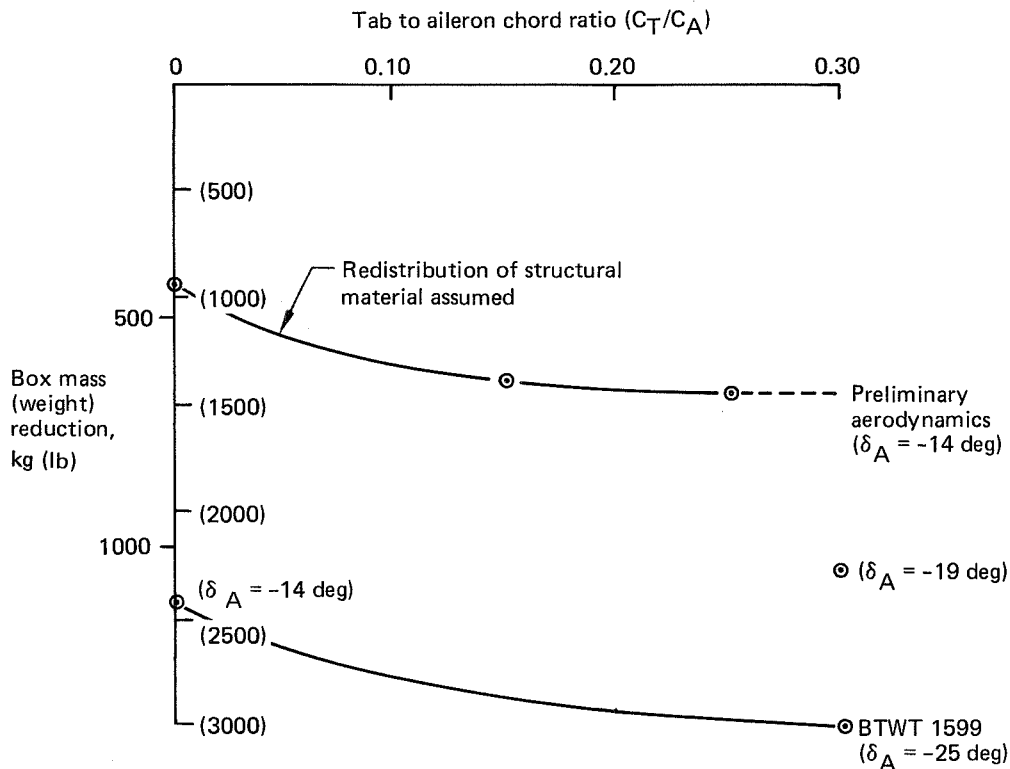


Figure 74. Effect of Tab Chord Ratio on Wing Box Weight

will blowdown less because the hinge moment is reduced by the increased chord balance tab. The lower curve shows the plain aileron and the 30% chord tab wind tunnel data. It can be seen that the most benefit occurs with about a 30% chord tab.

The effect of the resulting resized wing stiffness on design loads, due to changes in aeroelastic effects, was not evaluated.

The major concern of increased torsion levels is that additional structural material (weight) must be added to the wing panels. A secondary concern is the resultant need to strengthen the front spar. It was expected that the use of a balance tab would allow maneuver load alleviation to be implemented with significantly less extensive front spar modifications than if a plain aileron were used. However, Figure 75 shows that a similar area of the basic wing is modified in either case. An additional study also was conducted to see if this conclusion was valid for the wing with a 1.83-m (6-ft) tip extension. The figure shows this to be the case; i.e., the tab did not eliminate the need to modify the front spar.

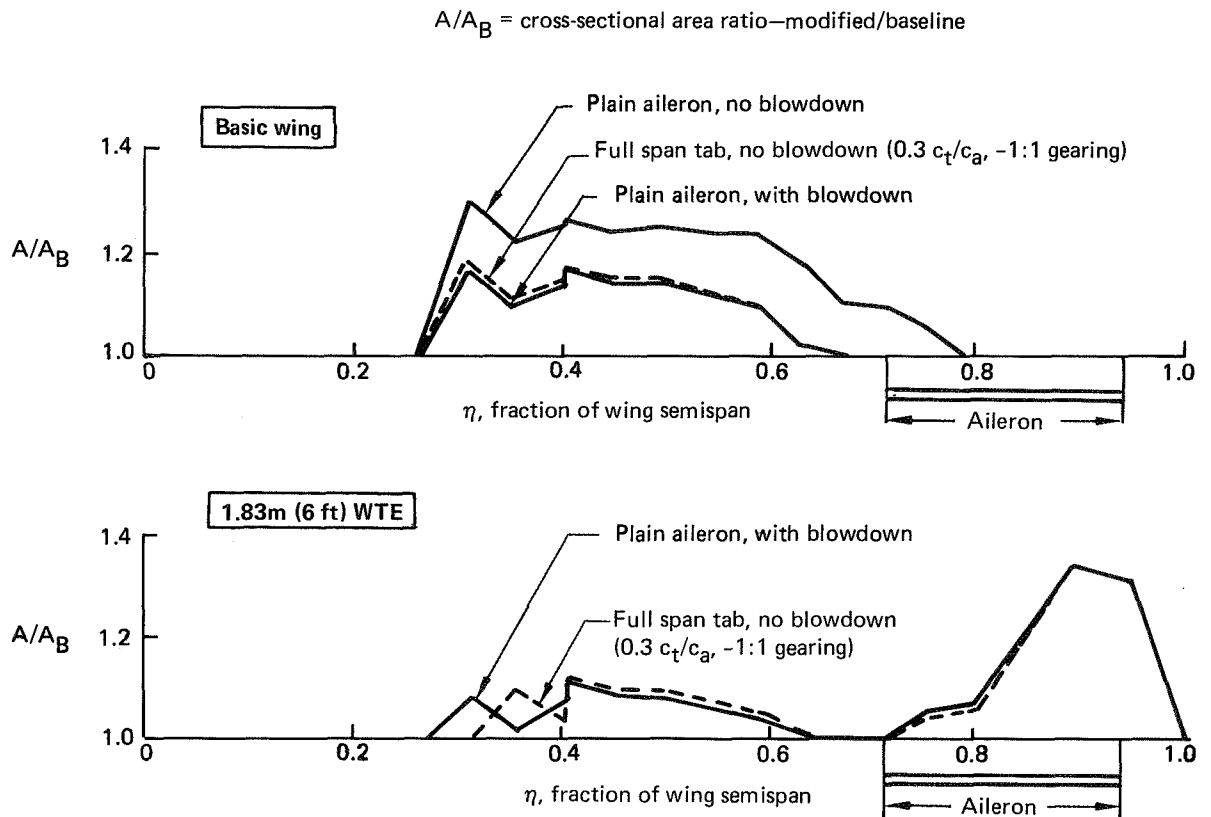


Figure 75. Effect of MLC Aileron Configuration on Front Spar Web Sizings

To determine the overall weight benefits of a tabbed aileron configuration to the airplane, weight estimates of the system and aileron/tab structural changes were made. Table 4 is a summary of the weights associated with the system (preliminary estimate for the initial system configuration), the aileron structural changes (including additional balance weights), and a tab lockout mechanism. The system weight (tab linkages and lockout excluded) is independent of the tab configuration. The tab lockout mechanism is required to lock the tab out during flaps down flight so that outboard aileron roll authority is maintained.

Table 4. Weights for WLA System and Aileron/Tab Changes

Increment per airplane—mass (weight), kg (lb)								
Configuration	System: Computers, servos, sensors, other		Aileron structural changes and balance weights		Tab lockout mechanism		Total per airplane	
Plain aileron	204	(450)	0	(0)	0	(0)	204	(450)
0.55 span tab	204	(450)	70	(155)	20	(45)	295	(650)
Full span tab	204	(450)	118	(260)	41	(90)	363	(800)

After choosing a tab configuration with a 30% chord, a sizing study was conducted consisting of a loads/stress/weights cycle on the wing box. Loads were generated at the positive high angle of attack (+HAA) 2.5g maneuver condition for a plain aileron; a 55% span, 30% chord tab with a -0.7:1.0 gearing (WLA Demonstrator study); and a full span 30% chord tab with a -1.0:1.0 gearing. These loads were used in a stress analysis to resize the wing structure. The baseline wing structure was initially resized to zero margins of safety. Each study wing structure then was further resized to zero margin, and the incremental changes in size were used to evaluate wing weight benefits from the MLC system.

The loads data used for this study were based on the results from wind tunnel testing of the tabbed aileron configuration (BTWT 1599). Blowdown was taken into account, based on existing actuator capability. The weight summary included a weight allowance of 204 kg (450 lb) for installation of the MLC system (initial configuration with separate WLA servos) on the airplane, plus the changes to the aileron configuration that included tab lockout and balance weights of 91 kg (200 lb) for the 55% span tab and 16 kg (350 lb) for the full span tab. The weights data generated for the wing when using MLC assumed that a gust alleviation system had been utilized to reduce the gust design requirements below those for the +HAA maneuver case. Also, when using MLC flaps-down, it was assumed that the flaps-down design loads are less than those for flaps-up maneuver.

This study had the following inherent assumptions:

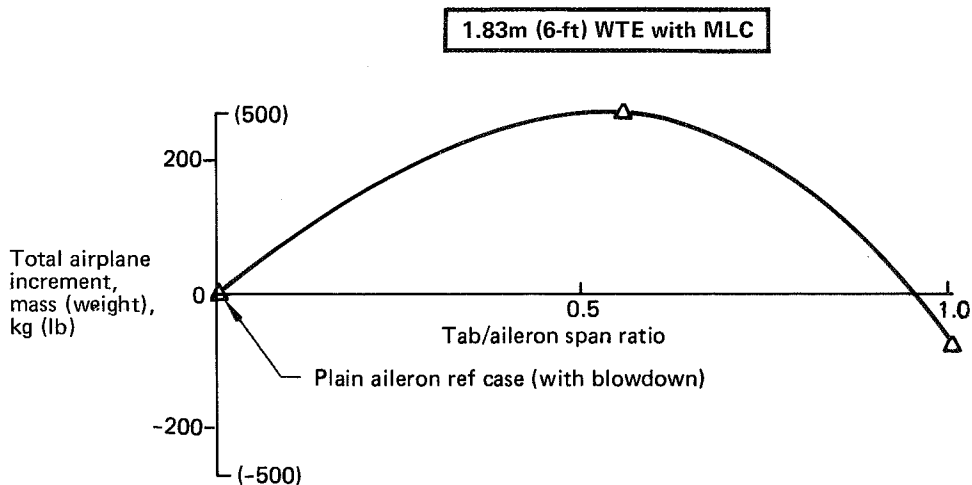
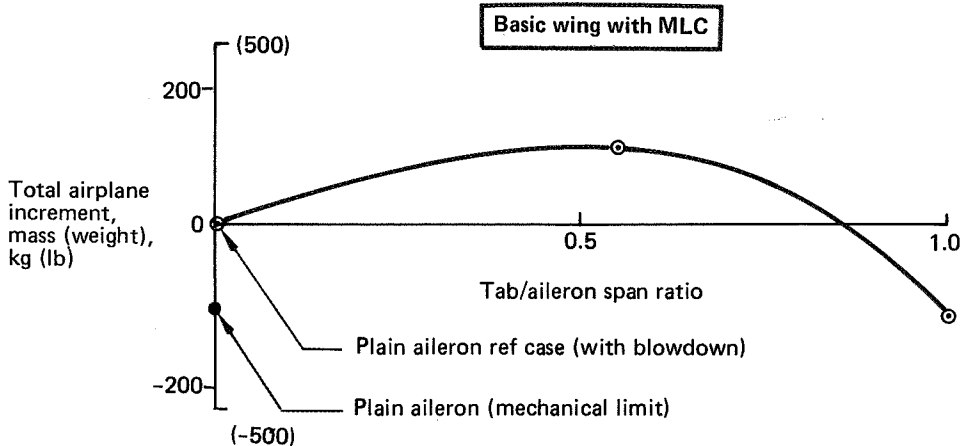
- Flaps-up, +HAA maneuver case designs the wing
- Aileron tab is locked out for use of MLC flaps down
- No credit for aeroelastic lift redistribution due to the stiffness change on the resized wing structure
- No allowance made for flutter or fatigue material

The potential airplane weight changes resulting from this study are shown in Figure 76.

The aileron balance tab shows very little weight benefit; in fact, the part span tab with 0.7:1 gearing actually adds weight as compared to the plain aileron. Also shown in this figure is a data point taken from an actuator sizing study (sec. 7.3.1) in which the weight reduction for a plain aileron utilized to mechanical limit was evaluated. This configuration gave nearly as much incremental weight reduction as the full-span tab configuration.

Results for the wing tip extension configuration also are depicted in Figure 76 and show the same trends as the basic wing.

Note: Increment relative to airplane with plain aileron MLC



Tab/aileron span ratio	Aileron blowdown angle (deg)	Tab gearing
0	-14	0
0.55	-19	-0.7:1
1.0	-25 (mechanical limit)	-1:1

Figure 76. Airplane Weight Trends for Variations in MLC Aileron Tab Span

6.1.4 Selection and Rationale

The primary factors bearing on the aileron configuration selection and a plus/minus (good/bad) comparison of the plain and tabbed configurations are summarized in Figure 77. As previously discussed, the tab offered no advantage in terms of airplane weight savings or minimization of spar modifications. However, there were several disadvantages:

Factor considered	Aileron configuration	
	Plain	Full-span tab (0.33 c_t/c_a)
● Airplane weight savings (combined structure/system)	+	+
● Front spar modification	-	-
● Low-speed roll control	0	-
● High-speed holddown	0	-
● Tab flutter risk	0	-
● System complexity	-	-

● No significant difference if hinge-moment limited
 ● If not hinge-moment limited, more weight savings and spar modifications for plain aileron

Plus/minus comparisons—plain versus tabbed

+ Favorable effect	}	Relative to baseline 747
- Unfavorable effect		
0 No effect		

Figure 77. MLC Aileron Configuration Selection

Low-Speed Roll Control—A balance tab reduces the effectiveness of the ailerons as low-speed roll control surfaces.

High-Speed Hold-Down—The requirement to prevent an overbalanced aileron from floating hardover following a single hydraulic system failure was identified as an area of concern. Hinge moment trade studies for various aileron configurations were conducted, primarily as part of the Boeing WLA Demonstrator program. These showed that a full chord tab with 1:1 gearing is unacceptable with the existing aileron PCUs, but that the hold-down requirement can be met by a half-span tab with reduced gearing and uprig. The uprig would be undesirable for a production system due to the drag penalty.

Hold down is not a problem for the plain aileron.

Aileron/Tab Flutter—The tab tends to induce an unstable slope into the aileron hinge moment versus deflection curve. This is undesirable and could lead to flutter.

System Complexity—Use of the aileron as a MLC device requires addition of an input in series with the roll command to the PCUs. This is true whether a plain or tabbed configuration is selected. The tabbed configuration becomes more complex because of the additional linkages, hinges, and balance weights (possibly) associated with the tab. In addition, a tab lockout is likely to be required for flaps down conditions to maintain current low speed roll control capability. This would considerably add to the complexity.

Rationale for Selection—In view of the added complexity and other disadvantages associated with adding a balance tab to the 747 outboard aileron, the tabbed aileron would have to offer significant advantages in terms of reduced structural weight and/or modifications to warrant selection over a plain aileron. No such advantages for 747 EET applications of MLC are apparent, although the conclusion might be different for other models or applications.

6.2 STRUCTURAL BENEFITS

The purpose of active wing load alleviation is to reduce the aerodynamic loads at the design load conditions and thus reduce structural weight. Many parameters enter into the study to determine the optimum control surface for such an application. Definition of the aileron configuration was discussed in Section 6.1, together with aileron effectiveness determination, bending/torsion trades, and wing box weight trends. It is evident from these data that a tabbed aileron configuration did not provide a significant weight advantage to the airplane relative to a plain aileron. The tab also was investigated as a possible device to minimize the spar web changes when adding MLC to either the baseline wing or the wing with a 1.83-m (6-ft) tip extension, but again it was found that no benefit resulted.

The real structural benefit from the active aileron comes in the upper and lower surface wing panel weight reductions attainable. In fact, for the 747 wing the most benefit comes from the MLC function, with some additional benefit possible from GLA.

Designing for satisfactory fatigue quality is a major effort in any airplane structure. Benefits from MLC can, in some areas of the wing, be restricted by fatigue requirements due to the fact that, although MLC can reduce strength design loads and fatigue alternating loads, it does not alter the nominal 1-g flight condition loads. Thus the 1-g flight stress levels will increase, because of reduced sizing of structure. The ground-air-ground (GAG) stress levels may be increased or decreased depending on the effectiveness of the WLA system. The MLC system for this study was linear (no dead zone) for the low-g maneuvers considered in the GAG cycle. Fatigue sizing results without GLA showed that fatigue material must be redistributed (due to the MLC system related load changes), but the weight of the fatigue material was essentially unchanged. The GLA system can reduce some of the gust induced fatigue loadings and hence yield some benefit, but overall this is relatively small.

In obtaining wing box structural weight estimates, a significant interaction is required between the structural disciplines of loads, stress, flutter, and the weight engineer. A typical flow chart for a design cycle is shown in Figure 78.

6.2.1 Loads

Maneuver—The plain aileron with existing actuator authority was selected for this study, as discussed in Section 6.1.2, and was used for both flaps-up and down maneuvers. A comprehensive set of maneuver conditions was analyzed. This set included all the conditions used for design and certification of the study baseline wing, plus additional conditions critical with operation of the WLA system. A reduced spectrum of fatigue loads was analyzed. The airplane data and methods are the same as used for certification of the baseline airplane.

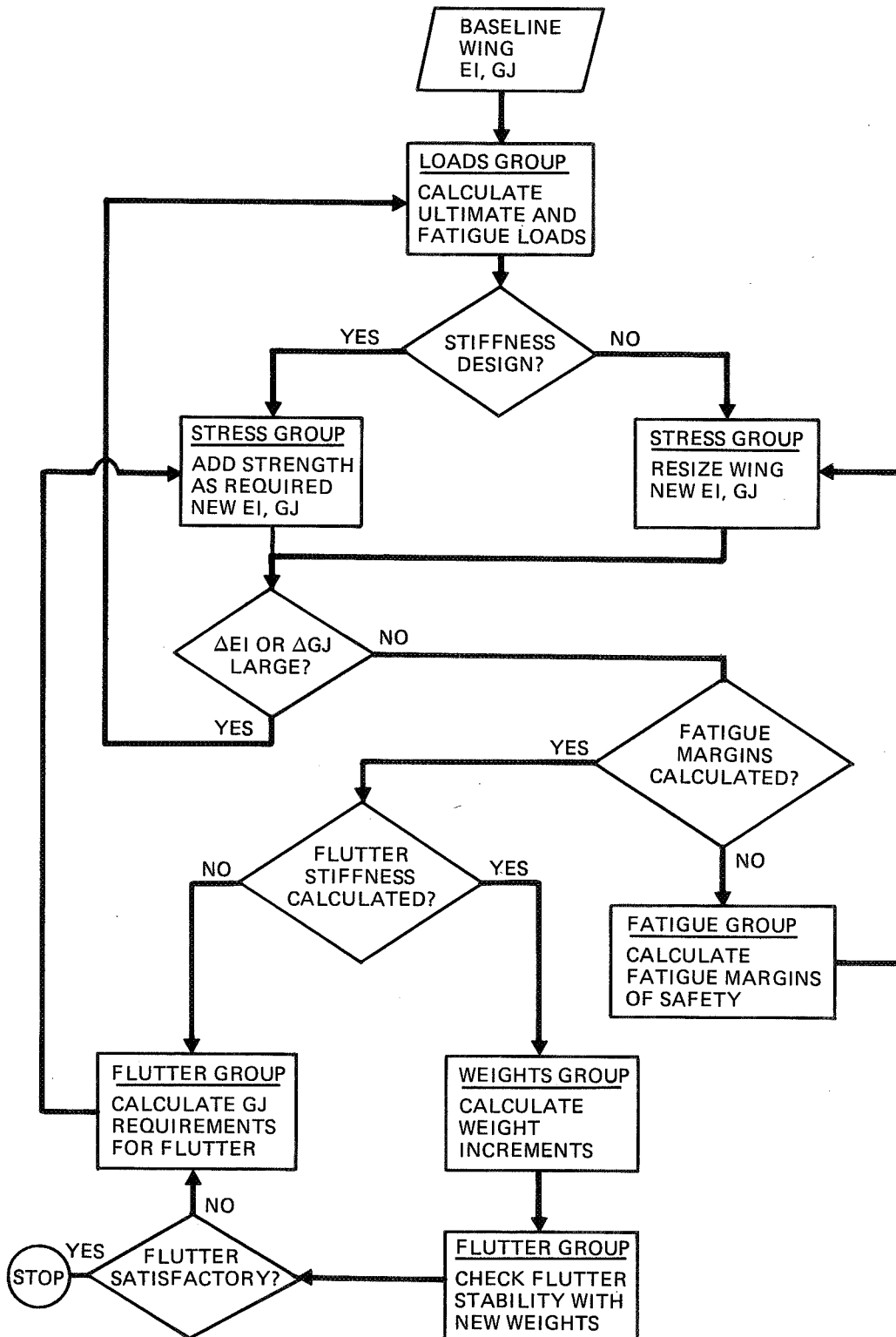


Figure 78. Wing Structural Resizing Procedure

Figure 79 shows the effect of WLA on the wing bending moment envelope due to maneuvers. Flaps up maneuver results are compared, based on aileron effectiveness from the BTWT 1599 and BTWT 1642 wind tunnel tests. Aileron effectiveness data for the flaps down analysis was based on wind tunnel test results with deflected ailerons in a flaps down roll configuration. For flaps up maneuvers, the loads with the BTWT 1599 data base were used for the WLA benefits study on the base wing. The benefits study was not updated following the BTWT 1642 test because only a small change in load benefit was predicted (fig. 79). Although the wing section aerodynamic coefficients were lower from the BTWT 1642 test, as discussed in Section 6.1.1, the associated blowdown angles were higher, with the net effect that only a small loss in load benefit was predicted using the BTWT 1642 data.

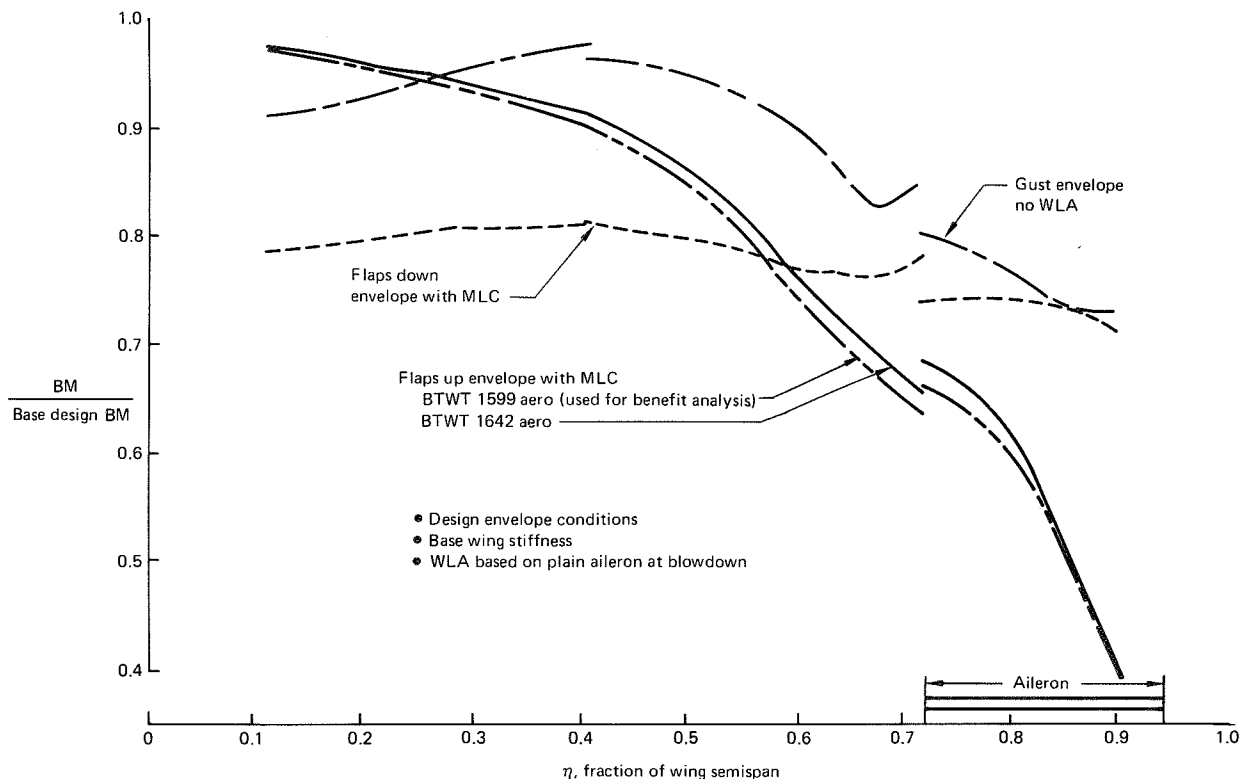


Figure 79. Effect of MLC on Base Design Bending Moments

Gust—The gust loads used for the structural benefits assessment were for the baseline configuration with no WLA system included (open-loop analysis). The bending moment envelope due to gust is shown in Figure 79 and the gust load analysis method is discussed in Section 6.2.5.

Cruise Twist—Figure 80 shows the change in wing twist for the cruise flight condition due to resizing the structural gages of the wing for MLC. As expected, the reduced structural material resulted in increased wing washout. The effect of increased wing washout was included in aerodynamic performance estimates.

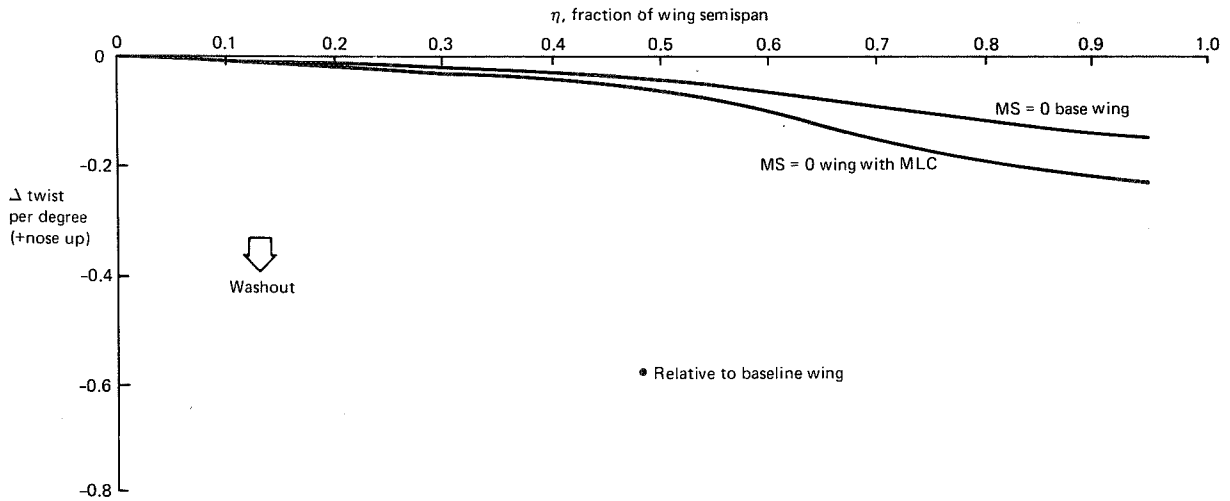


Figure 80. Incremental Wing Twist for MLC on Base Wing

6.2.2 Wing Resizing

Flutter investigations were conducted to determine the stability impact due to stiffness variations resulting from a MLC designed wing. The standard analyses were performed on the baseline 747 airplane without WTE or WTW. Figure 81 shows the change between stiffness for the baseline and MLC configurations when both are sized to zero margin of safety (MS = 0).

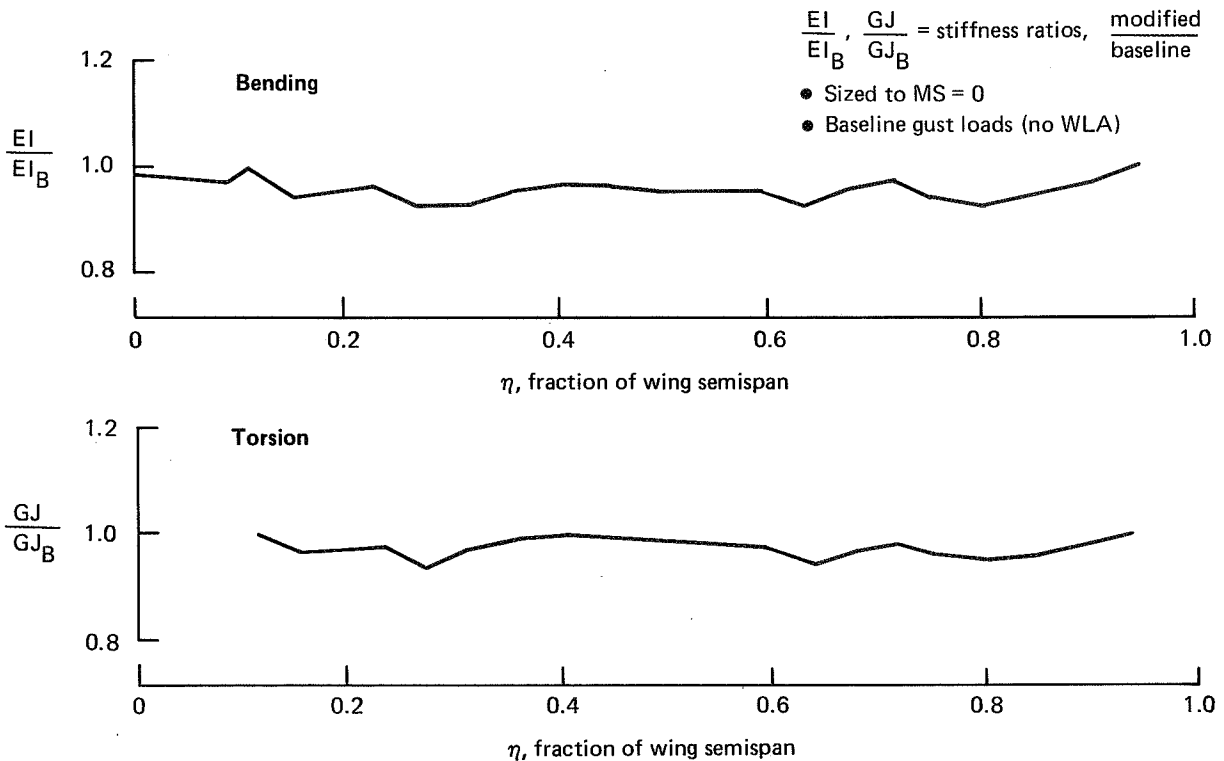


Figure 81. Structural Stiffness Ratios of Basic Wing With MLC

Figure 82 shows the small difference in flutter characteristics for the two wing stiffnesses as the variation of flutter speed with outboard nacelle strut side bending frequency. These results indicate that no added flutter material is required.

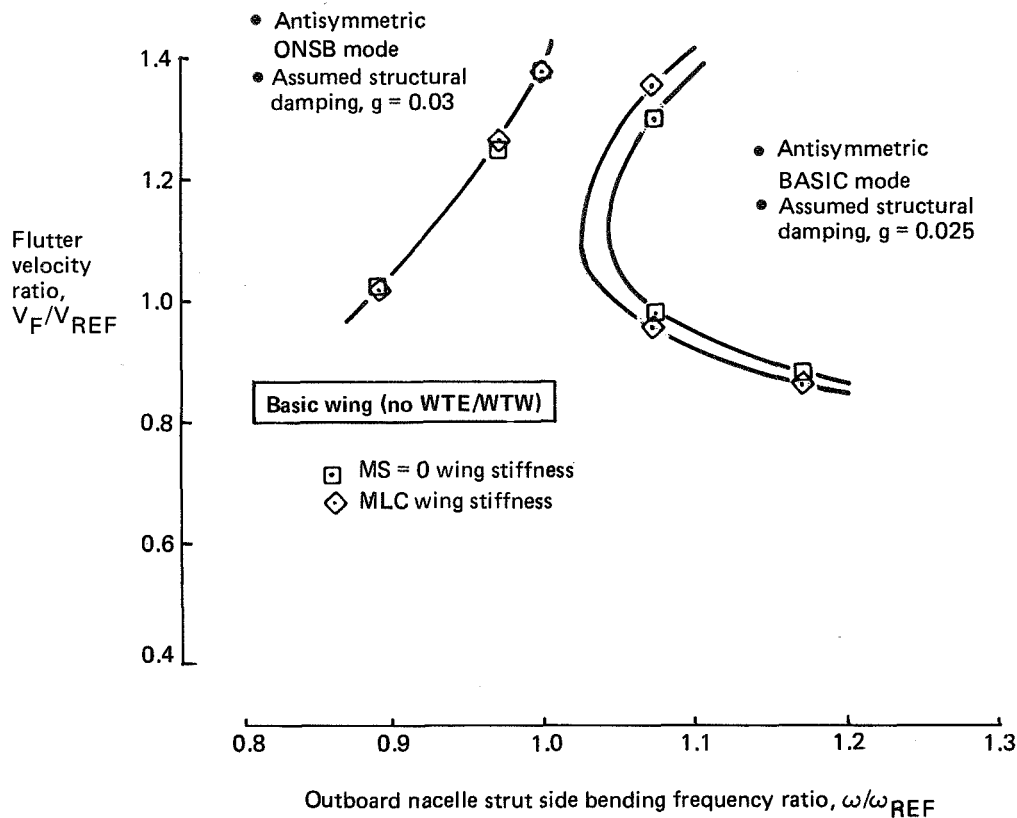


Figure 82. Wing Stiffness Design Change Effects

Structural Resizing For MLC—The MLC system gives reduced wing bending moments and increased wing torsions, which combine to give smaller panel skin-stringer areas. Installation of the MLC system would require changes to the front and mid-spar webs to support the increased torsions, and reinforcement of the outboard aileron and wing trailing-edge panels (illustrated in sec. 6.4.3). To determine the benefits of MLC, the wing box was resized to have panel margins of safety of zero and was compared to a baseline wing box similarly resized. Critical spar web loads were not calculated; therefore, spar web gages on both wings were increased to bring negative margins of safety up to zero, but were not reduced where positive margins of safety remained. The side-of-body joint sizing was not reduced due to fatigue considerations. All other general analysis procedures were the same as given in Section 4.2.3. The sizing results are contained in Figures 81 and 83.

A/A_{B_0} = Cross-sectional area ratio, $\frac{\text{modified}}{\text{zero margin baseline}}$

A/A_B = Cross-sectional area ratio, modified/baseline

- Sized to MS = 0
- Baseline gust loads (no GLA)

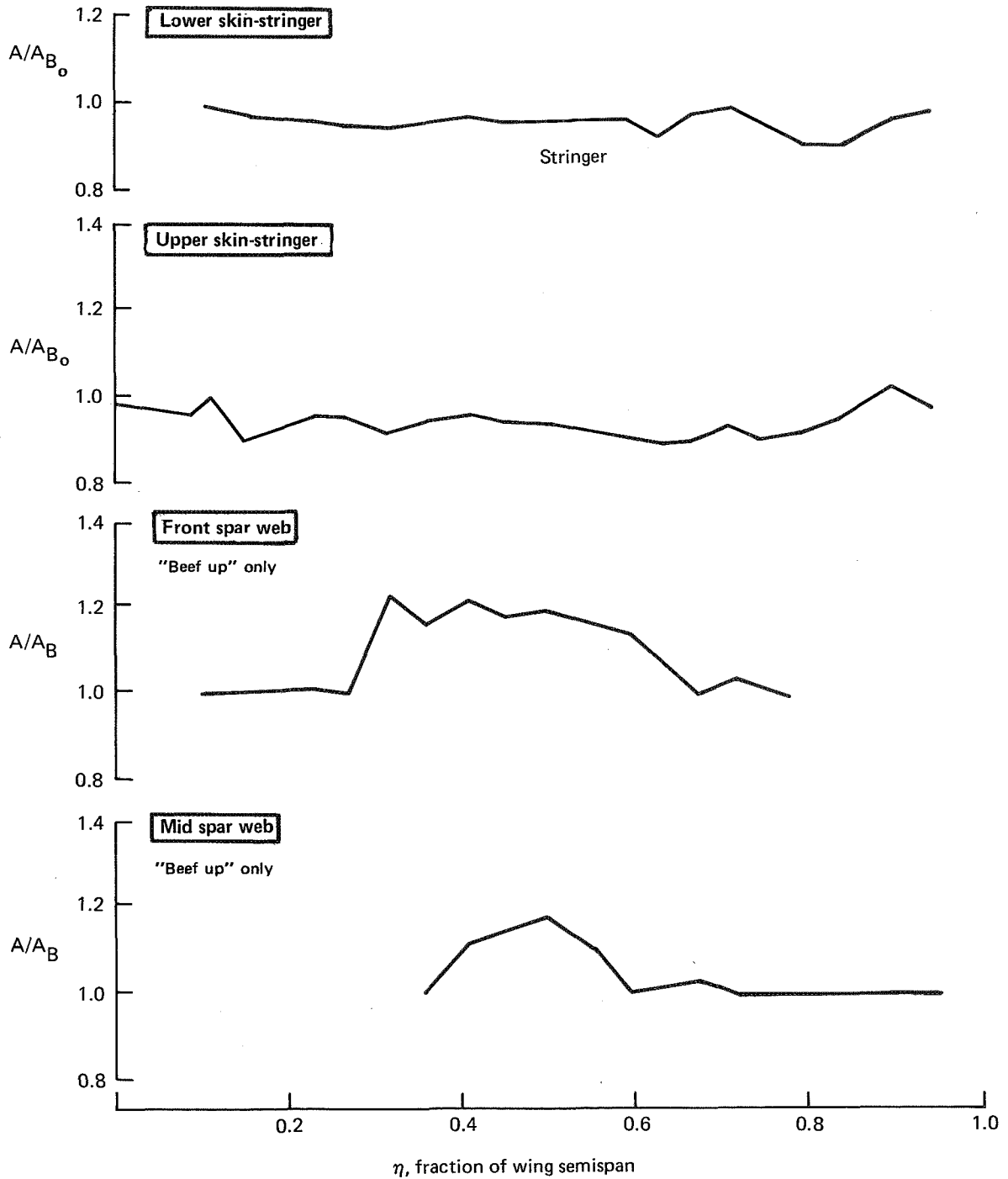


Figure 83. Structural Sizing of Basic Wing with MLC

With maneuver loads reduced by the MLC system, more structure becomes critical for gust loads as shown in Figure 84. The incremental sizing above maneuver loads is not large.

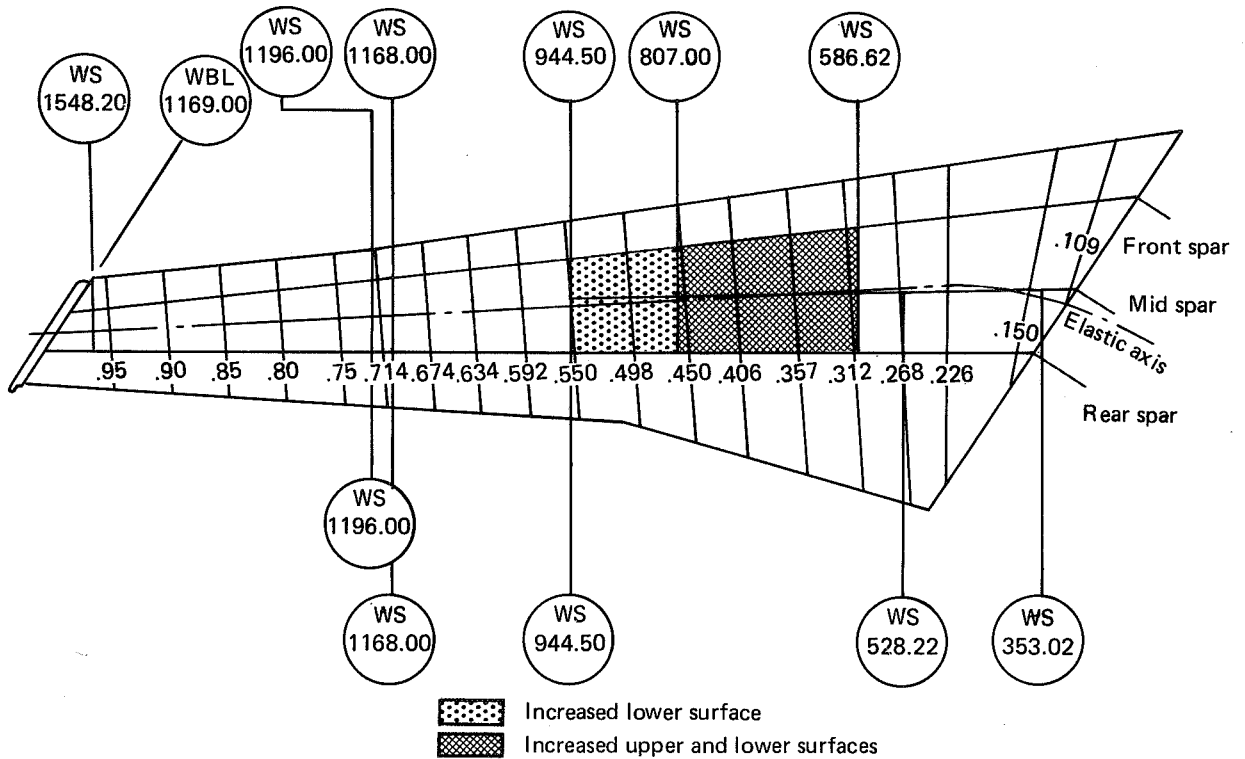


Figure 84. Effect of MLC on Wing Panel Sizing for Ultimate Gust Loads

The majority of the fatigue damage comes from the GAG cycle, which is the stress excursion from maximum compression to maximum tension occurring once per flight. The MLC system may increase or decrease the GAG cycle, depending upon the wing station and stringer being analyzed. Typical fatigue stresses with and without MLC are shown in Figure 85. (Note the increase in l-g stress levels caused by smaller sizing with MLC.) The locations where material was redistributed for fatigue are shown in Figure 86.

There was no requirement to add material for flutter stiffness on either the baseline or MLC wings.

A study indicated that retrofitting a MLC system is not practical because of the extensive spar web changes required.

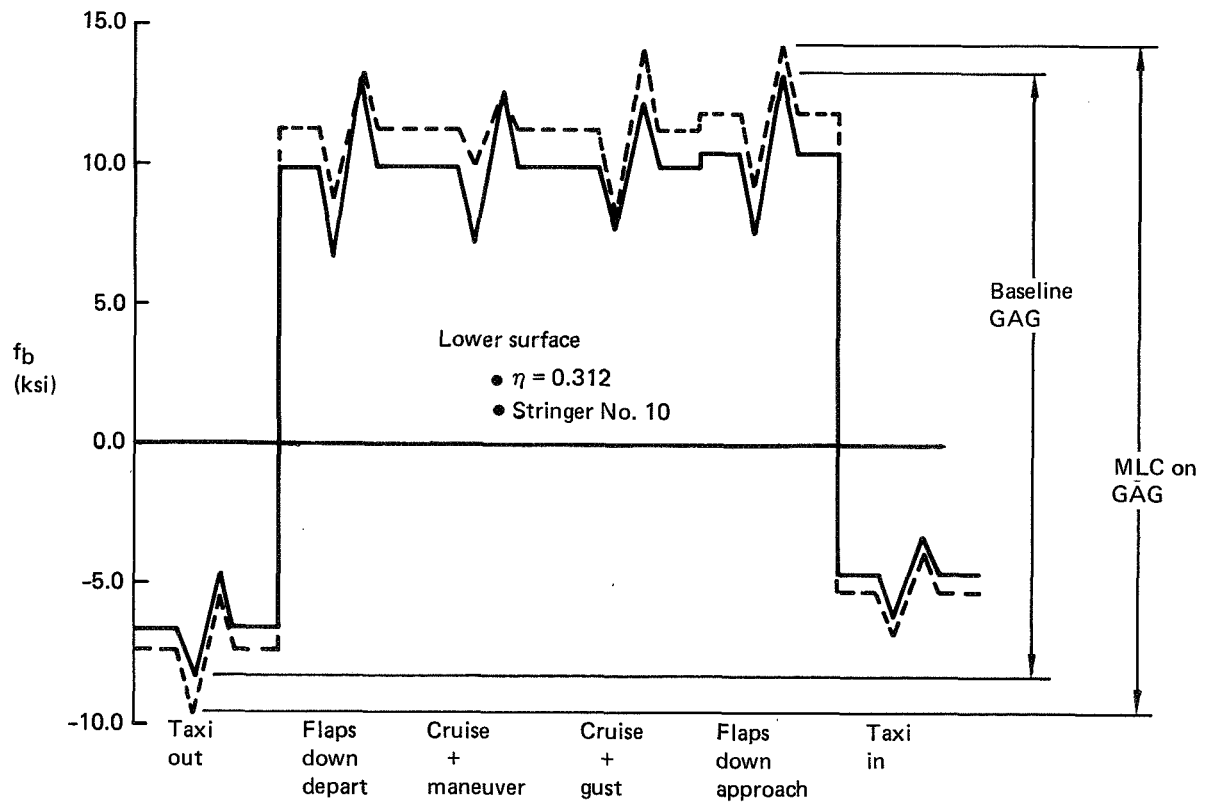
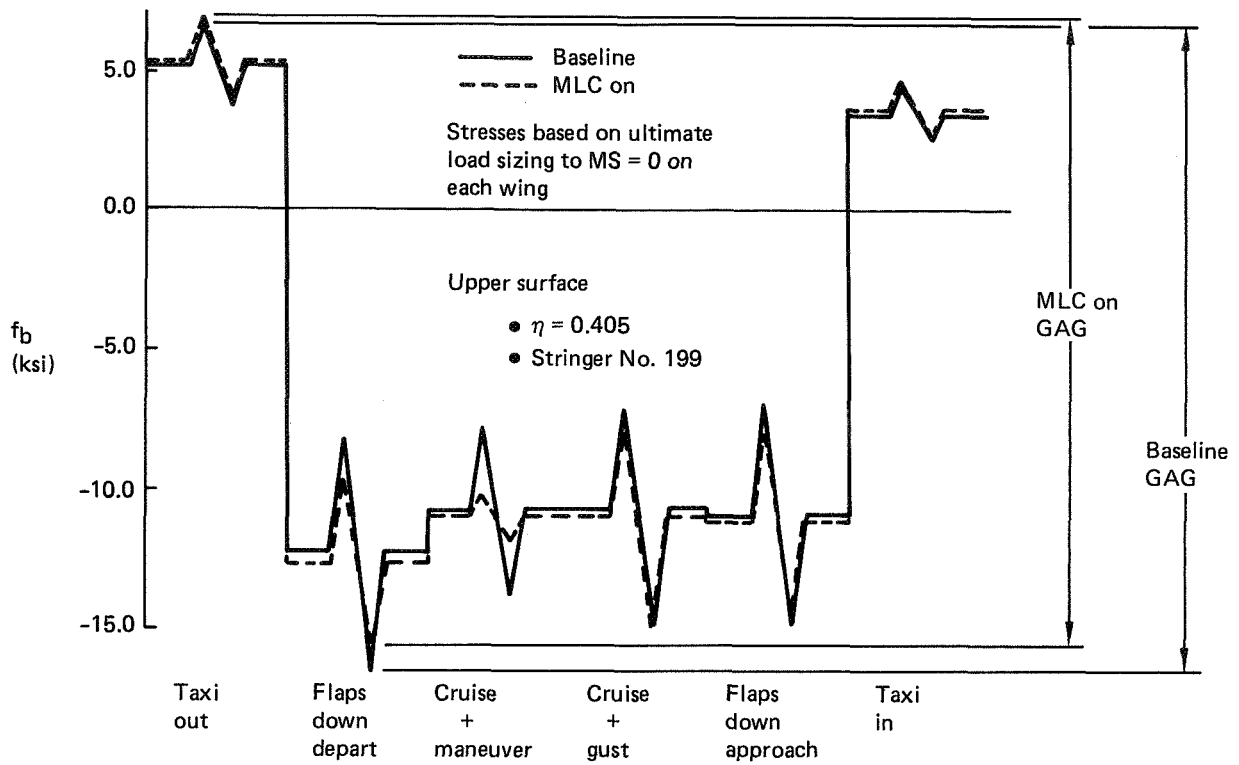


Figure 85. Fatigue Stresses at Specific Locations

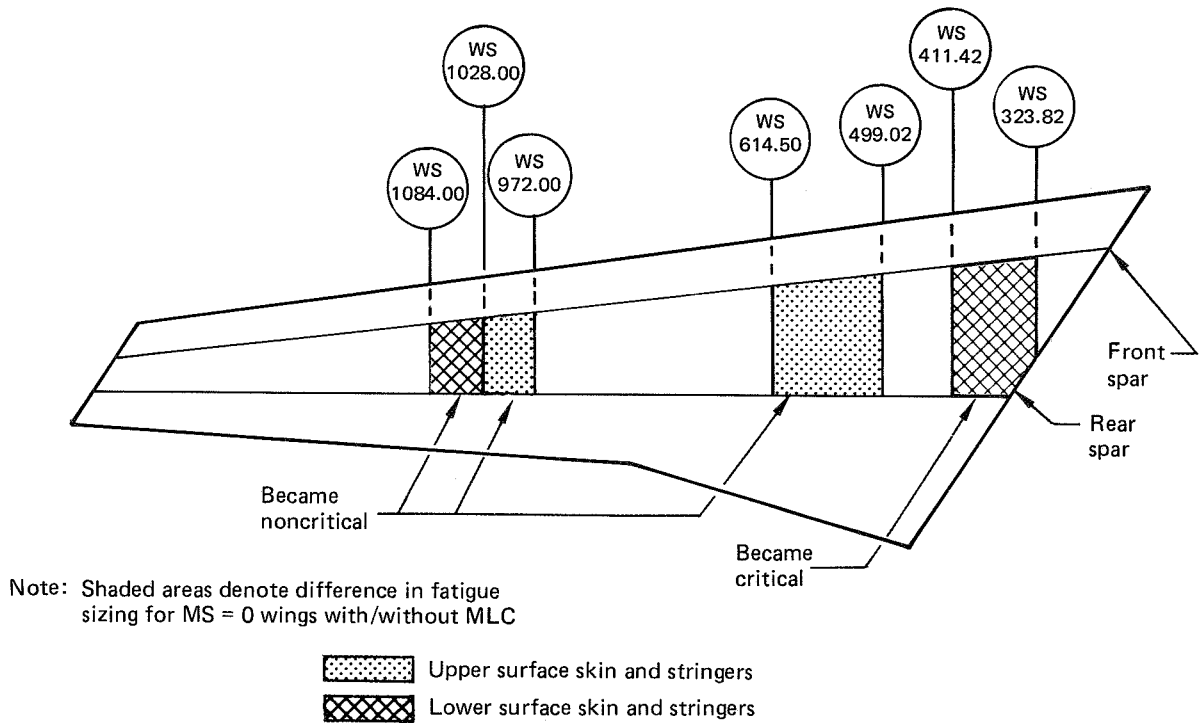


Figure 86. Effect of MLC on Fatigue Sizing

6.2.3 Weights

From the structural sizings of the baseline wing and the MLC wing, both with margins of safety zero, incremental weight changes were calculated to determine the benefits of MLC. Static maneuver and gust design conditions were evaluated together with weight increments for fatigue. No additional material was required for either the baseline or MLC wings to meet flutter stiffness requirements.

Estimated weight benefits of the MLC and GLA functions are indicated in Figure 87. The WLA system allows a wing box weight reduction relative to a baseline wing optimized without WLA. Not all of the wing box weight reduction can be realized in terms of reduced airplane operational empty weight, however, because of the added system weight (Table 5) as indicated on the figure.

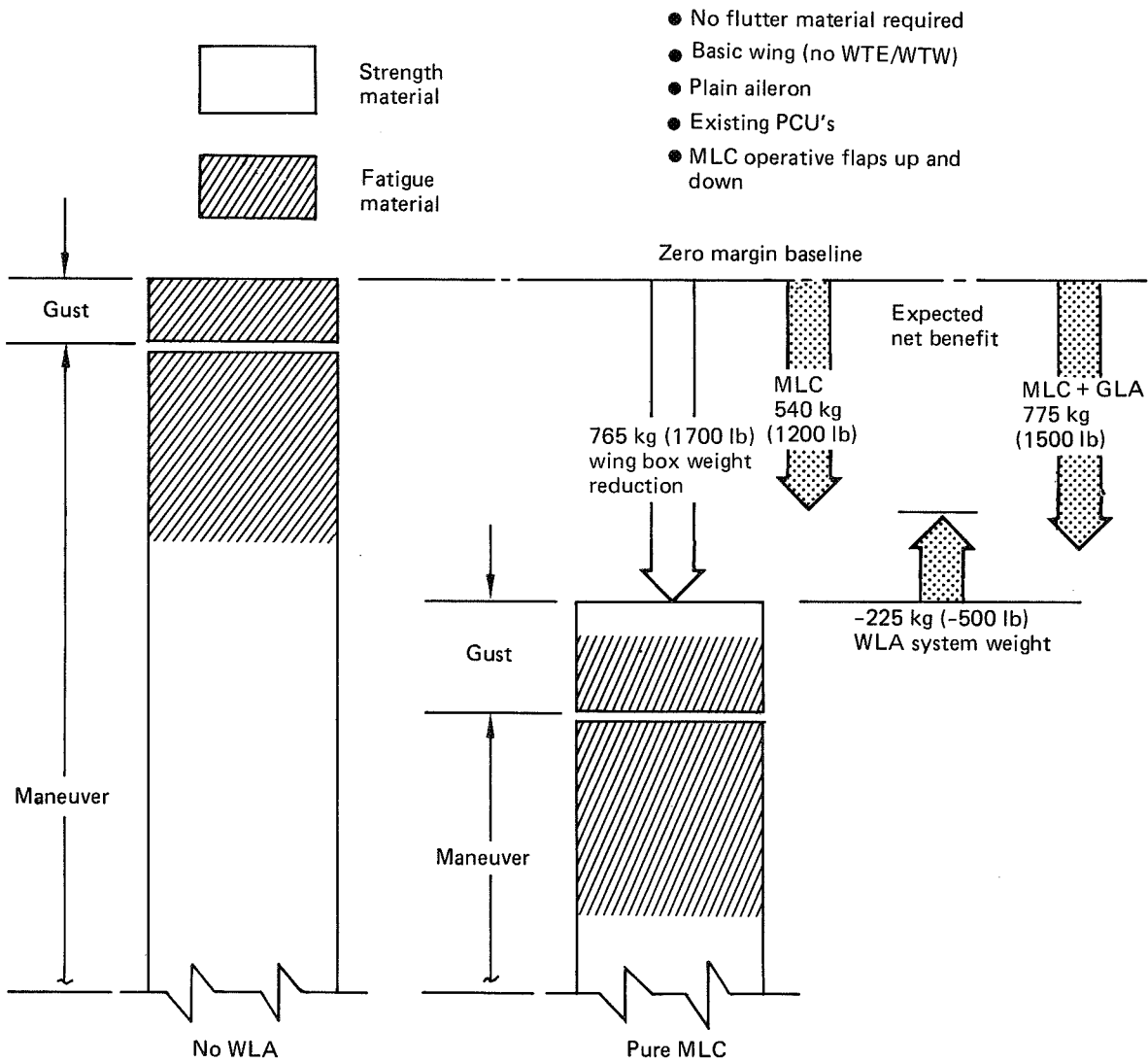


Figure 87. Wing Mass (Weights) with MLC

Table 5. Weights Breakdown for Final WLA System

	Per airplane		Total per airplane	
	Mass, kg	Weight (lb)	Mass, kg	Weight (lb)
Outboard plain aileron modification	—	—	136.1	(300)
Wing trailing-edge modification	—	—	22.7	(50)
WLA electrohydraulic control system			91.0	(200)
Outboard aileron control				
Integral servo/PCU	9.1	(20.0)		
Wing structural provisions	9.1	(20.0)		
Lateral control deletions	-17.5	(-38.6)		
	<u>0.7</u>	<u>1.4</u>		
Outboard elevator control				
Integral servo/PCU	9.1	(20.0)		
Elevator control system deletions	-12.3	(-27.2)		
	<u>-3.2</u>	<u>(-7.2)</u>		
Hydraulic tubing and fluid				
Outboard aileron	6.4	(14.0)		
Outboard elevator	6.4	(14.0)		
	<u>12.8</u>	<u>(28.0)</u>		
Electrical wiring				
Outboard aileron control	32.2	71.0		
Outboard elevator control	16.8	37.0		
	<u>49.0</u>	<u>(108.0)</u>		
System electronics				
System computers (2) GE-MCP-701A	18.1	(40.0)		
Accelerometers (6) QA-1200	4.1	(9.0)		
Pitch rate sensor (2) GE-VYROCRS-3	1.4	(3.0)		
Elevator signal transducer (2)	1.4	(3.0)		
Control panels	0.9	(2.0)		
	<u>25.9</u>	<u>(57.0)</u>		
Miscellaneous and roundoff	5.8	(12.8)		
Total MLC system + aileron modification			<u>+249.8</u>	<u>+(550)</u>

The wing box weight increment for the pure MLC function corresponds to alleviation of maneuver loads only. The actual WLA system also influences gust design loads, increasing them for some wing locations and reducing them for others. For the wing with pure MLC, about 272 kg (600 lb) of material is required for gust design. This is indicative of the maximum potential weight benefit for an ideal GLA system. It was estimated that only about half of the potential GLA weight benefit would be achieved by the actual system. Comparison of the shaded areas of Figure 87 shows about the same weight of fatigue material is required with or without MLC. The fatigue material required for gusts could be reduced by the GLA function.

6.2.4 Actuator Sizing

A study was conducted to evaluate the effect on wing box weight of the outboard aileron blowdown speed. Blowdown speed relates directly to actuator hinge moment capability. The results of the study allowed determination of an optimum aileron actuator size for maneuver load control.

Four wing structure sizings were made for the study. Wing structure was sized both with and without aileron blowdown at both high angle of attack (+HAA) and dive speeds (V_D). The resulting wing box weights were calculated from the sizings. Figure 88 shows the results plotted relative to a zero structural margin baseline wing. The data for the 2.5-g +HAA condition shows considerable weight reduction in the wing box as the aileron angle is increased. Conversely, the data for the 2.5-g V_D condition show how structural weight would have to be put back in the wing box as the aileron angle is increased to its mechanical position limit. The figure shows that to achieve the maximum weight benefit from using the aileron to its mechanical position limit, speed scheduling would be required such that the 2.5-g V_D conditions would not be critical for design. The current blowdown characteristics are such that the 2.5-g V_D condition would not be critical. Also, using the aileron to its mechanical position limit at +HAA speed would only achieve an additional 104 kg (230 lb) of wing box weight saving above that obtained at current blowdown levels.

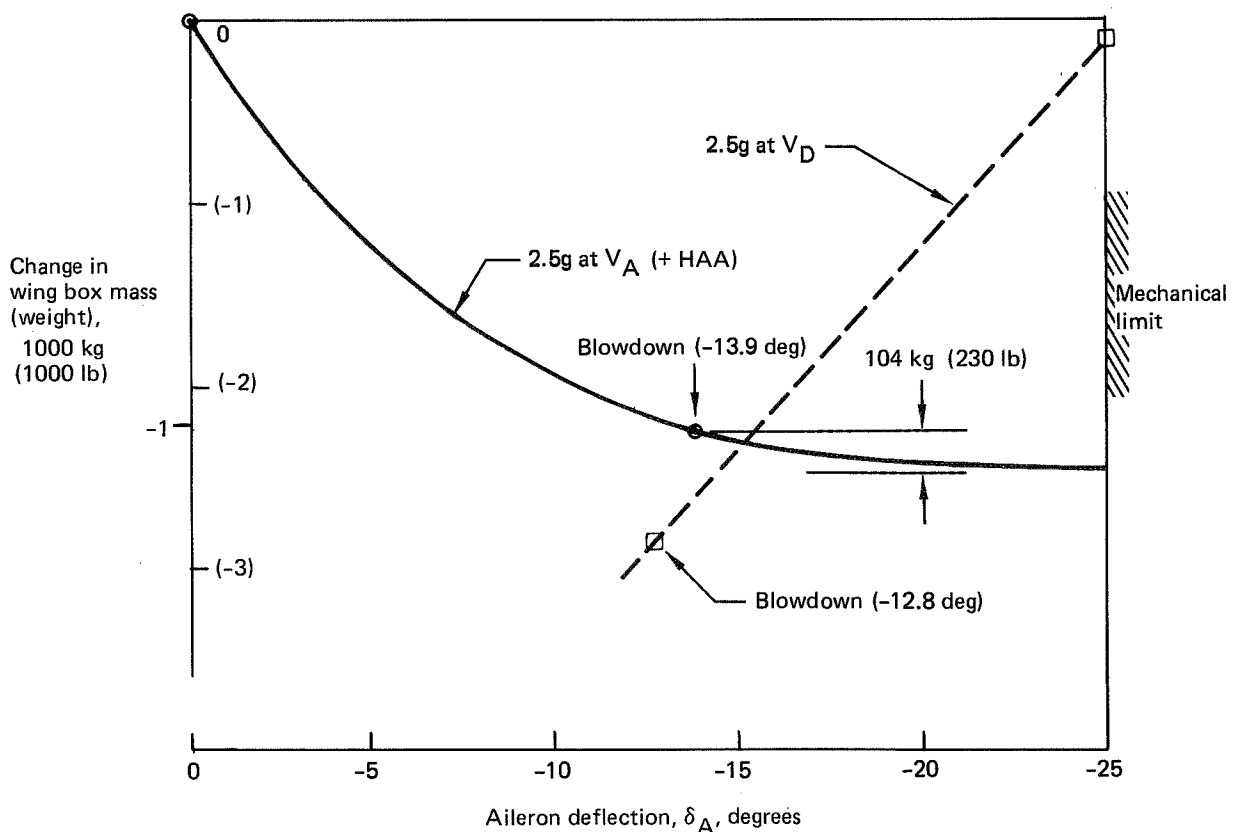


Figure 88. Effect of Aileron Deflection Capability on MLC Benefits

This study shows only a relatively small wing box weight reduction due to using the aileron to its mechanical position limit. An actual airplane weight benefit would be less than this because of increased actuator weight due to requirement for increased power, increased strength of aileron and back-up structure due to increased loads, and additional aileron balance weights.

Because of this relatively small weight benefit from use of the aileron to its mechanical position limit, it was decided to retain the existing actuator size (force capability) for the EET studies.

6.2.5 Gust Loads With Wing Load Alleviation

This section summarizes the gust load analysis for the WLA system on the basic wing. Results are shown for the base airplane (open-loop analysis) and with the WLA system (MLC + GLA) active (closed-loop analysis). The gust loads from the open loop analysis (i.e., controls fixed), were used for the structural benefits study. The closed loop results provide an indication of the GLA effectiveness of the WLA system.

The dynamic analysis used was similar to the analysis used for certification of the basic 747-200B airplane, except for modifications to include the WLA active control surfaces. The analysis is summarized in the following discussion, and the method used to account for the nonlinearities of the WLA system is shown. Selected results from a time domain simulation that modeled the rate and position limits of the WLA actuators are presented. Other results from the time domain simulation are reported in Section 6.3.1.

Airplane Model—Vertical translation, pitch, outboard aileron, outboard elevator, and 11 free-free symmetric structural modes were used to represent the airplane responses. The structural modes were derived using beam theory to represent the flexibility of the wing, fuselage, and horizontal tail. The aerodynamic forces were derived using strip theory with adjustments to match wind tunnel static pressure data for the analysis Mach number. Unsteady aerodynamic effects were accounted for using incompressible, infinite aspect ratio Wagner and Kussner functions. Structural damping of 0.03g was used, and gradual gust penetration effects were included. The loads were determined using the load summation method. The plain aileron was selected for the study, as discussed in Section 6.1.4, and the aileron effectiveness was based on the BTWT 1642 wind tunnel test.

The aerodynamic data used for the dynamic analysis, when reduced to steady state, showed good agreement with similar data from the static maneuver load analysis and the engineering flight simulator. Also, selected gust load results from the analysis were compared with results from an analysis using the Doublet Lattice lifting surface unsteady aerodynamic theory, and satisfactory agreement was demonstrated.

Analysis Approach—A PSD design envelope rather than a mission profile approach was used to determine the design gust loads. A mission analysis was not conducted because it was expected to be noncritical for the WLA configuration. This was because the critical high-speed design conditions that exhibit reduced WLA effectiveness due to blowdown and related aeroelastic losses are not included in the mission analysis method.

The design envelope loads were determined using the VonKarman spectrum of atmospheric turbulence with a scale of turbulence of 762m (2500 ft). The nonlineari-

ties of the WLA system were accounted for using the same method as that used for analysis of the 747 yaw damper system gust response. This method is discussed further below.

Results—Figure 89 shows the rms bending moment due to a 1 fps rms gust velocity. Results are shown for a gust penetration speed condition ($V_B = 310 \text{ KCAS/M} = 0.85$) and for a structural cruising speed condition ($V_C = 375 \text{ KEAS/M} = 0.875$).

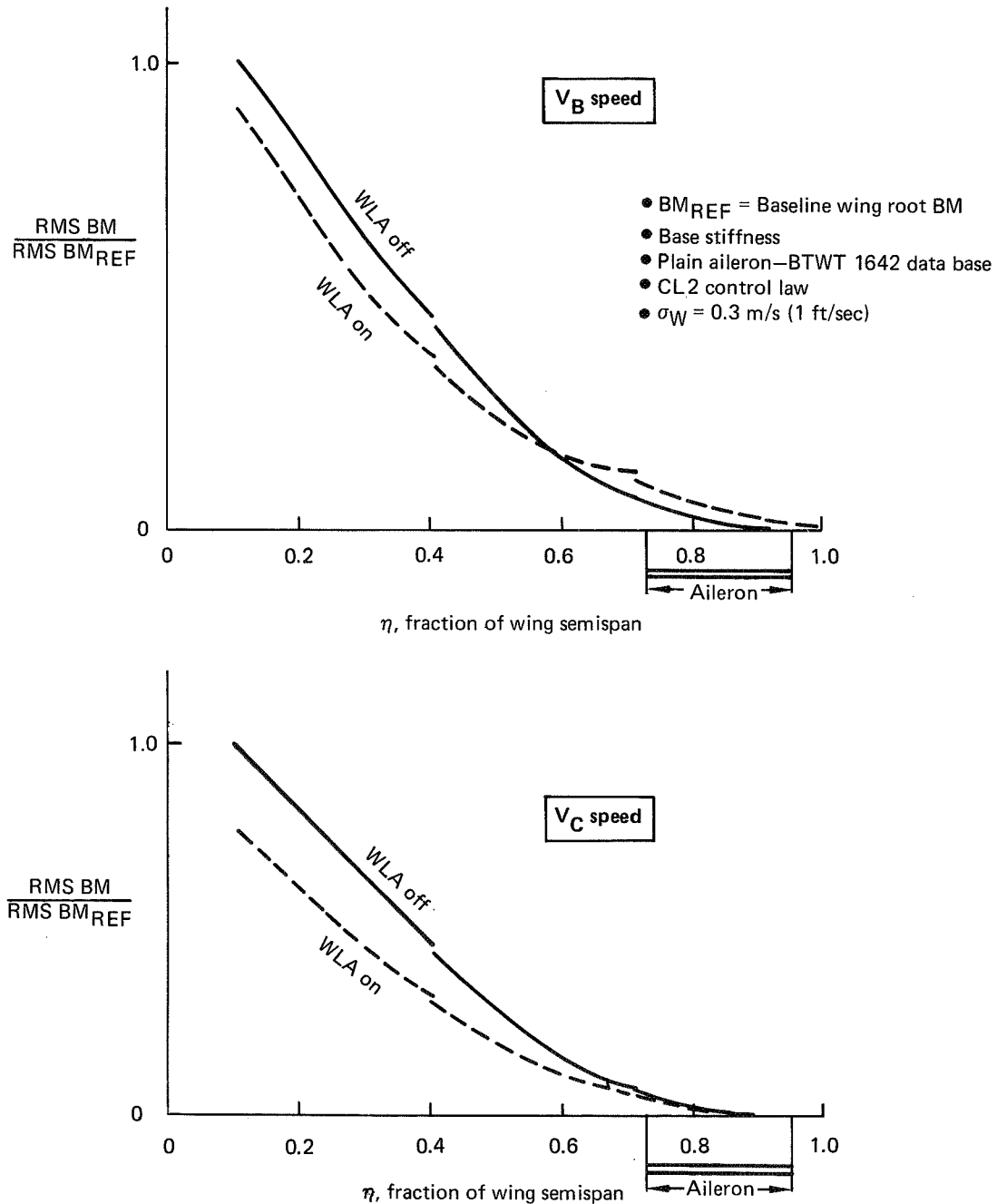


Figure 89. Effect of WLA on Wing RMS Bending Moments Due to PSD Gust

The WLA system significantly reduced the rms bending moment near the wing root but caused some increase outboard of $\eta = 0.57$ for the VC condition. The control law used for the GLA function was designed to provide maximum reduction in wing root bending moment for the VB condition that was the critical gust condition for the base airplane. This control law (denoted CL2) is shown and discussed in Section 6.4.2. Other control laws, also shown in Section 6.4.2, included variations in gain schedules that gave improved results over the outboard wing.

The effect of the WLA system on the net bending moment envelope due to gust is summarized in Figure 90. Results are shown for the base airplane (no WLA), for the

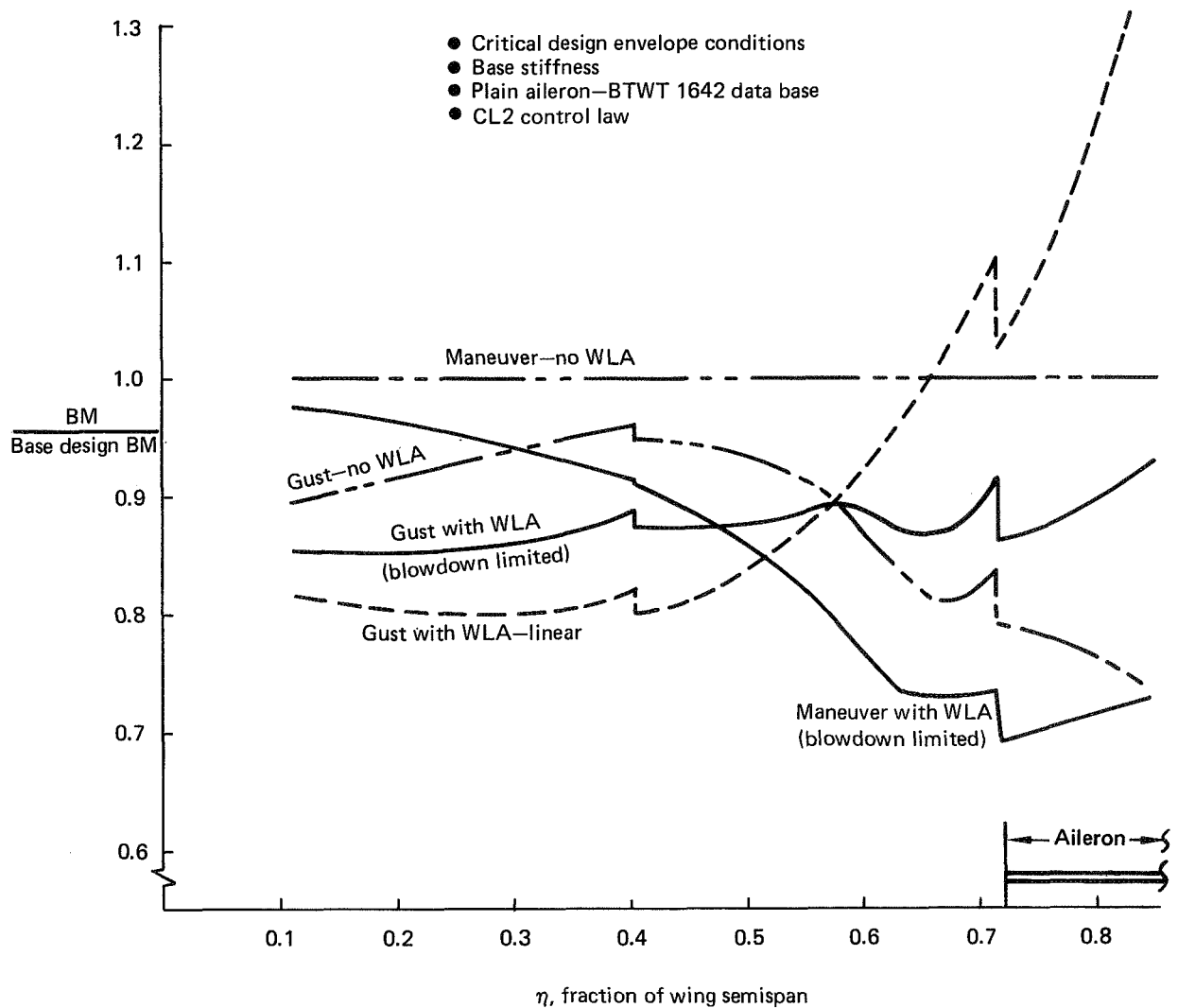


Figure 90. Effect of WLA on Wing Design Bending Moment Envelope—PSD Design Envelope Gust Versus Maneuver

WLA system active with unlimited authority (WLA on, linear), and with the effects of position limits included (WLA on, nonlinear). Similar results from the maneuver analysis reported in Section 6.4.1 are shown for comparison. This figure shows that the bending moment envelope for the base wing was formed by maneuver conditions. When the maneuver loads were alleviated by the MLC system, unalleviated gust conditions formed the envelope outboard of $\eta = 0.30$. When the WLA system was active for both maneuvers and gusts, the portion of the bending moment envelope formed by gust was limited to outboard of $\eta = 0.48$.

Nonlinear Analysis Method—Nonlinear results (with WLA on) were computed using the method illustrated in Figure 91. Load exceedance curves were constructed by numerically integrating the appropriate exceedance equation. The variation of rms load and zero crossing rate with rms gust velocity used for the exceedance calculations was based on an approximate method developed by Dempster and Roger (ref. 2) for analysis of the B-52 with active controls. Incremental gust loads were determined using the design envelope gust intensity value (U_{σ}) for the base airplane and with the WLA system active with unlimited authority. These values were used to derive allowable load exceedance rates for the design envelope conditions. The incremental gust loads with nonlinear WLA response were then read from the load exceedance curves using the derived exceedance rates.

Time Domain Simulation Results—As described in the next section, the time domain simulation used for WLA system development was modified for use in exploring the effects of aileron actuator rate and position limit effects on flexible wing dynamic loads. Data obtained from the simulation are shown in Figure 92 for several levels of turbulence. It was apparent from these data that actuator rate and position limit effects greatly reduced the gust load alleviation capability of the WLA system at the higher gust intensities, particularly on the outboard portions of the wing. Since the potential structural weight benefits of a GLA system were previously determined to be small even for an ideal system, an effort to "fine tune" the control law to obtain an optimum GLA function was not completed, nor was a full structural analysis conducted to determine the weight benefit for the GLA control law.

6.3 CLOSED-LOOP DYNAMIC ANALYSES

Closed-loop dynamic analyses were conducted to explore the effects of the WLA system on:

- Wing dynamic response to gusts (for the basic wing without WTE/WTW)
- Flutter (for the wing with the Z13 WTW)

In addition to conventional linear system analysis reported elsewhere, a time domain simulation incorporating actuator rate and position limits was used in examining gust response. One concern was whether or not aileron rate-limiting in severe turbulence would destabilize the wing bending mode. Results of frequency/amplitude sweeps indicated this was not a problem. Wing bending moment data obtained during the study were used in the evaluation of GLA effects on gust loads.

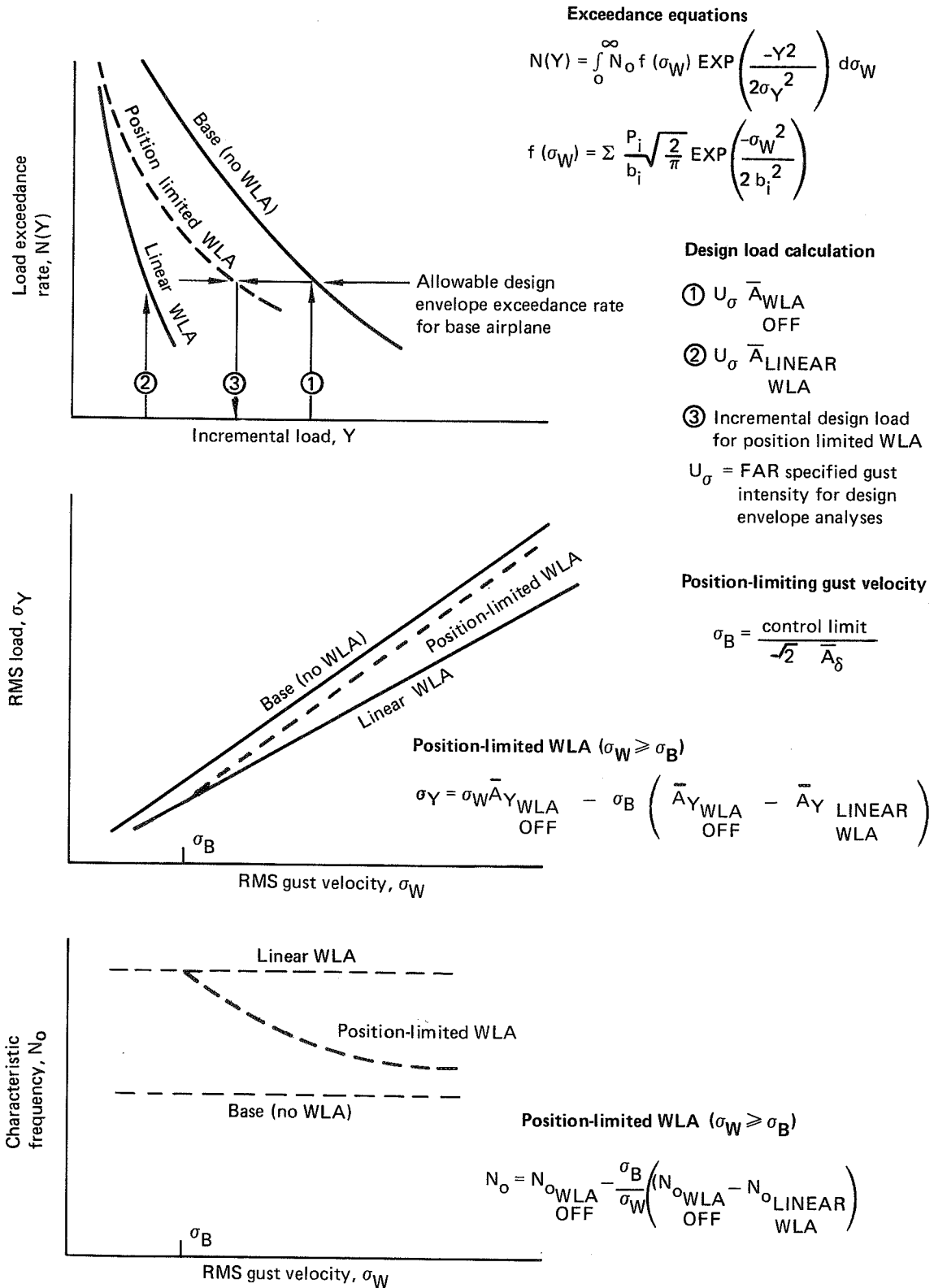


Figure 91. Design Envelope Gust Method for WLA System With Position Limits

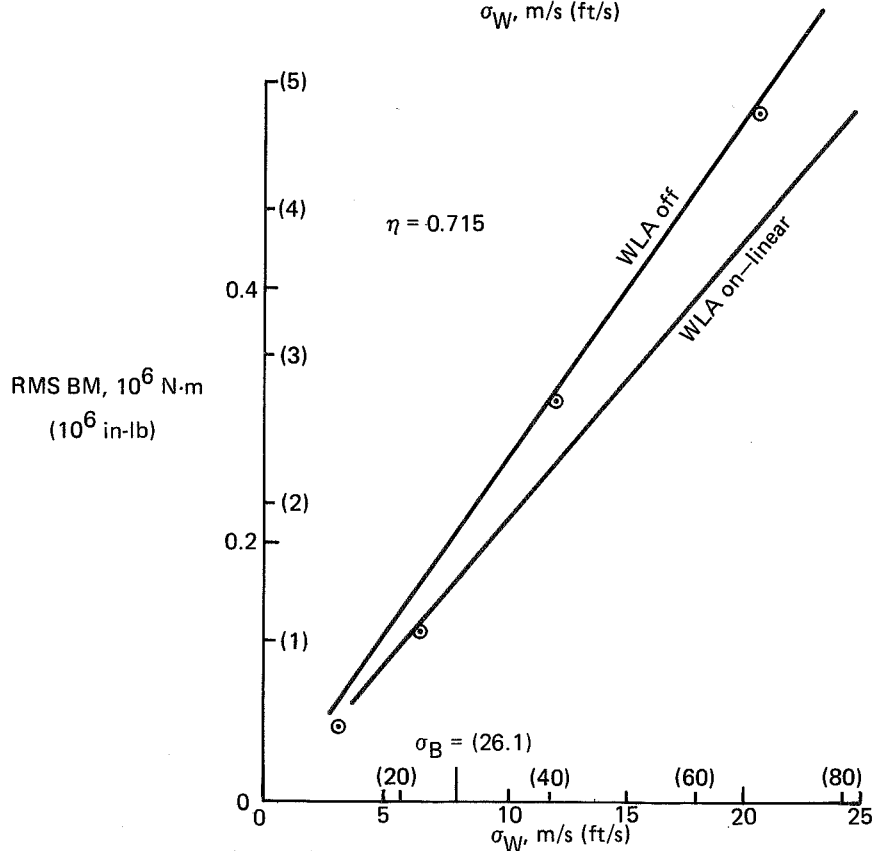
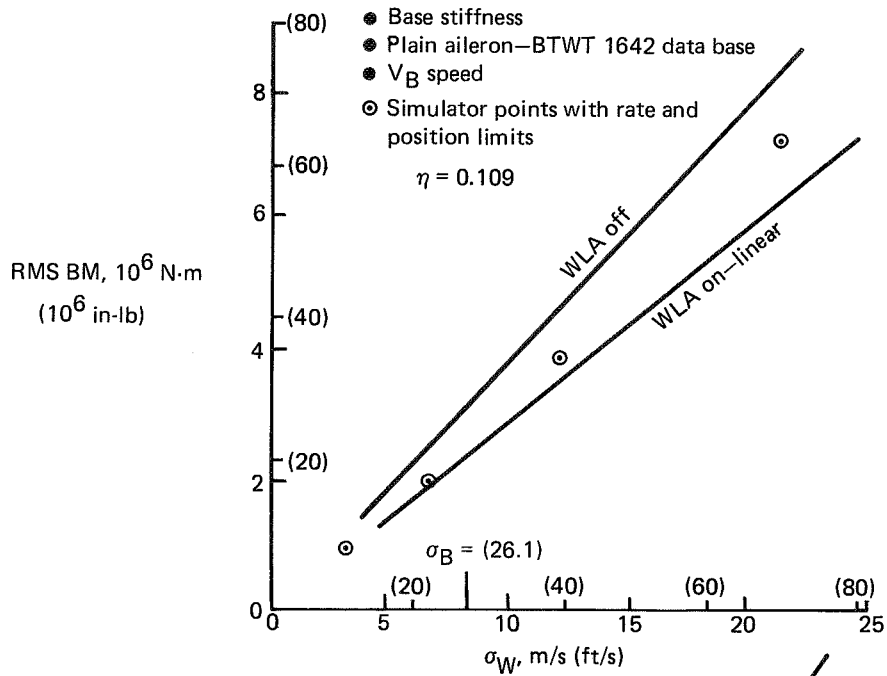


Figure 92. Effect of WLA Rate and Position Limits on Wing RMS Bending Moments Due to PSD Gust

Closed loop flutter evaluations were conducted for the wing with WTW by incorporating a linear representation of the WLA system into the conventional flutter analysis. Results indicated closed loop flutter speeds are lower than open loop.

The MLC/GLA control law (incorporating cg and wing accelerometers, and pitch rate feedback) was used for both studies. The gust studies were conducted using structural dynamics for the basic wing so as to provide continuity with the other WLA system/benefits analysis. The flutter studies were conducted for the wing with the Z13 WTW because 1) closed loop analysis for the basic wing were accomplished as part of the Boeing WLA Demonstration program, and 2) the symmetric flutter mode from the winglet configuration was considered to be more likely to couple adversely with the WLA system (than the antisymmetric flutter mode of the basic wing).

6.3.1 Rate/Position Limit Effects on Gust Load Alleviation

The benefits of gust load alleviation are limited by the control surface actuator capabilities. In high-intensity turbulence the control surface actuators experience both position and rate limiting. Only a portion of the potential weight savings for GLA can be attained by the actual GLA system. The effect of the saturated actuator response on closed loop stability is summarized in this section.

For this study the system equations were developed in the time domain. Equations of motion for the flexible airplane were reduced from the set used in the dynamic loads analyses (sec. 6.2.5). The airplane degrees of freedom modeled were two rigid body modes, pitch and plunge; three flexible body modes, the first, second, and fourth; and the elevator and outboard aileron control surfaces. Unsteady aerodynamics were represented with the Kussner and Wagner functions for an aspect ratio of six in lieu of infinite aspect ratio. This was done to simplify the simulation math model representation by reducing the order of the filter. The effect of gradual gust penetration was not included.

A schematic of the actuator model is shown in Figure 93. Aerodynamic loading was represented as a simple spring. This force results in nonlinear valve flow rate as well as elastic deflections of the control surface, the actuator rod, and the actuator support structure. Rate and position limiting due to the control surface hinge moment are implied by the nonlinear valve flow rate. Additional actuator nonlinearities are limited valve and cylinder travel.

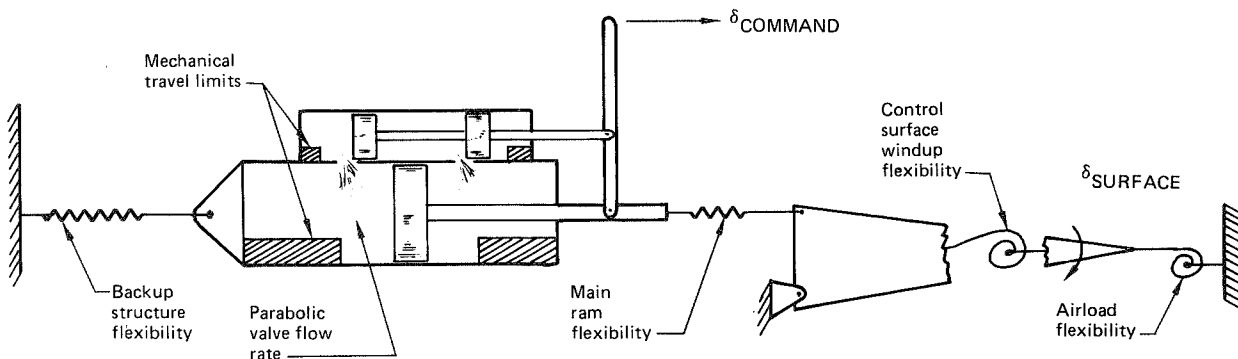


Figure 93. Power Actuator Model

A block diagram of the control laws used in this study is shown in Section 6.4.2.

Turbulence intensity rms levels are listed in Reference 1 for clear air turbulence and thunderstorm turbulence. For thunderstorm turbulence a level of 6.4 m/sec (21 ft/sec) is stated. The WLA system is predicted to respond linearly in clear air turbulence. However, in more severe turbulence the control surface actuators experience both position and rate limiting.

In addition to closed-loop stability analysis, the purpose of the simulation was to determine the variation of rms responses at turbulence intensities ranging to several times the thunderstorm level. System stability, however, had to be confirmed to establish the validity of these rms measurements.

To evaluate the closed-loop stability the airplane was forced with sinusoidal gusts at each modal frequency. Any tendency toward instability depends on the magnitude and frequency of the gust. As opposed to random turbulence, the sinusoidal excitation allows this situation to be clearly identified. The atmosphere was modelled with the Dryden spectrum, and the gust amplitude was weighted accordingly at each frequency. At the short period mode frequency the gust amplitude was approximately 30% of a given level of gust intensity. At the structural mode frequencies the gust was attenuated considerably more.

Figure 94 shows time histories of the WLA system motion sensors and the outboard elevator and aileron position, and rate responses to a large amplitude gust. A sinusoidal gust at the short period mode frequency is stepped to zero after several cycles. Blowdown limits the position and rate capability of both the elevator and aileron actuators. However, the system remains stable throughout the continuous input and the responses achieve a steady state. After the gust is stepped to zero no oscillations are sustained, and the transient response decays to zero.

The effect of the nonlinearities is not as evident at the structural mode frequencies as a result of the rolloff of the Dryden spectrum. Only aileron rate limiting occurs at the first elastic mode frequency, and the system remains stable. At the second and fourth elastic mode frequencies the response is linear.

The significance of the actuator nonlinearities on surface rates and position at various levels of random turbulence is illustrated in Figures 95 and 96. Effects on rms loads were also recorded and are discussed in Section 6.2.5. The aileron rms position and rate are shown in Figure 95 for the linear and nonlinear WLA systems. Position and rate limiting are reflected in the rms response as expected. In light turbulence, less aileron than the linear system predicts is the result of the flexibility of the actuator backup structure and windup of the control surface. The elevator response, as shown in Figure 93, for the nonlinear system is greater than that for the linear system. Although the aileron experiences rate and position limiting in heavy turbulence, the effect of blowdown on the outboard elevator is much less. Consequently, the elevator deflection to compensate the aileron pitching moment is more than needed, and the airplane becomes more pitch responsive. The additional pitch rate results in more elevator being commanded through the pitch rate control path. As is evident in the response of both control surfaces, the actuator nonlinearities are not significant in this case for turbulence up to the thunderstorm level.

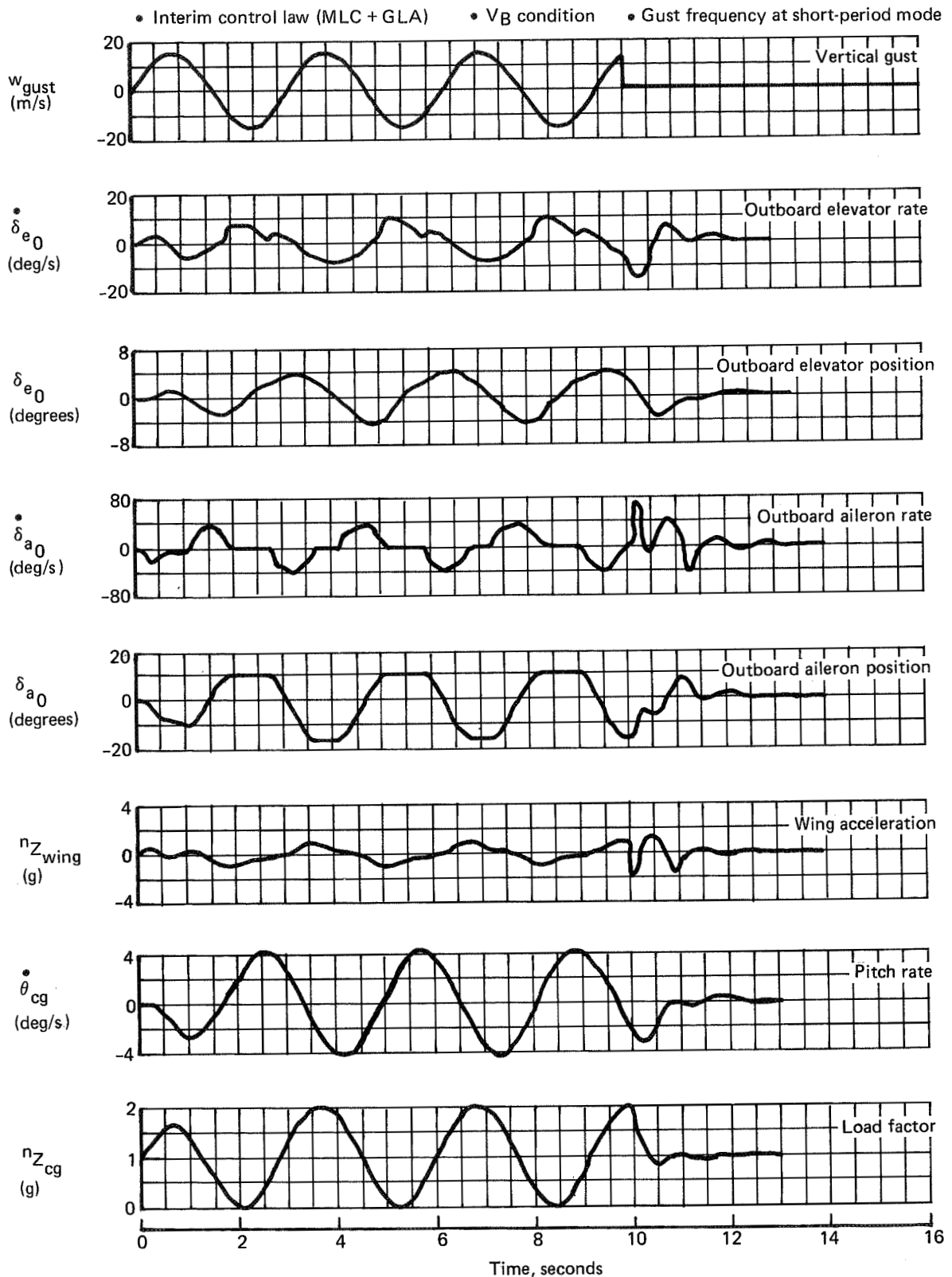


Figure 94. WLA Stability Evaluation with Blowdown in Large Amplitude Gust

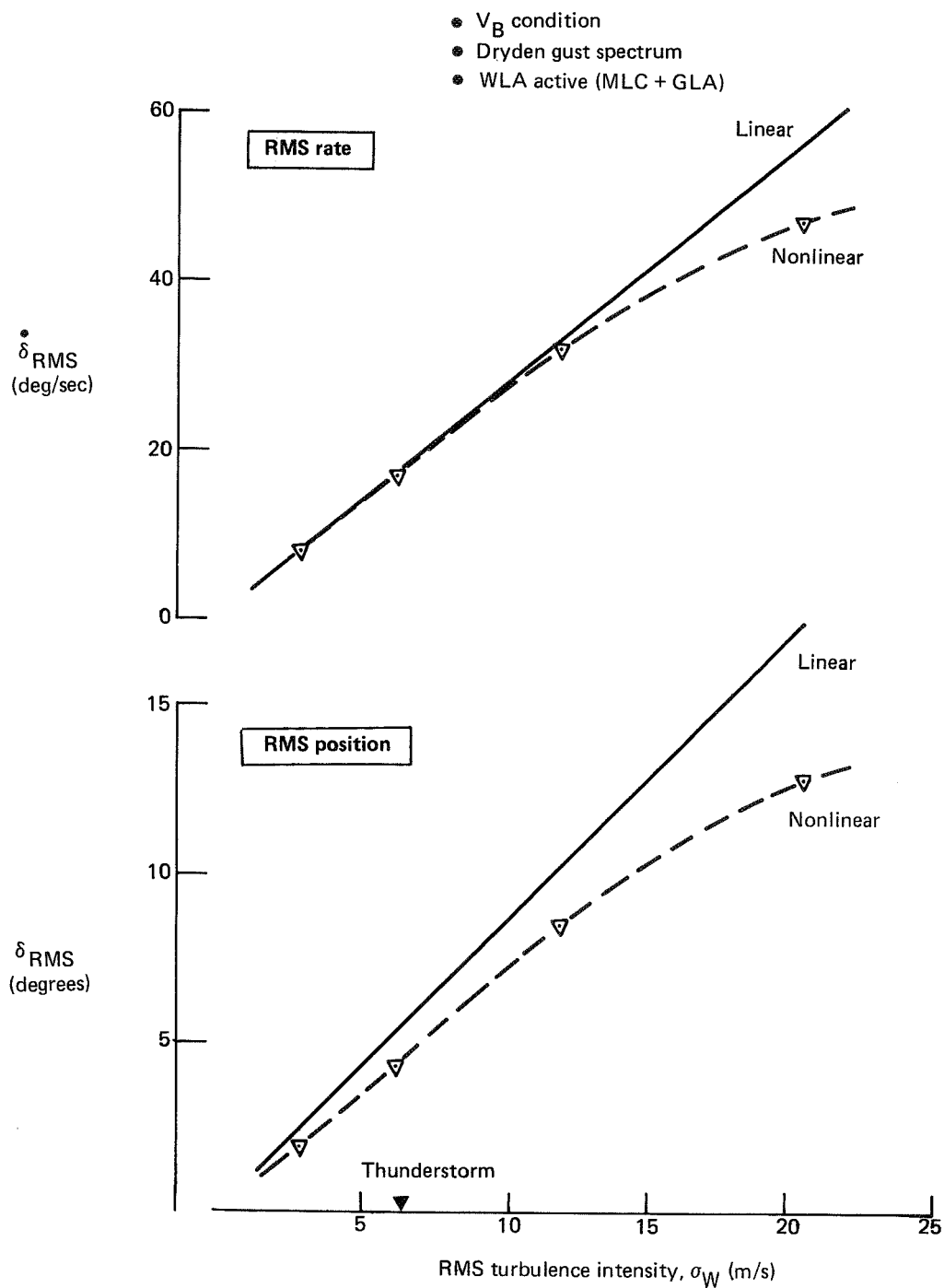


Figure 95. WLA Aileron Response to Turbulence

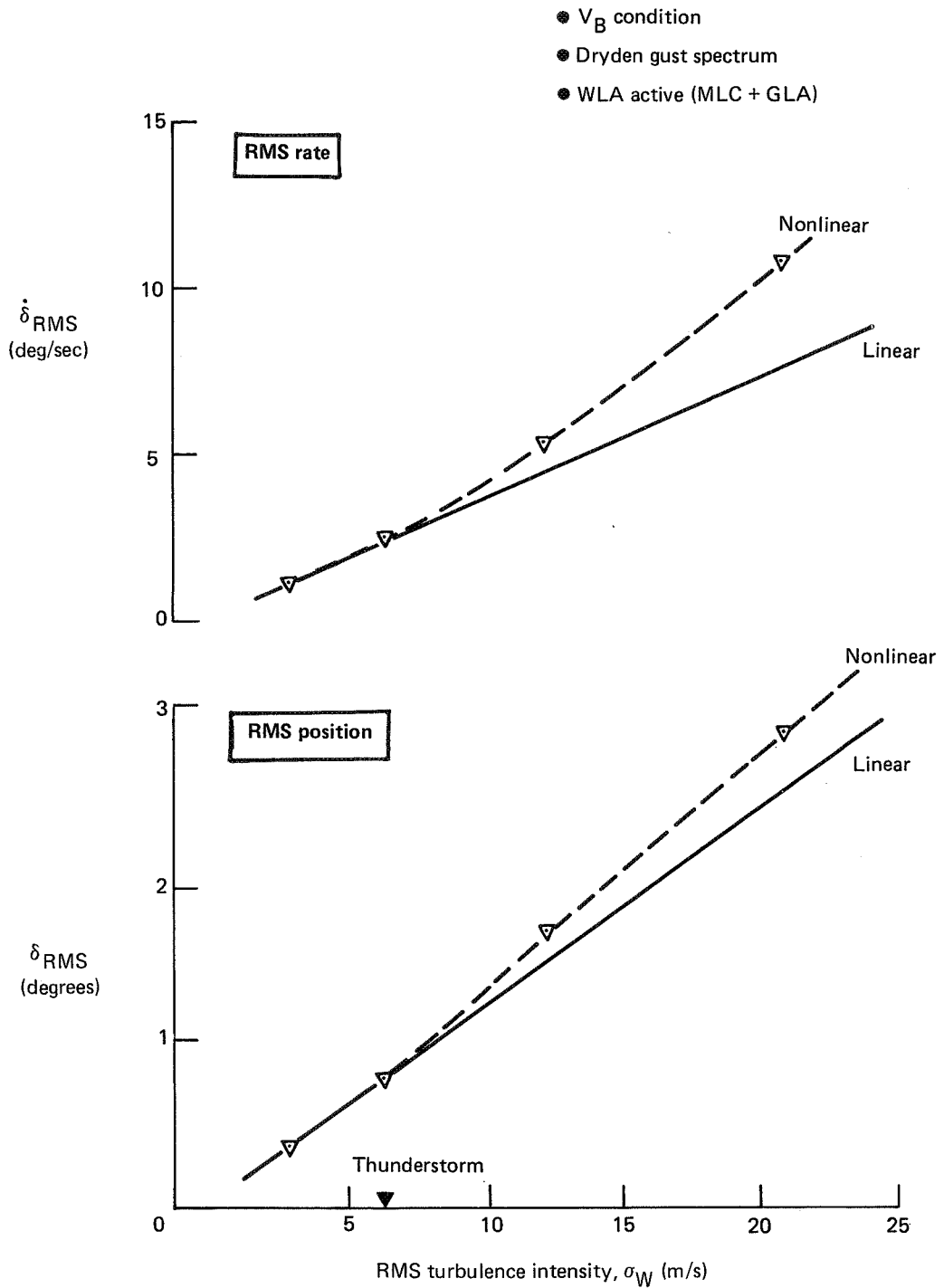


Figure 96. WLA Elevator Response to Turbulence

6.3.2 Maneuver Load Control/Gust Load Alleviation Effects On Flutter

Closed-loop studies were accomplished on the 747 EET/Z13 MLC plus GLA configuration to assess the feedback effects of the MLC and GLA systems on flutter stability.

Closed-loop flutter analyses with the MLC/GLA system were performed only in combination with the wing tip winglets. The results and descriptions of these studies are reported here as appropriate to the overall closed-loop dynamic analyses. Descriptions of the final WTW configuration are found in Section 7.1.3 in conjunction with the open-loop flutter studies.

Figure 97 is a schematic of the system analyzed. Inputs from body center of gravity and wing accelerations and body pitch rate are used to control maneuver and gust

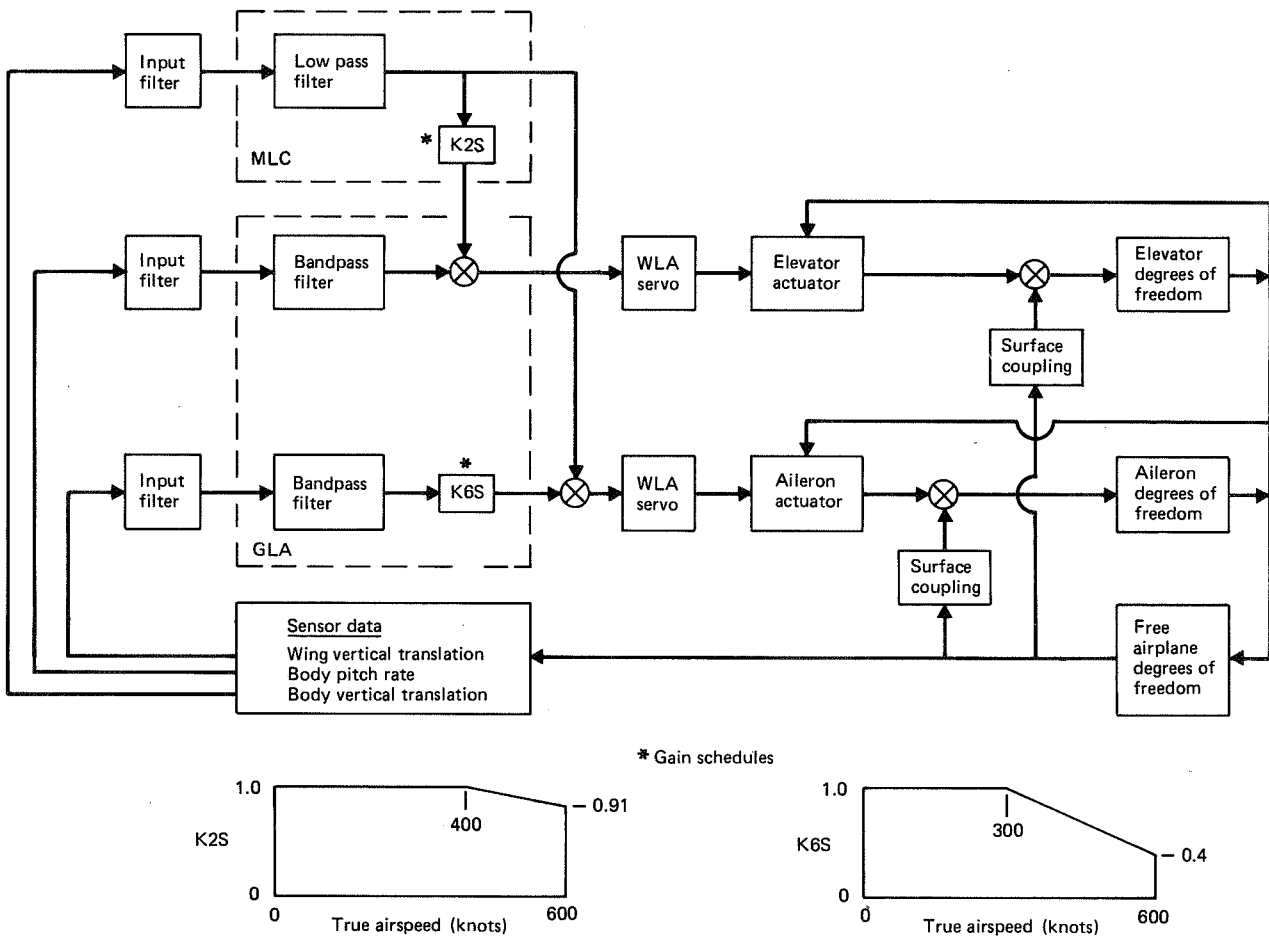


Figure 97. MLC/GLA Control Law and Gain Schedules for Flutter Analysis

loads with the outboard ailerons and outboard elevators. The system as designed can only affect the symmetric modes. Figures A-6 and A-7 of Appendix A show the structural and aerodynamic models used. The open-loop analysis used the improved methodology with the addition of aileron and elevator rotation degrees of freedom.

The closed-loop analysis adds the feedback effect with the transfer functions and actuator properties to the open-loop formulation in the S-plane. The problem is then solved for the usual flutter parameters of velocity, frequency, and damping.

Figure 98 shows the comparison of the critical open and closed-loop symmetric flutter modes for the final WTW configuration. The closed-loop solution results in flutter speeds lower than those of the open-loop solution. As noted on the schematic, the MLC and GLA systems have gain scheduling that is used to reduce the authority of the feedback loop at higher airspeeds. The flutter speeds are in the velocity range where the reduced gains apply. With an assumed structural damping ratio of 0.015 in the symmetric mode, the result of the closed-loop solution with reduced gains is considered acceptable. No other gain or phase variations were analyzed.

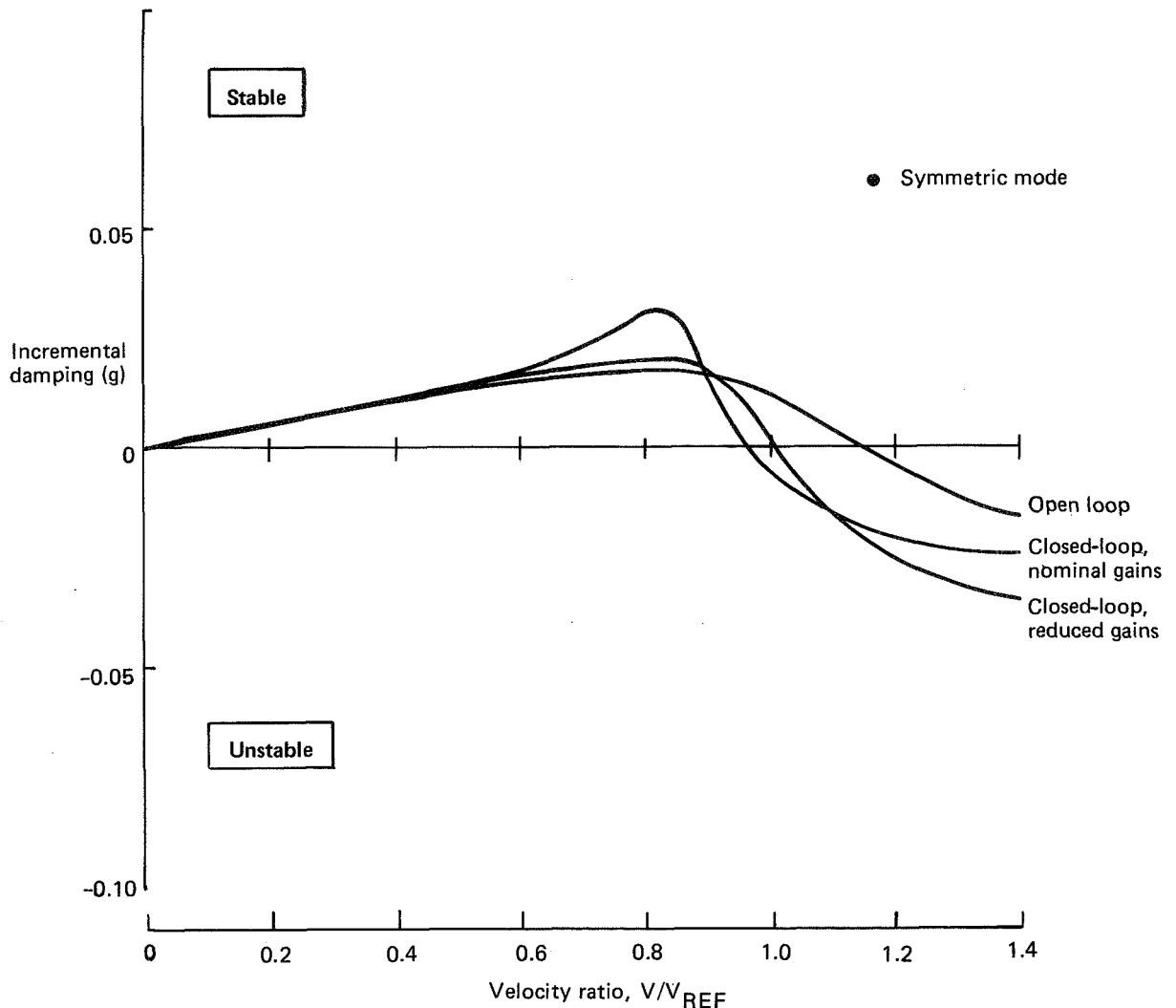


Figure 98. Flutter Stability Comparisons for MLC and GLA With WTW

6.4 SYSTEM CONFIGURATION DEFINITION

The recommended WLA system is a digital, dual channel configuration with fail-operate capability. In-line monitoring techniques are applied and electrohydraulic power actuators for both the outboard elevators and ailerons are implemented for cost and weight savings. The system installation includes provisions for electrically transducing primary flight control commands. These primary flight control commands are summed with the WLA commands in the servo electronics. In the final control law design, the GLA function (which includes first elastic mode suppression) and the MLC function are incorporated through the use of wing accelerometers. For fail-operate capability the sensors are triple redundant. Failure detection and signal selection are performed in each computer. High reliability, comparable to that of a dual, independent yaw damper system, is achieved with the final system mechanization.

6.4.1 Study Approach and Criteria

Control Law—A review of past active controls applications (ref. 3 and 4) provided a baseline for the development of the 747 EET WLA control laws. The functions selected for study on the basic wing (no WTE/WTW) were MLC and GLA. These were judged to potentially have greater payoff with less design complexity than other active control functions.

The objective of the MLC function was to reduce wing design bending moments for maneuvers by deflecting the outboard ailerons symmetrically. For this conceptual development study the aileron command was scaled to provide full deflection, trailing edge up at 2.0g; i.e., 0.5g before the design load factor of 2.5g was reached. Significant reductions in this gain could probably be achieved without adversely affecting the structural benefits since the aileron is blowdown-limited at critical flaps-up load conditions. A gain reduction would be favorable in several areas (e.g., gust loads, compensation for MLC-induced pitching moments, buffet margins in maneuvers) and should be considered in a production hardware development program. The objective of the GLA function was to reduce the wing root bending moment due to random turbulence (a PSD approach). To accomplish this, the outboard ailerons were used to provide quasi-steady lift reduction in low-frequency gusts and to increase the damping of the first wing bending mode. In preliminary studies, the outboard elevators were used to damp the airplane pitch response in gusts, but this feedback path (and the associated feed-forward path to augment the pilot input to the elevators) was not included in the final system configuration.

Studies were conducted for the basic 747 configuration without WTE or WTW. Design concepts for the control law were assumed to be independent of wing tip modification. The effect of WLA combined with either WTE or WTW is discussed in Section 7.0. Control law analysis was conducted with the existing (untabbed) aileron configuration.

The following stability criteria were applied to the control law design:

- Control system coupling with structural modes other than the first symmetric wing mode be minimized
- The system remain stable with sensor location variations up to 1.52m (60 in) in any direction
- The structural modes have the gain and phase margins shown in Table 6

Table 6. Gain and Phase Margins

Modal frequency (Hz)	Airspeeds up to V_D		Airspeeds between V_D and $1.2 V_D$	
	Gain margin (dB)	Phase margin (deg)	Gain margin (dB)	Phase margin (deg)
<0.75	+4.5	± 45	±3.0	± 30
0.75-5.0	+6.0	± 60	+4.5	± 45
>5.0	+8.0	+180	+6.0	+180

With WLA active no degradation of the basic airplane ride and handling qualities were to occur. Ride improvement was a desirable objective but not a requirement for this study. Activation of WLA also was required to be compatible with the performance of other flight control systems, such as the autopilot.

System Mechanization—A dual channel, fail-passive configuration was baselined for the initial WLA mechanization studies. Reliability analysis of this configuration indicated the need to retain system operation following a single failure. In judging the reliability, a dual yaw damper system, being similar in function, was used as a guideline. For the final system implementation the goal was to achieve minimum complexity and cost with reliability comparable to that of a dual yaw damper system.

In-line monitoring techniques were applied to gain fail-operate capability with a dual channel configuration. This approach increased parts count relative to the fail-passive configuration but required significantly fewer parts than a triple channel "brick-walled" approach. New integrated actuator packages for the outboard elevators and ailerons were selected to provide hydraulic redundancy for the WLA system. From trade studies with a hydromechanical concept, an electrohydraulic package was recommended as being lighter, cheaper, and having better performance. The existing actuator force capabilities were retained. Rationale for the actuator sizing is discussed in Section 6.2.4.

A digital computer was determined to be the most cost effective means to provide built-in test capability for fault monitoring and preflight and maintenance tasks. Other considerations in the selection of a digital computer were its reliability and the compatibility of the WLA system with future systems. Criteria for fault isolation required that identification of a failed component to a line replaceable unit be 90% successful. The probability of an active (hardover or oscillatory) failure was required to be extremely remote (less than 10^{-9}).

For the final WLA system, dispatch with no flight restrictions was allowed with only one channel operational. Dispatch without WLA was permitted, but restrictions on takeoff gross weight and maneuver limits were imposed. Complete loss of the system during flight did not impact safety. Continuation of the flight was possible with precautionary measures, such as avoiding steep turns or other high-g maneuvers, necessary.

6.4.2 Control Law

The control law for the final WLA system incorporates first elastic mode suppression with the primary function, MLC. Two flight conditions, the gust penetration speed condition, V_B , and the structural cruising speed condition, V_C , were analyzed for elastic mode dynamics. The flexible airplane model was the same as that used for dynamic loads analyses (sec. 6.3.4) but without the effect of gradual gust penetration. Additional flight conditions were analyzed with quasi-static aeroelastic equations of motion to evaluate handling qualities.

Final Control Law—A block diagram of the final control law is shown in Figure 99. From an accelerometer mounted on each wing, symmetric vertical motion is sensed by averaging the two signals. The filtered signal commands symmetric outboard aileron for elastic mode suppression as well as maneuver load control. The gains are reduced when the flaps are extended. To compensate for the aileron pitching moment, the outboard elevators are commanded proportionately. During lateral maneuvers, with the flaps extended, the WLA authority is reduced to give roll control priority. Engage/disengage transients are minimized with an easy on/off circuit.

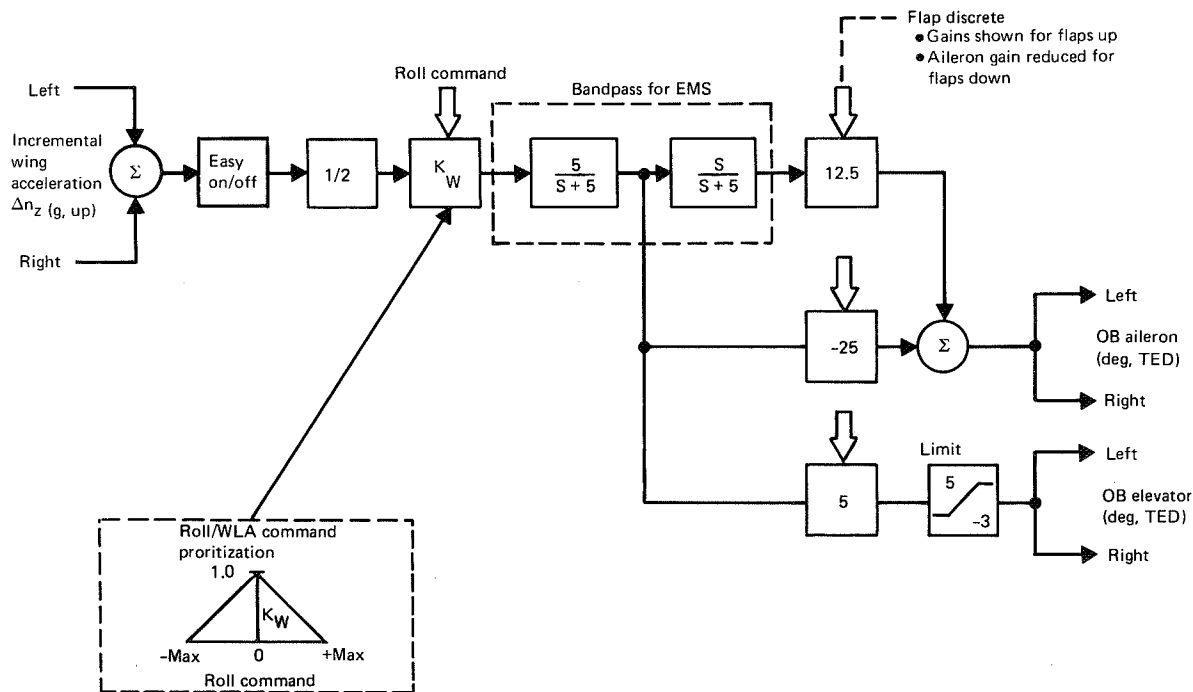


Figure 99. Final Control Law Diagram

The mode line for the first elastic mode, which is predominantly first wing bending, is on the wing. Use of cg acceleration feedback to the outboard ailerons for the MLC function results in adverse coupling with this mode. A wing accelerometer to outboard aileron path augments the first elastic mode stability in a manner advantageous for load alleviation. This sensor also measures rigid body motion that is required for the MLC function. To facilitate the filter design, the wing accelerometer is located where motion of the first mode is appreciable, while activity of the other elastic

modes is slight. Near the outboard nacelle is a region of confluence of node lines for the second through sixth elastic modes. The sensor was located in this region on the front spar for this feasibility study. The practicality of this sensor location must be further evaluated in a hardware development program, considering the effects of the vibration and climatic environment and the effects of accelerometer tilt due to variations in steady-state wing deflections.

The feedback signal is filtered to the outboard aileron in two parts. For MLC, the rigid body motion is sensed with a low pass filter. The break frequency is chosen to minimize the phase lag at the short period mode frequency. Implementation of this filter in the computer hardware also eliminates high-frequency input signals to prevent aliasing. This feedback path provides good MLC performance but couples excessively with the elastic modes. The second filter path controls this coupling to achieve elastic mode suppression. Activity of the elastic modes is sensed with a high pass filter. The filter in series with the low pass filter forms a bandpass network centered near the frequency of the first elastic mode. The output of this filter is subtracted from the MLC signal and results in the proper augmentation of the first mode stability. Also, coupling with other elastic modes is reduced.

Feedback to the outboard elevators has a negligible effect on the elastic modes. This signal is scaled in proportion to the aileron MLC command to compensate for the aileron pitching moment. The effect of the aileron and elevator path gains on the short period mode damping and frequency is shown in Figure 100. With only the outboard aileron loop, the WLA system significantly alters the short-period mode characteristics. However, damping and frequency not appreciably different from that of the basic airplane are achieved with the outboard elevator loop included. The small differences can be attributed to a compromise value of the elevator path gain for various flight conditions and to unbalanced lift changes from the aileron and elevator. In a typical mission, scheduled gain variations have not been found necessary to maintain acceptable performance, flaps up. The pitch compensation is limited to that needed with the ailerons fully deflected.

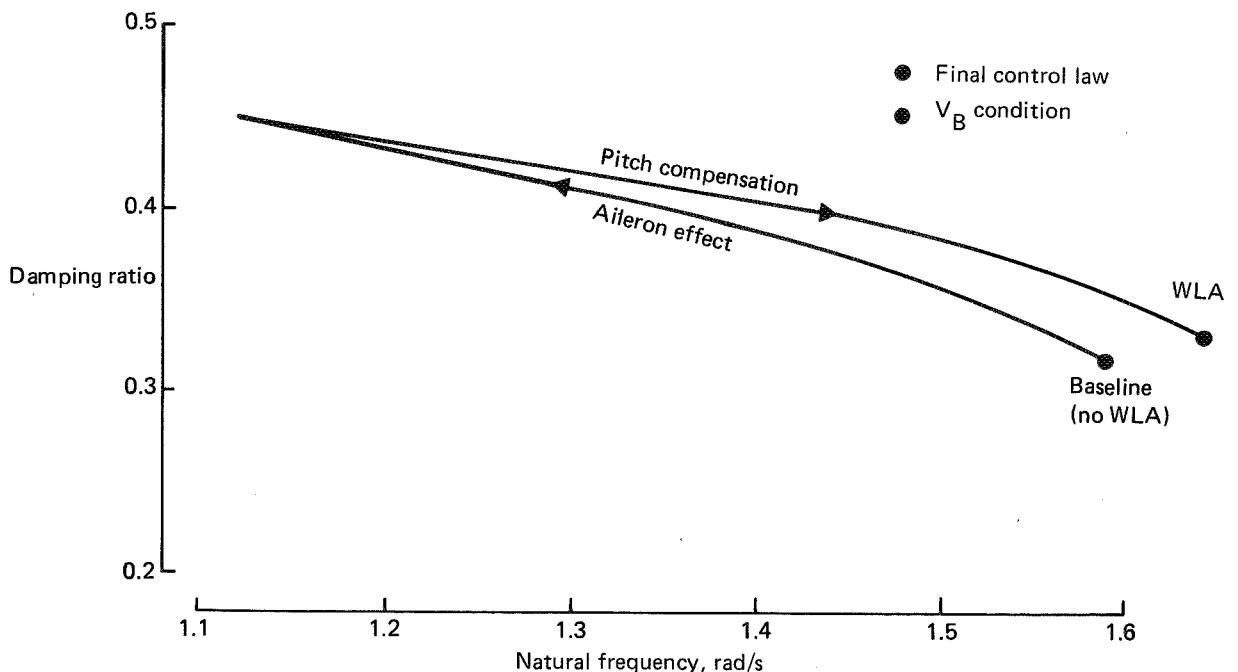


Figure 100. Effect of WLA on Airplane Short-Period Characteristics

Stability—The stability of the final WLA system at the V_B condition is shown in Figure 101. Relative to the basic airplane, the first elastic mode has increased frequency and approximately twice the damping. The fourth elastic mode is modified but has increased stability. System stability at the V_C condition is shown in Figure 102. At this condition the aileron is less effective. Very little change to the first elastic mode characteristics occurs. Coupling with the fourth and sixth modes is appreciable. The stability of both, though, is increased. At both conditions, the short period mode damping and frequency have not significantly changed.

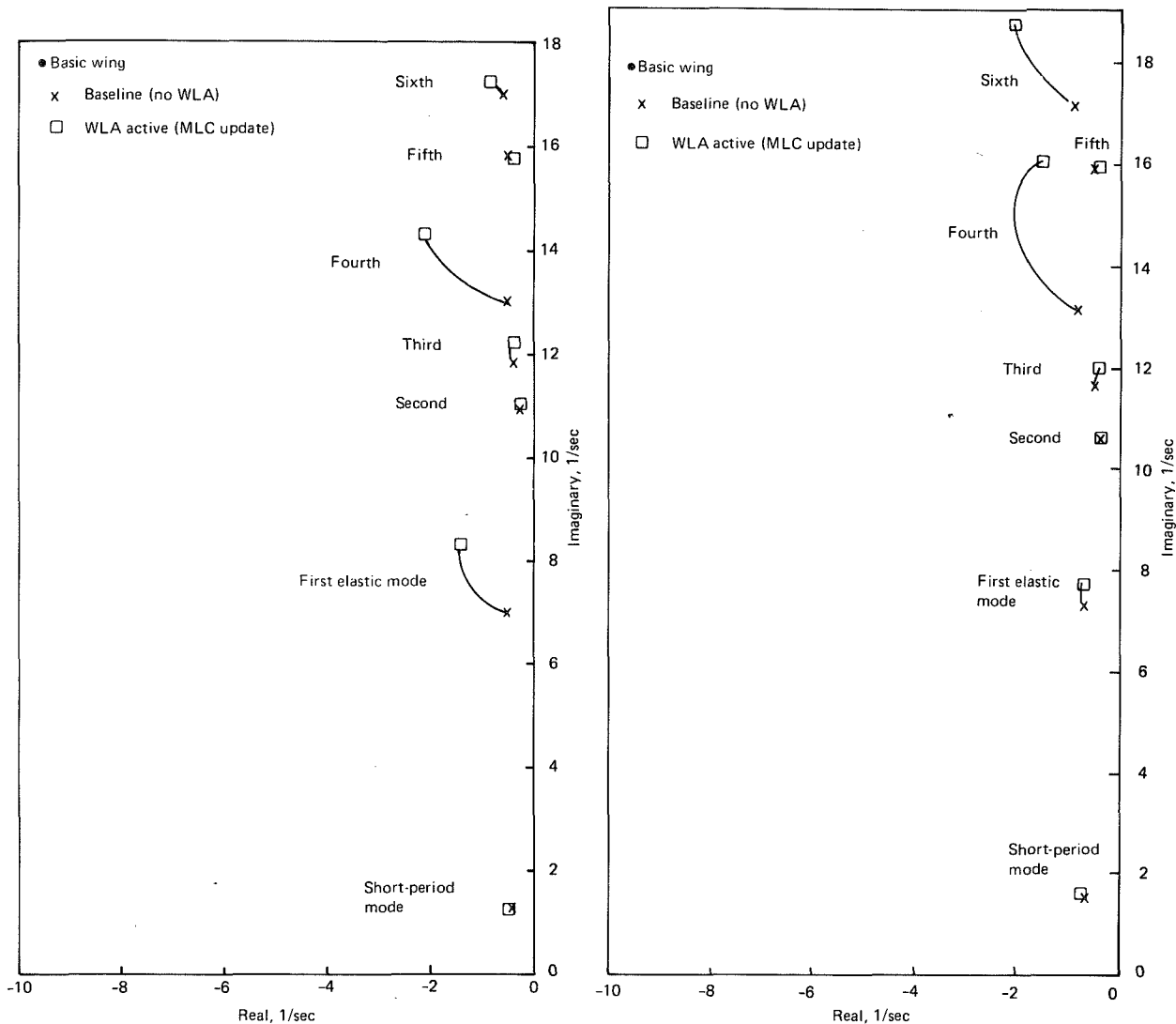


Figure 101. Final WLA System Stability at V_B Figure 102. Final WLA System Stability at V_C

At the V_B condition the structural modes have the required stability margins. The fourth mode has the minimum phase margin of 64 deg lag. With the exception of the fourth and sixth modes the stability margins also satisfy the criteria at the V_C condition. Both modes have a phase margin of 55 deg lag, which is close to the required 60 deg. The criteria can be satisfied with a refinement to the filter design or a small reduction of the gains.

For stability analysis, mode shape variations were simulated by varying the location of the sensor. Movement of the wing accelerometer of 1.52m (60 in) fore and aft, as well as inboard and outboard, results in only small root movements of the first seven elastic modes, and the system remains stable. Higher frequency modes are decoupled with filtering and are not affected by mode shape variations.

MLC Performance—MLC performance is compared in Figure 103 with the basic airplane response to a step column command. The aileron tracks load factor and reduces bending loads. With WLA active the load factor response is the same as the baseline response. As the feel system of the basic airplane has not changed, the final WLA system does not impact the stick force per g handling quality.

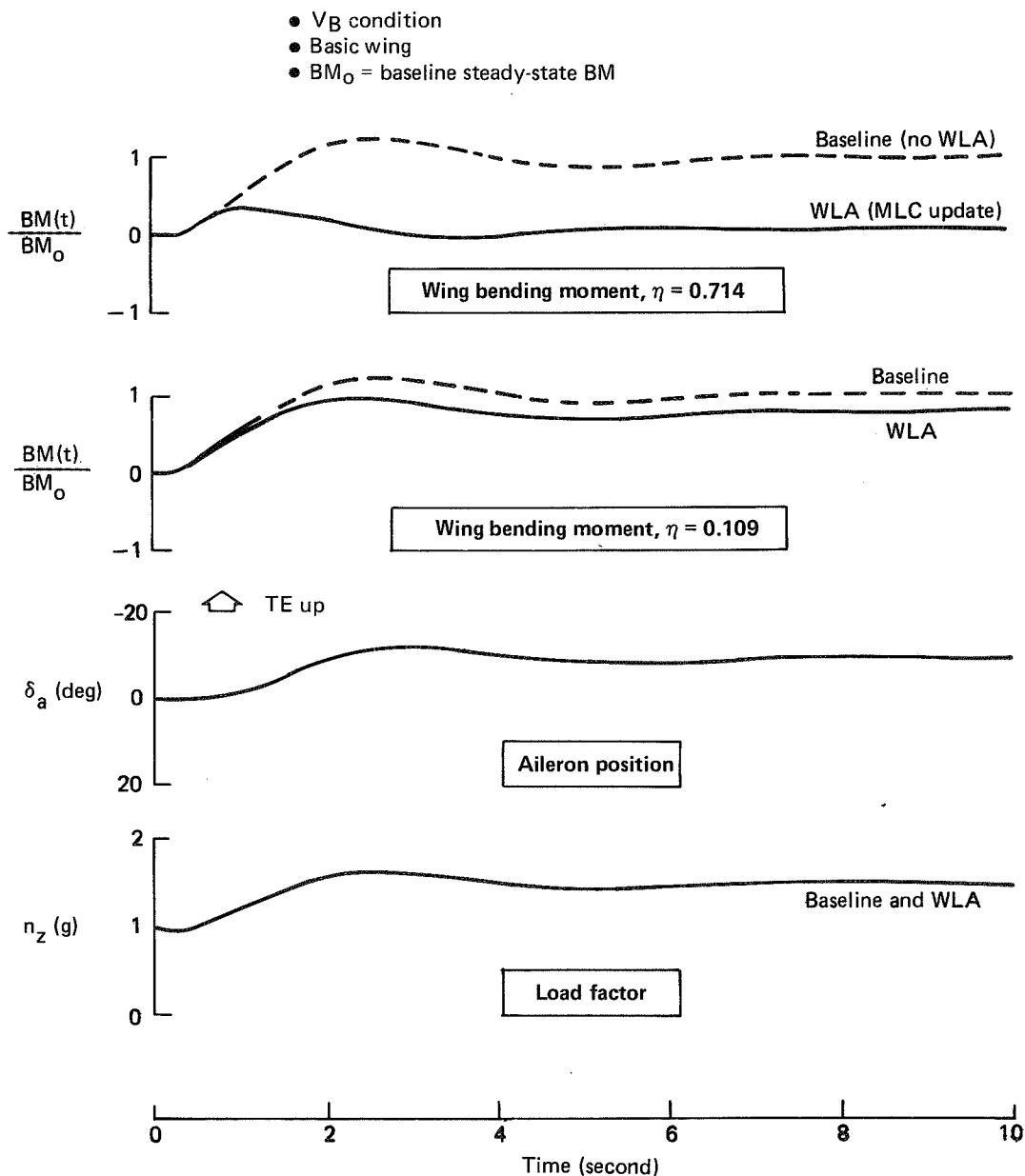


Figure 103. Step Column Maneuver Response, Final Control Law

Gust Performance—At the V_C condition, gust loads near the outboard aileron are a concern with the WLA active as these are greater than the maneuver loads. The final control law is an attempt to reduce the number of sensors needed to perform WLA without making gust loads more critical. The effect of the final control law on the PSD of wing root bending moment is illustrated in Figure 104. The response is contrasted with the responses for the basic airplane and for a MLC + GLA system. Although the short period mode damping and frequency are not altered, the MLC function of the final control law does reduce the gust load at this frequency. The MLC + GLA system with pitch rate feedback reduces the power more. At higher frequencies the final control law has improved performance. With either control law a similar reduction of the rms load is achieved as discussed in Section 6.2.5.

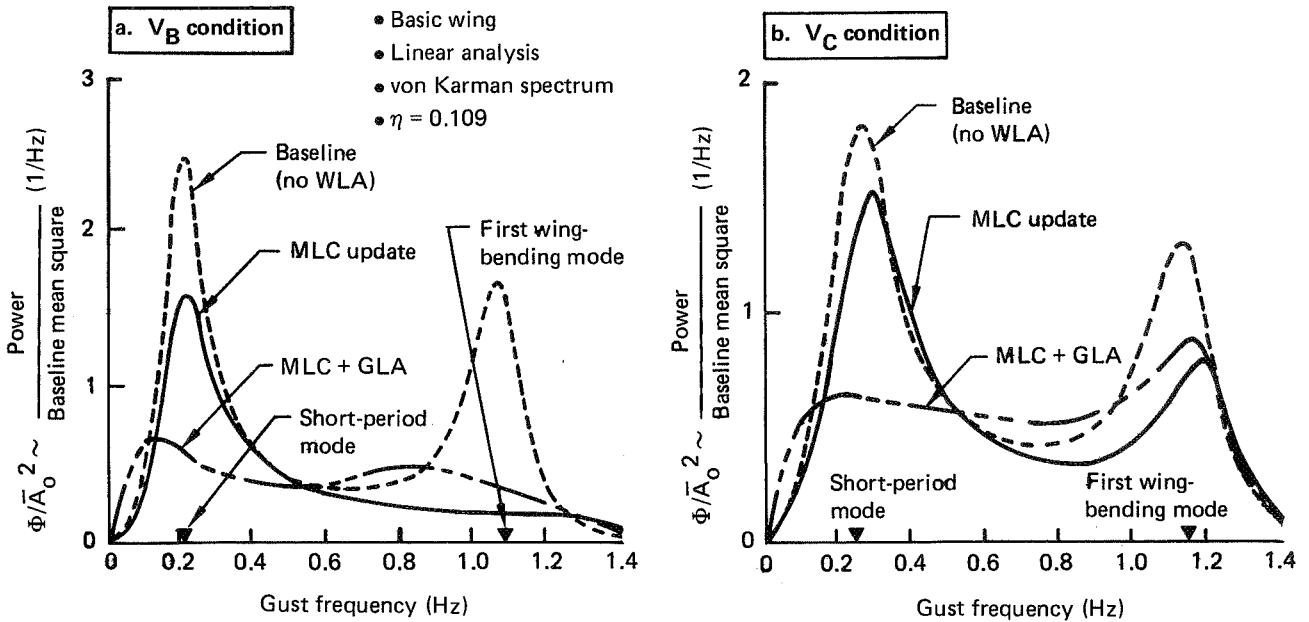


Figure 104. Effect of Control Law on Bending Moment Power Spectrum Near Wing Root

The effect of the control law (linear system) on the bending moment near the outboard aileron is shown in Figure 105. These data are presented for purposes of control law comparisons only. (Structural design loads for gust conditions are discussed in sec. 6.2.5.) At V_B condition the final control law provides more bending moment reduction than the preliminary MLC + GLA system. At V_C condition the outboard bending moment is increased with either control law. With the final control law, power is increased at the short period and first elastic mode frequencies. The MLC + GLA system also shows more response between the two modal frequencies due to the closed loop filter dynamics for the wing accelerometer. In comparison, the rms increase is reduced with the final control law.

The outboard gust loads at the V_C condition can be reduced with a modification to the control law. The effect of the accelerometer gain on the rms gust loads is shown in Figure 106. As the WLA system is gradually activated, the outboard bending moment and shear are reduced. These loads eventually increase as the gain increases, with bending moment becoming greater than the baseline value. Torsion outboard increases linearly with gain. At the wing root, alleviation of the bending moment improves as the gain increases. Beyond 50% of nominal gain, though, its sensitivity diminishes.

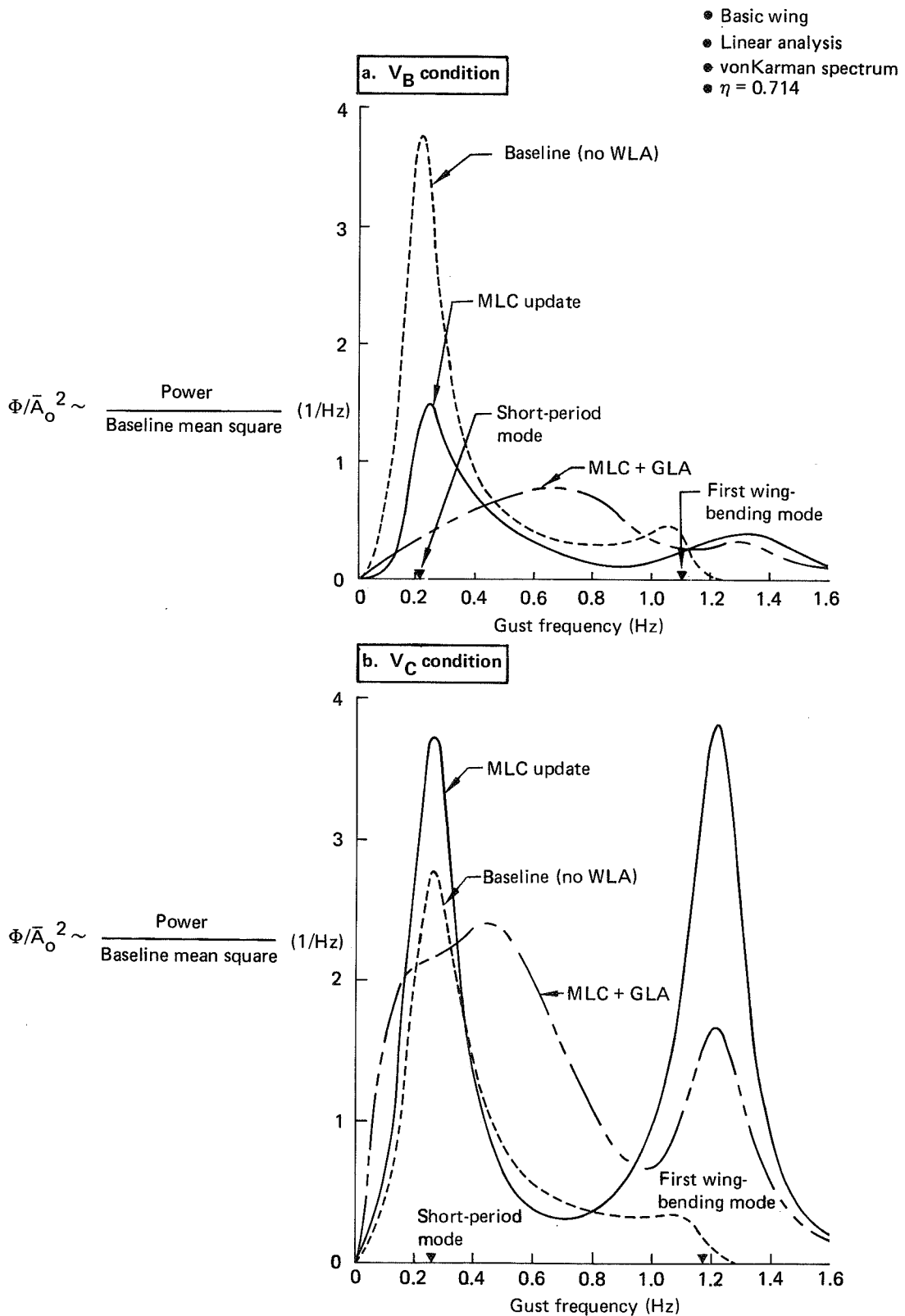


Figure 105. Effect of Control Law on Bending Moment Power Spectrum Near Outboard Aileron

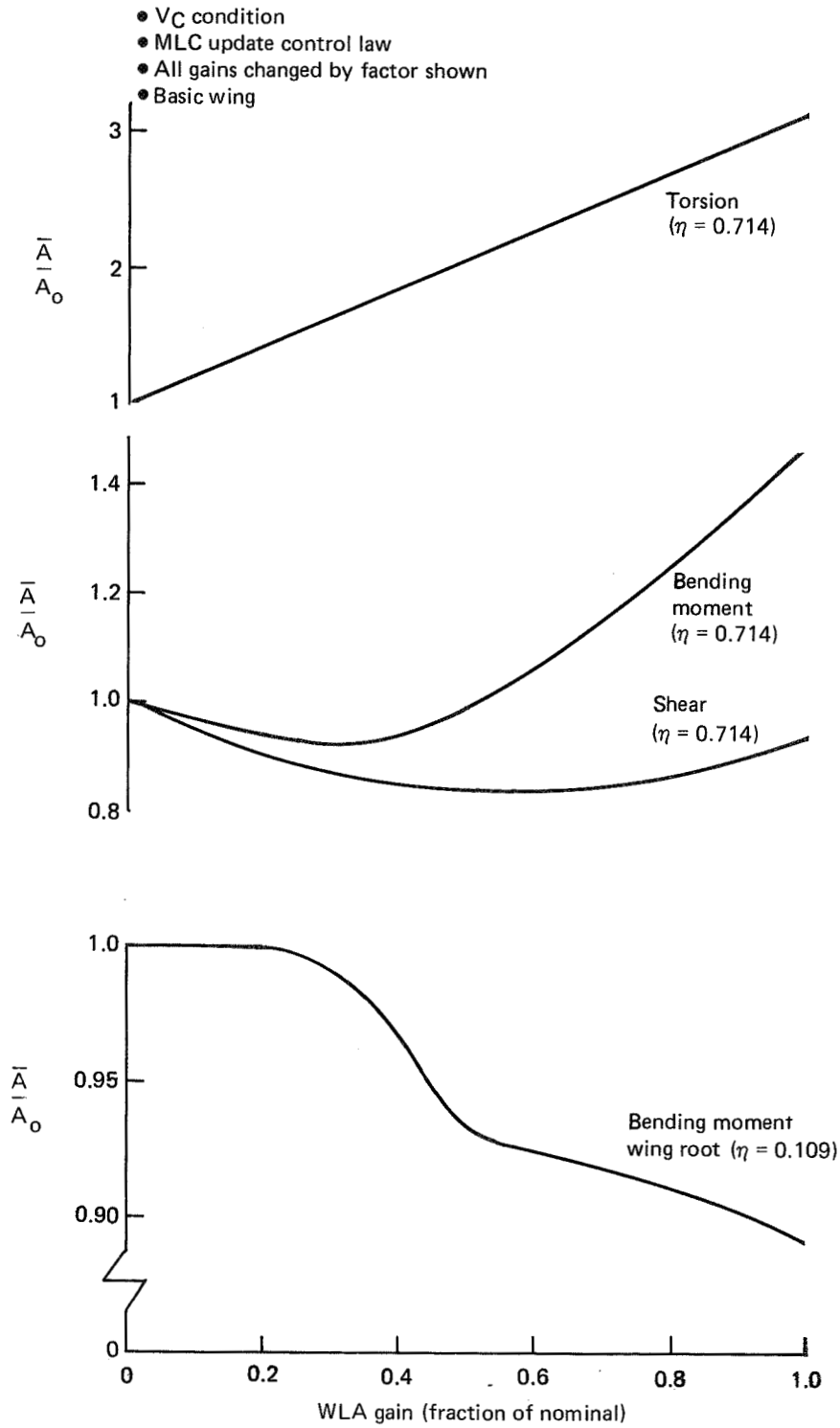


Figure 106. Effect of MLC Gain on Gust Loads

The major factor in the selection of the nominal gain is the MLC function. When slowdown is considered, a small gain reduction does not affect MLC performance. Therefore, the gust loads can be adjusted, if necessary, in this manner without impacting the MLC function.

Another improvement to the gust performance can be attained with the elevator loop removed. The effect on the wing root bending moment PSD is shown in Figure 107 for the V_B and V_C conditions. Power at the short period mode frequency is further reduced. At other frequencies the effect is negligible. The incremental rms improvement is approximately 2% at both flight conditions. Outboard the improvement is slightly better.

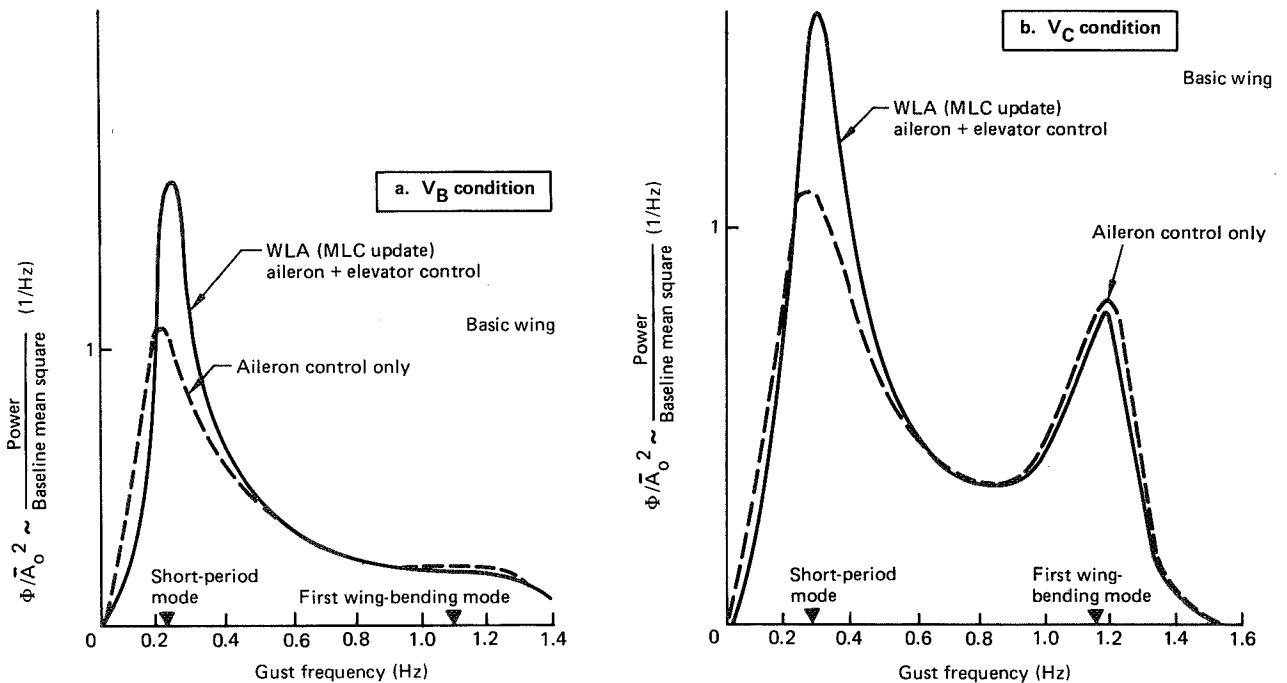


Figure 107. Effect of Elevator on Wing Root Bending Moment Power Spectrum

During gust penetration longitudinal stability produces a restoring force to pitch the airplane into the gust. Aileron motion for load alleviation also opposes this pitching motion. Removal of the outboard elevator path, which normally compensates for the aileron pitching moment, allows the WLA system to damp the short period mode gust response. However, this modification must be compatible with handling qualities and the autopilot operation.

The performance of the final control law in discrete gusts has also been evaluated. The wing root bending moment and aileron responses to a discrete gust are shown in Figure 108. With WLA, active peak loads are significantly reduced. Most apparent is damping of the first elastic mode dynamics. Reduction at the initial peaks is better than the performance of the MLC + GLA system. This improvement is the result of less phase lag between the aileron and accelerometer.

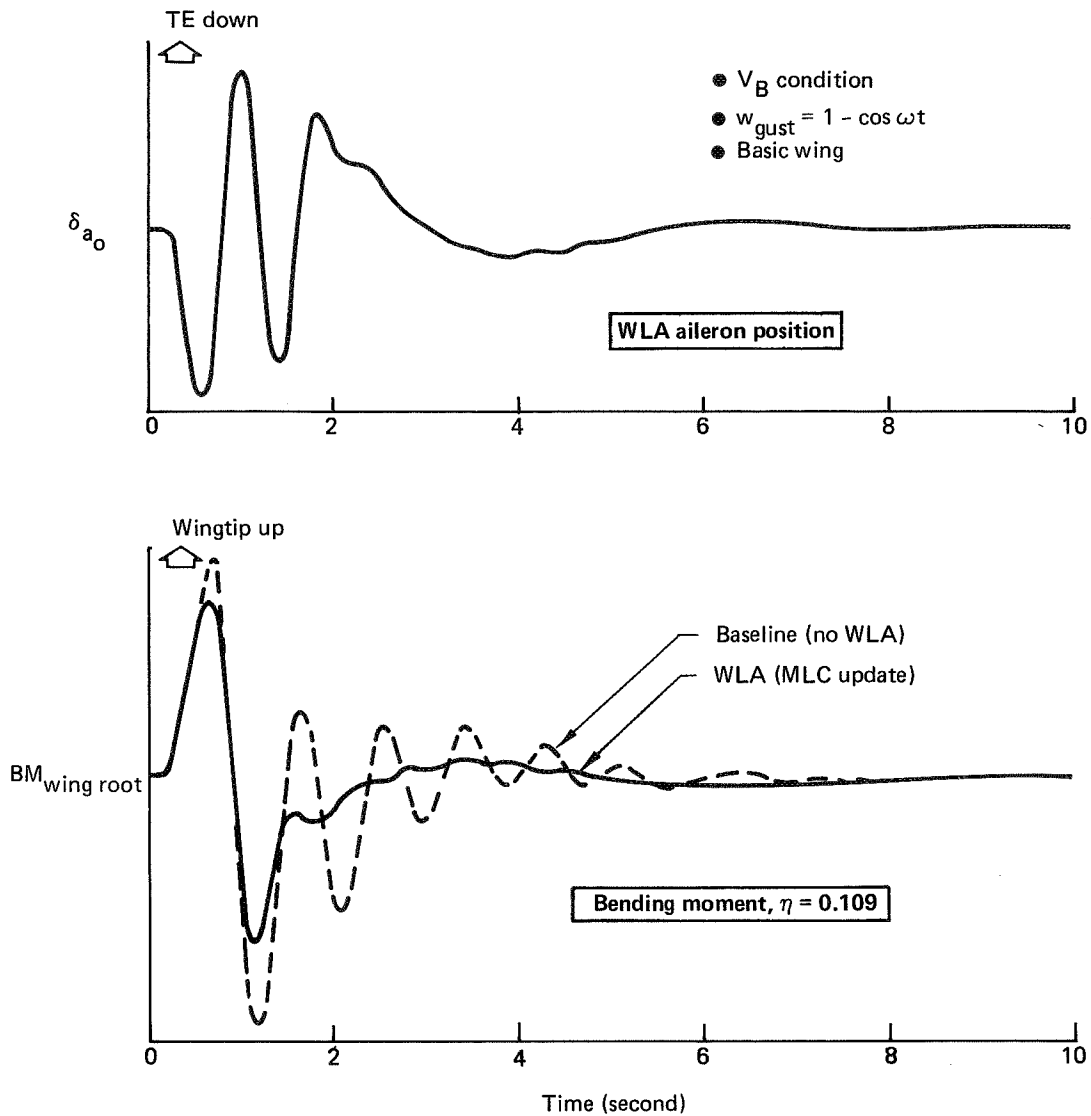


Figure 108. Discrete Gust Response, Final Control Law

Ride Qualities—Ride qualities at the V_B condition are changed slightly by the final control law. At the aft fuselage, gust-induced rms accelerations are approximately 5% less. Essentially no change occurs at the cg. At the pilot station, the level of acceleration is approximately 15% higher. This effect should be considered in a refinement to the control law.

Autopilot Performance—The pitch compensation path of the control law restores the piloted response characteristics to those of the basic airplane. Consequently, performance of the pitch autopilot is not expected to be impacted by the WLA system. The performance of the basic autopilot mode, attitude hold, following a step attitude command is shown in Figure 109. Activation of the WLA system is apparent in the elevator dynamics; however, the attitude response is very close to that with WLA inactive. The WLA function is expected also to be compatible with the performance of the other autopilot modes. Automatic disengagement of WLA prior to landing is

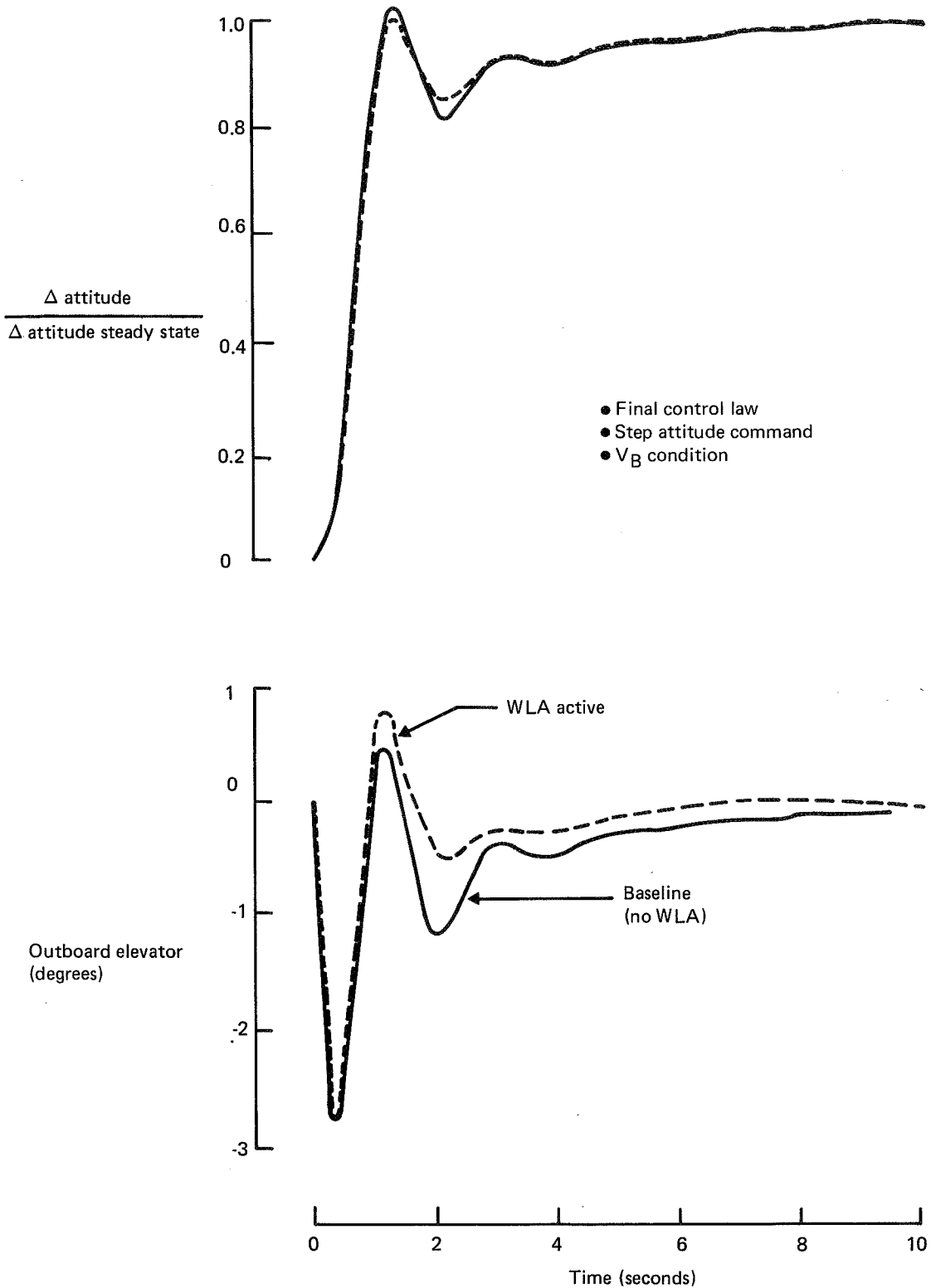


Figure 109. Autopilot Performance with WLA

envisioned. In this case, autoland performance is not affected. If the WLA system remains active during landing, the flight path response to column inputs will be a little more sluggish due to the apparent decrease in wing lift curve slope resulting from MLC aileron deflection. However, this is not expected to have significant impact on landing performance.

Low-Speed Roll Control—The outboard aileron performs two functions, lateral control and wing load alleviation with the flaps extended. To retain the existing low-speed lateral control capabilities, the roll control function is given priority at large wheel commands (fig. 110). WLA commands are reduced linearly with wheel angle; at 50 deg wheel, its authority is zero.

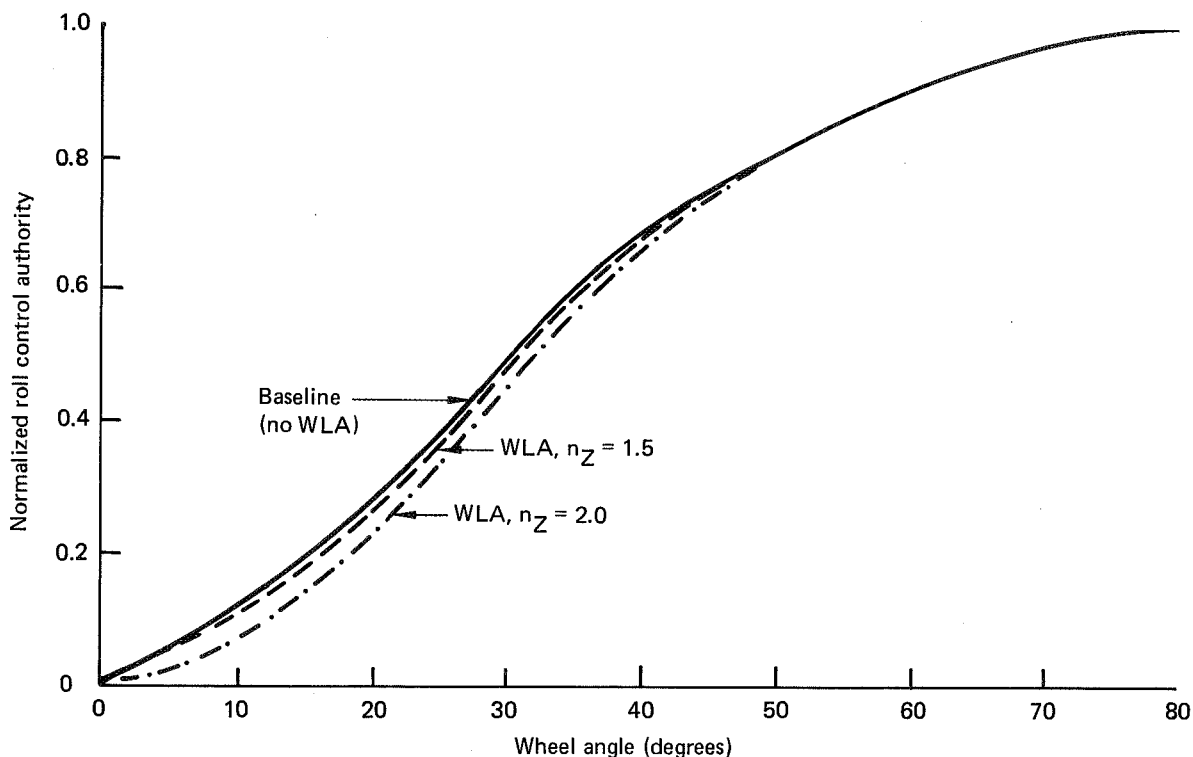


Figure 110. Flaps-Down Roll Control With WLA

Control Law Development—In the first design cycle for the MLC system, an accelerometer located near the cg provided an incremental load factor feedback signal. Without filtering of this feedback signal the damping of the first and sixth elastic modes was reduced. A structural mode filter was designed to decouple the MLC system from the elastic modes.

Control laws for the GLA function then were added. To control the short period mode response in turbulence, pitch rate was fed back to the outboard elevators. Symmetric wing motion was sensed and commanded outboard ailerons to damp the first elastic mode response.

The pitch rate path of the GLA control law modified the short period mode dynamics and handling qualities. A feedforward path in the GLA control law restored the short period dynamics. Pilot and autopilot commands were sensed by a linear variable

differential transformer mounted on the inboard elevator PCU. The signal was filtered to cancel commands from the pitch rate feedback path that result from maneuvers in still air. With the appropriate gain, the feedforward signal had the effect of masking the short period mode dynamics of the augmented airplane with simulated dynamics representing the basic airplane.

The first cycle control law increases gust loads at some frequencies. The problem is illustrated in Figure 111. The power spectral density of incremental wing root bending moment for the unaugmented airplane is contrasted with the spectrum for both MLC and GLA active at the V_B condition. At the short period mode frequency the functions perform together to reduce the response. At the frequency of the first elastic mode, the outboard aileron path of the GLA control law suppresses the response. However, at frequencies between the two airplane modes, a power increase is evident. The reason is apparent from an examination of the MLC filter. A Bode plot of the filter frequency response is shown in Figure 112. At frequencies near 4 rad/sec, the filter amplifies the feedback signal and produces an out-of-phase command. The resulting control surface deflections increase the wing load.

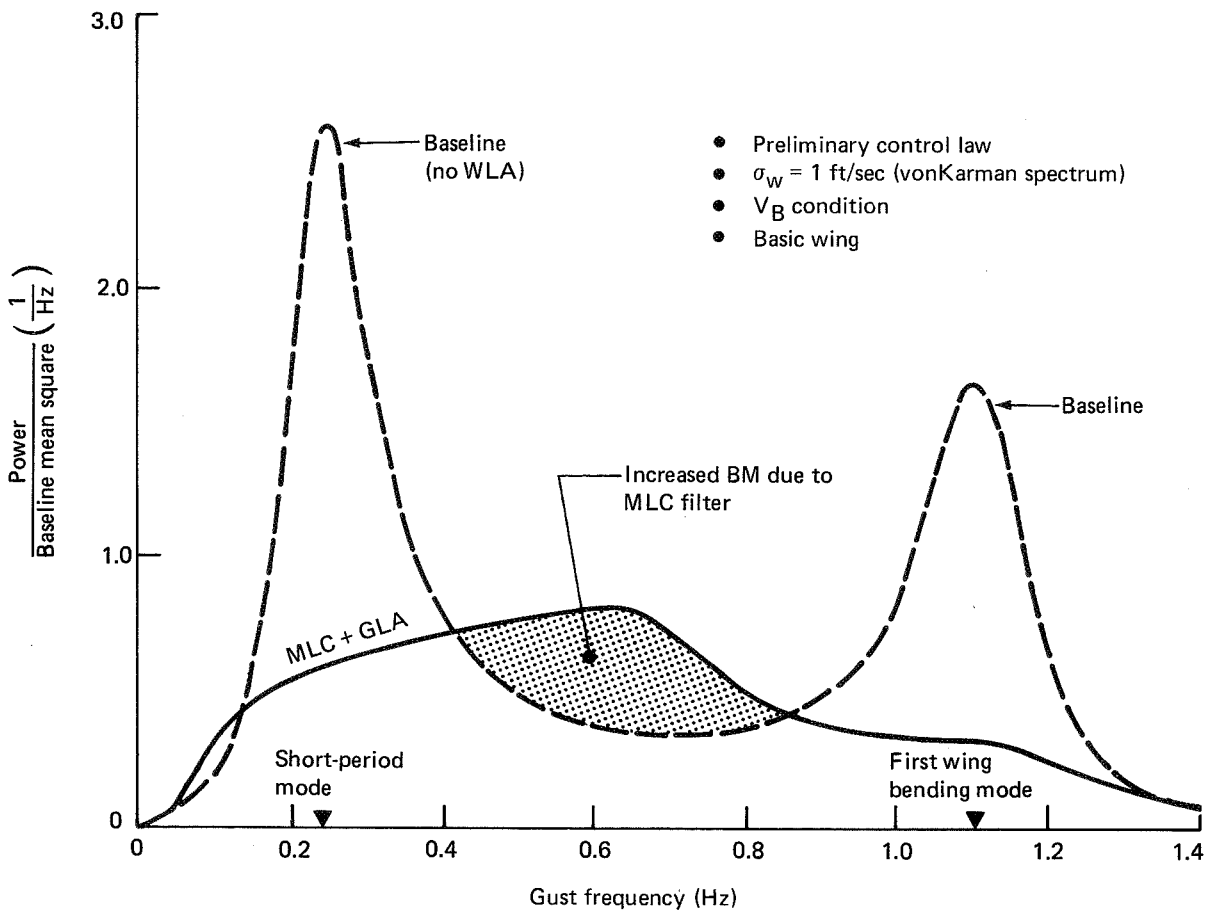


Figure 111. Wing-Root Bending Moment Power Spectrum

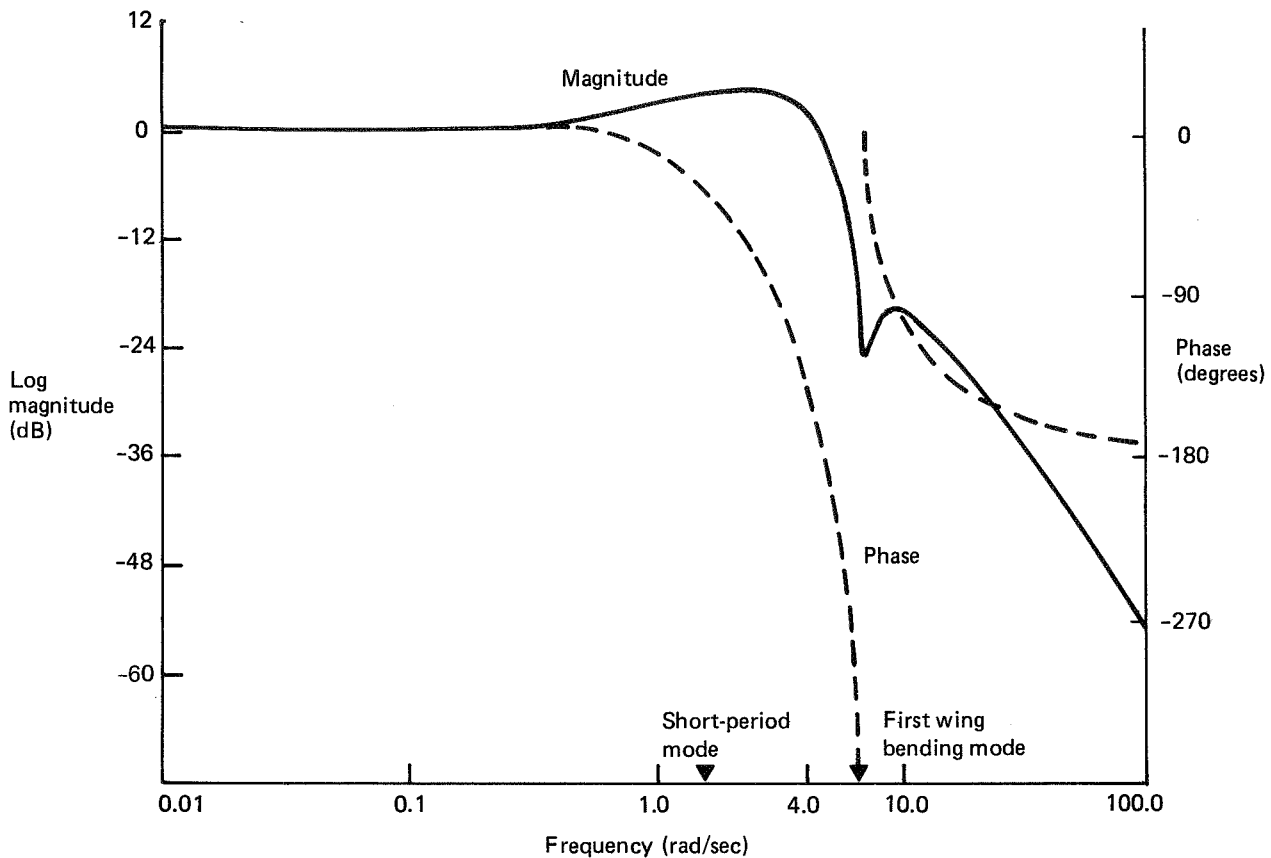


Figure 112. First Cycle MLC Filter Frequency Response

In the second design cycle, a modification of the MLC structural mode filter greatly alleviated the gust problem. The improvement was realized with an integration of the MLC and GLA control law designs. The increased stability of the first elastic mode derived from the GLA control law afforded a relaxation of the MLC structural mode filter design requirements. With less stringent attenuation requirements beyond the short period mode frequency, the MLC control law had improved performance during gust penetration and dynamic maneuvers.

These control laws, shown in Figure 113 and denoted CL2, were interim to the final design. The control functions and sensors identified in the first design cycle were retained. Representative anti-aliasing filters in the digital computer hardware also were included.

As discussed in Section 6.2, the structural benefit of MLC for the basic wing is approximately 771 kg (1700 lb). The same studies show the potential benefit of GLA is considerably less. Only a portion of the GLA potential probably can be realized when the effects of blowdown, torsion introduced by the aileron, and performance uncertainties in the actual implementation of the control law are considered. Mechanization of these functions in a fail-operational arrangement requires three sensors for MLC but 11 additional for GLA. The small weight savings associated with GLA for the basic wing does not justify the added complexity. In the final design cycle,

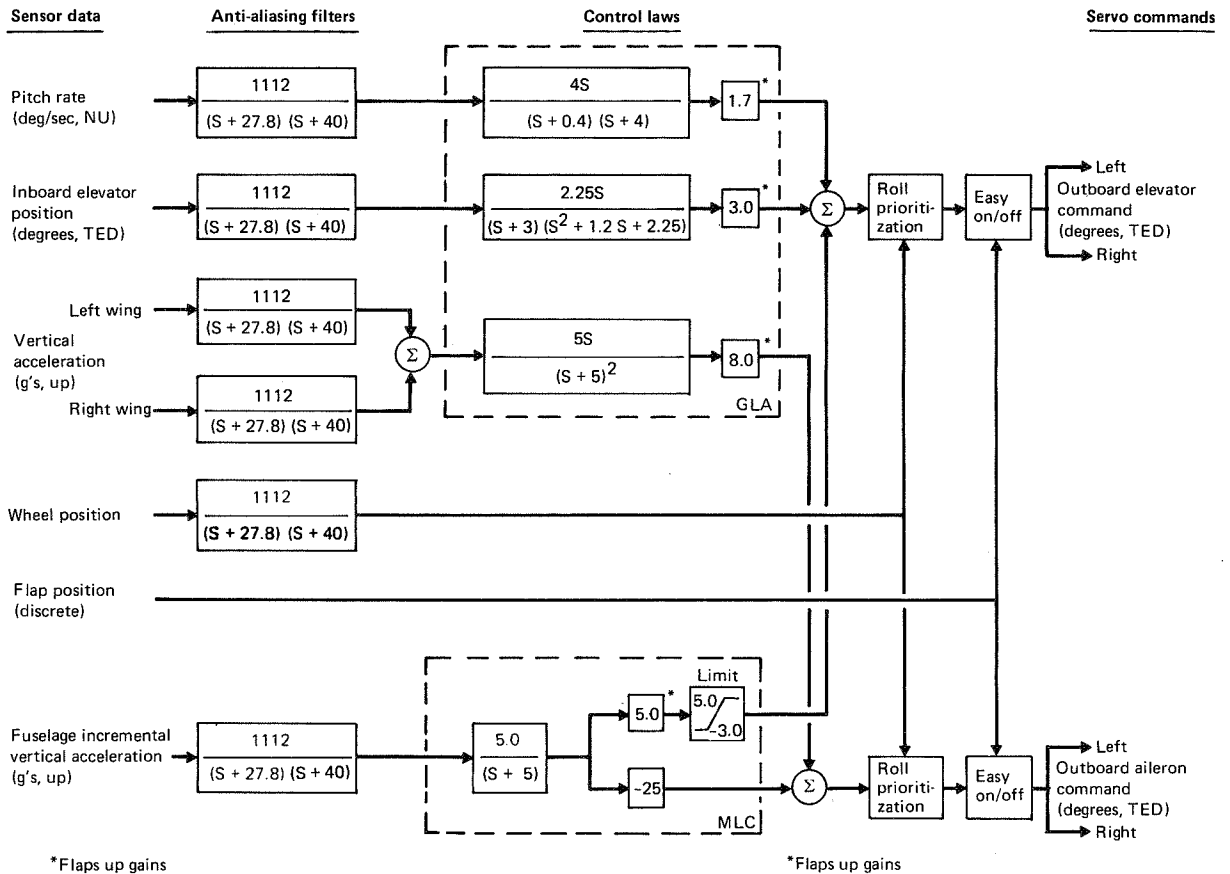


Figure 113. Interim Control Laws, CL2

simplification of the control law to only the MLC function was desirable. With the MLC + GLA control law, gust loads near the outboard aileron were increased at the V_C condition. The objective in the final control law design was to determine if the number of sensors could be reduced without making the gust loads more critical.

6.4.3 System Mechanization and Installation

The WLA system is mechanized as a dual channel, digital, fail-operational system. For cost and weight savings, in-line monitoring techniques are employed and electro-hydraulic power actuators are implemented. High reliability, comparable to that of a dual, independent yaw damper system, is achieved.

Selected System Description—A schematic of the final system mechanization is shown in Figure 114. Dual, self-monitored, digital computers are the central components. Control law computation is dual redundant in each channel (dual-dual). In addition to control law computation, the system functions that reside within the computer unit are as follows:

- Provisions for interface with the external system components.
- Inflight failure monitoring, failure status annunciation, and system shutdown.

- Automated pre-flight test that verifies operational integrity of the entire WLA system.
- Semi-automated maintenance test to be performed, especially in the areas of the automated pre-flight testing, maintenance testing, and inflight monitoring. The automated test features lead to the selection of a digital computer with necessary input/output electronics.

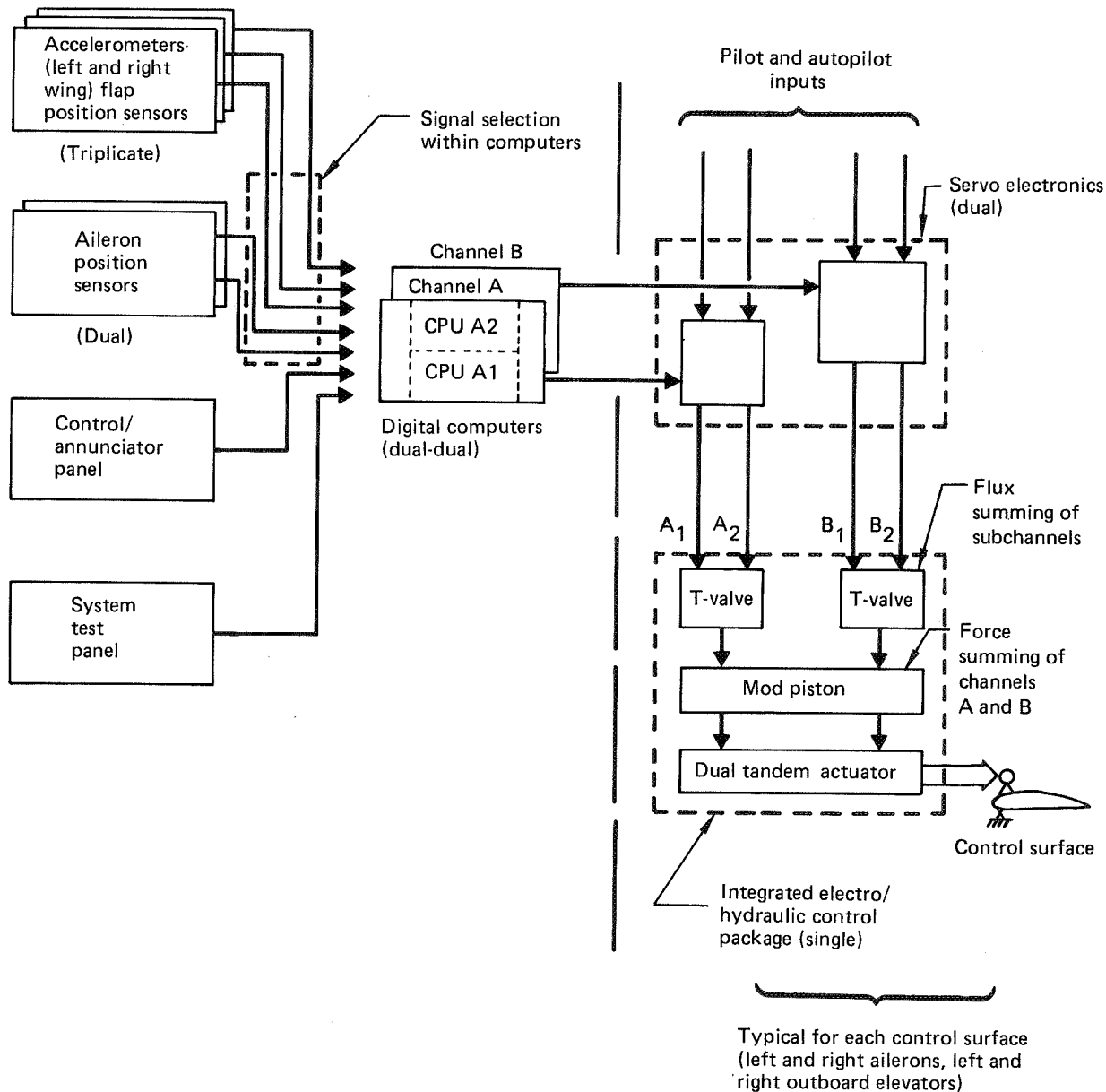


Figure 114. Final WLA System Mechanization

The two digital computers are packaged in two one-half ATR long boxes that are installed in the electronics bay. The location of the components is shown pictorially in Figure 115.

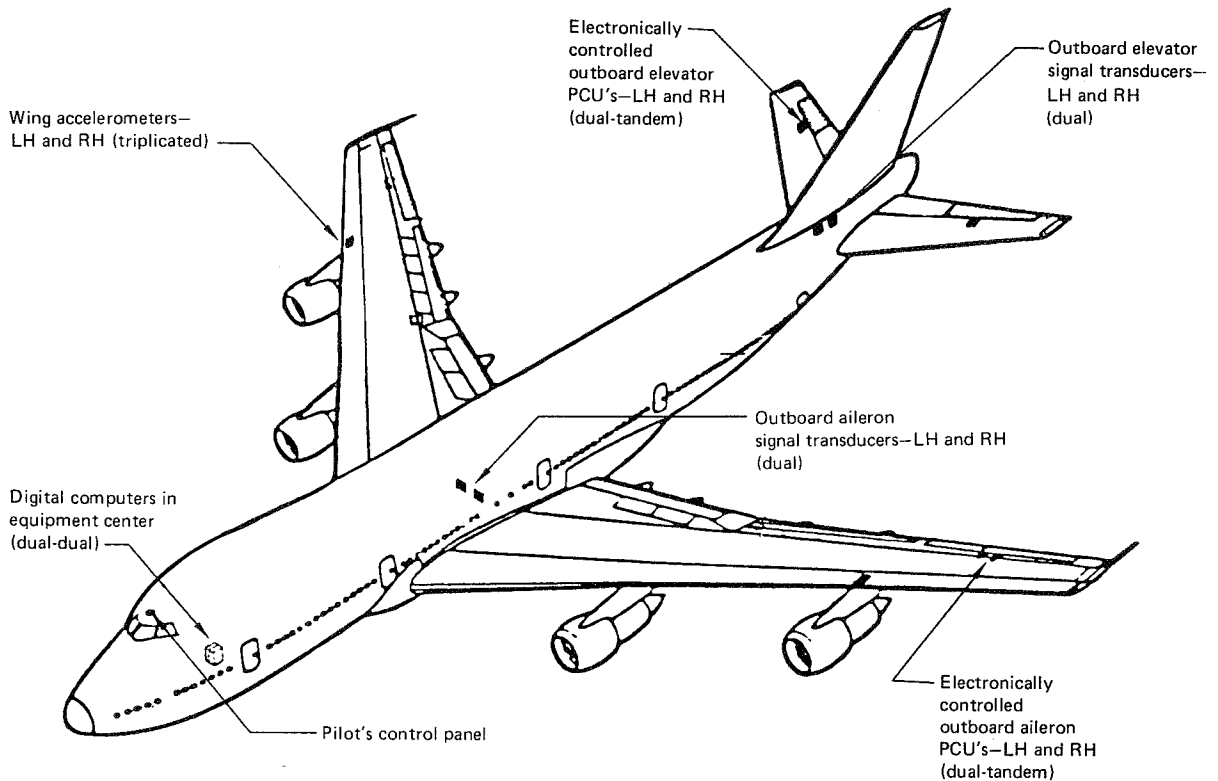


Figure 115. WLA Control System Installation

Six accelerometers equivalent to Sundstrand Model WA-1200 are installed, three each at WS 1180 on the left and right front spars. The flap position sensors are installed in the flap extension system. One set of dual linear variable differential transformers (LVDT) installed at each aileron programmer is shared with the lateral control system.

The existing outboard aileron PCU is replaced with the new actuator having the same stroke and force output. LVDTs are installed at each aileron programmer to provide lateral control input signals to the respective outboard aileron PCU. The aileron programmers are revised to drive the new signal transducers. The existing aileron lockout (fig. 116), control cables, and control linkages are removed.

The new PCU installation is shown in Figure 117 for the left outboard aileron. The new PCU is installed on the existing structural supports. Balance weight for the outboard aileron control surfaces is increased to counteract the weight increment from reinforcement of the aileron skin panels. Modifications to the aileron and local back-up structure, which were included as part of the incremental cost of the system, are illustrated in Figure 118.

The new outboard elevator PCU has the same stroke and force output as the present single actuator. Dual LVDTs are installed at the elevator aft quadrant to provide pilot commands to both outboard elevator actuators. The existing linkages, control

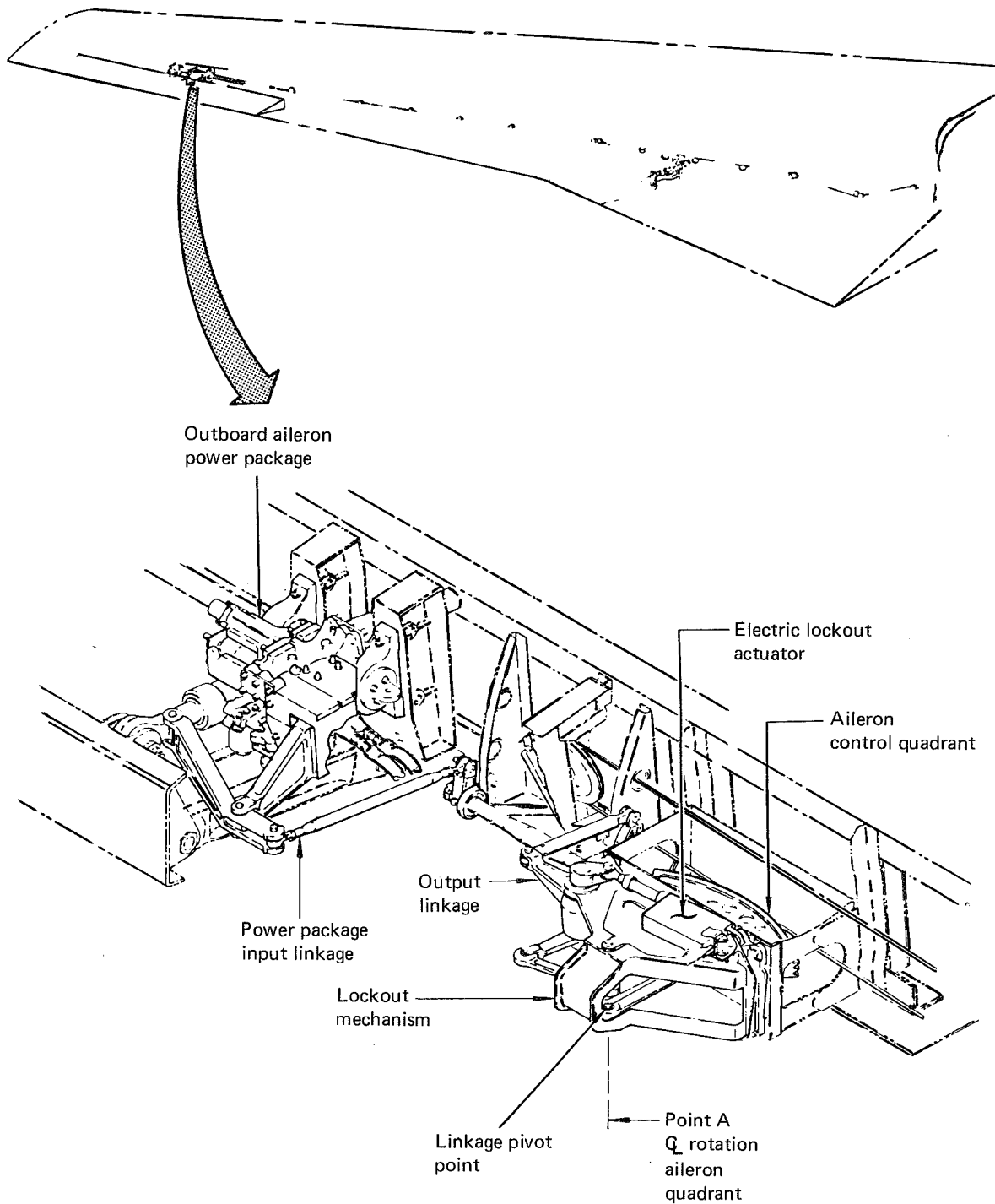


Figure 116. Existing Outboard Aileron PCU and Lockout Mechanism

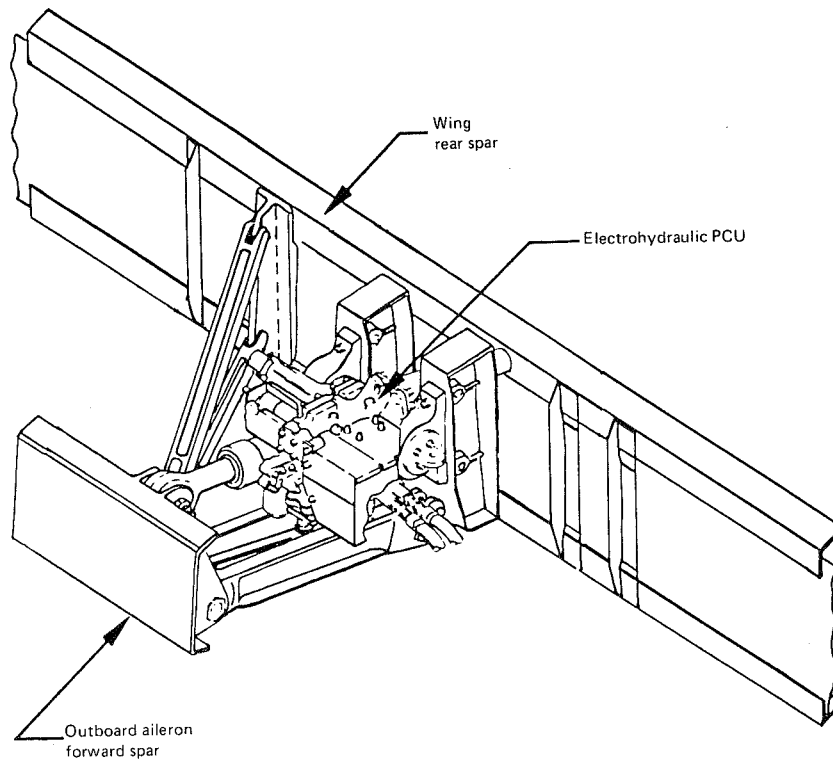


Figure 117. Outboard Aileron Electrohydraulic Power Control Unit (PCU) Installation

Note: Does not reflect wing box resizing for MLC loads

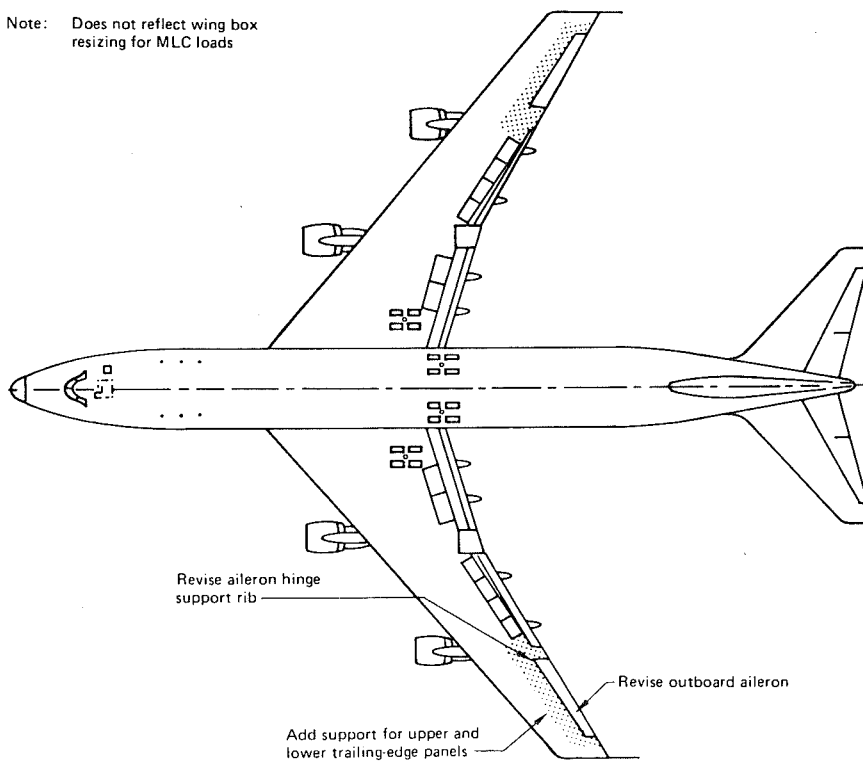


Figure 118. Local Structural Revisions for MLC Aileron Installation

quadrants, and cables between the outboard elevator PCUs and the opposite inboard elevators are removed. The new electrohydraulic PCU installation is shown in Figure 119 for the left outboard elevator. The new actuator is installed on the existing structural supports.

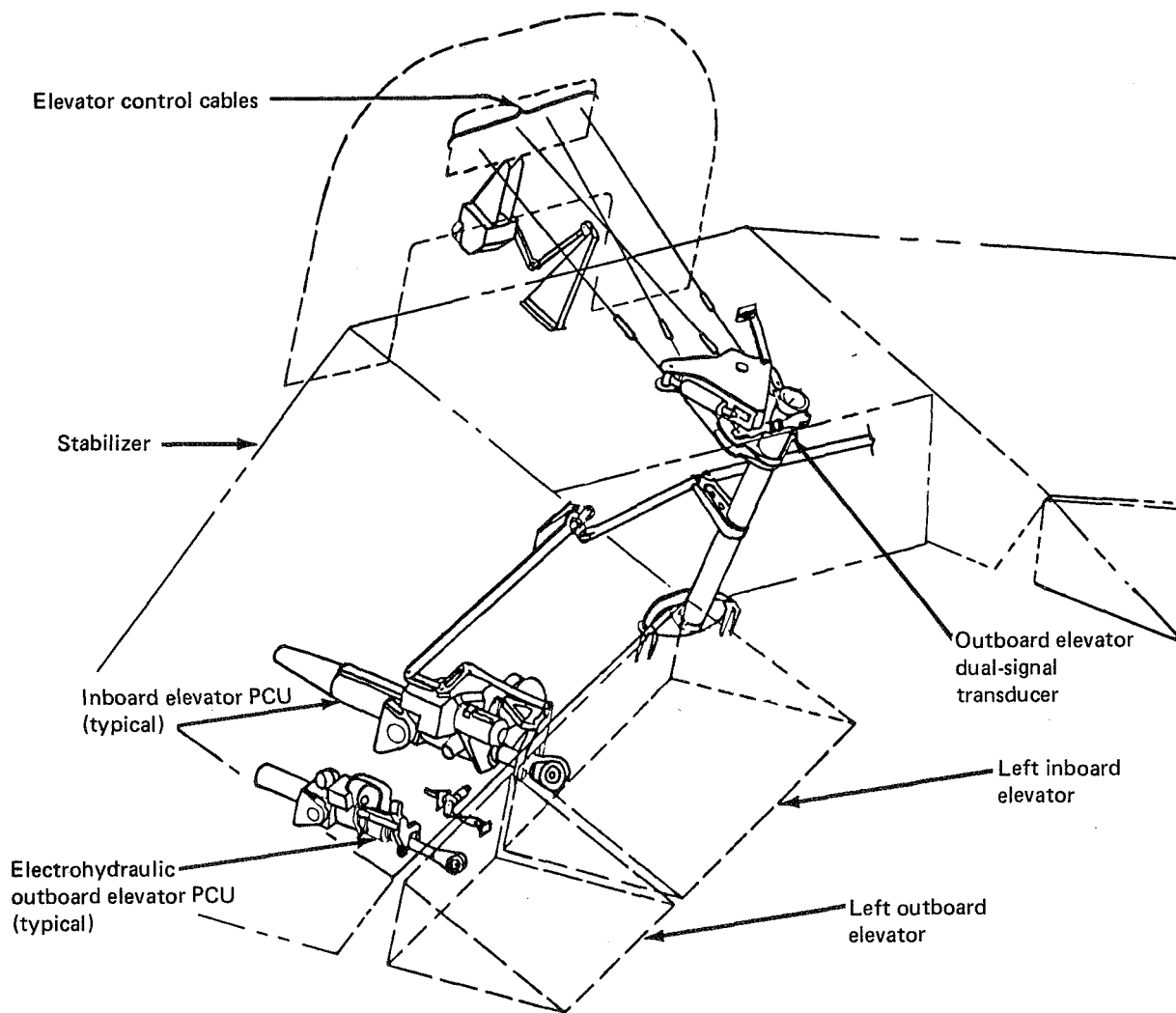


Figure 119. Outboard Elevator Electrohydraulic Power Control Unit (PCU) Installation

Sensor data are cross strapped to both computers, and signal selection is performed within each. For fail-operate capability the motion sensors (wing accelerometers) and the flap position sensors are triple redundant. The pilot roll input sensor is self-checking and need only be dual. Redundant sensors are packaged together as a unit to enable precise input axis alignment and calibration at the assembly level, thus minimizing sensor signal variations. To eliminate the aliasing problem, the sensor signals are connected to the digital processor through a prefilter.

The power actuators for the outboard elevators and ailerons are electrohydraulic. Each actuator has fail-operate capability with two electrical and two hydraulic

channels. Dual redundant servo electronics receive WLA computed commands and electrically transduced pilot/autopilot commands. In each set of servo electronics two series sums are formed by combining the pilot/autopilot command with each of the two commands from one WLA computer. The two sums are then combined by flux summing in the armature of a T-valve to position a mod piston. Force voting by the mod piston in each channel positions the main valve for the dual tandem main pistons.

The mode control and display panel provides flight crew interface with the WLA system. The mode control and display functions are divided between two panels, the overhead panel and the master caution panel. The overhead panel contains a master WLA system engage/disengage (ON/OFF) switch which provides crew override on WLA system operational status. The panel also contains the controls and displays necessary to perform the preflight test. All inflight detected failures are annunciated on the master caution panel to the flight crew. The interface between the maintenance personnel and WLA system is the system test panel. Failure identification is displayed on, and system maintenance tests are initiated from, this panel.

The purpose of the system test function is to provide an assessment of the operational integrity of the WLA system and to provide maintainability enhancement. The preflight or ground test is an automated built-in test and diagnostic function that checks for failures within the WLA system and localizes them to a line replaceable unit.

Electrical power (110 Vac 400 Hz and 28 Vdc) is supplied to Channel A from the essential flight instrument busses and to Channel B from the flight instrument busses.

Selected Systems Reliability—The Computer Aided Redundant Systems Reliability Analysis (CARSRA) computer program (ref. 5) has been used to investigate the WLA system reliability. Appendix A contains a discussion of the reliability modelling.

System reliability is essentially determined by the probability of occurrence of computer failures that are not detected and isolated by the in-line monitors. During dual channel operation, force summing in the actuator provides failure protection. In-line monitors detect and isolate the failure, and the failed channel is deactivated. If the failure is not detected and isolated, the two channels force fight and the system function is lost. In this case, operation following first failure is not possible and system reliability is degraded.

Due to lack of in-service experience with self-monitored digital computers, the ability of this failure detection technique to identify all failures for fail-operational capability cannot be clearly defined. However, a survey of vendor capability indicates that at least 97% failure coverage and possibly 100% is attainable with state-of-the-art technology. The sensitivity of failure probability for the final system mechanization to computer failure coverage is shown in Figure 120. The probability of system failure is greatly increased with less than perfect failure detection. Complete failure coverage is necessary to achieve reliability comparable to that of a dual yaw damper system. For long flight times, even 99% coverage is less than desirable. The impact warrants a better definition of in-line monitoring performance to adequately predict the system reliability.

During single channel operation, flux summing and in-line monitoring provide failure protection. Undetected failures can cause hardover or oscillatory control surface motion. Test data for the active failure rate of a self-monitored digital computer are

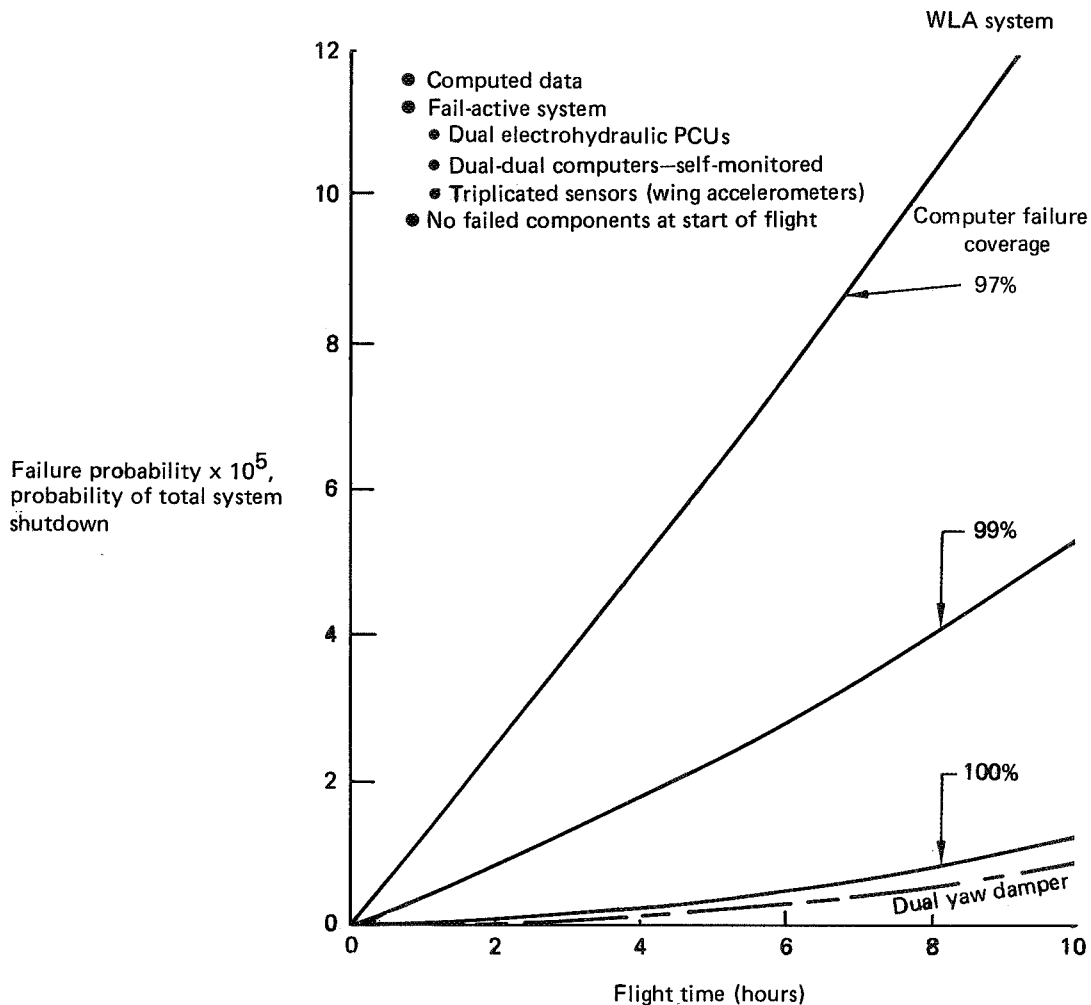


Figure 120. Final WLA System Reliability (MLC Only)

reported in Reference 6 and has been used in WLA failure probability calculations. With only one channel operational at dispatch, the probability of an active failure (hardover or oscillatory failure) of the WLA system is predicted to be 5.2×10^{-7} during an average flight length of 4 hours. If single channel dispatch happens less frequently than once every 520 departures, the probability of WLA failing active can be considered extremely remote. This rate of deferred repair is quite high considering airline normal maintenance practice with the yaw damper system. With both WLA channels operational at dispatch, the probability of two failures, the second being an active failure, is 0.4×10^{-9} during an average flight length, and this is an extremely remote occurrence.

Selected System Development—Through several design cycles the WLA system reliability progressed substantially toward the goal of high reliability with reasonable complexity and cost. A functional diagram of the first cycle mechanization, a fail-passive system, is shown in Figure 121. It consists of dual sensors, dual computers, and dual secondary servos. A sensor set is associated with each computer. The dual servo

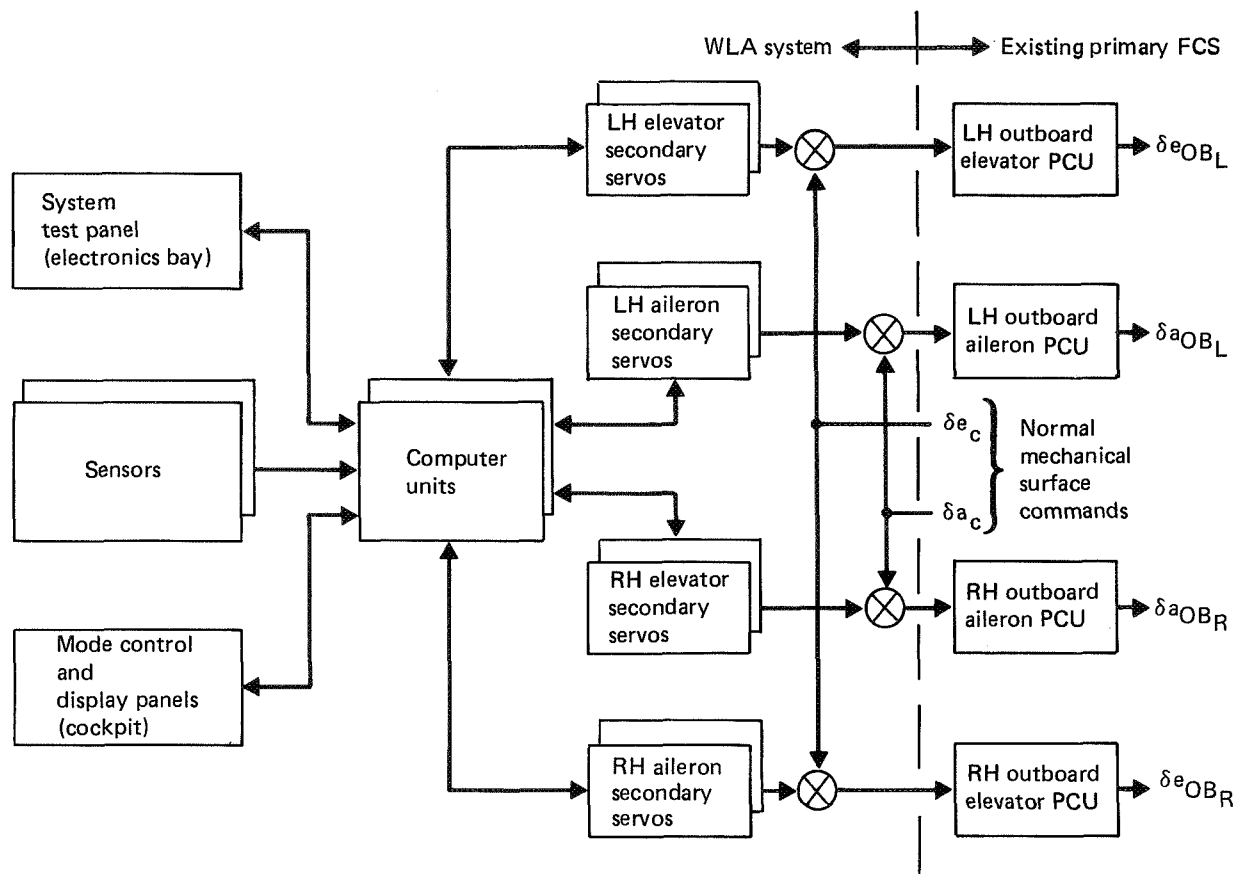


Figure 121. Preliminary WLA System General Arrangement

outputs are force summed through internal force detent mechanisms that provide hardware protection against failures. The mechanical outputs of the servos are series summed with the normal mechanical path commands to form the total surface deflection command inputs to the PCUs. The failure probability after 1 hour of flight is shown in Figure 122. Equivalently, the mean time between failure is 1250 hours. This poor reliability indicates the need to retain system operation following a single failure.

In-line monitoring techniques, which allow each channel to be self-monitored, were applied, thereby providing fail-operate capability with a dual rather than triple channel configuration. Not only was reliability improved, but the technique was cost effective. This approach increased parts counts relative to a dual channel, fail-passive configuration but required significantly fewer parts than a triple channel "brick-walled" approach. Discussions with vendors have indicated that this concept is feasible for both the digital computer and the actuator with state-of-the-art technology.

In the first cycle mechanization the major feature of the dual servo, force summed concept is the built-in mechanical protection against hardover type failures originating upstream of the actuator pistons. This feature is provided by a hydraulic pressure regulated detent located between the actuator piston and the output linkage. The

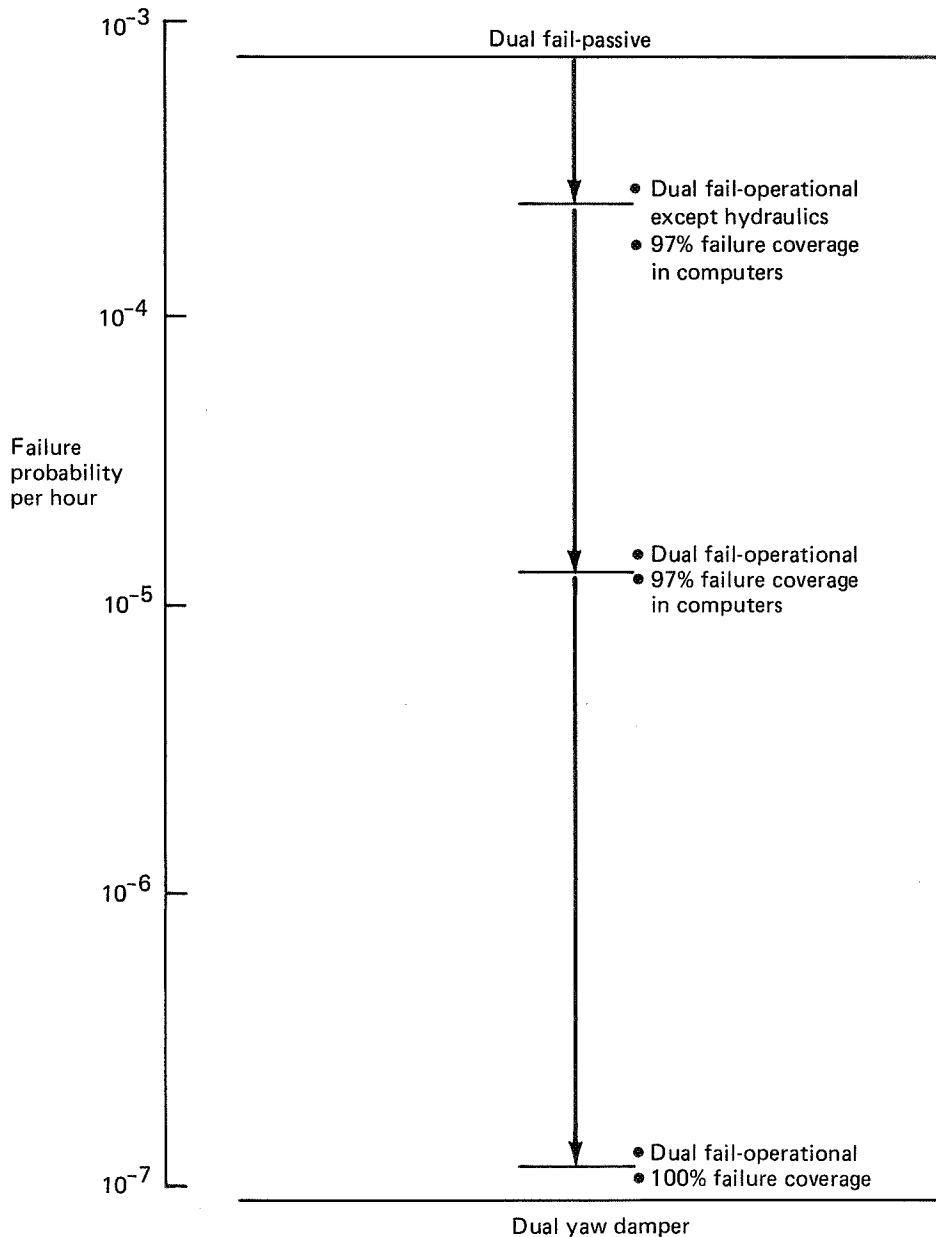


Figure 122. Progression of WLA System Reliability

function of the detent is to limit the output force capability of the secondary servo. Sufficiently dissimilar piston commands result in a force fight greater than the detent force and in at least one piston immediately camming out. In a triple channel, fail-operate configuration, this capability is retained after the first channel failure.

The eight secondary servos in the first cycle mechanization, however, contributed significantly to the system cost and weight. As a first update, a single secondary servo replaced the dual force summed concept. In-line monitoring of dual servo electronics and flux summing of the two channels were employed for failure protection. The hydraulics to the outboard elevator power actuator were supplied by

one system, and the single servo concept was consistent with this redundancy, maintained commonality of parts, and retained the retrofit capability of the baseline mechanization. Except for hydraulic failures, WLA was mechanized as fail-operational. The improvement to system reliability is shown in Figure 122. The mean time between failure increased from 1250 to 4000 hours. The dependency on a single hydraulic failure, however, made this WLA system configuration much less reliable than dual, independent yaw dampers.

Studies, as discussed in Section 6.4.4, show advantages in the areas of system weight, cost, and performance can be achieved by replacing the secondary servos and existing power actuators with electrohydraulic power actuators. Although the primary flight control system must be revised, the implementation with these actuators has attendant benefits in that weight is reduced, reliability is improved, and maintenance costs are reduced. Furthermore, the new actuator installation allows the hydraulic supply to the outboard elevators to be revised to a dual system. The final mechanization with these actuators is fail-operational for hydraulic as well as electrical failures. Although one aileron actuator is at half boost following one hydraulic failure, the WLA computer reconfigures the system to maintain symmetric control surface deflection.

The current 747 yaw damper system is used as a basis for comparison since it performs a function similar to WLA. However, it has some unique characteristics that allow a simpler mechanization than that required for WLA. A brief description of this system follows. The yaw damper system is comprised of two independent channels; one that controls with an upper rudder segment, and one that controls with a lower rudder segment. Following the failure of one channel, dutch roll damping continues to be augmented by the remaining channel, although with approximately one half the effectivity. Each channel has limited authority of 3.6 deg. Failure detection and protection against hardover or oscillatory failure are not as critical as with the WLA system because of the limited authority. At least one yaw damper channel must function for dispatch. However, no limitations or placards on airplane operation occur following failure of the second channel in flight. Because the two yaw dampers are independent and the system is relatively simple, high reliability is easily achieved.

As shown in Figure 122, system reliability has improved appreciably. Assuming both channels are functional at takeoff, the system mean time between failure has increased to 75 000 hours with 97% coverage of computer failures. With complete failure coverage the system reliability is improved to a level comparable to that of a dual yaw damper system.

Actuation System Trades—The outboard aileron and elevator control surface actuators must incorporate provisions for series summing WLA commands with normal pilot and autopilot commands. Essentially two approaches are possible; a conventional PCU with remote servos to provide WLA commands, or an integrated actuator with pilot/autopilot and WLA commands summed internally. An integrated PCU can be, in general, either a combination electrohydraulic-hydronechanical scheme or an exclusively electrohydraulic scheme. For the 747 WLA application an entirely electrohydraulic integrated PCU is judged to be lighter, cheaper, and to have better performance.

A proposed electrohydraulic scheme, shown in Figure 123, consists of two electrical and two hydraulic channels. In each electrical channel, two servo amps receive commands from one WLA computer and electrically transduced pilot/autopilot commands. The two servo amps drive a transfer valve (T-valve) with each amp energizing

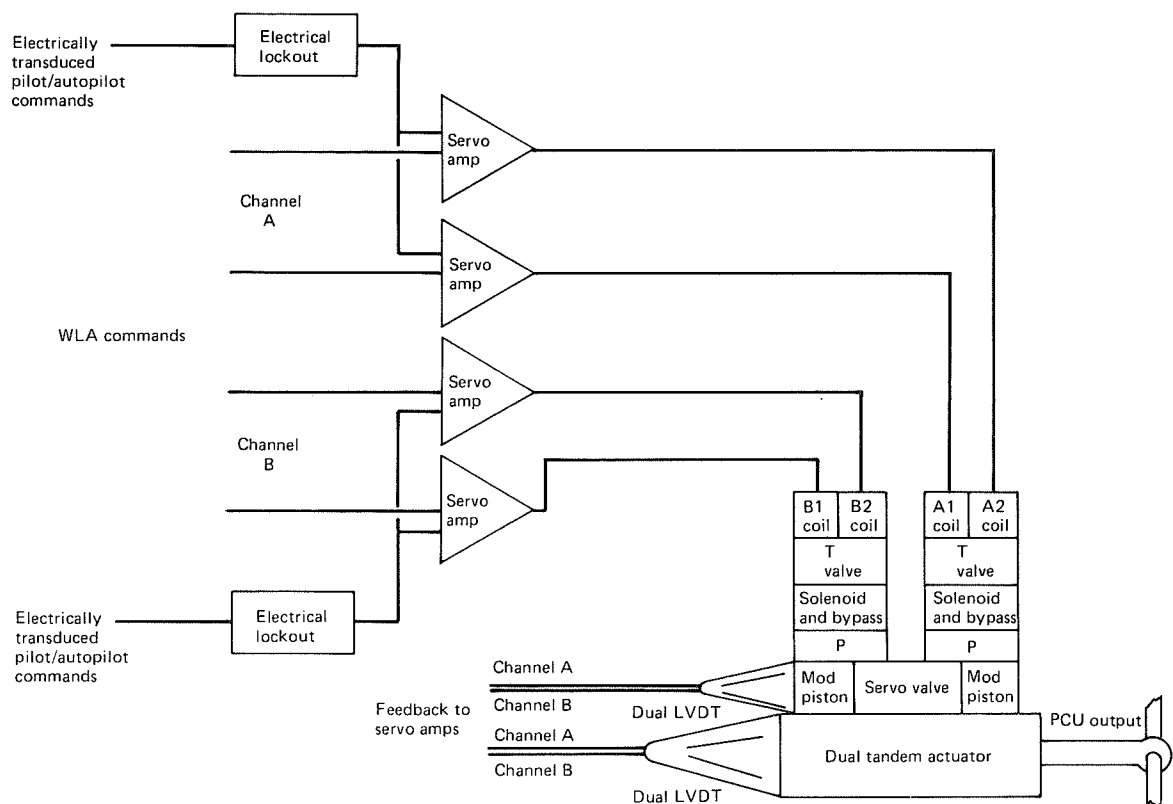


Figure 123. Electrohydraulic Actuation, Outboard Aileron

one T-valve coil. This provides flux summing of the electromagnetic commands upstream of the actuator hydraulics. Control pressures from the T-valve position a secondary or mod (modulating) piston and simultaneously the main control valve. Commands from the two electrical channels to the mod pistons are combined by force summing on a common shaft. The resulting motion controls a dual tandem main servo valve. The mod pistons position and main ram position are fed back electrically. Tolerances and null bias of the valves can cause force fights between the mod pistons resulting in command dead zones. To prevent this, the mod piston pressure differentials (ΔP) can be fed back for equalization. This scheme requires cross channel comparison. Another scheme, the active on-line scheme, renders one mod piston a "slave" with ΔP feedback to that channel. The other mod piston, without ΔP feedback, becomes the master. This scheme has very desirable performance characteristics after failures. Either application of ΔP feedback is feasible. Studies are required to choose the best approach.

Pilot and autopilot electrical commands replace the existing mechanical paths. The command to the outboard elevator is sensed with an LVDT at the elevator aft quadrant. This arrangement improves the elevator system performance after certain failures because the outboard elevator is no longer dependent on the inboard elevator function. The outboard aileron command is sensed at the aileron programmer output. The asymmetrical program needed for the outboard aileron is produced directly in the transducer. Furthermore, electronic lockout controllers replace the present lockout mechanisms. For both outboard elevator and aileron control, dual electrical channels take the place of single mechanical command paths. Relative to the existing primary flight control installation, weight is saved and the reliability is enhanced.

Failure detection of each PCU channel is employed to be consistent with a fail-operational mechanization for WLA. In dual channel operation the force summing feature protects against active failures. Monitors identify the failed channel. During single channel operation, flux summing and in-line monitoring minimize failure transients. Single channel considerations require a current comparator for the servo amp outputs, self-monitored T-valve, and self-monitored feedback LVDTs for failure identification. Self-checking T-valves are relatively new devices, and their reliability must be investigated.

An integrated hydromechanical actuator package is illustrated in Figure 124. Two secondary servos are incorporated with the power control unit; each servo is commanded by a WLA computer and employs flux summing. The two mod pistons are position summed and the average position is mechanically combined with pilot/autopilot commands to control the servo valve. These mod pistons require electrical feedback just as in the electrical scheme. However, equalization or slaving is not needed. The existing lockout mechanism and mechanical control paths are retained.

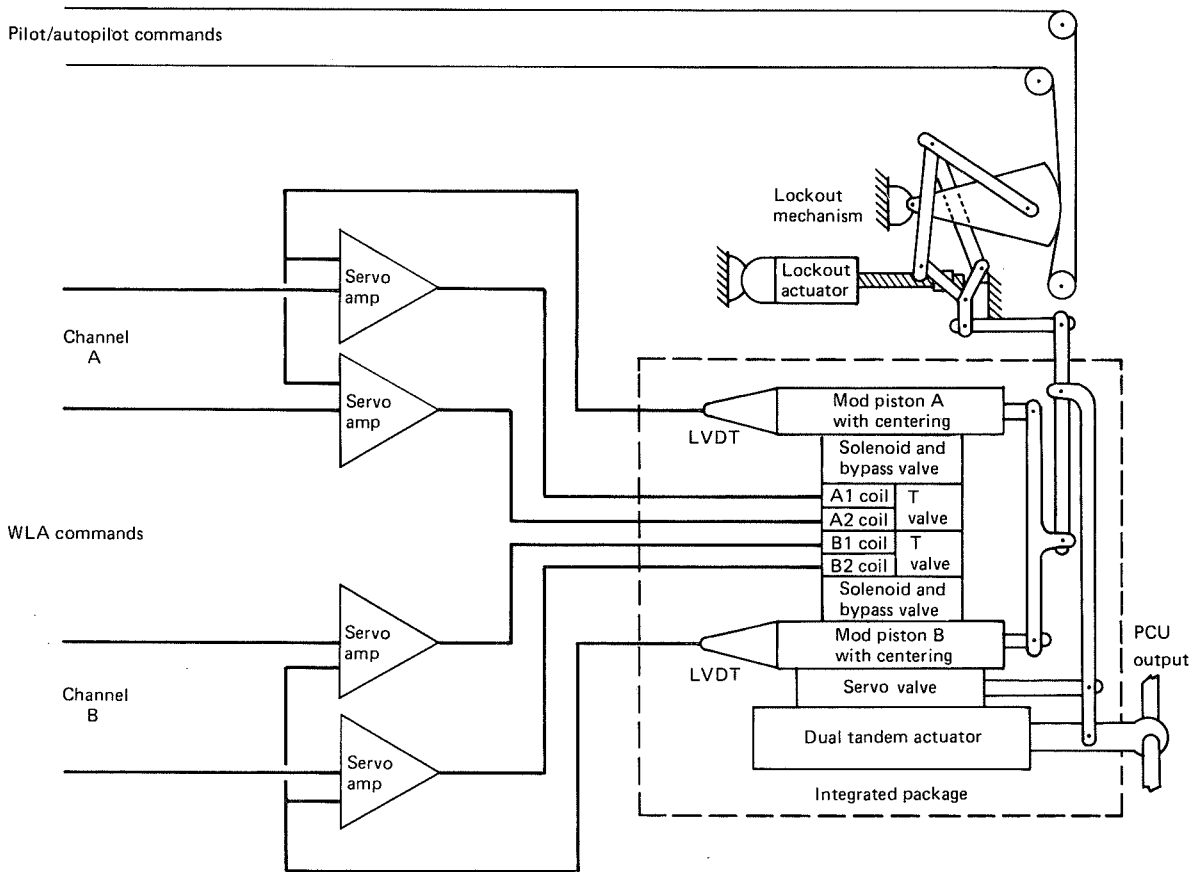


Figure 124. Integrated Hydromechanical Actuation, Outboard Aileron

During dual channel operation, this actuator scheme relies on in-line monitoring for failure protection. This is not as desirable as the force summing concept. Following the first failure the command gain for the remaining secondary servo is doubled to retain the WLA authority. In single channel configuration, failure detection is similar to that employed for the electrohydraulic actuator.

The electrical scheme has an apparent advantage in several areas; weight, cost, design simplicity, and reliability. The chief advantage of implementing an exclusively electrohydraulic actuator is design simplicity. It does not need a complex linkage to provide command summing or aileron surface deflection asymmetry and lockout. Linkages inherently have compliance and backlash. This leads to design difficulties in surface position resolution and PCU stability. Beyond that, the limited space available in which to package the outboard aileron PCU amplifies these problems.

The position resolution possible with electrical feedback is about an order of magnitude better than that possible with a linkage. The position resolution required for WLA renders electrical feedback desirable.

Because of design simplicity the WLA system mechanized with electrohydraulic actuators is expected to cost about a third that of the system with hydromechanical actuators. Mechanical paths for the outboard elevator and aileron portion of the primary flight control system are replaced with electrical paths which contribute to a lighter system weight. It is approximately half of the mechanical system weight.

Also, substitution of redundant electrical channels improves the reliability of the basic pitch and roll functions. Exclusively electrohydraulic actuators are recommended for WLA on the 747 EET derivative airplane.

6.5 RECOMMENDED DESIGN APPROACH AND ASSESSMENT

6.5.1 Recommended Design Approach

This subsection outlines the approach to system design and structural sizing recommended as a starting point for more detailed definition if a development program for production application of the WLA concept to the commercial 747 fleet is initiated. Recommendations and rationale are discussed for the following areas:

- Aileron configuration
- System configuration
- WLA authority limiting
- Flaps-down operation
- System redundancy and structural sizing philosophy

Aileron Configuration

Recommendation—Use an untabbed aileron strengthened as required for operation at high-speed conditions. Consider extending the aileron span for applications of WLA in combination with a wing tip extension.

Rationale—Selection of the untabbed aileron is discussed in Section 6.1.4. An aileron span extension could be beneficial in combination with a WTE because the extended tip twists (aeroelastically) in a direction to increase the tip load when the aileron is deflected (sec. 7.1.2). The local aerodynamic influence (α/δ effect) of the extended

aileron would provide more load reduction, and the larger aileron would also be beneficial for roll control. However, the aileron would have to be stiffened, and increased actuator force capability would probably be required.

System Configuration

Recommendation—Use the final system configuration defined in Section 6.4.

Rationale—This configuration achieves high reliability with a reasonable degree of complexity. Although designed primarily to provide the MLC function, it incorporates EMS of the first wing bending mode and (if desired) can provide most of the GLA attainable with any practical system.

WLA Authority Limiting

Recommendation—Retain existing actuator force capability. Maintain symmetric WLA aileron deflections following single hydraulic system failures by reducing the WLA commands at blowdown-limited flight conditions. Based on further trade studies, set the WLA system gains and authority limits as low as possible without significantly reducing the weight benefits.

Rationale—The recommended system configuration incorporates new electrohydraulic actuators (outboard ailerons and outboard elevators) that could be sized to provide more force capability if desired. However, preliminary trade studies (sec. 6.2.4) showed very little additional wing box weight benefit could be obtained by installing more powerful aileron actuators.

Reduction of the MLC gain was found to be favorable with respect to closed-loop gust loads on some areas of the wing but was not further explored in this study. Other potential advantages of reduced MLC aileron commands include: reduced and less abrupt aileron motion and less effect on buffet boundaries for normal maneuvers, better ability to compensate for aileron-induced pitching moments (because the C_m vs δ_a curve becomes more nonlinear at larger deflection), and less unporting of the aileron balance weights.

At high-speed conditions critical for wing box sizing, the MLC aileron was hinge-moment limited to about half of the mechanical deflection limit. It is possible that the WLA command authority could be similarly limited without incurring a structural weight penalty.

Symmetric MLC inputs are desirable to avoid roll disturbances. The four hydraulic systems are paired with the dual-tandem PCUs such that none of the systems is common to both the left and right outboard ailerons. Consequently, if one hydraulic system fails, the MLC gain should be reduced such that the commanded deflection does not exceed the hinge moment capability of the PCU operating on one hydraulic system. With this approach, the WLA capability of the system at some flight conditions would be reduced following a hydraulic failure.

Flaps Down Operation

Recommendation—Use the WLA system for takeoff. Conduct studies to determine if the system is required for landing.

Rationale—Structural weight trend studies showed very little weight benefit could be obtained if the WLA system were used only for flaps up conditions. Hence, the WLA system was assumed to be operational for all flight conditions for purposes of computing the loads used in the structural benefits study. The critical flaps down load condition was a takeoff case. The weight penalty, if any, associated with deactivating the system for landing was not determined.

Deactivating the system for landing would eliminate the "negative direct lift control" effect of WLA in the flare and could allow existing roll control sensitivity to be retained for landing without concern for roll/WLA command prioritization (neither is a major concern). The WLA requirement for landing also would be of interest in determining system reliability requirements and possible placards for dispatch with system failures.

System Redundancy and Structural Sizing Philosophy

Recommendation—Use dual tandem PCUs and fail operational WLA system electronics. Reliability of the WLA system (including the effects of hydraulic system failures) should be comparable to current dual, independent yaw damper systems.

Structural sizing should be based on design envelope load conditions assuming normal WLA system and hydraulic system status, except the capability for continued safe flight and landing following system failures (regardless of their computed probability of occurrence) should be assured as follows:

- The structure should be capable of sustaining limit loads, treated as ultimate, following a passive failure of the WLA system
- At normal flight conditions (i.e., routinely encountered in commercial transport operations), the structure should be able to accommodate hardover or oscillatory type failures of the WLA system.

Rationale—The foregoing recommendations are intended to apply only to the WLA system concept considered in this study for the 747 or to a similar installation. Criteria applicable to WLA systems in general should relate system reliability requirements to the level of benefits provided or, stated alternatively, to the possible consequences of a system failure.

In the case of the 747, a WLA system employing active ailerons provides wing load alleviation comparable to the fin load alleviation provided by the current yaw damper (except in the region of the wing near the aileron where, percentage-wise, WLA is more effective). Consequently, reliability comparable to the current yaw damper was used as a WLA system design objective and appears to be attainable with system complexity reasonably compatible with the benefits.

Dual tandem PCUs are recommended because, first of all, the current 747 aileron PCUs are dual tandem. It would be impractical to consider triplicated PCUs solely for WLA implementation; and, due to the effect of hydraulic system reliability, the WLA system reliability objective could not be met with WLA inputs to a single PCU. Fail-operational electronics are required to meet the reliability objective and to provide more operational flexibility for dispatching with one WLA channel failed. Use of dual electronic channels with in-line monitoring appears to be the most cost effective way of meeting the fail operational requirement for this particular system application.

6.5.2 Assessment

The outboard ailerons of the 747 were found to be effective for use as wing load alleviation (WLA) control surfaces to reduce wing design bending moments. Torsion loads and local loads on the ailerons and attachment structure are increased, but the net effect of WLA is favorable in terms of reducing the wing box weight. Since the outboard ailerons are currently used only as low-speed roll control surfaces, structural and flight control system modifications are required to allow symmetric aileron deflections throughout the operational flight envelope.

In general, the potential benefits of WLA fall in two categories:

- Wing box weight reduction relative to a wing optimized without WLA.
- Reduction of the extent of the structural modifications required for airplane gross weight growth or for installation of a wing tip modification such as a tip extension (Note: Application of WLA to airplane gross weight growth was not analyzed in this study.)

The potential of WLA for improving fuel efficiency is related to the first type of benefit; i.e., airplane gross weight can be increased or a wing tip extension can be added without a WLA system, but the structural weight increment would be greater. The second type of benefit (less extensive structural modifications) is related to implementation costs rather than fuel efficiency. For 747 derivative applications, WLA offers the first type of benefit, but (because of the structural modifications necessary to allow symmetric aileron deflections at high speed) not the second.

The structural benefit analysis conducted for the basic wing with WLA (sec. 6.2) showed that a net airplane operational empty weight reduction equivalent to 2% of the wing box weight could be achieved by means of MLC and that the benefit could be increased to perhaps 2.5% by also taking credit for the GLA capability of the system. When the wing structure was resized to take credit for MLC, redistribution of strength material and of fatigue material was required. The strength material weight was reduced while the fatigue material weight remained essentially unchanged. The combined effects of reduced bending stiffness and increased torsional stiffness were such that flutter characteristics were not adversely affected.

Aeroelastic twist was increased for the wing sized with MLC (sec. 6.2.3). Since the jig twist of the baseline wing was not changed, the cruise twist was modified (more washout) resulting in a small L/D penalty. As indicated in Figure 125, the beneficial effect of the airplane weight reduction more than offsets the L/D penalty, providing a net fuel savings of about 0.2% attributable to WLA.

Because of the aileron and wing structural modifications necessary to use the outboard ailerons at high speeds (increased aileron loads and wing torsion loads), the WLA system offers no significant benefit in terms of reduced structural modification costs for a wing tip modification. Somewhat less structural material is required with WLA, but the same general regions are affected. With current manufacturing techniques (numerically controlled machines) the costs for making small modifications to the wing box are more sensitive to the number of parts affected and the nature of the changes (which influence the nonrecurring costs for drawing revisions, recertification, etc.) than to small differences in the skin/stringer thicknesses or spar gages.

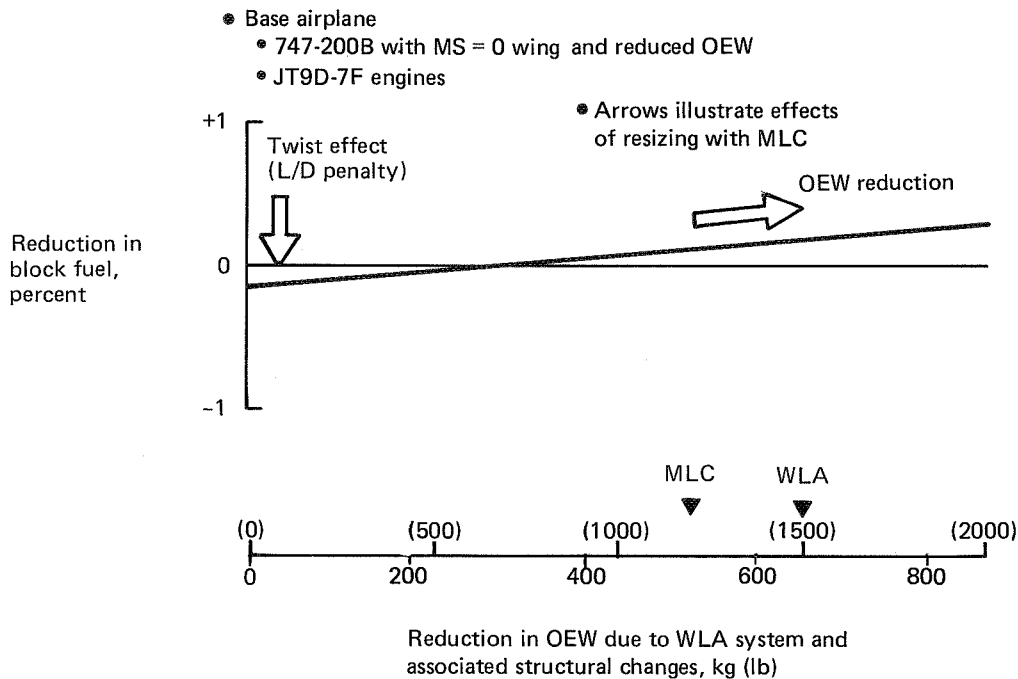


Figure 125. Fuel Saving With WLA

In short, study results show the principal economic benefits of WLA for 747 derivative applications would accrue from an airplane operational empty weight reduction relative to the same model without WLA. By providing increased damping of the first wing bending mode and reduced pitching in turbulence, the WLA system also should have a favorable effect on ride qualities.

It is expected that FAA certification of a derivative 747 equipped with a WLA system could be accomplished by application of existing FAR 25 requirements, without the need for new special conditions. However, there are some areas where interpretation is required, such as the relationship of system reliability to structural sizing requirements, the applicability of existing static destruction test results, etc., some of which are partially addressed in the following section. These areas of interpretation can be resolved only through discussion with the FAA, which was beyond the scope of this feasibility study.

Page intentionally left blank

7.0 FINAL CONFIGURATIONS STUDIES

This section provides comparisons of wing tip extensions (WTE) and winglets (WTW) with and without maneuver load control (MLC); discusses the potential benefits of a flutter mode control (FMC) system, in combination with wing tip winglets, and presents economic comparisons of the final candidate configurations. Some operational considerations, such as gate and maintenance hangar access and possible takeoff weight restrictions with an inoperative WLA system, are discussed.

Study Approach—The original plan had been to select one final wing tip configuration at the conclusion of the individual concept studies to be further analyzed in combination with a wing load alleviation system. This approach was altered (largely due to the additional time required for aerodynamic design and flutter analyses of the winglet configuration) such that the final configuration task was oriented toward developing comparative data for selecting the best configuration rather than toward a more detailed analysis of a single configuration.

Emphasis was on the Z13 WTW combined with MLC, but weight, performance, and economic data also were generated for two [1.83-m (6-ft) and 2.74-m (9-ft)] tip extensions with MLC. Wind tunnel test data and detailed structural resizing analyses (sec. 4.0) were available for the 1.83-m (6-ft) WTE without MLC. Therefore, it was decided to conduct wind tunnel testing and detailed analyses for the same [1.83-m (6-ft)] WTE combined with MLC. Weight estimates for the 2.74-m (9-ft) WTE were then developed using the previously established trend data (sec. 4.0). Those data were then used to compute L/D and fuel-saving comparisons.

This approach (1) provided a solid data base for determining MLC benefits for the 1.83-m (6-ft) WTE, (2) gave a realistic assessment of the fuel-savings potential of the 2.74-m (9-ft) WTE for comparison with the Z13 WTW, while retaining a lower-cost WTE (no leading-edge flaps on the shorter WTE) in the economic comparisons, and (3) avoided the need to build additional wind tunnel model parts to test the 2.74-m (9-ft) WTE. One cycle of strength, fatigue, and flutter sizing was completed for both the 1.83-m (6-ft) WTE and Z13 WTW with MLC. Loads were then recycled for the WTE to account for stiffness changes and final sizing was completed. The sizing activity was terminated for the WTW/MLC configuration after the first cycle because (1) it became apparent that much of the weight that could be removed by virtue of MLC would have to be replaced to meet flutter stiffness requirements, (2) large expenditures of engineering time and computing resources would be required to converge on a final sizing, and (3) precise weight estimates were not essential to economic comparisons of the WTE/WTW/WLA concepts because of the relatively weak effect of weight on fuel savings (fig. 125) as compared with the effect of L/D on fuel savings.

It was judged that a choice could be made between tip extensions and winglets based on costs and performance data estimated for the WTE/WTW concepts without WLA. The benefit of WLA was assessed on the basis of data obtained for the basic wing tip (sec. 6.0).

Although definitive structural sizing and weight comparisons of WTE and WTW configurations were not completed, the comparison attempt provided valuable insight concerning aeroelastic effects. At the conclusion of the first cycle of strength,

fatigue, and flutter sizing with MLC, it was found that maneuver loads were much lower for the WTW with MLC than for the WTE with MLC. Part of the reason was that aeroelastic twist of the wing outboard of the aileron caused an increase in the loads on the extended tip. This led to a recommendation to consider an aileron span extension for subsequent WTE/MLC studies. The most significant reason was the effect of the winglet loads on aeroelastic wing loads. Small changes in orientation of the winglet normal force vector and the effects of wing deflections in bending were found to have a very strong effect on bending moments for the inboard portions of the aeroelastic wing. Though not isolated in the flutter analyses, these "static" aeroelastic effects observed in the loads results probably contribute significantly to the difference in flutter characteristics between tip extensions and winglets.

Since the 747 EET program objective is to promote near-term commercial fleet implementation of fuel efficiency concepts, the marketability of the various configurations was considered. This was accomplished by computing the economic return to the customer airline considering the purchase price of the equipment, fuel cost savings, and other factors.

7.1 WING TIP (WTE/WTW) COMPARISONS WITH AND WITHOUT MANEUVER LOAD CONTROL

The data for tip extensions and winglets without WLA were generated as part of the individual concept study tasks. Emphasis in this section is on comparison of WTE/WTW characteristics. Details regarding development of the data are provided in Sections 4.0 and 5.0.

7.1.1 Basic Concepts

Aerodynamics—Winglets and wing tip extensions are devices which decrease induced drag, thereby improving the lift-to-drag ratio (L/D). Wing tip extensions increase the real aspect ratio of the wing, while simple end plates increase the effective aspect ratio. Winglets are more than simple end plates because of the cambered lifting surfaces that produce a forward component of the winglet normal force (fig. 126) in the same manner as a sail. The winglet concept was extensively evaluated by Dr. Richard T. Whitcomb (ref. 6). The winglet loading is integrated with that of the wing to efficiently produce significant side forces. These side forces act to reduce the lift-induced inflow above the wing tip or outflow below the wing tip. Both wing tip extensions and winglets load up the outboard wing, as shown by the span loadings on Figure 127. Aerodynamic twist (washout) of the existing wing, as well as increased structural weight, penalize the drag improvement. The resultant benefit of winglets for the 747 was found to exceed that of wing tip extensions for a given increment in airplane structure weight.

Loads—This section discusses the wing load advantages of a winglet configuration as compared to a wing tip extension. The results shown are for the Z13 winglet and the 1.83-m (6-ft) tip extension configurations, but the basic differences demonstrated are general.

Figure 128 illustrates the relative magnitude and orientation of the normal force vectors and the effects of aeroelasticity on wing section lift coefficients. The condition illustrated is a 2.5-g maneuver condition critical for wing root design loads.

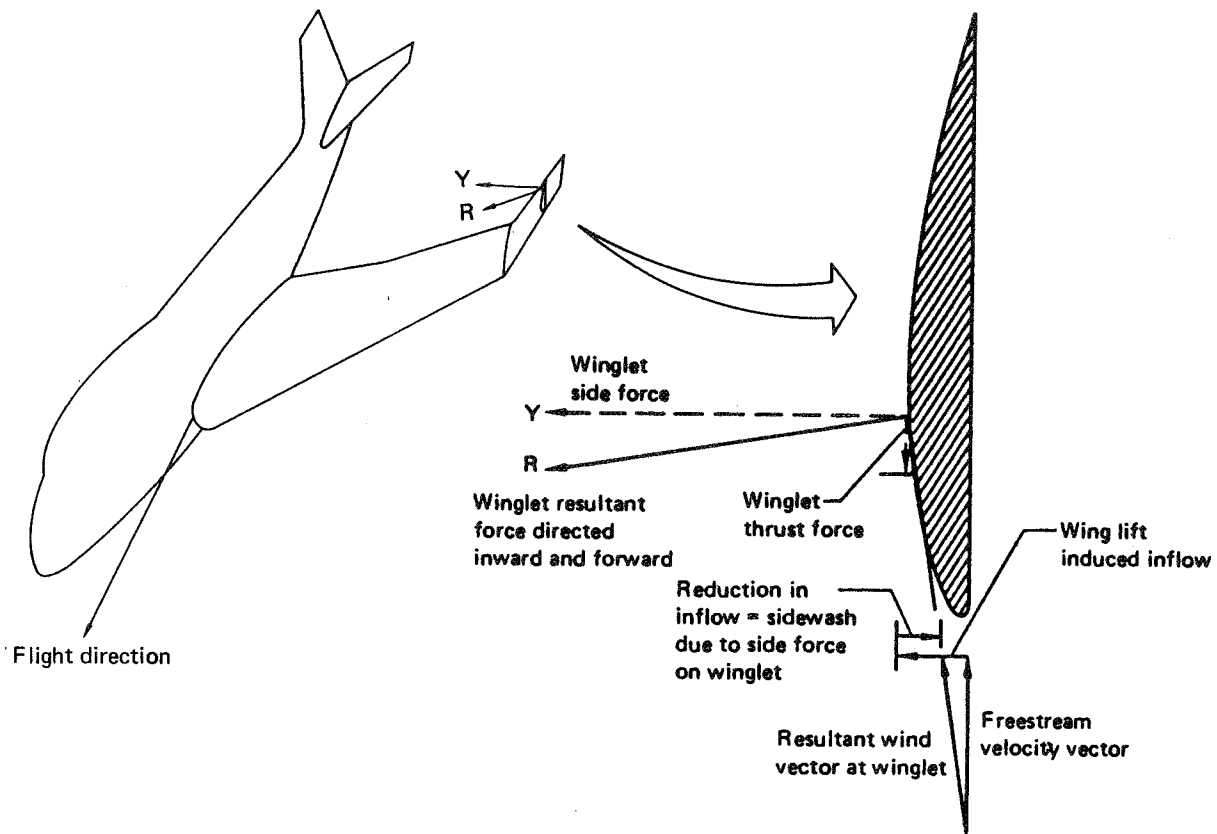


Figure 126. Winglet Force Vector Illustration

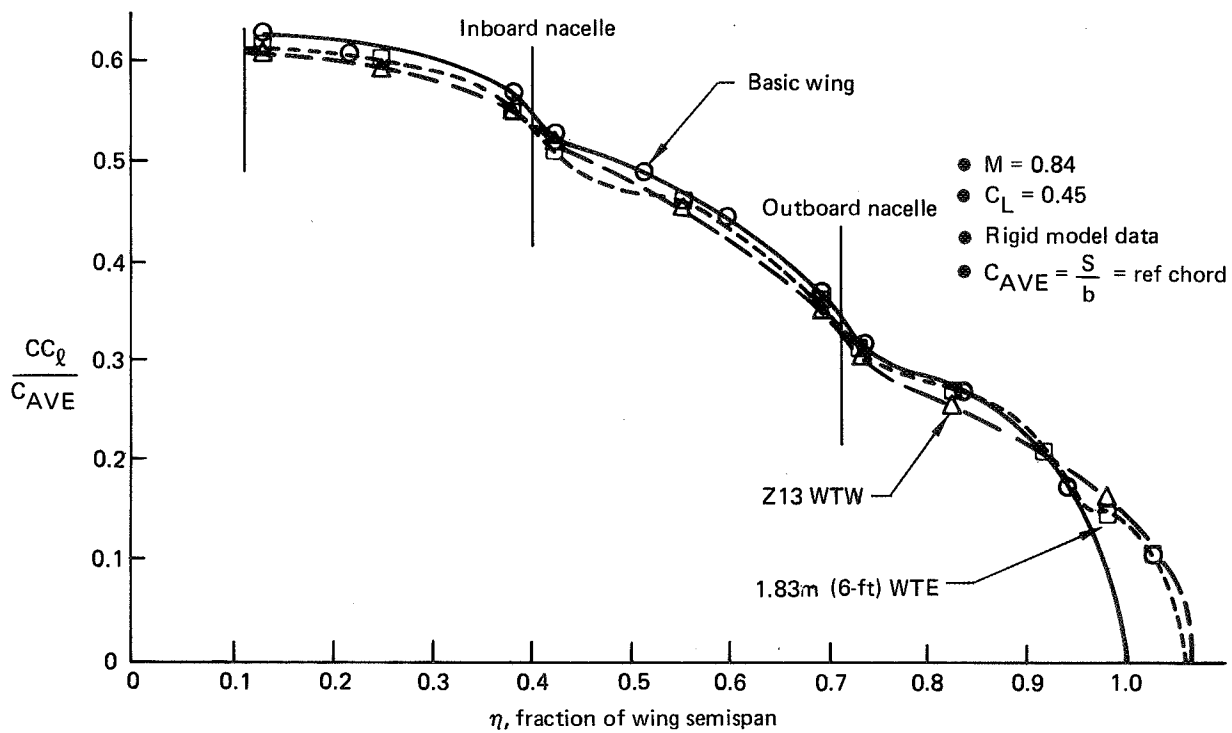


Figure 127. Span Loadings

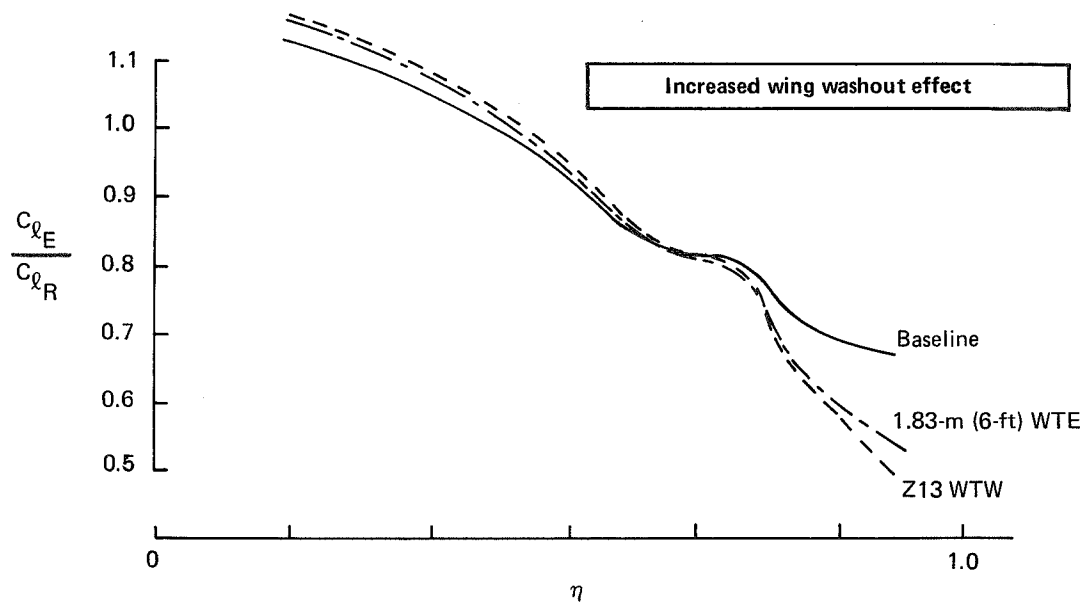
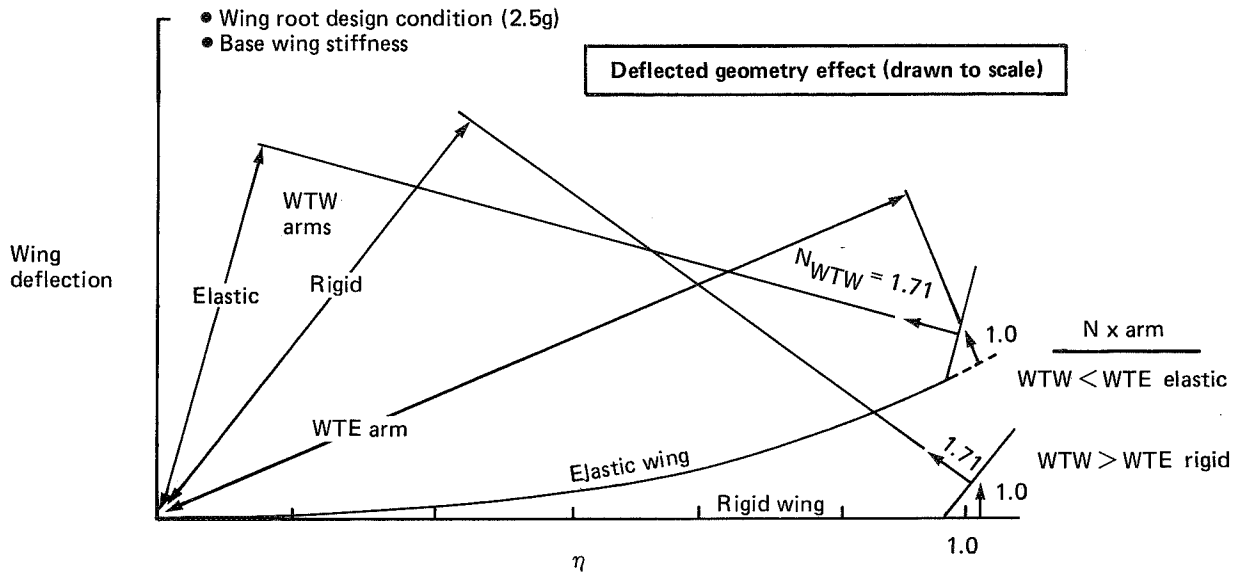


Figure 128. Effect of Aeroelasticity on WTE/WTW Loads

For this condition the winglet produced the largest local load (i.e., normal force vector), due primarily to its larger area and, when applied to the geometry of a rigid wing, it also produced the largest bending moment near the wing root. However, when the elastic bending of the wing was accounted for, the orientation of the normal force vector was changed more for the winglet, resulting in a significant reduction in the moment arm for the winglet but with virtually no change for the tip extension. As indicated, the resulting bending moment near the wing root was lower for the winglet than for the tip extension, which reversed the trend for the rigid wing.

A second advantage for the winglet configuration was that it produced increased aeroelastic washout in the outboard wing area due to its higher local moment. This resulted in shifting the wing spanwise center of pressure slightly inboard relative to the 1.83-m (6-ft) tip extension configuration. The increased washout with the winglet, a disadvantage for performance, was less pronounced at 1-g cruise conditions.

The combination of these effects produced a more favorable wing loading for the winglet configuration even though the winglet had more than 40% greater area and was designed to approximately the same normal force coefficient.

Flutter—The basic concept of wing surface extension is common to both the planar wing tip extension and the wing tip winglet configurations. From a pure flutter standpoint, the addition of wing tip mass and aerodynamic surface area is generally conducive to degradation of damping in the critical modes for flutter. Wind tunnel testing confirmed that the aerodynamic effect, rather than the mass effect, was the dominant factor in 747 flutter speed degradation with winglets. It also was concluded from test and analysis that a WTW addition was more flutter critical than a WTE of equal area.

Specific parameters responsible for the relatively poor flutter performance of the winglets have not been isolated. On a qualitative basis, some unique winglet differences can be assessed by considering the additional air force increments described in Figure A-9 of Appendix A. Normal force due to winglet spanwise motion is unique to the WTW. Wing chordwise bending motions (observed in both test and analysis) suggest that incremental forces due to fore and aft motion could be significant. Unique spatial relations of the WTW normal force vector will obviously create different force/moment effects tending to bend and twist the basic wing. Phase relationships could be destabilizing for some of these WTW induced air force increments. In addition to the unsteady motion effects unique to winglets, the large dihedral break results in increased steady-state induction effects as seen in Figure 48 of Section 5.2.2. Winglets show large local section lift curve coefficients when defined on the basis of local panel rotations. In summary, the configuration and motion effects of the WTW create larger unsteady aerodynamic forces than do comparable co-planar WTEs, thus the WTW configuration exhibits degraded flutter performance relative to the WTE configuration.

7.1.2 Loads and Twist

This section summarizes the load results for the 1.83-m (6-ft) tip extension and Z13 winglet configurations in combination with WLA. Maneuver, fatigue, and gust conditions critical for design of the wing structure were analyzed. Aileron effectiveness was based on results from the BTWT 1642 wind tunnel test. A sample of these results is shown in Appendix B.

Figures 129 and 130 show bending moment results for the wing root design condition. The winglet configuration had the highest wing bending moments when analyzed on a rigid wing but gave the lowest bending moments when wing flexibility was included. The classic washout effect and the effect of wing-up bending were accounted for separately to identify the contribution of these effects to the flexible wing loads. The more favorable aeroelastic effects for the winglet configuration are evident from the figures.

In addition to the basic winglet aeroelastic benefits identified above, two secondary benefits were noted and are discussed below.

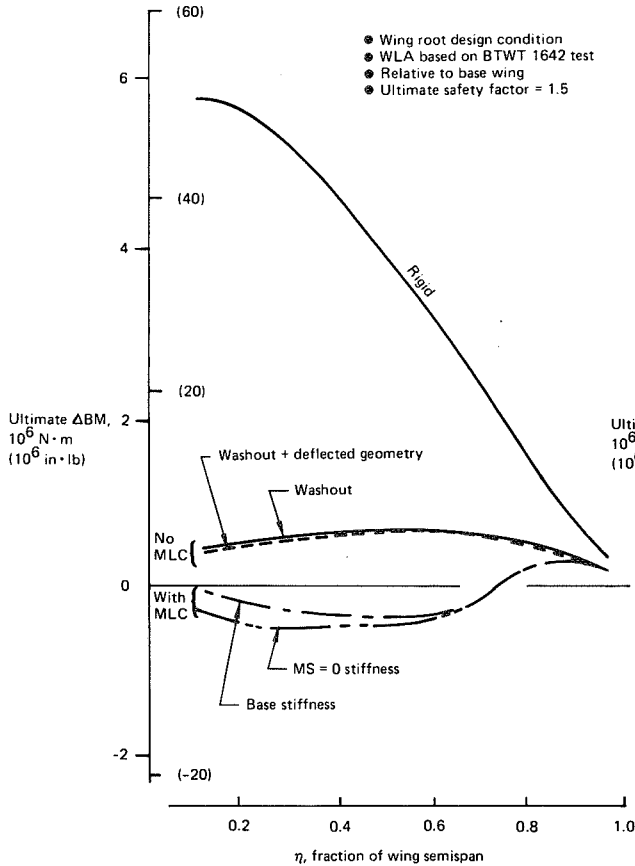


Figure 129. Effect of Aeroelasticity on Wing Bending Moments for 1.83m (6-ft) WTE

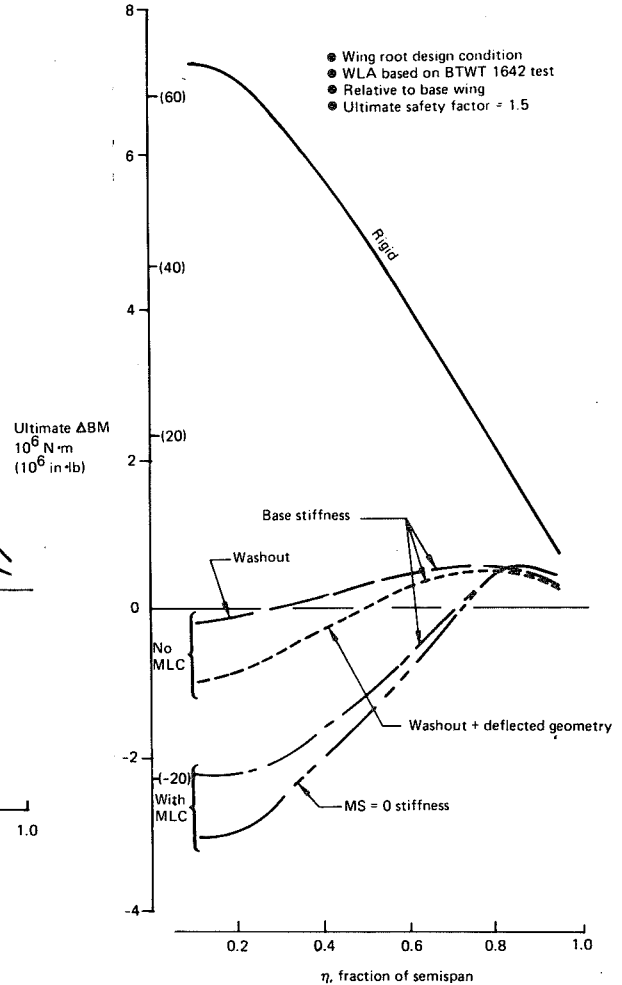


Figure 130. Effect of Aeroelasticity on Wing Bending Moments for Z13 WTW

Effect of Aeroelasticity on Aileron Effectiveness—As can be seen from Figures 129 and 130, the load reduction due to WLA was greater for the Z13 winglet configuration. This effect is illustrated further in Figure 131 where the wing bending moment reduction due to WLA is plotted. Results are shown for the rigid wing and with aeroelastic effects included. Note that the aileron effectiveness was about the same for the rigid wing configurations and, as expected, was reduced significantly due to wing flexibility. The loss of aileron effectiveness due to wing flexibility was caused by aileron induced wing "wash in" wherein, when the aileron is deflected up to produce a down load on the wing, the wing twists to a higher angle of attack and produces an offsetting up load. This is a classic effect that is well known; however, as can be seen from Figure 131B, the loss of aileron effectiveness due to wing flexibility was greater for the modified tip configurations than for the base wing. This was because these configurations produced load increases at the tip due to the respective aerodynamic surfaces attached outboard but with no corresponding load increase for the base wing, which had no additional surface outboard.

Figure 131C shows that when the effect of wing "up-bending" was accounted for, the aileron was more effective for the winglet configuration than for the 1.83-m (6-ft) tip extension configuration. The load due to aileron induced wash in produced a greater net loss in aileron effectiveness for the 1.83-m (6-ft) tip extension than for the Z13 winglet configuration, which is the expected result because of the way the winglet load is attenuated inboard when the wing is deflected up.

Effect of Structural Resizing on Final Loads—The more favorable loading characteristics for the winglet configuration resulted in reduced wing structural sizing for strength design. When the reduced stiffness was cycled in the load analysis, further load reduction resulted, as can be seen in Figures 129 and 130.

Envelope Load and Cruise Twist Results Summary—Figures 132 and 133 summarize the final bending moment envelope load and wing cruise twist results for the Z13 winglet configuration and the tip extensions in combination with WLA. These results are based on wing stiffness for a zero margin strength and fatigue design and do not include flutter stiffness requirements for the winglet configuration. The load results in Figure 132 are for the 1.83-m (6-ft) tip extension. Cruise twist results are shown in Figure 133 for both 1.83- and 2.74-m (6- and 9-ft) tip extensions. As shown in Figure 132, the winglet configuration gave significantly lower envelope load results than did the 1.83-m (6-ft) tip extension. The structural analysis for these configurations, and the predicted weight results, are reported in Sections 7.1.4 and 7.1.5. The cruise twist results were used in the aerodynamic analyses reported in Section 7.1.6.

7.1.3 Flutter

Final configuration studies were conducted for purposes of evaluating which of the two concepts was structurally more efficient while providing the required flutter margins. Throughout this comparison each concept is considered as an addition to an existing 747 wing and the conclusions could be quite different for a new wing integrated design concept. The uncertainties in flutter analysis/test evaluation were not equal for each configuration considered. The wing tip extensions were not wind tunnel tested in this program, whereas the Z13 WTW benefitted from a Z9 flutter test at a 30-deg cant angle.

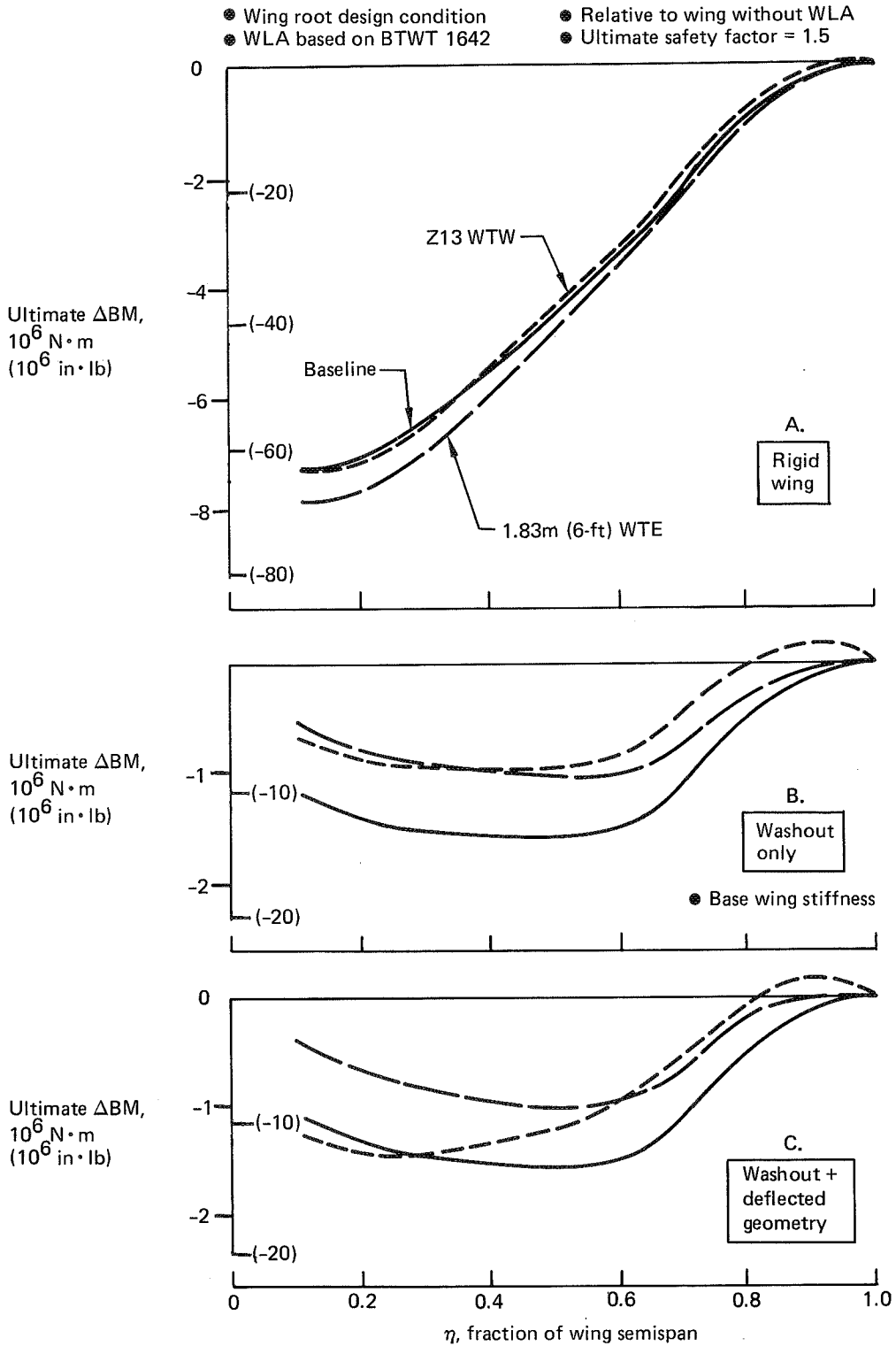


Figure 131. Effect of MLC on Wing Bending Moments for Base Wing and Wing With 1.83m (6-ft) WTE and Z13 WTW

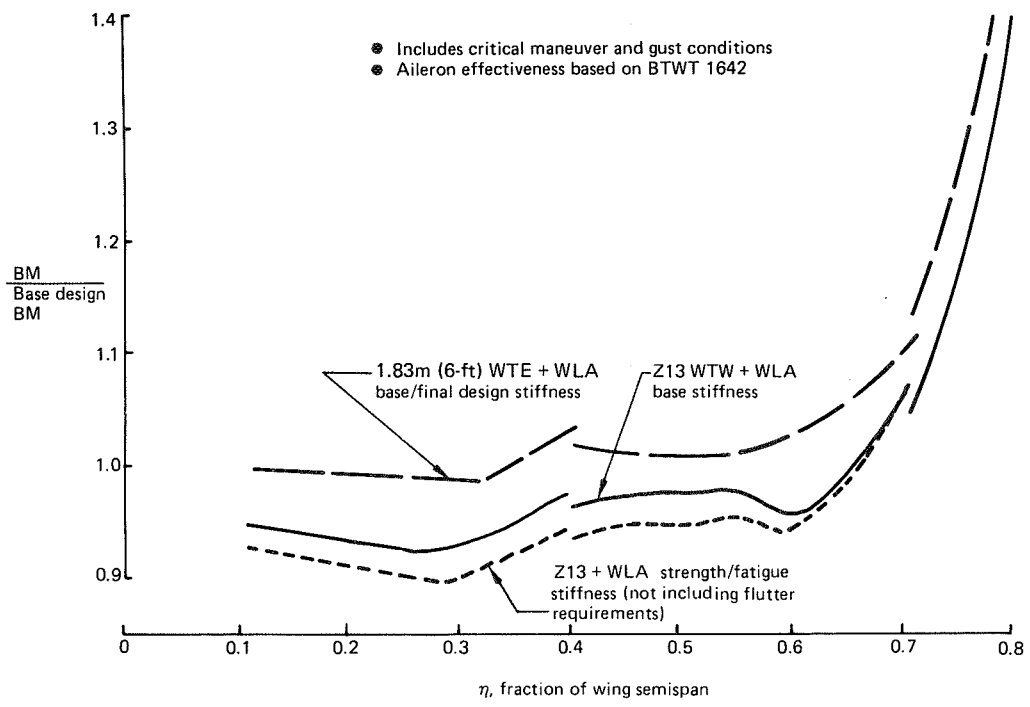


Figure 132. Effect of Combined WTW or WTE and WLA on Wing Bending Moment Envelope

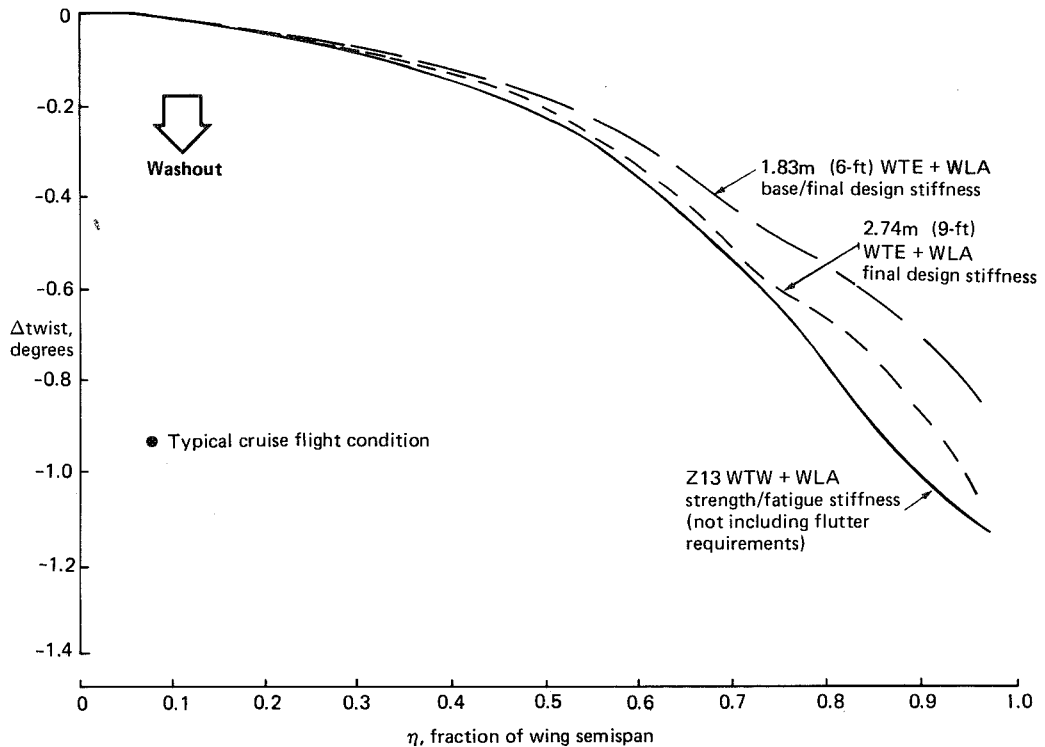


Figure 133. Effect of Combined WTE or WTW and WLA On Wing Elastic Twist

Figure 134 summarizes and compares the flutter stability characteristics of wing tip extensions and wing tip winglets considered as final configuration candidates. The WTE data are based on analysis only, and the WTW data presented here are purely experimental. The data represent a production wing configuration with nominal nacelle strut frequencies. Certain flutter stability conclusions can be supported from these comparisons. For surface extension areas up to about 9.3 m² (100 ft²), the flutter stability for the WTE concept appears acceptable and definitely superior to the winglet concept. None of the winglet candidates shown would satisfy FAA flutter requirements without a wing structural stiffness increase. High confidence data are not available on wing tip extensions in the 2.74-m to 3.66-m (9-to 12-ft) range, but analysis data show such configurations are feasible from a flutter standpoint. Beyond the 1.83-m (6-ft) extension, the appearance of a low damped symmetric mode could potentially require stiffness increases for acceptable ride comfort and/or flutter margin clearance. Additional pressure distribution tests, low-speed flutter tests, and analyses would be required to establish a flutter weight comparison. Moreover, transonic testing of winglet configurations would be required to ensure a correct evaluation of flutter safety.

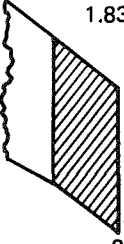
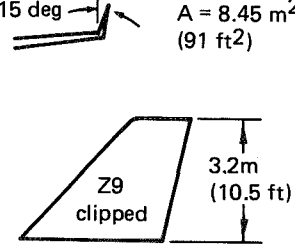
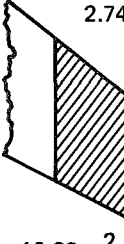
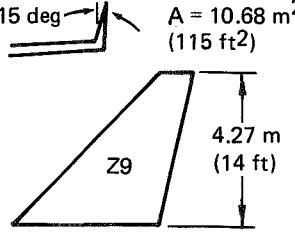

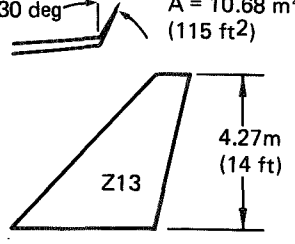
Extensions	Critical modes	V _F /V _{REF}	Winglets	Critical mode	V _F /V _{REF}
 <p>1.83m (6 ft)</p> <p>A = 7.43 m² (80 ft²)</p>	<p>Antisymmetric outboard nacelle side bending 1.98 Hz</p> <p>Antisymmetric BASIC mode 1.76 Hz</p>	<p>Flutter 1.305</p> <p>Stable (g_{min} = 0.037)</p>	 <p>15 deg</p> <p>A = 8.45 m² (91 ft²)</p> <p>Z9 clipped</p> <p>3.2m (10.5 ft)</p>	<p>Antisymmetric outboard nacelle side bending 1.95 Hz</p>	<p>Flutter 1.085</p>
 <p>2.74m (9 ft)</p> <p>A = 10.22 m² (110 ft²)</p>	<p>Symmetric 2.65 Hz</p> <p>Antisymmetric outboard nacelle side bending 1.98 Hz</p> <p>Antisymmetric BASIC mode 1.76 Hz</p>	<p>Low-damped 0.68 to 1.11</p> <p>Flutter 1.325</p> <p>Stable (g_{min} = 0.034)</p>	 <p>15 deg</p> <p>A = 10.68 m² (115 ft²)</p> <p>Z9</p> <p>4.27 m (14 ft)</p>	<p>Symmetric 2.35 Hz</p>	<p>Flutter 0.985</p>
 <p>3.66m (12 ft)</p> <p>A = 14.86 m² (160 ft²)</p>	<p>Symmetric not defined</p> <p>Antisymmetric BASIC mode 1.70 Hz</p>	<p>Symmetric not defined</p> <p>Low-damped (g_{min} = 0.009)</p>	 <p>30 deg</p> <p>A = 10.68 m² (115 ft²)</p> <p>Z13</p> <p>4.27m (14 ft)</p>	<p>Wing tip flutter 5.67 Hz</p>	<p>Flutter 0.965</p>
Analysis			Wind tunnel test		

Figure 134. Flutter Comparisons for Extensions and Winglets

Final configuration flutter analyses were carried out on three selected configurations including wing tip extensions of 1.83m (6 ft) with constant chord and 2.74m (9 ft) with constant taper and the Z13 winglet. Figure 135 shows the significant aerodynamic parameters of these three configurations. Each of the configurations was analyzed with the required stiffness for the incorporation of a maneuver load control system with that configuration.

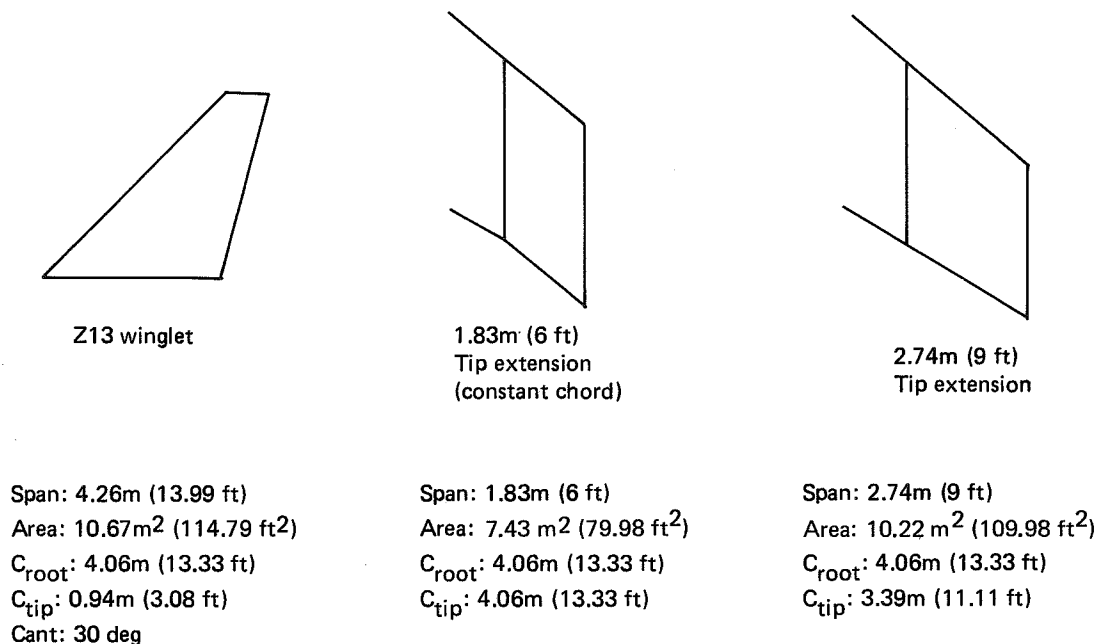


Figure 135. Configurations for Final Flutter Analyses

The highest level of confidence in the results exists for those modifications that only affect the familiar antisymmetric flutter modes—the wing tip extensions. Even then, new modes are introduced as the span increases. The wing tip winglets are considered less amenable to standard methodology and require more experimental data than wing tip extensions.

Figure 136 compares each of the final configurations with MLC wing stiffness for the appropriate critical flutter mode. The configuration with the least damping at the lowest velocity is the 2.74-m (9-ft) wing tip extension. It is assumed that the inherent structural damping would provide adequate total damping characteristics. The most critical configuration is the Z13 winglet with the symmetric mode flutter. The 1.83-m (6-ft) wing tip extension is not considered critical.

Figure 137 compares the flutter modes for the 1.83-m (6-ft) wing tip extension with and without the MLC wing stiffness. The antisymmetric BASIC mode is slightly degraded and the antisymmetric outboard nacelle side bending (ONSB) mode is slightly improved with the MLC wing stiffness.

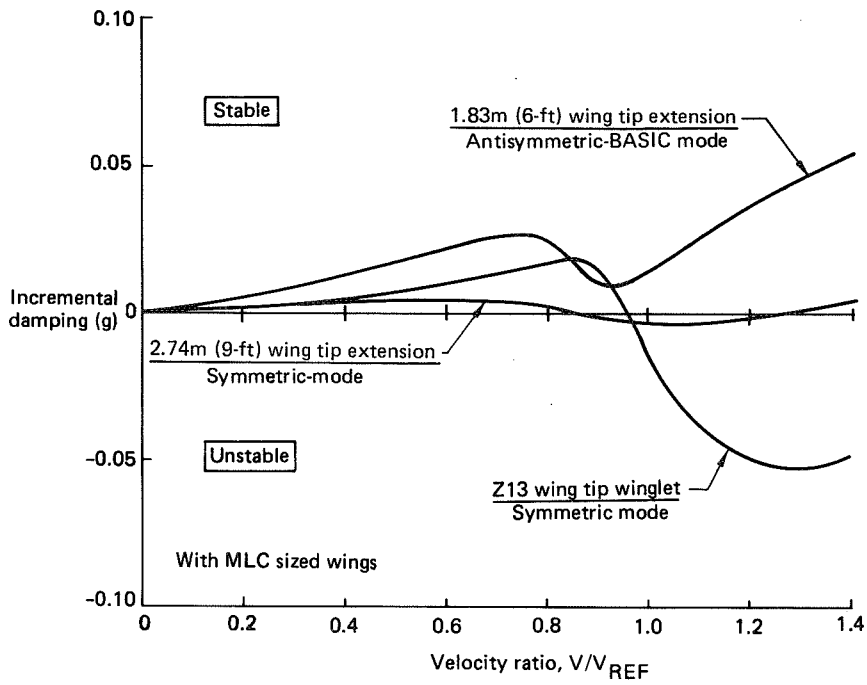


Figure 136. Flutter Stability Comparisons for Final Configurations

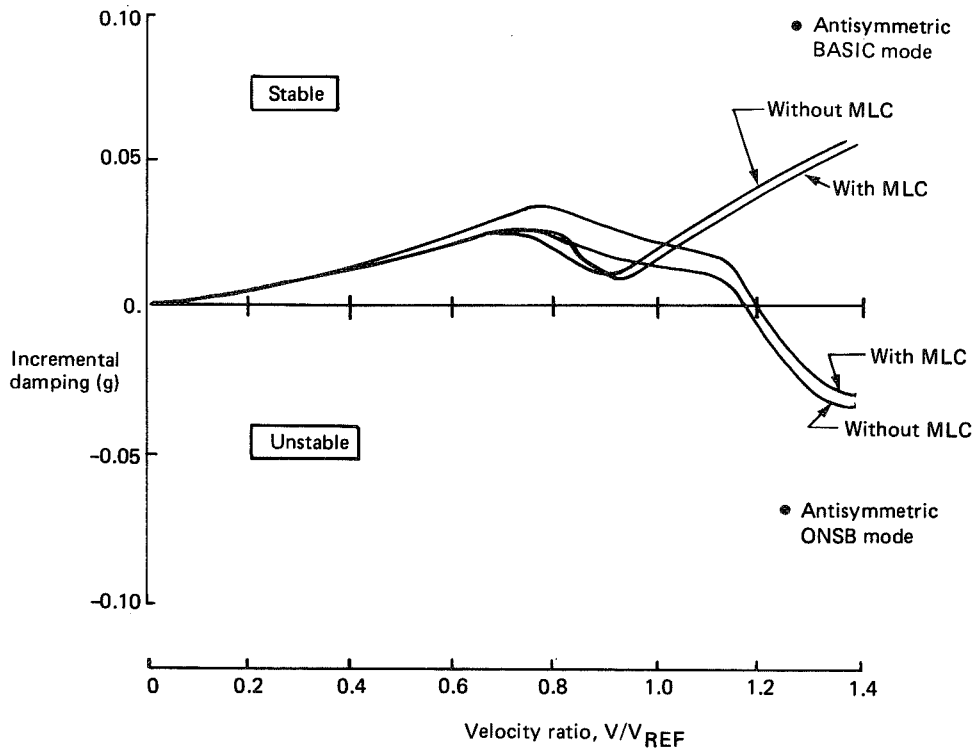


Figure 137. MLC Effect for a 1.83m (6-ft) Wing Tip Extension

Figure 138 compares the flutter modes for the 2.74-m (9-ft) wing tip extension with and without the MLC wing stiffness. This tip extension introduces a low damped symmetric flutter mode that is slightly better with the MLC wing stiffness. The antisymmetric ONSB mode is slightly worse with the MLC wing stiffness. The antisymmetric BASIC mode shows little change due to the MLC wing stiffness.

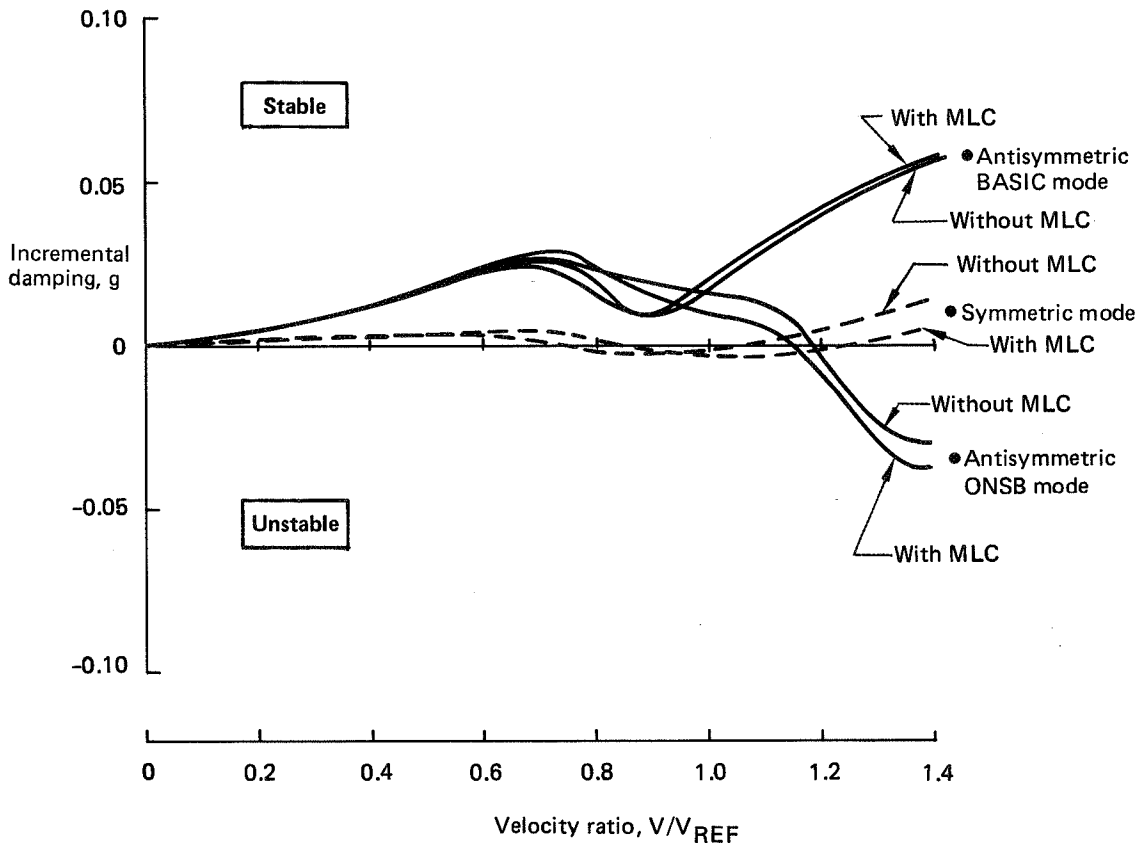


Figure 138. MLC Effect for a 2.74m (9-ft) Wing Tip Extension

Figure 139 compares the flutter modes for the Z13 winglet with and without the MLC wing stiffness. The Z13 winglet flutter solution with the baseline wing stiffness shows that the wing tip flutter mode occurs at a slightly lower airspeed than the symmetric mode. With the MLC sized wing, the flutter mode criticality is reversed and the symmetric mode now occurs at the lower airspeed. This is caused by the torsional stiffness redistribution that results in a softer inboard wing and a stiffer outer wing. Since the symmetric mode flutter requires inboard stiffness to raise its flutter speed, the MLC wing necessitates the larger flutter weight penalty to clear FAA margins.

The final configuration closed-loop flutter studies are contained in Section 6.3.2 as part of the closed-loop dynamic analyses with wing load alleviation.

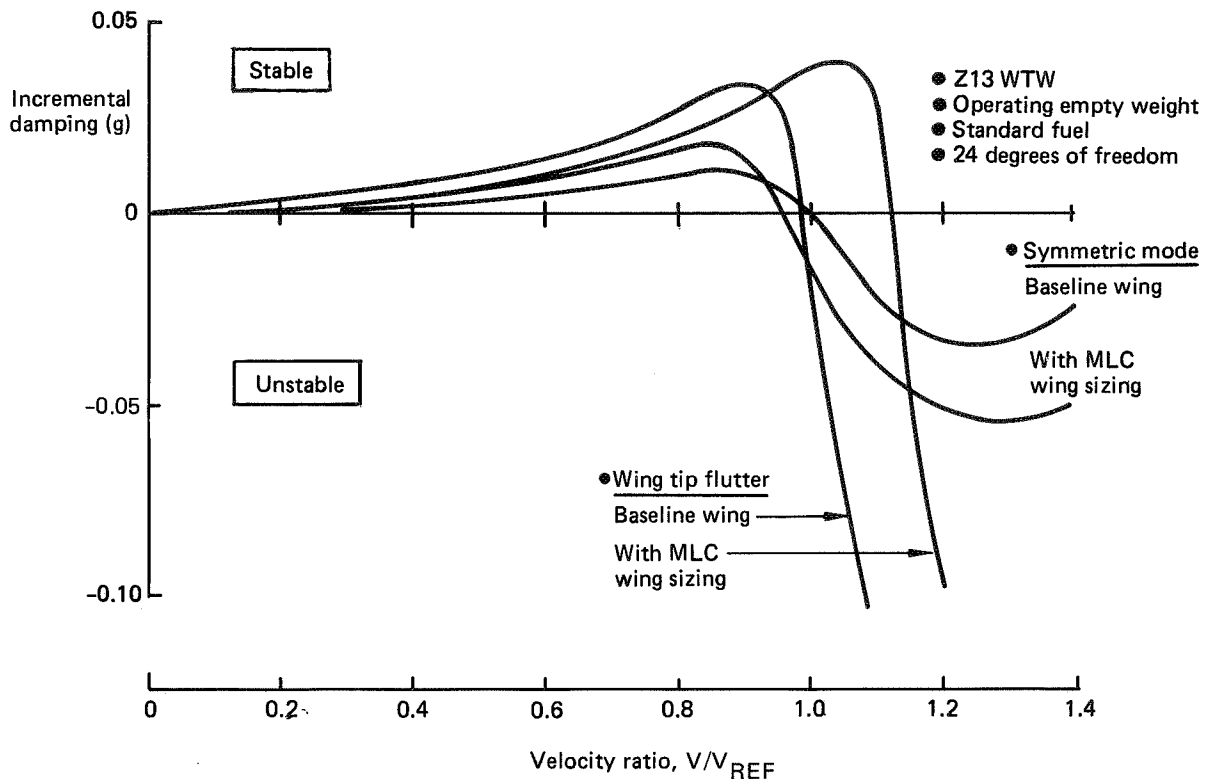


Figure 139. MLC Sizing Effect for Wing Tip Winglets

7.1.4 Structural Resizing with MLC

Resizing of the wing box structure to accommodate tip extensions and winglets without MLC is discussed in Sections 4.2.3 and 5.3.3. The wings with wing tip modifications (WTE/WTW) combined with MLC were resized to zero margin of safety using the same general analysis procedures used for resizing the basic wing with MLC (sec. 6.2.2). The resultant sizing for the 1.83-m (6-ft) tip with MLC is shown in Figure 140. The effects of MLC on the bending and torsional stiffness of the wing with the 1.83-m (6-ft) tip are shown in Figure 141.

The wing with a Z13 winglet and MLC required less material for ultimate and fatigue loads than the wing with a 1.83-m (6-ft) tip and MLC, but required large stiffness increases for flutter. No flutter material was required for the 1.83-m (6-ft) tip configuration with or without MLC.

The wing with the Z13 winglet and MLC was not further resized after the addition of the large stiffness increase for flutter. It was not considered worthwhile to iterate to a final optimum sizing because the flutter requirements tended to negate the possible advantages from MLC.

Figure 142 shows the wing structural modification required to add the WTE or the WTW without MLC to the baseline wing. In this case, the existing baseline margins of safety are absorbed as required and the wing "beefed up" where required to give zero margins of safety. The different extent of changes required for the WTE and WTW can be seen from this figure.

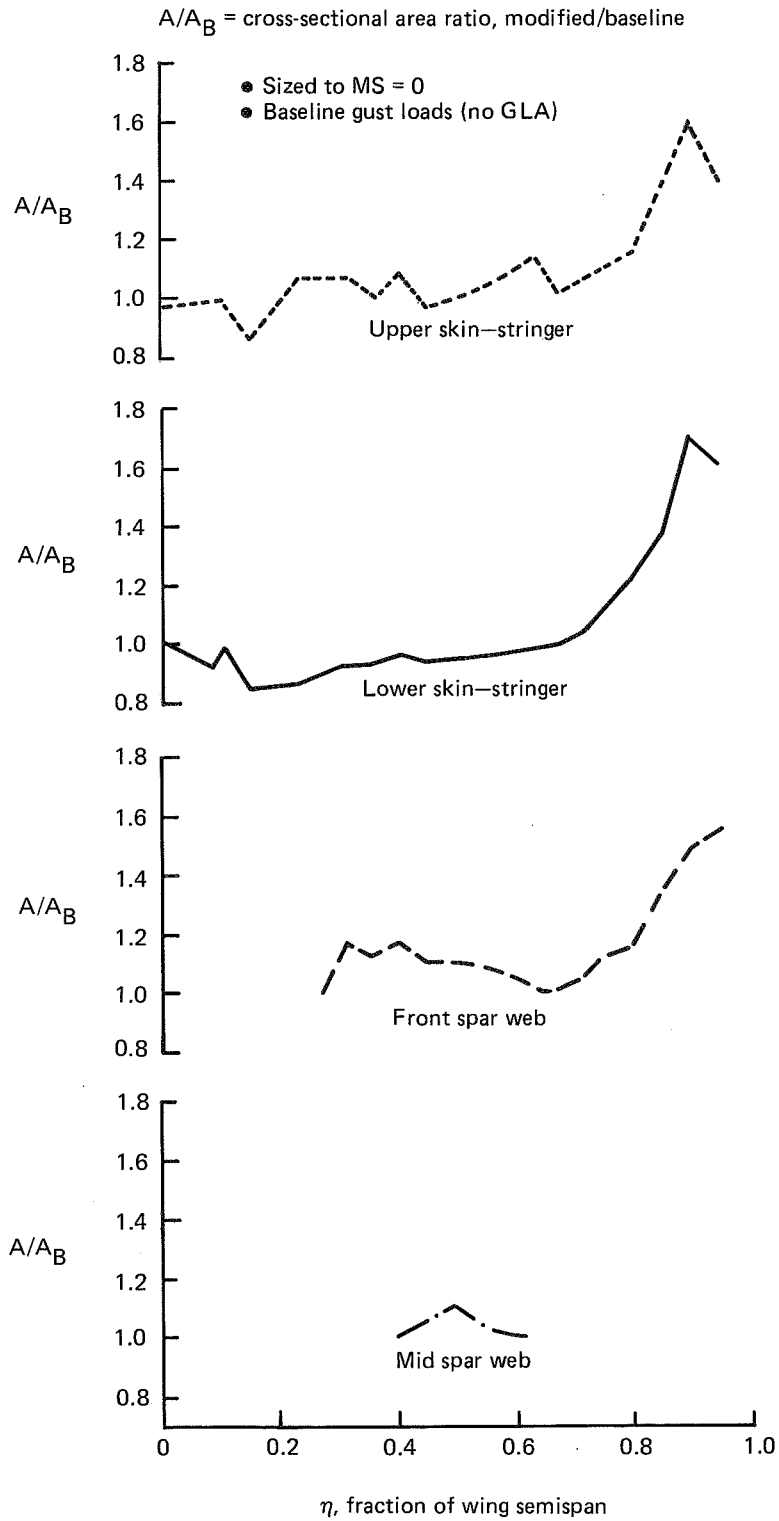


Figure 140. Structural Sizing of Wing With 1.83m (6-ft) WTE and MLC

- $\frac{EI}{EI_B} \frac{GJ}{GJ_B}$ = stiffness ratios – $\frac{\text{modified}}{\text{baseline}}$
- Baseline MS absorbed where ratios > 1.0
- Sized to MS = 0 for ratios < 1.0

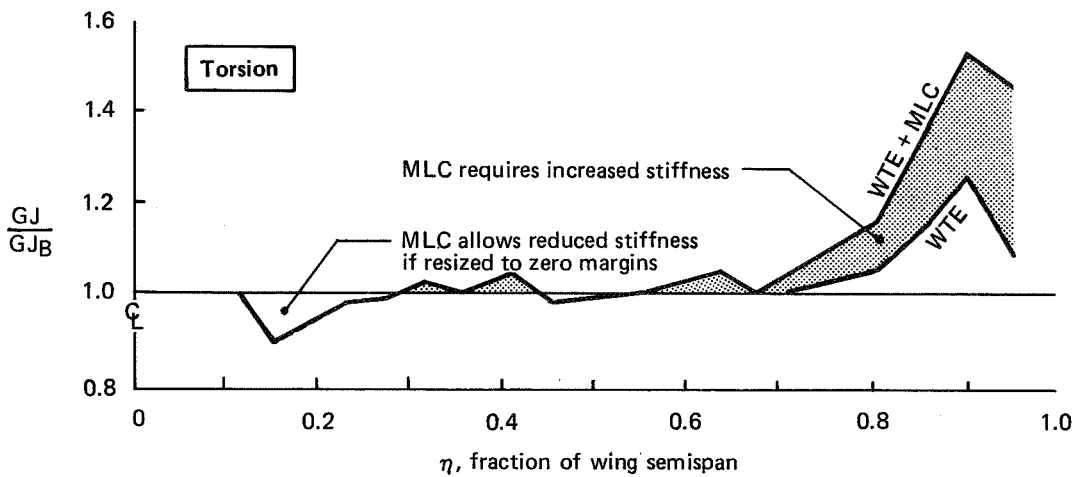
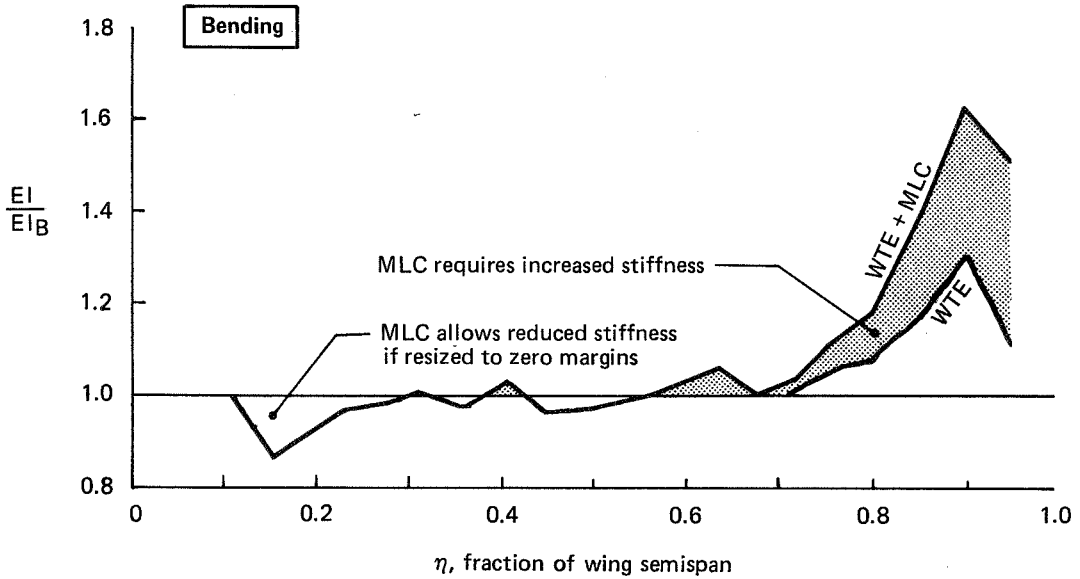
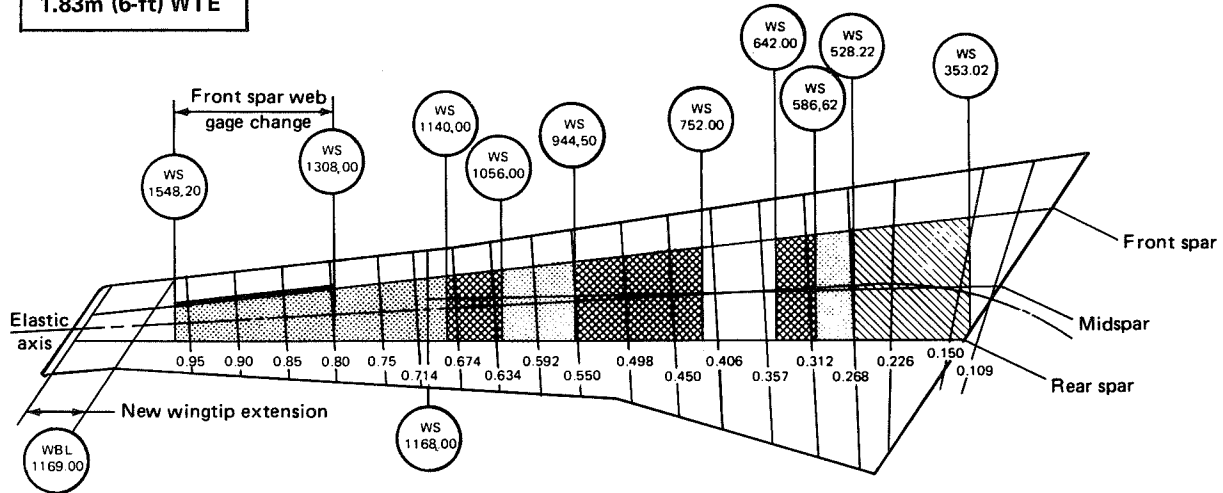


Figure 141. Effect of MLC on Wing Structural Stiffness Requirements for 1.83m (6-ft) WTE

- Baseline margins absorbed
- Shading denotes skin-gage and stringer-area changes relative to baseline wing
- ▨ Increased upper surface skin gages and stringer areas
- ▩ Increased lower surface skin gages and stringer areas
- ▧ Increased upper and lower surface skin gages and stringer areas

1.83m (6-ft) WTE



Z13WTW

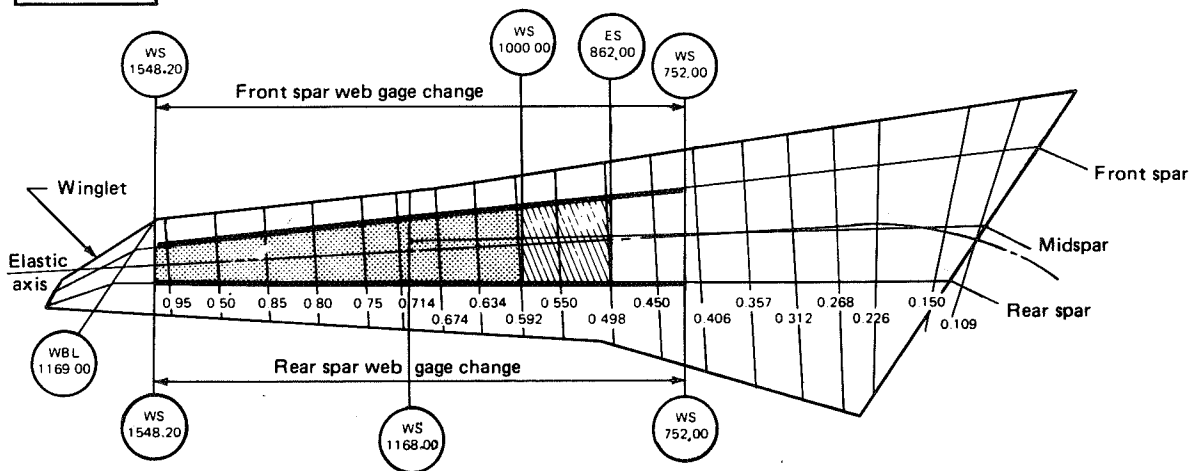


Figure 142. Wing Structural Modifications Required to Add WTE/WTW Without MLC to Baseline Wing

The wing structural modifications required to add the WTE and MLC to the baseline wing are shown in Figure 143. Again the existing margins of safety were absorbed and the wing beefed up where required. The final sizing used loads generated with MS = 0 stiffness. Changes in loads with stiffness corresponding to "beef-up" only sizing were negligible. Final sizing was not completed for the Z13 WTW with MLC, thus the structural modifications are not shown.

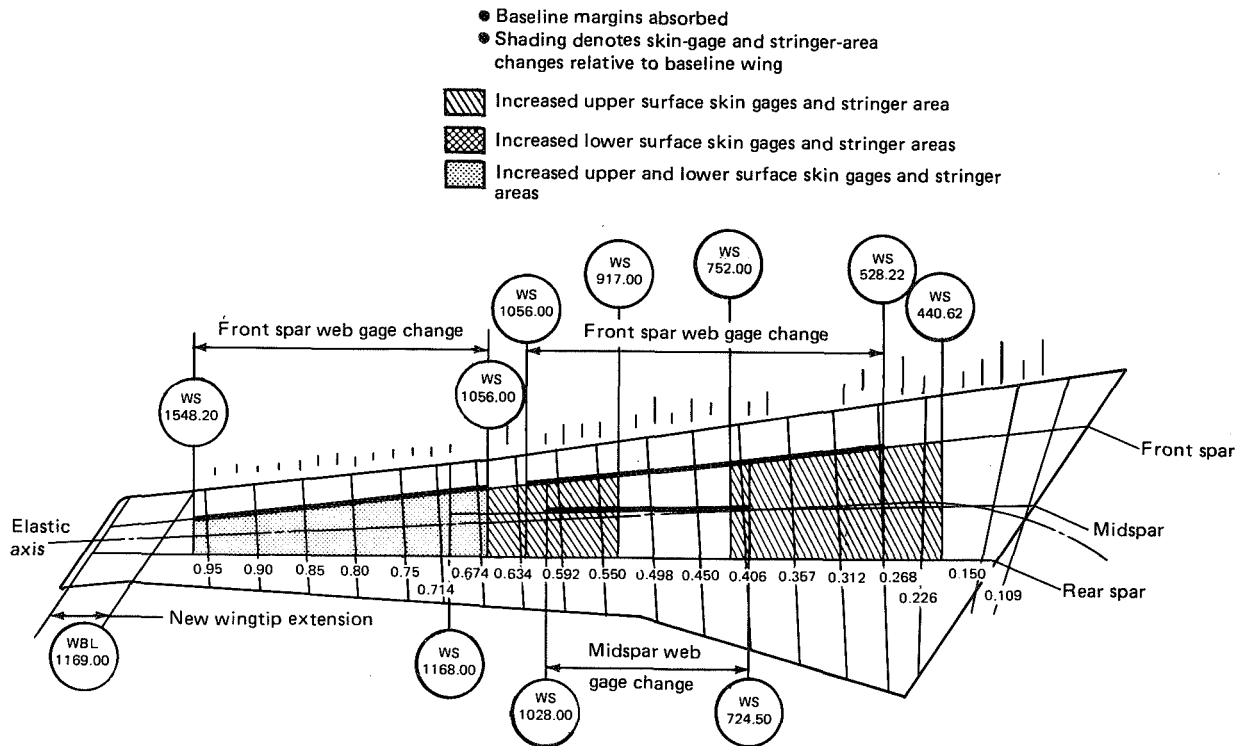


Figure 143. Wing Structural Modifications Required to Add WTE + MLC to Baseline Wing

The wing structural modifications required to add the WTE and MLC to a zero margin wing are shown in Figure 144. No existing positive margins of safety exist and, therefore, the changes are larger than those shown in Figure 143.

Retrofitting a tip device and MLC is not practical because of the extensive structural changes required.

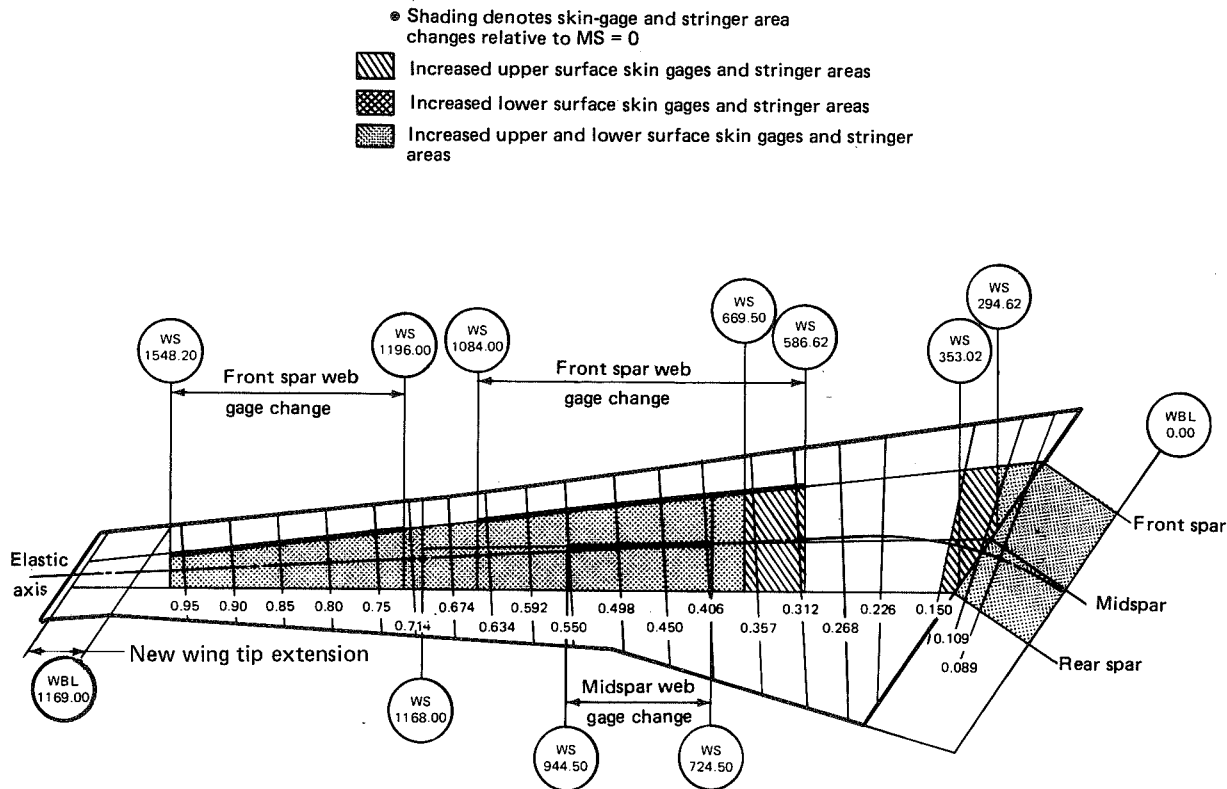


Figure 144. Wing Structural Modifications Required to Add WTE + MLC to a Zero-Margin Baseline Wing

7.1.5 Weights

WTE/WTW without WLA—The increases in airplane operational empty weight (OEW) necessary for installation of wing tip modifications without WLA are compared in Figure 145 for the two sets of structural resizing ground rules. The data shown for the 3.66-m (12-ft) WTE are probably optimistic since only a partial set of load conditions was considered and flutter sizing was not conducted. Weights for the 1.83-m (6-ft) WTE and Z13 WTW were based on complete resizing analyses, including flutter sizing (no flutter material required for the WTE).

Results show that a winglet can be added with less increase in total airplane OEW than a panel of the same length installed as a wing tip extension. The weight advantage for the winglet was found to be more pronounced when existing structural margins of safety were maintained. These data (margins maintained) give an indication of the weight increments for tip modifications on a wing having no positive margins in the baseline wing box structure. The weight increments for strength material should be reasonably representative of the corresponding increments for a zero margin wing, but the fatigue and flutter material requirements would be greater for the zero margin wing.

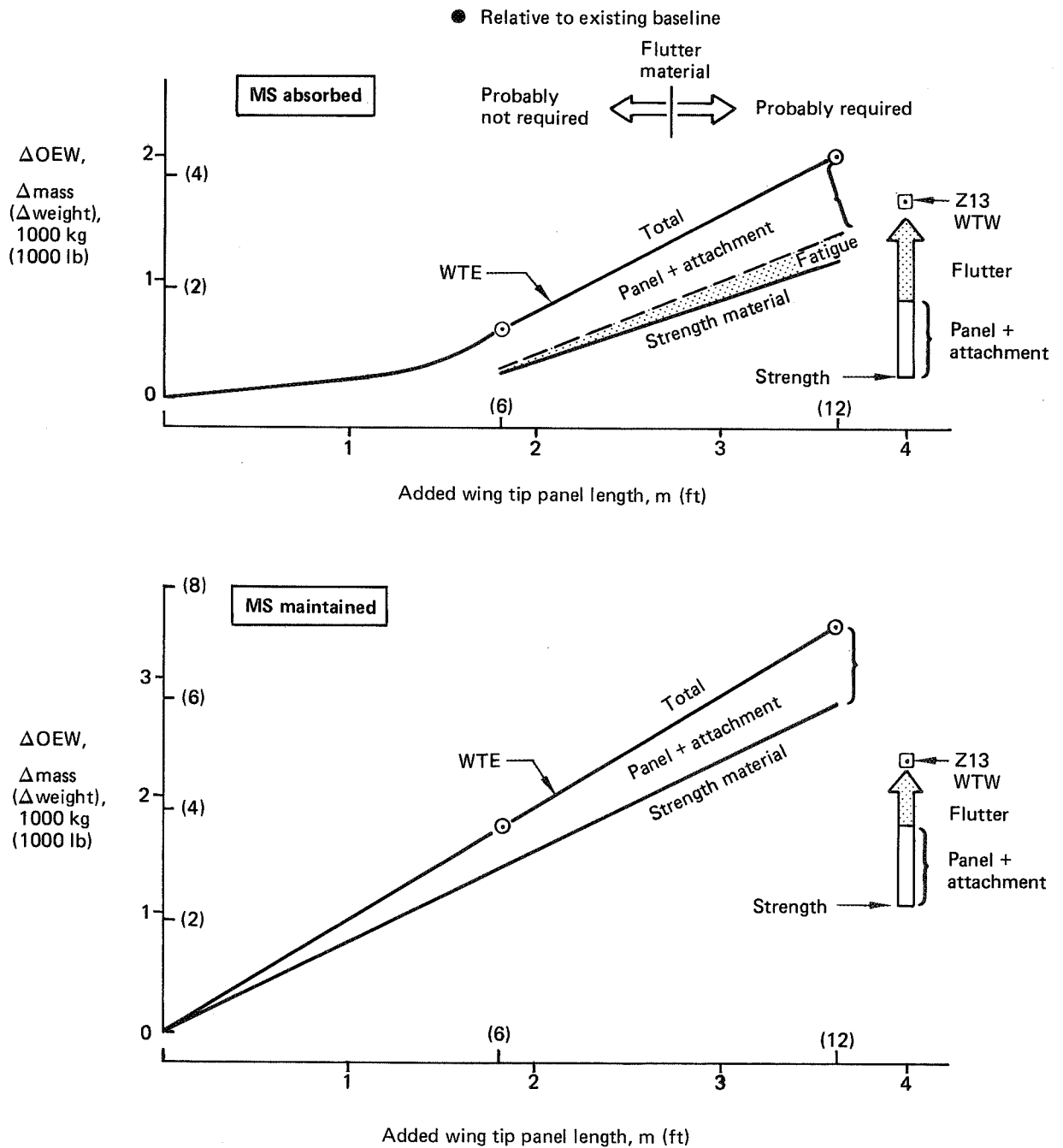


Figure 145. Weight Comparison of WTE/WTW Without WLA

Configurations With MLC—Airplane OEW increments for several wing tip configurations (basic wing tip, tip extensions, Z13 winglet) combined with MLC are shown in Figure 146. These increments are relative to a baseline airplane (having the wing box structure sized to zero margins without WTE, WTW, or WLA) that is lighter than the baseline used for the data shown in Figure 145. As explained in the introduction to this section, different baselines were used because of differences in objectives, ground rules, and methods between the studies of configurations with and without WLA. Due to these differences, weight increments have not been shown in the same figure for configurations with and without WLA. The data without WLA (fig. 145) are consistent as a set, and the data with MLC (fig. 146) also are consistent as a set; but the weight benefits of MLC for the WTE/WTW configurations should not be inferred from the difference in weights between Figures 145 and 146. However, some observations regarding MLC effects on weights can be made as follows:

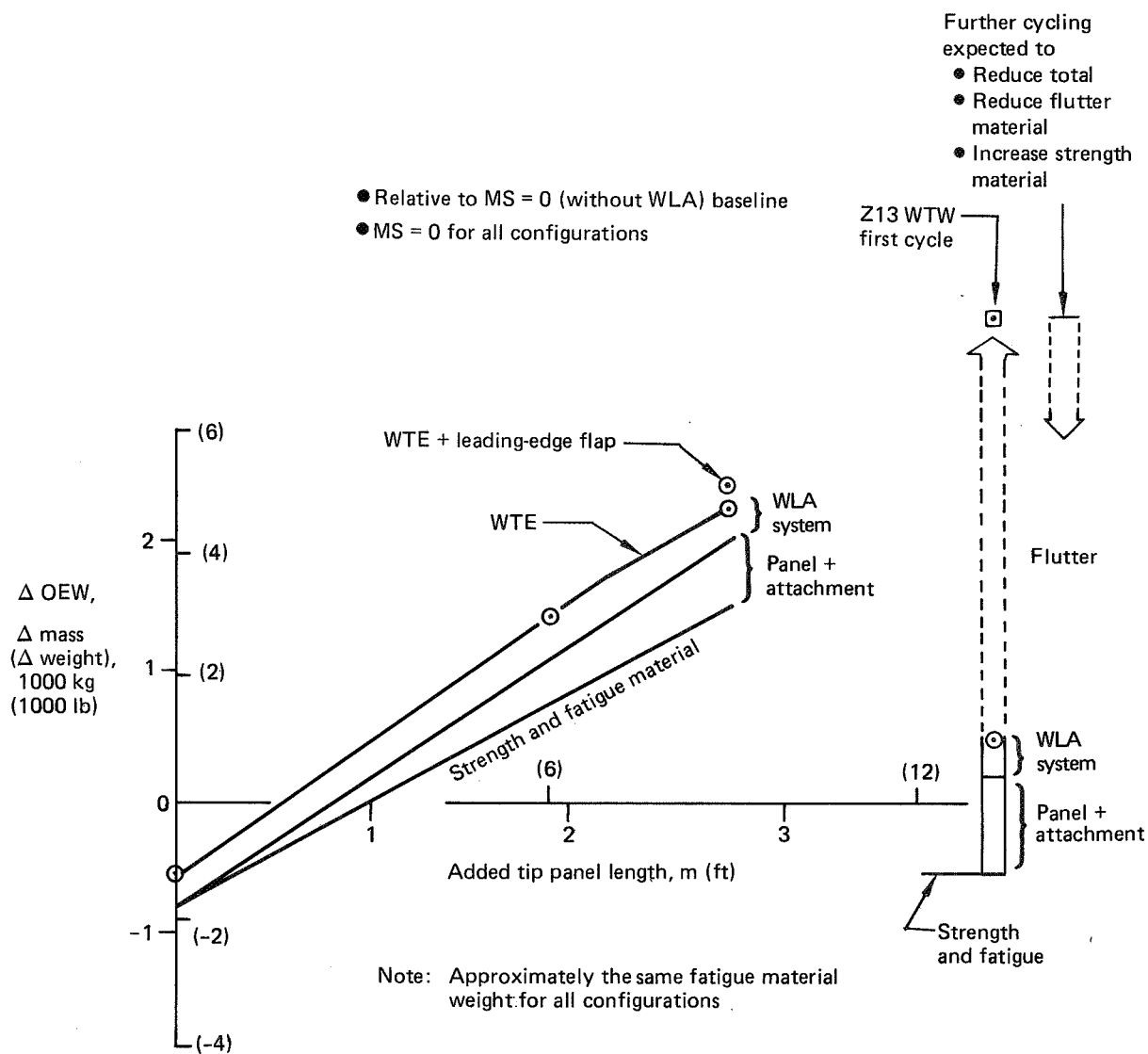


Figure 146. Weight Comparison of WTE/WTW with MLC

- **MLC Benefit For Basic Wing Tip**—The total weight increment shown in Figure 146 for a zero length WTE corresponds to the MLC benefits discussed in Section 6.2.3 for the basic wing. The fatigue increment illustrated in that section (fig. 87) was shown with and without MLC on a zero margin wing. The fatigue increment is not illustrated in Figure 146 because it was quite small relative to the $MS = 0$ baseline and was approximately the same for all of the configurations.
- **MLC Effect For WTE**—A direct comparison of weights for a given WTE with and without MLC is not shown. The slope of the weight vs. span curve is a little greater for the wing with MLC (fig. 146) than the slope of the corresponding curve for the wing without MLC (fig. 145, existing structural margin maintained). This implies that the benefit of MLC with the existing aileron span is a little less than the benefit predicted for the basic wing tip (sec. 6.2.3). This observation correlates with the increased load on the extended tip resulting from aeroelastic effects discussed in Section 7.1.2. The MLC benefits could be increased with the WTE by extending the aileron span.
- **WTE/WTW Comparisons With MLC**—Before considering the WTE/WTW weight increments shown in Figure 146, it should be recognized that the strength-fatigue material and flutter material weights indicated for the WTW/MLC configuration are unrealistic because resizing analyses were terminated after the first cycle of sizing for reasons outlined in the Section 7.0 introduction. If the WTW/MLC sizing were further cycled to optimize the flutter material distribution and to reflect the effects of flutter stiffness on strength sizing, the flutter weight increment would be much less than indicated, but the strength material requirements would be greater. The total weight increment would be reduced, but probably not enough to give the WTW/MLC configuration a significant weight advantage relative to the WTE/MLC configuration.

Although final sizing of the WTW/MLC configuration was not completed, the data resulting from the fairly extensive resizing analyses that were accomplished are of considerable academic interest and are presented for that reason. The wing box strength material requirements (fig. 146) are seen to be much less for the WTW/MLC configuration (prior to resizing for increased flutter stiffness) than for the WTE/MLC configurations (not flutter critical). This result, which was unexpected since rigid wing aileron effectiveness was the same for both, was due to differences in aeroelastic effects on loads (discussed in sec. 7.1.2).

The weight of the added panel (WTE/WTW) and attachment is greater for the winglet, unless leading-edge flaps (table 7) are required on the WTE, in which case the added panel weights are similar. A weights breakdown for the 2.74-m (9-ft) WTE (without leading edge flaps) is provided in Table 8.

The WLA system weights, including strengthening of the existing aileron, were the same for all wing tip configurations. A breakdown is shown in Section 6.2.3.

No flutter stiffness material was required with the tip extensions. With the winglet, much more flutter material was required with MLC (fig. 146) than without (fig. 145). Some increase in flutter material for the WTW/MLC wing was expected because the baseline wing for MLC studies (zero margin) had less inherent stiffness, and resizing the baseline wing to take credit for MLC capability further reduced the stiffness. However, the magnitude of the flutter weight increase resulting from the first cycle

Table 7. Weight Breakdown for Variable Camber Flaps on 2.74m (9-ft) WTE

	Mass, kg/airplane	Weight (lb/airplane)
Linkage	64.0	(141)
Actuators	32.2	(71)
Actuator support structure	5.9	(13)
Pneumatic drive unit (2)	42.2	(93)
Drive unit support structure	7.6	(16)
Pneumatic ducting	2.3	(5)
Drive shaft	3.2	(7)
Rib modifications	21.8	(48)
Folding nose panel	14.5	(32)
Nose flippers	26.3	(58)
Existing skin panel	-10.4	(-23)
Miscellaneous + round-off	4.1	(9)
Total	+213.7	(+470)

Table 8. Mass (Weight) Breakdown for 2.74m (9-ft) WTE

Panel weight	Mass (weight) per airplane,	
	kg	(lb)
Wing box extension	337	(745)
Leading-edge extension	122	(270)
Trailing-edge extension	44	(97)
Additional access doors	10	(21)
Deletions	-61	(-134)
Systems relocation and round-off	10	(21)
Total	462	(+1020)

of flutter sizing was exceptionally large. In fact, the wing with winglet was a great deal heavier in absolute terms (not shown) when sized with MLC (fig. 146) than without (fig. 145), even though the baseline wing for the MLC studies was lighter. This made it apparent that the flutter material distribution selected for the first cycle of sizing was not optimum for the WTW/MLC configuration. The flutter material was added to the wing between the engine nacelles and outboard (as had been done for winglet flutter sizing without MLC), whereas strength material had been removed inboard (when resized with MLC). This suggests that flutter material for the WTW/MLC configuration could be reduced by distributing part of the material further inboard to restore some of the stiffness lost in MLC sizing.

Although flutter material requirements could be reduced, it should be noted that further recycling of the loads and strength sizing would result in increased requirements for strength material due to the effects of the flutter stiffeners (sec. 7.1.2). Because of the flutter-critical nature of the 747 wing with winglets, it is doubtful that the weight advantage of winglets relative to tip extensions would be any greater with MLC than without.

Incremental Mass (Weight) Distributions—The change in wing mass (weight) distribution is illustrated in Figures 147 and 148 for wing tip modifications without WLA, expressed relative to the existing baseline wing. Similar data for configurations resized with MLC are provided in Figures 149 and 150, expressed relative to the zero margin baseline. A smaller scale was selected for presenting the winglet data (fig. 150) due to the larger flutter increment.

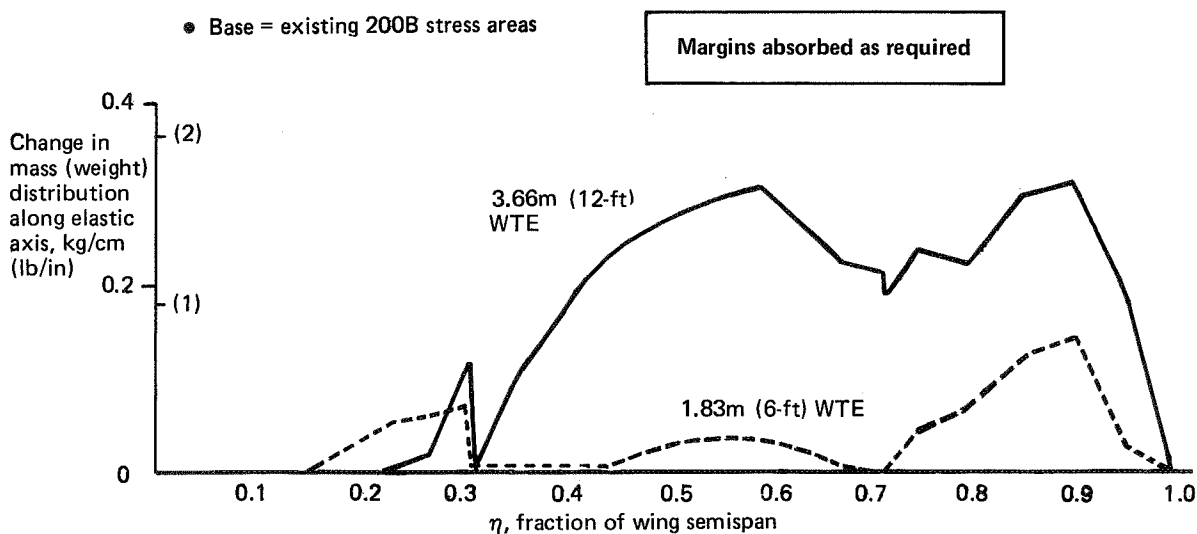


Figure 147. Change in Wing Box Weight Distribution for WTE Without WLA

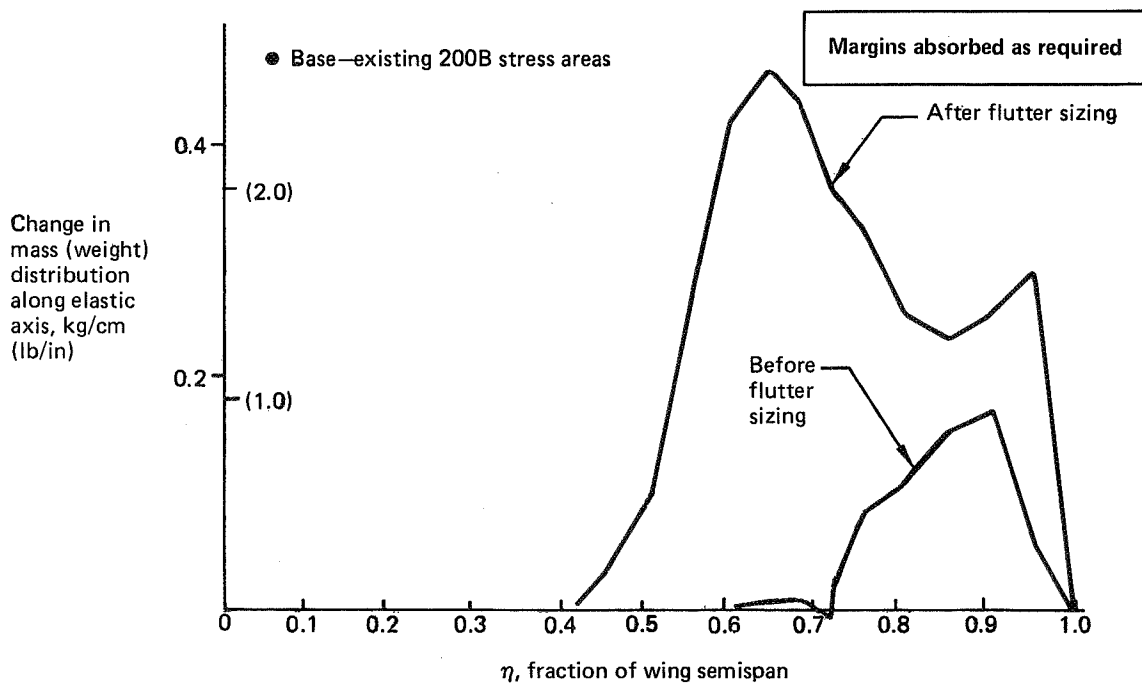


Figure 148. Change in Wing Box Material Distribution for Z13 WTW Without WLA

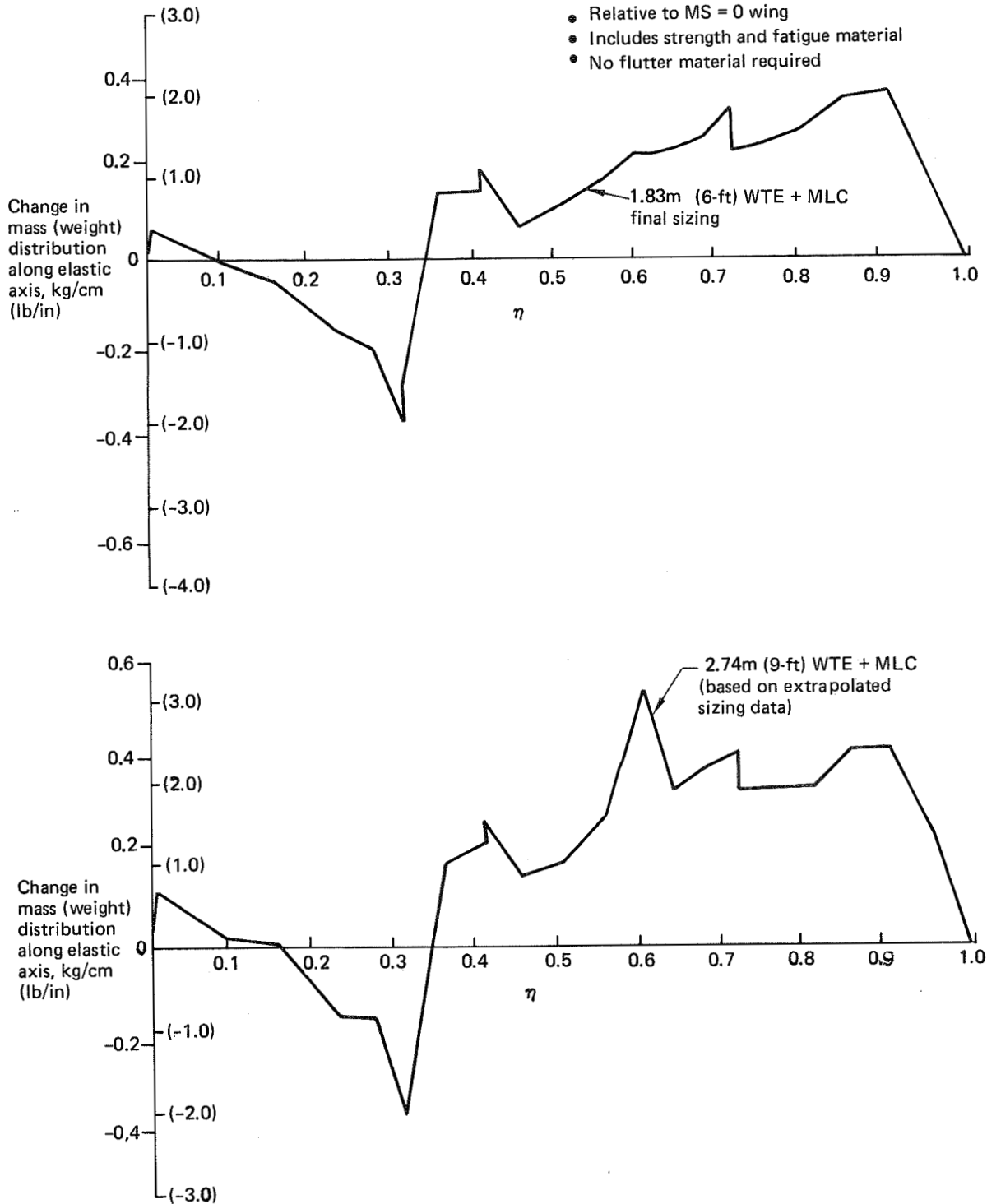


Figure 149. Wing Box Mass (Weight) Distributions for WTE's + MLC

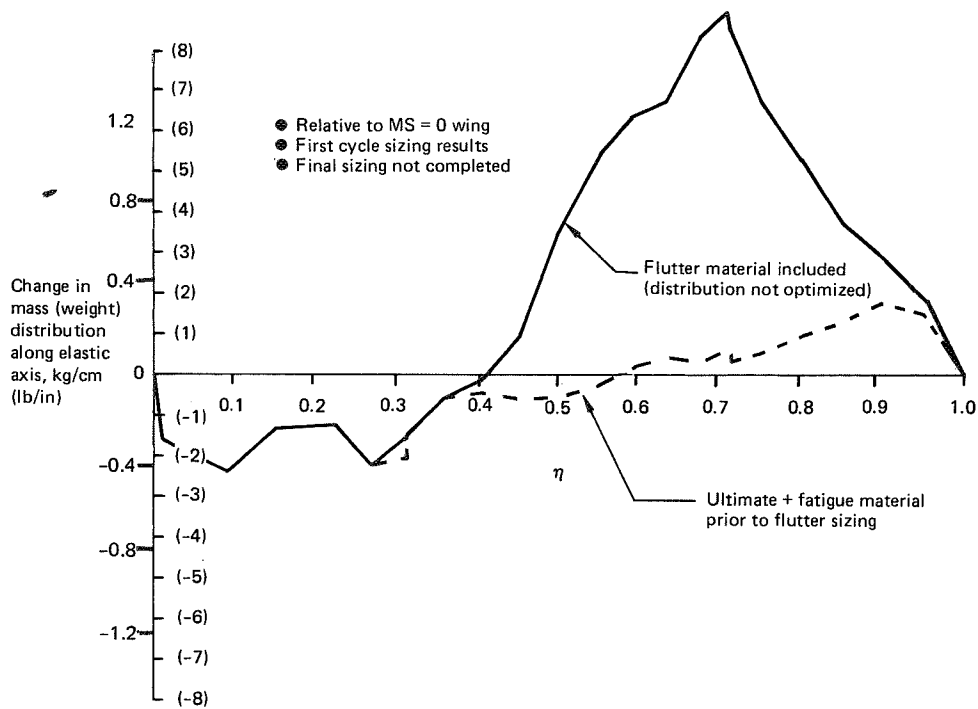


Figure 150. Wing Box Mass (Weight) Distribution for Z13 WTW + MLC

7.1.6 Aerodynamics

Cruise L/D—Figure 151 compares cruise $(L/D)_{MAX}$ ratio for the 1.83-m (6-ft) WTE, 2.74-m (9-ft) WTE, and Z13 WTW. The effect of adding MLC to the 1.83-m (6-ft) WTE configuration was insignificant. Again, the (L/D) equivalent of the increased OEW was obtained using trade factors which are valid for non-takeoff gross weight limited missions [e.g., 5556 km (3000 nmi)]. Net $(L/D)_{MAX}$ improvement was 2.5% for the Z13 WTW compared with 1.9% for the 2.74-m (9-ft) WTE plus MLC.

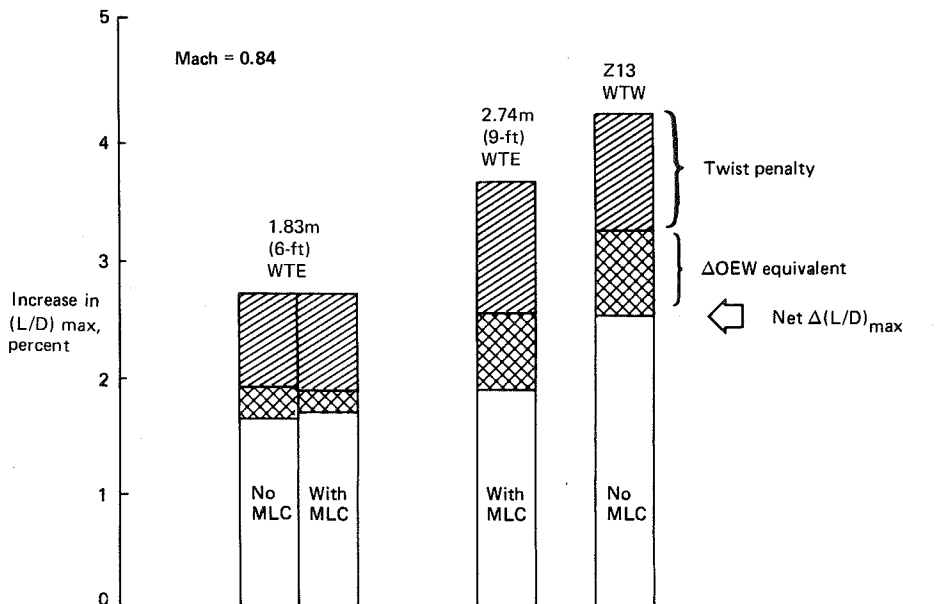


Figure 151. Lift-to-Drag Comparison, WTE Versus WTW

The relative aerodynamic/structural efficiency of the wing tip extensions and winglets is indicated by percent improvement in $(L/D)_{max}$ plotted versus airplane weight increase as shown in Figure 152. The winglet is more efficient than the wing tip extensions if existing structural margins are absorbed as required and decidedly more efficient if existing structural margins are maintained. Differences between "trend study" data and "final" data include updated methodology for evaluating drag due to twist and weight differences as indicated.

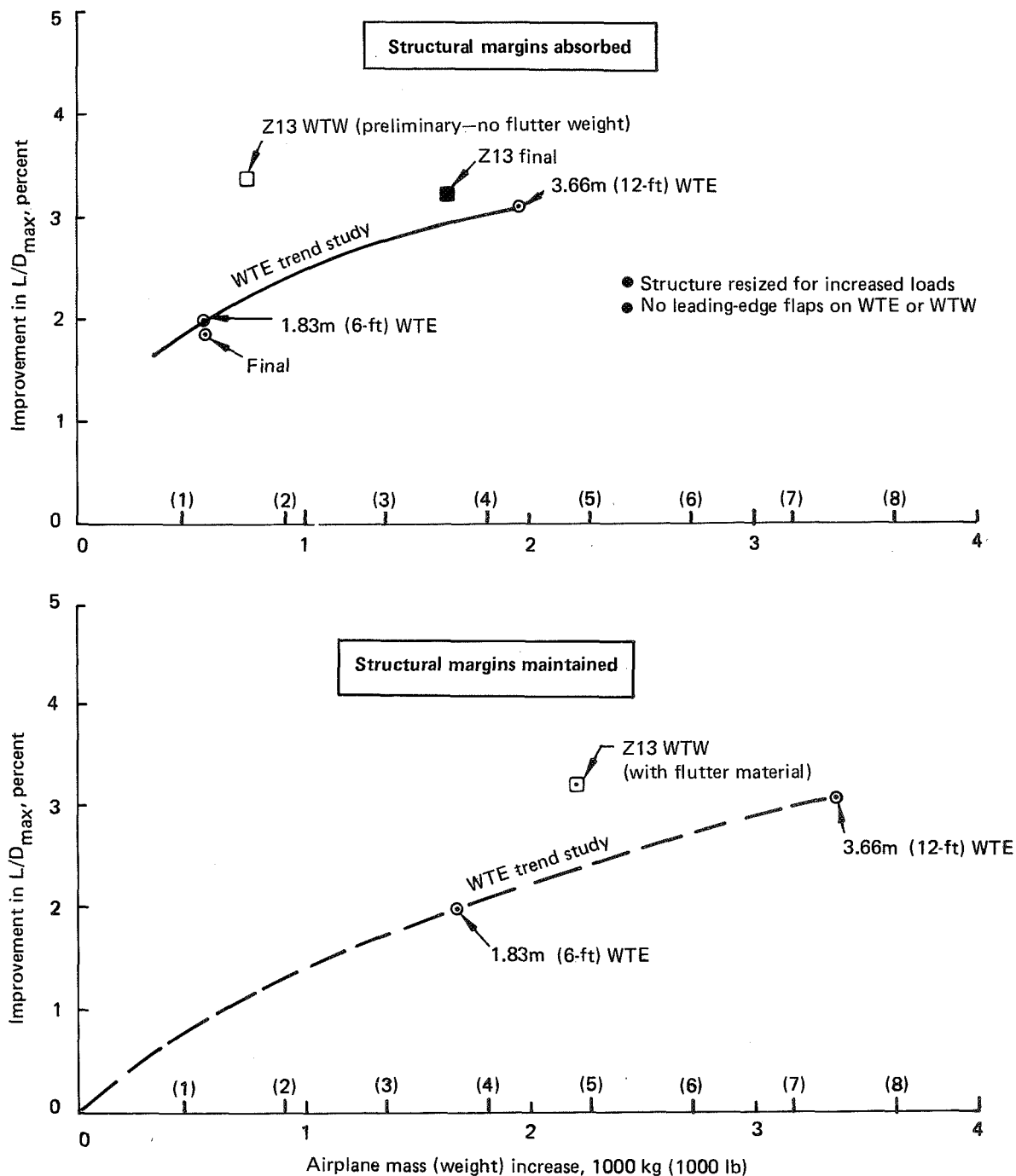


Figure 152. WTE/WTW Relative Aerodynamic/Structural Efficiency

Initial Buffet—Initial buffet predictions are shown on Figures 153 and 154 for the 1.83-m (6-ft) WTE and Z13 WTW, respectively. Full-scale estimates were made using wind tunnel increments of lift coefficient applied to a flight test baseline (winglet off). In each case the initial buffet boundary was improved with the wing tip modification.

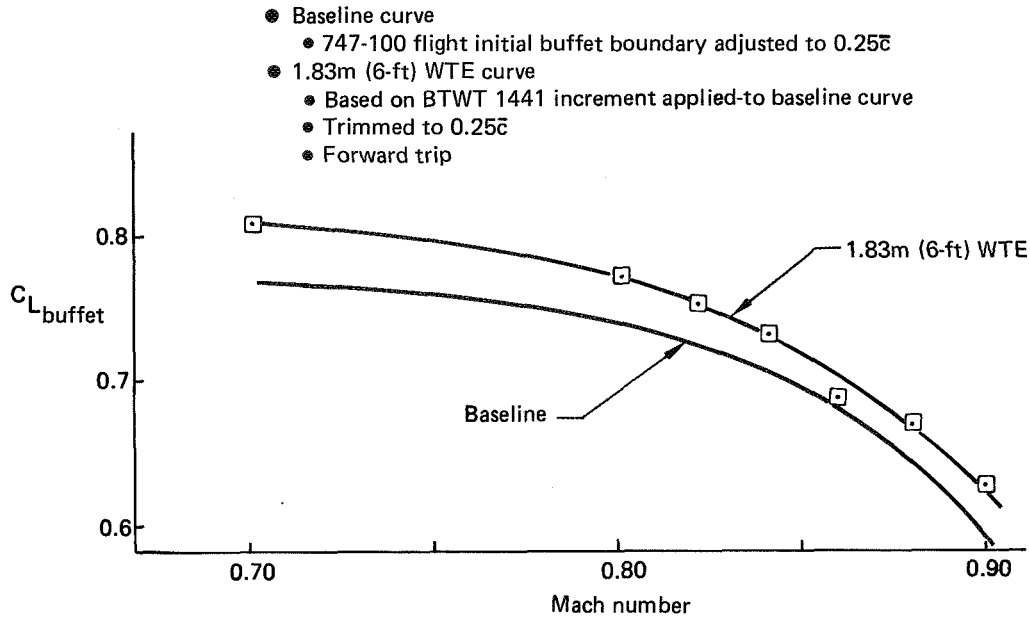


Figure 153. Effect of 1.83m (6-ft) WTE on Initial Buffet

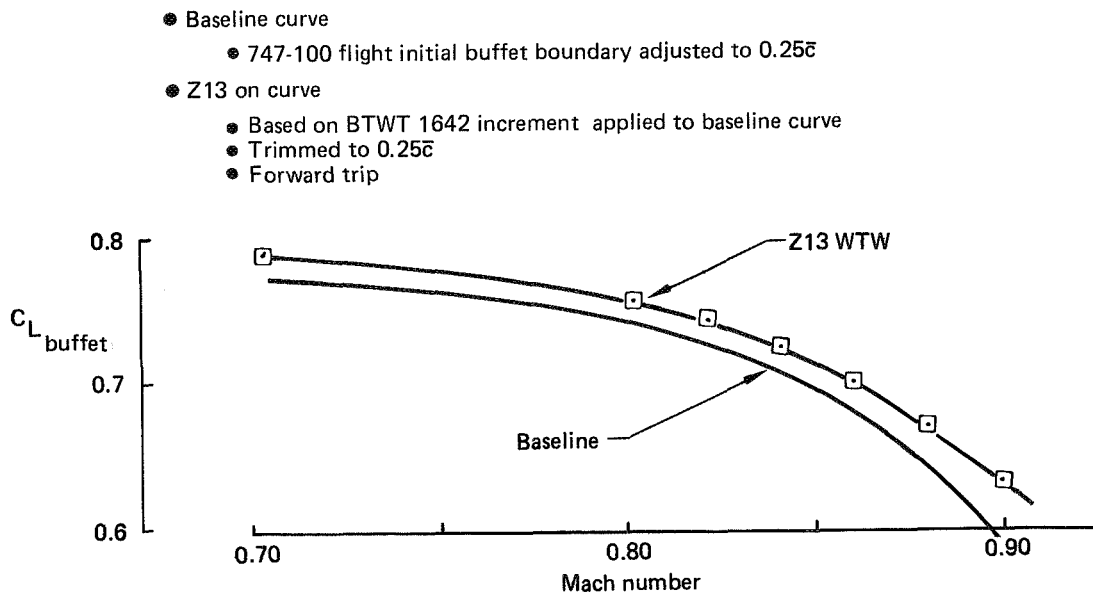


Figure 154. Effect of Winglet Z13 on Initial Buffet

Low Speed—Results of a potential flow analysis of a 747-200 with a 2.74-m (9-ft) WTE indicate that wing tip stalling will likely occur near the critical one-engine inoperative climb-out condition (V_2) in the takeoff configuration. Stalling is not predicted at the approach condition with flaps 30. Low-speed wind tunnel testing is necessary to determine what additional leading-edge flap span would be required to eliminate problems due to premature stall. However, the theoretical analysis indicates that an extension of the leading-edge flap to WBL 1234 (about 50% of the span extension) should be adequate to protect the extended wing up to C_{LMAX} .

The potential reduction in approach speed is shown on Figure 155 for wing tip extensions. Assuming the leading-edge flaps are extended out to wing buttockline (WBL) 1234, the approach speed increment is 1.6 knots for the 1.83-m (6-ft) WTE and 2.3 kn for the 2.74-m (9-ft) WTE.

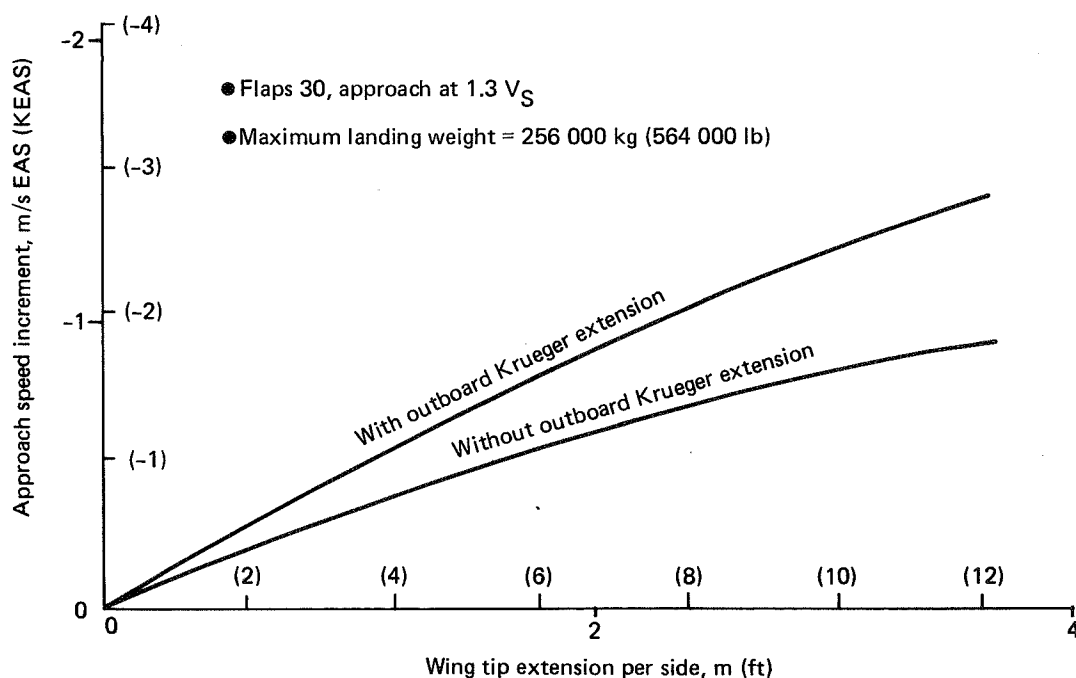


Figure 155. Estimated Approach Speed Improvement Due to WTE

Figure 156 shows a potential reduction in approach speed with flaps 30 of less than 0.5 kn with winglets installed on the 747-200. This estimate was based on 1976 low-speed test results of an early winglet design. Similar results could be anticipated with winglet Z13, provided there are no separation or buffet problems. Low-speed wind tunnel tests would be required to evaluate flow separation and buffet onset points. However, Z13 was designed at slightly less than optimum winglet loading, and it is conceivable that no premature winglet/wingtip stalling will occur. If future low-speed testing uncovers an early stall problem, a first attempt at a fix would be to incorporate more leading-edge camber and, possibly, a greater nose radius.

Approach attitude does not change significantly with the addition of either tip extensions or winglets.

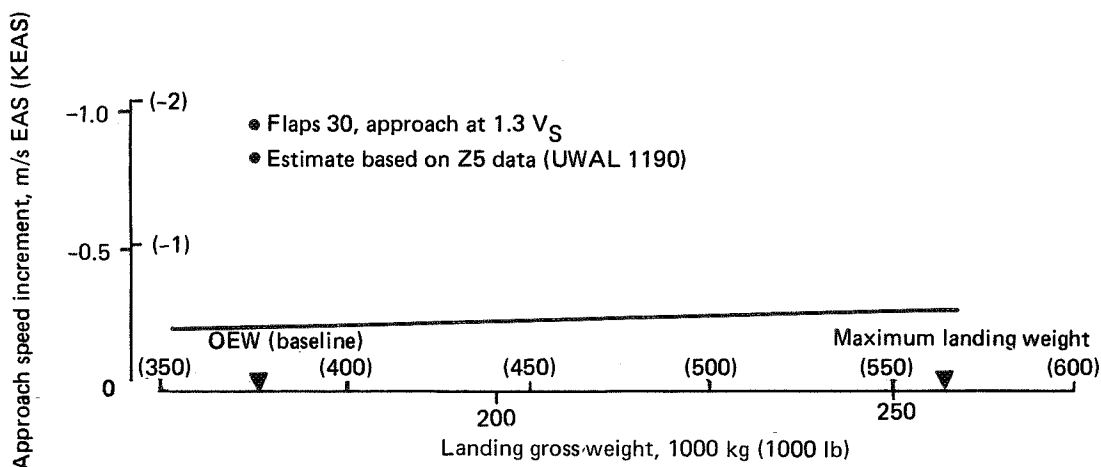


Figure 156. Estimated Approach Speed Improvement Due to Winglets

Noise—From the standpoint of approach noise, it may not be advantageous to utilize the approach speed reduction associated with the wing tip modifications. However, the changes in noise characteristics would be insignificant.

7.1.7 Stability and Control

Stability and control characteristics of the basic 747 are slightly altered by the introduction of either a wing tip extension or wing tip winglet. The effects of the wing tip extensions on longitudinal characteristics are larger than those of winglets. Minor revisions to the longitudinal flight control system will compensate for the changes. Lateral-directional effects of winglets are larger than those of tip extensions. Although these are not a major factor, the effects tend to favor the tip extension.

A comparison of wing tip extension and winglet effects is summarized in Figure 157. Both produce an increase in longitudinal stability and a trim shift. The stability increase is approximately 2% mean aerodynamic chord (MAC) greater with the tip extension than with the winglet over most of the Mach range. As indicated in Figure 157, similar modifications to the longitudinal flight control system may be necessary to compensate for the effects of either tip configuration.

Directional stability ($C_{N\beta}$) is increased by the winglet but is essentially unchanged by the WTE. The increased directional stability would slightly reduce directional controllability during landing rollout in crosswinds.

The increase in rolling moment due to sideslip ($C_{l\beta}$) relative to the increase in directional stability ($C_{N\beta}$) is proportionately greater for the WTW than for the WTE. Since the aileron roll control effectiveness ($C_{l\delta_a}$) is about the same for both the WTE and WTW, roll control margins would be less with winglets in demonstrations of engine-out "tameness" (Boeing criteria). However, controllability should be satisfactory, and no adverse impact on FAA certification of crosswind landing or engine-out control is anticipated. Changes in dutch roll characteristics are expected to be minor as increases in ($C_{l\beta}$), ($C_{N\beta}$) and roll damping have offsetting effects.

Longitudinal effects	Wing tip extension	Wing tip winglet
Increased static stability	✓	✓
FAA speed/trim stability	Small effect	Small effect

Longitudinal FCS components possibly requiring revision	Wing tip extension	Wing tip winglet
Pitch feel system	✓	✓
Elevator rigging (downrig)	✓	✓
Stabilizer electrical trim limits	✓	✓
Takeoff trim greenband	✓	✓

Lateral/directional effect	Wing tip extension	Wing tip winglet
Increase in $c_{l\beta}/c_{l\delta_a}$	Negligible effect	✓
Increased directional stability	No effect	✓
Reduced crosswind capability	No effect	✓
Reduced tameness	No effect	✓
Dutch roll dynamics	Negligible effect	Negligible effect

Figure 157. Effects of WTE/WTW on Flight Control System and Flying Qualities

7.1.8 Installation Design

Wing Tip Extensions—The 1.83-m (6-ft) wing tip extensions shown in Figure 158 are of conventional construction and can be spliced to a suitably prepared wing.

A 2.74-m (9-ft) extension is shown installed on the baseline wing in Figure 159. Figure 160 shows the planform of the 1.83- and 2.74-m (6- and 9-ft) extensions. The 2.74-m (9-ft) extension has the same chord taper and thickness-to-chord ratio (t/c) as the basic wing. The twist remains constant at 3.5 deg outboard of the existing tip location. Installation of the 1.83-m (6-ft) extension is described in Section 4.3.1.

Installation of leading-edge devices are possible in both configurations, if required. One V/C flap can be installed in the 1.83-m (6-ft) extension, two in the 2.74-m (9-ft) extension.

The leading-edge flap drive system is revised as shown in Figure 161 and the existing actuation mechanism, as shown in Figure 162, can be installed for the new flaps in the 2.74-m (9-ft) extension.

Tip extensions provide an easier splicing arrangement to the wing and less disturbance of the electrical/electronic systems located in the tip than a winglet installation. Consideration of reinforcing an existing wing to accept an extension indicated that, while it is possible to apply external skin doublers, difficulty is encountered in applying

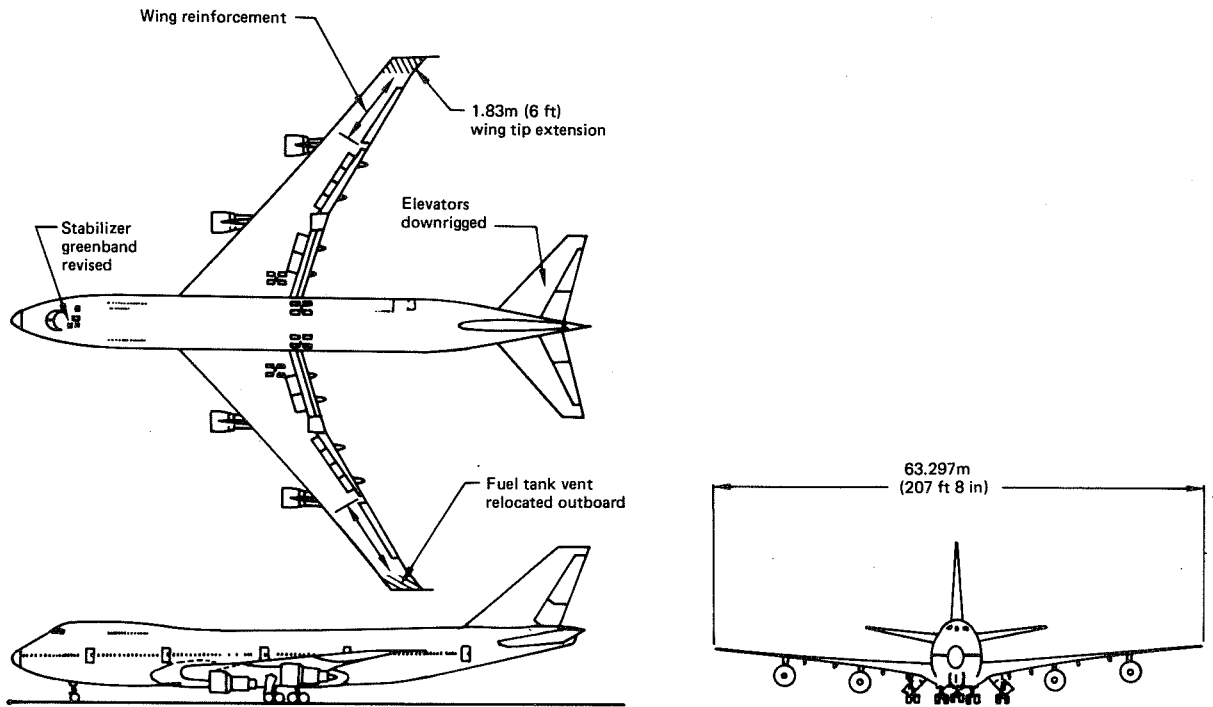


Figure 158. Airplane Modifications for 1.83m (6-ft) WTE Installation

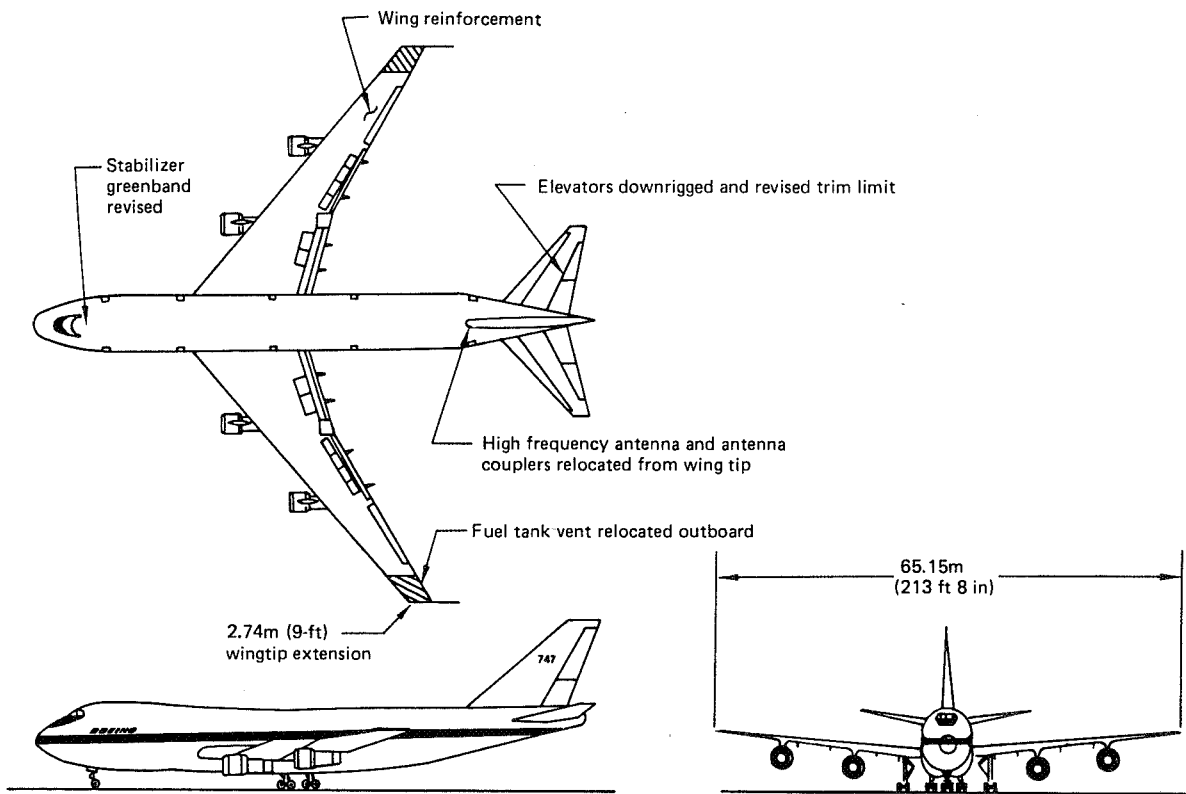


Figure 159. Airplane Modifications for 2.74m (9-ft) WTE Installation

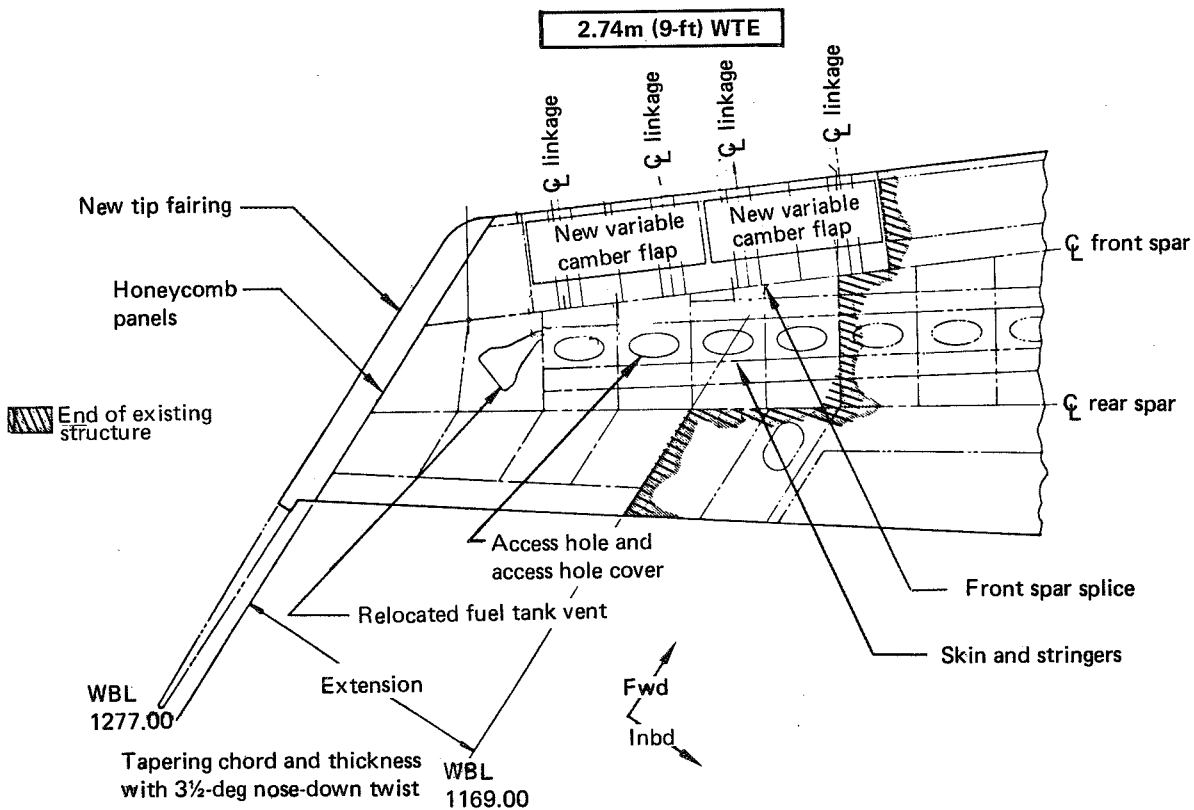
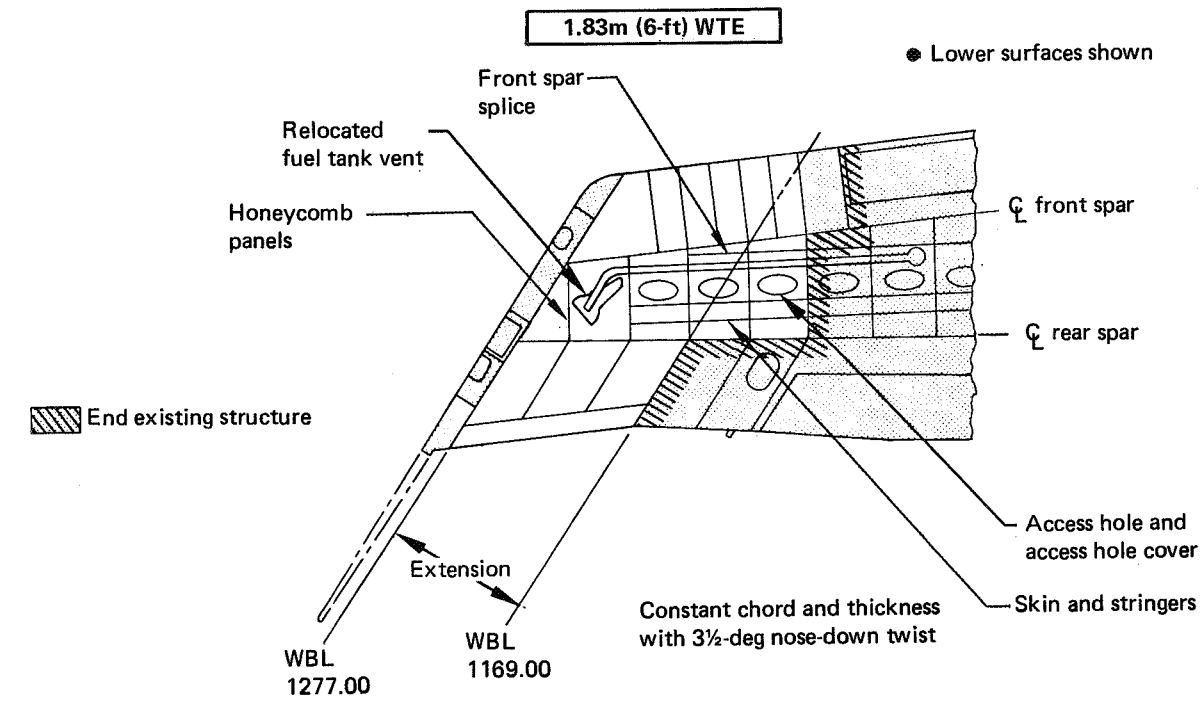


Figure 160. WTE Installation Design Concepts

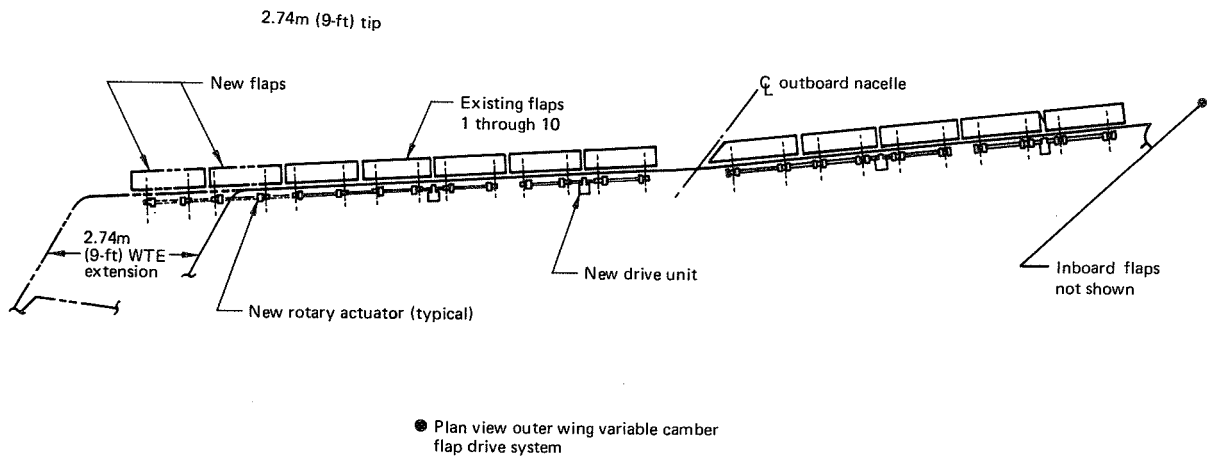


Figure 161. New Variable Camber Flap Drive for 2.74m (9-ft) WTE

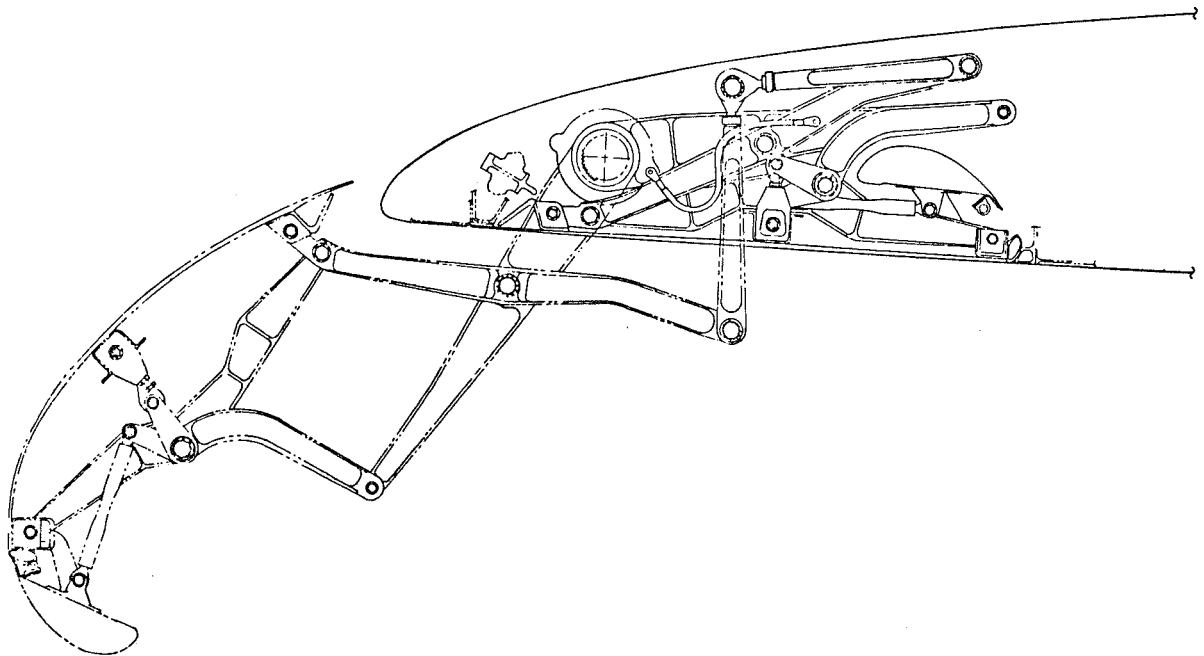
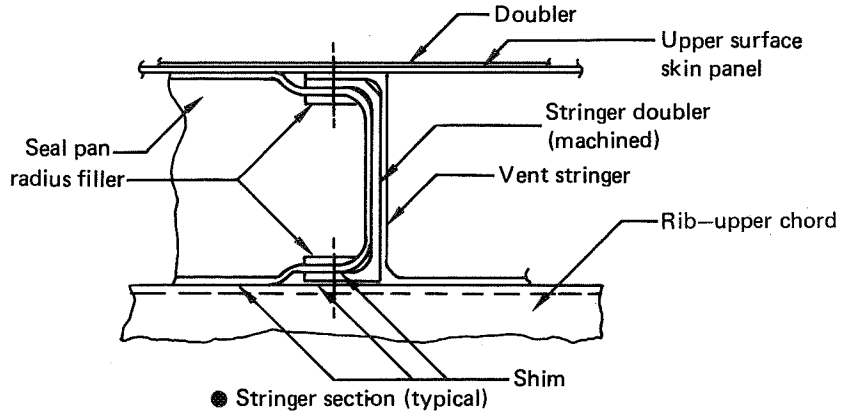
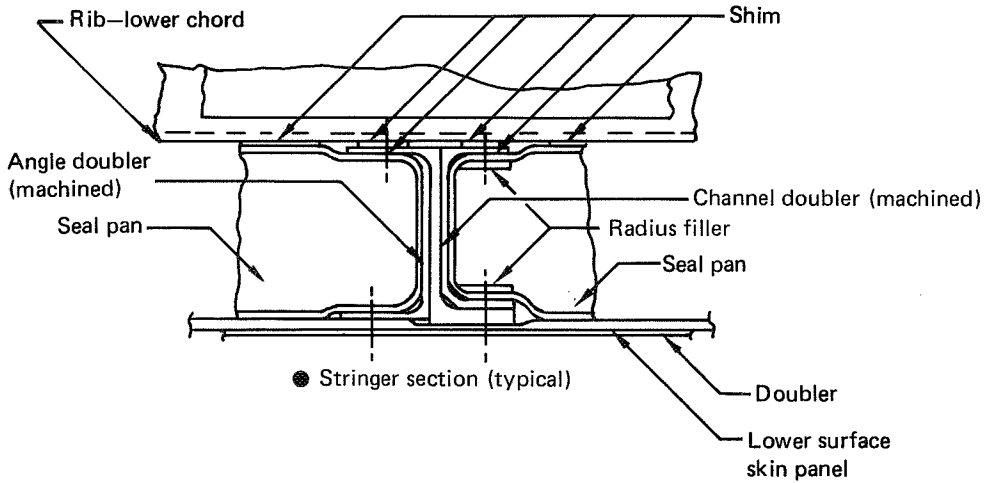


Figure 162. 747 Wing Leading-Edge Variable Camber Flap Mechanism

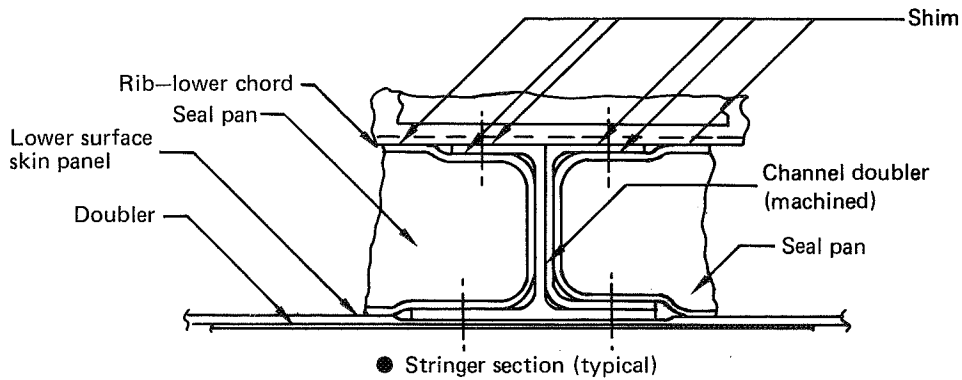
doublers to the spar and stringers. Removal of numerous fasteners from the spars and skins makes retention of jig position almost impossible, and jig position is imperative for reinstallation of close tolerance fasteners. The doubler installations are shown in Figure 163. To derive benefit from the installation of a WLA system, the inboard upper and lower surface panels should be reduced in thickness. The front spar web and outboard skin panels, however, must be increased to react the increased torsional load. Retrofit of tip extensions with or without WLA could reduce fatigue life in addition to being very expensive.



Upper surface stiffener reinforcement for retrofit



Lower surface stiffener reinforcement for retrofit—Z section



Lower surface stiffener reinforcement for retrofit—J section

Figure 163. Stiffener Reinforcement for Retrofit

Wing Tip Winglets—Study of wing/winglet attachment methods produced two candidate configurations. The first for the Z9 winglet utilized the previously proposed approach of bolting together mating fittings in the winglet and wing tip (sec. 5.0, fig. 64). The fittings were fairly complex since they must match the spar geometry in the wing and also in the winglet, splice, and the adjacent rib, and they must be capable of fail-safe operation. The resulting attachment required large diameter bolts and even then provided a relatively soft joint.

A multi-spar configuration was devised for the Z13 winglet which was capable of accommodating the higher bending moments at the wing/winglet junction and provided a stiffer load path (sec. 5.0, fig. 65). The multi-spar approach provides better possibilities for the winglet construction and attachment.

Attachment of a winglet to the wing is more complex than the attachment of a tip extension. It also has a more adverse effect on the systems located at the existing wing tip.

Revision to the inboard wing for the winglet (fig. 164) is similar to the tip extension. Therefore the observations for retrofitting a wing to accept a tip extension are also applicable for a winglet installation.

Modifications to the flight control systems are similar for the tip extension and winglet installations. When WLA is incorporated, the wing upper and lower surface panels are increased in thickness for the outboard approximately 50% span and decreased in thickness for the inboard 50% span. The front and mid-spar webs are increased in thickness to react the increased torsion from the ailerons being activated at higher air speeds.

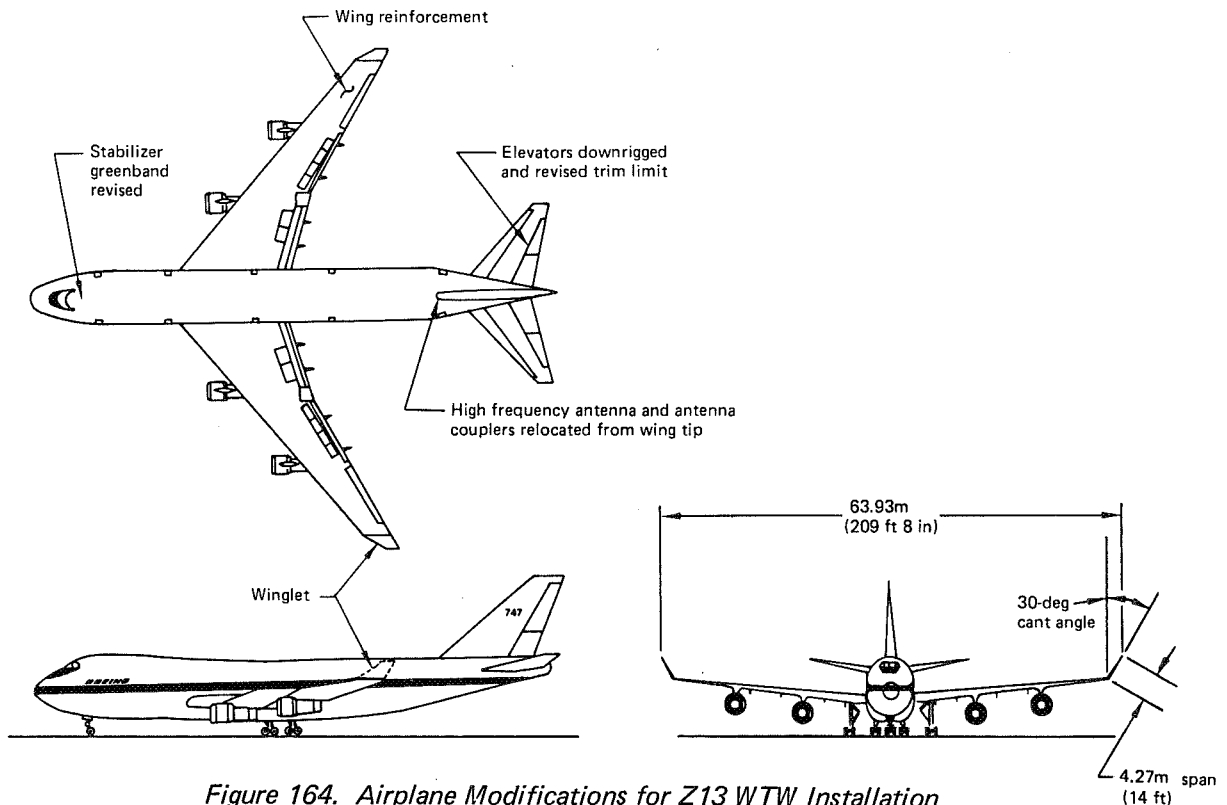


Figure 164. Airplane Modifications for Z13 WTW Installation

7.2 BENEFITS OF WING LOAD ALLEVIATION FUNCTIONS

Structural benefits of WLA for the WTE and WLA configurations are discussed in this section. Benefits for the basic wing are discussed in Section 6.2.

As previously noted (sec. 6.5.1), application of WLA in combination with tip extensions or winglets was considered for the purpose of reducing the structural weight penalty and/or the extent of the wing box modifications associated with the WTE/WTW installation. Major emphasis was on the MLC function. However, the GLA potential was determined by means of the same procedure used for the basic wing (with MLC), and a preliminary evaluation of the potential benefits of FMC for the wing with winglets also was conducted.

7.2.1 Manuever Load Control/Gust Load Alleviation For Wing Tip Extensions and Wing Tip Winglets

Weight Benefit—Isolation of the structural weight reduction attributable to MLC requires sizing the structure for the same wing tip configuration with and without MLC, using the same ground rules and methodology for both sizings. This was done for the basic wing (sec. 6.2.2), and the result, in terms of the percentage of wing box weight reduction, was assumed to be also applicable to the WTE and WTW configurations for purposes of assessing the fuel savings attributable to WLA.

Resizing studies for wing tip modification combined with MLC were directed toward obtaining a weight estimate for production installation of the combined concepts rather than toward isolating the weight benefit of MLC. Relative to the production baseline airplane (no WTE/WTW/WLA), the change in airplane OEW for a wing tip modification combined with the MLC system (neglecting effects on gust loads) was found to be as follows:

<u>Wing Tip Modification with MLC</u>	<u>Change in Airplane Mass (Weight)</u>
1.83-m (6-ft) WTE	+421 kg (930 lb)
2.74-m (9-ft) WTE with LE Flaps	+1450 kg (3200 lb)
Z13 WTW	Final sizing not completed

The weight for the 1.83-m (6-ft) WTE was based on complete loads and stress analyses, while the wing box weight for the 2.74-m (9-ft) WTE was based on extrapolation of the 1.83-m (6-ft) WTE sizing data. The potential weight benefit for a GLA system was found to be about the same for a wing tip extension as for the basic wing.

These weight increments are not directly comparable with the WTE/WTW studies of Sections 4.0 and 5.0 because all of the wings with MLC were sized to zero structural margin of safety, and the fatigue analyses were conducted in more detail with MLC. Shear interaction due to the high torsion loads induced in the wing as a result of the active outboard aileron was an important consideration in the study. In this evaluation, the fatigue quality of the structure was obtained by increased structural material, but it is possible in areas affected by the shear loadings to improve the DFR (detail fatigue rating) by change in detail design rather than increased sizing. This would lead to a lighter configuration but would be more expensive from a design and manufacturing standpoint.

Structural sizing of the Z13 winglet configuration with MLC was complicated by the necessity for a stiffness designed wing to satisfy flutter clearance requirements (sec.

7.1.4). The basic Z13 WTW configuration sized to absorb existing margins required about 862 kg (1900 lb) of flutter stiffness material. When MLC was added to the winglet configuration, the first cycle of strength and fatigue sizing (prior to flutter sizing) showed that the Z13 WTW/MLC configuration would weigh about the same as the zero margin basic wing (no MLC) configuration; hence, less than the 747-200B study baseline production model. Unfortunately, the stiffness reductions associated with strength resizing of the winglet configuration with MLC caused large reductions in flutter speeds. Past experience had suggested that additional wing torsional material spread from zero at the inboard nacelle to a maximum at the outboard nacelle would probably be optimum for the symmetric flutter mode. An attempt was made to stabilize the symmetric flutter mode by adding material in this manner while leaving the inner wing sizing at the values dictated by MLC design. Material was also added in the wing tip region outboard of the outboard nacelle to stabilize the wing tip flutter mode. This approach to stabilizing the symmetric mode was found to be nonoptimum because the outer wing became heavier as stiffness was added, which further degraded the symmetric flutter mode. The WTW/MLC configuration with first cycle flutter sizing included was much heavier than the WTW configuration without MLC. This indicates that the flutter weight penalty for the WTW/MLC configuration could be reduced by adding flutter stiffness material to the inboard section of the wing where stiffness was reduced by strength sizing; however, this tends to negate the potential weight benefits of MLC. These results suggest a significant benefit could be obtained from flutter mode control for the WTW/MLC configuration.

Extent of Structural Modifications—Apart from the weight benefits, a WLA system would be quite valuable if it reduced the extent of structural modifications associated with a wing tip modification. Figure 165 shows the nature and extent of the wing box resizing associated with a WTE installation with and without MLC. In both cases, any existing margins in the baseline (747-200B) wing have been absorbed, as required, before adding material. The associated structural modifications are illustrated in Figures 166 and 167.

The effect of MLC is to require the addition of more material outboard, while allowing removal of material inboard. If the material were not removed (i.e., not resized to zero margin with MLC), the WTE configuration would be considerably heavier with MLC than without. Whether or not the inboard material were removed, the structural modifications required to the baseline wing would be more extensive with MLC than without. Hence, MLC does not facilitate retrofit of a wing tip modification or reduce structural modification costs for production implementation.

7.2.2 Flutter Mode Control

A limited survey of flutter mode control benefits and feasibility of such a system was conducted for the winglet configuration. Survey results indicate significant weight savings could be accomplished, especially in the case of wing tip winglets combined with MLC where substantial flutter weight penalty is incurred to clear 1.2 V_D margins. Current results for the Z13 WTW without MLC indicate a potential mass (weight) savings of about 454 kg (1000 lb). The potential savings are dependent upon the nature of the modes to be suppressed and the proposed stability criteria. Figure 168 shows the high frequency 5.6-Hz wing tip flutter mode and the lower frequency 2.4-Hz symmetric wing mode associated with the Z13 WTW. The estimated weight savings is based on clearing both modes structurally to V_D speed, clearing the wing tip flutter structurally to 1.2 V_D , and using FMC to suppress the symmetric mode to 1.2 V_D . The potential benefits of FMC would be greater for the WTW/MLC configuration.

- $\frac{EI}{EI_B}, \frac{GJ}{GJ_B}$ = stiffness ratios – $\frac{\text{modified}}{\text{baseline}}$
- Baseline MS absorbed where ratios > 1.0
- Sized to MS = 0 for ratios < 1.0

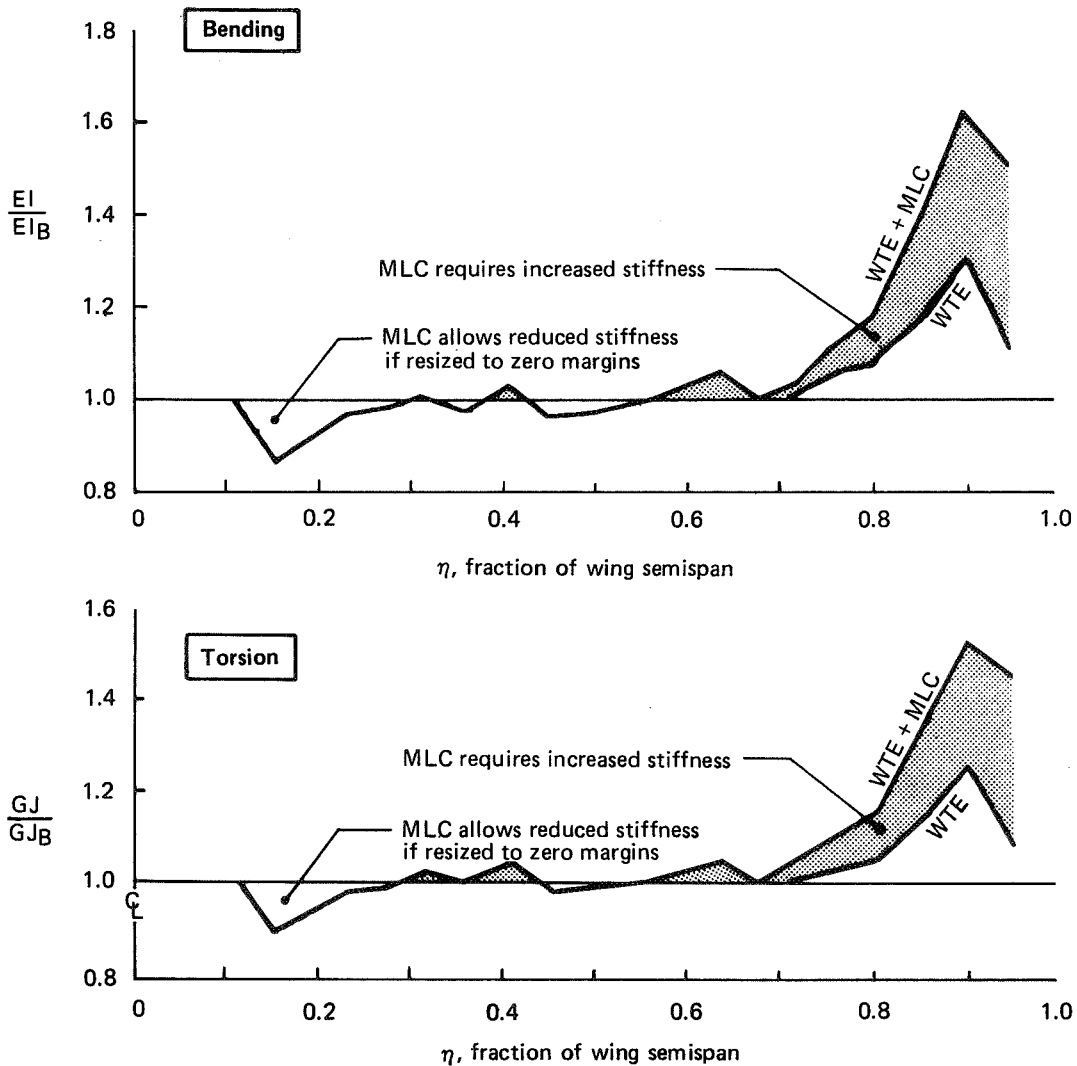
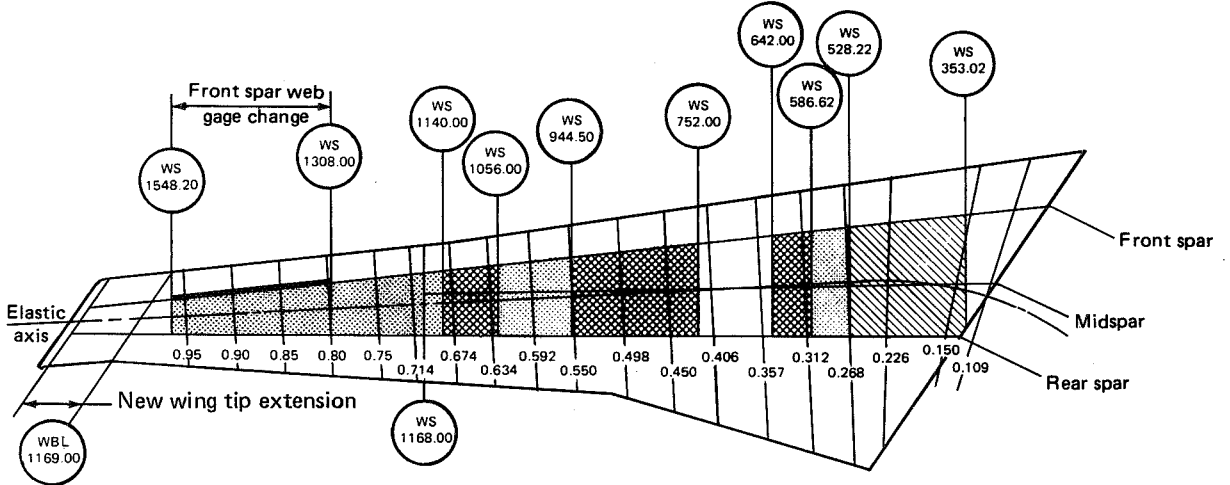


Figure 165. Effect of MLC on Wing Structural Stiffness Requirements for 1.83m (6-ft) WTE

The critical flutter modes of interest as shown in Figure 168 are wing modes involving bending/torsion motion and some fore and aft chordwise bending motion primarily in the outer wing area extending outboard from the outboard nacelle location. Use of the outboard aileron is considered the logical choice for future closed loop investigations involving FMC systems with winglets. Figure 169 shows phase change and amplitude response at the left hand outboard aileron input quadrant as a function of frequency. Amplitude is not expected to be a problem, particularly if the system operates on the

- Baseline margins absorbed
- Shading denotes skin-gage and stringer-area changes relative to baseline wing
- ▨ Increased upper surface skin gages and stringer areas
- ▩ Increased lower surface skin gages and stringer areas
- ▧ Increased upper and lower surface skin gages and stringer areas

1.83m (5-ft) Wingtip Extensions



Z13 Winglet

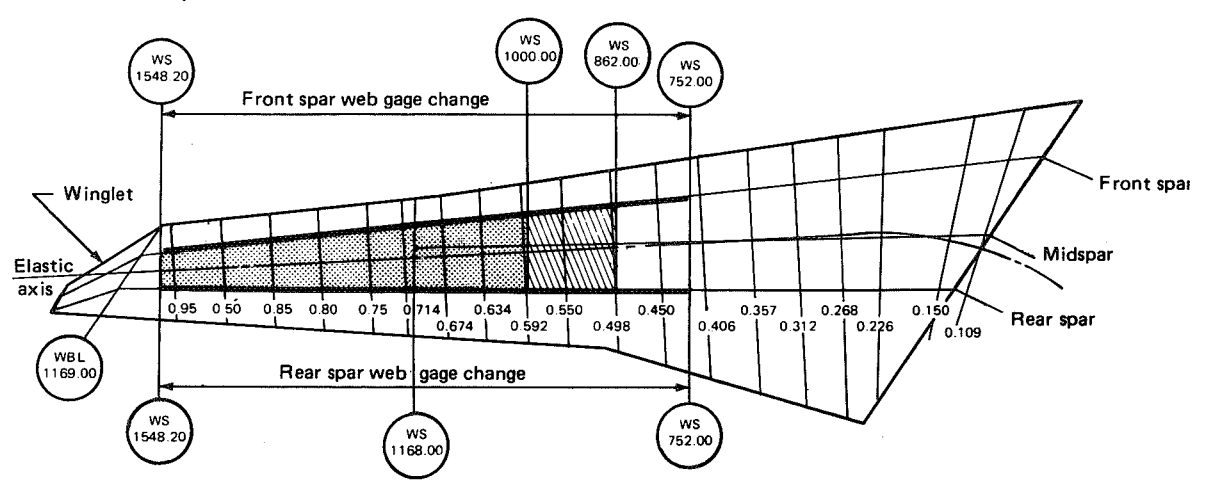


Figure 166. Wing Structural Modifications Required to Add WTE/WTW Without MLC to Baseline Wing

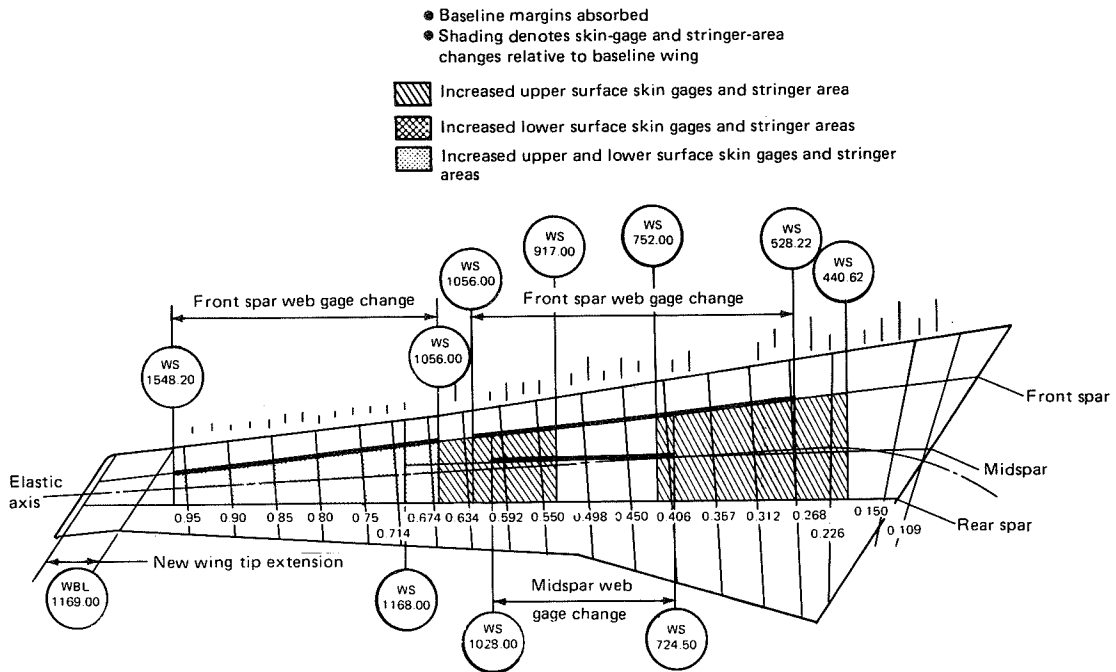


Figure 167. Wing Structural Modifications Required to Add WTE + MLC to Baseline Wing

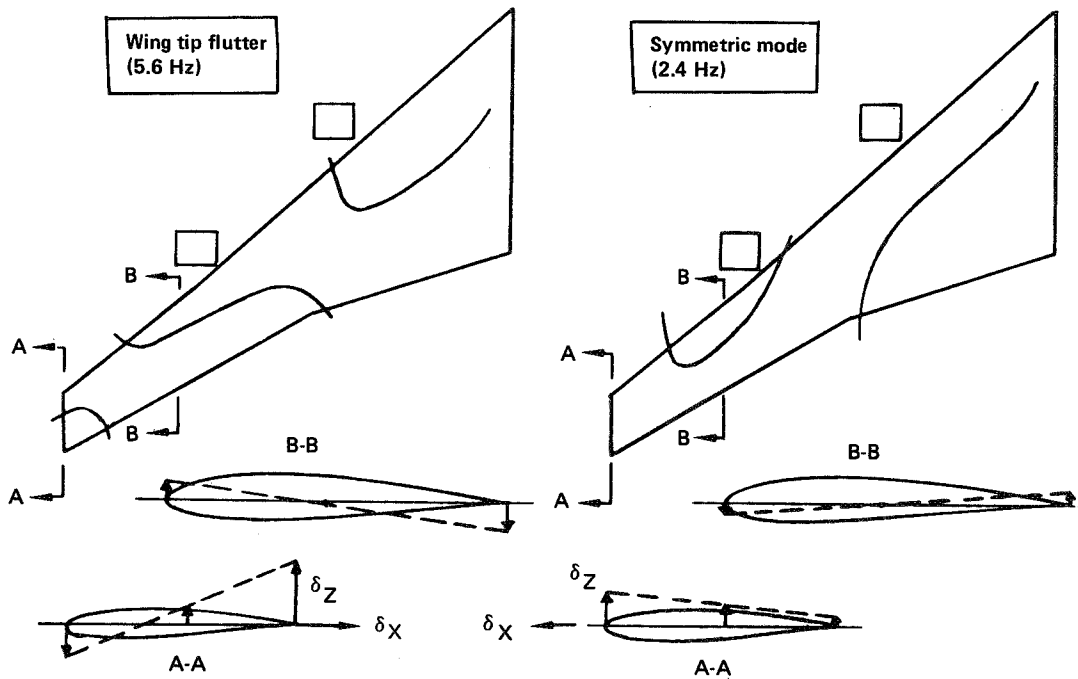


Figure 168. Flutter Modes for the 747 EET/Z13 Winglet Configuration

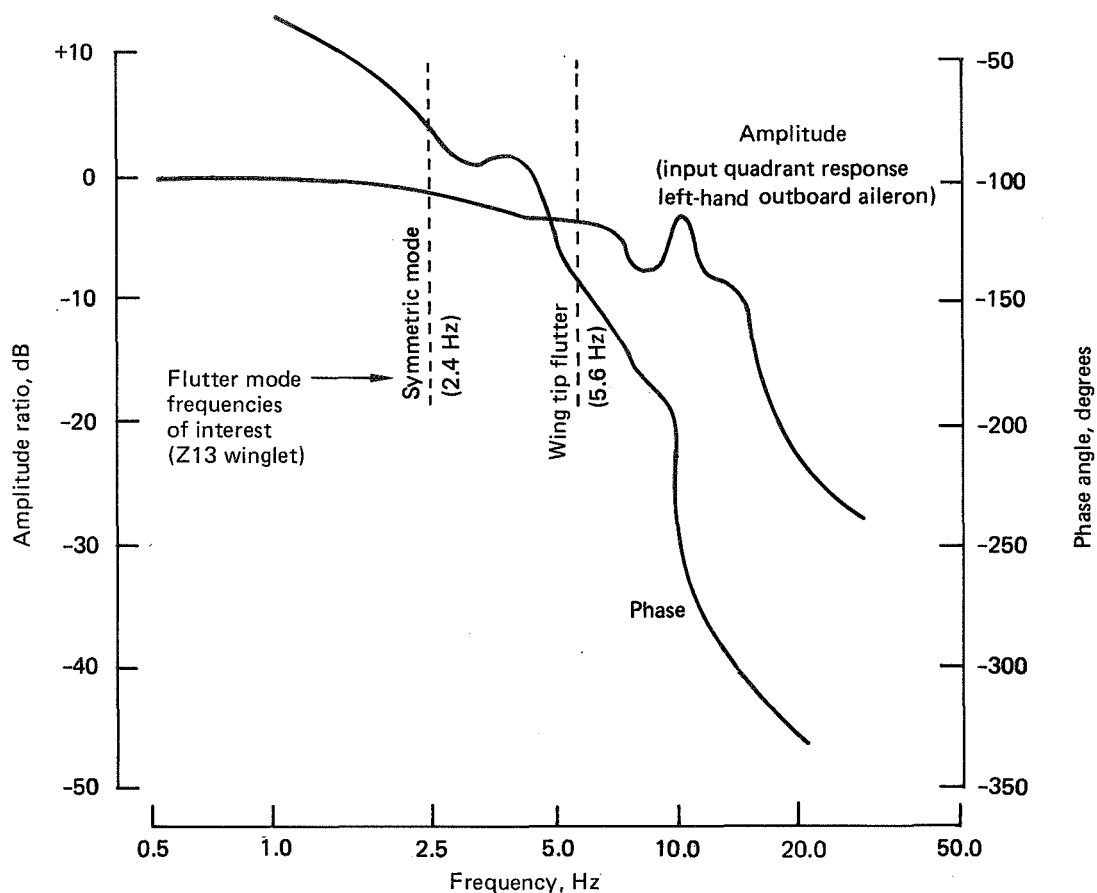


Figure 169. Outboard Aileron Frequency Response

2.4-Hz low-frequency symmetric mode only and a split aileron concept is employed. Based on other work such as the B-52 active flutter suppression demonstrations (ref. 8 and 9), it appears that phasing between the incremental wing lift and the wing displacement will be the key parameter, and existing hardware capabilities may require modification to achieve the necessary responses. In-flight tuning would be necessary to establish requirements, but the B-52 conclusions indicate that if adequate analysis methods are developed to predict winglet flutter the controllability of the flutter is also predictable.

The question of design concept must consider not only weight saving potential, but also the implications of hardware modification and flight safety. Suppressing the high frequency 5.6-Hz wing tip flutter mode would most certainly require more severe response characteristics and more extensive modifications. The symmetric mode at 2.4 Hz has been shown to easily clear V_D speed without increased stiffness but is relatively difficult to stabilize to $1.2 V_D$. Hence the use of FMC to suppress only the symmetric mode from V_D to $1.2 V_D$ appears to be the optimum concept.

In summary, the FMC concept appears feasible, has significant weight saving potential, and would require a significant amount of analysis and test activity to develop successfully. For the winglet application, it is recommended that any future investigations initially concentrate on the 2.4-Hz symmetric mode and explore capabilities of the existing plain outboard aileron system including balance weights attachments for flutter safety.

7.3 FINAL EVALUATION

The final evaluation was concerned with selection of the best type of configuration, considering performance, economics, operational factors, and other data generated during the study. Performance analyses were made for the configurations noted in Figure 170. In the economic comparisons, it was assumed that the fuel savings data for all configurations applied without MLC and that additional fuel savings of about 0.2% could be attained by combining WLA with any of the wing tips (because this was the WLA benefit determined from studies of the basic wing that had been conducted specifically to isolate WLA benefits).

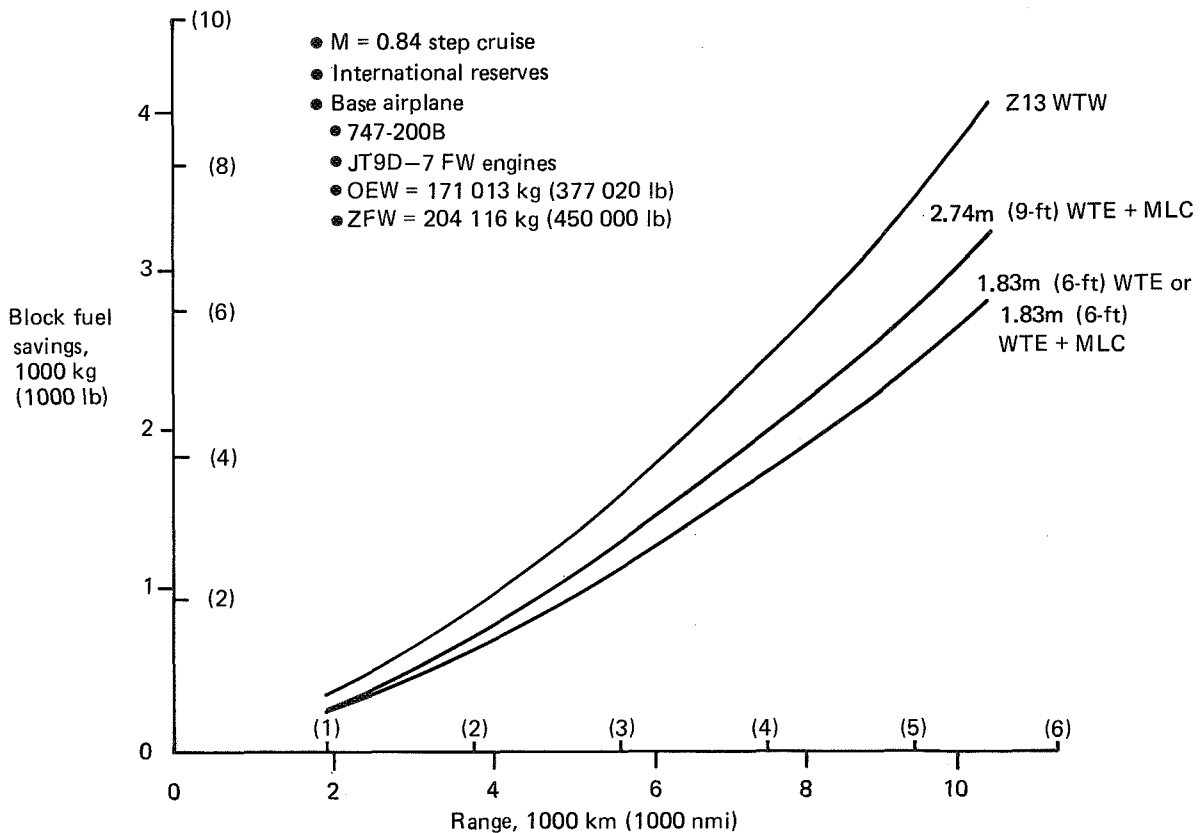


Figure 170. Block Fuel Savings

7.3.1 Performance Comparisons

Fuel Savings—Block fuel savings per trip are shown on Figure 170 in kilograms (pounds) of fuel and on Figure 171 in percent for the several EET concepts. This comparison is made for a constant payload based on a 60% passenger load factor. Figure 172 shows the sensitivity of fuel savings to zero fuel weight (payload) at 5556 km (3000 nmi) for the 1.83-m (6-ft) WTE and Z13 winglet. Discontinuities in the performance comparison curves are caused by different step cruise patterns than those of the basic airplane. Mission performance was based on constant Mach 0.84 step cruise at altitudes of 9500, 10 670, and 11 890m (31 000, 35 000, and 39 000 ft). This allows the airplane with the tip modifications to fly at higher cruise altitudes than the basic airplane (if optimum) to take full advantage of the improved aerodynamics.

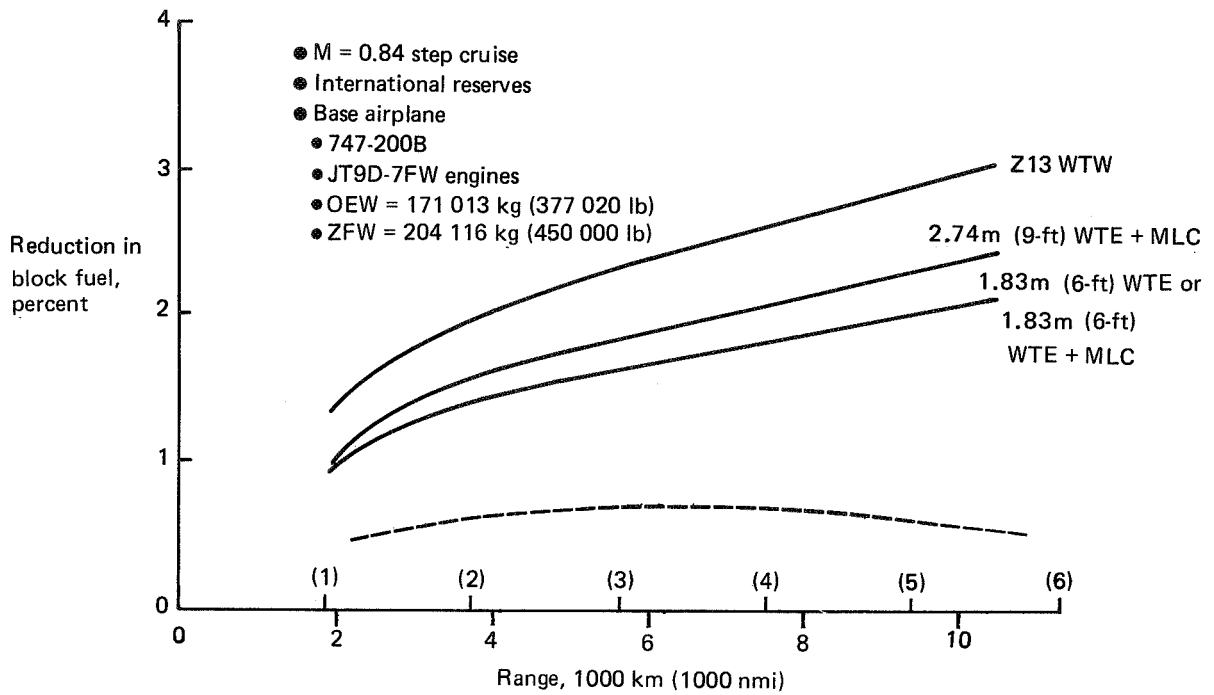


Figure 171. Percent Block Fuel Savings

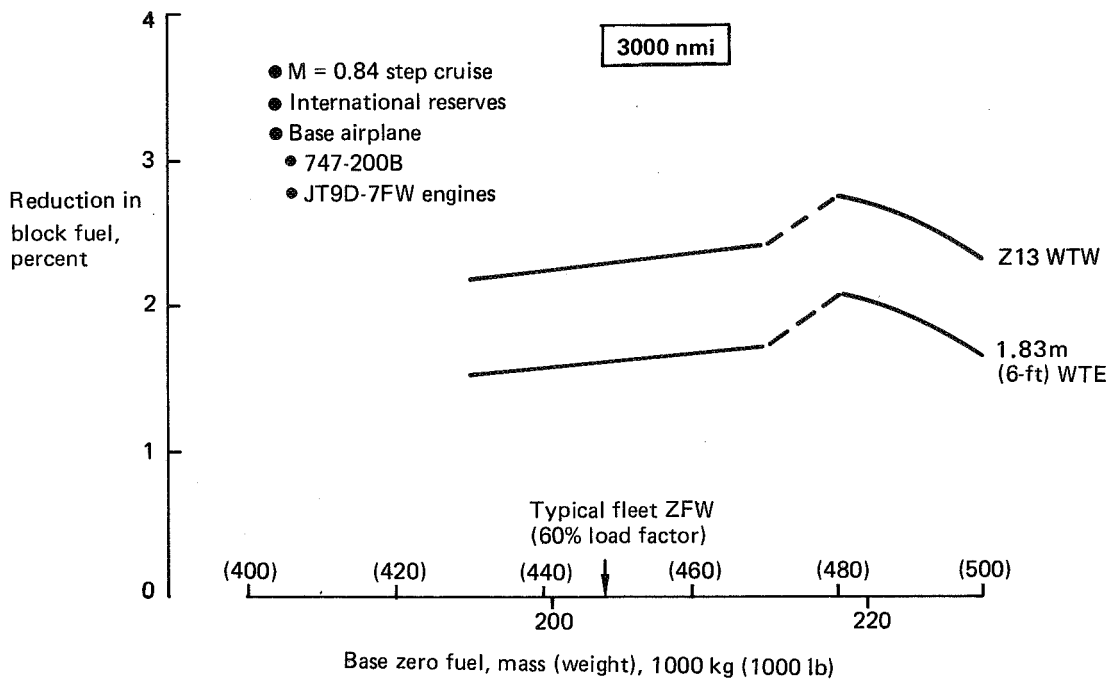


Figure 172. Block Fuel Trades With Zero Fuel Weight

Fuel cost savings per trip are compared on Figure 173 based on 60 cents per gallon. Fuel cost savings per year for a range of fuel cost per gallon are shown on Figures 174 and 175 for the 1.83-m (6-ft) WTE and Z13 winglet, respectively. All concepts are more effective at long range, with the winglets providing the most savings.

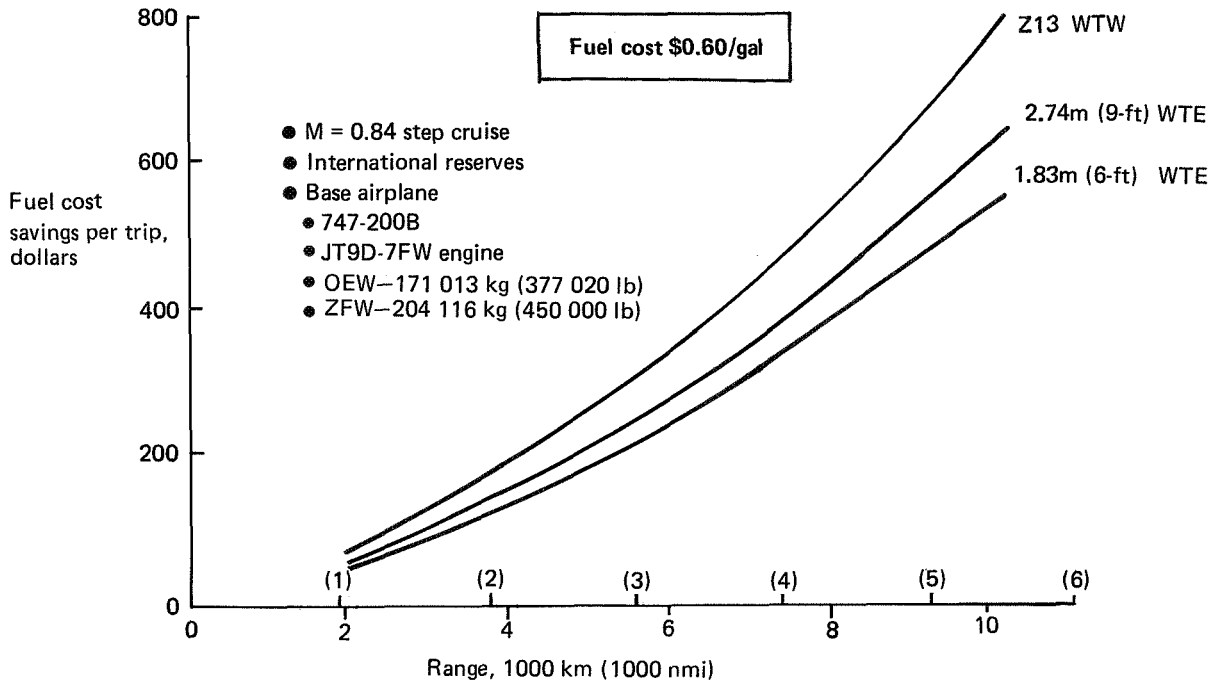


Figure 173. Fuel Cost Savings Per Trip Comparison

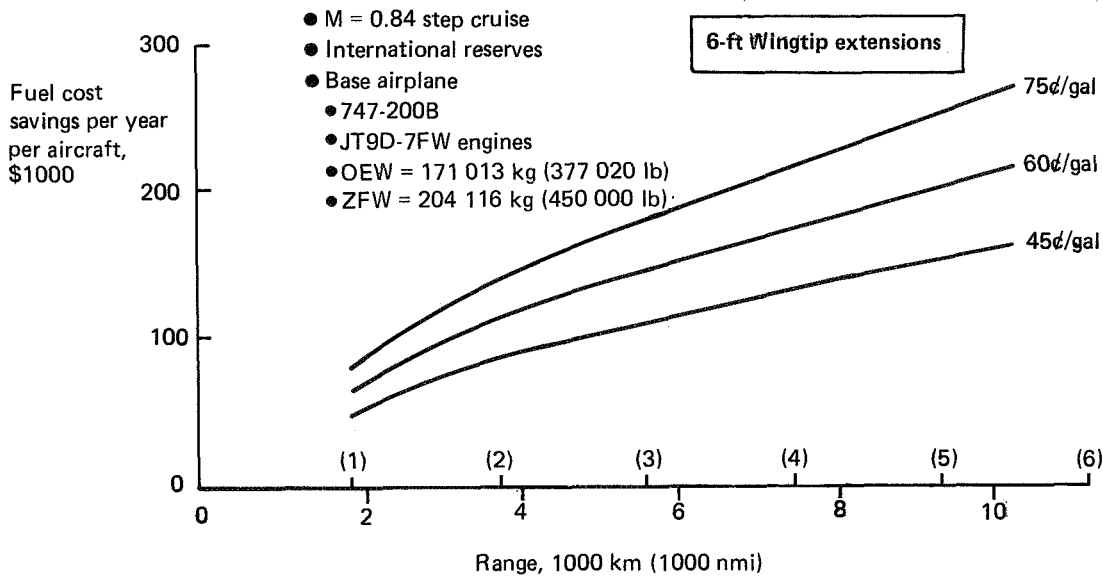


Figure 174. Fuel Cost Savings Per Year—747-200B With 1.83m (6-ft) WTE

- M = 0.84 step cruise
- International reserves
- Base airplane
- 747-200B
- JT9D-7FW engines
- OEW = 171 013 kg (377 020 lb)
- ZFW = 204 116 kg (450 000 lb)

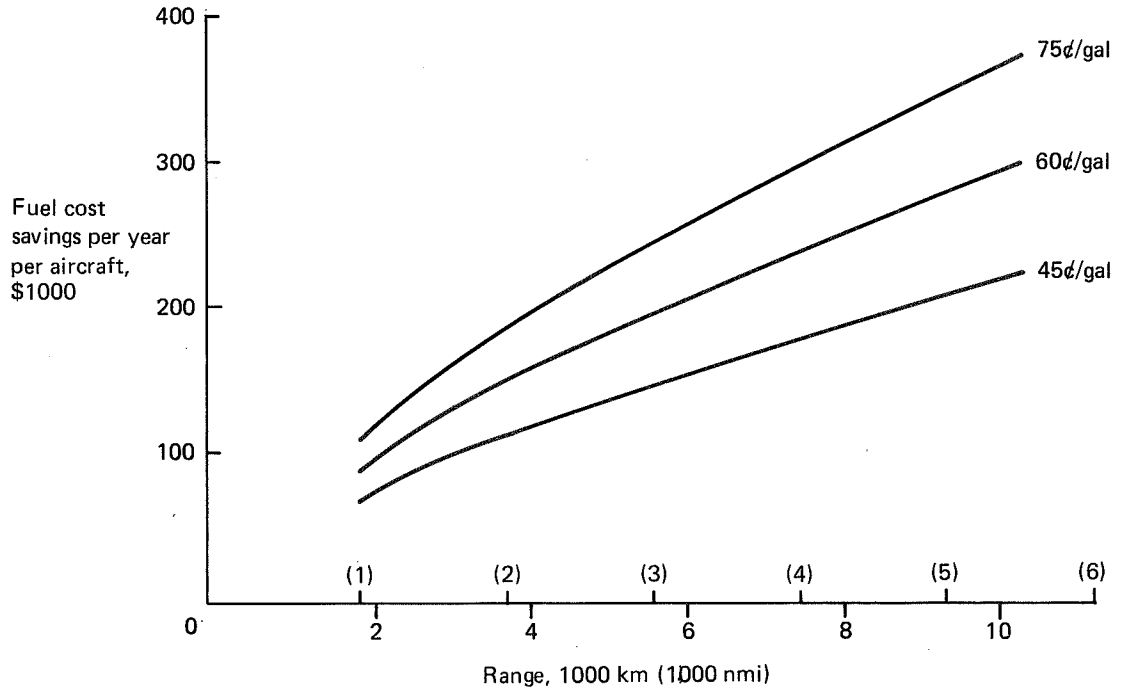


Figure 175. Fuel Cost Savings Per Year—747-200B With Z13 Winglet

Payload/Range—For 747 passenger models, there is no payload penalty or benefits for any of the EET concepts up to about 8334-km (4500-nmi) range due to airplane volume limits; i.e., with a full passenger payload, the cargo compartments can be filled with average density cargo before weight limits become constraints. Significant payload increases are available for the WTE and winglet at very long ranges, however, as shown on Figure 176.

7.3.2 Economic Comparisons

The concepts studied in the program are intended to improve fuel efficiency on existing routes, as contrasted with concepts intended to provide a new capability or open up new routes. For modifications of this type, the potential return on the customer airline's investment (ROI) is usually considered in deciding between alternate configurations. The ROI calculation takes into account the costs of the concepts in addition to the performance benefits.

- M = 0.84 step cruise
- International reserves
- Base airplane for WTW and WTE
 - 747-200B (wing 4)
 - JT9D-7FW engines
 - OEW = 377 020 lb (Except base airplane for WLA has MS = 0 wing with reduced OEW)

Note:
Small Δ OEW has no effect on payload at shorter ranges for passenger models due to payload volume limit

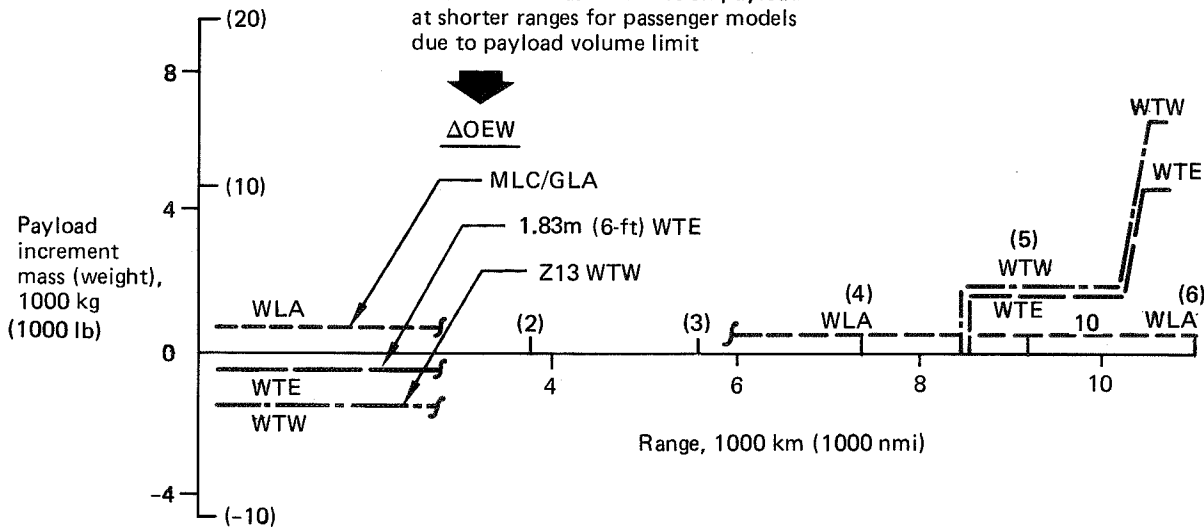


Figure 176. Effect of EET Modifications on Maximum Payload

Purchase Price—The major cost to the airline associated with any of these concepts would be the purchase price of the equipment. In an actual program, the price would be established after a market survey had been conducted to determine the expected number of units to be produced. Since a market survey was not conducted as part of the study, the estimated prices are shown parametrically as a function of market base (fig. 177). Prices shown for the tip extensions and the winglet do not include the WLA system. The price indicated for WLA is the incremental price associated with the system if installed concurrently with one of the wingtip modifications, and it is based on the final system configuration for this study (fail operational, electrohydraulic power control unit, existing aileron). The WLA system price increment includes strengthening of the aileron and backup structure but excludes wing box modification costs, which are included as part of the wing tip modification costs. The price curves for all of the concepts include a return to the airframe manufacturer and amortization of the nonrecurring costs for production engineering, certification, and tooling.

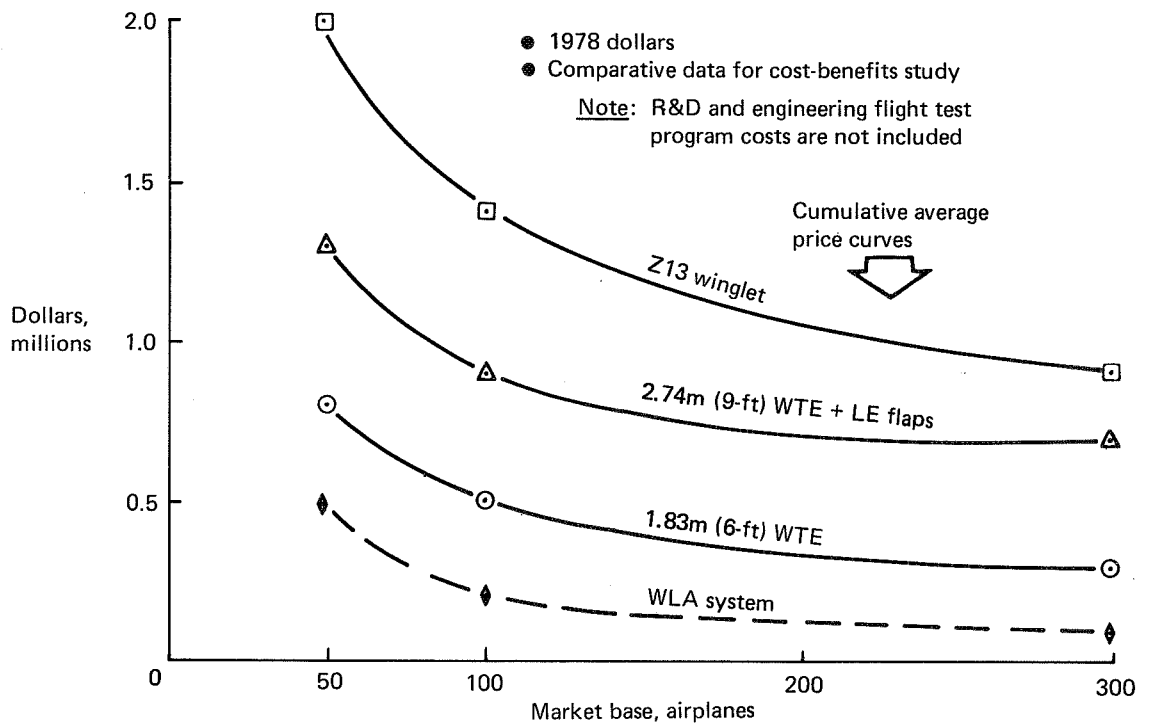


Figure 177. Study Prices for 747 EET Modifications

An important ground rule used in estimating production costs for this study was that research, development, and engineering flight test program costs were excluded. These costs were excluded because the winglet is a relatively new concept which would require much more development than wing tip extensions. The prices would be higher, particularly for the winglet, if these costs were included. The intent was to get a comparison of actual production program costs, assuming an equal technical development status for all of the concepts.

Preliminary design descriptions (work statements) developed during the study were used to define the configurations for cost estimation. In addition, detailed drawings from a prior Boeing study were available for the 1.83-m (6-ft) WTE. The number of new parts required was carefully determined for this WTE and was used as a basis for estimating manufacturing costs. Estimates for the 2.74-m (9-ft) WTE and the winglet were obtained by considering the additional parts and complexity relative to the 1.83-m (6-ft) WTE. In the case of the WLA system and leading-edge flaps, costs for major components (e.g., aileron actuators, computers, flap drive) were obtained from historical data or current prices for similar components.

The nonrecurring engineering, ground test, and certification flight test resource requirements for all of the concepts were estimated with reference to historical data. Tooling costs for the WTEs were estimated from experience and extrapolated to the winglet, considering the increased complexity.

The increased complexity of the winglet relative to the 1.83-m (6-ft) WTE is illustrated in Figure 178. This figure shows the winglet projected in the same plane as the wing tip extension. Spars and ribs are indicated, but most of the stringers have been omitted for clarity. For purposes of comparing complexity, consider the winglet installation to consist of three parts. First, the existing wing tip must be modified. This is somewhat more complex for the winglet. Second, there is a transition section for the winglet containing nine aluminum forgings and the highly contoured wing-winglet juncture. This section does not exist for a tip extension. Third, there is the winglet panel with construction similar to the WTE. This panel, about twice the length of the 1.83-m (6-ft) WTE but with a smaller chord, has more parts than the WTE. Tooling is obviously more expensive for the winglet; and recurring manufacturing costs are estimated to be about three times greater due to the larger size and more complex construction and contours.

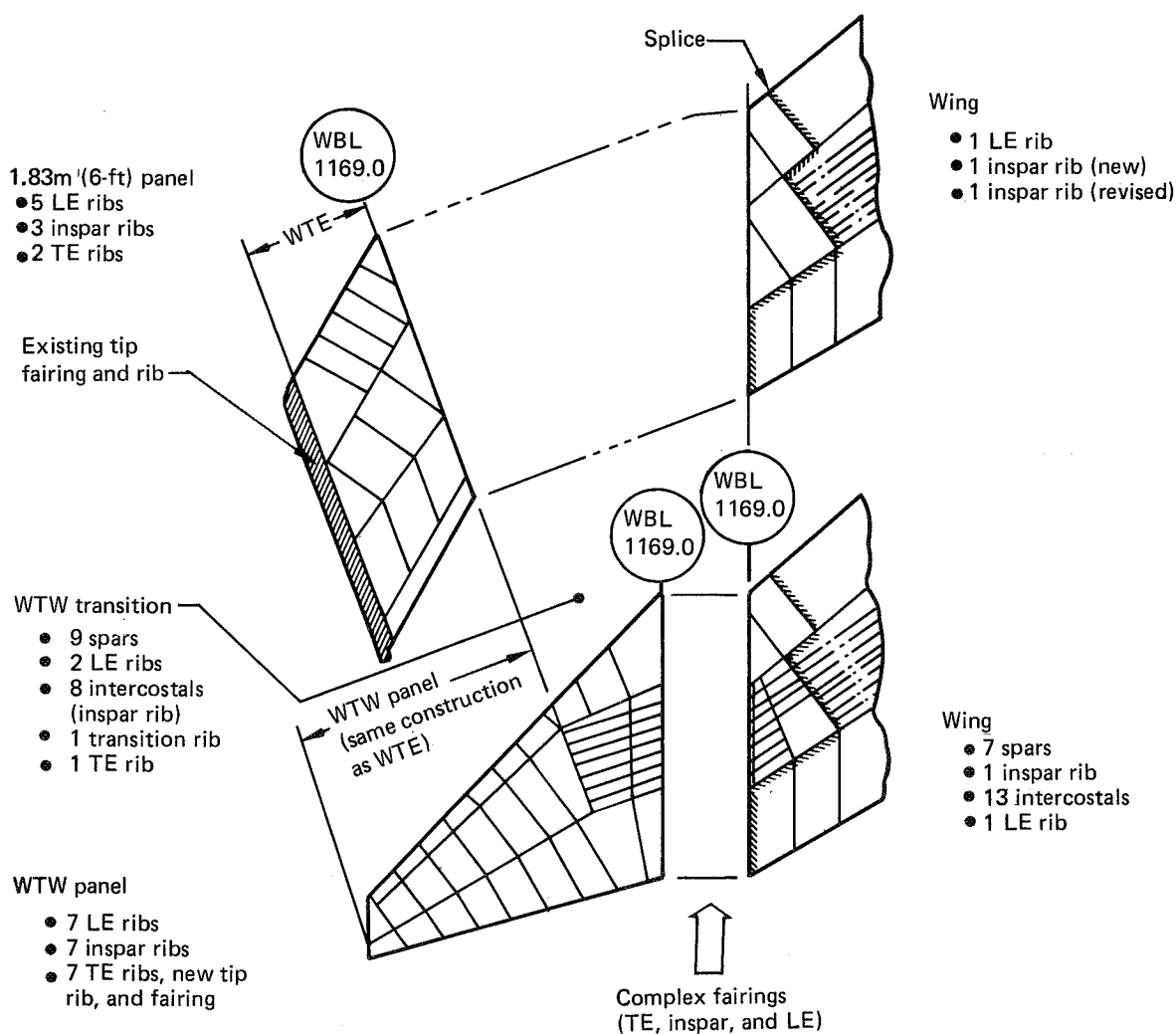


Figure 178. Structural Complexity Comparison of WTE/WTW

Return on Investment—The economic analysis of the 747 EET used incremental ROI analysis. This means that each configuration is analyzed as though the changes to the baseline 747 were options offered to a customer, and the customer was evaluating each option without regard for the desirability of the basic airplane. This analytical approach illuminates the economic desirability of each modification. The ROI analysis is a costs-benefits analysis based on present value of net cash flows, referred to as net present value (NPV), as indicated in the following equation:

$$\text{NPV} = -\text{Investment} + \sum_{n=1}^{\text{useful life}} (\text{cash in} - \text{cash out}) (1 + r)^n$$

ROI is the discount rate that makes the sum of the projected annual cost savings equal to the initial investment (i.e., when NPV = 0, r = ROI = discount rate). It is the best comparator of alternative investment opportunities in a general business context. ROI recognizes the value of money over time, and it can be directly related to any airline's cost of capital to show how much a modification is above or below the hurdle rate.

In this study's context, the hurdle rate is the ROI required before an airline would consider undertaking an investment opportunity. It should be noted that there is an inherent uncertainty in any generalized figure of merit applied to a specific airline due to considerable variation in individual airline operations, rules, and evaluation criteria. A specific ROI analysis using an airline's individual rules and hurdle criterion could produce considerably different results. In general, however, a hurdle rate of 15% after taxes is considered an acceptable criterion and is used by several major airlines.

Cash flows were calculated using constant (1978) dollars, considering the purchase price of the airplane modification as the initial investment. The costs for airport gate and maintenance facility modifications were not included. The fuel cost savings were the only cash inflows considered. Incremental costs for insurance were included as a cash outflow for all concepts. It was assumed that operational maintenance costs would be unchanged by the wing tip modification. Though negligible, the net change in flight control system maintenance costs (\$0.29 per flight hour increase) due to the WLA system was included in ROI calculations for that concept. Other pertinent ground rules were:

- 15 years useful life
- 48% tax rate
- Depreciation based on sum of years digits, 10 years to 10% residual value
- 10% investment tax credit taken over 3 years
- 3704-km (2000-nmi) range
- 850 trips per year utilization

The ROI comparisons were made for a 3704-km (2000-nmi) range because that is approximately the average range for current 747 fleet operations.

The results shown in Figure 179 indicate that a wing tip extension without leading-edge flaps and without wing load alleviation is the only study configuration that could be expected to provide an ROI in excess of the hurdle rate. Though parametric increases in fuel prices are shown, it should be recognized that increased fuel price alters the ROI comparisons only to the extent that fuel prices escalate relative to the overall inflation rate.

Fuel Price

- 1978 dollars
- 3700-km (2000-nmi) range
- 866 trips/year

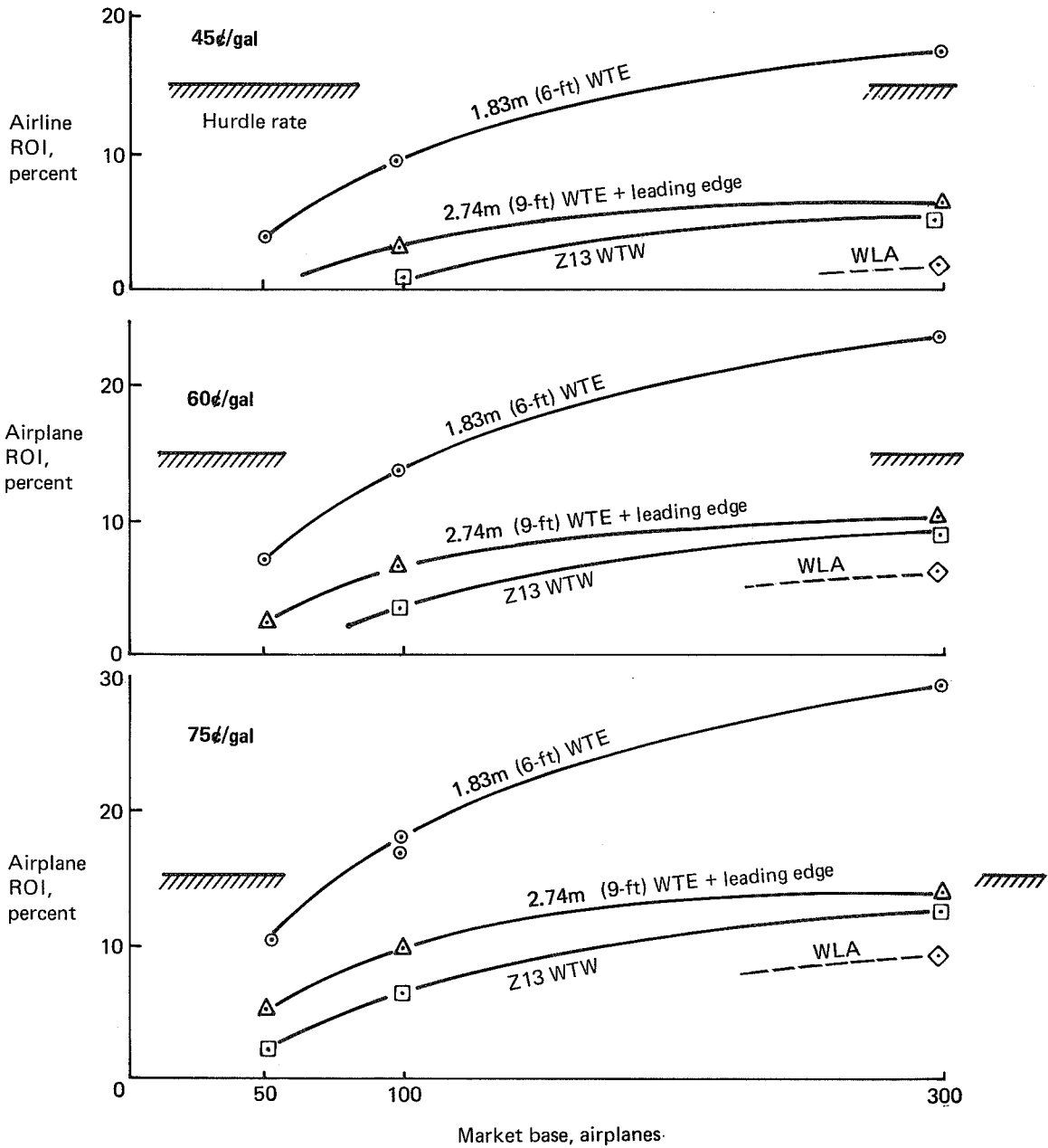


Figure 179. After Tax Return on Modification Investment

The trades between initial purchase price and fuel cost savings for the 1.83-m (6-ft) WTE and the winglet are illustrated in Figures 180 and 181. The purchase price appears as an initial cash outlay. The slope of the lines reflect the annual fuel cost savings only; i.e., taxes, depreciation, etc., are not included in these illustrations. The points where the curves pass through zero give an indication of the relative time required to recover the initial investment for the various concepts. Comparison of the figures indicates that the winglet becomes more competitive at longer ranges and escalated fuel prices. The effect of varying the purchase price can be visualized by parallel displacement of the curve(s) of interest.

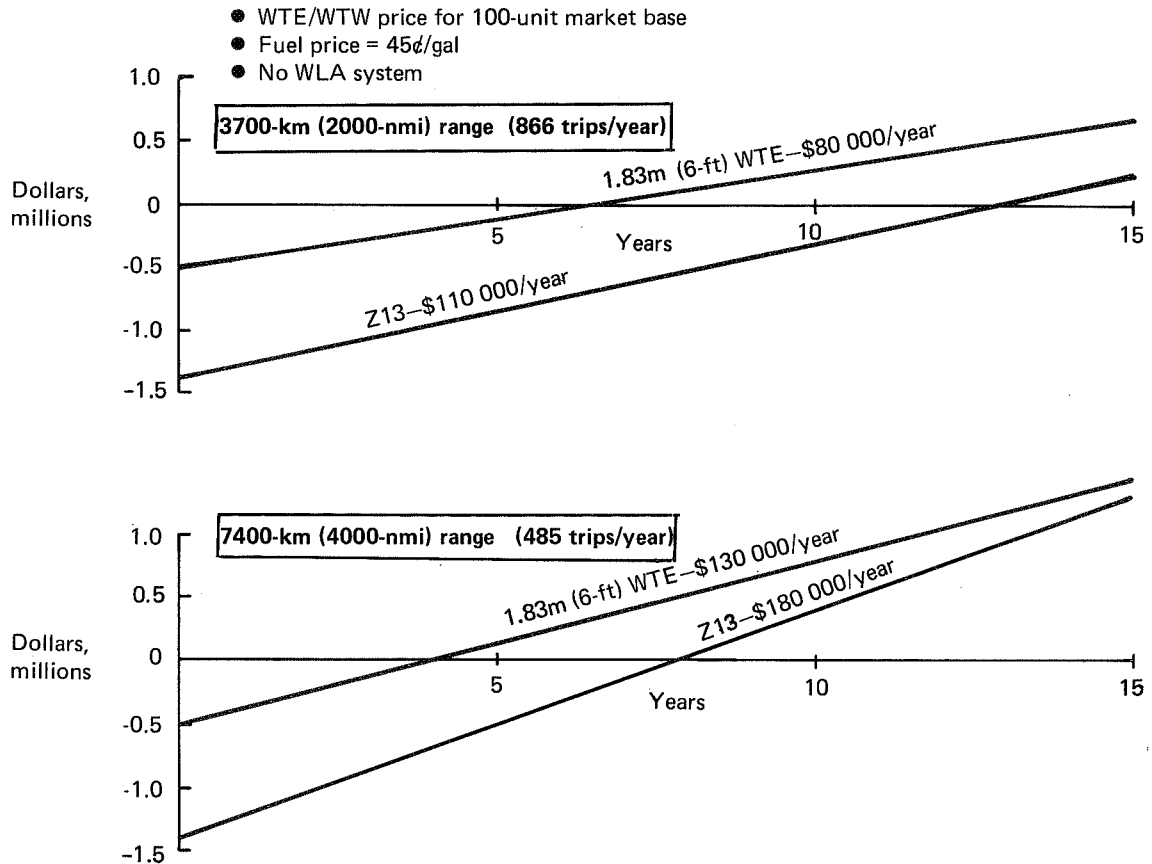


Figure 180. WTE/WTW Price/Payback Comparison for Current Fuel Price

Based on the assumption that all parameters affecting ROI, except fuel price, remain constant, the ROI offered by the winglet improves as the price of fuel is increased. The winglet would yield an acceptable return at around \$1.00/gal fuel cost, assuming the price of the installed winglet did not also escalate. That is undoubtedly an unrealistic assumption as increased energy costs invariably affect other parameters in the ROI equation, particularly production costs. The conclusion drawn from these economic comparisons was that it is unlikely that winglet price can be reduced enough or that fuel costs will escalate enough to warrant near-term development of the winglet for commercial 747 implementation.

- WTE/WTW price for 100-unit market base
- Fuel price = 60¢/gal
- No WLA system

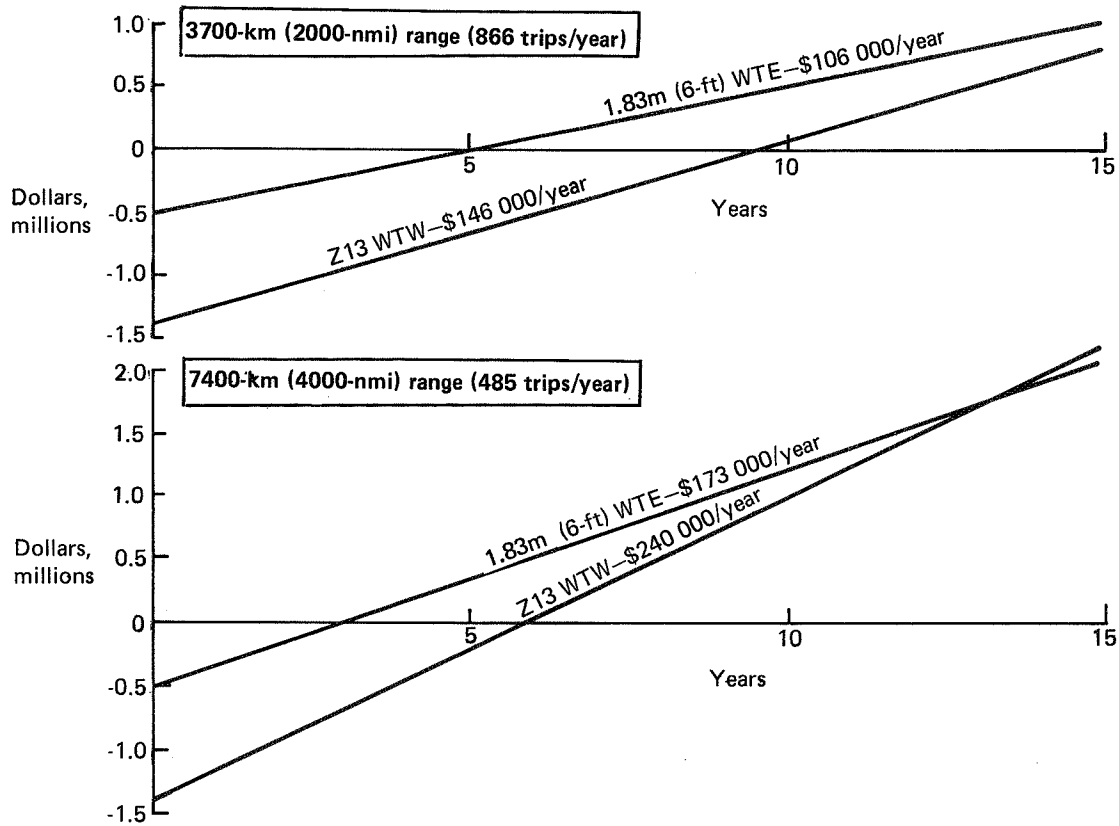


Figure 181. WTE/WTW Price/Payback Comparison for Escalated Fuel Price

The fuel savings attributable to WLA were insufficient for the 747 EET to provide a positive ROI for the system; therefore, ROI curves are not shown for wing tip modifications combined with WLA. The ROI could be more favorable for other 747 applications or for other airplane models.

7.3.3 Operational Considerations

Reliability and Maintenance Cost—WLA for the 747 EET derivative is mechanized as a simple system with high reliability and with only a small increment to the total airplane maintenance cost. As discussed in Section 6.4.3, the mean time between system failure is predicted to be better than 75 000 hours and the reliability approaches that of a dual yaw damper system. Maintenance of the WLA system is facilitated by the built-in test, which identifies a failed component to the line replaceable unit (LRU) level.

The maintenance cost with WLA is an additional \$0.29 per flight hour. On a component by component basis this is similar to the cost for a dual yaw damper

system. Dispatch with only one WLA channel operational is an objective for all except very long range routes. Thus no delay or cancellation costs were included in the maintenance cost estimates.

Effect of System Failures—This subsection summarizes the structural analysis for failures of the WLA system. The failures analyzed included both passive and hardover failures of the aileron control surface with the wing resized to zero margin of safety with MLC.

Inflight Failures—With the surface failed in the neutral position (passive failure) the structure was analyzed for the design limit load envelope using a safety factor of 1.0. In addition the structure was estimated to be failsafe for a passive failure of the WLA system using limit loads for a normal operating condition and a failsafe factor of 1.0. Finally, limit loads were computed for a hardover failure of the aileron for a normal operating condition. The bending moment results from this condition for a safety factor of 1.0 were shown to be less than the design envelope.

Placards For System Off Dispatch—Figure 182 shows design bending moment envelope results for the WLA system inactive and a takeoff gross mass (weight) reduction of 22 680 kg (50 000 lb). The wing design bending moments for this configuration exceeds the design envelope for the basic configuration with active WLA but the torsions are reduced. A penalty of 91 kg (200 lb) was predicted to provide required wing strength for this configuration.

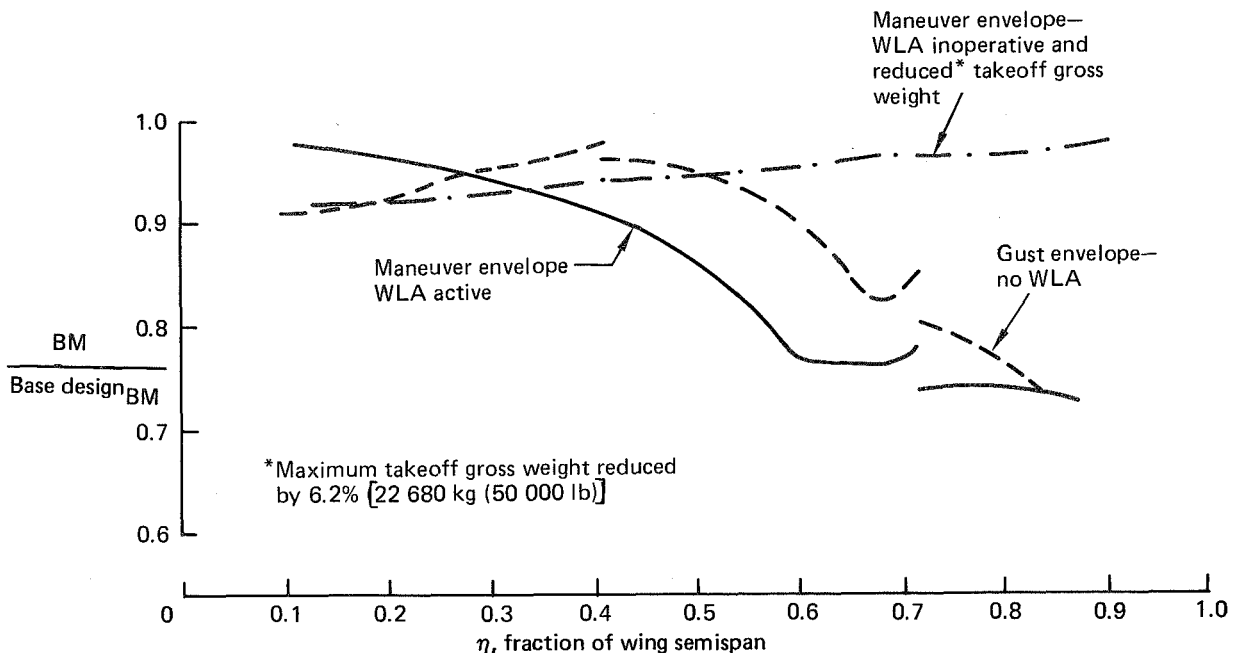
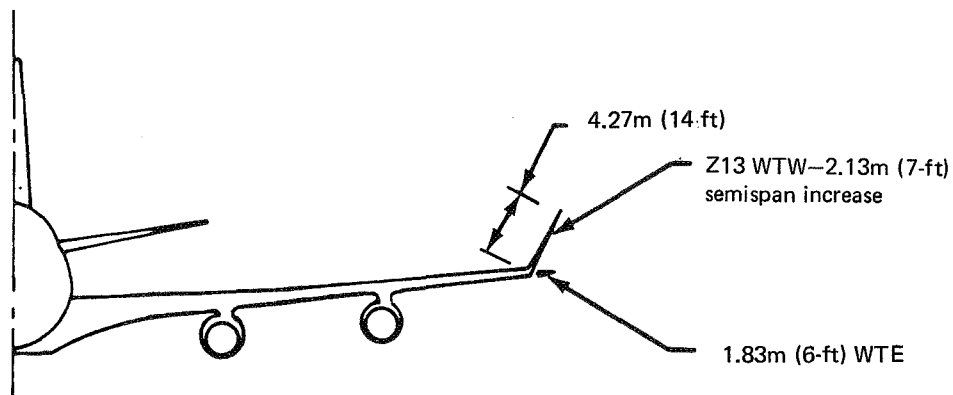


Figure 182. Wing Bending Moment Envelope Ratio for Reduced Takeoff Gross Weight With WLA System Inoperative

Gate and Hangar Access—A brief survey of the impact of WTE or WTW on airport ground operations and maintenance facilities was conducted by United Airlines (UAL) as a subcontract study item. Some of the concerns expressed by

UAL are outlined in Figure 183. In general, it was concluded that these concerns would not be a factor in choosing between tip extensions and winglets for the 747, provided the winglet did not extend below the wing tip. Winglets below the wing tip could interfere with parking and flight line maintenance/refueling operations. Costs for modifying maintenance facilities (docks, etc.) were estimated and found to be relatively minor. A more detailed examination involving cost/benefit trades for the selected configuration was recommended by UAL prior to committing the selected concept to production.



- UAL study identified potential problem areas:
 - Terminal area
 - Taxi lanes
 - Aprons
 - Parking gate clearances
 - Maintenance facilities—some hangar and dock modifications required (relatively minor)
 - Not a factor in choosing between 1.83m (6-ft) WTE versus Z13 WTW
- } Reduced clearances and loss of gates at some airports

Figure 183. Increased Semispan Operational Concerns

7.3.4 Retrofit Feasibility

Feasibility of retrofit using doublers to strengthen the wing box, was considered for the WTE and WTW configurations with and without MLC. It was concluded that retrofit would not be practical for any of the configurations.

Retrofit of a winglet (Z9) with a 15 deg cant angle probably would be technically feasible if flutter stiffness requirements could be limited to the relatively small portion of the outboard wing where strength material was required. Even if this could be achieved (not likely) costs for retrofit would be considerably higher than for a production line installation. Tip extensions require strength "beef-up" further inboard than winglets (flutter neglected). The length of the required stringer doublers would prohibit their entry into the wing interior through fuel tank access doors. Disassembly of the wing would be so extensive that jig position could not be held.

7.4 RESULTS SUMMARY

Wing tip Modifications without WLA—Final L/D comparisons were made for the 1.83-m (6-ft) WTE, 2.74-m (9-ft) WTE, and Z13 WTW using wing twist distributions corresponding to wing box structure resized to accommodate the wing tip modifications, assuming the existing structural margins were absorbed before adding new material. To give an indication of the relative fuel efficiency, an equivalent L/D increment based on an L/D versus weight trade factor, also was estimated to account for the effects of the added WTE/WTW panel and wing-box weights. The L/D versus weight trade factor of 0.2% equivalent L/D decrease per 453.5 kg (1000 lb) increase in airplane mass (OEW) is valid for missions not limited by takeoff gross weight; i.e., 5556 km (3000 nmi). The final comparisons showed the following L/D relationships:

	<u>Actual</u>	<u>L/D increase without WLA, % Net (adjusted for ΔOEW)</u>
1.83-m (6-ft) WTE	1.9	1.7
2.74-m (9-ft) WTE	2.6	1.9 (includes leading-edge flap weight effect)
Z13 WTW	3.2	2.5

The relative efficiency of the concepts can be inferred from the net L/D comparisons. The actual percentage fuel savings vary with trip distance, as discussed in Section 7.3.1.

Wing Load Alleviation—Application of WLA to the basic wing of the 747 (sec. 6.0) was found to offer the potential for an airplane OEW reduction of approximately 2.5% of the wing-box weight. When the adverse effects of the L/D reduction associated with the twist modification resulting from wing structural resizing were combined with the favorable effects of the airplane OEW reduction, the net fuel savings attributable to WLA was quite small; approximately 0.2%. Because payload is volume-limited rather than gross-weight limited for typical 747 passenger routes, the airplane OEW benefit of WLA could not be converted to additional revenue in the form of increased payload.

Final structural sizing was not completed for the WTW/MLC configurations for reasons noted above. A judgement was made that the WLA benefits determined for the basic wing would apply to either wing tip modification combined with WLA. Therefore, the net L/D improvements listed above for the WTE/WTW without WLA could be increased about 0.2% if combined with WLA.

Economic Comparisons—Although the winglet provides the best improvement in L/D and fuel efficiency, manufacturing costs were estimated to be about three times those of the 1.83-m (6-ft) WTE. Manufacturing costs for the 2.74-m (9-ft) WTE also were higher than for the shorter WTE, largely because of the cost increment associated with the leading-edge flaps. Economic studies that considered the costs to the airplanes as well as the fuel savings, showed the 1.83-m (6-ft) WTE to be the most economically attractive.

8.0 CONCLUSIONS AND RECOMMENDATIONS

This study has been valuable in providing complete aerodynamic and structural comparison data for the concepts, based on consistent sets of ground rules relative to the same baseline model. The analyses and wind tunnel testing conducted in this program will be useful for reference in subsequent studies, has promoted a better understanding of the concepts (particularly as applied to a flexible wing), and has identified some problem areas concerning winglet applications.

A number of conclusions and recommendations of interest to specific technical disciplines were made during the study and are contained in the main body of the report. Only those of more general interest are presented in the following sections.

8.1 CONCLUSIONS

WTE and WTW without WLA

- Fuel efficiency of current 747-200 production models (heavier than the original 747-100) can be improved by the addition of wing tip extensions or winglets. Block fuel reductions on the order of 1.5 to 3% can be achieved, depending on the length of the added wing tip extension/wing tip winglet (WTE/WTW) panel and the route length considered. As expected, the percentage fuel savings are greater for the longer routes.
- Selection of the best wing tip modification for the 747 is a compromise between performance, cost, stability and control, flutter, and operational (gate clearance, etc.) considerations. Winglets have advantages in the areas of performance and gate clearance, while tip extensions are less expensive and are also preferable in the other areas noted. The cost vs benefit trades are such that a tip extension would provide a better return on investment to customers with a typical route structure. Winglets might be advantageous for extremely long range routes with escalated fuel prices.
- When viewed in terms of return on customer investment, a 1.83 to 2.74-m (6 to 9-ft) wing-tip extension appears optimum. The requirement for leading-edge flap protection and other structural design, manufacturing, and operational concerns would be considered in making the final selection.
- The full-chord, sub-optimally-loaded winglet aerodynamic design approach was successful. The winglet design resulting from this study achieved nearly all of the theoretical potential for a winglet of that span ($0.135 b/2$) and cant (30 deg out from vertical). Therefore, further significant drag improvements cannot be expected from aerodynamic design refinements alone; but instead could be achieved only through increased winglet size (flutter penalty), cant angle variations (possibly), and reductions in aeroelastic and/or structural weight penalties. The performance penalty associated with increased aeroelastic washout of the basic wing might be reduced through an iterative design/test/analysis process wherein the winglet design and cruise twist of the wind tunnel model were modified to reflect the new cruise shape of the wing with winglets. This procedure was not used in this study.

- Relative to simple wing span extensions, winglet design is a considerably more difficult task. Winglet configuration development is more sensitive to aerodynamic/structural interactions. Winglet analysis techniques are still in the developmental stage and have not been adequately correlated against full-scale flight results. Structural design and tooling are complicated by the curvilinear intersecting surfaces. Consequently, a production winglet installation would require a more extensive development and manufacturing program with attendant higher production costs. The question of whether the performance potential of the winglet could be realized at an attractive cost would require a full-scale development program to be determined with confidence.

Wing Load Alleviation

- The existing 747 outboard aileron can be used to reduce wing design bending moments in maneuvers and turbulence. Although torsion loads are increased, a plain aileron is preferable to a tabbed configuration. The tab provides no more net airplane operational empty weight reduction than does the plain aileron, and has several disadvantages such as increased complexity and reduced roll control power.
- A maneuver load control (MLC) system would allow an airplane operational empty weight reduction equivalent to 2% of the wing box weight. If a gust load alleviation (GLA) system were able to make the maneuver load control designed wing entirely non-gust-critical, a further 1% reduction in wing box weight would be possible. However, due to torsion loads induced by the ailerons, adverse effects of phase lag induced by the filters, and effects of actuator rate/position limits, only about half of the gust load alleviation (GLA) potential can be realized by an actual system. The final maneuver load control system, which utilizes wing acceleration as the only feedback parameter, provides elastic mode suppression of the first wing bending mode and is effective in reducing power spectral density gust loads. However, it may be preferable to retain some of the gust material in the wing to minimize possible loading restrictions for dispatch with the system inoperative.
- Fatigue material distribution had to be modified when the wing box was resized with maneuver load control, but the total weight of the fatigue material was essentially unchanged. If further resized to take credit for gust load alleviation, a small reduction in fatigue material weight could be achieved.
- Fuel savings associated with the weight reduction potential of MLC/GLA are small for the 747. Aerodynamic efficiency (L/D) is slightly reduced by the increased aeroelastic washout resulting from resizing with wing load alleviation (WLA). The airplane operational empty weight benefits are limited by the system weight and the added structural weight necessary to use the outboard aileron as a high-speed control surface. At typical operating ranges, a mass (weight) reduction of 2268 kg (5000 lb) would be necessary to achieve a 1% fuel savings.
- The wing load alleviation system offers little potential for increased revenue through increased payload, because passenger models of the 747 are typically volume-limited rather than weight-limited at all except very long ranges.

- Although the wing load alleviation system would be reliable and relatively inexpensive (if installed concurrently with another modification requiring wing box resizing and recertification), return on investment to the airline probably would be unattractive due to the small revenue/fuel cost benefits. The operational empty weight reduction and return on investment should be better for an airplane already equipped with high speed outboard ailerons because the aileron and wing box would contain most of the material required by the higher torsion and local aileron loads. Further improvements in the return on investment attributable to wing load alleviation could be expected if provisions were incorporated in a new airplane design, since aeroelastic twist penalties (L/D) and most of the flight control system component costs (e.g., actuators, computers) could be avoided.
- The new electrohydraulic outboard aileron and outboard elevator power control units recommended as part of the maneuver load control system installation would improve the existing actuation system in terms of reduced weight and complexity, and improved functional availability.
- A flutter mode control system would offer no weight benefits for the 747 basic wing or the wing with wing tip extensions since no additional material is required for flutter clearance with or without MLC/GLA. However, flutter mode control would be beneficial for the wing with winglet, particularly in combination with maneuver load control. The winglet introduces a symmetric flutter mode that could be damped by a flutter mode control system employing the outboard aileron.

8.2 RECOMMENDATIONS

At the conclusion of this Phase I study effort, recommendations were to be made regarding final configuration selection and continuation of the program into Phase II for further development and flight test. These are described below.

8.2.1 Final Configuration

Wing Tip Modification--Wing tip extensions rather than winglets should be considered for near term implementation on 747 derivatives.

Wing Load Alleviation System--Results of this study do not support a general recommendation to incorporate a wing load alleviation system into 747 derivative passenger models, solely for the purpose of reducing operational empty weight, due to the low return on investment. However, the system may offer benefits for specific 747 applications and the economic trades would be more favorable for aircraft designed with provisions for high-speed outboard aileron actuation. Potential benefits should be reviewed after flight test data from the Boeing Wing Load Alleviation Demonstrator program are available.

Design recommendations regarding the wing load alleviation system configuration and system/structural design approach are presented in Section 6.5.

8.2.2 Phase II

Flight testing of MLC/GLA concepts has been accomplished as part of a separate Boeing-funded IR&D program, and flight testing of a WTE/WLA combination on the L-1011 is included in the NASA EET program. No further NASA-funded research appears necessary for application of WTE/WLA concepts to the B-747 and near-term commercial application of winglets appears unlikely. As a result, no further NASA/Boeing 747 EET Phase II work is recommended in these technical areas.

9.0 REFERENCES

1. MIL-F-8785B; Military Specification, "Flying Qualities of Piloted Airplanes"; Aug. 7, 1969.
2. Dempster, J. B. and K. L. Roger; Paper No. 66-998; "Evaluation of B-52 Structural Response to Random Turbulence with Various Stability Augmentation Systems", AIAA Meeting, Dec. 1966.
3. "C-5A Active Load Alleviation System"; *J. of Spacecraft*, Vol. 14, No. 2; Feb. 1977.
4. Paper No. 77-1220; "Use of Active Controls for Fuel Conservation of Commercial Transports"; AIAA Aircraft Systems and Technology Meeting; Aug. 1977.
5. NASA CR-145024; "Airborne Advanced Reconfigurable Computer System (ARCS)"; Contract NAS1-13654; Aug. 1976.
6. Bailey, D. G. and K. Folkesson; "JA-37 Digital Automatic Flight Control System (DAFCS) Self Test Development"; *AGARDograph*, AGARD-AF-224; April 1977.
7. Whitcomb, R. T.; NASA TN-8260; "A Design Approach and Selected Wind-Tunnel Results at High Subsonic Speeds for Wing-Tip Mounted Winglets"; 1976.
8. Roger, K. L., G. E. Hodges, and L. Felt; "Active Flutter Suppression--A Flight Test Demonstration"; *AIAA J. Aircraft*; June 1975.
9. Redd, L. T., J. Gilman Jr., D. E. Cooley, and F. D. Severt; "Wind-Tunnel Investigation of a B-52 Model Flutter Suppression System", *AIAA J. Aircraft*; Nov. 1974.

**APPENDIX A
METHODOLOGY**

CONTENTS

	Page
1.0 AERODYNAMICS (A372 and A230 Computer Programs)	A-3
2.0 FLUTTER	A-7
3.0 FLIGHT CONTROLS (Reliability Estimates)	A-9
4.0 REFERENCES	A-11

FIGURES

	Page
A-1	Typical Representation of Wingtip and Winglet in A372 by a Multihorseshoe Vortex Lattice A-3
A-2	Wing Spanload Theory Versus Experiment A-4
A-3	Typical A230 Source Paneling for Wing and Winglet A-5
A-4	Typical A230 Source Paneling for Wingtip and Winglet A-6
A-5	Winglet Z9 Spanload Theory Versus Experiment A-6
A-6	Structural Model for Flutter Analyses A-7
A-7	Flutter Aerodynamic Model for Wing Tip Winglet and Control Surfaces A-7
A-8	Flutter Aerodynamic Models for Wing Tip Extensions A-8
A-9	Static Effects on Oscillatory Winglet Air Forces A-8
A-10	Typical Static Normal Force Effect on Flutter Speeds A-9
A-11	Reliability Model Dependency Tree—Final WLA Mechanization A-10

APPENDIX A—METHODOLOGY

1.0 AERODYNAMICS

A372 and A320 Computer Programs—Computer programs A372 and A230 were used for the analysis and design of wing/winglet configurations in three dimensional flow. The 747 EET winglets were designed using the A372 program. Program A230 was used to calculate the potential flow pressure distributions with and without winglets (Mach number = 0.70). Nacelle and body effects are relatively small at the wing tip region and were not included in either program paneling model.

A372 is an incompressible, potential flow program in which each lifting surface (wing and winglet) is represented by a multihorseshoe vortex lattice. This lattice is placed along the camber line, and airfoil thickness is not simulated. Figure A-1 shows a typical wing/winglet paneling configuration for A372. The dashed outline indicates the wing/winglet planforms. Strengths of individual vortex elements are determined by satisfying tangent flow boundary conditions at specific points on the camber surface. The boundary points are shown as + signs on the figure. Since the fuselage was not modeled, the wing surface extended to the plane of symmetry. Lift, induced drag, and moments for the configuration were obtained in the program by a vector summation of the net force (and force times moment arm) acting on each vortex panel.

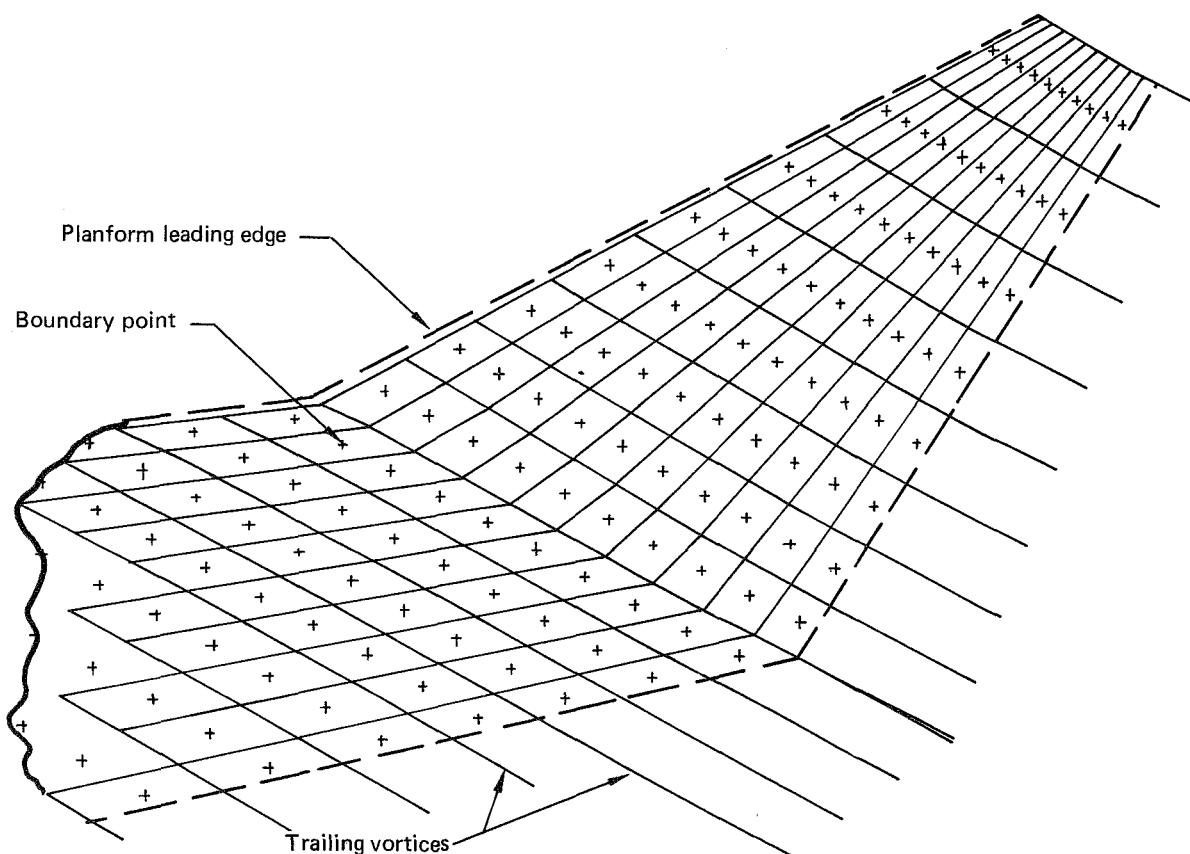


Figure A-1. Typical Representation of Wing Tip and Winglet in A372 by a Multihorseshoe Vortex Lattice

Program A372 can be used for both analysis and design. In the design mode, a part of the configuration can be held in a fixed position while other parts are allowed to move about a reference position. A372 determines the locations of the moveable portions that give optimum (i.e., minimum) induced drag for the total configuration. For the analysis mode all geometry is fixed.

Two types of A372 design optimization runs were made. The first allowed the winglet airfoil sections to twist to give minimum induced drag. This type of optimization was used to establish the winglet section lift required prior to selection of a compatible initial airfoil for the A372 winglet design cycle described in Section 5.0. The second type allowed both twist and camber of winglet sections to vary and was used for the A372 winglet design mentioned in Section 5.0. Both types of design yield the same minimum CD_i because it is a function of spanwise loading, but not of chordwise load distribution. Only the winglet geometry is varied when minimizing induced drag with A372 because the wing is an existing configuration and must be maintained. Another capability is addition of optional constraints. During the 747 EET winglet design program it was found necessary to use suboptimum winglet loading. This was accomplished in A372 by specifying the winglet side force for which the winglet geometry was to be optimized.

Figure A-2 shows a comparison of the wing (alone) spanload for A372, A230, and experimental results. The agreement between A372 and the experimental spanloading is quite good. The A230 spanloading is slightly high over the outboard portion of the wing.

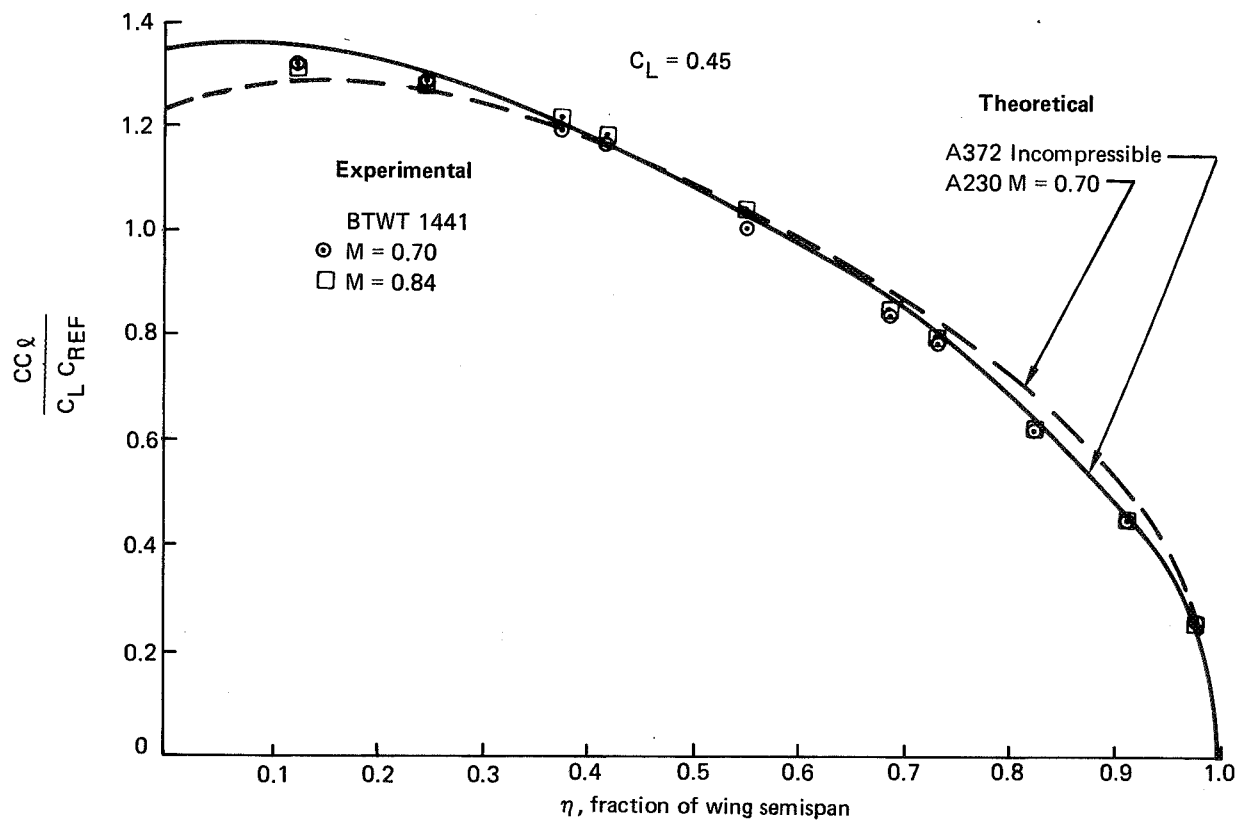


Figure A-2. Wing Spanload Theory Versus Experiment

A230 is a subsonic potential flow program that analyzes arbitrary configurations with thickness. Source panels and vortex lattices are distributed over the configuration to represent thickness and lifting effects, respectively. Singularity strengths are calculated by solving a set of linear algebraic equations that express exact tangent flow boundary conditions. Force and moment calculations are made only on the source panel surfaces. They are based on an integration of pressures where the pressure is assumed constant over a source panel. Figures A-3 and A-4 show typical A230 paneling.

The A230 program uses Gothert's rule as a model to calculate subsonic flow. The program is limited to use where no significant shock waves would likely occur since these cannot be properly accounted for. Usage with slight supervelocities where no strong shocks occur would not be unreasonable. Because the flow on the winglet is strongly linked to viscous effects, the A230 prediction of winglet loadings is too high (Figure A-5).

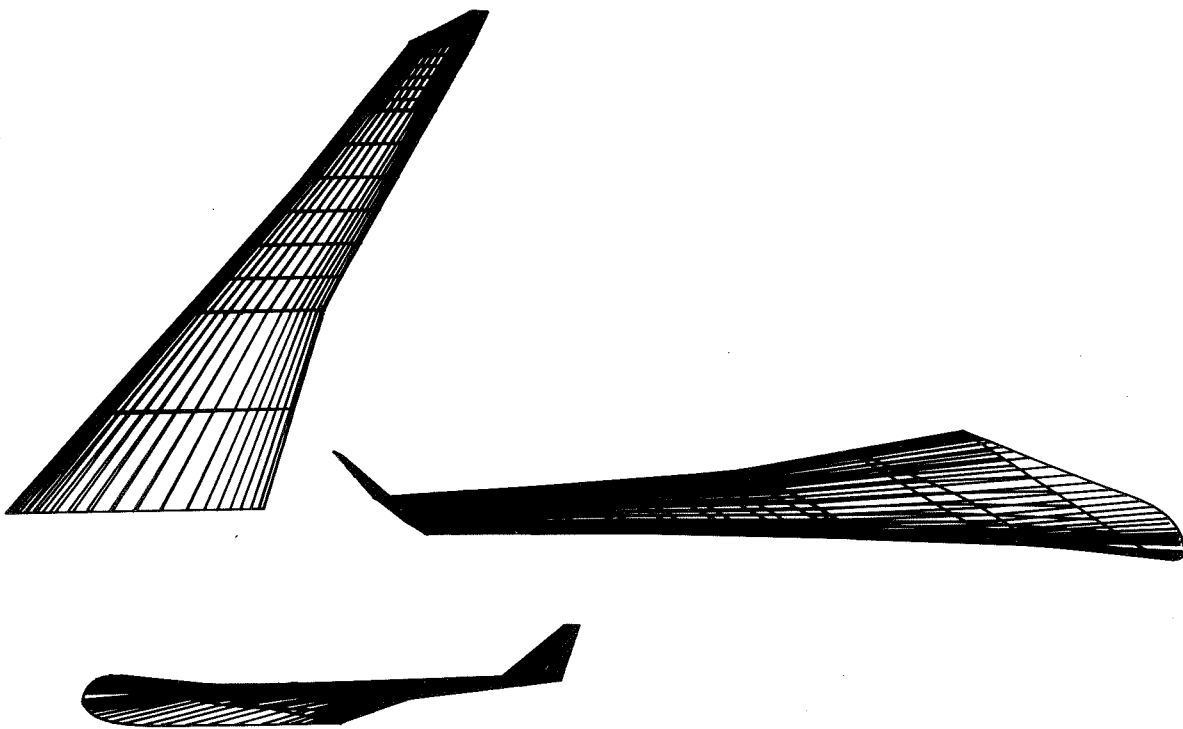


Figure A-3. Typical A230 Source Paneling for Wing and Winglet

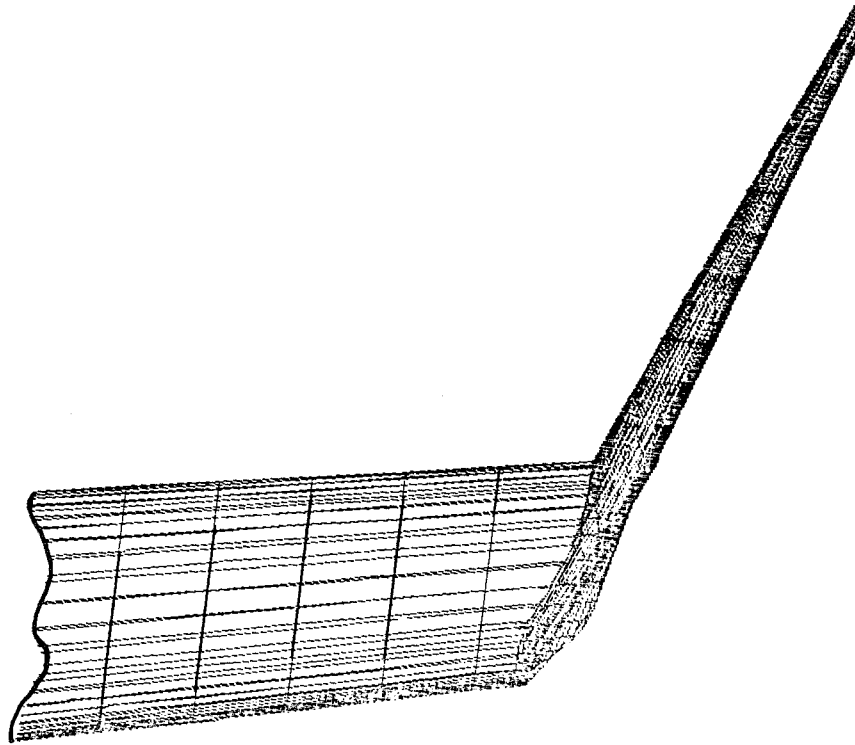


Figure A-4. Typical A230 Source Paneling for Wing Tip and Winglet

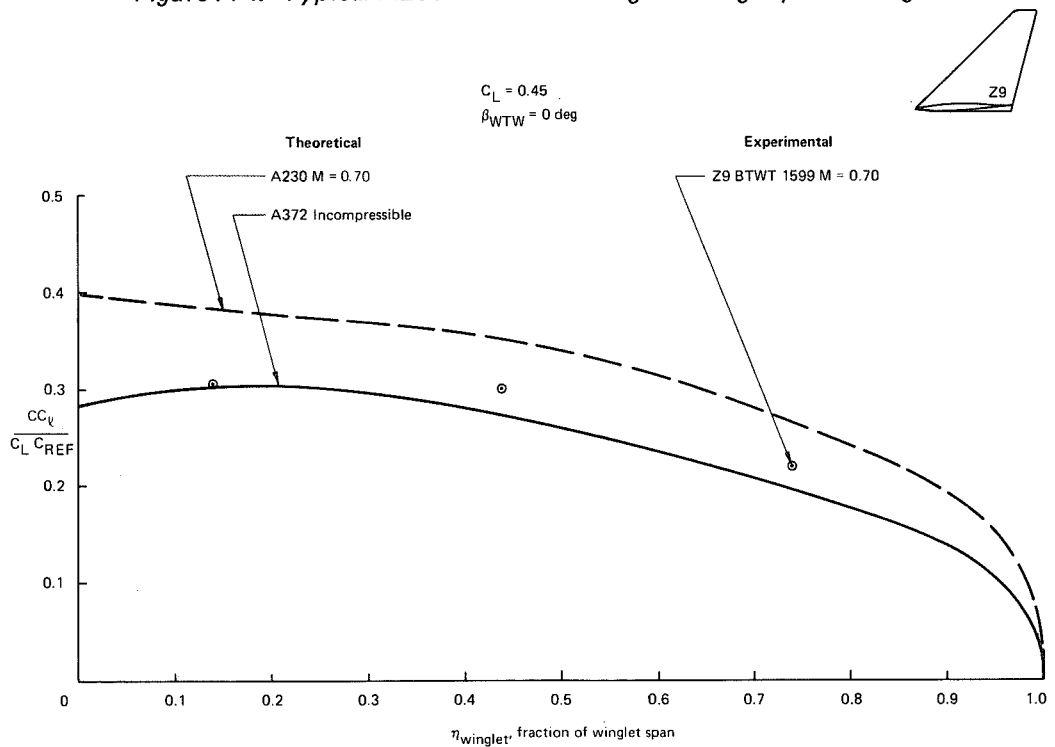


Figure A-5. Winglet Z9 Spanload Theory Versus Experiment

2.0 FLUTTER

Phase I studies for wing tip winglets and wing tip extensions have utilized basic 747 methodology where possible with methodology developments applied as necessary to correlate with wind tunnel flutter test results.

The standard structural model used was a finite element stick model as shown in Figure A-6. The figure shows the stick beam modeling necessary for the closed loop maneuver load control (MLC) analysis including elements providing the correct nacelle frequencies and mode shapes, control surface hinge points, and wing and body sensors.

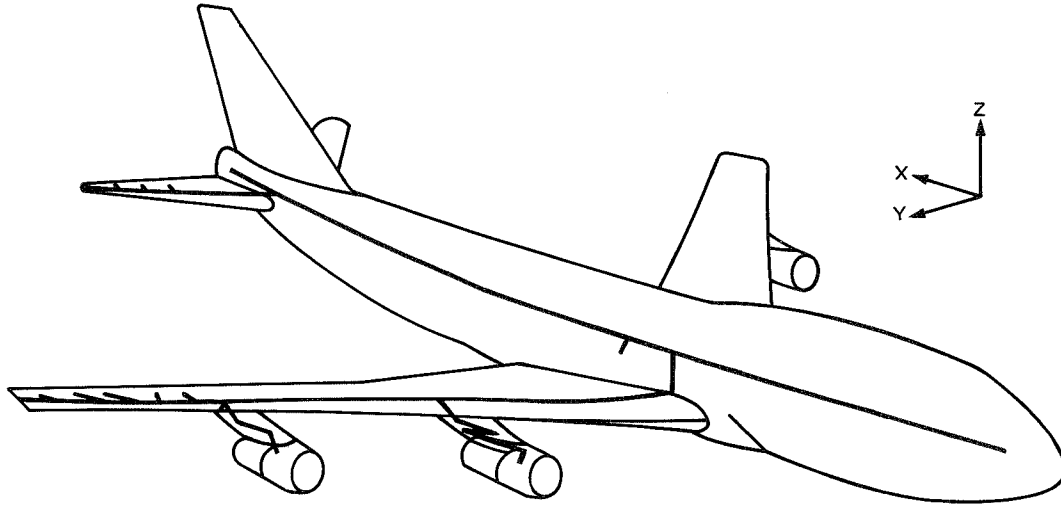


Figure A-6. Structural Model for Flutter Analyses

Figure A-7 shows the aerodynamic model for the closed loop MLC analysis with wing tip winglets and includes outboard ailerons and outboard elevators. The aerodynamic program uses Theodorsen's strip-theory with three-dimensional induction effects and experimentally derived scale factors. Figure A-8 shows the equivalent planforms and aerodynamic paneling for the wing tip extension analyses.

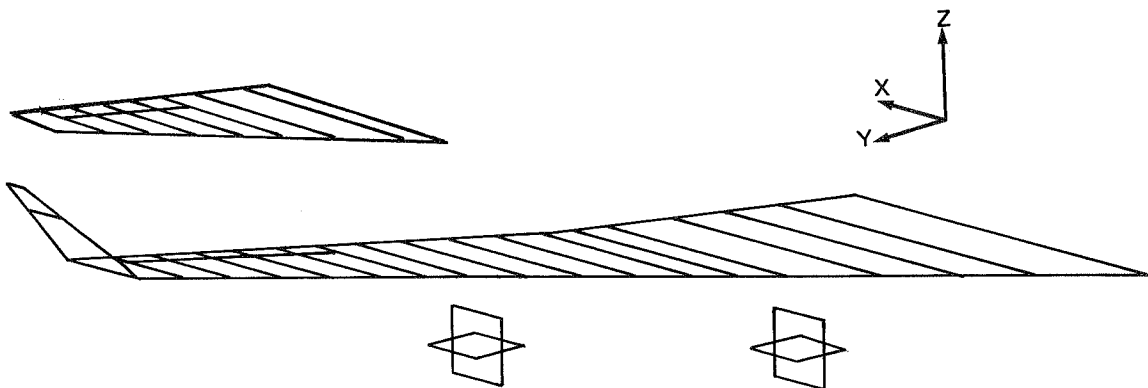


Figure A-7. Flutter Aerodynamic Model for Wing Tip Winglet and Control Surfaces

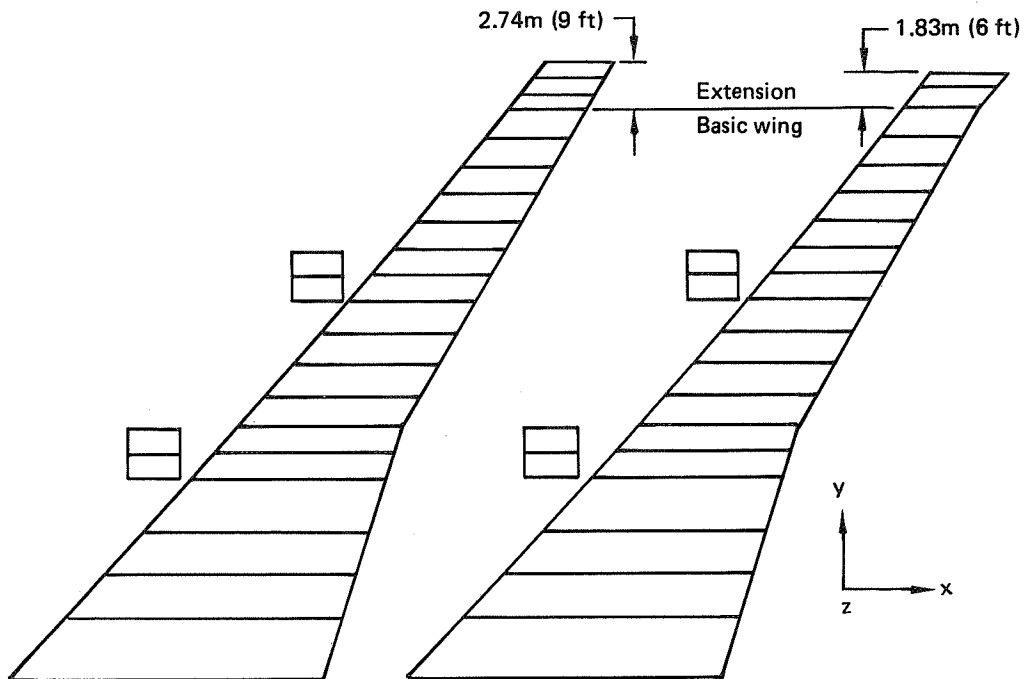
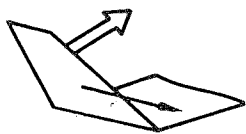


Figure A-8. Flutter Aerodynamic Models for Wing Tip Extensions

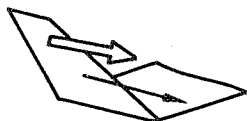
Figure A-9 shows the additional aerodynamic forces included in the improved methodology for the analysis of wing tip winglets. The magnitude of the winglet forces is determined from static normal force and chord force experimental data. These forces are then made oscillatory using Theodorsen's function, $C(k)$, and added to the normal flutter air forces.

Effects accounted for:

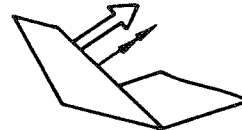
1. Normal force due to fore and aft motion



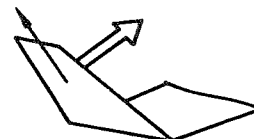
2. Chordwise force due to fore and aft motion



3. Normal force due to winglet "pitch"



4. Normal force due to winglet spanwise motion



5. Spanwise force due to roll

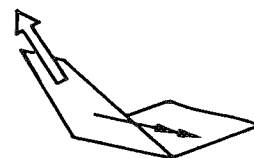


Figure A-9. Static Effects on Oscillatory Winglet Air Forces

The static effects on the oscillatory winglet air forces represent a key variable in the empirical tuning of the flutter solution to match experimental results. Figure A-10 shows the effect of the winglet static normal force on the symmetric mode flutter and wing tip flutter modes. A normalized force ratio of 1.0 represents the level selected for the improved methodology. At this point the symmetric mode flutter speed becomes nearly constant and any increase in force level is ineffective for this mode, while the wing tip flutter mode is rapidly stabilized.

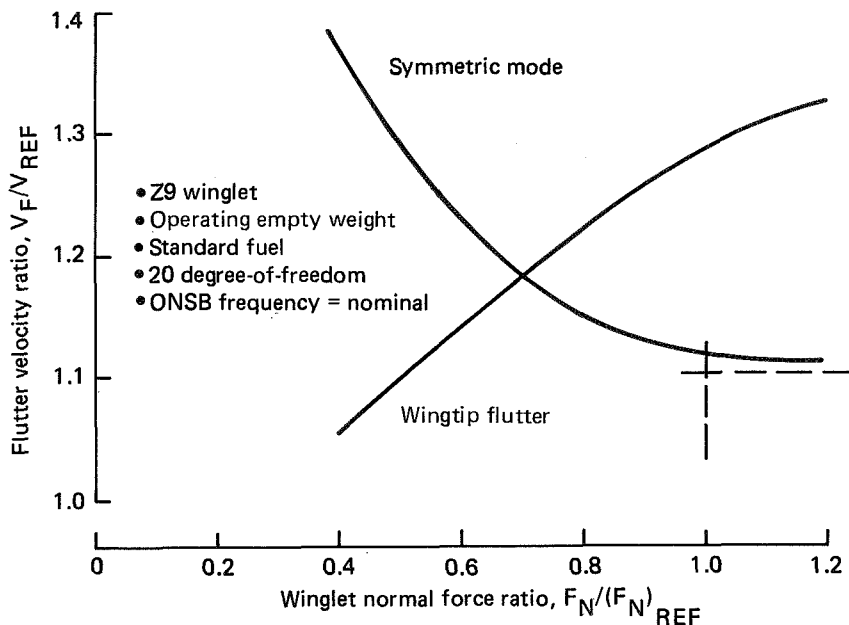


Figure A-10. Typical Static Normal Force Effect on Flutter Speeds

3.0 FLIGHT CONTROLS

Reliability Estimates—The EET program work statement specifies that the Computer Aided Redundant Systems Reliability Analysis (CARsRA) computer program (ref A-1) be used to investigate the wing load alleviation (WLA) system reliability characteristics. The CARsRA approach is to partition the system into stages, each of which consists of a set of identical redundant modules. A module is the smallest functional entity treated by the program, and is assumed to have a known constant failure rate. The operational status of each stage is modeled by a finite order Markov process in which each state corresponds to a particular redundancy state. The system failure probability then is evaluated by computing the contribution from each stage.

The operational status of a module in a particular stage can depend on modules in other stages being operational. A module which, when failed, causes the loss of function of another module in a different stage is termed a "dependency module", and the corresponding stage a "dependency stage". The reliability model dependency tree for the final system mechanization is shown in Figure A-11. The lines connecting the different stages indicate the dependency structure. For the WLA function the actuators are dependent on the survival of the computer stage and the hydraulic stages. Cross strapping and signal selection of the sensor data allows the sensor stages to be independent. CARsRA treats dependency between stages by "exhaustive

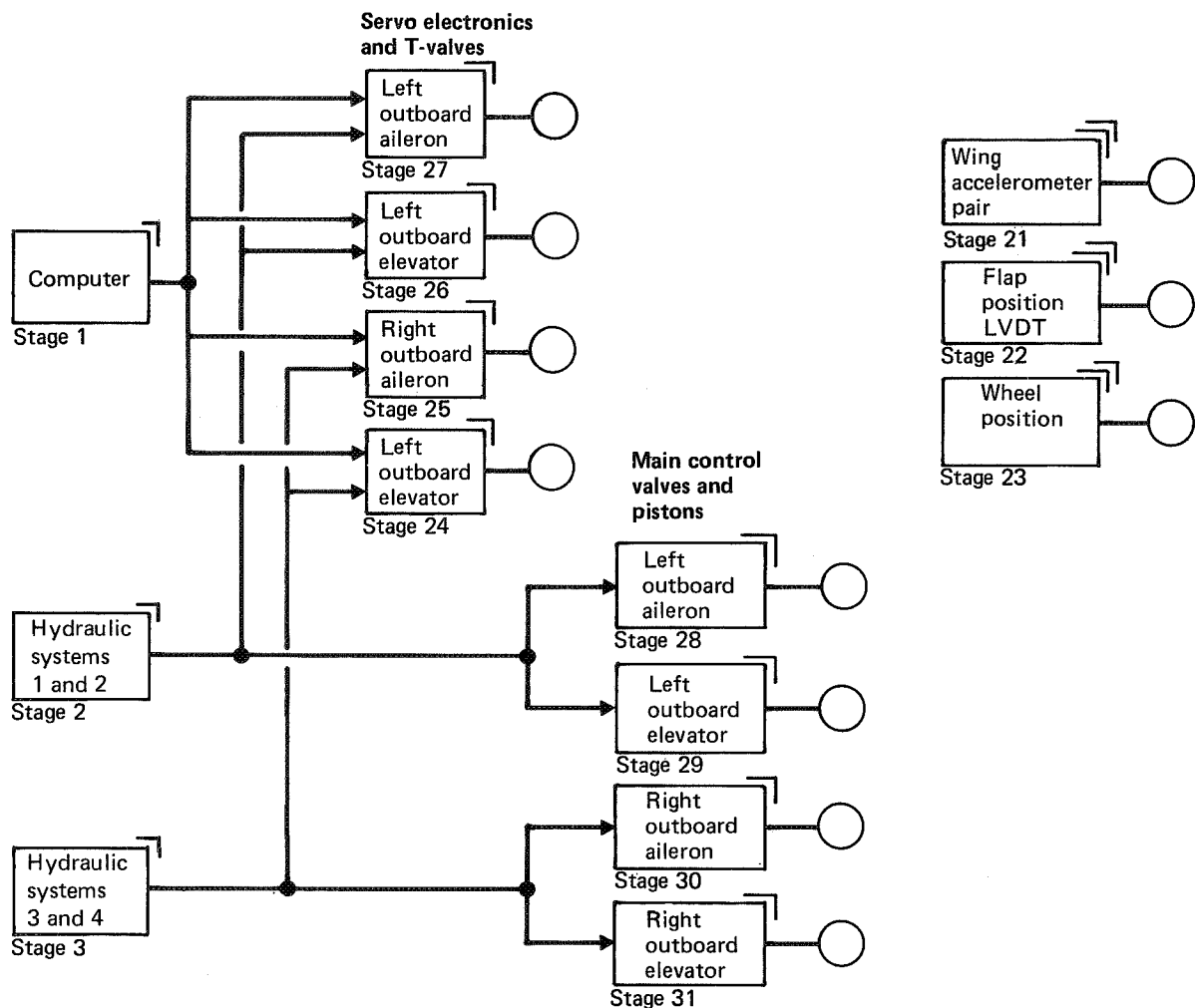


Figure A-11. Reliability Model Dependency Tree—Final WLA Mechanization

conditioning". The essence of this approach is to make the nondependency stages independent via conditioning upon the failure status of the dependency stages. The signal consolidation points or voting nodes, shown as circles in the figure, represent functions needed for system survival. Besides the trivial state of no stage failures, several success configurations exist. WLA is considered to function successfully following the loss of either outboard elevator function but not both, or the loss of the wheel position sensor data either separately or in combination with one outboard elevator failed.

Failure rates as input to the CARSRA program are assumed to be constant; i.e., not time varying. Actual time-to-failure data satisfies this assumption if the number of failures of a specific module type is exponentially distributed in time, Poisson distributed. This failure rate is the instantaneous failure rate due to hazards, rather than to "burn-in" or "wear-out" causes which are time dependent.

The failure rate data used in this analysis have been collected from several sources. The primary sources of failure information are the airlines' component installation and removal records. The records generally specify reason for removal and the mainten-

ance shop determination, from which the failure mode can be identified. Time to failure can be determined by noting the aircraft flight time when the component was installed, and the time when removed. These "raw" data are processed and are summarized in terms of unscheduled component removals per 1000 unit flight hours, and percentage of those removals that were justified. Another source is a previous reliability analysis (ref A-2). Still other sources are miscellaneous airline service reports and Customer Service records. Finally, for lack of any data at all, the reasonable guess or estimate based on similarity is used.

4.0 REFERENCES

- A-1 NASA CR-145024; "Airborne Advanced Reconfigurable Computer System (ARCS)"; Contract NAS1-13654; Aug. 1976.
- A-2 NASA CR-145271; "Flight Control Electronics Reliability Maintenance Study"; Contract NAS1-13654; Dec. 1977.

APPENDIX B
SUPPORTING DATA

CONTENTS

	Page
1.0 AERODYNAMICS	B-4
1.1 Pressure Data	B-4
1.2 Lampblack Flow Visualization Photographs	B-16
2.0 FLUTTER	B-19
3.0 LOADS	B-29

FIGURES

		Page
B-1	Winglet Z9 Pressures	B-4
B-2	Winglet Z9 Flow Visualization	B-5
B-3	Winglets Z4 and Z11 Pressures Near Root Section	B-6
B-4	Winglets Z4 and Z11 Pressures Near Tip Section.	B-7
B-5	Winglets Z4 and Z12 Pressures Near Root Section.	B-8
B-6	Winglets Z4 and Z12 Pressures Near Tip Section	B-9
B-7	Winglets Z9 and Z13 Pressures Near Root Section.	B-10
B-8	Winglets Z9 and Z13 Pressures Near Tip Section	B-11
B-9	Effect of Winglets and Wingtip Modification on Upper Surface Wing Pressure	B-12
B-10	Outboard Wing Pressures With Z11 Winglets Installed	B-13
B-11	Outboard Wing Pressures With Z12 Winglets Installed	B-14
B-12	Outboard Wing Pressures With Z13 Winglets Installed	B-15
B-13	Winglet Z10 With Wing Mod Flow Visualization	B-16
B-14	Winglet Z10 Flow Visualization.	B-17
B-15	Winglet Z11 Flow Visualization	B-17
B-16	Winglet Z12 Flow Visualization.	B-18
B-17	Winglet Z13 Flow Visualization.	B-18
B-18	Velocity-Damping Results Without Static Effects on Winglets	B-19
B-19	Velocity-Damping Results With Static Effects on Winglets. . .	B-20
B-20	Velocity-Damping Results With Improved Methodology	B-21
B-21	Velocity-Frequency Results With Improved Methodology. . . .	B-22
B-22	Velocity-Damping Results for Z13 Winglet Symmetric Analysis	B-23
B-23	Velocity-Frequency Results for Z13 Winglet Symmetric Analysis	B-24
B-24	Velocity-Damping Results for Z13 Winglet Antisymmetric Analysis	B-25
B-25	Velocity-Frequency Results for Z13 Winglet Antisymmetric Analysis	B-26
B-26	Critical Still-Air Mode Shape for Z13 Symmetric Flutter Mode	B-27

	Page	
B-27	Critical Still-Air Mode Shape for Z13 Wing Tip Flutter Mode	B-27
B-28	Flutter Torsional Stiffness Requirements for Wing with Z13 Winglet	B-28
B-29	Effect of WTW and WTE on Wing Lift Distribution	B-29
B-30	Z9 WTW Force Coefficients Based on Integrated Pressures (C_n , C_m , C_T)	B-30
B-31	Z9 WTW Force Coefficients Based on Integrated Pressures (C_n and C_m)	B-31
B-32	Effect of WTW and WTE on Aileron Effectiveness	B-32

APPENDIX B—SUPPORTING DATA

1.0 AERODYNAMICS

1.1 PRESSURE DATA

Figure B-1 shows the pressure distribution on winglet Z9 at three spanwise stations at $C_L = 0.45$, $M = 0.84$. The lowest station has a peak local Mach number (normal to quarter-chord span line) approaching a value of 1.3. A shock wave was in evidence on the inboard surface during a lampblack flow visualization run (fig. B-2) which corresponds to the pressure distribution of Figure B-1. The midspan pressure stations on the left and right hand winglets were used for on-line verification of the winglet incidence angle to avoid any flow asymmetry problems.

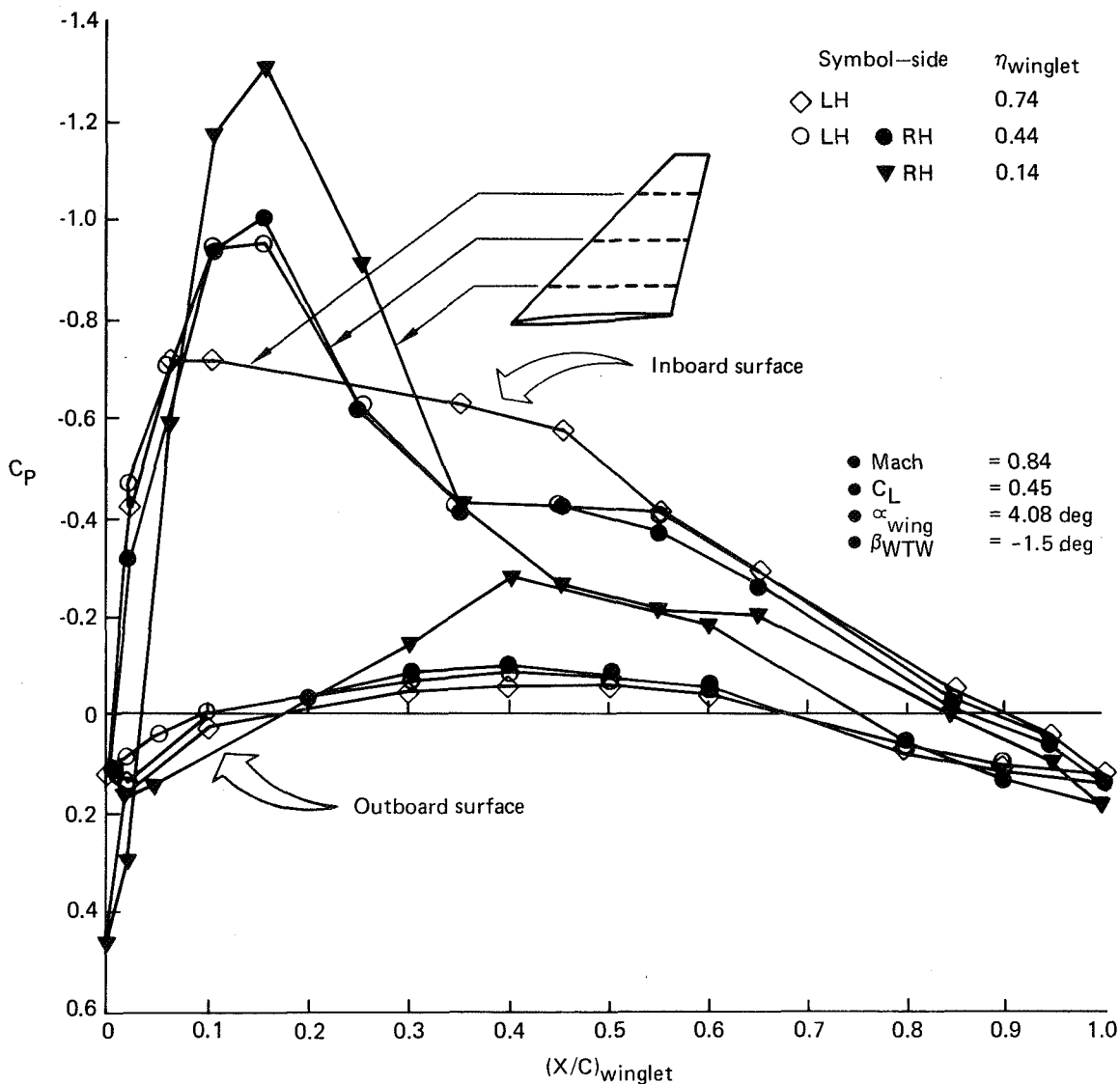
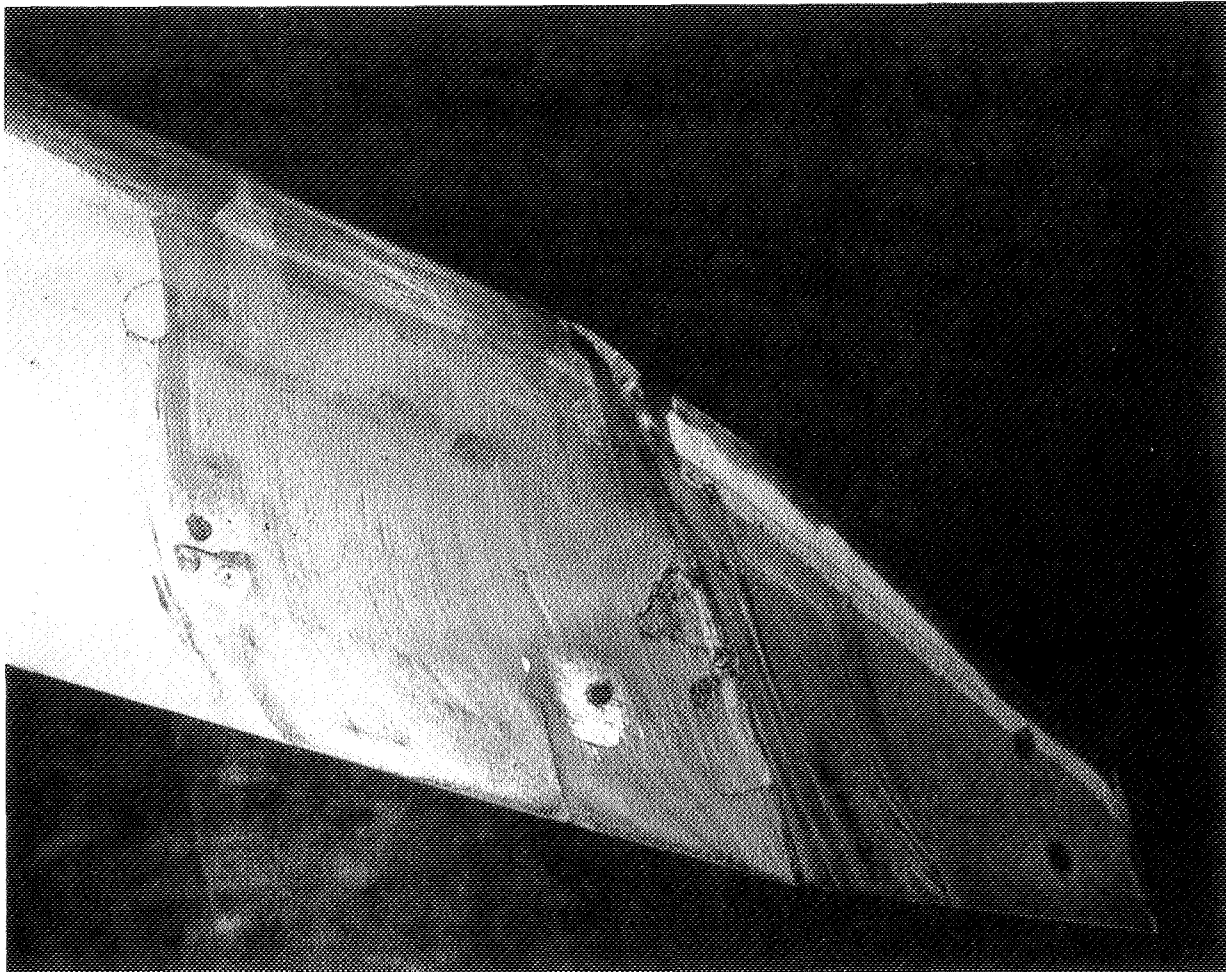


Figure B-1. Winglet Z9 Pressures



● Lampblack oil flow at mach = 0.84, $C_L = 0.45$ ● BTWT 1599 ● $\beta_{WTW} = -1.5$ deg ● Wing upper surface

Figure B-2. Winglet Z9 Flow Visualization

Figures B-3, B-4, B-5, and B-6 compare experimental pressure distributions for a previous study winglet (Z4) to theoretical pressure distributions for Z4, Z11, and Z12 winglets at a root and a tip span station. The important differences between winglet Z4 and winglets Z11 and Z12 are the much lower leading-edge velocities and increased aft loading found on Z11 and Z12. Figures B-7 and B-8 compare experimental pressure distributions for winglet Z9 with theoretical pressure distributions for Z9 and winglet Z13 at a root and a tip span station, respectively. The Z13 winglet has lower leading-edge velocities and more aft loading than Z9. This is similar to the comparison between winglet Z4 and winglets Z11 and Z12, but the shape of the pressure distribution for winglet Z13 is distinctly different from that of winglets Z11 and Z12.

Figure B-9 shows the effect of winglets Z9, Z10, and wing tip modification on the outboard wing upper surface pressure distribution at near cruise conditions. The Z9 winglet produced a substantial shock at approximately 50% chord. A wing tip airfoil modification was designed in an attempt to relieve the shock. At the same time, some of the camber of the root section of the winglet was removed by filling in the inboard contours (Z10). The combination succeeded in moving the peak velocity well forward, but any drag gains were limited due to a leading-edge shock (at approximately 10% chord) and a midchord velocity level that was still excessively high. When winglet Z10 was tested without the wing tip modification, only a slight improvement over the Z9 pressure distribution was noted.

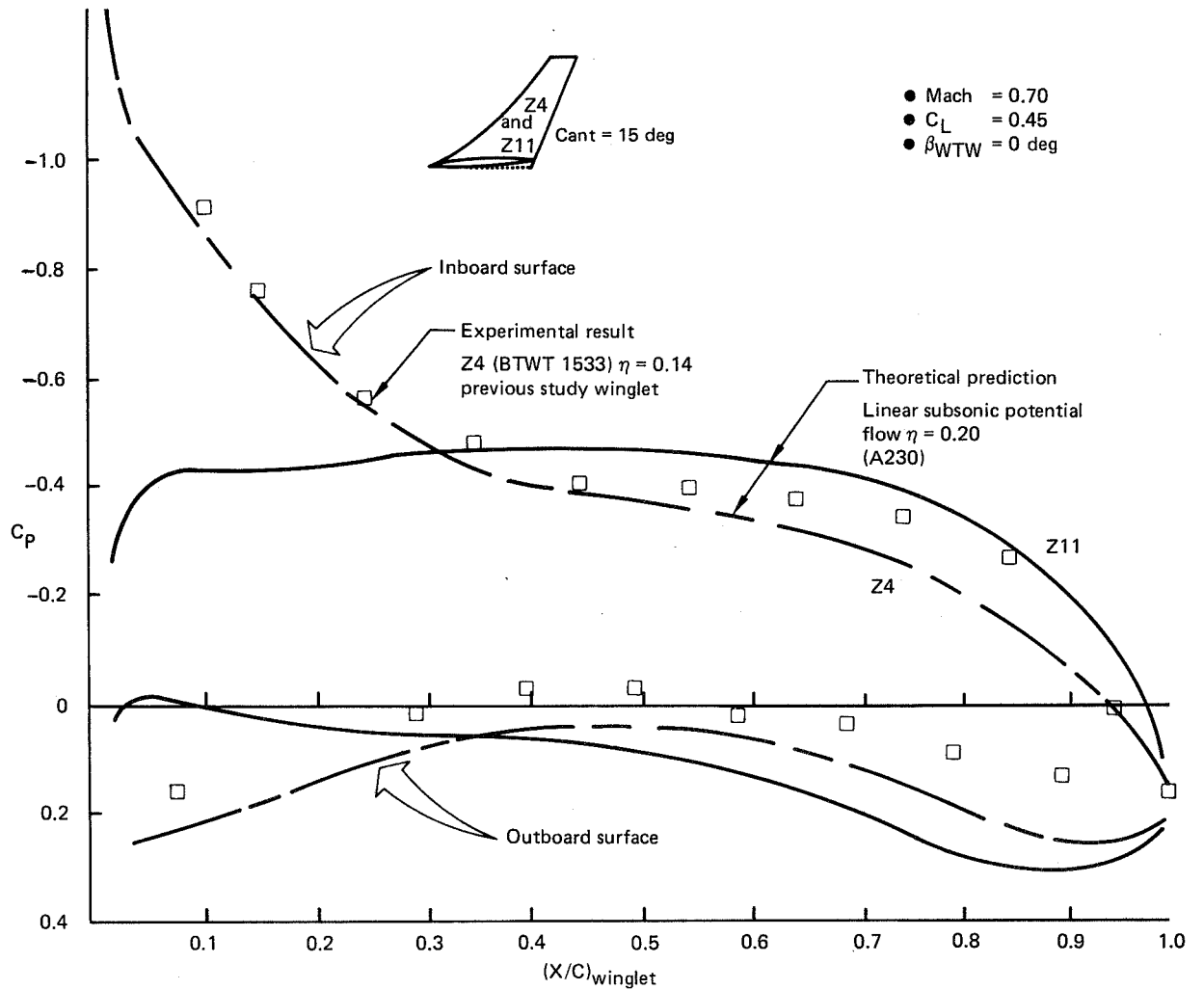


Figure B-3. Winglets Z4 and Z11 Pressures Near Root Section

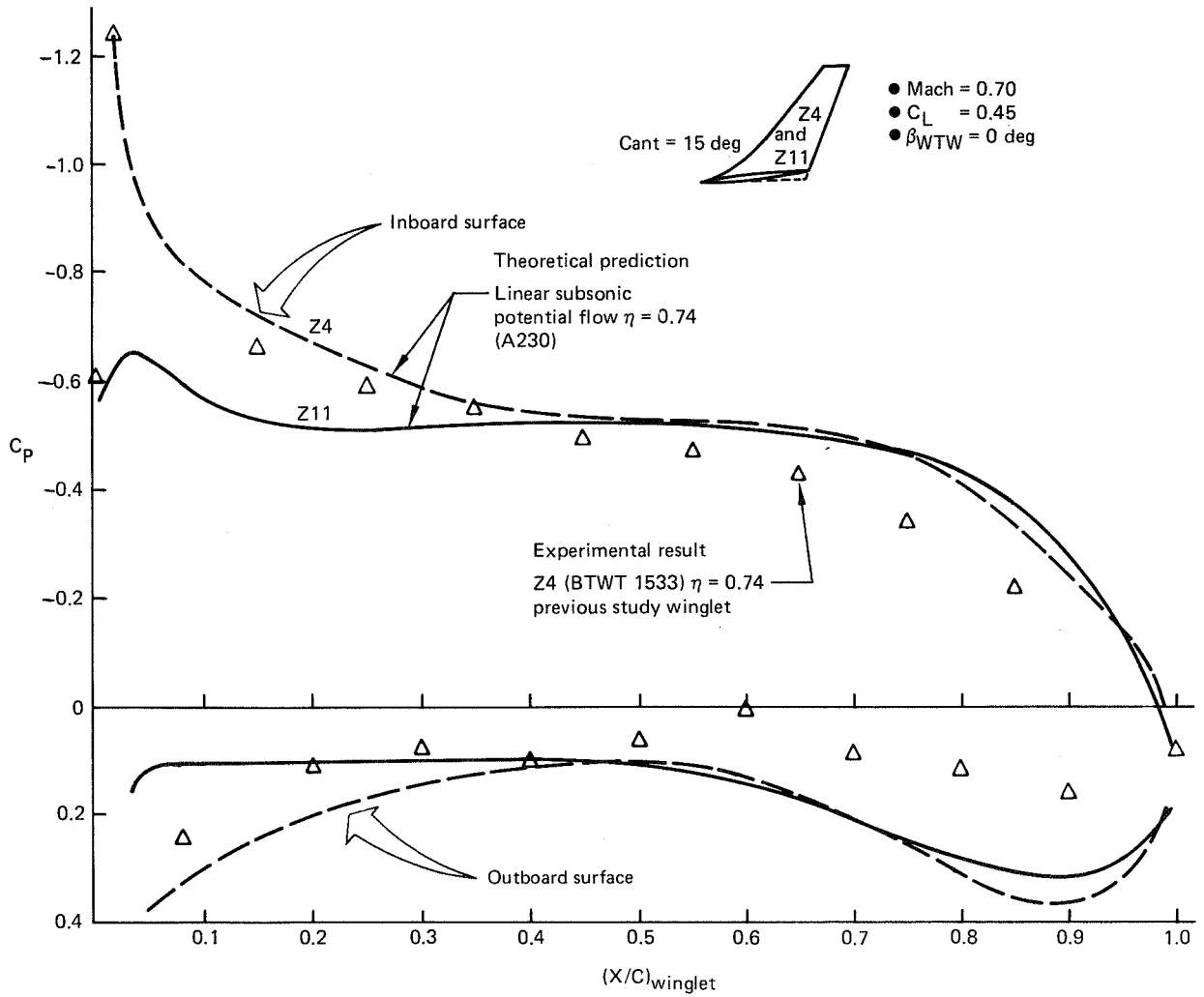


Figure B-4. Winglets Z4 and Z11 Pressures Near Tip Section

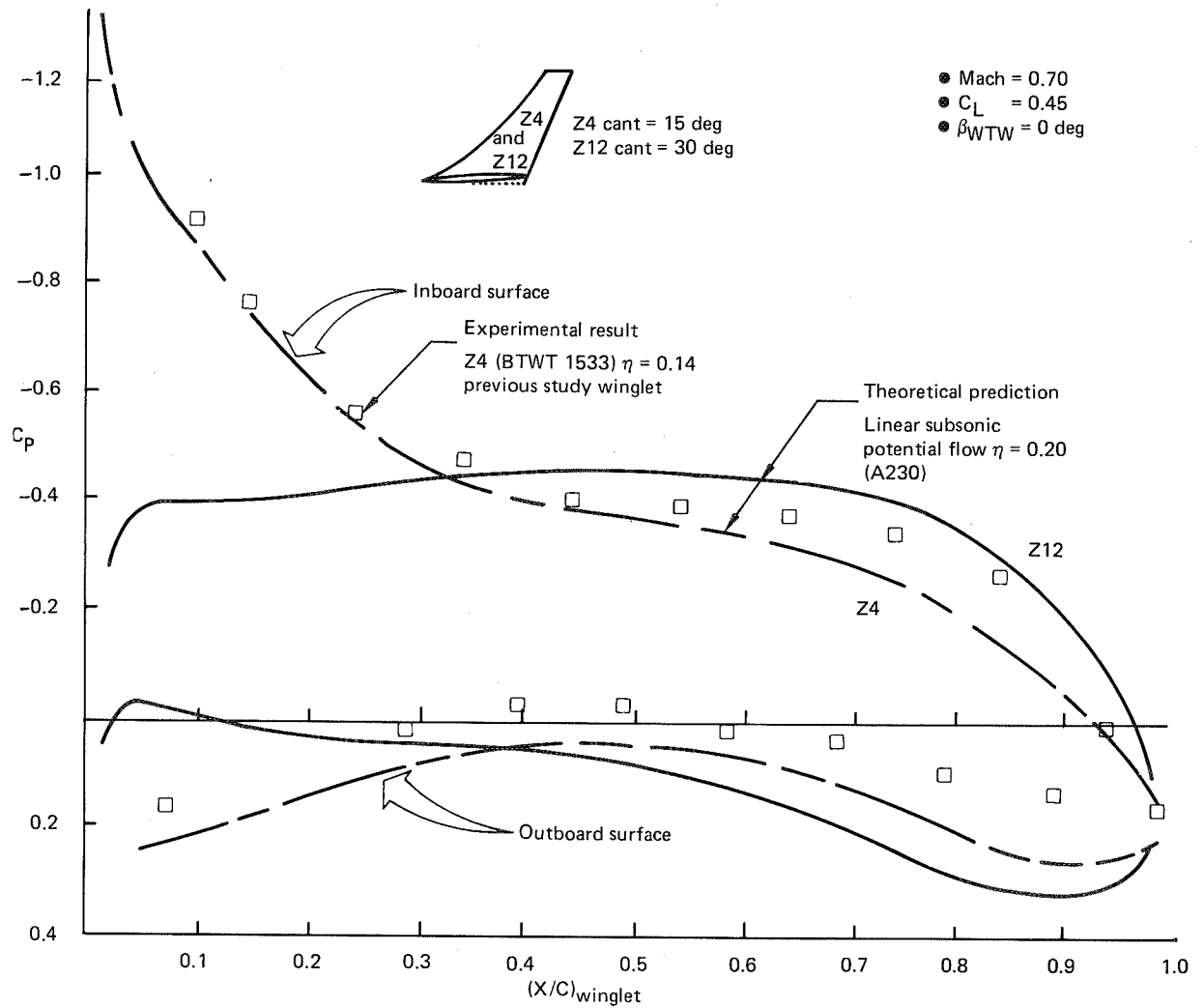


Figure B-5. Winglets Z4 and Z12 Pressures Near Root Section

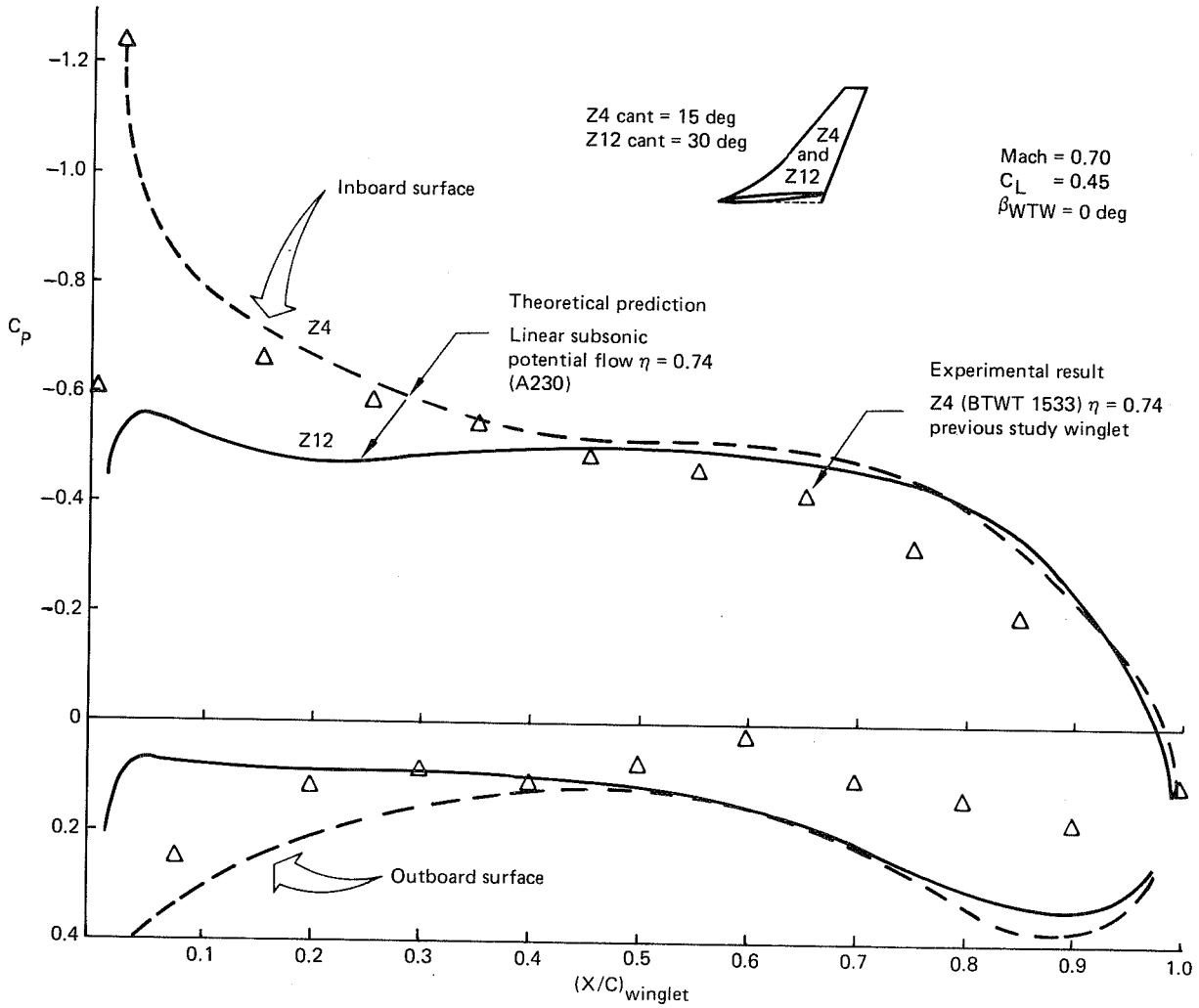


Figure B-6. Winglets Z4 and Z12 Pressures Near Tip Section

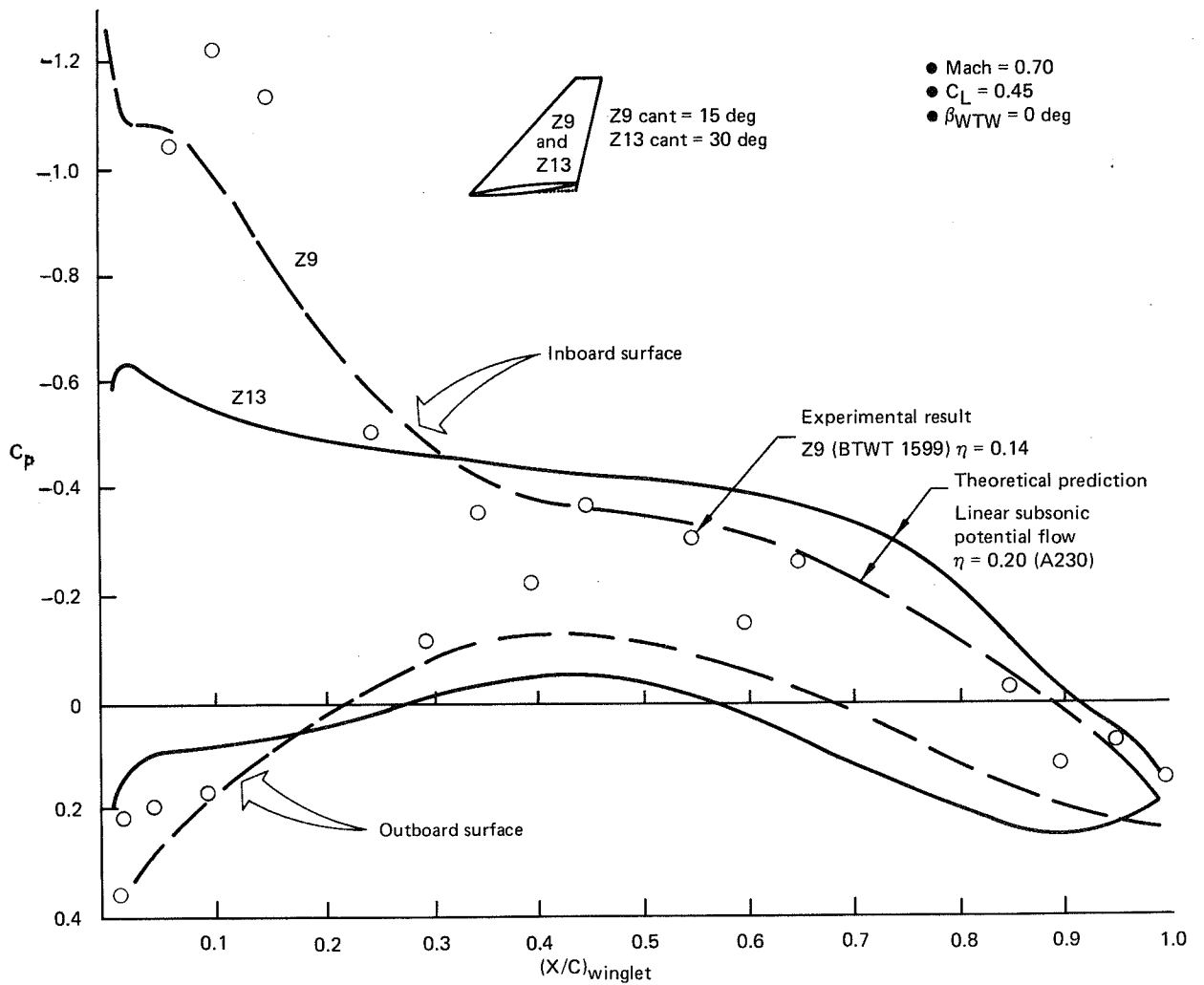


Figure B-7. Winglets Z9 and Z13 Pressures Near Root Section

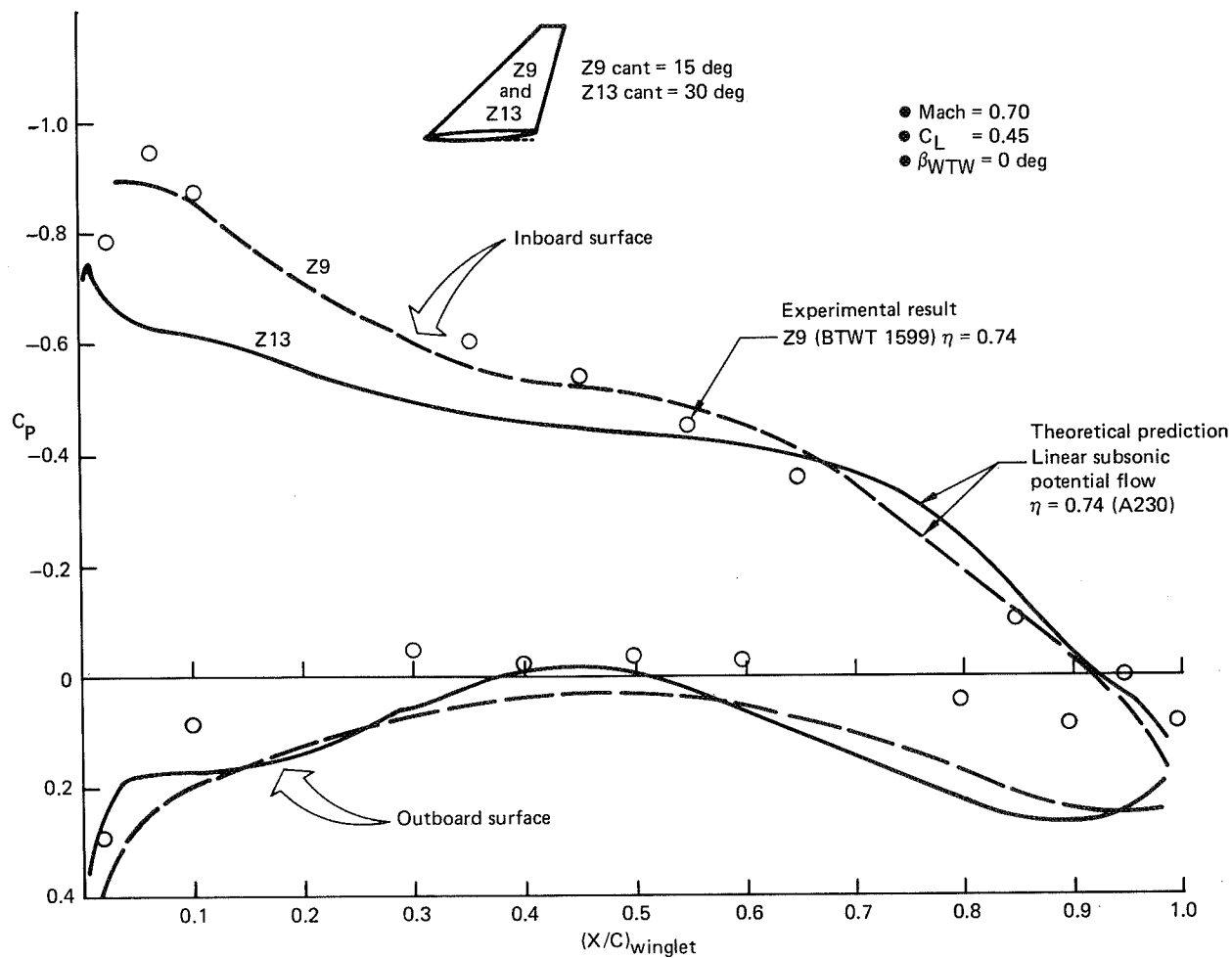


Figure B-8. Winglets Z9 and Z13 Pressures Near Tip Section

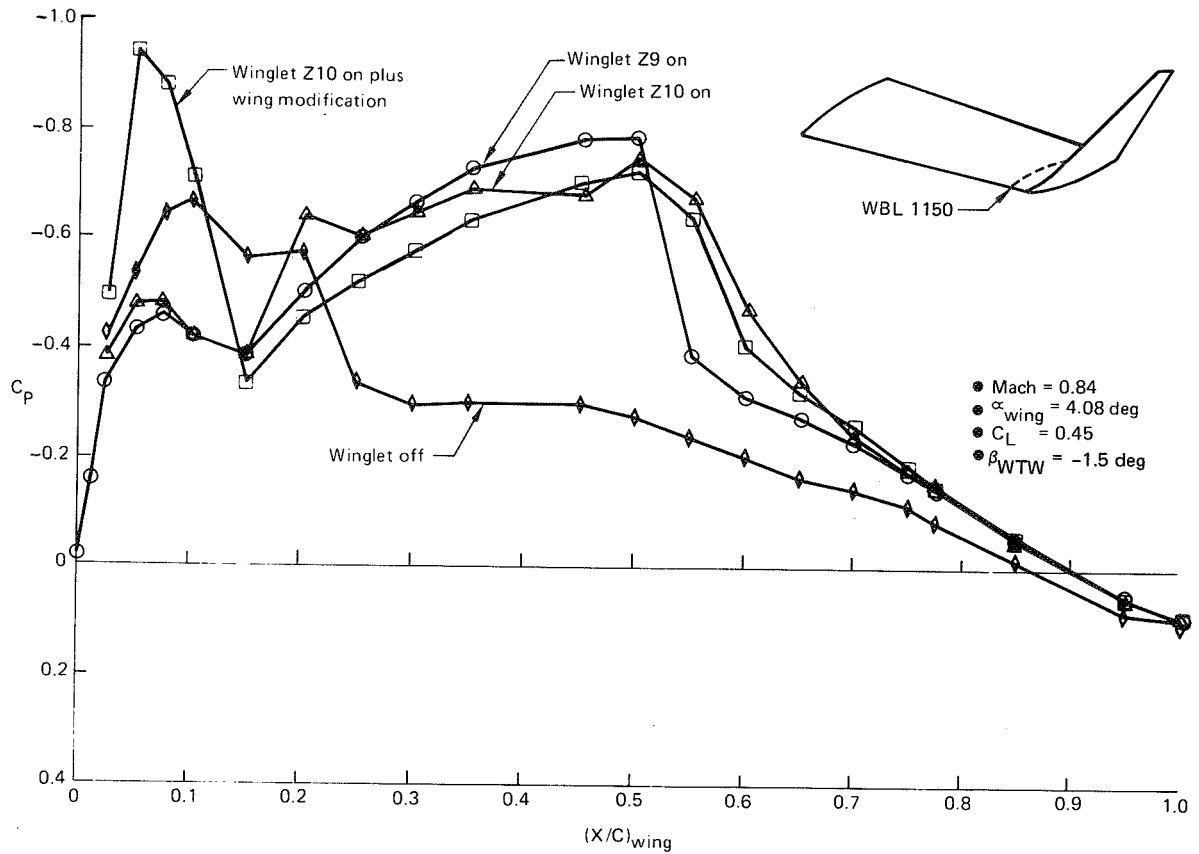


Figure B-9. Effect of Winglets and Wing Tip Modification on Upper Surface Wing Pressure

Figures B-10, B-11, and B-12 show, for $M = 0.7$, the experimental and theoretical effects on wing tip pressure distribution of winglets Z11, Z12, and Z13, respectively. The additional experimental distribution at $M = 0.84$ shows no evidence of strong shocks or excessive winglet interference.

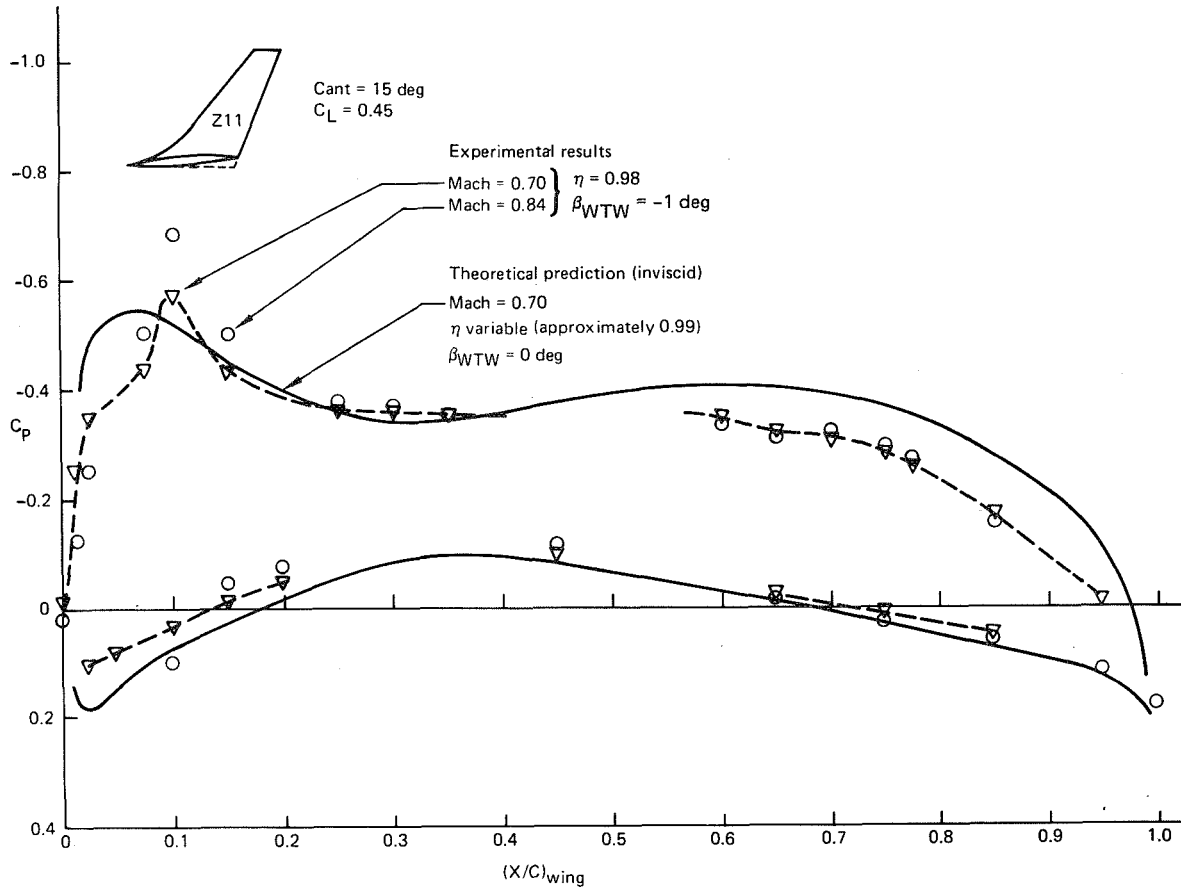


Figure B-10. Outboard Wing Pressures With Z11 Winglets Installed

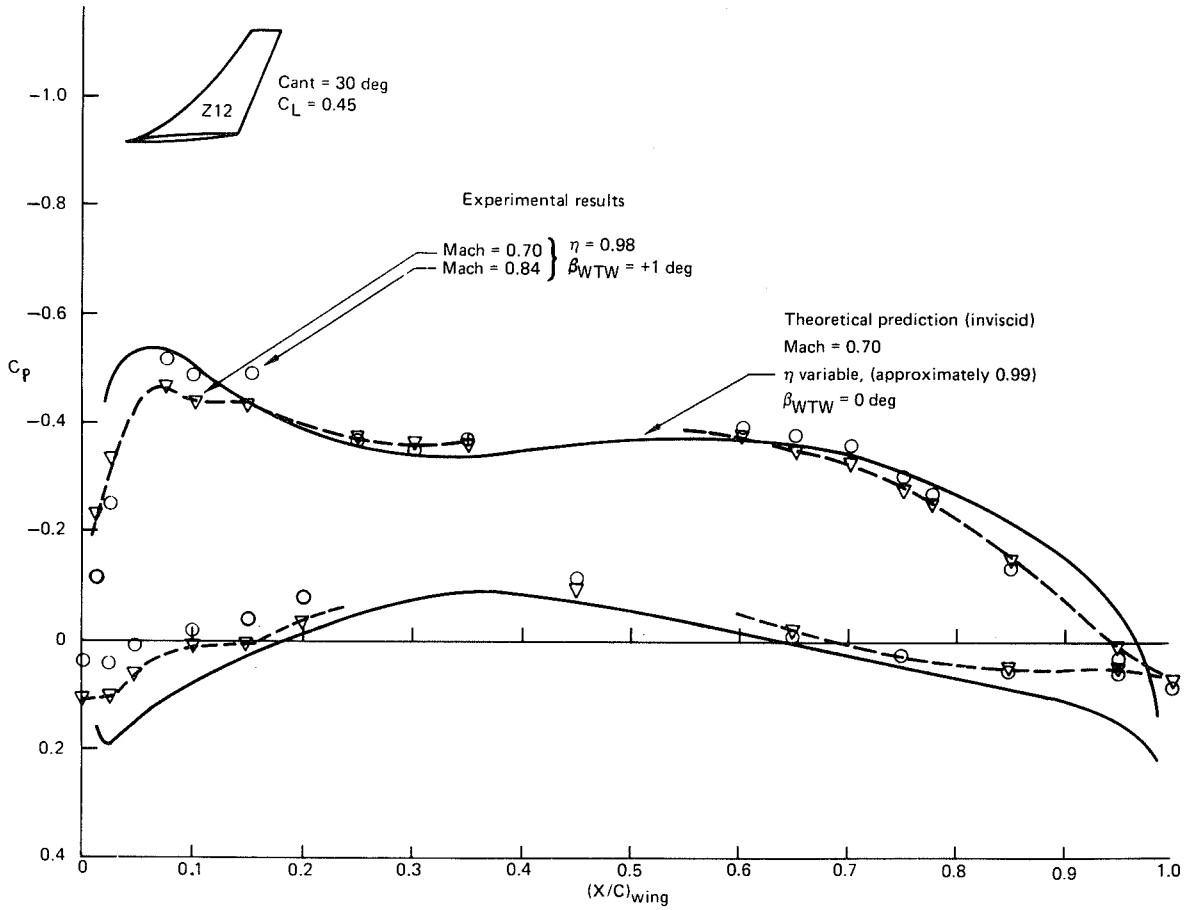


Figure B-11. Outboard Wing Pressures With Z12 Winglets Installed

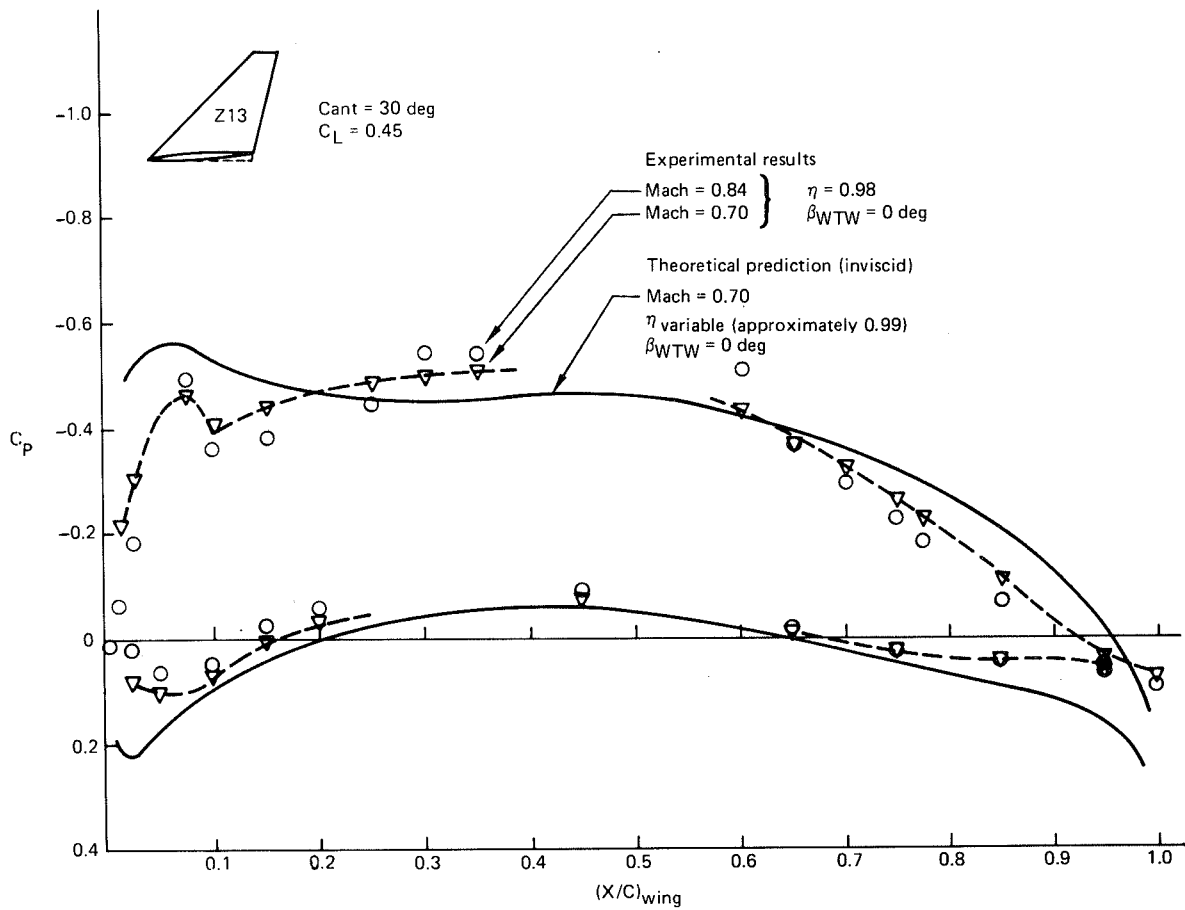
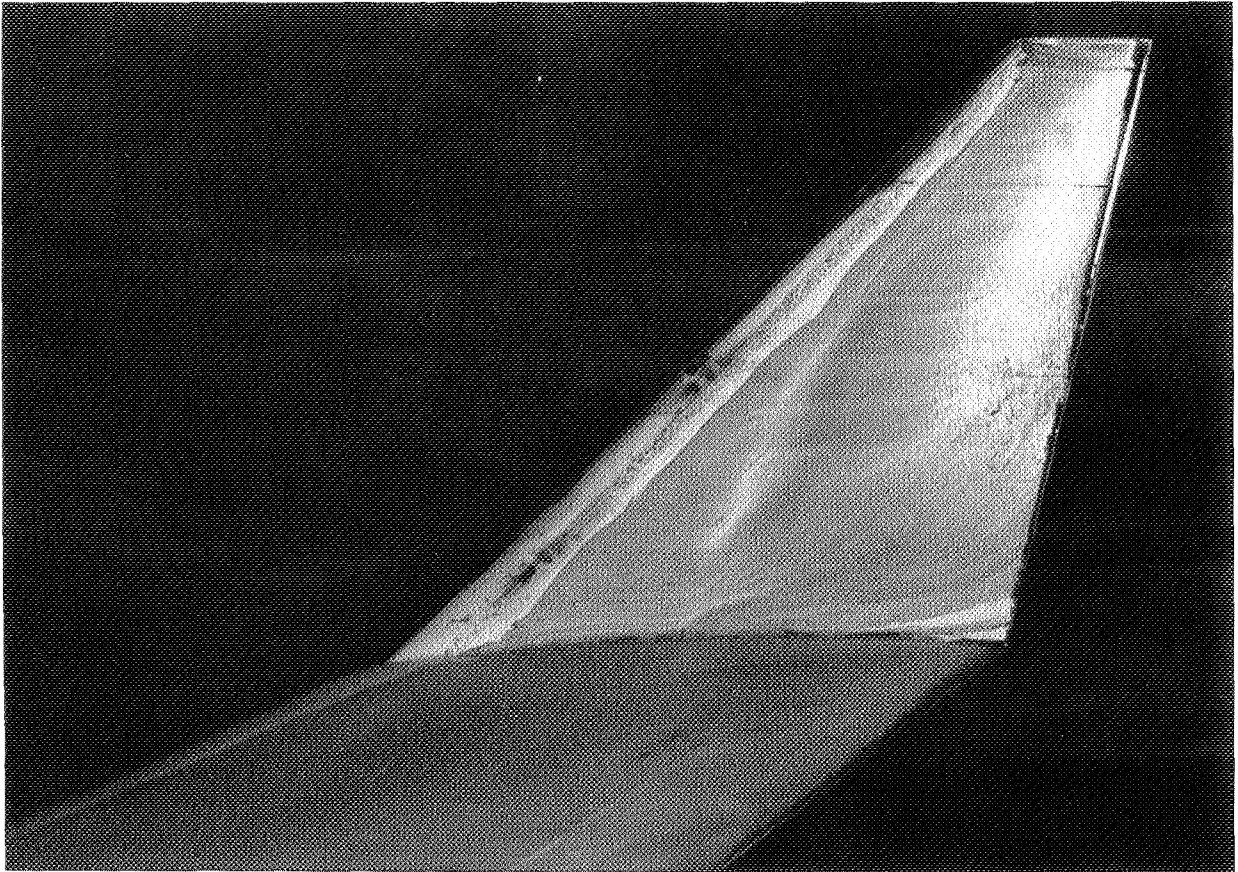


Figure B-12. Outboard Wing Pressures With Z13 Winglets Installed

1.2 LAMPBLACK FLOW VISUALIZATION PHOTOGRAPHS

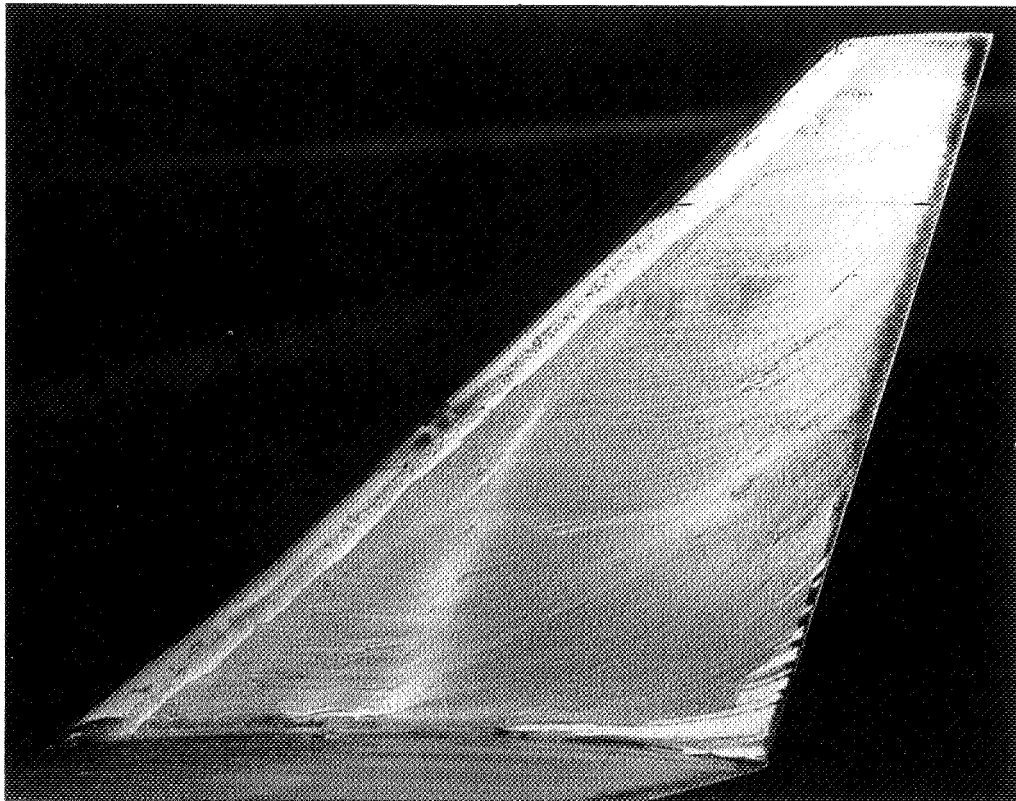
Figure B-2 shows the wing tip and winglet Z9 flow for incidence angle = -1.5 deg. The winglet Z9 shock wave indicated by the pressure distribution shown in Figure B-1 is visible in the flow photograph. Figure B-13 shows the flow on the wing tip and winglet Z10 with the wing tip modification and Figure B-14 shows the flow without the wing tip modification. The flow quality for winglet Z10 (with or without the wing tip modification) is generally improved relative to winglet Z9, but the winglet shock wave is still present.

Figure B-15 shows the flow on winglet Z11. Inboard surface flow on winglet Z11 shows some trailing-edge separation in the last several percent chord over most of the span. Winglet Z12 has more extensive separation on the inboard surface (fig. B-16). It is apparent that these two winglets incorporated too much aft camber. Figure B-17 shows the flow on winglet Z13 with no appreciable trailing-edge separation.



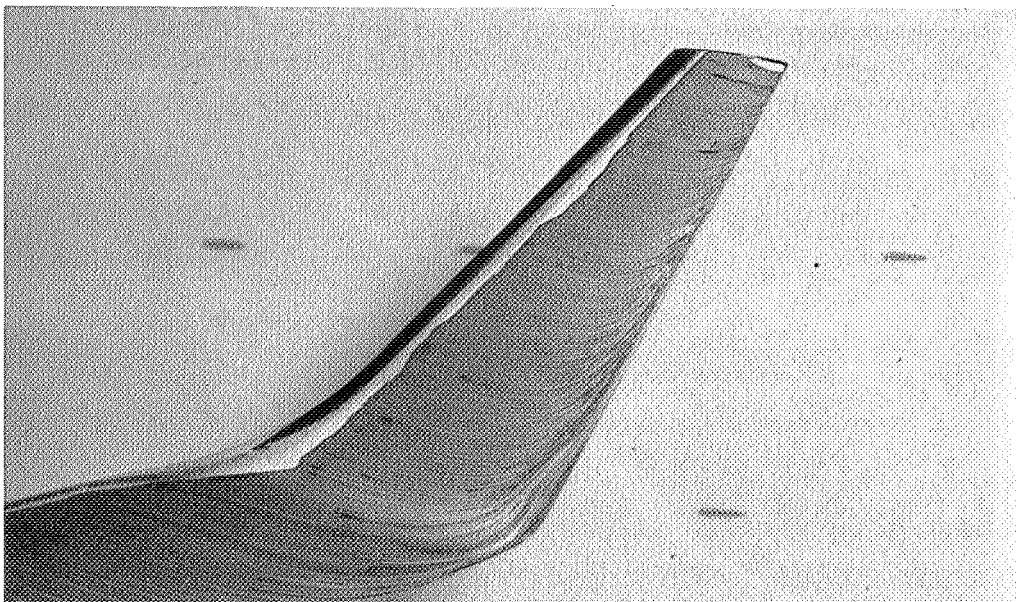
● Lampblack oil flow at Mach = 0.84, $C_L = 0.45$ ● BTWT 1602 ● $\beta_{WTW} = -1.5$ deg ● Wing upper surface

Figure B-13. Winglet Z10 With Wing Mod Flow Visualization



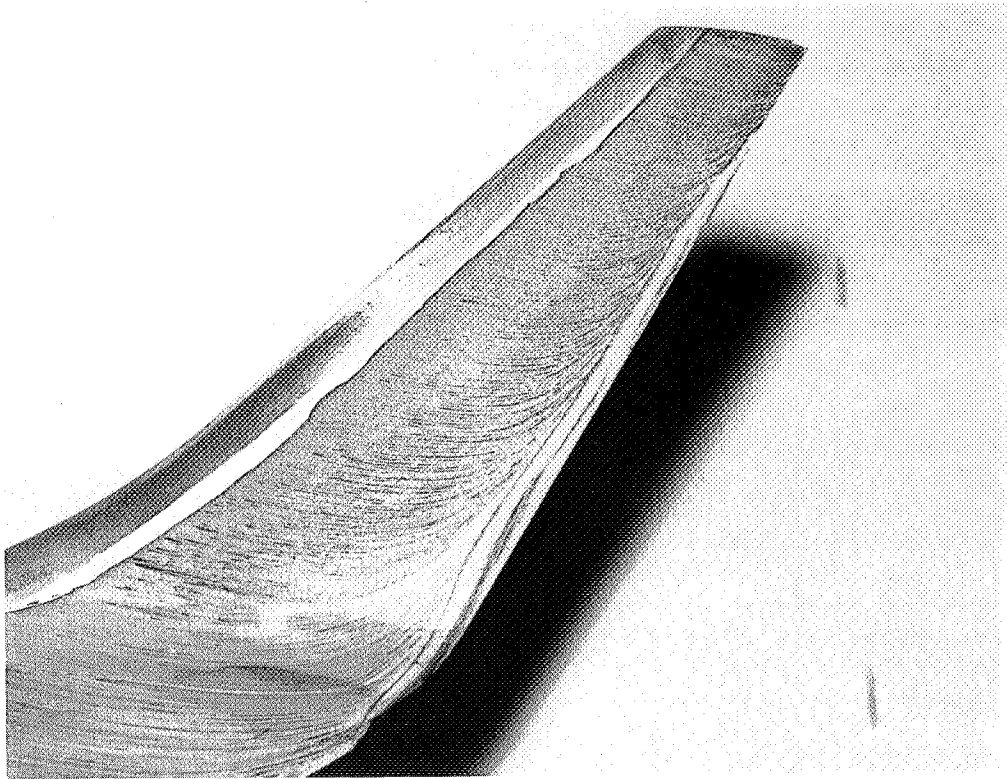
• Lampblack oil flow at Mach = 0.84, $C_L = 0.45$ • BTWT 1602 • $\beta_{WTW} = -1.5$ deg • Inboard surface

Figure B-14. Winglet Z10 Flow Visualization



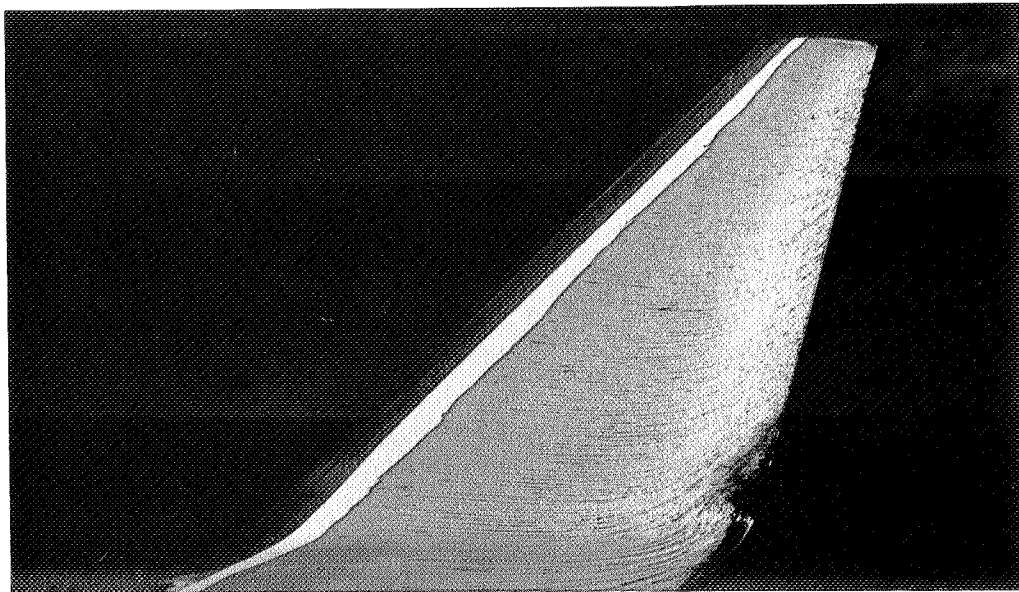
• Lampblack oil flow at Mach = 0.84 • BTWT 1642 • $\beta_{WTW} = -1.0$ deg • Inboard side

Figure B-15. Winglet Z11 Flow Visualization



• Lampblack oil flow at Mach = 0.84 • BTWT 1642 • $\beta_{WTW} = +1.0$ deg • Inboard side

Figure B-16. Winglet Z12 Flow Visualization



• Lampblack oil flow at Mach = 0.84 • BTWT 1642 • $\beta_{WTW} = 0$ deg • Inboard side

Figure B-17. Winglet Z13 Flow Visualization

2.0 FLUTTER

Selected flutter analysis results are presented in this appendix to provide additional visibility of the characteristics of the wing tip winglet flutter modes. Supplemental data is in the form of velocity-damping (V-g) plots and velocity-frequency (V-f) plots showing the trends with air speed for critical modes in the solution. The $g = 0$ crossing represents the point at which the total damping in the mode is equal to its inherent structural damping. For reference purposes assumed structural dampings, based upon experience, associated with flutter boundaries in the main text are as follows:

- Antisymmetric ONSB mode $g = 0.030$
- Antisymmetric BASIC mode $g = 0.025$
- Symmetric mode $g = 0.015$
- Wing tip flutter mode $g = 0.010$

Figures B-18 and B-19 show the V-g comparisons for the Z9 preliminary methodology results without and with the static effects on the winglets as defined in Figure A-9 of Appendix A. The critical mode for the symmetric flutter (Mode 5) does not go unstable unless the static effects are included. Figures B-20 through B-25 show

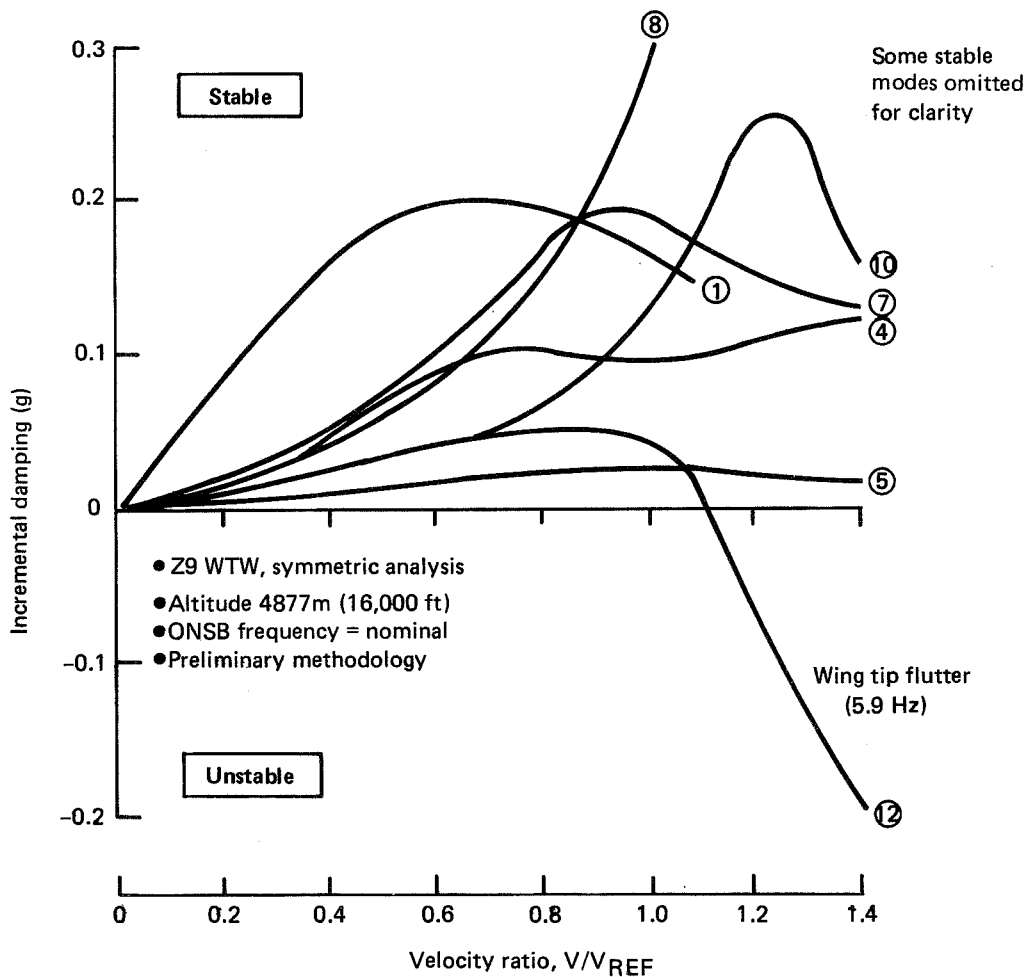


Figure B-18. Velocity-Damping Results Without Static Effects on Winglets

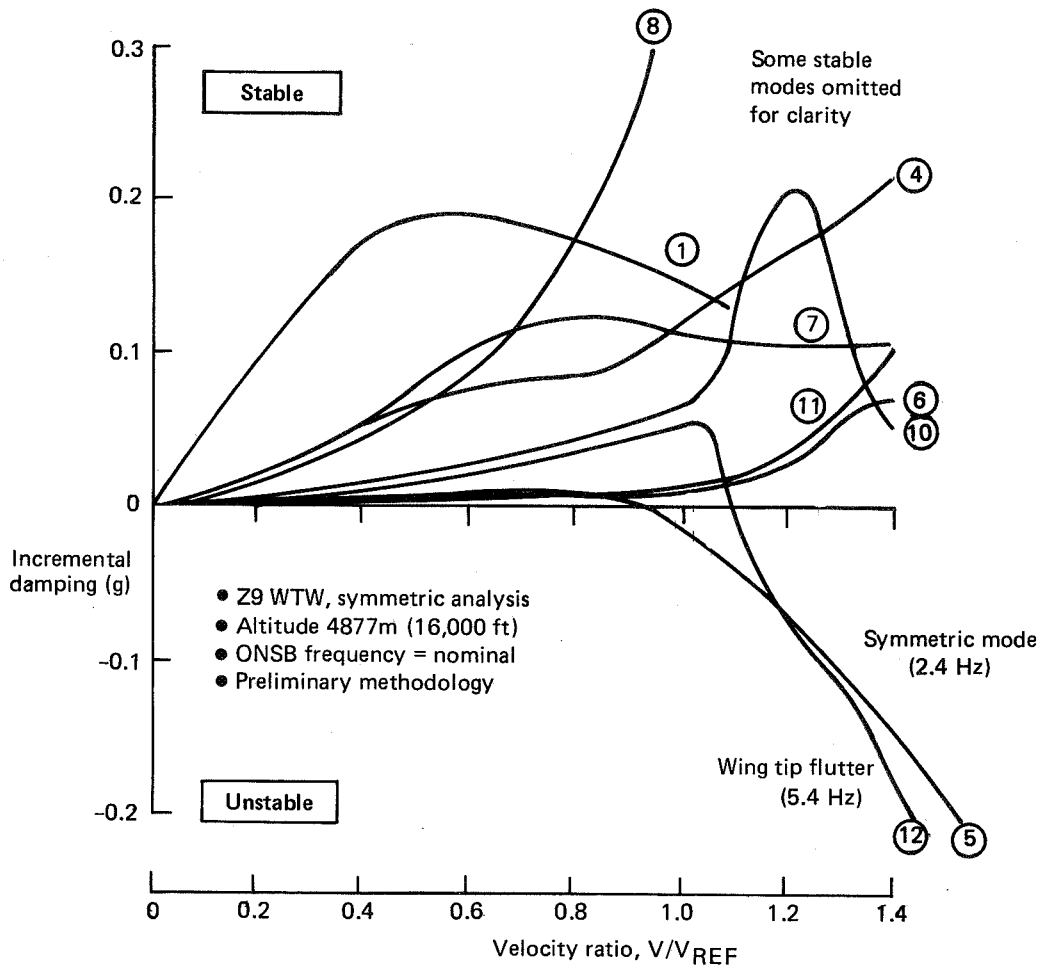


Figure B-19. Velocity-Damping Results With Static Effects on Winglets

corresponding pairs of V-g and V-f plots for solutions using the improved methodology with the static effects on the winglets. Figures B-20 and B-21 show the Z9 WTW results. A comparison of methodologies can be seen for the Z9 winglet by looking at Figures B-19 and B-20. Note that two wing tip flutter modes (Mode 10 and Mode 12) appear with the improved methodology and the "bucket" type flutter (Mode 12) is the lower speed mode. In both cases the 12th flexible mode decreases rapidly in frequency with air speed and eventually goes unstable as a wing tip flutter. Figures B-22 and B-25 show final Z13 results for the symmetric and antisymmetric solutions. The wing tip flutter corresponding to experimental results observed in the CVAL wind tunnel test is the 5.6 Hz wing tip flutter (12th flexible mode) in the symmetric solution. Antisymmetric flutter modes were not observed experimentally at the nominal outboard nacelle strut side bending frequency.

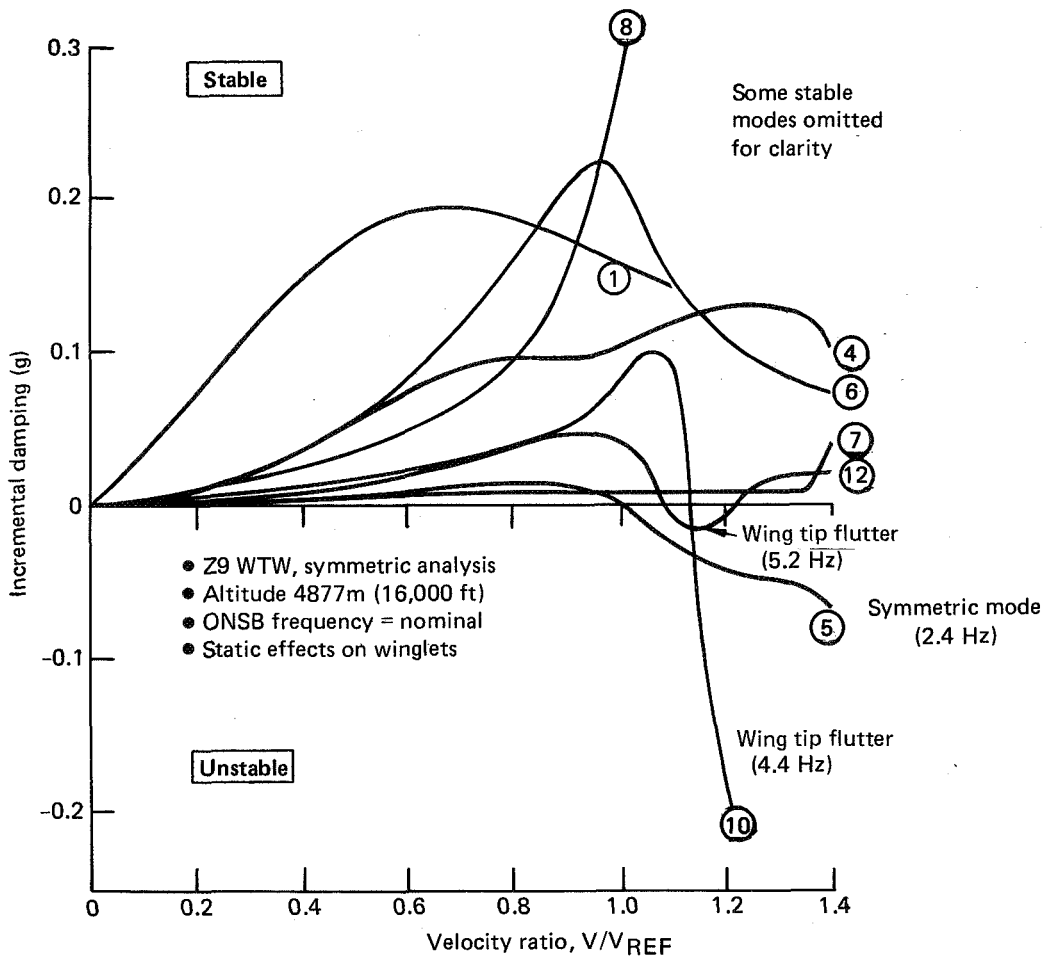


Figure B-20. Velocity-Damping Results With Improved Methodology

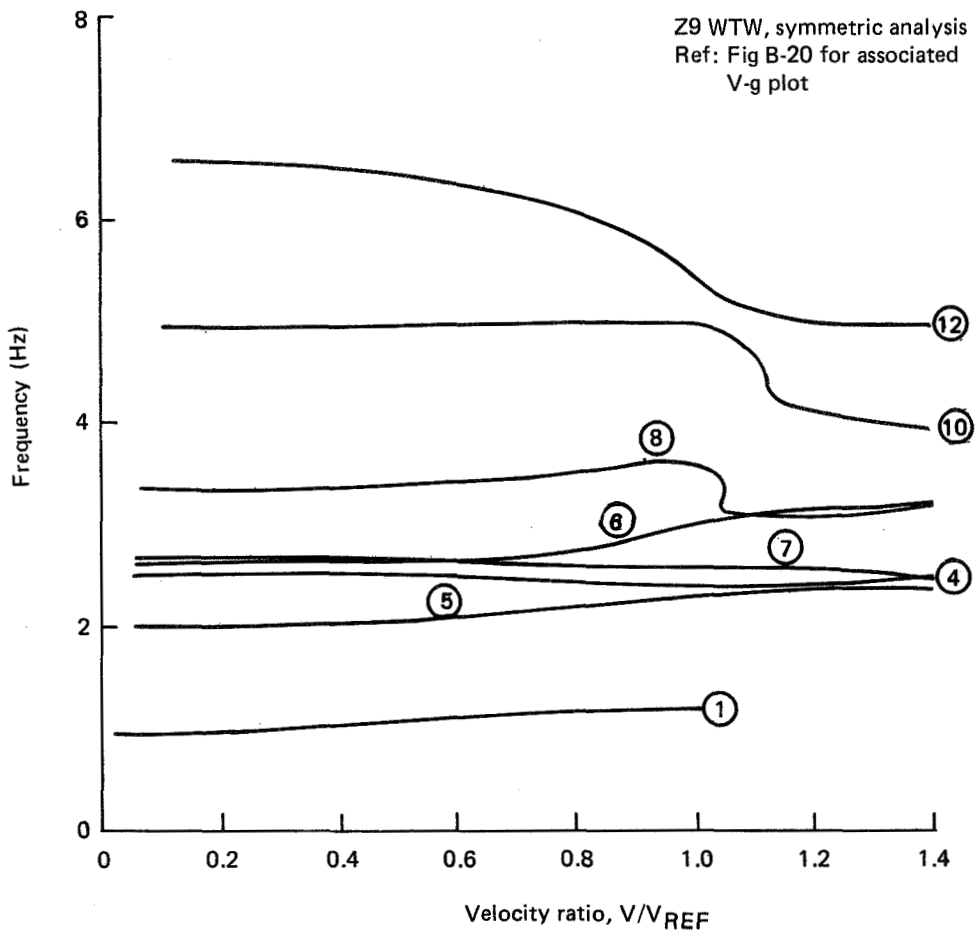


Figure B-21. Velocity-Frequency Results With Improved Methodology

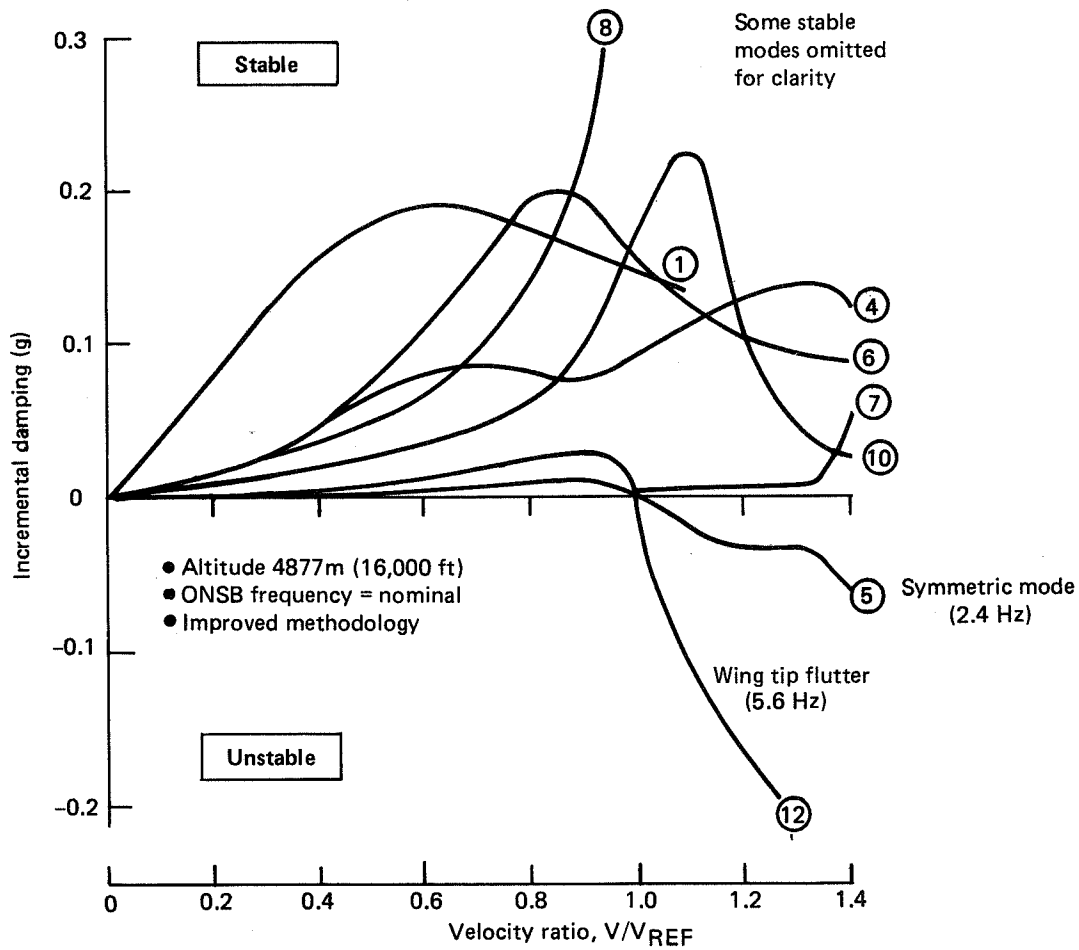


Figure B-22. Velocity-Damping Results for Z13 Winglet Symmetric Analysis

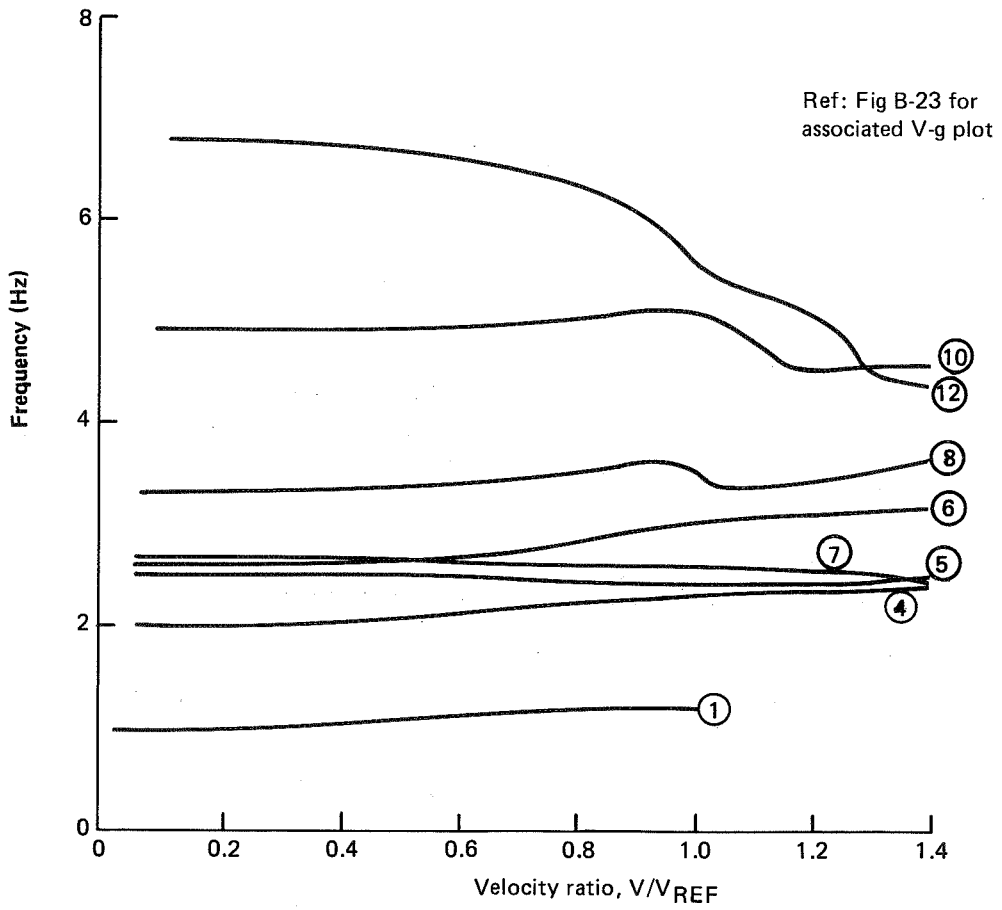


Figure B-23. Velocity-Frequency Results for Z13 Winglet Symmetric Analysis

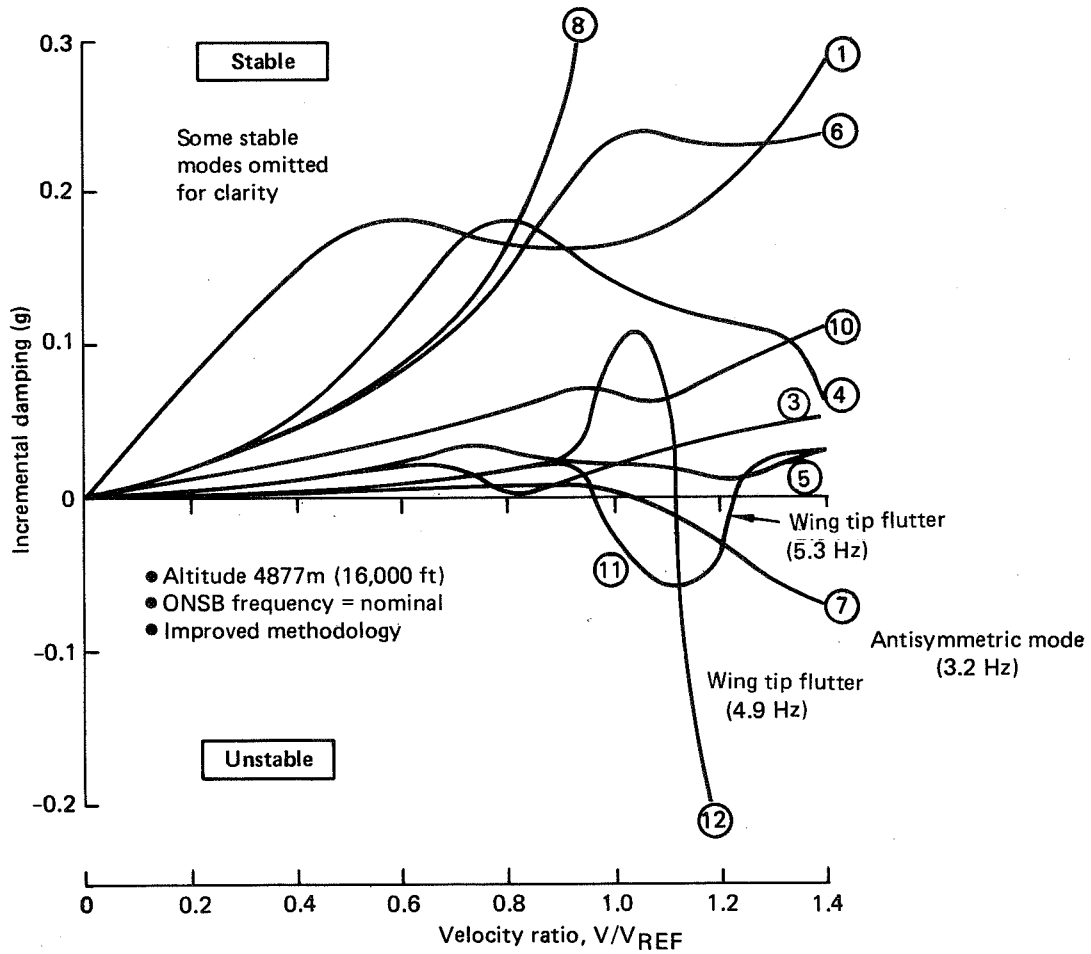


Figure B-24. Velocity-Damping Results for Z13 Winglet Antisymmetric Analysis

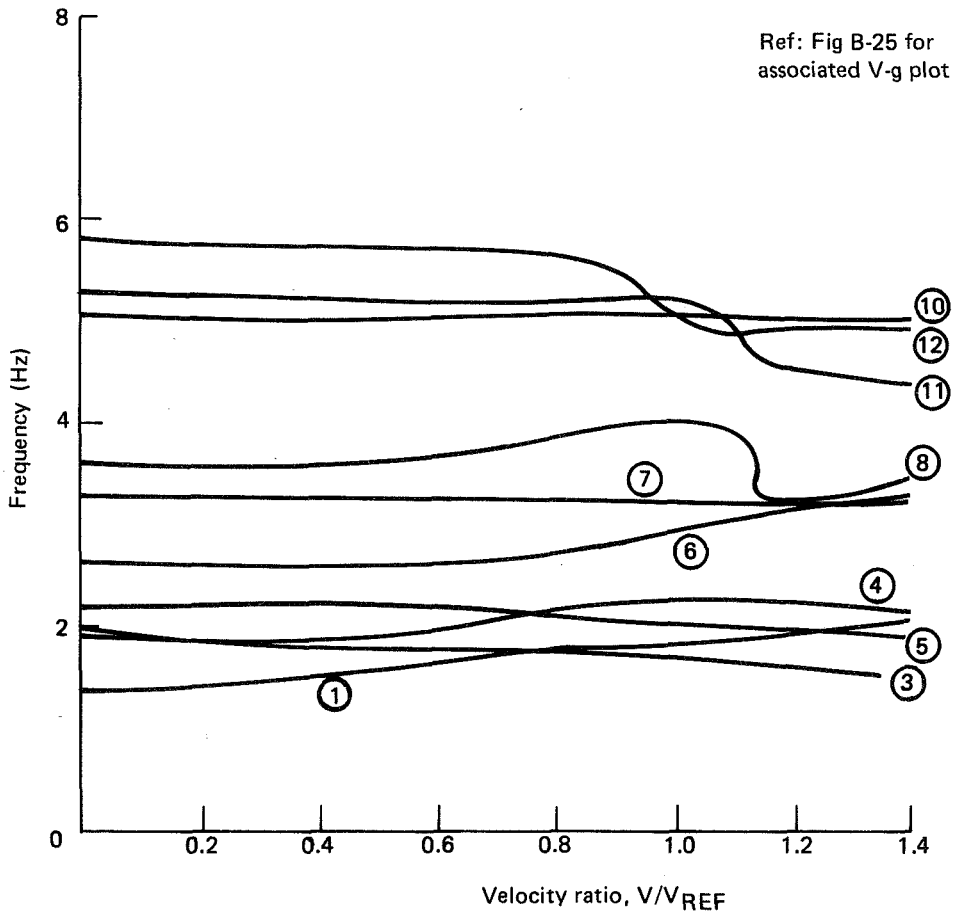


Figure B-25. Velocity-Frequency Results for Z13 Winglet Antisymmetric Analysis

Figures B-26 and B-27 show the symmetric still air modes that develop into the symmetric and tip flutter modes. The structural model presented is designed for the MLC closed loop analysis and shows the fuselage, nacelles, wing elastic axis, and control surface hinge line deflections. The large amount of wing tip twist in the wing tip flutter mode may be noted by the opposite deflections at the aileron hinge line and the wing elastic axis.

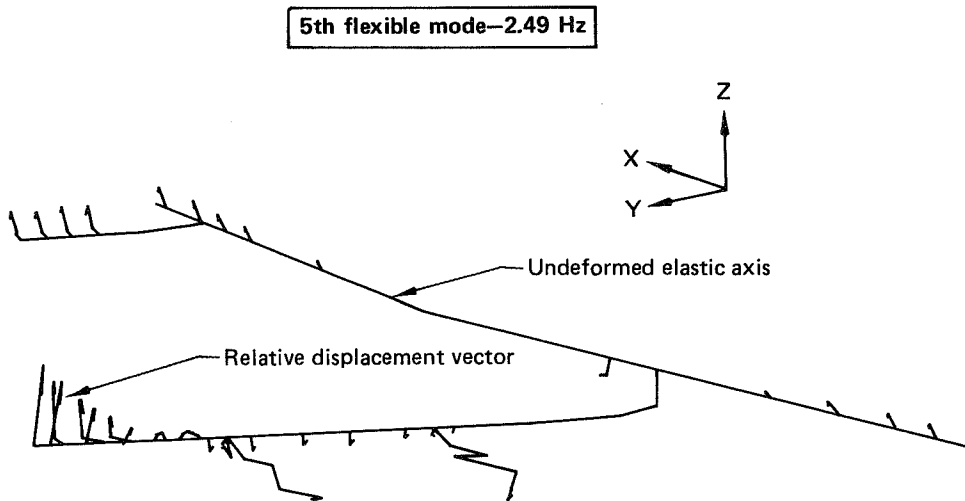


Figure B-26. Critical Still-Air Mode Shape for Z13 Symmetric Flutter Mode

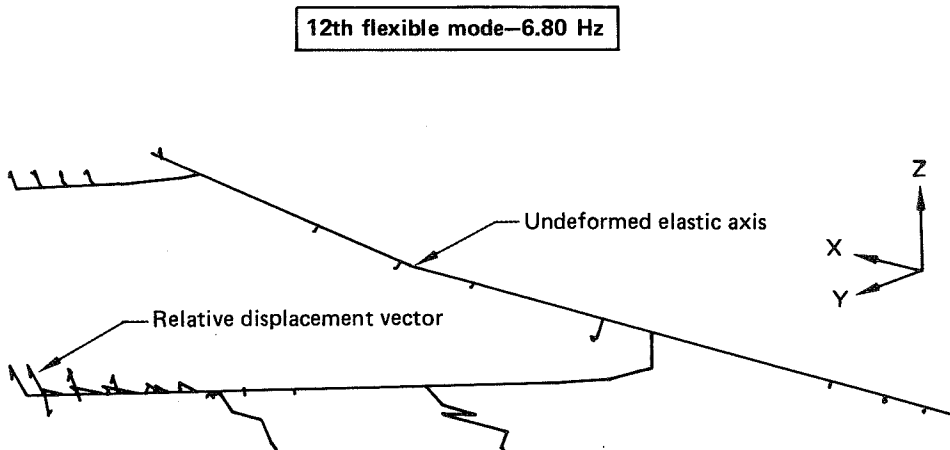


Figure B-27. Critical Still-Air Mode Shape for Z13 Wing Tip Flutter Mode

Figure B-28 wing illustrates the type of wing torsional (GJ) stiffness increases that were required to clear 1.2 V_D flutter margins with the Z13 winglet configuration. On a pure structural approach, one can note that there is excess margin for wing tip flutter when the requirements for the symmetric mode are met. These data were used as first cut guidelines and generally required reiteration with the increased bending stiffness and mass increments associated with GJ requirements.

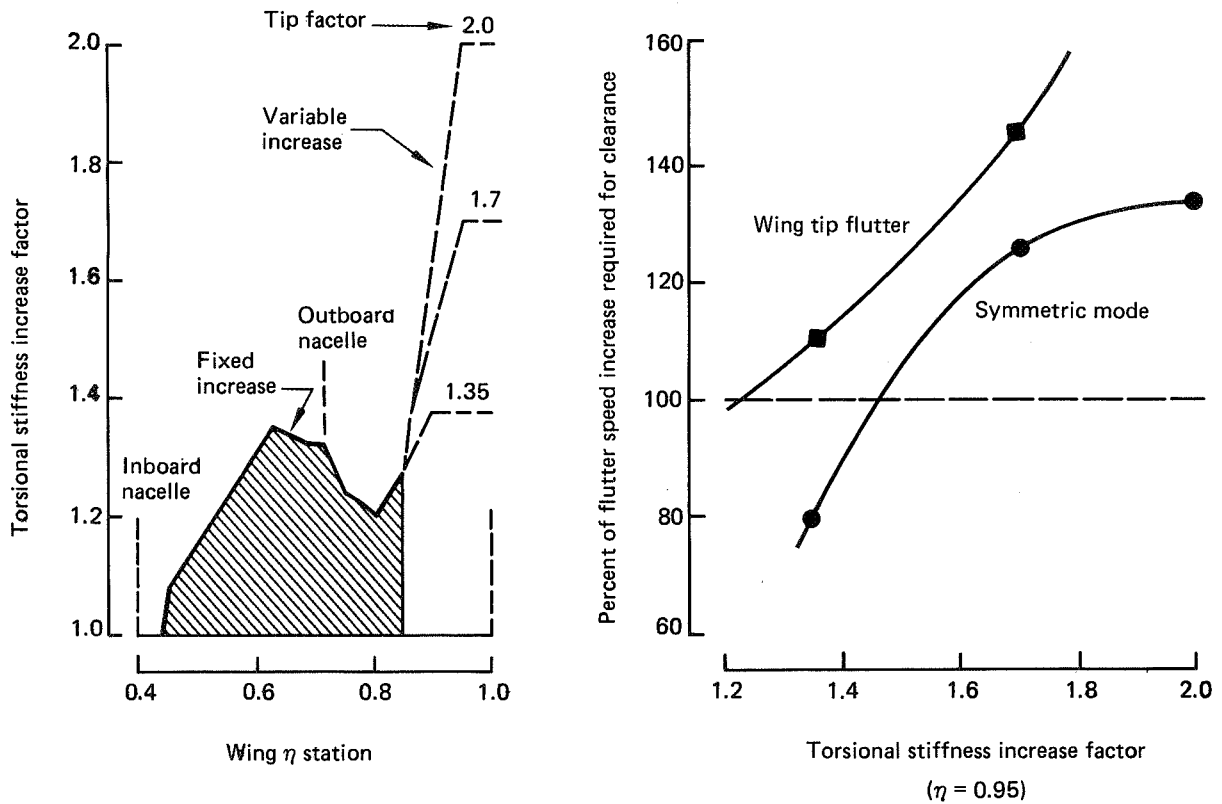


Figure B-28. Flutter Torsional Stiffness Requirements for Wing With Z13 Winglet

3.0 LOADS

This section contains sample force coefficient data derived from wind tunnel pressure tests. Figure B-29 shows the effect of the Z13 WTW and 1.83-m (6-ft) WTE on the wing spanwise lift distribution at Mach 0.85 as derived at maximum airplane C_L using wind tunnel pressure data. Similar data were derived at other Mach numbers as a function of wing angle of attack and added to the base wing lift (and moment) distributions for use in the aeroelastic loads analyses of the WTW and WTE configurations.

Figures B-30 and B-31 show the force coefficients for the Z9 winglet at Mach = 0.875 as derived from wind tunnel pressure data. Similar data were derived at other Mach numbers. These results were used to establish linearized force coefficients for use in the aeroelastic loads analysis of the Z9 WTW configuration. Z13 winglet force coefficients and associated design loads were derived based on the Z9 winglet results.

Figure B-32 shows the variation of aileron effectiveness associated with the Z13 WTW and 1.83-m (6-ft) WTE as determined by wind tunnel test. Except for the "carry over" airload on the 1.83-m (6-ft) WTE configuration, which was included in the aeroelastic loads analysis, the aileron effectiveness for these configurations was similar to the effectiveness for the base wing. Some simplification to the aeroelastic loads analysis was achieved by taking advantage of this similarity where appropriate.

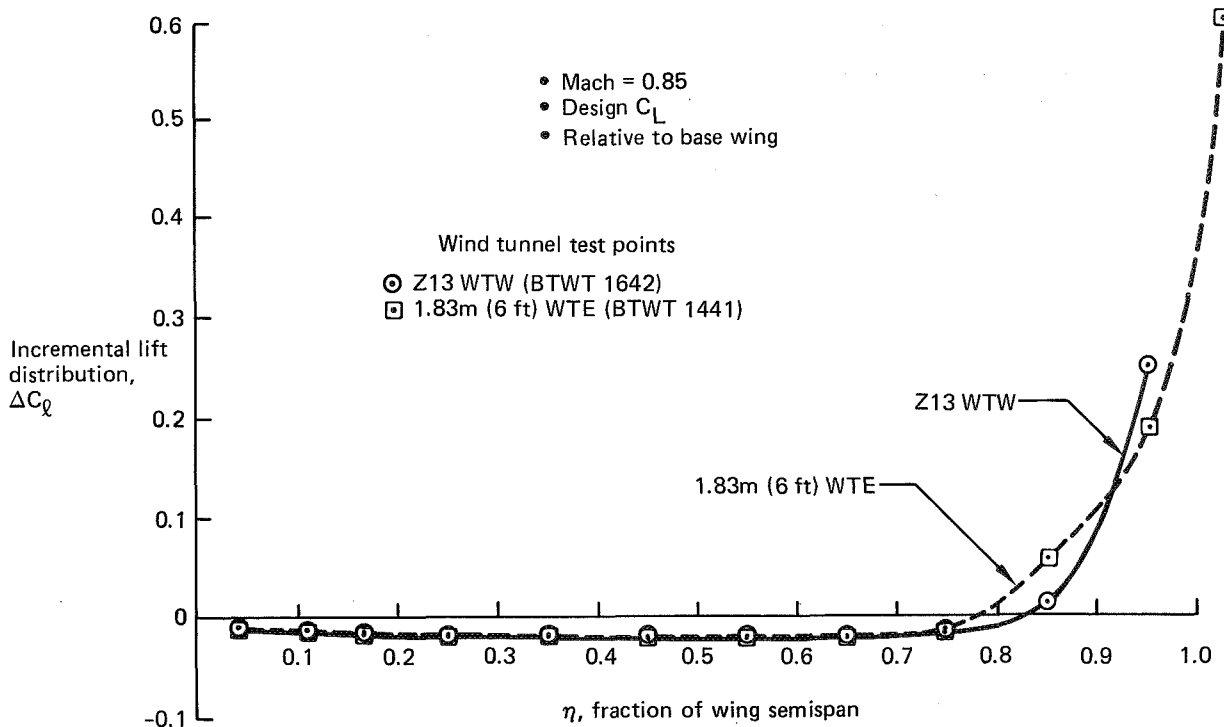


Figure B-29. Effect of WTW and WTE on Wing Lift Distribution

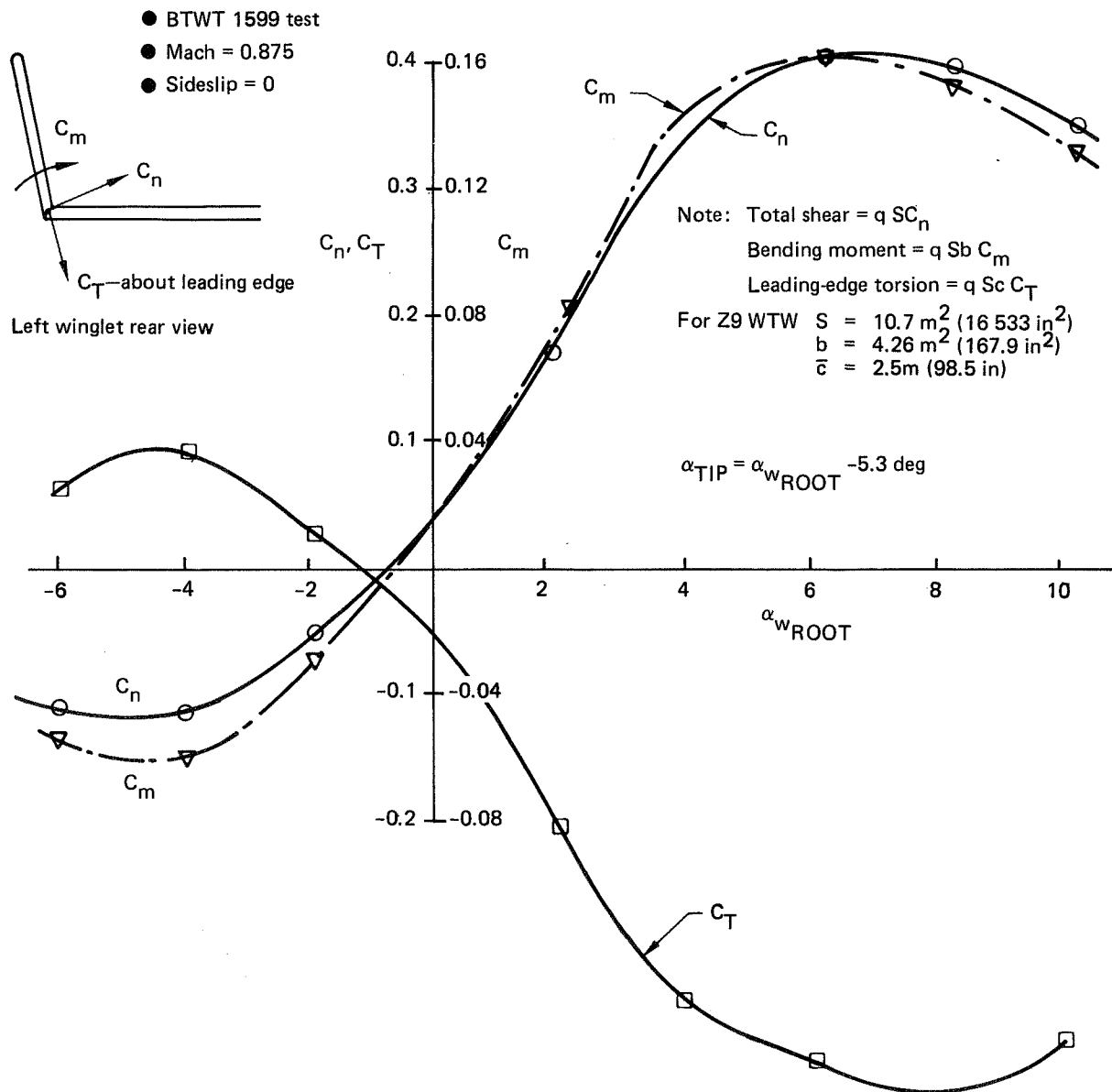
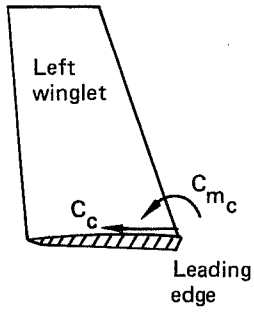


Figure B-30. Z9 WTW Force Coefficients Based on Integrated Pressures (C_n , C_m , C_T)



- BTWT 1599 test
- Mach = 0.875
- Sideslip = 0

Note: Total chord shear = $q S C_c$
 Chord moment = $q S b C_{m_c}$

For Z9 WTW $S = 10.7 \text{ m}^2 (16\,533 \text{ in}^2)$
 $b = 4.26 \text{ m}^2 (167.9 \text{ in})$

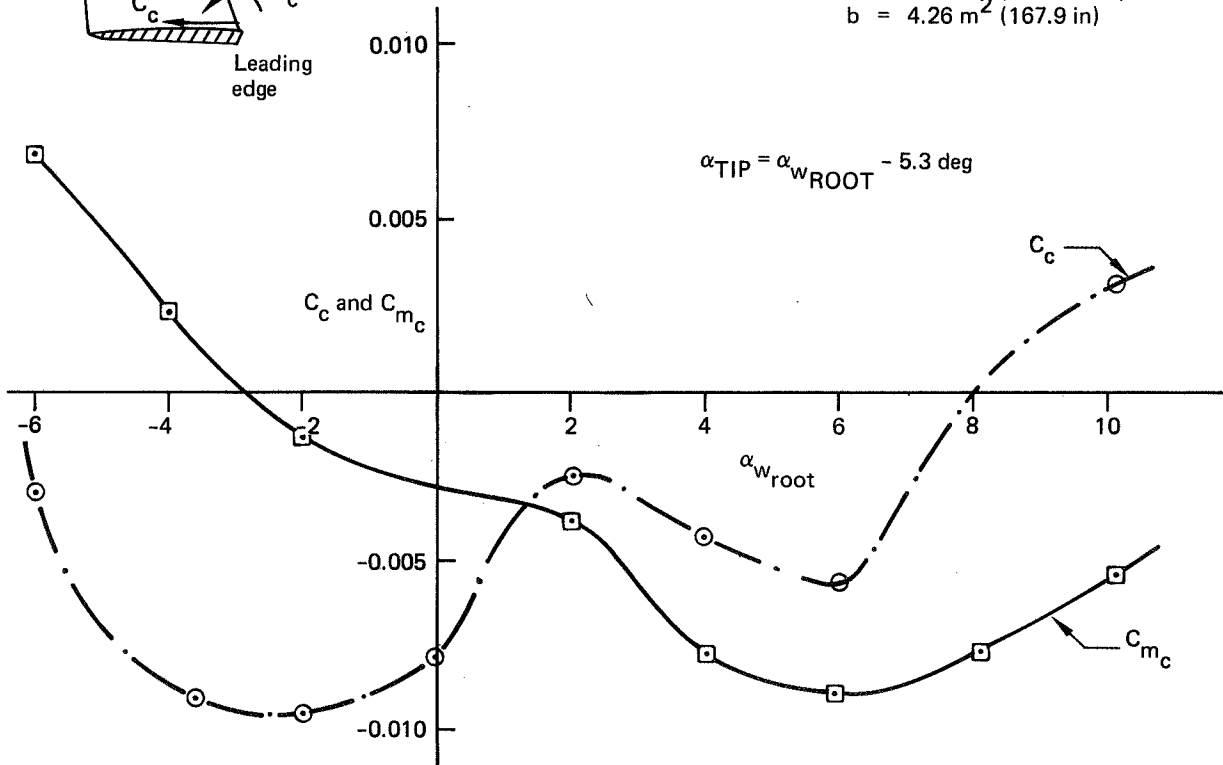


Figure B-31. Z9 WTW Force Coefficients Based on Integrated Pressures (C_c and C_{m_c})

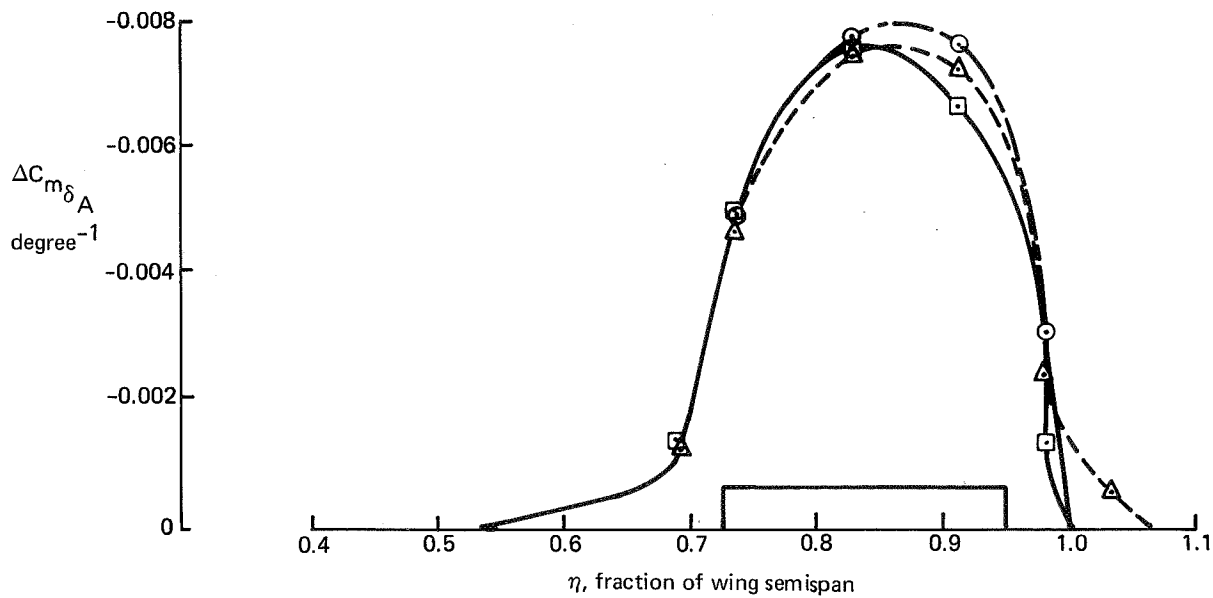
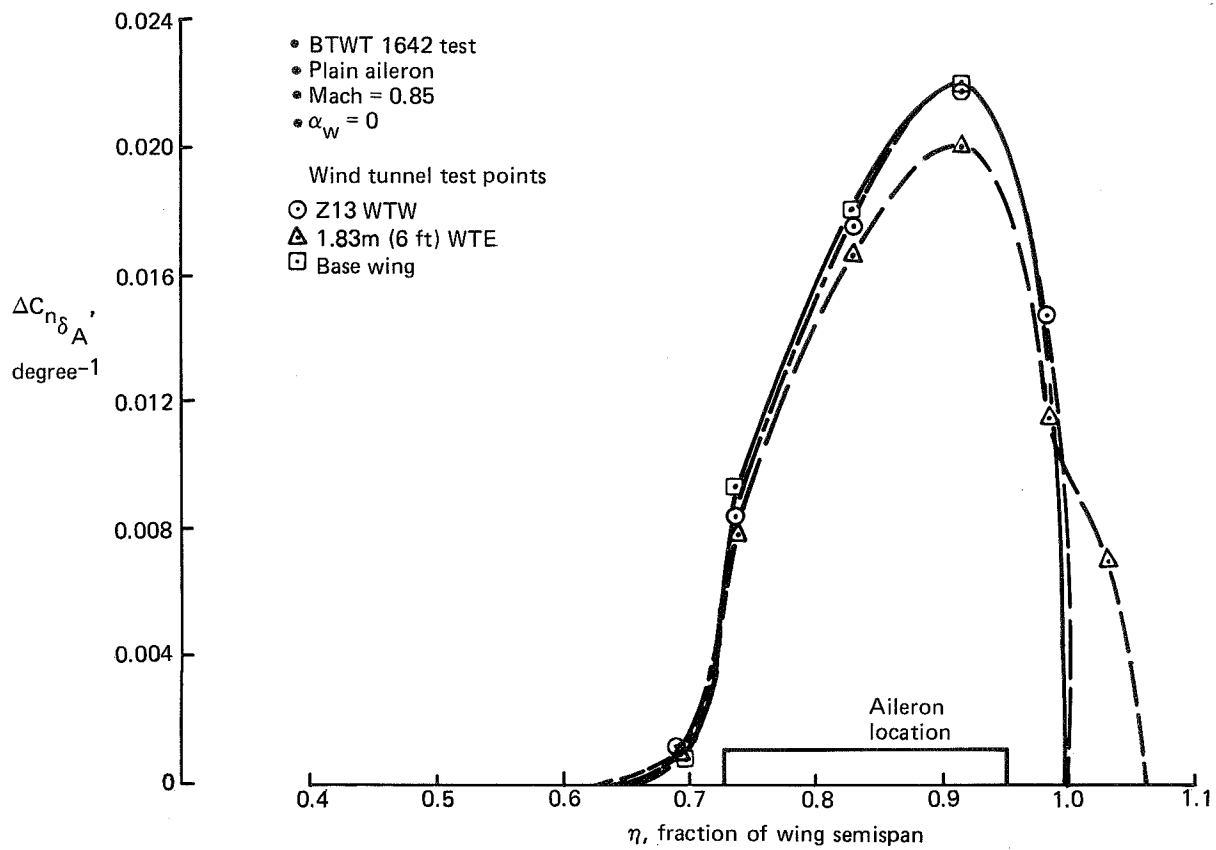


Figure B-32. Effect of WTW and WTE on Aileron Effectiveness

APPENDIX C
WIND TUNNEL TESTING

CONTENTS

	Page
1.0 FORCE AND PRESSURE TESTING	C-3
1.1 Model and Facilities Description	C-4
1.2 Winglet Test Summary	C-6
1.3 MLC Aileron Test Summary	C-9
1.4 Data Reduction	C-10
2.0 FLUTTER TESTING	C-11
2.1 Model and Facilities Description	C-11
2.2 Winglet Test Summary	C-15

FIGURES

	Page
C-1 Winglet High-Speed Wind Tunnel Test Model	C-4
C-2 Wing Pressure Port Locations for 747 Wind Tunnel Model	C-5
C-3 Winglet Blended Junction (View Looking Aft)	C-6
C-4 Wind Tunnel Configurations for Loads Testing.	C-10
C-5 Wind Tunnel Test Installation (CVAL)	C-12
C-6 View of Flutter Test Model With Winglets—Side View	C-12
C-7 Flutter Model Winglet Installation.	C-14
C-8 Winglet Z9 Geometry	C-14
C-9 Flutter Model Accelerometer Installation	C-15
C-10 Winglet Effect on Flutter Characteristics	C-17
C-11 Effect of Winglet Mass and Aerodynamics	C-17
C-12 Effect of Wing Tip Winglet Cant	C-18

TABLES

C-1 Test Condition Summary for Aerodynamics Testing	C-7
C-2 Wind Tunnel Run Log Summary for Loads Testing	C-8
C-3 Wind Tunnel Test Summary for Stability and Control Testing	C-9
C-4 Subsonic Flutter Model Scale Factors	C-13
C-5 Flutter Test Configuration	C-16

APPENDIX C

WIND TUNNEL TESTING

Two types of wind tunnel testing were conducted during this program:

- High-speed force and pressure model testing of winglets and maneuver load control (MLC) ailerons
- Flutter model testing of winglets (low-speed model scaled to represent high-speed conditions)

The program emphasized development and analysis of a satisfactory high-speed configuration; therefore, flaps-down configuration testing was not accomplished.

Force and pressure data were obtained during two 747 EET test entries in the Boeing Transonic Wind Tunnel (BTWT). The first winglet design (Z9) and two MLC aileron configurations (plain and full-span tab) were tested in the first entry (BTWT 1599). Shortly after this EET test, the opportunity presented itself to experiment with modifications (Z10) to the Z9 configuration as an add-on to another Boeing test (BTWT 1602). In the second EET entry (BTWT 1642), three winglets (Z11, Z12, Z13) were tested, and the untabbed aileron was tested in combination with the best winglet (Z13) and the 1.83-m (6-ft) WTE. The run sequence in both entries encompassed aerodynamics, stability and control (S&C), and loads testing.

Flutter tests were accomplished during two low-speed tunnel entries. The first entry was in the University of Washington Wind Tunnel (UWAL 1215), while the second entry was in the Convair Aeronautical Laboratory (CVAL 731).

Only the UWAL entry had been planned, but baseline correlation runs (routinely accomplished during all flutter tests) showed a model part was defective that could influence the quality of the results. An abbreviated set of data were obtained to provide an indication of winglet effects. The winglet testing disclosed the existence of a symmetric mode that significantly reduced flutter speeds. Following additional analysis and repair of the model part, a more extensive test was conducted at the CVAL where the existence of the symmetric mode was confirmed and a wing tip flutter mode was encountered.

1.0 FORCE AND PRESSURE TESTING

Force and pressure testing were accomplished to support winglet aerodynamic design development and performance, S&C, and loads analyses of the various study configurations. Wing pressure data were obtained in both BTWT entries. Due to time and budget constraints, winglet surface pressure data were obtained only for the Z9 configuration. Both plain and tabbed ailerons were tested in the first wind tunnel entry, while only plain ailerons were tested in the second. To conserve test time in the second entry, loads and S&C testing were conducted only for the best (Z13) WTW configuration.

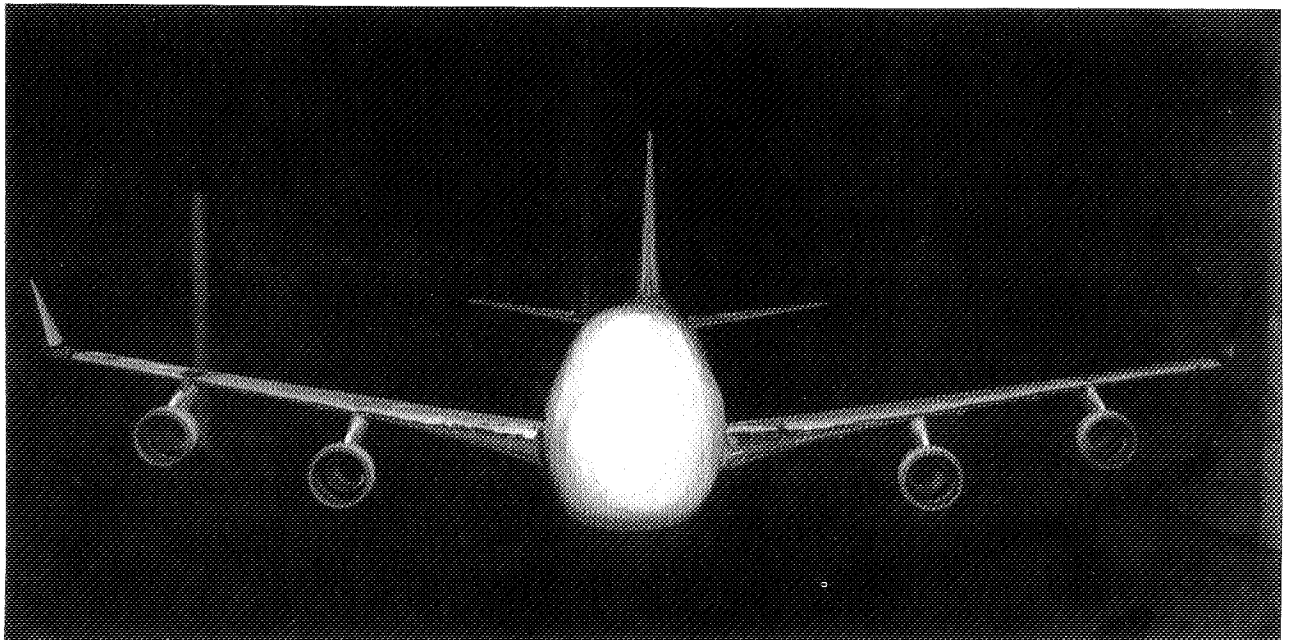
1.1 MODEL AND FACILITIES DESCRIPTION

Testing was performed in the Boeing Transonic Wind Tunnel, a closed-circuit single-return type with a 2.44-by-3.66m (8-by-12 ft) slotted-wall test section. The model was mounted on a sting strut using an internal force balance. Mach numbers ranged from 0.40 to 0.97.

The testing (BTWT 1599 and 1642) was performed on the existing 0.03-scale full-span pressure model (TE 1007) of the 747-200. Figure C-1 shows an overall view of the model with winglets installed. The left wing was instrumented to read upper-surface pressures and the right wing instrumented to read lower-surface pressures. Ten chordwise rows of pressure ports were located spanwise, as shown in Figure C-2.

Figure 22 (sec. 5.1.1 of the basic document) shows the Z9 and Z10 winglet planforms with typical airfoil sections. The Z10 winglet was a modification to the Z9 winglet. An outboard wing modification also was tested with the Z10 winglet. The Z9 (and Z10) winglets were equipped with three rows of pressure ports. Figures 25, 26, and 27 (sec. 5.1.1) show winglets Z11, Z12, and Z13 planforms and airfoils. No pressures were available on these three winglets. Figures 28 (sec. 5.1.1) and C-3 show details of the wing/winglet junctions that were modeled.

The 1.83-m (6-ft) wing tip was a constant chord extension of the present tip as shown in Figure 4 (sec. 4.1.1 of the basic document). This model was developed for a previous Boeing-sponsored test (BTWT 1441) and was used during the BTWT 1642 test to determine aileron effectiveness for the combined WLA and WTE configuration. The tip extension was equipped with one row of pressure ports located midway along the wing tip extension (WTE).



747-200 model with Z13 winglets
(0.03 scale)
BTWT installation

Figure C-1. Winglet High-Speed Wind Tunnel Test Model

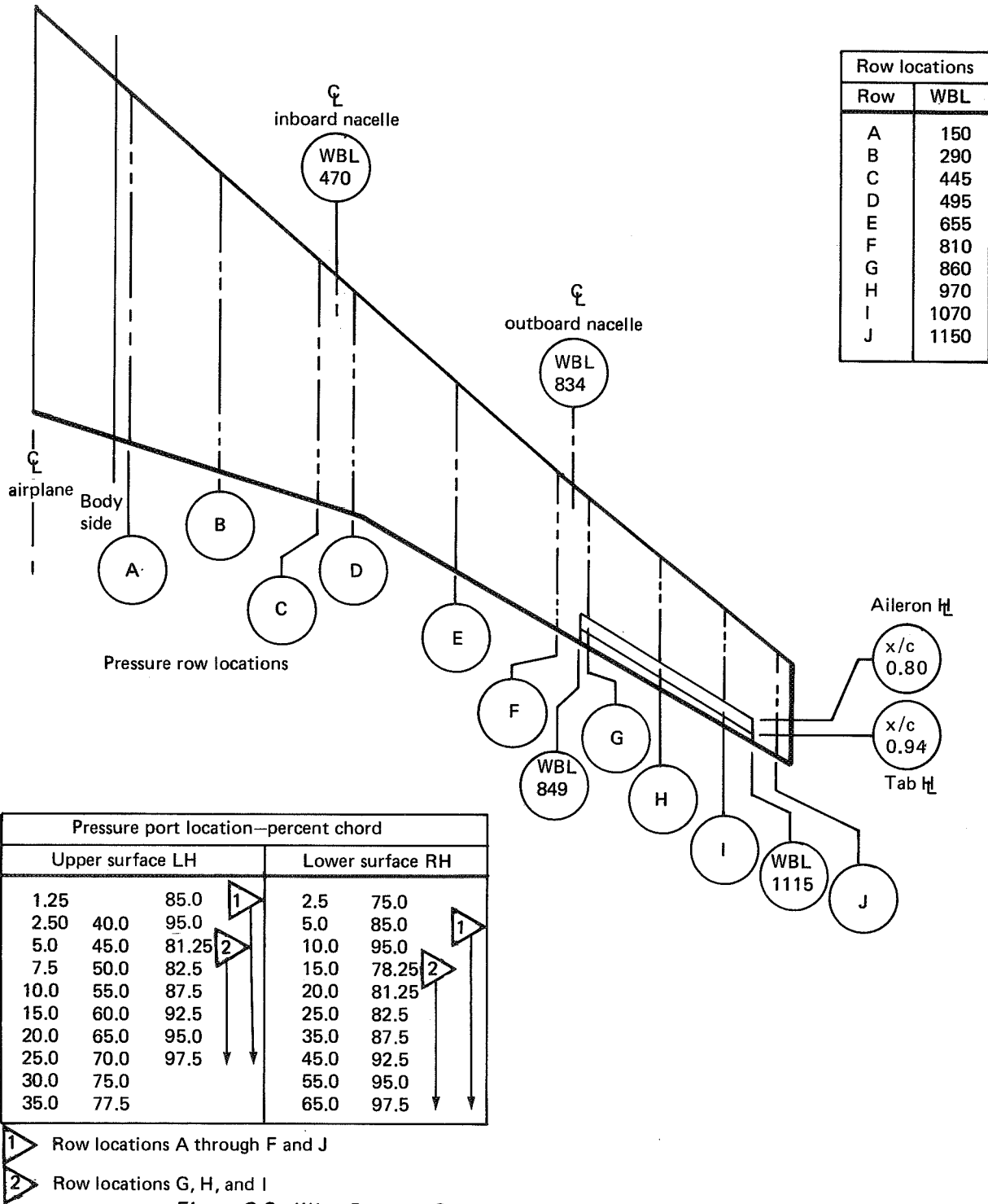


Figure C-2. Wing Pressure Port Locations for 747 Wind Tunnel Model



Figure C-3. Winglet Blended Junction (View Looking Aft)

1.2 WINGLET TEST SUMMARY

Aerodynamics—Winglet testing was conducted in two phases. The first phase consisted of two tests (BTWT 1599 and 1602) conducted during November and December of 1977. The second phase occurred in June of 1978 (BTWT 1642). A summary of the data acquired during these three tests is presented on Table C-1.

Initial testing used winglet Z9, but this winglet failed to achieve its performance goal due to excessive leading-edge velocities that caused significant wave drag plus undesirable wing tip interference losses. Winglet Z10, a modification to Z9 to reduce the root camber, resulted in some improvement, but still fell short of the goal. Winglet Z10 also was tested with an outboard wing modification designed to improve the pressure distribution. Little or no benefit was obtained.

Three new winglets were designed for the second phase of testing. The design philosophy incorporated use of aft-loaded airfoils, blended junctions between wing and winglet, and greater cant angle as follows:

- Z11—Partial chord planform with leading-edge strakelet and 15-deg cant angle
- Z12—Partial chord planform with leading-edge strakelet and 30-deg cant angle
- Z13—Trapezoidal planform and 30-deg cant angle

Winglet Z13 was the best of these three winglets and achieved nearly all of its theoretical potential; winglets Z11 and Z12 fell short of their goals. Trailing-edge separation on the low pressure (inboard) surfaces indicated that the latter two winglets incorporated too much aft camber.

Table C-1. Test Condition Summary for Aerodynamics Testing

First BTWT entry (BTWT-1)

BTWT 1599														BTWT 1602							
WTW	Off		Off		Z9			Z9		Z9		Z9	Z9	Off	Z10			Z10 + wing modification			
β_{WTW}	Off		Off		0 deg			15 deg		-3.0 deg		-1.5 deg	-1.5 deg	Off	-1.5 deg			-1.5 deg			
ΔFRL	0 deg		Off		Off			Off		Off		-1 deg	0 deg	0 deg	0 deg			0 deg			
Data Mach	F	P	F	VIZ	F	P	VIZ	F	P	VIZ	F	VIZ	F	F	F	F	P	VIZ	F	P	VIZ
0.70	▷	▷	▷		▷	▷		▷	▷		▷		▷	▷	▷	▷	▷		▷	▷	
0.80																					
0.82																					
0.84		▷		▷	▷	▷	▷		▷	▷	▷	▷	▷				▷	▷		▷	▷
0.86												▷									
0.88																					
0.90																					

Second BTWT entry (BTWT-2)

BTWT 1642																					
WTW	Off	Z12	Z12	Z12	Z12			Z13	Z13	Z13			Z11	Z11	Z11			Off	Z13	Z13	Z13
β_{WTW}	Off	-2 deg	-1 deg	0 deg	+1 deg			+1 deg	-1 deg	0 deg			+1 deg	0 deg	-1 deg			Off	0 deg	0 deg	0 deg
ΔFRL	0 deg	0 deg	0 deg	0 deg	0 deg			0 deg	0 deg	0 deg			0 deg	0 deg	0 deg			0 deg	0 deg	-1 deg	+0.5 deg
Data Mach	F	F	F	F	F	P	VIZ	F	F	F	P	VIZ	F	F	F	P	VIZ	F	F	F	F
0.40																		▷	▷	▷	▷
0.70	▷	▷	▷	▷	▷	▷		▷	▷	▷	▷		▷	▷	▷	▷					
0.80																					
0.82																					
0.84	▷	▷	▷	▷	▷	▷	▷	▷	▷	▷	▷	▷	▷	▷	▷	▷	▷				
0.86																					
0.88																					
0.90																					
0.92																					

Notes:

- Boundary layer trip strip on wing located at 10% chord, all runs
- F indicates force data
- P indicates pressure data
- VIZ indicates flow visualization

α_W series

- ▷ 0 deg to 7 deg by 0.2-deg increments
7 deg to maximum by 0.5-deg increments
- ▷ α for tail off $C_L = 0.35$
 $C_L = 0.45$
- ▷ α for tail off $C_L = 0.45$
- ▷ 0 deg to 7 deg by 0.2-deg increments
- ▷ -6 deg to 9 deg by 0.5-deg increments
0 deg to 7 deg by 0.2-deg increments
7 deg to maximum by 0.5-deg increments

Testing performed during this study was limited by budget constraints and tunnel availability. The potential of the Z12 partial chord winglet was theoretically about equal to Z13, but an effort to refine the Z12 winglet trailing edge to improve its performance had to be curtailed. The concept of using a wing glove to further improve junction loading was never fully explored. However, the testing which was done was adequate to complete the cost/benefit study. More extensive testing is necessary prior to flight testing.

Loads—Wing pressure data were obtained for the Z9 and Z13 winglet configurations for a complete range of Mach and α points as summarized in Table C-2. Winglet pressures were obtained only on the Z9 configuration due to budget limitations. Selected data are presented in Appendix B.

Table C-2. Wind Tunnel Run Log Summary for Loads Testing

δ_A (deg)	BTWT 1599									BTWT 1642									
	0	-10	-10	-25	+10	+10	0	-10	0	0	-10	-25	0	-10	0	-10	0	-10	
δ_T (deg)	0	0	+10	0	0	-10	0	0	0	0	0	0	0	0	0	0	0	0	
WTW	Off	Off	Off	Off	Off	Off	Z9	Z9	Z9	Off	Off	Off	Z13	Z13	Off	Off	Off	Off	
1.83m WTE	Off	Off	Off	Off	Off	Off	Off	Off	Off	Off	Off	Off	Off	Off	On	On	Off	Off	
Trip strip	On	On	On	On	On	On	On	On	On	On	On	On	On	On	On	On	Off	Off	
Yaw (deg)	0	0	0	0	0	0	0	0	± 4	0	0	0	0	0	0	0	0	0	
Mach																			
0.40	1	2	2	2	2	1	1			3	1	1	1	1	1	1	1		
0.55																			
0.70																		1	1
0.80																			
0.85										1	3							1	1
0.875															4				
0.90																			
0.925																			
0.95										1									
0.97											3								

Notes:

- All tests recorded wing pressures and force balance loads
- All tests conducted with horizontal tail removed
- Boundary layer trip strip located at 10% chord line
- Z9—cant = 15 deg, incidence = -1.5 deg (negative outboard)
- Z13—cant = 30 deg, incidence = 0 deg

α_W series

- 1 -6 deg to max by 2-deg increments
- 2 -4 deg, 0 deg, 4-deg and max
- 3 0 to 10 deg by 2-deg increments
- 4 -2 deg. to max by 2-deg increments

Stability and Control—Pitch runs and a limited number of yaw runs were made for the Z9 and Z13 configurations to determine the effects on longitudinal and lateral/directional stability characteristics. A summary of the stability and control testing is presented in Table C-3.

Table C-3. Wind Tunnel Test Summary for Stability and Control Testing

WTW	BTWT 1599														BTWT 1642								
	Off	Off	Off	Off	Off	Off	Off	Off	Off	Z9	Z9	Z9	Z9	Z9	Off	Off	Off	Off	Off	Z13	Z13	Z13	Z13
Horizontal tail	Off	On	On	On	On	On	On	On	On	Off	On	On	On	On	On	On	On	On	On	On	On	On	On
Ψ	0	0	0	0	0	0	0	0	4	0	0	0	4	-4	0	0	0	0	4	0	0	2	4
δ_A L/R	0	0	-25	-10	10	10	10/-10	10/-10	0	0	0	-10	0	0	0	-25	-10	15	0	0	-10	0	0
δ_T L/R	0	0	0	0	0	-10	0	-10/10	0	0	0	0	0	0	0	0	0	0	0	0	0	0	0
Mach																							
0.40	X	X	X	X	—	X	X	X	X	X	X	X	X	X	X	X	X	X	X	X	X	X	X
0.70	X	X	X	X	X	X	X	X	—	X	X	X	—	—	X	X	X	X	X	X	X	X	X
0.80	X	X	X	X	X	X	X	X	—	X	X	X	—	—	X	X	X	X	X	X	X	X	X
0.82	X	X	X	X	X	X	X	X	—	X	X	X	—	—	X	X	X	X	—	X	X	—	—
0.84	X	X	X	X	X	X	X	X	0.85	X	X	X	0.85	0.85	X	X	X	X	X	X	X	X	X
0.86	X	X	X	X	X	X	X	X	—	X	X	X	—	—	X	X	X	X	—	X	X	—	—
0.88	X	X	X	X	X	X	X	X	0.875	X	X	X	0.875	0.875	X	X	X	X	X	X	X	X	X
0.90	X	X	X	X	X	X	X	X	—	X	X	X	—	—	X	X	X	X	—	X	X	—	—
0.92	—	X	—	X	—	X	0.925	0.925	0.925	—	X	X	0.925	0.925	X	X	X	X	X	X	X	X	X
0.95	—	—	—	—	—	—	X	X	—	—	—	—	—	—	X	X	X	X	—	X	X	—	—
0.97	—	X	—	X	—	X	X	X	X	—	X	X	—	—	X	X	X	X	—	X	X	—	—

Notes:

- Wing trip strip at 10% local chord
- Z13: Cant = 30 deg (outboard tilt)
Incidence = 0 deg
- Z9: Cant = 15 deg (outboard tilt)
Incidence = -1.5 deg (leading edge outboard)
- Horizontal tail on configurations set at $\delta_{FR_L} = 0$ deg

*With and without balance weights

1.3 MLC AILERON TEST SUMMARY

Loads Testing—The various configurations tested during the two BTWT tunnel entries are summarized in Figure C-4 and the associated Mach and angle of attack ranges are tabulated in Table C-2. Force balance data was recorded for all loads tests with the horizontal tail removed.

Sample data from the tests is shown in Section 6.1.1 of the basic document for the basic wing and in Appendix B for the Z9 winglet and 1.83-m (6-ft) tip extension.

Stability and Control Testing—Force balance data were obtained to determine the effects of symmetrically deflected ailerons on airplane lift and pitching moment. Both tail-on and tail-off data were obtained. The test conditions are presented in Table C-3.

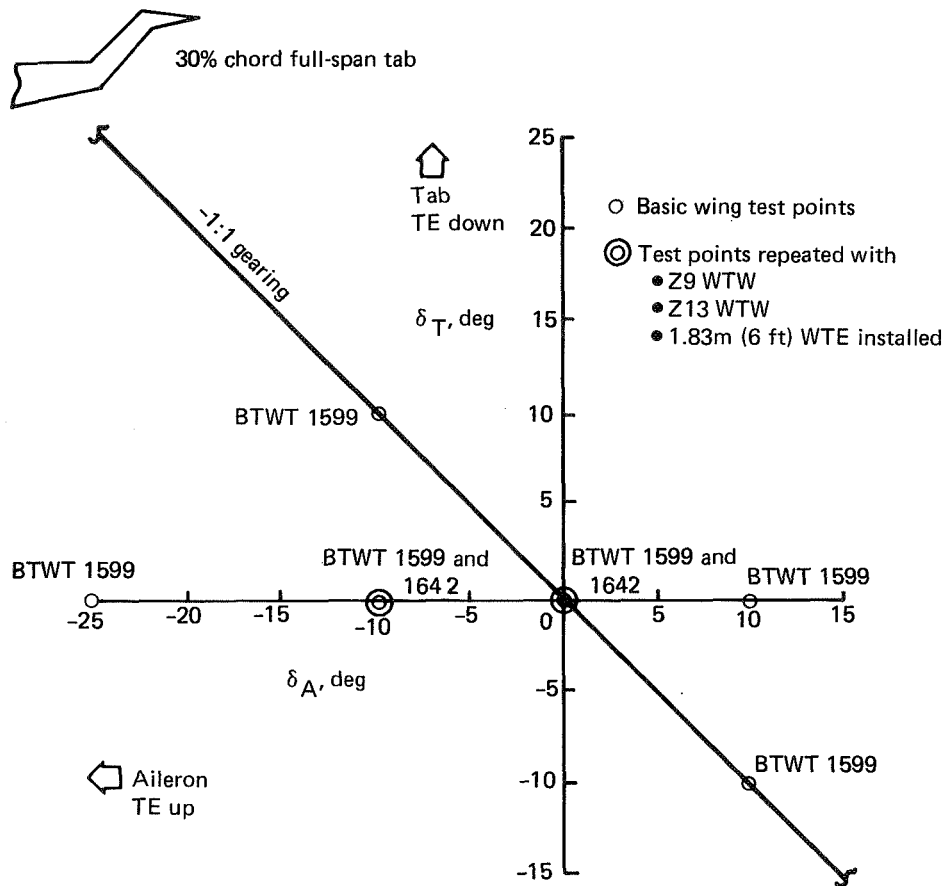


Figure C-4. Wind Tunnel Configurations for Loads Testing

1.4 DATA REDUCTION

Force and Moment Data—The wind tunnel test data were reduced using standard BTWT data reduction procedures.

Data Reduction Corrections—The following corrections were used during test data reduction:

- Wind-off zeros
- Initial loads
- Balance output corrected for interactions and temperature effects
- Static weight tares
- Sting-balance deflections
- Moment transfers to the wing 0.25 mean aerodynamic chord
- Wall interference corrections
- Static pressures recorded in the cap plenum corrected to test section centerline conditions (11% porosity walls)
- Upflow corrections
- Stability axis conversions
- Skin friction drag corrections

The upflow used in final data reduction was obtained experimentally during the BTWT 1603 test which followed the Z10 test.

Skin friction drag was corrected for deviations in temperature to a nominal Reynolds number per foot.

Prior to use in the aerodynamic analysis, the force data were faired using the curve fairing routine option available in the data manipulation program.

Pressure Data—Data generated in the test section were first reviewed with the aid of online pressure plots and limited force balance plots. The on-line pressure plots, in conjunction with periodic leak checks of the pressure ports, were used to determine the functional status of the ports. A list of nonfunctional ports was used to derive a preliminary set of pressure plots. These plots were thoroughly reviewed to verify the proper consideration of nonfunctional ports. A further iteration generated a set of corrected pressure plots with a tabulated set of integrated pressure data in the form of section aerodynamic coefficients.

The integrated pressure data were linearized and incremental coefficients for the winglet, tip extension, and aileron configurations determined. The incremental data were combined with existing base wing data. This approach was used to preserve the basic wing aerodynamic data that had previously been adjusted to correlate with flight test load measurements.

2.0 FLUTTER TESTING

The unique nature of the WTW configuration and lack of analytical and test experience with such configurations dictated the necessity of an early wind tunnel flutter test program to provide confidence in the preliminary design evaluation. Because the scope of Phase I preliminary design studies was limited due to the resources available, the WTE configurations were considered to be more conventional and amenable to analysis, with a better level of confidence relative to winglet analysis. For these reasons, it was elected to delete the WTE concept from initial wind tunnel investigations and concentrate the test effort on the winglet configuration. The approach was to gain early verification of whether or not winglets were a critical flutter problem for the 747 EET airplane. From these experimental results, any flutter data obtained then could be used to develop the analysis programs to a state where they could economically provide the answers to what structural penalties would be incurred to design a flutter-free winglet configuration. Finally, the wind tunnel model was designed to economically provide design development data, including the effects of winglet geometry variations and flutter sensitivity to the usual airplane flight configurations such as payload and wing fuel distribution. Summary descriptions of the 747 EET/WTW wind tunnel flutter test program are provided in the following subsections. Section 2.1 describes the model, test techniques, and facility used. Section 2.2 presents a summary of major results obtained.

2.1 MODEL AND FACILITIES DESCRIPTION

An existing dynamically scaled 747 flutter model was modified to support wind tunnel investigations of wing tip winglet effects on 747 flutter characteristics. The model tested was a 0.046-scale dynamic model of the 747-200B airplane. Figures C-5 and C-6 show the model installed in the Convair Aeronautical Laboratory wind tunnel. The

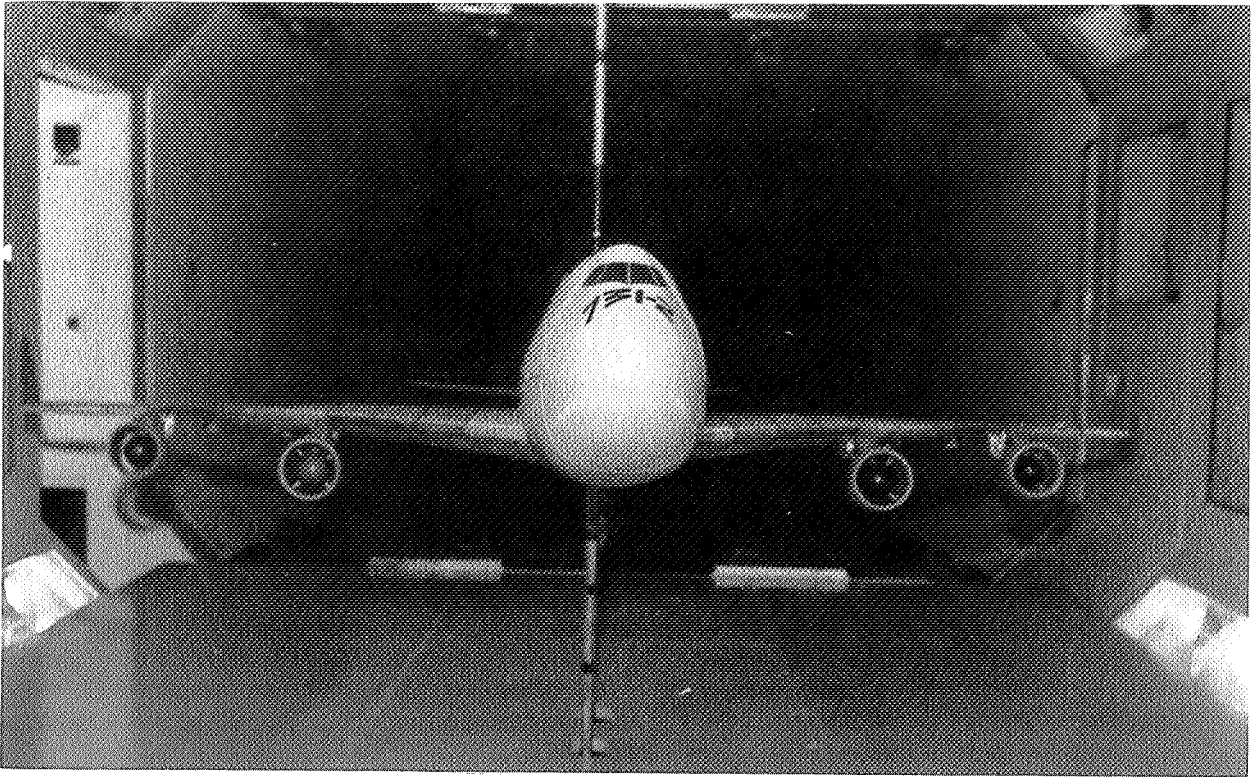


Figure C-5. Flutter Model Wind Tunnel Test Installation (CVAL)

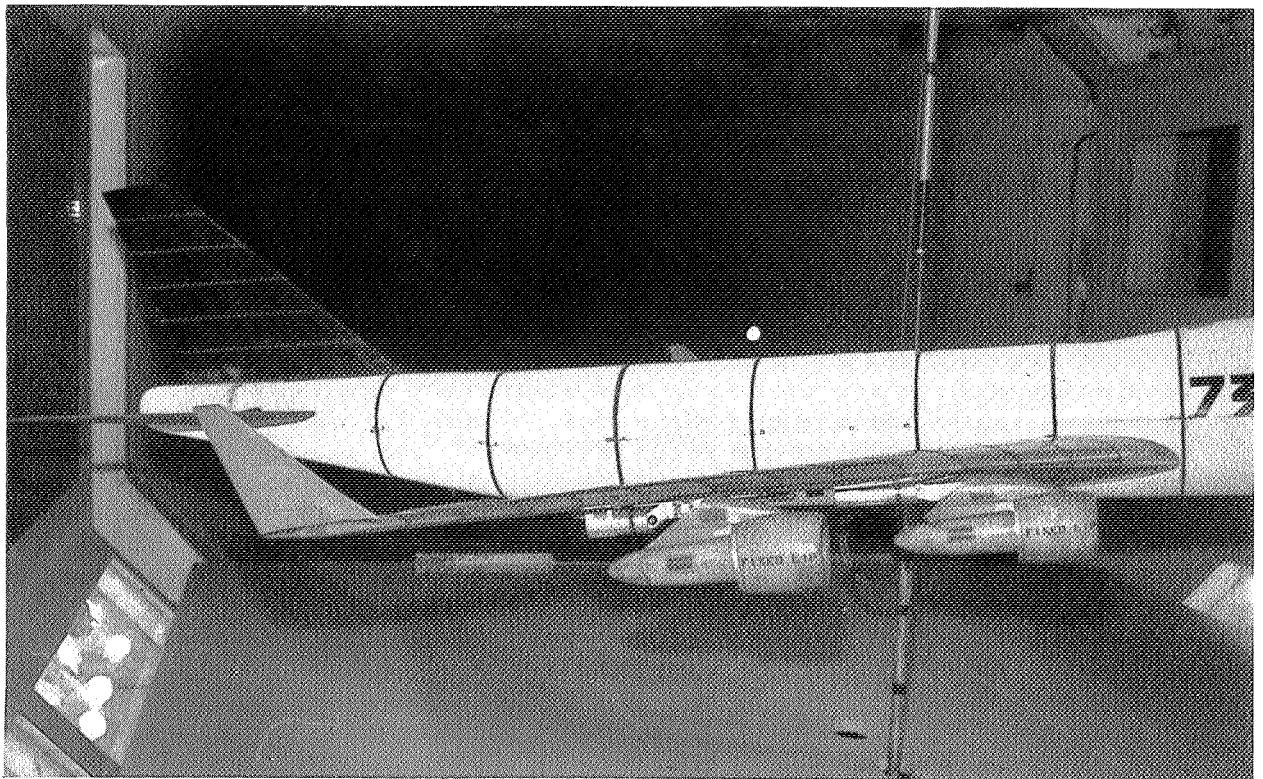


Figure C-6. Flutter Test Model With Winglets—Side View

dynamic scale factors are listed in Table C-4. The model was scaled to represent the airplane at an altitude of 4877m (16 000 ft) based upon a wind tunnel density altitude of 152m (500 ft). The model was attached to a vertical rod in the center of the tunnel working section. The rod allowed freedom in pitch, yaw, and vertical translation and provided a low frequency restraint to the model in roll, side translation, and fore and aft translation. The model was "flown" in the tunnel by remote control of the horizontal stabilizer trim. The model nacelles had flow-through fan cowls scaled to give an inlet mass flow ratio equivalent to the airplane at the design dive speed.

Table C-4. Subsonic Flutter Model Scale Factors

● Dimension (L)	$\frac{L_M}{L_A}$	0.046
● Density (ρ)	$\frac{\rho_M \text{ 152m (500 ft)}}{\rho_A \text{ 4877m (16000 ft)}}$	1.618
● Speed (V) (incompressible flow)	$\frac{V_M}{V_A}$	0.1956
● Stiffness (K)	$\frac{K_M}{K_A} = (L_M/L_A)^4 (\rho_M/\rho_A) (V_M/V_A)^2$	0.277×10^{-6}
● Weight (W)	$\frac{W_M}{W_A} = (L_M/L_A)^3 (\rho_M/\rho_A)$	0.158×10^{-3}
● Mass moment of inertia (I)	$\frac{I_M}{I_A} = (L_M/L_A)^5 (\rho_M/\rho_A)$	0.333×10^{-6}
● Frequency (ω)	$\frac{\omega_M}{\omega_A} = (L_A/L_M) (V_M/V_A)$	4.252
● Dynamic pressure (q)	$\frac{q_M}{q_A} = (V_M/V_A)^2 (\rho_M/\rho_A)$	0.0619
● Fraction of model weight to be supported	—	0.168

M = Model A = Airplane

The winglets were installed as shown in Figure C-7. Figure C-8 shows the winglet geometry. The following parts were made for testing winglets:

- A set of Z9 winglets
- A set of attachment brackets to allow three different incidence angles and a different cant angle at one incidence angle
- A pair of weights and attachment fittings to represent the mass, center of gravity, and inertia of the winglets to allow evaluation of the winglet mass effects alone

Existing nacelle struts provided a range of side bending and vertical bending frequencies. Existing fuel weights provided fuel quantity increments of 25%. Existing payload weights provided full and empty payload configurations.

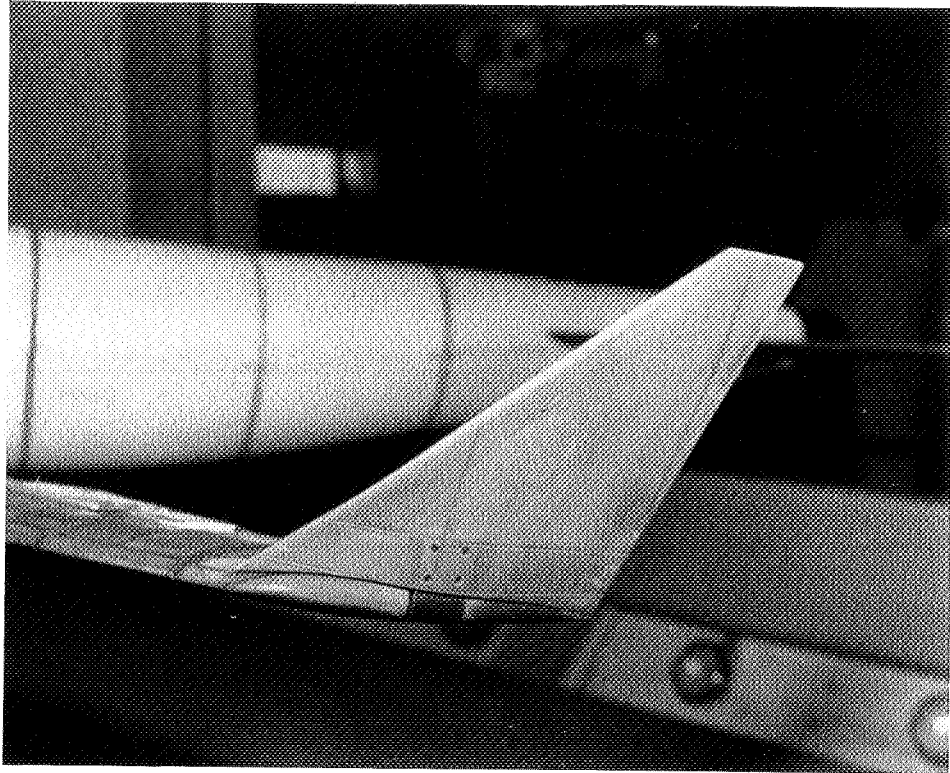


Figure C-7. Flutter Model Winglet Installation

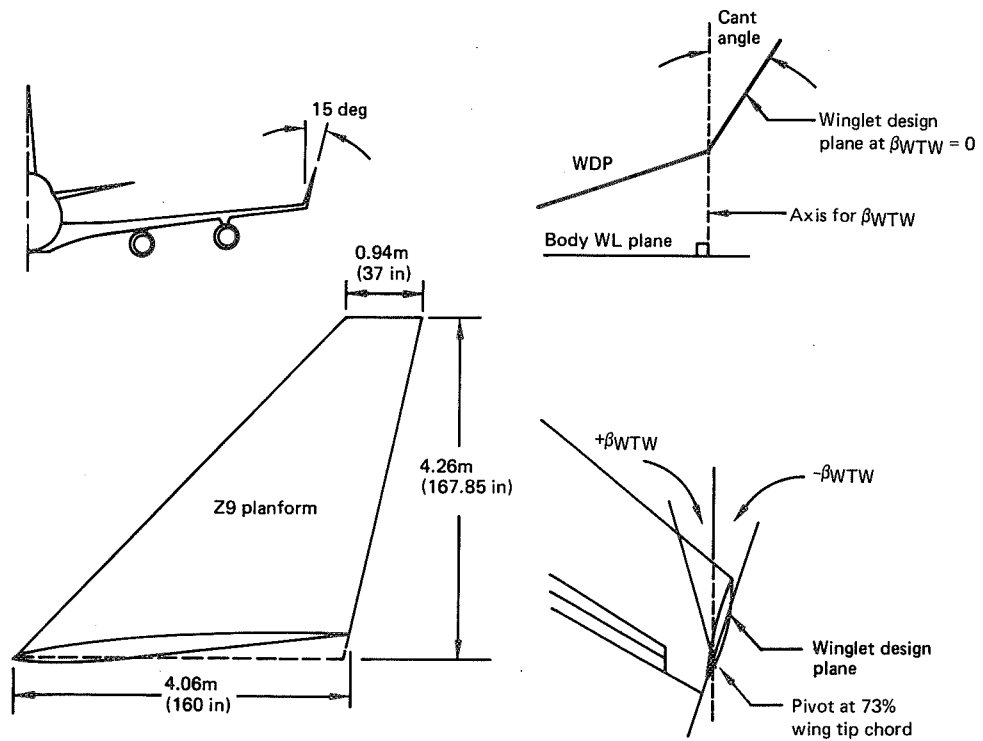


Figure C-8. Winglet Z9 Geometry

Nine calibrated accelerometers were installed in the model, as shown in Figure C-9. These accelerometers provided modal frequency, phasing, and relative amplitude. Convair provided wind tunnel temperature, pressure, and airspeed at each test point. High-speed motion pictures (250 frames per second) were taken at selected test points from the tunnel bellmouth and side. The accelerometer traces and motion pictures were used for modal identification, in addition to visual observations made during the test.

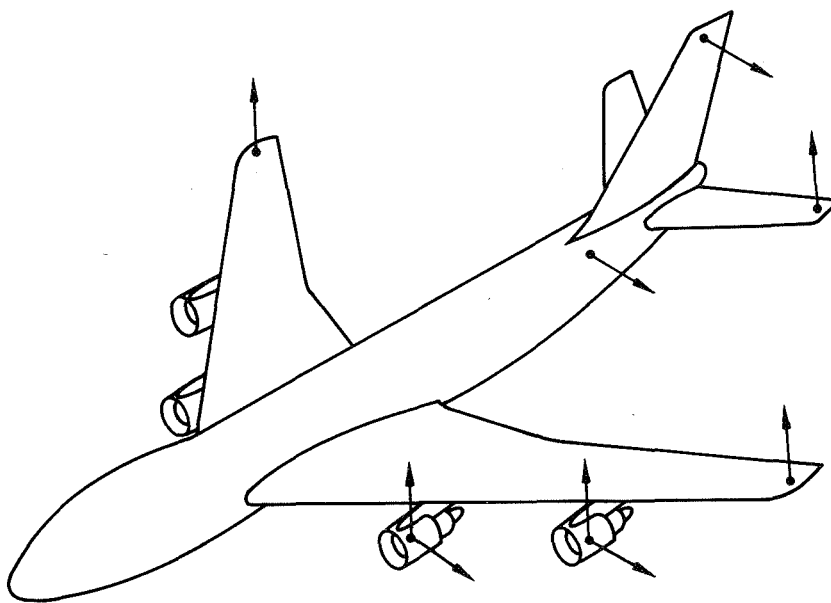


Figure C-9. Flutter Model Accelerometer Installation

2.2 WINGLET TEST SUMMARY

Wind tunnel flutter tests were accomplished in the CVAL facility to define the flutter characteristics of the 747 airplane with wing tip winglets. Table C-5 contains a list of the test parameters. Specific objectives were to determine:

- The effect of wing tip winglets, WTW cant angle, and WTW incidence angle on flutter characteristics
- The critical payload and wing fuel condition for flutter with winglets installed
- The effect of outboard nacelle strut frequencies on wing flutter with winglets installed

The addition of winglets had a significant effect on the flutter characteristics, including the introduction of a symmetric flutter mode and a wing tip flutter mode. The following conclusions are based on the flutter model test results:

- The addition of wing tip winglets had a significant effect on flutter characteristics by lowering flutter speeds and introducing a symmetric flutter mode. A wing tip flutter mode also was evident for certain configurations.
- Winglet mass effects lowered flutter speeds.
- Winglet aerodynamics significantly lowered flutter speeds.

- Flutter speeds with winglets were affected by changes in payload in the same manner as the basic airplane is affected by changes in payload.
- The effect of cant angle was small.
- Flutter speed decreased as the winglet incidence became more positive.
- Flutter speeds with winglets were not significantly affected by inboard nacelle strut side and vertical bending frequencies. Flutter speeds and modal characteristics with winglets were significantly affected by outboard nacelle strut side bending frequency. The symmetric flutter mode speed was significantly increased with a decrease in outboard nacelle strut vertical bending frequency.
- Flutter speeds with winglets increased with a reduction in outboard main fuel and, to a lesser extent, with a reduction in inboard main fuel. However, no usable fuel placard was defined that would not require some other means of raising flutter speeds.

Table C-5. Flutter Test Configuration

Test parameter	Notation	Description
Payload	OEW Full	Operating empty weight Aft cg, dumbbell-loaded
Fuel	—	Fuel variation: Inboard mains—25% to 100% Outboard mains—25% to 100% Standard reserves—full or empty Extended range fuel—full or empty
Strut	—	Outboard nacelle strut side bending frequency variation (5 struts) with full wing fuel, $\omega/\omega_{ref} = 0.89$ to 1.39
Winglet	Off On Weight	Nominal airplane Z9 winglet installed Mass, cg, inertia representation of Z9
Cant	15 deg 30 deg	Nominal winglet cant angle Alternate winglet cant angle
Incidence	-1.5 deg 1.5 deg -4.5 deg	1.5-deg toe out—nominal incidence 1.5-deg toe in—plus incidence 4.5-deg toe out—minus incidence

Figures C-10, C-11, and C-12 are included to show the effect of winglet mass, aerodynamics, and cant angle on the flutter characteristics of the baseline airplane. The results are presented as flutter speed versus outboard nacelle strut side bending frequency for each of the winglet parameters.

Figure C-10 shows the effect of adding the winglet to the baseline airplane, introducing the wing tip flutter and symmetric flutter modes. Figure C-11 shows the effect of winglet mass and aerodynamics separately on the flutter characteristics of the baseline airplane. Figure C-12 shows the effect of changing the 15-deg cant angle of the Z9 winglet to the 30-deg cant angle of the Z13 winglet.

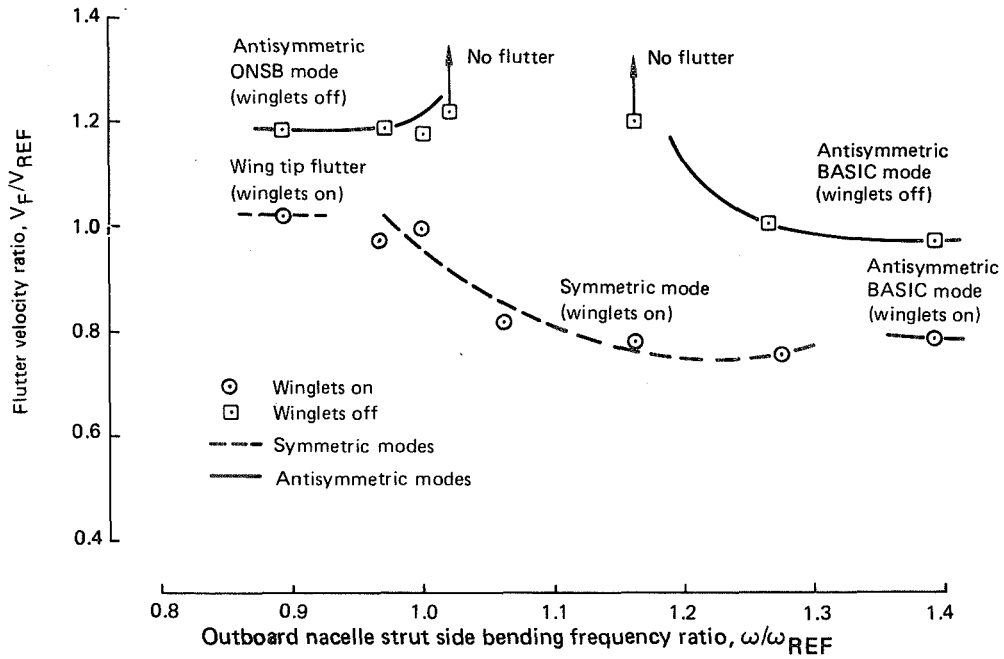


Figure C-10. Winglet Effect on Flutter Characteristics

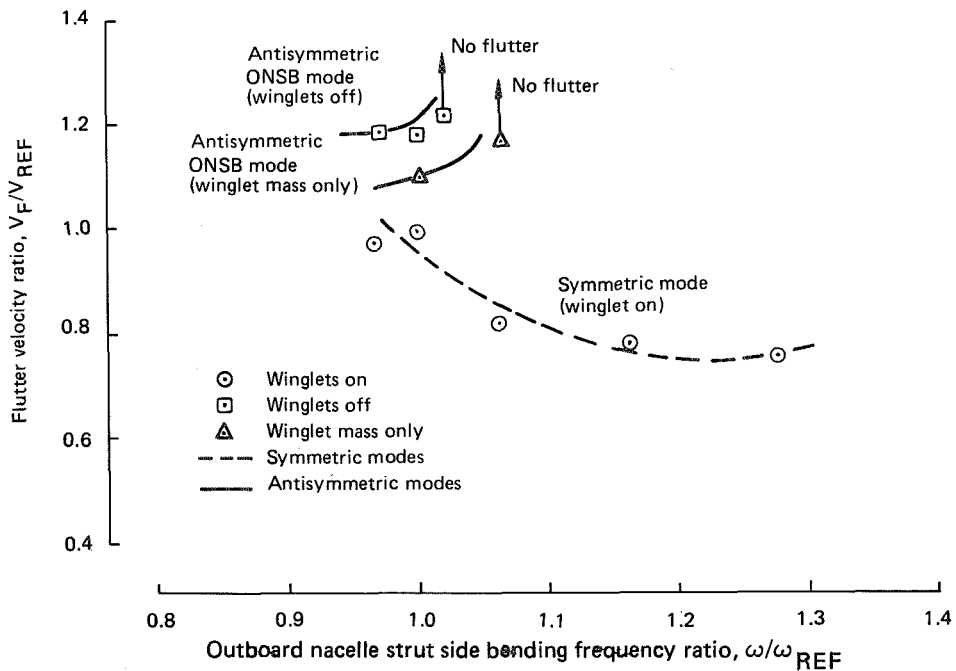


Figure C-11. Effect of Winglet Mass and Aerodynamics

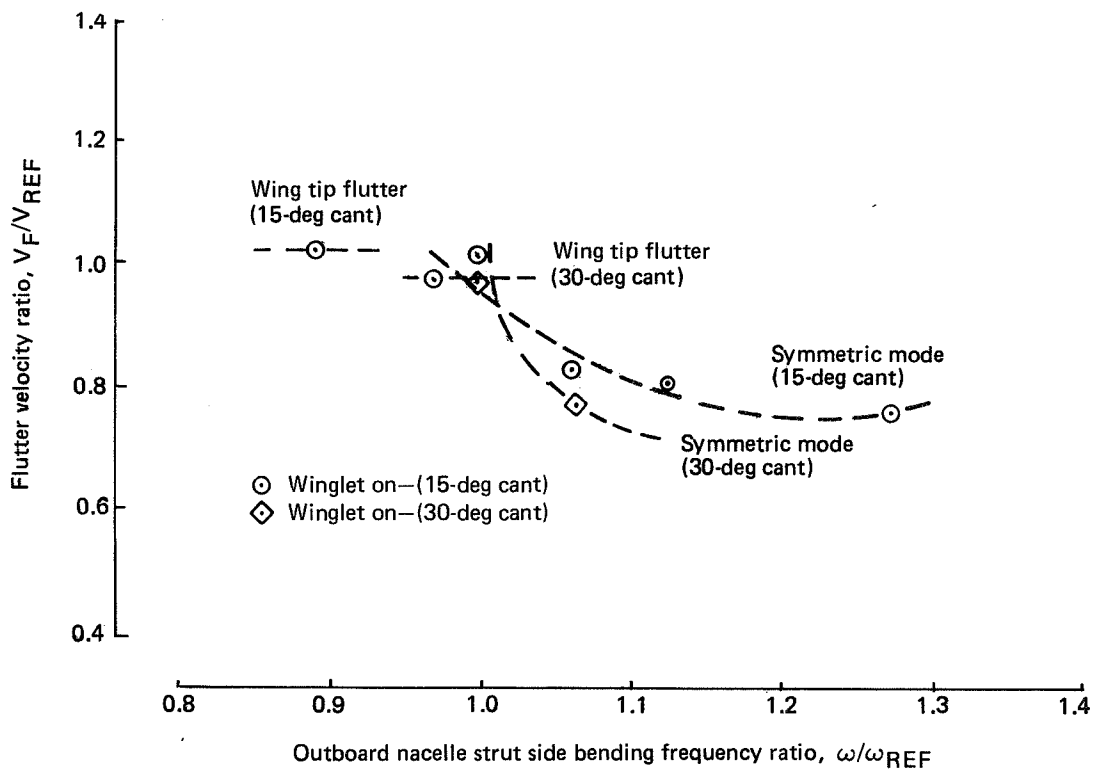



Figure C-12. Effect of Wing Tip Winglet Cant

1. Report No. NASA CR-3164		2. Government Accession No.		3. Recipient's Catalog No.	
4. Title and Subtitle Selected Advanced Aerodynamics and Active Controls Technology Concepts Development on a Derivative B-747—Final Report				5. Report Date July 1980	
				6. Performing Organization Code	
7. Author(s) Staff of Boeing Commercial Airplane Company (747 Product Development)				8. Performing Organization Report No. D6-48664	
				10. Work Unit No.	
9. Performing Organization Name and Address The Boeing Commercial Airplane Company P.O. Box 3707 Seattle, Washington 98128				11. Contract or Grant No. NAS1-14741	
				13. Type of Report and Period Covered Contractor Report May 1977 - May 1979	
12. Sponsoring Agency Name and Address National Aeronautics and Space Administration Washington, D.C. 20546				14. Sponsoring Agency Code	
15. Supplementary Notes Langley Technical Monitor: David B. Middleton Final Report					
16. Abstract Analyses, conceptual design, and wind tunnel test evaluations covering the feasibility of applying wing tip extensions, winglets, and active control wing load alleviation to the Boeing 747 are described. Winglet aerodynamic design methods and high-speed wind tunnel test results of winglets and of symmetrically deflected ailerons are presented. Structural resizing analyses to determine weight and aeroelastic twist increments for all the concepts and flutter model test results for the wing with winglets are included. Control law development, system mechanization/reliability studies, and aileron balance tab trade studies for active wing load alleviation systems are discussed. Results are presented in the form of incremental effects on L/D, structural weight, block fuel savings, stability and control, airplane price, and airline operating economics.					
17. Key Words (Suggested by Author(s)) Wing tip extensions, winglets, active controls, wing load alleviation			18. Distribution Statement  Subject Category 05		
19. Security Classif. (of this report) Unclassified		20. Security Classif. (of this page) Unclassified		21. No. of Pages 300	22. Price